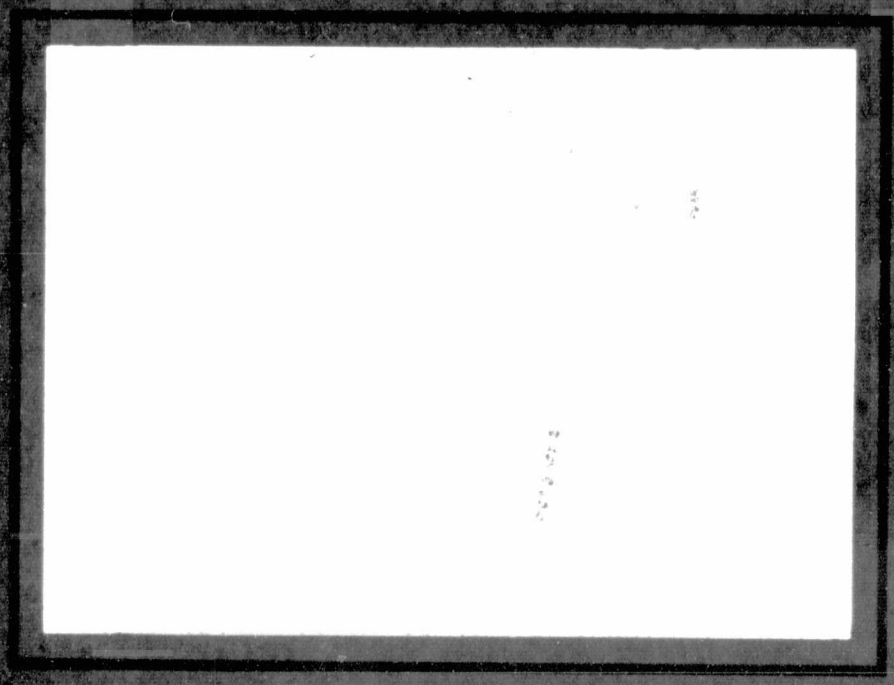

UNIVERSITY OF CALIFORNIA
SAN DIEGO

La Jolla, California

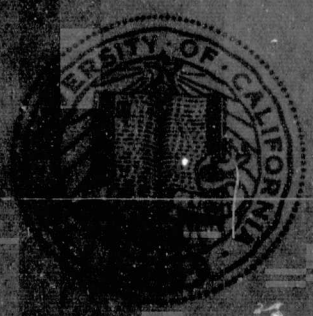

Center for Astrophysics and Space Sciences

Publications Resulting from:

"Infrared Astronomy Research /
Hign Altitude Observations."

1973 - 1983 Grant No. NGR 05-005-055

B. Jones,
Center for Astrophysics
and Space Sciences, C-011,
University of California, San Diego,
La Jolla, CA 92093.

Principal Investigators:

W. A. Stein / B. T. Soifer	12/15/73 -	8/31/78
S. P. Willner	9/ 1/78 -	10/31/80
B. Jones	11/ 1/80 -	4/30/83

The NASA Technical Officer for this grant is:

Dr. L. C. Haughney,
NASA Ames Research Center,
University Affairs Office,
Mail Stop 241-25,
Moffett Field,
California 94035.

Bibliography

1974

1. "4 - 8 Micron Spectrophotometric Observations from the NASA Flying 36-inch Telescope" Russell R. W., Soifer B. T. and Forrest W. J. 1974, BAAS, 6, 470.

1975

2. "Spectrophotometric Observations of Mu Cephei and the Moon from 4 to 8 microns." Russell R. W., Soifer B. T. and Forrest W. J. 1975, Ap. J. 198 , L41.

3. "Spectrophotometry of CRL 2688 from 2 to 24 microns." Forrest W. J., Merrill K. M., Russell R. W. and Soifer B. T. 1975 Ap. J. 199, L181.

4. "The Peculiar Object HD 44179 (The Red Rectangle)." Cohen M. L., Anderson C. M., Cowley A., Coyne G. V., Fawley W. M., Gull T. R., Harlan E. A., Herbig G. H., Holden F., Hudson H. S., Jakoubek R. O., Johnson H. M., Merrill K. M., Schiffer III F. H., Soifer B. T. and Zuckerman B. 1975, Ap. J. 196, 179.

1976

5. "Infrared Observations of Ices and Silicates in Molecular Clouds." Merrill K. M., Russell R. W. and Soifer B. T. 1976, Ap. J. 207, 763.

6. "16 - 25 micron Spectroscopy of the Trapezium and BN-KL Source in Orion." Forrest W. J. and Soifer B. T. 1976, Ap. J. 208, L129.

1977

7. "Observations of Jupiter and Saturn from 5-8 microns." Russell R. W. and Soifer B. T. 1977, Icarus 30, 282.

8. "Spectra of Late Type Stars from 4 - 8 Microns." Puetter R. C., Russell R. W., Sellgren K. and Soifer B. T. 1977 PASP, 89, 320.

9. "The 4 - 8 Micron Spectrum of the BNKL Source in Orion." Russell R. W., Soifer B. T. and Puetter R. C. 1977, Astr. Ap., 54, 959.

10. "Infrared Spectra of Protostars." Puetter R. C., Russell R. W., Soifer B. T. and Willner S. P. 1977, BAAS, 9, 571.

11. "The Infrared Spectrum of BD +30 3639 and Possible Celestial Grain Constituents." Soifer B. T., Russell R. W., Peutter R. C., and Willner S. P. 1977, BAAS, 9, 582.

12. "2 to 8 Micron Spectrophotometry of M82." Willner S. P., Soifer B. T., Russell R. W., Joyce R. R. and Gillett F. C. 1977, Ap. J. 217, L121.

13. "The 4 to 8 Micron Spectrum of NGC 7027." Russell R. W., Soifer B. T. and Willner S. P. 1977, Ap. J. 217, L149.

1978

14. "Spectrophotometry of OH 26.5 +0.6 from 2 to 40 microns." 1978 Forrest W. J., Gillett F. C., Houck J. R., McCarthy J. F., Merrill K. M., Pipher J. L., Puetter R. C., Soifer B. T. and Willner S. P. Ap. J. 219, 114.

15. "The Infrared Spectra of CRL 618 and HD 44179 (CRL 915)." Russell R. W., Soifer B. T. and Willner S. P. 1978, Ap. J. 220, 568.

16. "Infrared Spectra of HM Sagittae and V1016 Cygni." Puetter R. C., Russell R. W., Soifer B. T. and Willner S. P. 1978, Ap. J. 223, L93.

17. "Instrumentation for Infrared Astronomy." Soifer B. T. and Pipher J. L. 1978, Ann. Rev. Astr. Ap. 16, 335.

18. "An Analysis of Infrared Spectra of some Gaseous Nebulae with Emphasis on the Planetary Nebula NGC 7027." 1978, Russell R. W. PhD Thesis, University of California, San Diego.

1979

19. "Spectrophotometry of Compact HII Regions from 4 to 8 Microns." Puetter R. C., Russell R. W., Soifer B. T. and Willner S. P. 1979, Ap. J. 228, 118.

20. "The 4 - 8 Micron Spectrum of the Galactic Center." Willner S. P., Russell R. W., Puetter R. C., Soifer B. T. and Harvey P. M. 1979, Ap. J. 229, L65.

21. "Unidentified Infrared Spectral Features." Willner S. P., Puetter R. C., Russell R. W. and Soifer B. T. 1979, Astrop. & Sp. Sci., 65, 95.

22. "The 4 - 8 Micron Spectrum of the Infrared Source W33A." Soifer B. T., Puetter R. C., Russell R. W., Willner S. P., Harvey P. M. and Gillett F. C. 1979, Ap. J. 232, L53.

23. "Infrared Spectra of IC 418 and NGC 6572." Willner S. P., Jones B., Puetter R. C., Russell R. W. and Soifer B. T. 1979, Ap. J. 234, 496.

1980

24. "Infrared Molecular Absorption Features." Willner S. P., Puetter R. C., Russell R. W. and Soifer B. T. 1980, IAU Symp No. 87, 381.

25. "The Infrared Spectrum of the Carbon Star Y CVn Between 1.2 and 30 Microns." Goebel J. H., Bregman J. D., Goorvitch D., Strecker D. W., Puetter R. C., Russell R. W., Soifer B. T., Willner S. P., Forrest W. J., Houck J. R. and McCarthy J. F. 1980, Ap. J. 235, 104.

1981

26. "Measurements of Forbidden Line Radiation of Ar II (6.99 microns) in W3 IRS1." Herter T., Pipher J. L., Helfer H. L., Willner S. P., Puetter R. C., Rudy R. J. and Soifer B. T. 1981, Ap. J. 244, 511.

27. "Observations of Saturn in the 5 to 8 Micron Spectral Region." Witteborn F. C., Pollack J. B., Bregman J. D., Goebel J. H., Soifer B. T., Puetter R. C., Rudy R. J. and Willner S. P. 1981, Icarus, 45, 653.

28. "Identification of New Infrared Bands in a Carbon Rich Mira Variable." Goebel J. H., Bregman J. D., Witteborn F. C., Taylor B. J. and Willner S. P. 1981, Ap. J. 246, 455.

29. "Abundances of Argon, Sulfur, and Neon in Six Galactic HII Regions from Infrared Forbidden Lines." Herter T., Helfer H. L., Pipher J. L., Forrest W. J., McCarthy J., Houck J. R., Willner S. P., Puetter R. C., Rudy R. J. and Soifer B. T. 1981, Ap. J. 250, 186.

30. "4 - 8 Micron Spectrophotometry of OH 0739 -14, Implications for Interstellar Grain Chemistry." Soifer B. T., Willner S. P., Capps R. W. and Rudy R. J. 1981, Ap. J. 250, 631.

1982

31. "Infrared Spectra of Protostars: Composition of the Dust Shells." Willner S. P., Gillett F. C., Herter T., Jones B., Krassner G., Merrill K. M., Pipher J. L., Puetter R. C., Rudy R. J., Russell R. W. and Soifer B. T. 1982, Ap. J. 253, 174.

32. "Observations of Interstellar Ammonia Ice." Knacke R. F., McCorkle S., Puetter R. C., Erickson E. F. and Kratschmer W. 1982, Ap. J. 260, 141.

33. "Abundances in Five Nearby Galactic HII Regions from Infrared Forbidden Lines." Herter T., Helfer H. L., Pipher J. L., Briotta D. A., Forrest W. J., Houck J. R., Rudy R. J. and Willner S. P. 1982, Ap. J. 262, 153.

1984

34. "Abundances in Galactic HII Regions, III; G25.4-0.2, G45.5+0.06, M8, S159 and DR22." Pipher J. L., Helfer H. L., Herter T., Broitta Jr. D. A., Houck J. R., Willner S. P., and Jones B. 1984, Ap. J., 285.

BULLETIN
OF THE
AMERICAN ASTRONOMICAL SOCIETY
PUBLISHED BY THE AMERICAN INSTITUTE OF PHYSICS INC.

VOLUME 6, NUMBER 4, PART I Page 470 *1974*

24.09.04 4 μ - 8 μ Spectrophotometric Observations from the NASA Flying 36" Telescope. R. W. RUSSELL, B. T. SOIFER, & W. J. FORREST, Univ. of Calif., San Diego - Spectrophotometric observations from 4 μ - 8 μ with a liquid nitrogen cooled filter wheel having resolution $\Delta\lambda/\lambda \sim 0.012$ were obtained on αLyr, βPeg, μCeph, Jupiter, and the Moon, using the NASA flying 36" telescope on the Airborne Infrared Observatory. The lunar spectrum shows that it is not a black body emitter, with a depression between 6 μ and 8 μ.

The spectrum of μCeph, an M supergiant, shows no excess over the stellar continuum from 5 μ - 8 μ. This implies that the previously identified silicate grains are the only infrared active circumstellar material in this star. The implications of this will be discussed.

The Jovian spectrum shows a deep minimum at 6 μ, characteristic of ammonia in the atmosphere, as well as further spectral structure.

This work was supported by NASA grant NGR 05-005-055.

THE ASTROPHYSICAL JOURNAL, 198:L41–L43, 1975 May 15

SPECTROPHOTOMETRIC OBSERVATIONS OF MU CEPHEI AND THE MOON FROM 4 TO 8 MICRONS

R. W. RUSSELL, B. T. SOIFER, AND W. J. FORREST
Department of Physics, University of California, San Diego
Received 1974 December 11; revised 1975 February 14

ABSTRACT

We have obtained the first 4–8 μ spectrophotometric observations ($\Delta\lambda/\lambda \sim 0.01$) of μ Cep and the Moon, using the NASA Airborne Infrared Observatory. The lunar spectrum shows nongray behavior from 6.5 to 8 μ. The spectrum of μ Cep, an M2 Ia star with circumstellar emission, shows no evidence for circumstellar excess emission from 4 to 8 μ; we conclude that silicates provide the only infrared-active component of the circumstellar material.

Subject headings: circumstellar shells — Moon — spectra, infrared

I. INTRODUCTION

Infrared observations have established the existence of a broad 10-μ emission feature in many highly evolved late-type (oxygen-rich) stars. This has been interpreted as positive evidence for associated circumstellar matter, and in particular, evidence for the existence of silicate mineral grains surrounding these stars (Woolf and Ney 1969). The star μ Cep, an M2 Ia supergiant, was one of the stars used to identify the silicates observationally. Spectrophotometry ($\Delta\lambda/\lambda \sim 0.01$) of μ Cep in the atmospheric windows from 3 to 14 μ clearly established the existence of the 10-μ emission feature while showing the stellar continuum for $\lambda < 5$ μ (Gillett, Low, and Stein 1968).

Direct observations of the μ Cep spectrum from 5 to 8 μ, not observable with ground-based telescopes due to very strong H_2O atmospheric absorption, are important to define the stellar continuum, and to establish properly the strength and extent of the 10-μ emission feature. These observations can be used to search for other infrared-active circumstellar materials to test current theories of grain formation in stellar atmospheres (Gilman 1969; Salpeter 1974). We report here spectrophotometric observations from 4 to 8 μ, obtained on a flight of the recently commissioned NASA flying 36-inch (91 cm) infrared telescope (the Airborne Infrared Observatory).

II. EQUIPMENT

The observations were obtained with a cooled filter-wheel spectrometer designed by F. C. Gillett (see Gillett and Forrest 1973 for details) and built at UCSD specifically for airborne observations. The circular variable filter wheel covered the wavelength range 4.1–8.1 μ (mostly inaccessible from ground-based telescopes) with a resolution $\Delta\lambda/\lambda \approx 0.011$. In addition to the narrow-band observations, the spectrometer had broad-band filters ($\Delta\lambda/\lambda \sim 1/10$–$\frac{1}{4}$) covering the wavelengths 2–8 μ to allow for photometric observations of sources, for calibration, and for intercomparison with ground-based photometry.

The spectrometer was mounted at the bent Cassegrain focus of the telescope using a beam-splitter photometer, and used the chopping secondary mirror available on the AIRO. This allowed continuous viewing of the focal plane for guiding and for infrared observations. The signal was processed with the usual phase-sensitive amplifier, sampled through an analog-to-digital converter, recorded and displayed by the on-board computer system to give real-time signal-to-noise ratios for a given measurement.

III. THE OBSERVATIONS

The observations of μ Cep were obtained on an AIRO flight on the night of 1974 September 5/6. The aircraft altitude for most of the flight was 41,000 feet (12.5 km), and the precipitable water vapor above the aircraft (monitored in flight) was 7 ± 1 μm.

Since these are the first observations of stellar objects in this wavelength range, the spectral calibration of the observations is most important. Photometry and spectrophotometry of α Lyr, β Peg, and the Moon were used to calibrate the observations. The primary standard was α Lyr, which was taken to be a blackbody with a temperature of 10,000 K. Broad-band observations from 2 to 8 μ and narrow-band observations from 4.5 to 6.5 μ of α Lyr served to calibrate the observations of β Peg. The narrow-band observations of α Lyr were necessary to calibrate the β Peg spectrum in this wavelength range, where there is a slight depression (at $\sim$5 μ) in the β Peg spectrum, probably due to molecular opacity of CO (Solomon and Stein 1966). Broad-band observations at 6.5 μ ($\Delta\lambda \approx 3$ μ) and 8.4 μ ($\Delta\lambda \sim 0.8$ μ) verified that β Peg behaves as a hot blackbody for $\lambda \gtrsim 5.5$ μ.

The calibrated spectrum of β Peg was used in turn to deduce the lunar spectrum. This spectrum, taken with a 17″ diameter aperture at the approximate Selenographic coordinates 6° S, 67° W, is shown in Figure 1. The shape from 4.5 to 6.5 μ and at 8 μ fits a 355 K blackbody fairly well, but the depression from 6.5 to 8.0 μ shows that this particular position is not a gray body in this wavelength range. Murcray, Murcray, and

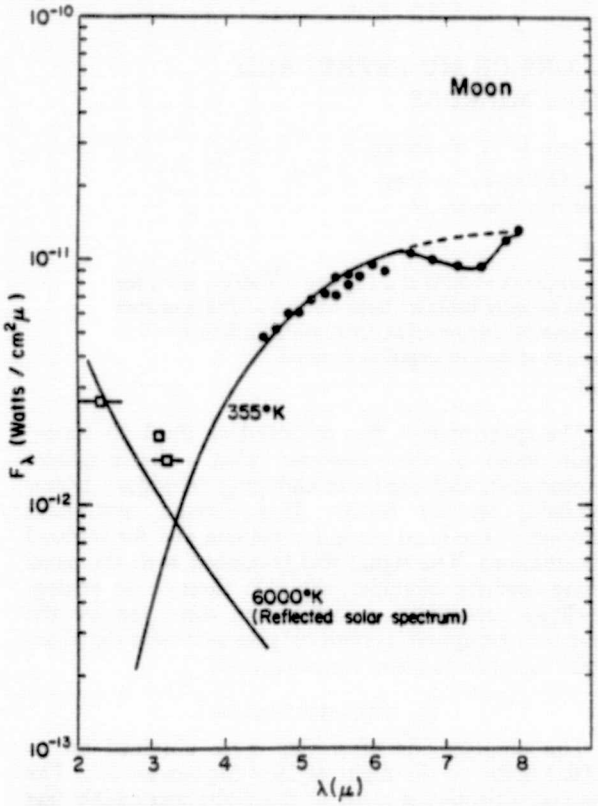

FIG. 1.—The lunar spectrum, obtained on the AIRO. Broad-band data (*open squares*) and narrow-band data (*closed circles*) were calibrated using α Lyr and β Peg as standards. The filter bandpasses are shown when larger than plotted points. The scatter in the narrow-band data reflects the noise in the calibration of the standards β Peg and α Lyr, not noise in the lunar spectrum. The system solid angle is 5.5×10^{-9} sr, so that the 355 K curve corresponds to emissivity = 1. The reflected solar curve corresponds to an albedo of 0.08.

Williams (1970) have previously found this nongray behavior in the lunar spectrum. We attribute this wavelength dependence of the lunar emissivity to the chemical/physical composition of the surface layer which was observed. Possible materials with spectral features in this region are carbonate minerals and silica glasses (Hunt, Wisherd, and Bonham 1950). The question of the source of the 7-μ lunar depression should be investigated further in light of the present knowledge of the composition of the surface layers of the Moon.

Finally, the lunar spectrum, smoothed from Figure 1, was used to calibrate the 4.5–8 μ spectrum of μ Cep (Fig. 2). (The seemingly circuitous route to the calibration of the Cep spectrum was necessary because the data on β Peg were less complete than those for the Moon or μ Cep.) We have included in Figure 2 infrared observations of μ Cep from 2 to 14 μ, including ground-based broad-band and narrow-band observations of Forrest, Gillett, and Stein (1974), as well as broad-band and narrow-band AIRO observations, and our previously unpublished narrow-band observations at 2 and 3 μ.

The broad-band observations from the AIRO and ground-based observations show excellent agreement. The 8.4-μ broad-band magnitudes, obtained with identical filters, agree to 0.03 mag between airborne and ground-based observations.

IV. DISCUSSION

The main features of the 4–8 μ spectrum of μ Cep are the slight depression at $\sim$5 μ, and the blackbody nature of the spectrum from 5.5 μ to 8 μ. The 5-μ depression is attributed to CO absorption in the stellar atmosphere (Solomon and Stein 1966).

The 5.5–8 μ flux appears to be long-wavelength emission from a blackbody at a higher flux level than that deduced from the $\lambda < 5$ μ observations. This could be due, for instance, to decreased stellar opacity in this wavelength region—allowing us to see to a higher temperature level ($T \sim 4200$ K) than is observed shortward of 5 μ ($T \sim 3500$ K). An alternate explanation of this flux would have excess emission from circumstellar dust combining with the stellar continuum to mimic closely a hot blackbody. This is unlikely, both because of the temperature requirements on such particles ($T > 1000$ K) and the peculiar optical properties such grains would require (virtually no emission for $\lambda < 5$ μ and featureless spectra from 5 to 8 μ).

If the entire 5–8 μ flux were attributed to stellar emission, there would be several consequences. First, the strength of the 10-μ emission feature, which we derive by subtracting a hot blackbody fitted to the short-wavelength data, is slightly reduced, while the emission profile rises more sharply from 8 to 9 μ compared with the result using the technique of Forrest *et al.* (1974). This new profile is also shown in Figure 2. The lack of evidence for any other infrared-active circumstellar material in the 5–8 μ spectrum of μ Cep confirms the assumption that "silicates" are the only grain material observed in this star. This is consistent with theories of grain formation in the atmospheres of oxygen-rich red giants, which predicts that silicates will be the dominant grains formed in these stars (since all C will be in the form of CO—see Gilman 1969; Salpeter 1974 for descriptions of the theory).

Finally, there is no evidence (to 20% of the continuum) for molecular opacity due to SiO, which would peak at 7.8 μ (Gillett, Stein, and Solomon 1970).

We would like to thank R. M. Cameron, C. Gillespie, and the entire staff of the AIRO, both for putting the Observatory into service, and for their assistance to us.

The UCSD instrument was constructed largely through the efforts of P. Brissenden. F. C. Gillett provided the detector. We thank F. C. Gillett and W. A. Stein for many helpful discussions. D. Strecker provided valuable assistance at Ames Research Center. R. Settnick provided much valuable in-flight vocal assistance.

This research was supported under NASA grant NGR 05-005-055.

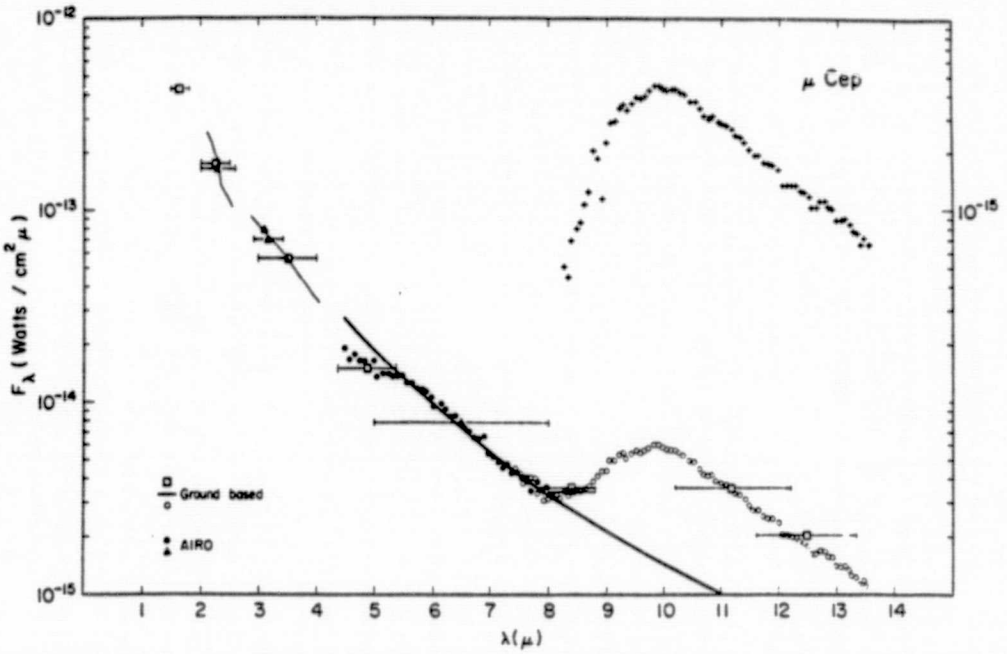

FIG. 2.—The spectrum of μ Cep from 2 to 14 μ. The ground-based data are broad-band observations (*open squares*), and narrow-band observations from 8–13 μ (*open circles*, Forrest *et al.* 1974), and narrow-band observations from 2 to 4 μ (*thin lines*, previously unpublished observations of Soifer and Russell). The AIRO data are broad-band (*filled triangles*), and narrow-band (*filled circles*) observations. Filter bandpasses are shown where they are larger than the plotted points. The errors are about 5% of the flux for the AIRO data, and $\lesssim$3% for the ground-based data. The heavy line is the fit of a 4200 K blackbody to the narrow-band data between 5.5 and 8 μ. The 8–13 μ excess spectrum (*pluses*) is the difference between the observed flux and the 4200 K fit to the data. The scale factor on the right side of the figure refers to the 8–13 μ excess flux.

REFERENCES

Forrest, W. J., Gillett, F. C., and Stein, W. A. 1975, *Ap. J.*, **195**, 423.
Gillett, F. C., and Forrest, W. J. 1973, *Ap. J.*, **179**, 483.
Gillett, F. C., Low, F. J., and Stein, W. A. 1968, *Ap. J.*, **154**, 677.
Gillett, F. C., Stein, W. A., and Solomon, P. M. 1970, *Ap. J. (Letters)*, **160**, L173.
Gilman, R. C. 1969, *Ap. J. (Letters)*, **155**, L185.
Hunt, J. M., Wisherd, M. P., and Bonham, L. C. 1950, *Anal. Chem.*, **22**, 1478.
Murcray, F. H., Murcray, D. G., and Williams, W. J. 1970, *J. Geophys. Res.*, **75**, 2662.
Salpeter, E. E. 1974, *Ap. J.*, **193**, 579.
Solomon, P. M., and Stein, W. A. 1966, *Ap. J.*, **144**, 825.
Woolf, N. J., and Ney, E. P. 1969, *Ap. J. (Letters)*, **155**, L181.

W. J. FORREST: Center for Radiophysics and Space Research, 220 Space Sciences Blvd., Cornell University, Ithaca, NY 14850

R. W. RUSSELL and B. T. SOIFER: Department of Physics, University of California, San Diego, Mail Code C-011, La Jolla, CA 92037

THE ASTROPHYSICAL JOURNAL, 199:L181–L183, 1975 August 1

SPECTROPHOTOMETRY OF CRL 2688 FROM 2 TO 24 MICRONS

W. J. FORREST, K. M. MERRILL, R. W. RUSSELL, AND B. T. SOIFER
Department of Physics, University of California, San Diego
Received 1975 March 20

ABSTRACT

Medium-resolution spectrophotometry ($\Delta\lambda/\lambda \approx 0.01$) of CRL 2688 from 2 μ to 24 μ are reported. No significant features are found from 3 μ to 24 μ, although the spectral flux distribution is broader than that of a single-temperature blackbody.

Subject headings: infrared sources — nebulae — spectrophotometry

I. INTRODUCTION

This *Letter* reports infrared spectrophotometric observations of the infrared source in Cygnus associated with twin symmetric reflection nebulae which has been recently catalogued by the Air Force Cambridge Research Laboratories Rocket Survey (Walker and Price 1974), where it will be designated as CRL 2688. (Following the convention of using 1950.0 right ascension and declination as a source designation, often used in radio astronomy, one might refer to this source as IR 2100+36.) Spectrophotometry from 2 to 24 μ ($\Delta\lambda/\lambda \sim 0.015$) was obtained at the UCSD–University of Minnesota 152-cm Mount Lemmon infrared telescope between 1974 May 3 and December 27. Table 1 gives a journal of these observations. See Ney *et al.* (1975) and Crampton, Cowley, and Humphreys (1975) for complementary observations and discussions.

II. OBSERVATIONS

The 2–4 μ and 8–13 μ data were obtained using techniques and systems described elsewhere (Merrill, Soifer, and Russell 1975; Gillett and Forrest 1973). The 16–24 μ data were obtained using a newly developed liquid-helium–cooled grating spectrometer, built at UCSD, and which will be more fully described in another publication (Forrest and Soifer 1975). The 2–4 μ observations used α Lyr and α Cyg as calibration standards, and the 8–13 μ observations used α Tau and β Peg as standards. The 16–24 μ observations used the Moon as the spectral calibration, while the absolute level was taken from the 18-μ broad-band data of Ney *et al.* (1975).

TABLE 1

OBSERVING LOG

Date (1974)	Wavelength Region (μ)	Observers
May 3	8–13	KMM
May 20	8–13	BTS & RWR
October 20	2–4	KMM
October 25	2–4	KMM & RWR
November 1	8–13	BTS & RWR
November 4	2–4	KMM
November 5	2–4	EPN & KMM
November 27	8–13	BTS & RWR
December 25	16–24	WJF
December 28	16–24	WJF

The 2–4 μ observations were taken with a 9″ aperture centered on the 3.5-μ flux peak (centered between the optical sources but not completely containing them) to minimize the contribution to the flux from the reflection nebulae. Beam size effects were noted at 1.65, 2.3, and 3.5 μ between concentric 9″ and 18″ beams. No beam size effects were seen at 8–13 μ, and data using apertures between 9″ and 22″ were combined. The 16–24 μ data were taken with an 18″ aperture.

III. DISCUSSION

The spectrum (Fig. 1) shows several qualitative characteristics of note. The entire 3–24 μ spectrum is generally a featureless continuum at this spectral resolution. Although the 16–24 μ data can be fitted by a 120 K blackbody, it is clear that the overall spectrum is too broad to be fit by a single blackbody. The 8–13 μ data suggest a 200 K equivalent blackbody which is hotter than the 10–20 μ color temperature of ~150 K (Ney *et al.* 1975). If, as suggested by Ney *et al.*, the intense infrared flux from this source is due to thermal radiation by warm dust grains, the observed broad flux distribution probably suggests that a range of dust temperatures is being observed. This could be due to the radiation transfer process through an extended dusty envelope and/or geometrical effects in an asymmetric source allowing us to see some warmer dust (e.g., a slightly tilted torus in the model of Ney *et al.*).

The 8–13 μ spectrum of CRL 2688 appears completely smooth and featureless. This lack of features is quite unusual: most objects where the infrared radiation is attributed to thermal reradiation of dust do show features characteristic of the emitting material in this wavelength interval (see Forrest, Gillett, and Stein 1975, and references therein). Thus the overall grain emissivity (due to chemical composition, particle size, etc.), combined with the large optical depth local to the source (inferred from the good agreement between color temperature and surface brightness at 10 μ—Ney *et al.* 1975) must mask these characteristic signatures.

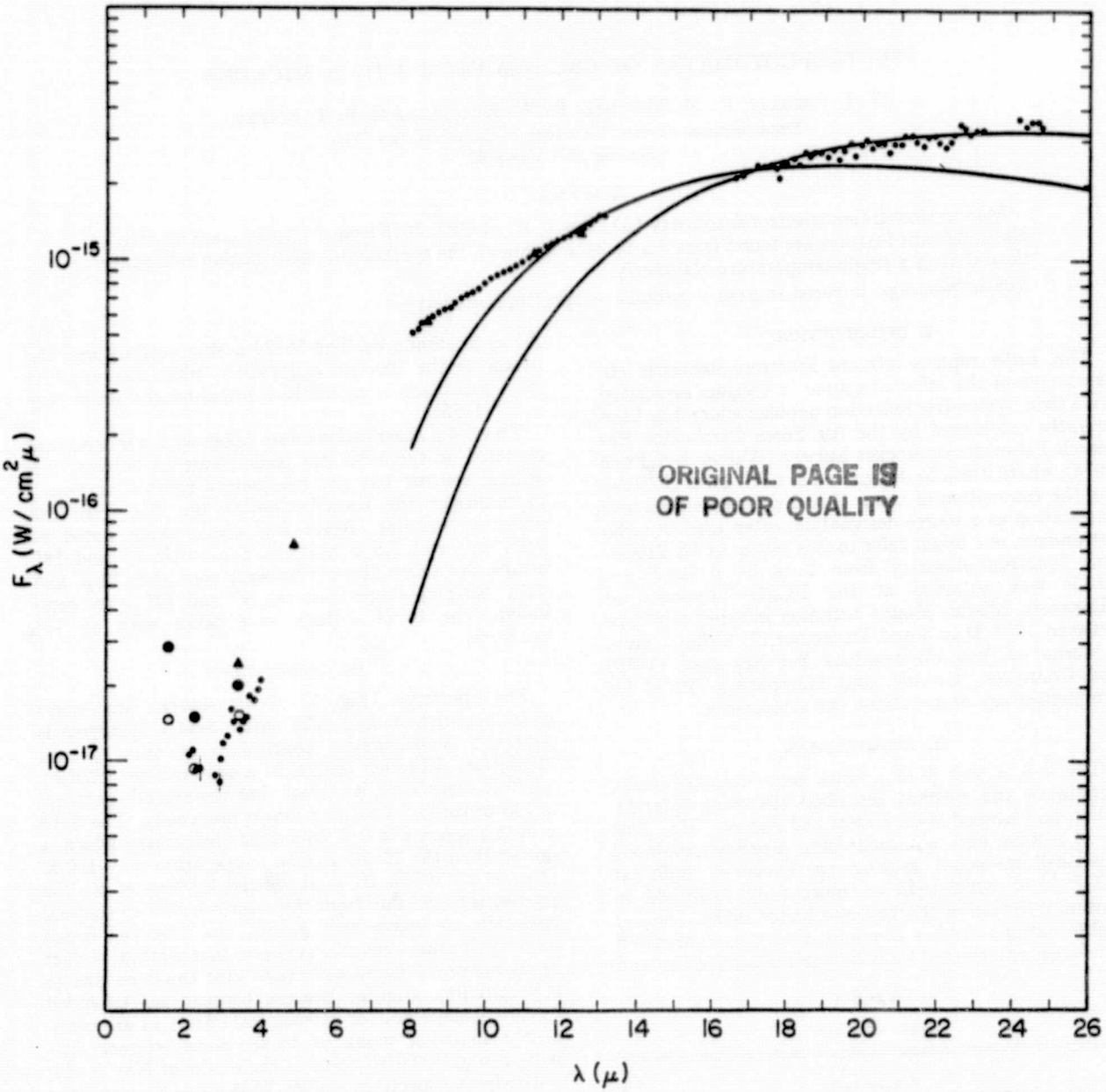

FIG. 1.—The spectrum of CRL 2688 from 2 to 24 μ. *Small filled circles*, narrow-band observations. *Open circles*, *large filled circles*, and *triangles*, broad-band data taken with 9″, 18″, and 22″ apertures. Typical statistical errors in the 2–2.4 μ and 3–4 μ data are shown in the figure. The errors from 8 to 13 μ are typically less than 5%, while the scatter in the measured points is indicative of the errors from 16 to 24 μ. Blackbody curves for 150 K and 120 K (the solid line which is higher at 26 μ) are shown.

Also the absence of any absorption centered near 9.7 μ indicates that there is not a substantial amount of cooler ($T \lesssim 100$ K) silicate dust in the line of sight to this source.

The 2–4 μ region of the spectrum contains the only evidence of structure. The rise toward shorter wavelengths is almost certainly due to the rapidly increasing contribution of reflected light from the obscured central source, as suggested by the marked aperture dependence between concentric 9″ and 18″ apertures (see Fig. 1) as more of the optical sources are contained within the beam (see Ney *et al.* 1975). The 22″ observations, taken on 1974 May 3, were obtained under totally different circumstances from the later 9″ and 18″ observations, and the disagreement between 18″ and 22″ may not be real.

There is no evidence for ice absorption near 3.1 μ, which is not surprising, since at the observed 150 K brightness temperature of the source, the evaporative lifetime of ice is very short. The lack of ice absorption indicates that there is not a significant amount of cold ice ($T \ll 100$ K) in the line of sight to the source, consistent with the lack of observed silicate absorption. A possible emission feature near 3.3 μ is suggested by the data, but this requires further observations for confirmation.

We would like to thank E. P. Ney for calling our attention to this source and for assistance in obtaining some of the data, and W. A. Stein for helpful discussions. Infrared astronomy at UCSD is supported in part by the National Science Foundation and by NASA through grant NGL 05-009-230.

REFERENCES

Crampton, D., Cowley, A. P., and Humphreys, R. M. 1975, *Ap. J.* (*Letters*) (submitted for publication).
Forrest, W. J., Gillett, F. C., and Stein, W. A. 1975, *Ap. J.*, **195**, 423.
Forrest, W. J., and Soifer, B. T. 1975, in preparation.
Gillett, F. C., and Forrest, W. J. 1973, *Ap. J.*, **179**, 483.
Merrill, K. M., Soifer, B. T., and Russell, R. W. 1975 (to be submitted).
Ney, E. P., Merrill, K. M., Becklin, E. E., Neugebauer, G., and Wynn-Williams, G. C. 1975, *Ap. J.* (*Letters*) (submitted for publication).
Walker, R., and Price, S. D. 1974, AFCRL Infrared Sky Survey, preprint.

W. J. Forrest: Center for Radiophysics & Space Research, Space Sciences Bldg., Cornell University, 220 Space Sciences Blvd., Ithaca, NY 14850

K. M. Merrill, R. W. Russell, and B. T. Soifer: Department of Physics, Mail Code C-011, University of California, San Diego, La Jolla, CA 92037

THE ASTROPHYSICAL JOURNAL, 196:179–189, 1975 February 15

THE PECULIAR OBJECT HD 44179 ("THE RED RECTANGLE")

MARTIN COHEN,[1] CHRISTOPHER M. ANDERSON,[2] ANNE COWLEY,[3] GEORGE V. COYNE,[4] WILLIAM M. FAWLEY,[1] T. R. GULL,[5] E. A. HARLAN,[6] G. H. HERBIG,[6] FRANK HOLDEN,[6] H. S. HUDSON,[7] ROGER O. JAKOUBEK,[2] HUGH M. JOHNSON,[8] K. M. MERRILL,[7] FRANCIS H. SCHIFFER III,[2] B. T. SOIFER,[7] AND BEN ZUCKERMAN[1,9]

Received 1974 July 22; revised 1974 September 3

ABSTRACT

A strong infrared source detected in the AFCRL sky survey is confirmed, and is identified with the binary star HD 44179, embedded in a peculiar nebula. *UBVRI* and broad-band photometry between 2.2 and 27 μ are combined with blue, red, and near-infrared spectra, polarimetry and spectrophotometry of the star, and a range of direct and image-tube photographs of the nebula, to suggest a composite model of the system. In this model, the infrared radiation derives from thermal emission by dust grains contained in a disklike geometry about the central object, which appears to be of spectral type B9–A0 III and which may be in pre–main-sequence evolution. Two infrared emission features are found, peaking at 8.7 and 11.3 μ, the latter corresponding to the feature seen in the spectrum of the planetary nebula NGC 7027. The complex nebular structure is discussed on the basis of photographs through narrow-band continuum and emission-line filters. The polarization data support the suggestion of a disk containing some large particles. No radio continuum emission is detected.

Subject headings: binaries — infrared sources — nebulae — stars, individual

I. INTRODUCTION

In a systematic photographic survey by one of us (M. C.) of infrared sources seen in the AFCRL sky survey (Walker and Price 1975), a number of interesting identifications have been made on the *National Geographic Society–Palomar Sky Survey* prints. One such source coincides with a ninth magnitude star embedded in nebulosity. The object is AFCRL 618–1343 = HD 44179 = BD −10°1476. The reality of the rocket infrared source was confirmed by ground based photometry in 1973 October, and direct photographs of the nebula were secured in 1973 November on the Kitt Peak 4-m reflector.

From 1973 November until 1974 March, a wide range of observational techniques was applied to this object. This paper describes these observations and suggests a composite model of the system based upon all the available data. The categories of observation discussed below are : § II, photography of the nebula; § III, spectroscopy; § IV, spectrophotometry; § V, broad-band photometry; § VI, infrared spectrophotometry; § VII, polarimetry; § VIII, radio observations; and § IX, the binary nature of HD 44179. Each section carries the names of those who have contributed to the observations.

[1] Berkeley Astronomy Department, University of California, Berkeley.
[2] Washburn Observatory, University of Wisconsin–Madison.
[3] Dominion Astrophysical Observatory.
[4] University of Arizona.
[5] Kitt Peak National Observatory.
[6] Lick Observatory.
[7] Department of Physics, University of California, San Diego.
[8] Lockheed Palo Alto Research Laboratory.
[9] University of Maryland.

II. PHOTOGRAPHY OF THE NEBULA

R. BROWN, T. R. GULL, E. A. HARLAN, AND R. KRON

At the position of the infrared source, the Palomar prints show a closely nebulous star in the blue, and a crisp, rectangular object in the red (figs. 1*a* and 1*b* [pl. 3]). Direct photographs of the nebulosity were obtained in 1973 November and December at the prime focus of the Kitt Peak 4-m reflector. These plates, and subsequent ones taken with the 4-m and other telescopes, were intended to investigate the detailed structure of the "red rectangle," both in the continuum and in a variety of emission lines. Figure 1*c* shows the nebula through a broad red (RG 610) filter (15-minute exposure, O98-02, 1″–2″ seeing), and *f* shows a 30-minute exposure, also on O98-02 emulsion, in Hα + [N II], using a narrow-band filter (90 Å). In order to provide information on the central portions of the nebula, figures 1*d*, 1*e*, and 1*f* present a sequence of 90 Å passband Hα + [N II] photographs with exposures of 1, 6, and 30 minutes, respectively. The spikes first become apparent in the 6-minute exposure. A 6-minute exposure with a 90 Å bandpass filter centered at λ6470 in the continuum reveals essentially everything seen of the nebular structure in the 6-minute Hα exposure, and a 30-minute, 90 Å bandpass filter which isolates the $\lambda\lambda$6730 [S II] doublet shows no difference from the same length of exposure in Hα. However, a 90 Å bandpass photograph in the blue at λ4400 in the continuum, using the Kitt Peak No. 1 92-cm reflector with a Carnegie image tube, shows only a stellar image. A second (broad) blue plate taken at the prime focus of the Lick 3-m reflector reveals only a faint suggestion of nebulosity about the star.

Several other photographs have been secured of the nebula with various filters: a 93-minute near-infrared exposure (λ_{eff} ~ 8500 Å; hypersensitized I-N plate,

RG 8 filter) on the 76-cm telescope of Leuschner Observatory at Berkeley only faintly indicates the northern pair of spikes, although adjacent star images have appreciable dimensions; a 30-minute yellow photograph (103aG plate, O64 filter) with the 92-cm refractor of Lick Observatory begins to show all four spikes emerging from the image of HD 44179. To investigate the region in which the sodium D-lines arise (see § III), a Kron tube was used on the Mount Hopkins 1.5-m telescope; the star image is slightly extended N–S into an elliptical nebulosity, rather like the appearance in the shortest Hα exposure (fig. 1*d*).

Extracting the salient features from this wide range of photographs, we may summarize the character of the nebulosity as follows: in the blue, a very weak amorphous nebula is present, very close to the star; in the yellow, a bright, small elliptical nebulosity surrounds the star, and this oval structure is seen in the D-lines, whereas the spikes are not, only becoming visible in a broad filter; in the red, the nebula shows an inner, bright, apparently rectangular core close to the star, with prominent bright spikes emanating symmetrically from its corners. Both rectangle and spikes are continuum features rather than line structure; in the near-infrared the spikes are weakly visible. The highly symmetrical appearance of the nebulosity is striking, and much detail is apparent beyond the bright rectangular core; for example, there is a second, fainter nebulosity present within the north and south quadrants which terminates sharply and linearly, parallel to the shorter edges of the rectangle. This fainter nebulosity meets the spikes at four small, bright knots which also limit the extent of the brightest portions of the spikes. The spikes persist beyond these knots but with a much reduced surface brightness. The nebula is about 40″ in N–S extent, although wispy extensions can be traced further out.

It should be noted that the spikes are not merely telescopic diffraction effects, for they maintain essentially the same appearance both in the Palomar Schmidt (with north–south and east–west diffraction patterns) and in the Kitt Peak 4-m reflector (with patterns rotated 45° to the cardinal directions). Figure 1 includes purely stellar diffraction patterns from the 4-m plates along with the images of HD 44179.

III. SPECTROSCOPY

ANNE COWLEY, WILLIAM M. FAWLEY, E. A. HARLAN, AND G. H. HERBIG

The spectroscopic material consists of 12 plates and an echelle spectrogram of HD 44179. Seven plates were taken at the coudé focus of the Lick Observatory 3-m reflector, two in the region λλ5800–6800, three in the region λλ7600–8600 at 34 Å mm^{-1}, using a cooled Varo intensifier, one covering λλ5600–6200 at 17 Å mm^{-1}, and one centered at Hα with a dispersion of 10 Å mm^{-1}. Two plates were taken on the 2.1-m reflector at Kitt Peak using the feed for the coudé spectrograph; these cover λλ5200–6800 at 25 Å mm^{-1} and λλ3600–5000 at 17 Å mm^{-1}. Two plates were obtained on the coudé auxiliary telescope of Lick Observatory in the region λλ5800–6800 at 33 Å mm^{-1}. A spectrogram was obtained with the Wisconsin 91-cm reflector using an echelle spectrometer (Schroeder and Anderson 1971) and a Carnegie image intensifier; this was centered at λ5890 and covered roughly half the spectrum between 5400 and 6400 Å. Sensitometric calibration was that of Anderson and Schiffer (1975).

The blue plate taken at Kitt Peak is very narrow, but shows that no emission lines are present in this spectral region. The hydrogen lines are broad absorptions, and a weak narrow interstellar K-line is present. The collection of red plates shows Hα to be a strong narrow emission centrally placed in a broad absorption; narrow sodium D-lines are present in emission. Na I λ5889 is weaker than the component at λ5895, although the reverse is to be expected. It is possible that interstellar absorption overlies the Na I emission producing this anomaly, although it is more likely that the region producing the lines is optically thick so that both lines are completely saturated.

At 10 Å mm^{-1} the structure of Hα is quite complex; the absorption is steep on the blue side but shallow and prolonged on the red, while the central sharp emission core is superposed on much broader emission wings within the overall absorption. The Wisconsin echellogram also shows He I λ5876 in absorption, and suggests that the D-line emissions are superposed on absorption features (fig. 2). In the near-infrared there are no emission lines; lines of the Paschen series appear in absorption as do those of O I λλ7771–7775 and 8446. No diffuse interstellar features are seen throughout the region from blue to near-infrared.

According to the HD catalog, the spectral type of star is B8. An objective prism plate, at 108 Å mm^{-1} in the blue, taken with the Curtis Schmidt at CTIO in late 1967, shows an apparently normal late B giant, classified independently by Houk and by Cowley as B9 II–III. The absorption strength at Hα is that expected from a star of type late B to early A, while in the near-infrared a type of AO III is appropriate. A spectrum of θ Aur (B9.5pv) taken at Wisconsin with the same echelle spectrograph used for HD 44179 shows He I λ5876 to be of comparable strength in the two stars, confirming a late B spectral type. Radial velocities have been determined from the emission lines in the red and from the absorption lines in the blue and the near-infrared. The velocities are Hα + 19.3, Na I λ5895 + 20.4, Na I λ5889 + 20.8 km s^{-1} in the red (errors ± 0.7), while the mean radial velocity from the Paschen lines and the O I absorptions in the near-infrared is +18 ± 2 km s^{-1}, and from eight hydrogen lines in the blue is 19 ± 9 km s^{-1}.

No definite statements can yet be made concerning the spectrum of the nebula, but a 30-minute red exposure at the coudé focus of the Lick 3-m reflector fails to show even the presence of Hα emission, in accordance with the photographic information on the similarity of nebular structure in Hα and in the red continuum.

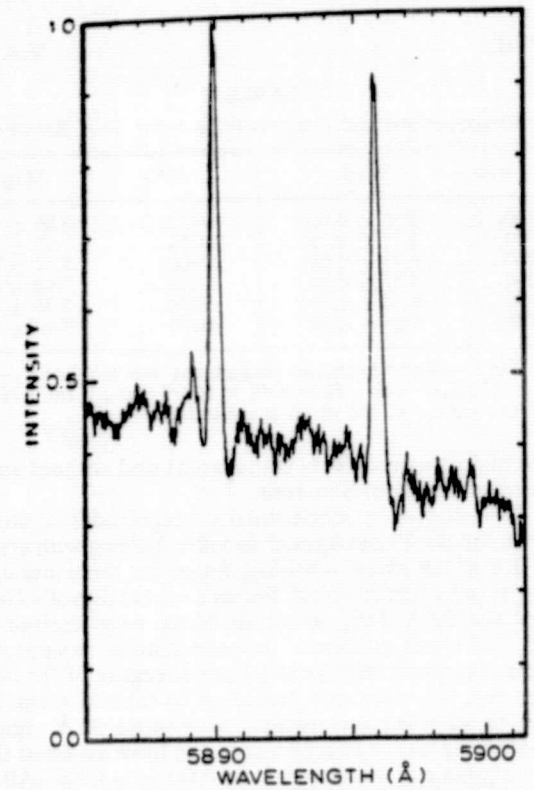

FIG. 2.—Direct intensity tracing of the Wisconsin echelle spectrogram of 1973 December 16–17 in the region λλ5885–5901, showing the D lines. In this plot, the exposure due to scattered light and image tube phosphor dark glow have been subtracted, in intensity, after processing through the characteristic curve obtained from sensitometric strips applied to a plate from the same glass blank as used for the stellar spectrogram and developed with it.

IV. SPECTROPHOTOMETRY

CHRISTOPHER M. ANDERSON, WILLIAM M. FAWLEY, ROGER O. JAKOUBEK, FRANCIS H. SCHIFFER III, AND HYRON SPINRAD

On the night of 1973 December 20–21, low resolution spectrophotometric observations of HD 44179 were obtained with the Washburn Observatory 41-cm reflector and computer controlled scanner. The observations were made with a 40 Å bandpass at the 17 standard wavelength points of Oke (1965) in the range λλ3390–5840 with a 7′ beam. Because of the prohibitively low slew rates of this telescope in the subzero (°F) conditions, it was not possible to obtain a full set of standard star observations for extinction and instrumental-sensitivity calibration. Instead the nearby unreddened (Crawford 1963) B9 star HD 44037 was also observed, and both stars were reduced to monochromatic magnitudes $AB(\lambda^{-1}) = -2.5 \log F_\nu + C$ on the system of Oke and Schild (1970) with mean extinction coefficients and instrumental sensitivities. The night was of good quality and the colors, defined as $AB(\lambda^{-1}) - AB(1.8)$, of HD 44037 are in excellent agreement with observations of other stars of its spectral type obtained with the standard procedure. We thus feel that these colors can be considered good to about ± 0.04 mag.

The results of this spectrophotometry are given in table 1 and plotted as a function of frequency in reciprocal microns in figure 3. In this figure the open triangles are the observed colors of HD 44037 and the filled circles are those of HD 44179. The latter is substantially reddened. If we assume that the intrinsic spectral energy distribution in the Paschen continuum of HD 44179 can be represented by that of HD 44037, the color excesses can be determined. The $E(B - V)$ is approximately 0.5 and the excess between 1.8 and

TABLE 1

LOW RESOLUTION SPECTROPHOTOMETRY

λ	λ^{-1}	HD 44037	HD 44179	Reddening Curve	HD 44179 minus Reddening
3390.....	2.950	+0.70	+2.20	+0.81	+1.22
3448.....	2.900	+0.72	+2.22	+0.78	+1.28
3509.....	2.850	+0.73	+2.17	+0.76	+1.25
3571.....	2.800	+0.71	+2.11	+0.74	+1.22
3636.....	2.750	+0.71	+1.69	+0.71	+0.83
3704.....	2.700	+0.58	+0.89	+0.68	+0.07
3862.....	2.589	−0.16	+0.37	+0.62	−0.38
4032.....	2.480	−0.37	+0.29	+0.54	−0.36
4167.....	2.400	−0.35	+0.26	+0.50	−0.35
4255.....	2.350	−0.32	+0.24	+0.45	−0.31
4464.....	2.240	−0.25	+0.19	+0.37	−0.26
4566.....	2.190	−0.23	+0.18	+0.34	−0.23
4785.....	2.090	−0.18	+0.15	+0.25	−0.15
5000.....	2.000	−0.12	+0.14	+0.18	−0.08
5263.....	1.900	−0.04	+0.08	+0.09	−0.03
5556.....	1.800	0.00	0.00	0.00	0.00
5840.....	1.712	+0.14	−0.01	−0.07	+0.08

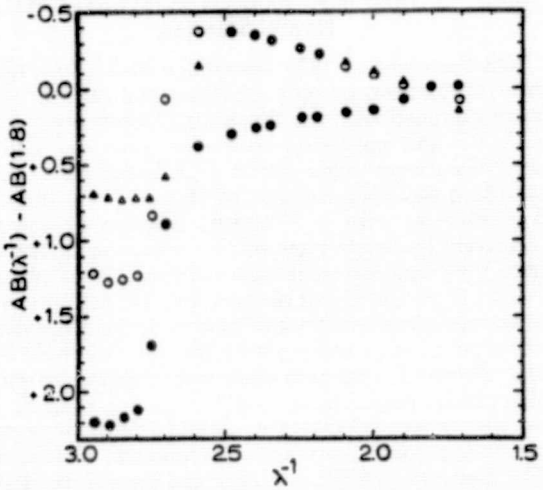

FIG. 3.—The observed and computed monochromatic colors as a function of frequency in reciprocal microns. *Open triangles*, the observations of HD 44179; *open circles*, the de-reddened colors of HD 44179.

2.4 μ^{-1} is 0.61. The latter value, along with the mean field reddening curve of Anderson (1970) which is given in column (5) of table 1, can be used to remove the reddening. The results of this process are shown in figure 3 by the open circles, and in column (6) of table 1. It is seen that the Paschen continua are in quite good agreement up to 2.48 μ^{-1}. However, the Balmer continuum of HD 44179 is depressed by about 0.5 mag relative to HD 44037. Considering the temperature inferred from the presence in absorption of He I, this Balmer jump, if stellar in origin, would imply a very large surface gravity (Mihalas 1970). On the other hand, 40 Å bandpass observations at the two points at 2.589 (between H8 and H9) and 2.700 μ^{-1} (which includes H14 to H18) are usually seen to be depressed with respect to either models or very narrow band scans, and this depression increases with higher gravity due to the Stark broadening of the hydrogen lines. In this case these points are significantly brighter in HD 44179 than in HD 44037. This could be an instrumental discrepancy (e.g., due to poor centering of HD 44037 in the diaphragm), but should be kept in mind.

Spectrophotometric data on HD 44179 were obtained on two nights in 1974 February with the prime focus scanner and 91-cm reflector of the Lick Observatory. The entrance aperture was 1 mm, corresponding to 42″ on the sky. On the first night, HD 44179 was observed with a 30 Å bandpass at wavelengths used by Hayes (1970) longward of 7000 Å. Air-mass corrections for this night were empirically determined by observations of Hayes's standard stars. On the second night, 90 Å bandpasses were used and the star was scanned at 100 Å intervals between 6000 and 10800 Å. Air-mass corrections (ranging between 0.02 and 0.05 mag) for this night were derived by interpolation between values given by Hayes; the night was relatively transparent and without smog interference from San Jose.

TABLE 2

SPECTROPHOTOMETRIC OBSERVATIONS WITH 30 Å BANDPASSES

λ(Å)	Mag	λ(Å)	Mag
7100.....	8.36 ± 0.03	9832.....	8.09 ± 0.07
7530.....	8.35 ± 0.05	10256.....	7.93 ± 0.08
7780.....	8.43 ± 0.06	10400.....	8.02 ± 0.11
8090.....	8.37 ± 0.04	10610.....	7.90 ± 0.08
8370.....	8.34 ± 0.06	10796.....	7.75 ± 0.13
8708.....	8.25 ± 0.04	10870.....	7.80 ± 0.15

NOTE.—Monochromatic magnitudes are tabulated: $-2.5 \log (F_\nu/F_0)$ with $F_0 = 3.46 \times 10^{-20}$ ergs s^{-1} cm^{-2} Hz^{-1}. Errors are 1 σ of the mean magnitudes.

The relative monochromatic magnitudes obtained from the 30 Å data appear in table 2 along with errors of 1 σ of the mean. Absolute fluxes for these measurements came directly from Hayes's calibration of γ Gem. For the 90 Å data, absolute fluxes were derived by the following method: monochromatic magnitudes were computed relative to γ Gem (because of the large number, these are not presented in tabular form but can be supplied on request). For those 90 Å regions containing Hα or Paschen lines, we have assumed that the equivalent widths of these lines in γ Gem (A0 V) are equal to those of α Lyr. The widths in α Lyr were determined from 10 Å bandpass scans kindly made available by L. Kuhi. This procedure of determining the flux depression probably is internally accurate to only 0.05 mag. Finally, absolute fluxes from the 90 Å data for γ Gem, and hence of HD 44179, were computed by interpolation between the wavelengths used by Hayes, making the above-described allowance for hydrogen line absorptions. The internal photometric errors (1 σ of the mean) for the 90 Å data are 0.05 mag or better below 10200 Å and increase to 0.10 mag at 10800 Å. Figure 4 presents all the

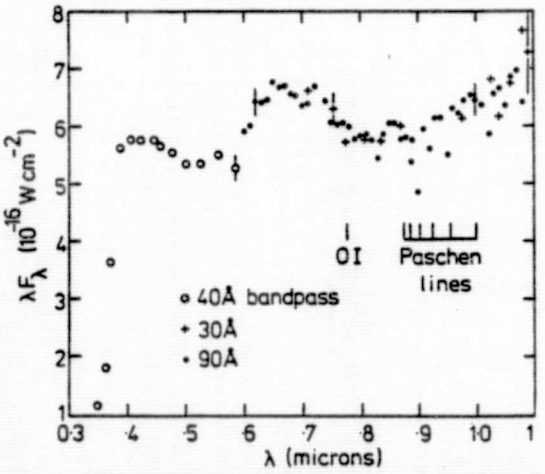

FIG. 4.—The combined spectrophotometry between 0.36 and 1.1 μ. Both axes are linear plots, and representative error bars (1 σ of the mean) are indicated, as are the positions of several absorption lines.

spectrophotometry between 3400 and 10800 Å in the form of a linear plot of λF_λ against λ.

The most remarkable features of the composite energy distribution of HD 44179 are the very broad apparent emission feature centered at 6900 Å and the general increase of flux between 8000 and 10800 Å. The depression at 7780 Å is most probably real and due to the absorption lines of the O I triplet near λ7774 (see § III). The curious bump in the distribution is also clearly seen in 2″ aperture observations of this object kindly obtained with the Cassegrain IDS scanner on the Lick Observatory 3-m reflector by H. Spinrad, H. E. Smith, and J. Liebert. Unfortunately these data are not as reliable as the spectrophotometry presented above because of cloudy conditions, and they have therefore not been shown in figure 4.

V. BROAD-BAND PHOTOMETRY

MARTIN COHEN, H. S. HUDSON, K. M. MERRILL, AND B. T. SOIFER

UBVRI photometry of HD 44179 was acquired on 1973 December 13 and 26 with the University of Minnesota–University of California, San Diego 1.5 m Mount Lemmon telescope using a 33″ circular diaphragm. The phototube was an RCA C31034 with a GaAs photocathode for red response and was operated in current mode. *UBV* and *R* are essentially the standard effective wavelengths and bandpasses, but *I* is somewhat shorter (0.82 μ) than that of Johnson, since the phototube response determines its long wavelength cutoff. The two sets of data are in excellent agreement and the magnitudes and photometric errors are presented in table 3.

Three sets of infrared photometric data were gathered in the period 1973 October to December with different aperture sizes. These comprise photometry between 2.2 and 18 μ with 4″ beams using a liquid-helium–cooled bolometer on the Lick 3-m reflector; between 2.2 and 22 μ with 11″ beams using a similar bolometer at Mount Lemmon; between 2.3 and 12.5 μ with 22″ beams using a photoconductor at Mount Lemmon. Observations of HD 44179 at 27 μ with 11″ beams were also obtained at Mount Lemmon on a very dry night in February. Table 4 displays these infrared magnitudes in three groups according to aperture. The total errors in these measurements (photometric statistics, uncertainties in calibrations, etc.) should not exceed ± 5 percent from 2.2 to 12.5 μ, ±15 percent at 18 and 22 μ, and ±25 percent at 27 μ, of which photometric errors alone contribute at most a few percent between 2.2 and 27 μ. Table 4 also includes the magnitudes obtained from the AFCRL rocket at 4, 11, and 20 μ. The differences in magnitude between the 11″ and 22″ data from 2 to 5 μ is almost certainly due to differing effective wavelengths caused by the responses of the germanium bolometer and the photoconductor; the former has a flat responsivity in this region, whereas the latter rises steeply at the shortest wavelengths in this range. Comparison of the various magnitudes in apertures from 4″ to 10′ × 3′ (that of the rocket survey) suggests that the infrared source is essentially pointlike, at least on a scale of a few arc seconds.

TABLE 3

UBVRI PHOTOMETRY OF HD 44179 WITH 33″ DIAPHRAGM, AND 1 σ OF THE MEAN ERRORS

Filter	λ_{eff}(Å)	Magnitude
U	3600	+9.51 ± 0.03
B	4380	+9.22 ± 0.02
V	5475	+8.83 ± 0.02
R	6800	+8.27 ± 0.02
I	8200	+7.97 ± 0.03

TABLE 4

INFRARED PHOTOMETRY OF HD 44179 WITH DIFFERENT BEAM SIZES

A. ROCKET DATA, 10′ × 3′ BEAM

[4]	+0.78	[11]	−2.63	[20]	−4.18

B. MOUNT LEMMON 1.5-METER REFLECTOR, 22″ BEAMS, PHOTOCONDUCTIVE DETECTOR

[2.3]	+3.19	[3.5]	+1.22	[4.9]	+0.09
[8.4]	−2.14	[11.2]	−2.63	[12.5]	−2.87

C. MOUNT LEMMON 1.5-METER REFLECTOR, 11″ BEAMS, BOLOMETRIC DETECTOR

[2.2]	+3.47	[3.6]	+1.26	[4.8]	+0.27
[8.6]	−2.08	[10.8]	−2.38	[11.3]	−2.64
[12.8]	−2.80	[18]	−4.0	[22]	−3.9
[27]	−4.7				

D. LICK 3-METER REFLECTOR, 4″ BEAMS, BOLOMETRIC DETECTOR

[2.2]	+3.53	[3.5]	+1.47	[4.8]	+0.60
[8.6]	−2.15	[11.5]	−2.56	[18]	−4.0

Figure 5 combines the *UBVRI* and infrared photometry into the energy distribution of HD 44179 in the form of λF_λ ($W\,cm^{-2}$) against λ (microns). A blackbody curve is also shown for comparison.

In order to evaluate the reddening we assume that both components of the binary (see § IX) have the same spectral type, B9–A0 III. Section VII demonstrates the likelihood of large grains being present around the star, and there might, therefore, be a component of neutral extinction. However, a reasonable lower limit can be placed on the true fluxes by correcting the observations for purely interstellar reddening. In this manner we find $E(B-V) = 0.39$ and $A_V = 1.2$ (from Lee 1968 for $T_{eff} = 10{,}000°$ K). Figure 5 shows broad-band fluxes de-reddened by this amount, again using Lee's tables (based on van de Hulst curve no. 15). Between *B* and *R*, the de-reddened curve has a slope like a Rayleigh-Jeans tail of a hot blackbody, but from *I* an appreciable near-infrared excess above this slope becomes apparent. This excess is also shown by the longer wavelength scanner spectrophotometry

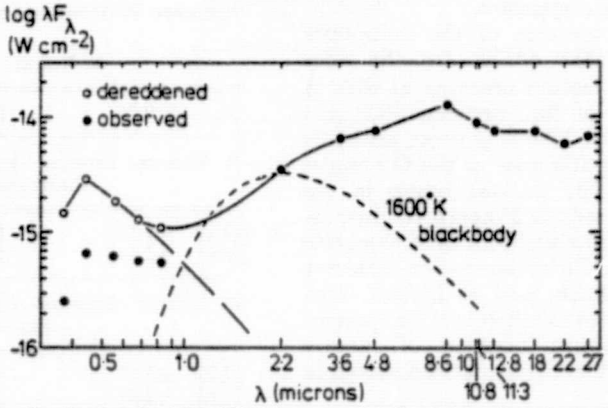

FIG. 5.—The composite energy distribution for HD 44179 between 0.36 and 27 μ, based on the broad-band observations. Both observed and de-reddened values of λF_λ are shown at the shorter wavelengths. Both axes are logarithmic and a blackbody curve is shown for comparison.

(fig. 4). It is possible to fit the Wien portion of a cool blackbody ($\sim$1600° K) into the de-reddened λF_λ distribution between about 0.8 and 2.2 μ in such a manner that the sum of the fluxes of this blackbody and of the Rayleigh-Jeans tail of the hot stellar component would roughly match the de-reddened observations from 3600 Å to about 2.2 μ. However, beyond 2.2 μ this simple blackbody curve cannot match the data, which present the appearance of a slowly rising broad distribution which reaches a peak somewhere near 8 μ. The composite λF_λ curve should be compared with that of HD 45677 (Swings and Allen 1971).

It is unreasonable to suppose that there is contamination of the broad-band near-infrared fluxes by emission lines (e.g., the Brackett series) when there is no evidence for emission lines of related species in the near-infrared spectra. Consequently there would appear to be a very broad yet relatively flat infrared continuum between 2 and 27 μ. This continuum is most probably due to thermal emission by dust grains at a range of temperatures and with a variety of compositions. There is strong independent evidence for dust near the star in the color and geometry of the nebula, in the large Balmer discontinuity, in the presence of spectral features near 10 μ (§ VI), and in the polarization data (§ VIII).

VI. INFRARED SPECTROPHOTOMETRY

K. M. MERRILL

Spectrophotometry covering the wavelength range 8–13 μ with a resolution of $\Delta\lambda/\lambda \approx 0.015$ was carried out during 1973 December with a cooled filter wheel spectrometer built at UCSD by F. C. Gillett. The observations, a total of four scans or 80 seconds total integration time per point, were taken with a 22″ beam at the UM–UCSD 1.5-m infrared telescope on Mount Lemmon, and were calibrated against α Tau. The averaged data shown in figure 6 have a statistical accuracy of better than ± 5 percent, although the absolute flux level is less certain.

Emission features are seen near 8.7 and 11.3 μ superposed on a smooth continuum which drops sharply from 8 μ and levels out beyond 10 μ. While far less complicated, this spectrum is strikingly similar to that of the planetary nebulae NGC 7027 and BD+30°3639 where the 11.3-μ feature, possibly due to mineral carbonates such as calcium magnesium carbonate (Gillett, Forrest, and Merrill 1973), is present at nearly the same strength relative to the continuum. The 8.7-μ feature, at best only marginally apparent in the two planetary nebulae spectra (where statistical uncertainty or a possible emission line prevents identification), is possibly due to mineral sulfates such as calcium magnesium sulfate which in the laboratory produce strong narrow absorption peaks in the vicinity of 9 μ (Lyon 1964). Consistent with an extremely low excitation region (as evidenced by the D-lines in emission), there is no evidence for the 9.0-μ [Ar III], 10.52-μ [S IV], or 12.78-μ [Ne II] lines seen in the planetaries.

VII. POLARIMETRY OF HD 44179

GEORGE V. COYNE

Polarimetric observations of HD 44179 were made in six spectral bands with a dual channel rotating half-wave plate polarimeter coupled to a NOVA computer. The observations are listed in table 5. They

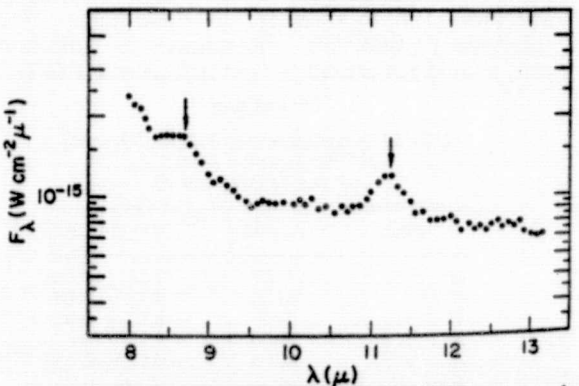

FIG. 6.—The 8–13 μ infrared spectrophotometry showing the two emission peaks.

TABLE 5

JOURNAL OF POLARIMETRIC OBSERVATIONS

$1/\lambda_0$ (μ^{-1})	Date 1973–1974	p (percent)	ϵ_p	θ (degrees)	ϵ_θ	Δp^* (percent)
2.72.....	Jan. 19	0.94	±0.05	41.6	±1.5	−0.01
	Jan. 23	0.98	±0.03	44.3	±0.9	−0.08
	Jan. 29	0.98	±0.03	44.0	±0.9	0.00
	Mean	0.97	±0.03	43.3	±1.4	...
2.32.....	Jan. 19	0.94	±0.02	39.6	±0.6	−0.02
	Jan. 23	0.96	±0.03	38.6	±0.9	−0.05
	Jan. 29	0.94	±0.01	39.7	±0.3	−0.01
	Mean	0.95	±0.01	39.3	±0.7	...
1.93.....	Jan. 19	0.94	±0.03	36.2	±1.0	−0.01
	Jan. 23	1.00	±0.04	37.2	±1.2	−0.05
	Jan. 29	1.03	±0.02	38.0	±0.6	0.00
	Mean	0.99	±0.05	37.2	±0.6	...
1.52.....	Jan. 23	1.07	±0.06	32.2	±1.7	−0.03
	Jan. 29	1.11	±0.18	37.1	±4.9	+0.24
	Mean	1.09	±0.08	34.7	±2.9	...
1.16.....	Dec. 8	1.38	±0.16	27.3	±3.5	+0.04
	Jan. 23	1.23	±0.04	29.5	±1.0	−0.05
	Mean	1.30	±0.08	28.3	±2.2	...
1.06.....	Dec. 8	1.26	±0.33	23.2	±7.8	+0.11
	Jan. 19	1.43	±0.31	22.7	±6.5	+0.08
	Jan. 23	1.38	±0.07	25.4	±1.5	+0.11
	Mean	1.36	±0.08	23.9	±1.6	...

* The measured sky-polarization corrections which were subtracted from the star-plus-sky data to obtain the polarization of the starlight listed in column (3). See text for explanation.

were made with the 1.5-m and 2.3-m telescopes of the University of Arizona. Corrections for instrumental polarization (less than $p = 0.05$ percent) have been applied. Corrections for the polarization of the background sky have been made by measuring at the four cardinal points at 15″ ± 3″ from the star with a 10″ diaphragm (the same as that used for the star-plus-sky measurements). Among these four sky measurements, the polarization differed by less than 10 percent of its mean value and the flux did not differ at all. The average polarization and flux were used to determine the sky corrections listed in the last column of table 5. These are the product of the sky polarization, the flux ratio of sky to star-plus-sky, and cos $2(\theta_m - \theta_s)$, where θ_m and θ_s are the position angles of the measured (star-plus-sky) polarization and the sky polarization, respectively. The corrections are small except for the $I(1/\lambda_0 = 1.06\,\mu^{-1})$ filter where they are about 3 times larger than the average sky correction and of opposite sign. The sky correction at the $O(1/\lambda_0 = 1.52\,\mu^{-1})$ filter for January 29 is anomalous. These polarimetric results are independent of aperture used in the range 5″ to 20″.

In figure 7 are plotted the mean percentage polarizations and position angles of table 5. These are the observed values corrected for instrumental and sky polarizations. The observations, including the position angle rotation, can be explained if one assumes three components of the observed polarization: electron scattering in the stellar atmosphere, Mie scattering from large grains in a circumstellar nebula, and interstellar polarization.

In order to sample the interstellar polarization ($l^{II} = 219°$, $b^{II} = -12°$), the polarization at the G filter ($1/\lambda_0 = 1.93\,\mu^{-1}$) was measured for two stars within 6′ of HD 44179 (for which $m_G = 8.7$ mag) with the following results: for HD 44219, $p = 0.02$ percent, $\theta = 129°$, $m_G = 7.7$ mag; for BD−10°1480,

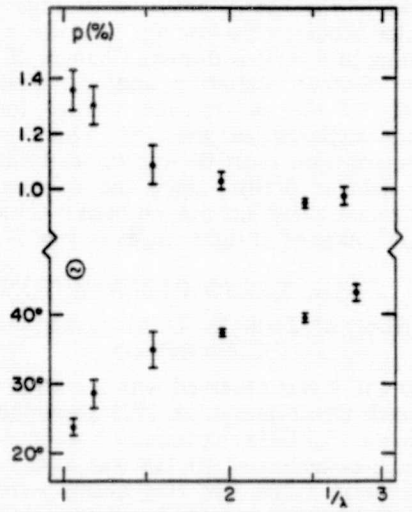

FIG. 7.—Percentage polarization (p) and position angle (θ) for HD 44179. The error bars give mean errors. The position angle rotation is due to a combination of electron scattering [$p = 0.95$ percent, $\theta = 42°$] and scattering from large grains [$p(\lambda)$, $\theta \approx 7°$].

TABLE 6

CORRECTED POLARIMETRIC DATA WHEN INTERSTELLAR AND ELECTRON SCATTERING POLARIZATION COMPONENTS HAVE BEEN REMOVED

$1/\lambda_0$ (μ^{-1})	2.72	2.32	1.93	1.52	1.1b	1.06
p(%)	0.07	0.15	0.24	0.37	0.69	0.86
θ(°)	...*	6	7	9	7	3

* The resultant position angle at 2.72 μ^{-1} is indeterminate.

$p = 0.13$ percent, $\theta = 86°$, $m_G = 9.8$ mag. The distance to these stars is not known and, for want of more information on them, the interstellar polarization is taken as the average of the two measured values: $p = 0.08$ percent, $\theta = 108°$. In the catalog of Mathewson and Ford (1970) for seven stars which have $b^{II} < -8°$ and lie within 4° of HD 44179 at distances from 350 to 650 pc, the polarization ranges from 0.09 to 0.40 percent. If the distance to HD 44179 is about 400 pc (see § X), our estimate of the interstellar polarization from the measurement of two nearby field stars appears to be essentially correct.

Polarization by electron scattering is neutral. If we assume that the observations between 2.3 μ^{-1} and 3.0 μ^{-1} in figure 7 represent the electron scattering component ($p = 0.95$ percent, $\theta = 42°$) and subtract this and the interstellar polarization from the observed polarization, we obtain the results given in table 6. The mean polarization position angle (giving one-half weight to the value at $1/\lambda_0 = 1.06\ \mu^{-1}$ because of the anomalous sky corrections) is $7 \pm 2°$. Thus by removing the interstellar and electron scattering components we obtain a component with a well determined plane of polarization (the plane of the electric vector maximum) which is approximately parallel to the nearly north–south edge of the rectangular nebular core (see fig. 1*d* where a line corresponding to $\theta = 7°$ is drawn). Changes of 0.1 percent in the electron scattering and/or interstellar components of the polarization change the resultant position angle by less than 10°. This component of the polarization must be due to scattering by quite large nebular grains, since the maximum of the polarization curve has not yet been reached at $1/\lambda_0 = 1.06\ \mu^{-1}$, aligned at right angles to $\theta = 7°$.

VIII. RADIO OBSERVATIONS

HUGH M. JOHNSON, D. MATSAKIS, AND BEN ZUCKERMAN

HD 44179 was observed with the 36-m dish of the Haystack Observatory[1] on 1973 December 6 and 7, UT, in the 15.5 GHz continuum. A standard technique of beam-switching at 10 Hz was used to minimize atmospheric noise. The two beams were separated horizontally 0.2, and each beam remained on source 32 s alternately, 10 times to constitute a scan. A total of nine such scans were made. The standard source DR 21 was observed each night with the same technique. Assuming that its flux density is 20.1 Jy at 15.5 GHz, the derived flux density of HD 44179 is -0.023 ± 0.025 Jy. Consequently only an upper limit to the strength of the source can be given.

Observations of HD 44179 were made on 1973 November 19, at a frequency of 8.4 GHz using the NASA–JPL Deep Space Network 64-m antenna at Goldstone, equipped with a right circularly polarized feed. Four drift scans were made through the position of the object. The average of these scans provides only an upper limit to the 8.4 GHz flux in a 2.1 beam of 0.022 Jy (1 σ).

[1] Radio astronomy programs at the Haystack Observatory are conducted with support from the National Science Foundation.

IX. THE BINARY

FRANK HOLDEN

The star HD 44179 is a visual double, ADS 4954, discovered by Aitken in 1915. Since its discovery, it has been observed on 13 occasions and resolved on 11 (see table 7). The observations indicate genuine duplicity and obvious motion, and suggest that the components were of equal brightness between 1915 and 1947, but have had $\Delta m \approx 0.4$ mag between 1951 and 1962. The separation slowly decreased from a maximum of 0.27 in 1921 to 0.17 in 1947, but van den Bos was unable to resolve the pair in 1948 (implying a separation $\leqslant 0.1$). Subsequently the pair reopened and the separation when last resolved was 0.21 in 1962. This scattered information does not enable the determination of an orbit.

Recent observations of HD 44179 have been made by Holden. The star was examined several times with the 92-cm refractor of Lick Observatory in late 1973, and with the 1.5-m reflector at Mount Wilson in early 1974. On none of these occasions was the seeing good enough to show duplicity of the star. The star was observed on 1974 April 10, 19, and 20, with good seeing using a 92-cm reflector at CTIO. The powers used were ×700, 1000, and 1700, but no duplicity was noted. Pairs with a separation <0.2 were clearly resolved with the same telescope on April 10, and a strong upper limit of 0.1 can be placed on the separation of HD 44179.

If the two stars are indeed of comparable brightness, then there are quite severe constraints on the spectral type of the companion. Throughout the region from the blue to the near-infrared, only a few absorption lines appear in the spectrum of HD 44179, and all of these are consistent with a late B or early A star. A late-type secondary, for example an M star, is precluded by the lack of molecular absorptions near 8000 Å. Equally, the presence of a hot star, for example an O star, is excluded by the *UBV* and scanner data which show no evidence of a continuum increasing to short wavelengths. If the early spectral type, B9–A0, is appropriate to the primary, then only the emission features at Hα and the D-lines remain unexplained, yet there is no significant difference in radial velocity between these emission lines and the absorption lines. Consequently, one is forced to conclude either that the companion has a spectrum close (B7–A2) to that of the primary, or that a simple

TABLE 7

BINARY OBSERVATIONS OF HD 44179

Date	Position Angle	Separation	Δm	Observer*	N†
1915.11....	141°.6	0".30	0	A	3
1921.82....	143.8	0.27	...	A	2
1930.19....	114.5	0.24	0	A	1
1941.08...	168.8	0.20	0.2	B	1
1944.06....	214.8	0.23	0.2	B	1
1945.17....	203.0	0.20	0	B	1
1947.22....	174.2	0.17	0	B	1
1948.10....	...	< 0.1	...	B	1
1951.07....	120.1	0.16	...	B	1
1958.03....	340.8	0.16	0.4	B	1
1958.09....	351.9	0.20	0.5	B	1
1959.17....	346.4	0.19	0.3	B	4
1962.03....	356.3	0.21	0.4	B	2
1974.29....	...	< 0.1	...	H	3

* Observer: A = Aitken; B = van den Bos; H = Holden.

† Number of nights on which measurements were made.

interpretation of the duplicity in terms of two stars is invalid. It is, however, unlikely that starlight scattered, for example, from some gas cloud in the vicinity of the primary would have a brightness comparable to that of the star or a convincingly stellar visual appearance, as the observations suggest. Therefore, an interpretation of the duplicity in terms of two stars seems entirely reasonable. Given the presence of considerable dust near the star, it is not impossible that protracted obscuration of one component of a binary might occur, so that one or both of the disappearances of the companion (1948 and 1973–1974) may not necessarily be due to orbital aspect. Indeed it may be that the difference in magnitudes noted by van den Bos between 1951 and 1962 foreshadowed the onset of such an obscuring phase. This hypothesis implies that in the past HD 44179 may have undergone slow changes in magnitude of small amplitude (~0.5 mag); as yet there is no evidence of such variability. It should be noted that the position angles of the binary (table 7) have not always been close to the plane of the dust disk, so one can invoke occasional disappearances of the companion.

X. DISCUSSION

We conclude that HD 44179 consists of one or two stars of spectral type B9–A0 III, and that a very low excitation region, in which the Hα and D-line emissions arise, is also present. It will be convenient now to summarize the evidence that dust is associated with the system, after which the color of the nebula and its geometry can be more easily discussed. Clues to the presence of circumstellar grains near HD 44179 are as follows, with the relevant sections of this paper in parentheses: (1) the large Balmer jump coupled with the lack of obvious widespread obscuration on the Palomar prints (§ IV); (2) the gross excess of infrared radiation over the Rayleigh-Jeans tail of a hot blackbody (§ V); (3) the presence of narrow spectral features attributable to dust particles in the 8–13 μ spectrum (§ VI); (4) the polarimetric data suggesting the existence of large grains which scatter the starlight producing the unusual $p(\lambda)$ curve (§ VII); (ξ) the possibility of local obscuration having caused a disappearance of the companion of HD 44179 (§ IX; see also the discussion below of the masses of the stars in the binary).

Paradoxically, despite the presence of an embedded blue star the nebula does not possess appreciable blue continuum, nor does its light arise significantly from emission lines. That the nebulosity is bright in red continuum remains to be explained. It would appear that the rectangular aspect of the nebula is a product of the brightness of HD 44179—were the star much fainter, the nebula would be seen to narrow to a small waist in the vicinity of the star. Consequently the geometry of the nebula seems to be that of a biconical structure (with axis $\theta \sim 7°$) in which the spikes represent a cone of higher surface brightness than the inner nebulosity. The nebula might be regarded as another example of an "hourglass" cometary nebula; or magnetic fields and plasma confinement might be invoked, or rotation, especially in the light of the high degree of symmetry.

If we are confronted by a cometary nebula, then the canonical picture of the hourglass morphology is relevant (e.g., Cohen 1974), but the wealth of observational material available on HD 44179 elevates this picture from circumstantial argument to a far stronger case. The geometry implies that surrounding HD 44179 there is an equatorial disklike structure of gas and dust close to whose plane we lie; in this model the inner edge of the toroid restricts the diffusion of light from the central object except into two cones of semiangle about 30° around the normal to the disk. The infrared radiation suggests considerable dust is about HD 44179, and it would be most unreasonable to assume that only relatively large grains, which dominate the polarization near 1 μ, are present. Within the two cones, starlight suffers local reddening by an admixture of small and large grains before escaping from the vicinity of the disk, eventually

to be scattered in our direction by an extensive enveloping halo of gas and perhaps small dust grains. The lack of aperture-dependence of the infrared fluxes suggests that only quite cold grains can be present in this halo ($T \leqslant 150°$ K). In this manner we can explain many of the features of the nebula, in particular the red continuum and the small nebulosity very close to the star seen in the blue (fig. 1*b*), in terms of scattering of reddened starlight. It should be noted that this would make HD 44179 the brightest star (visually) associated with a biconical nebula. Alternatively, the very symmetrical structure in the nebula might be explicable by a process of reconnecting magnetic fields following the collapse of an interstellar cloud from which HD 44179 was born (cf. the pattern of standing waves in fig. 1 of Priest 1973). There is one major restriction to be placed on a magnetohydrodynamic explanation, namely that no shock waves are involved in the system; this limitation arises from the lack of significant line emission within the nebula. However, in order to produce the strong red continuum and the spikes, it may be necessary to invoke both the reddening hypothesis and magnetic (and/or rotational) dominance of the overall structure. Although the 8–13 μ spectrum of HD 44179 has some similarities to those of two planetary nebulae, there is no justification for describing the nebulosity as a planetary, particularly since no radio continuum has been found.

Returning to the spectrophotometry, since photographs of the nebula indicate the presence of a strong continuum around 6500 Å but not in the near-infrared (~8500 Å), it is tempting to attribute the broad feature near 6900 Å to the nebula rather than to the star. This could, for example, be a feature in the scattering cross section of some circumstellar grains. It is not yet possible to make a definite statement about the origin of this feature; more spectrophotometry is planned using a variety of aperture sizes in order to define the precise contribution of the nebula to the spectrum.

An estimate of the distance of HD 44179 is clearly important. The simplest estimate can be made by assuming that the *UBV* data refer to a single B9 III star (and that the companion is presently hidden). this implies $M_V = -0.4$; and we find $V = 8.8$, $A_V = 1.2$ (see § V), $V_0 = 7.6$, and hence $D = 400$ pc. Perhaps more realistic estimates can be made by assuming that HD 44179 has the same *bolometric* luminosity as LkHα 208 or R Mon, stars also associated with conical or biconical nebulae which are bright infrared objects. Cohen (1973) gives $M_{bol} = -1.7$ for the former and -2.7 for the latter. For comparison with these objects, we require the total flux of HD 44179 ($\int_0^\infty F_\lambda d\lambda$). Since de-reddening the data increases the luminosity of HD 44179 by only 9 percent, we shall deal with the de-reddened spectral intensities (F_λ). A much more serious question relates to the unobserved radiation longward of 27 μ. A lower bound on this latter contribution (in the absence of spectral features) may be obtained from Appendix A of Cohen (1973), and yields an estimated 29 percent of the total luminosity beyond 27 μ. The appropriate values for the integrated spectral intensity in the ranges (0.36 μ, 27 μ) and (0.36 μ, ∞) are 2.23 (−14) and 3.13 (−14) W cm^{-2}. Comparison of the larger of these two figures with LkHα 208 gives a distance of 240 pc, and with R Mon, 370 pc. It would seem that a distance of 330 pc does justice to the three estimates above.

At 330 pc, the bolometric luminosity of HD 44179 is 1050 $L_\odot$, and the luminosity ratio of a 10,000° K blackbody, matched to the de-reddened data at *B* and *V*, to the observed spectrum between *U* and 27 μ, is 1:6. Replacing the blackbody by a model appropriate to a 10,000° K giant (e.g., Strom and Avrett 1965) reduces this ratio to 1:5 (of course allowance for energy beyond 27 μ increases the ratio). Thus arguing for a binary consisting of two normal B9 giants, both of which are presently visible despite their closeness in the sky, leads to a gross deficiency in the energy required to power the infrared emission. If one member of the binary is obscured now, but is another B9 giant, the deficiency is reduced to (>) 2.5. Only if the companion is both currently invisible and highly luminous can we escape this dilemma. From the observations of the binary we may attempt to estimate the sum of the masses of the two stars: provided that obscuration is responsible for one of the two "disappearances" of the companion, the period is no less than ~160 yr; for the apparent mean separation we take ~0".2. This yields $(M_1 + M_2) \approx 11\ M_\odot$ and suggests that we may require stars which are too luminous for their masses. If the disappearances of the companion in 1948 and 1974 are indeed due to orbital motion, then $P \approx 26$ yr—or perhaps ~52 yr, depending on the orientation of the orbit—which gives $(M_1 + M_2) \approx 400\ M_\odot$ (or 120), an absurd situation. Taken in context, the association of a dust disk, the peculiar nebula, and the large infrared energy argue for the pre–main-sequence nature of HD 44179. This conclusion suggests that perhaps rotation is responsible for the nebular symmetry rather than magnetic fields, for in the latter situation it is difficult to reconcile confinement of gas and dust with the lack of significant line emission in the nebula.

M. C. wishes to thank Drs. R. G. Walker and S. D. Price for providing a copy of the AFCRL rocket infrared survey, Drs. W. A. Stein and N. J. Woolf for observing time at Mount Lemmon and Dr. C. Worley of the USNO for supplying information on the binary data of HD 44179. The work at Berkeley was supported by the NSF under grant GP-31592X. Infrared astronomy at UCSD is supported by the NSF and by NASA under grant NGL 05–009–230. We thank Dr. R. Brown, Richard Kron, Dimitrios Matsakis, and Dr. Hyron Spinrad for their observational contributions also. G. V. C. thanks NSF for partial support of his work. F. H. acknowledges the financial support of NSF under grant GP-38468. H. M. J.'s contribution was made under contract NAS 2-7842 with NASA.

Note added in proof—A new blue spectrum of HD 44179 has been obtained by A. Cowley in 1974 October on the 1.8-m reflector of the Dominion Astrophysical Observatory. The plate covers the region λλ3600–4900 at 15 Å mm^{-1} on fine grain emulsion, and is well widened. Very narrow, weak emission components of calcium H and K are seen, at radial velocity +21.3 ± 1.4 km s^{-1} (cf. the velocity of the D-lines in § III), with red-displaced absorptions (velocity +55.1 ± 2.6 km s^{-1}) similar to, but stronger than, those seen near the D-lines (fig. 2). The difference in radial velocities between the sharp calcium emissions and the adjacent absorptions is the same as the corresponding shift measured for the D-lines. The stellar velocity, determined from 12 hydrogen lines, is +26.9 ± 4.3 km s^{-1}. Many weak absorption lines typical of late B stars are present in the spectrum, but four weak C I absorption lines are present with radial velocity +36.8 ± 4.2 km s^{-1}, different from the stellar velocity. No C II lines are seen, and no other late B star is known to show these C I lines, which are the four strongest lines in the appropriate multiplet tables.

REFERENCES

Anderson, C. M. 1970, *Ap. J.*, **160**, 507.
Anderson, C. M., and Schiffer, F. H., III. 1975, *AAS Photo Bulletin*, in preparation.
Cohen, M. 1973, *M.N.R.A.S.*, **164**, 395.
———. 1974, *Pub. ASP*, in press.
Crawford, D. L. 1963, *Ap. J.*, **137**, 530.
Gillett, F. C., Forrest, W. J., and Merrill, K. M. 1973, *Ap. J.*, **183**, 87.
Hayes, D. S. 1970, *Ap. J.*, **159**, 165.
Lee, T. A. 1968, *Ap. J.*, **152**, 913.
Lyon, R. J. P. 1964, *NASA Contract Report* CR-100.
Mathewson, D. S., and Ford, V. L. 1970, *Mem. RAS.*, **74**, 139.
Mihalas, D. 1970, in *Stellar Atmospheres* (San Francisco: Freeman), p. 190.
Oke, J. B. 1965, *Ann. Rev. Astr. and Ap.*, **3**, 23.
Oke, J. B., and Schild, R. E. 1970, *Ap. J.*, **161**, 1015.
Priest, E. R. 1973, *Ap. J.*, **181**, 227.
Schroeder, D. J., and Anderson, C. M. 1971, *Pub. ASP*, **83**, 438.
Strom, S. E., and Avrett, E. H. 1965, *Ap. J. Suppl.*, **12**, 1.
Swings, J. P., and Allen, D. A. 1971, *Ap. J. (Letters)*, **167**, L41.
Walker, R. G., and Price, S. D. 1975, in preparation.

Second note added in proof.—W. Liller has very kindly sampled 12 blue plates in the Harvard plate collection showing HD 44179 between 1897 and 1974, and has found no evidence of variability. The total range of blue magnitudes is 0.20 mag, and the mean error of a single measurement is 0.05 mag.

C. M. ANDERSON, R. O. JAKOUBEK, AND F. H. SCHIFFER III: Washburn Observatory, University of Wisconsin–Madison, 475 North Charter Street, Madison, WI 53706

M. COHEN and W. FAWLEY: Berkeley Astronomy Department, University of California, Berkeley, CA 94720

A. COWLEY: Dominion Astrophysical Observatory, 5071 W. Saanich Road, Victoria, BC V8X 3X3, Canada

G. V. COYNE, S.J.: Lunar and Planetary Laboratory, University of Arizona, Tucson, AZ 85720

T. R. GULL: Kitt Peak National Observatory, PO Box 26732, 950 North Cherry Avenue, Tucson, AZ 85726

E. A. HARLAN: Lick Observatory, Mt. Hamilton, CA 95140

G. H. HERBIG: Lick Observatory, University of California, Santa Cruz, CA 95064

F. HOLDEN: 302 S. Market Street, San Jose, CA 95113

H. S. HUDSON, K. M. MERRILL, and B. T. SOIFER: Department of Physics, Revelle College, University of California, San Diego, La Jolla, CA 92037

H. M. JOHNSON: Lockheed Palo Alto Research Laboratory, Lockheed Missiles and Space Company, Inc., 3251 Hanover Street, Palo Alto, CA 94304

B. ZUCKERMAN: Astronomy Program, University of Maryland, College Park, MD 20740

THE ASTROPHYSICAL JOURNAL, 207:763–769, 1976 August 1

INFRARED OBSERVATIONS OF ICES AND SILICATES IN MOLECULAR CLOUDS

K. M. MERRILL, R. W. RUSSELL, AND B. T. SOIFER
Department of Physics, University of California, San Diego
Received 1975 October 20

ABSTRACT

Spectrophotometric observations from 2 to 4 μ and from 8 to 13 μ of several infrared sources associated with molecular clouds are reported. Narrow absorption features at 3.08 μ, attributed to interstellar ices, appear in all sources with a molecular cloud in the intervening line of sight. All sources showing ice absorptions also show broad absorption features, attributed to cold silicates, from 8 to 13 μ.

The observed ice absorption profiles are all quite similar; however, they do not fit in detail Mie theory predictions of extinction for pure H_2O or NH_3 ices. The ratio of ice to silicate optical depths is found to vary, with most sources showing $\tau_{ice}/\tau_{silicate}$ in the range 0.1–0.4. The ratio of visual extinction to ice absorption is found to increase rapidly from inside to outside the molecular cloud in NGC 2024.

Subject headings: infrared sources: general — interstellar: matter — interstellar: molecules

I. INTRODUCTION

The determination of the constituents of solid particles in the interstellar medium has long been a subject of active study through many varied techniques. Infrared spectroscopy provides a fundamental means of approaching this problem because the absorption bands of solids occur at infrared wavelengths. It should ultimately be possible to identify quantitatively the major particulate constituents of the interstellar medium through infrared spectroscopy of a wide variety of objects, in much the same way as the gas-phase constituents can be determined through ultraviolet and optical spectroscopy of many objects.

Furthermore, because the cosmically abundant elements are relatively light (i.e., $z \lesssim 30$), the fundamental vibration bands of most materials are generally in the wavelength range 2–20 μ, and so are accessible, in large part, to observations from ground-based telescopes.

In this paper we report infrared spectrophotometric observations from 2 to 4 μ and from 8 to 13 μ that show absorption by interstellar ices and silicates in the infrared spectra of many objects. While the presence of silicates as a major constituent of the interstellar medium has been established observationally for some time (see, e.g., Woolf 1973; Gillett *et al.* 1975), the arguments for ices being abundant have been mostly indirect and theoretical in nature (see Greenberg 1964; van de Hulst 1973 for historical references). While ice absorption has been detected in the spectrum of the BN source in Orion (Gillett and Forrest 1973, hereafter GF), its abundance in interstellar matter remains uncertain. Our observations combined with other observations (Gillett *et al.* 1975*b*, hereafter GJMS), show that ices are common in the interstellar medium. However, their abundances are apparently small in comparison with silicates, and the ices are confined mainly to molecular-cloud regions.

II. THE OBSERVATIONS

All of the observations reported here were obtained with liquid-nitrogen-cooled circular variable-filter-wheel spectrometers spanning the 2.1–4.1 μ and 7.5–13.5 μ wavelength ranges. The equipment and data-taking procedures have been described by GF. All of the observations were obtained using the UCSD–University of Minnesota 1.5 m infrared telescope on Mount Lemmon.

The 2–13 μ spectra of the various sources are plotted in Figure 1. Where no error bars are shown, the statistical errors are less than 5 percent. Nearly all of the objects discussed here are known to be associated with molecular clouds, and were therefore thought likely to have large column densities of cold matter in the line of sight.

III. THE INDIVIDUAL SOURCES

CRL 490.—This source was originally found in the AFCRL infrared sky survey (Walker and Price 1975) and precisely located ($\alpha_{1950} = 3^h23^m44^s8$, $\delta_{1950} = +58°36'48''$) by workers at the University of Arizona (Low 1973). Millimeter emission lines of HCN and CS have been detected (Morris *et al.* 1974), indicating that a dense molecular cloud is associated with the infrared object, but no radio continuum flux to a limit of 0.03 Jy was detected (Morris *et al.* 1974). There is a faint (20 mag) red object at the position of infrared source (Low 1973). Our data show both ices and silicates in absorption.

NGC 2024 No. 1.—This is a highly reddened star ($A_v \approx 8$ mag) discovered by Johnson and Mendoza (1964), and suggested by them to be the exciting star of the H II region NGC 2024. This interpretation has recently been questioned (Grasdalen 1974), but this

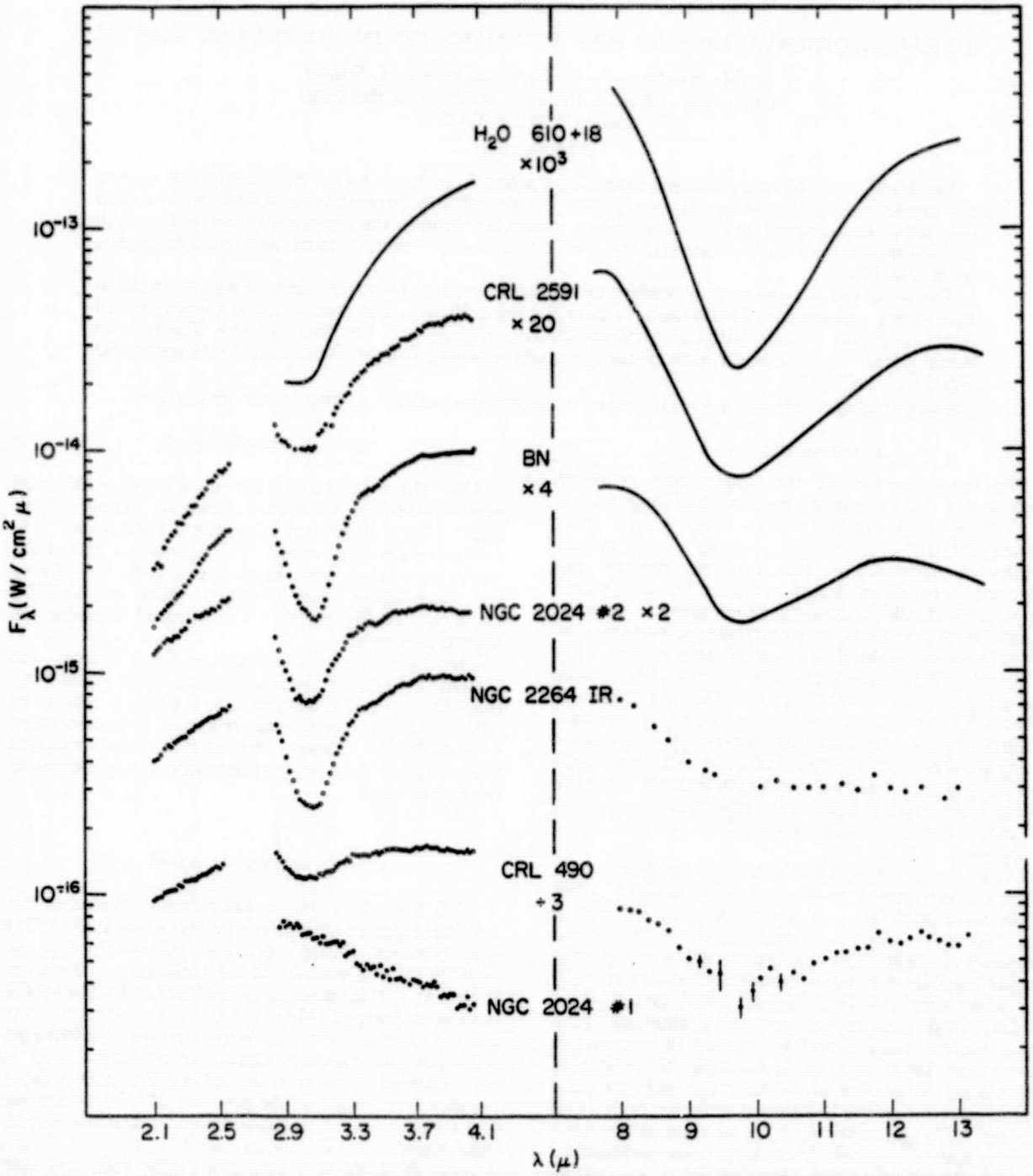

FIG. 1.—The 2.1–4.1 μ and 8–13 μ spectra of infrared objects associated with molecular clouds. Spectra represented by lines have been published elsewhere (see text). The 2–4 μ spectrum of BN is from GJMS. All objects, except NGC 2024 No. 1, show absorptions at 3.08 μ and around 9.7 μ, attributed to ice and silicate absorption, respectively. The wide variation in ratios of ice to silicate absorptions is evident from these spectra.

star could contribute a substantial fraction of the ionizing photons to the H II region (MacLeod, Doherty, and Higgs 1975). The 2–4 μ spectrum of this source shows no evidence for ice absorption ($\tau_{ice} \leq 0.05$), while broad-band photometry around 10 μ shows that the continuum at this wavelength is dominated by circumstellar dust emission (Grasdalen 1974).

NGC 2024 No. 2.—This infrared point source was discovered by Grasdalen (1974) and suggested by him to be the exciting star of the H II region. Whether or not this is a highly reddened star (if so, $A_v \approx 30$ mag is indicated), it lies in the line of sight to the large molecular cloud associated with NGC 2024 (Gilmore *et al.* 1976) and is nearly coincident with the peak of the 350 μ intensity distribution (Hudson and Soifer 1976). Both ice and silicate absorptions are prominent in this object.

NGC 2264 IR.—This infrared source, first reported by Allen (1972), is located at the head of a cometary nebula in NGC 2264. It is associated with a molecular cloud (Morris *et al.* 1974) and a far-infrared source (Harvey, Campbell, and Hoffmann 1975). The infrared spectrum shows deep ice absorption and some evidence for silicate absorption.

Several other previously observed infrared sources are associated with molecular clouds, and since ice and silicate absorption is evident in their 2–13 μ spectra, we include them in the discussion. These are the BN source in Orion (see, e.g., GF and references therein), CRL 2591 (Merrill and Soifer 1974), and H_2O 0610+18 (Pipher and Soifer 1976).

Infrared spectrophotometry of the BN source, the well-known infrared point source in or behind the Orion molecular cloud, has previously been reported by GF and GFMS, and shows the absorption features of both ices and silicates. Infrared spectrophotometry of CRL 2591 has been reported by Merrill and Soifer (1974), and also shows ice and silicate absorption in its spectrum (the 2–4 μ spectrum of this source reported here is new data obtained during 1974 October/November). Morris *et al.* (1974) report a dense molecular cloud coincident with this source, while Wendker and Baars (1974) and Brown (1974) report the detection of a weak, very compact radio source coincident with the infrared position. Observations of H_2O 0610+18, an infrared source associated with the H II region/molecular cloud complex IC 2162/S255/257, have been reported by Pipher and Soifer (1976). Once again, both ices and silicates are seen in absorption in the infrared spectrum.

IV. DISCUSSION

These sources, although representing a fairly heterogeneous group of infrared objects, are all associated with molecular clouds. In fact each, except NGC 2024 No. 1, is either imbedded in or behind its molecular cloud, so that they provide good background sources for absorption spectroscopy of material in the intervening line of sight. From the large value of A_v (~8 mag), the line of sight to NGC 2024 No. 1 samples a moderate amount of unshielded (i.e. non-molecular cloud) interstellar material.

a) Ice Absorption

It has long been supposed that ices are a major constituent of the interstellar medium. This supposition has been based on indirect evidence and theoretical calculations, rather than direct observations. In fact, observations have suggested (Knacke, Cudaback, and Gaustad 1969; GJMS), rather, that ices are at most a minor constituent of the general interstellar medium.

Our observations show that the feature that has been identified as ice absorption by GF is in fact quite commonly found in the spectra of sources associated with dense molecular clouds. What is more surprising is the similarity of all the ice absorptions in these spectra. This is shown in Figure 2 where we have plotted the absorption profile for each object (normalized to unit optical depth at τ_λ^{max}) derived by assuming the underlying continuum emission to be a smooth interpolation between the observed spectra at 2–2.5 μ and 3.5–4 μ. This simple approach to deriving τ_λ was chosen for two reasons. First, unlike the 10 μ feature, to be discussed later, we have no observations that indicate that this is ever seen in emission. Second, and more important, at temperatures required to produce such an emission feature, ices would rapidly evaporate. The absorption profiles for the different sources are nearly identical (certainly they must be regarded as identical to within the uncertainties in the underlying continua), suggesting nearly identical composition of the material causing the 3.1 μ absorption in the different clouds.

For comparison the absorption profiles of H_2O and NH_3 ices, calculated for 0.1 μ radius spheres using Mie theory and optical constants from Bertie, Labbé, and Whalley (1969) for H_2O ice, and Robertson *et al.* (1975) for NH_3 ice, are also shown in Figure 2, as is the effect of increasing the particle size for H_2O ice so that scattering becomes significant.

The observed absorption profiles agree qualitatively with absorption by water ice, although the detailed profile differs. The observational profile has more absorption for $\lambda < 3.08$ μ than solid H_2O, and a long-wavelength wing that does not appear in water ice. There appears to be no good agreement between the observations and the expected profile for solid ammonia. It seems possible to explain the observed profile by a mixture of H_2O and NH_3 ices (to produce the absorption shortward of 3.08 μ) with some extinction due to scattering by particles somewhat larger than 0.1 μ radius (to produce the long-wavelength wing on the absorption profile). It is somewhat disturbing that simple H_2O ice absorption cannot fit the observed profile; however, unless the optical constants of ice are wrong and/or Mie theory is inappropriate, the mixture of materials seems the most likely explanation. Further quantitative laboratory work on ice mixtures is necessary to reproduce the detailed profiles and to determine whether or not materials other than water ice are present.

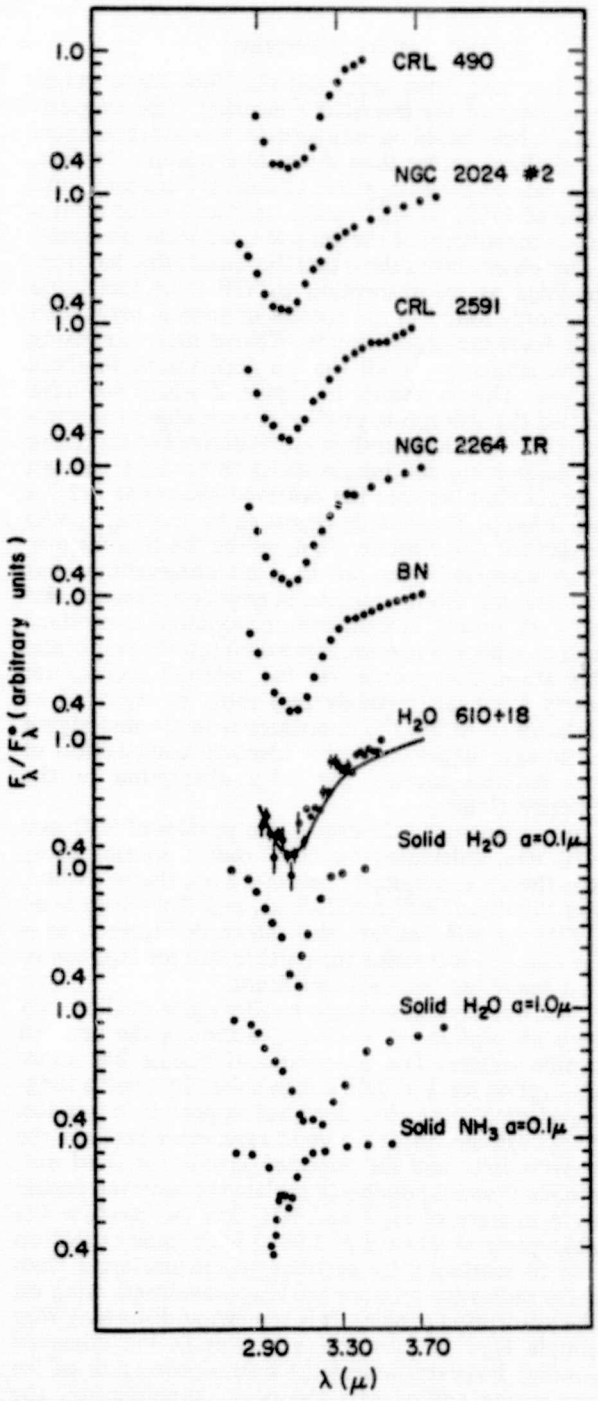

FIG. 2.—The absorption profiles of ices in the infrared sources. Each profile was obtained by assuming the underlying spectrum to be a smooth interpolation from the flux measured at 2–2.5 μ and 3.5–4.0 μ, deriving the absorption profile from this interpolated underlying spectrum, and normalizing the derived τ_λ to 1 at 3.08 μ. The solid line in the plot for H_2O 0610+18 shows the normalized "standard molecular cloud" ice absorption plotted with the derived profile. The three plots at the bottom show Mie theory calculations of the extinction profiles for pure H_2O ice (radii $a = 0.1\ \mu$, $1\ \mu$) and NH_3 ice (radius $a = 0.1\ \mu$) using optical constants determined by Bertie, Labbé, and Whalley (1969) for H_2O ice and by Robertson *et al.* (1975) for solid ammonia.

b) Silicate Absorption

All of the objects in our sample (except NGC 2024 No. 1) show the 10 μ absorption that is commonly attributed to cold silicate material in the line of sight (GF; Gillett *et al.* 1975*a*). To account properly for the observed width of the silicate absorption feature (generally narrower than that seen in emission in many objects), and to determine with reasonable confidence the correct absorption optical depth in silicates, it is necessary to make some assumptions about the unabsorbed spectrum of the object in question. In most of the sources, the correct underlying 8–13 μ emission is probably some sort of thermal dust continuum. We adopt the models described by Gillett *et al.* 1975*a*). These models postulate an underlying infrared source, with intervening cold dust absorbing significant radiation from 8–13 μ. The underlying source is either blackbody radiation (model I) or optically thin dust emission (model II). By assuming that the emitting and absorbing dust is similar to that found in emission in the Trapezium, we derive for both models the source temperature and maximum absorption optical depth (at 9.75 μ) in cold dust in the line of sight by χ^2 minimization (see Gillett *et al.* 1975*a* for a detailed discussion of the models).

Clearly, these are at best very simple approximations to the true physical conditions in these sources. However, such models do serve to estimate crudely the optical depth in cold silicate material in the line of sight. The hot-star underlying source is clearly a special case of Model I.

The best-fit values of T_{source} and $\tau_{9.75\,\mu}$, and the value of χ^2 per degree of freedom for the model fit are given in Table 1. Formal errors in the fitted parameters are difficult to assess, and are probably without much meaning, since the simplistic models probably make systematic errors much larger than any reasonable formal errors.

Unlike the H II regions studied by Gillett *et al.*, where model II fits were always better (i.e., smaller values of χ^2) than model I fits, in the case of these sources the model I fits were sometimes better, indicating that these sources are physically different from the H II regions. This result is not unexpected; the H II regions can be expected to produce optically thin emission, whereas some of these sources could very well be compact enough to be optically thick at 10 μ.

The best-fit models to the 8–13 μ spectra of some of the sources are shown in Figure 3; these fits show that the models reproduce the observed spectra quite well in most cases. Of particular interest is NGC 2264 IR, where the spectrum does not indicate a particularly pronounced absorption, but the observations can be fitted well with the parameters of the model I fit.

TABLE 1

PARAMETERS OF 8–13 μ SPECTRA FITS

Source	Number of Points Fitted	Model I T_{source}	Model I $\tau_{9.7\,\mu}^{abs}$	Model I χ^{2*}	Model II T_{source}	Model II $\tau_{9.7\,\mu}^{abs}$	Model II χ^{2*}
CRL 490	33	335	1.2	1.7	335	2.8	1.6
2264-IR	20	475	0.8	0.8	500	2.4	2.9
2024 No. 2†	4	10^4	1.7	3.8	...	...	...
H_2O 0610+18‡	32	270	3.7	1.8	325	5.6	1.4
BN§	67	470	1.7	2.5	480	3.3	1.0
CRL 2591	67	310	2.7	1.0	320	4.3	1.8

* χ^2 is per degree of freedom.

† Only model tried was $T_{source} = 10^4$ K (i.e., hot star), data from Grasdalen 1974.

‡ Results from Pipher and Soifer 1976.

§ Results from Gillett *et al.* 1975.

c) *Ice-to-Silicate Ratios in the Molecular Clouds*

The ice-to-silicate ratio is known to be extremely different (GJMS) for BN and VI Cyg No. 12 (a highly reddened star in Cygnus). Qualitatively the materials sampled in the two lines of sight are quite different, the former being predominantly molecular-cloud material, the latter being predominantly more tenuous "normal" interstellar material. How much variation exists within molecular-cloud material is important to the understanding of the process of ice formation in molecular clouds, and to the understanding of how abundant ices are in interstellar clouds.

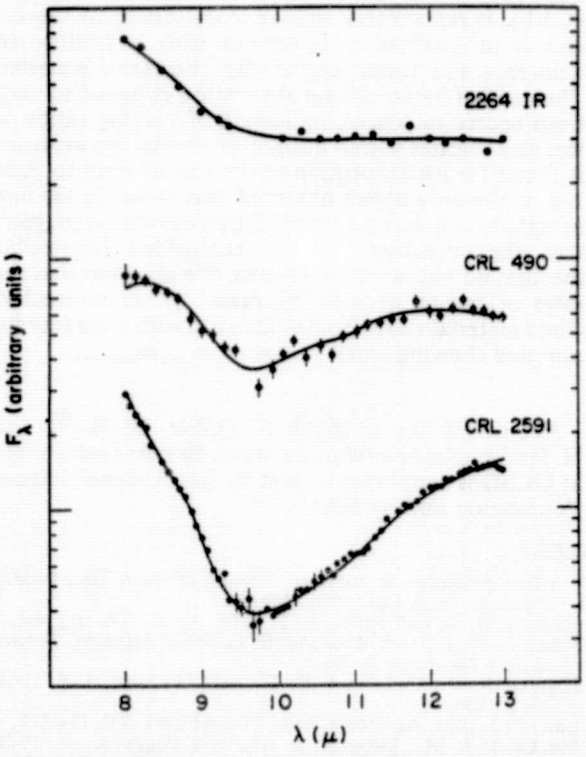

FIG. 3.—8–13 μ spectra of CRL 490, CRL 2591, and 2264 IR along with best model fits (*solid lines*) to these spectra. The models are described in the text, and the parameters of the best-fit lines are given in Table 1.

Inspection of Figure 1 shows that there is apparently a wide variation in the ratio of ice to silicate absorptions even within the infrared objects associated with molecular clouds. A measure of the ice-to-silicate ratio is given by the ratios of the optical depths at 3.08 μ and 9.75 μ. (For this to be a meaningful comparison it is necessary that the ices and silicates be occupying the same regions of space. The model fits to determine the silicate absorption optical depths implicitly assume this to be the case, since they determine the optical depths for cold silicates, i.e., that material absorbing at 10 μ. In any region where silicates emit significantly at 10 μ, ices should rapidly evaporate.) These data are compiled in Table 2, where we give the ice optical depths determined from Figure 1, and the optical depths at 9.75 μ from the model fits to the different sources. Ice-to-silicate ratios are shown for both model I and II fits to the 8–13 μ data. The ice/silicate ratio determined from the "best" estimate of $\tau_{9.7\,\mu}$ is noted.

There are several important points to notice about the results in Table 2. The range of $\tau_{ice}/\tau_{silicate}$ varies from 0.1 to 1.6 over the best-fit models. Unless these models substantially misrepresent the column densities of cold silicate materials to the sources, the ratio of ice to silicate absorptions appears highly variable. Further, there appears to be little or no correlation of this ratio with either ice or silicate optical depths. We conclude that there is no obvious correlation between the ratio of ices to silicates and any measure of the column density of particulate matter. If ices grow as mantles on core silicate grains, it is probable that the ratio of ice to silicate optical depths will be a function of the temperature and density history of the specific molecular cloud, and so it is not surprising that there are no apparent correlations from cloud to cloud.

d) *The Lack of Ice Absorption in NGC 2024 No. 1*

From the upper limit on the ice absorption in NGC 2024 No. 1 of $\tau_{ice} < 0.05$ (determined by fitting the "canonical" profile to the observed spectrum), we deduce, using Grasdalen's value of $A_v \approx 8.3$ mag that $A_v/\tau_{ice} > 165$ in the line of sight to this star. Models

TABLE 2

ICE/SILICATE RATIOS

Source	$\tau_{3.08\,\mu}$	$\tau_{9.7\,\mu}^{I}$	$\tau_{3.08\,\mu}/\tau_{9.7\,\mu}^{I}$	$\tau_{9.7\,\mu}^{II}$	$\tau_{3.08\,\mu}/\tau_{9.7\,\mu}^{II}$
CRL 490.....	0.27	1.2	0.2	*2.8*	*0.1*
2264-IR.....	1.29	*0.8*	*1.6*	2.4	0.5
2024 No. 2.....	1.22	1.7	0.7	...	...
H_2O 0610+18.....	0.9	3.7	0.2	*5.6*	*0.2*
BN.....	1.46	1.7	0.9	*3.3*	*0.4*
CRL 2591.....	0.71	*2.7*	*0.3*	4.3	0.2

NOTE.—Best-fit models are italicized.

of 2024 No. 2 suggest that it is extinguished by 30–50 mag of visual extinction (Grasdalen 1974; Hudson and Soifer 1976). The ratio of visual to ice extinction for 2024 No. 2 is then $A_v/\tau_{ice} \approx 22$–45. The discrepancy between this and the ratio for 2024 No. 1 is about a factor of 5.

While the lower limit to the ratio of A_v/τ_{ice} is greater for VI Cyg No. 12(500), the observations of 2024 No. 1 show that sharp gradients in A_v/τ_{ice} can exist over short distances in the interstellar medium. The two objects, 2024 No. 1 and No. 2, are physically very close, the major difference being that 2024 No. 2 is seen through a dense molecular cloud, while 2024 No. 1 is not. It must be that the conditions of this molecular cloud (cold, dense material, opaque to diffuse stellar radiation) favors the existence of ices, while the conditions of the more tenuous nearby interstellar medium do not. (However, simple molecular evaporation does not seem like a viable mechanism to inhibit ice growth: grain temperatures even in the interstellar medium are quite low, and should not prevent ice growth due to molecular evaporation).

e) The Fraction of Ice, Silicates by Volume

On the assumption that $\tau_{ice} = \tau_{sil}$ in the BN source, Greenberg (1973) derived a ratio of ices to silicates (by volume) of 0.21, and hence a mass ratio of ices to silicates of 1:10. The data presented in Table 2 allow us to conclude that within molecular-cloud material, this ratio varies over about an order of magnitude ($0.2 \leqslant \tau_{ice}/\tau_{sil} \leqslant 2$), so that the volume ratio of ices to silicates is $0.04 \leqslant v_{ice}/v_{sil} \leqslant 0.4$, with corresponding mass ratios of $0.02 \leqslant m_{ice}/m_{sil} \leqslant 0.2$. The majority of sources discussed here fall toward the low end of the τ_{ice}/τ_{sil} ratio, and so toward the low end of the v_{ice}/v_{sil} limits. Further, it must be emphasized that this applies to molecular-cloud material, i.e., material rich in ices. For material in the more tenuous interstellar medium, the contribution of ices to the particulate-matter component appears to be negligible.

V. CONCLUSIONS

Infrared spectrophotometry of a heterogeneous sample of infrared sources associated with molecular clouds has shown that ice and silicate absorption is quite common in these regions. The absorption feature at 3.1 μ is remarkably similar from source to source, and is in qualitative agreement with a mixture of ammonia and water ices in the absorbing material. The ratio of ice to silicate absorption is found to vary from source to source, indicative of varying ratios of ices and silicates within molecular clouds. No evidence is found for ice absorption in the line of sight to 2024 No. 1, the only object observed that is not in the line of sight to a molecular cloud. This observation suggests that the conditions of the unshielded interstellar medium do not favor ice growth. We also find that the ratio of ices to silicates (by mass) within molecular-cloud material varies from 0.02 to 0.2, with most sources sampled showing small values of $m_{ices}/m_{silicates}$.

We would like to thank F. Gillett, W. Stein, and H. Hudson for helpful discussions. Infrared astronomy at UCSD is supported in part by the National Science Foundation and by NASA.

REFERENCES

Allen, D. A. 1972, *Ap. J. (Letters)*, **172**, L55.
Bertie, J. E., Labbé, H. J., and Whalley, E. 1969, *J. Chem. Phys.*, **50**, 4501.
Brown, R. L. 1974, *Ap. J. (Letters)*, **194**, L9.
Gillett, F. C., and Forrest, W. J. 1973, *Ap. J.*, **179**, 483.
Gillett, F. C., Forrest, W. J., Merrill, K. M., Capps, R. W., and Soifer, B. T. 1975*a*, *Ap. J.*, **200**, 609.
Gillett, F. C., Jones, T. W., Merrill, K. M., and Stein, W. A. 1975*b*, *Astr. and Ap.*, **45**, 77 (GJMS).
Gilmore, W., Morris, M., Palmer, P., Zuckerman, B., and Turner, B. E. 1976, in preparation.
Grasdalen, G. 1974, *Ap. J.*, **193**, 373.
Greenberg, J. M. 1964, *Ann. Rev. Astr. and Ap.*, **1**, 267.
———. 1973, in *IAU Symposium No. 52, Interstellar Dust and Related Topics*, ed. J. M. Greenberg and H. C. van de Hulst (Boston: Reidel), p. 3.
Harvey, P. M., Campbell, M. F., and Hoffmann, W. F. 1975, paper presented at summer meeting of Astr. Soc. Pacific, Ensenada, Baja California, Mexico.
Hudson, H. S., and Soifer, B. T. 1976, *Ap. J.*, **206**, in press.
Johnson, M. L., and Mendoza, E. E. 1964, *Bol. Obs. Tonantzintla y Tacubaya*, **3**, 331.
Knacke, R. F., Cudaback, D. D., and Gaustad, J. E. 1969, *Ap. J.*, **158**, 151.
Low, F. J. 1973, Air Force Rept. No. AFCRL-TR-73-0371.
MacLeod, J. M., Doherty, L. H., and Higgs, L. A. 1975, preprint.
Merrill, K. M., and Soifer, B. T. 1974, *Ap. J. (Letters)*, **189**, L27.
Morris, M., Palmer, P., Turner, B. E., and Zuckerman, B. 1974, *Ap. J.*, **191**, 349.
Pipher, J. L., and Soifer, B. T. 1976, *Astr. and Ap.*, **46**, 153.
Robertson, C. W., Downing, H. D., Curnutte, B., and Williams, D. 1975, *Opt. Soc. Am.*, **65**, 432.

van de Hulst, H. C. 1973, in *IAU Symposium No. 52, Interstellar Dust and Related Topics*, ed. J. M. Greenberg and H. C. van de Hulst (Boston: Reidel), p. 569.
Walker, R. G., and Price, S. D. 1975, AFCRL Infrared Sky Survey, Vol. 1, Rept. No. AFCRL-TR-75-0373.
Wendker, H. J., and Baar, J. W. M. 1974, *Astr. and Ap.*, **33**, 157.
Woolf, N. J. 1973, in *IAU Symposium No. 52, Interstellar Dust and Related Topics*, ed. J. M. Greenberg and H. C. van de Hulst (Boston: Reidel), p. 485.

K. M. MERRILL: School of Physics and Astronomy, University of Minnesota, Minneapolis, MN 55455

R. W. RUSSELL and B. T. SOIFER: Department of Physics, C-011, University of California, San Diego, La Jolla, CA 92093

THE ASTROPHYSICAL JOURNAL, 208:L129–L132, 1976 September 15

16–25 MICRON SPECTROSCOPY OF THE TRAPEZIUM AND BN-KL SOURCE IN ORION

W. J. FORREST
Cornell University
AND
B. T. SOIFER
Department of Physics, University of California, San Diego
Received 1976 April 26; revised July 2

ABSTRACT

Spectrophotometric observations from 16 to 25 μ of the Trapezium and BN–KL object in Orion are reported. These observations were obtained with a newly developed liquid-helium–cooled grating spectrometer. The observations of the Trapezium show a relatively flat 16–25 μ spectrum, consistent with a 20 μ emission peak similar to that previously found at 10 μ. The BN–KL source has a smooth 16–25 μ spectrum, showing little absorption such as characterizes the 10 μ spectrum of this source. This lack of a deep 20 μ absorption is attributed to complex radiation transfer processes within the molecular cloud.

Subject headings: infrared: spectra — nebulae: Orion Nebula

I. INTRODUCTION

In recent years infrared spectroscopy has contributed greatly to our understanding of many types of bright infrared sources. Predominantly this spectroscopic work has been done in ground-based atmospheric windows at wavelengths less than 14 μ, primarily for technical reasons. In this paper we report spectroscopic observations from 16 to 25 μ of the Trapezium and KL nebulae in Orion, obtained with a liquid-helium–cooled grating spectrometer at the UCSD–U. Minnesota 1.52 m telescope of the Mount Lemmon Observatory. Previous ground-based 20 μ spectroscopy has been reported by Treffers and Cohen (1974).

Spectroscopic studies of the Trapezium (Gillett and Stein 1969) and Becklin-Neugebauer–Kleinmann-Low (BN–KL) (Gillett and Forrest 1973, hereafter GF) regions had previously shown the emission and absorption character of these specific regions. The spectroscopic observations have shown that the 8–13 μ emission of the Trapezium is reasonably well identified with thermal emission by warm silicate dust. The 8–13 μ spectrum of the BN–KL source can be explained (GF; Gillett *et al.* 1975) as emitted radiation from an underlying warm source absorbed by cold dust (similar in emissivity to the Trapezium dust) in the intervening line of sight. As silicates have a second resonance in the 20 μ region (Knacke and Thomson 1973), the present study of the 20 μ spectra of these objects was undertaken. In an accompanying *Letter* (Forrest, Houck, and Reed 1976, hereafter FHR), complementary observations from 16 to 40 μ are reported.

II. INSTRUMENTATION

The observations were obtained with a grating spectrometer built at UCSD for use in this wavelength range. The spectrometer is a standard Czerny-Turner optical design, with a 13.5 cm focal length, and using a diffraction grating blazed for first-order operation at 20 μ. Order separation is achieved by using a long-wavelength transmission ($\lambda > 15.5$ μ) interference filter, and wavelength scanning was done by rotating the grating. The spectrometer was operated at a resolution of $\lambda/\Delta\lambda \sim 75$ at 20 μ. The entire grating spectrometer was cooled to $\sim$5 K by mounting it on the work surface of a liquid-nitrogen–shielded liquid-helium Dewar. A Ge:Cu photoconductor built by F. C. Gillett was used as the detector.

III. OBSERVATIONS

Observations of the Trapezium were obtained in 1974 December, while those of BN–KL were obtained in 1974 December and 1975 January. Both objects were observed with the UCSD–U. Minnesota 1.5 m telescope of the Mount Lemmon Observatory. Standard dual-beam infrared observing techniques were employed; the two beams were separated by 25″ in declination, with a focal plane aperture of 17″. Data-taking procedures described in GF were employed.

Absolute and spectral calibration at 20 μ is difficult, because of the paucity of bright standards of accurately known flux. For this reason the procedures adopted to calibrate the spectroscopy were as follows. The flux of α Ori at 20 μ was assumed to be that reported by Morrison and Simon (1973); from the ratio of signals for α Ori and the lunar limb, the brightness temperature of the Moon at 20 μ was determined using the measured beam size of the spectrometer. The lunar spectrum was then assumed to be blackbody emission at the temperature determined by the above procedure. While this procedure makes the absolute flux levels quite sensitive to errors in the assumed flux level of α Ori, the lunar

spectral shape is relatively insensitive to the exact temperature, so that the spectral shapes determined for unknown sources using this calibration procedure should be relatively free from systematic errors.

The major obstacle to spectroscopic observations in the 20 μ atmospheric window is the significant absorption by atmospheric water vapor (see, e.g., Farmer and Key 1965). To illustrate the problem, Figure 1 shows the raw spectrum of the Moon taken through ~1–2 mm precipitable water. It was found that the depressions in the spectrum indicated on the figure could be identified with corresponding features in the spectra of Farmer and Key of the Earth's atmosphere which are presumably due to terrestrial water vapor. The wavelengths of these lines, taken from Farmer and Key, provided the final wavelength calibration of the spectrometer. In addition, terrestrial CO_2 made observations shortward of $\lambda \approx 16$ μ difficult.

To account properly for this atmospheric opacity, frequent calibration spectra were obtained of the lunar limb. From the lunar observations at different air masses, an effective atmospheric extinction coefficient at each wavelength in the spectrum was determined, and the observations of the Trapezium and the KL nebula were corrected for extinction by using the derived coefficients. If any narrow spectral feature coincides with a terrestrial absorption line, it will not appear in the derived spectrum if the Earth's atmosphere is optically thick at the wavelength in question.

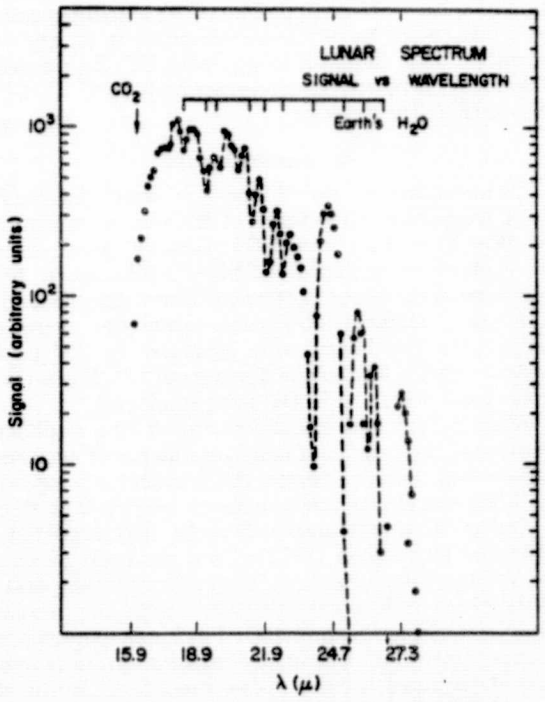

FIG. 1.—The lunar signal plotted versus wavelength from 16 to 27 μ. Some of the strong terrestrial water vapor features are noted in the figure.

IV. THE DATA

The spectra of the Trapezium and the KL nebula are shown in Figures 2 and 3, along with 8–13 μ spectra of these objects. The 8–13 μ spectrum of the Trapezium is taken from Forrest, Gillett, and Stein (1975), while that of KL is from GF.

The 8–13 μ spectrum of the Trapezium was obtained with 22″ apertures, so that a correction for the different apertures is necessary. In the case of the Trapezium, the 10 μ spectrum was reduced by a factor 0.65 which was the ratio of the present 16–20 μ flux to an earlier measurement made at Mount Lemmon with an 18 μ broad-band filter and 22″ focal plane aperture. This is only slightly larger than the ratio of beam size (~0.60), indicating the diffuse nature of this source.

In the case of the KL nebula, the spatial structure is very complex, and cannot be easily accounted for by scaling spectra taken with different apertures. We have included (in Fig. 3) 10 μ spectra of the regions obtained with 11″ and 22″ apertures (GF). We also include a curve corresponding to a blackbody at 86 K filling the 17″ aperture.

V. DISCUSSION

a) Trapezium

The 16–25 μ spectrum of the Trapezium (Fig. 2) shows a smooth continuum with no narrow features evident. The large statistical errors at $\lambda \sim 16$ μ and $\lambda > 22$ μ are due primarily to the attenuation of the flux by the Earth's atmosphere (cf. Fig. 1). The observed spectrum is narrower than a blackbody and indicates a dust emissivity which peaks at ~18–19 μ in this bandpass. This is in qualitative agreement with emission from small silicate grains. In the accompanying *Letter* (FHR) the observed spectrum is compared with a simple silicate emission model.

b) BN-KL

The 16–25 μ BN-KL spectrum (Fig. 2) also shows a smooth continuum with no narrow features. There is no evidence for a deep absorption feature analogous to the very strong 10 μ feature found by GF. There is a suggestion of a shallow absorption feature around 18–19 μ in that the spectrum has opposite curvature (though slight) to a blackbody fit to the data. In addition, the spectrum from 19 μ to 24 μ rises (slightly) faster than an 86 K blackbody (which is the brightness temperature at 24 μ); thus either the dust emissivity increases from 19 μ to 24 μ or absorption is occurring at 19 μ.

The spectrum from 16 to 25 μ has a brightness temperature of ~85–86 K. The point sources in BN-KL (Rieke, Low, and Kleinmann 1973) contribute less than 25 percent of the flux in the measuring aperture at 21 μ; therefore the dust temperature in the extended component of BN-KL must be greater than or equal to the brightness temperature. This temperature is very nearly equal to the peak 2.6 mm CO brightness temperature of 75 ± 7 K found by Liszt *et al.* (1974)

using a 1′ beam. The simplest explanation for these facts is that this dust is optically thick at 20 μ and that $T_{dust} \sim T_{gas} \sim 80$ K. From Figure 3 it is seen that dust at ~80 K would contribute negligible flux to the 10 μ spectrum; therefore, it is consistent that the same dust which is responsible for the deep 10 μ absorption found by GF can provide most of the radiation observed in the 20 μ region. The weak residual 20 μ depression could be a radiation transfer effect; at 17 and 24 μ, where the dust optical depth is less, we see deeper into the cloud and find a slightly higher brightness temperature. The lack of a deep 20 μ absorption feature in the presence of a strong 10 μ absorption is in agreement with the predictions of Kwan and Scoville (1975). The broad-band 20 μ observations of Simon and Dyck (1975) also showed a relatively small 20 μ absorption in two other sources with large 10 μ absorptions.

It is concluded that the 20 μ spectrum of BN-KL must be understood as the result of radiation transfer within a complicated source (Kwan and Scoville 1975; Merrill and Jones 1976); it cannot be easily inverted to give the strength and shape of the 20 μ silicate feature. If, as seems likely, silicates are a dominant form of interstellar dust, this is an important observational problem, since the temperature balance of many molecular clouds seems to be determined by transfer of the infrared radiation.

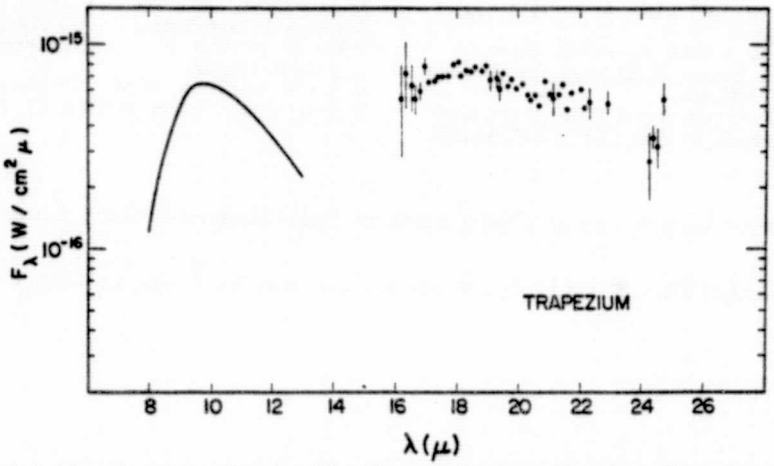

FIG. 2.—The spectrum of the Trapezium region from 8 to 25 μ. The solid line represents the 8–13 μ spectrum of the Trapezium (from Forrest *et al.* 1975) normalized in flux to the 17″ aperture used for the 16–25 μ observations (see text).

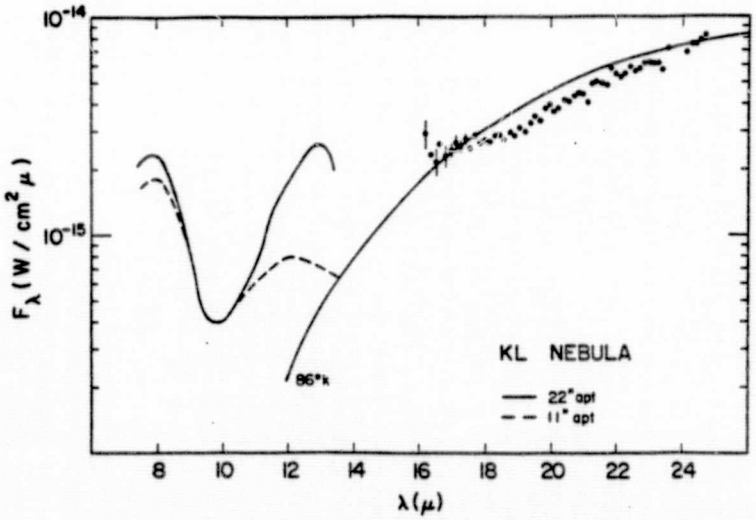

FIG. 3.—The spectrum of the BN-KL source from 7.5 to 25 μ. The 16–25 μ data was obtained with a 17″ aperture. The dashed and solid lines from 7.5 to 13.5 μ are data from GF obtained with 11″ and 22″ apertures, respectively. The solid line from 12 to 25 μ represents the flux emitted by an 86 K blackbody filling a 17″ aperture.

VI. CONCLUSIONS

1. The Trapezium region shows a second emission feature peaking at approximately 18–19 μ; this tends to confirm the identification of silicates as a major component of the dust in this region.

2. BN–KL shows only a weak 20 μ absorption feature ($\sim$1.5 K in brightness temperature or $\sim$30 percent in flux at 19 μ). The dust which was primarily absorbing at 10 μ can efficiently radiate at 20 μ; the resulting 20 μ spectrum must be understood as the result of radiation transfer in this dense cloud.

We would like to thank P. Brissenden for his assistance in building the grating-spectrometer. This research has been supported by the National Science Foundation and by NASA grant NGL 05-009-230.

REFERENCES

Farmer, C. B., and Key, P. L. 1965, *Appl. Optics*, **4**, 1051.
Forrest, W. J., Gillett, F. C., and Stein, W. A. 1975, *Ap. J.*, **192**, 351.
Forrest, W. J., Houck, J. R., and Reed, R. A. 1976. *Ap. J.* (*Letters*), **208**, L133 (FHR).
Gillett, F. C., and Forrest, W. J. 1973, *Ap. J.*, **179**, 483 (GF).
Gillett, F. C., Forrest, W. J., Merrill, K. M., Capps, R. W., and Soifer, B. T. 1975, *Ap. J.*, **200**, 609.
Gillett, F. C., and Stein, W. A. 1969, *Ap. J.* (*Letters*), **155**, L197.
Knacke, R. F., and Thomson, R. K. 1973, *Pub. A.S.P.*, **85**, 341.
Kwan, J., and Scoville, N. Z. 1975, preprint.
Liszt, H. S., Wilson, R. W., Penzias, A. A., Jefferts, K. B., Wannier, P. G., and Solomon, P. 1974, *Ap. J.*, **190**, 557.
Merrill, K. M., and Jones, T. W. 1976, in preparation.
Morrison, D., and Simon, T. 1973, *Ap. J.*, **186**, 193.
Rieke, G. H., Low, F. J., and Kleinmann, D. E. 1973, *Ap. J.* (*Letters*), **186**, L7.
Simon, T., and Dyck, H. M. 1975, *Nature*, **253**, 101.
Treffers, R., and Cohen, M. 1974, *Ap. J.*, **188**, 545.

W. J. FORREST: Center for Radiophysics and Space Research, Space Sciences Building, Cornell University, Ithaca, NY 14853

B. T. SOIFER: Department of Physics, C-011, University of California, San Diego, La Jolla, CA 92093

ICARUS 30, 282–285 (1977)

Observations of Jupiter and Saturn at 5–8 μm

R. W. RUSSELL AND B. T. SOIFER

Department of Physics, University of California, San Diego, La Jolla, California 92093

Received March 18, 1976; revised April 28, 1976

Moderate-resolution spectrophotometry ($\Delta\lambda/\lambda \sim 0.015$) has shown the effects of known atmospheric constituents (NH_3, CH_4, C_2H_6) on the 5–8 μm spectrum of Jupiter. Broadband observations of Saturn at 6.5 μm are also reported.

INTRODUCTION

Infrared spectroscopy of the Jovian planets has proved to be a powerful means of investigating the structure of the planetary atmospheres for both temperature structure and atmospheric constituents. In this paper we report spectrophotometric observations of Jupiter from 5 to 8 μm and photometric observations of Saturn at 6.5 μm ($\Delta\lambda = 3$ μm). This wavelength range, not available for ground-based observations because of strong water-vapor absorption, is accessible using the 91 cm telescope of the Kuiper Airborne Observatory (KAO).

OBSERVATIONS

The observations of Jupiter and Saturn from 5 to 8 μm were made using the KAO flying at an altitude of ~41,000 ft. The telescope system is described by Cameron *et al.* (1971). The 5–8 μm spectrophotometer is described by Russell *et al.* (1975). The spectrometer has a resolution of $\Delta\lambda/\lambda \sim 0.015$. The data-taking procedure is similar to that described by Gillett and Forrest (1973). A given wavelength is determined by positioning the cooled circular variable filter, and data are taken with the object in the signal and reference beam of the photometer until sufficient signal-to-noise is obtained; then the filter is rotated to a new wavelength.

On the KAO, the system is controlled by the onboard computer (ADAMS), which collects the data, rotates the filter wheel, and displays the results while data are being obtained. This results in maximum use of observing time.

The observations of Jupiter were obtained on a flight on 2/3 October 75, while those of Saturn were obtained on a flight on 8/9 October 75. The calibration objects were α Tau (for Saturn) and Mars (for Jupiter). The spectrum of α Tau was assumed to be that of a hot blackbody, except for a depression of ~20% at ~5μm. Mars, the primary calibrator for the Jupiter spectrum, was assumed to have a blackbody spectrum of 245°K from 5 to 8 μm. The deviations from this latter assumption are not more than 20% and do not significantly affect the reduction, since the Jovian spectrum shows intensity variations of greater than a factor of 20.

The 5–8 μm spectrum of Jupiter is displayed in Fig. 1. This spectrum was obtained with a 15 arcsec aperture centered on the planetary disk. There is some overlap in the wavelength coverage between this spectrum and that previously reported by Gillett, Low, and Stein (1968; hereafter GLS). The sharp decrease in surface brightness from 5 to 5.5 μm was reported by GLS, as was the high-intensity level

FIG. 1. The 5- to illustrate the over which seve tribute significa

between 7.5 and of this spectrum a in intensity to ~ crease beyond 6.3 be understood as molecular constitu sphere at various

Broadband obse ($\Delta\lambda = 0.7$ μm), . ($\Delta\lambda = 3$ μm), an with a 30 arcsec a a 10-min leg of th are shown in Fig analysis is not wa

ISSN 0019-1035

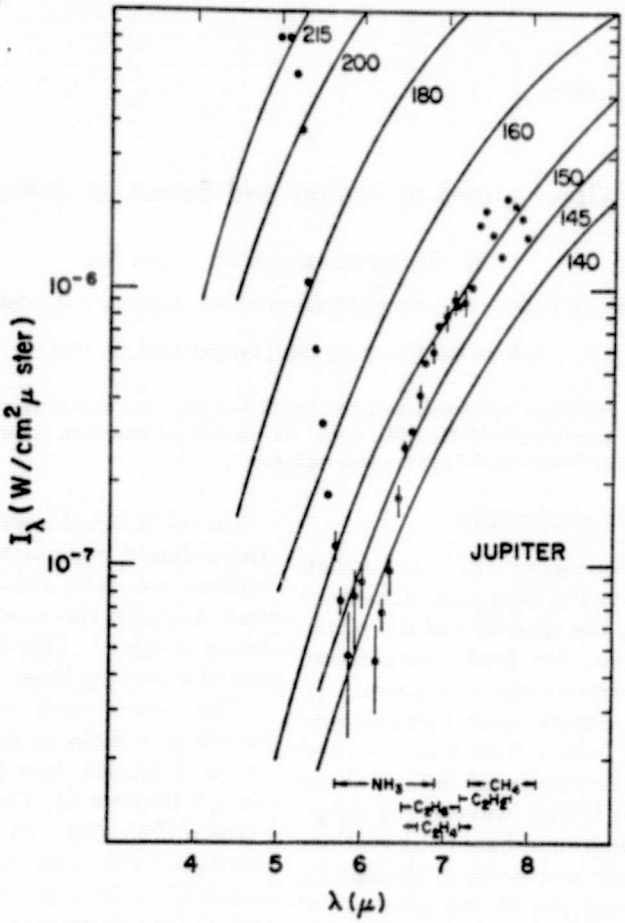

FIG. 1. The 5–8 μm spectrum of Jupiter. Blackbody curves at different temperatures are drawn to illustrate the brightness temperature variation in the Jovian spectrum. The wavelength ranges over which several molecules (known or believed to be present in the atmosphere) could contribute significant opacity are shown.

between 7.5 and 8 μm. The new features of this spectrum are the continued decrease in intensity to ~6 μm, then a rapid increase beyond 6.3 μm. These features can be understood as due to the opacity of the molecular constituents of the Jovian atmosphere at various levels.

Broadband observations of Saturn at 2.3 ($\Delta\lambda$ = 0.7 μm), 3.2 ($\Delta\lambda$ = 0.5 μm), 6.5 ($\Delta\lambda$ = 3 μm), and 8.5 μm ($\Delta\lambda$ = 1 μm) with a 30 arcsec aperture were obtained on a 10-min leg of the 8/9 October flight and are shown in Fig. 2. Although detailed analysis is not warranted, the broadband observation at 6.5 μm ($\Delta\lambda$ = 3 μm) is sufficiently interesting that it merits some discussion.

DISCUSSION

Jupiter

The 5–8 μm spectrum of Jupiter can be explained by a combination of atmospheric constituents already known to be present and those expected in the Jovian atmosphere. The high brightness temperature for $\lambda < 5.2$ μm has previously been observed by GLS and was interpreted by them as due to the transparency of the major atmo-

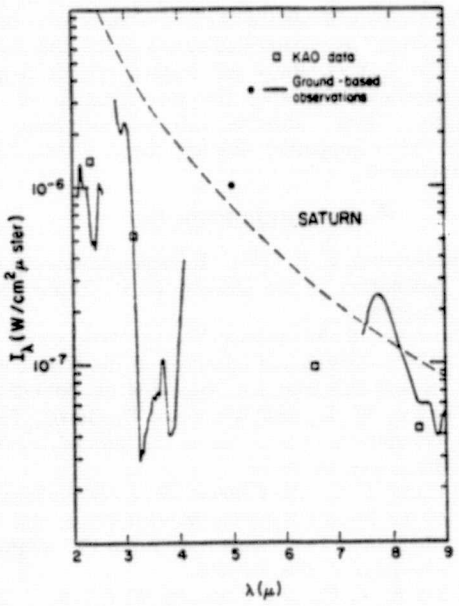

FIG. 2. Broadband and spectral intensity observations of Saturn. The open squares represent broadband data obtained on the KAO on 8/9 October 75, with a 30 arcsec aperture. Specific intensities were calculated from the observed fluxes using the solid angle of Saturn (disk plus rings) subtended by the observing aperture. The dashed curve represents the intensity of a perfect diffuse reflector at the distance of Saturn. The solid lines are ground-based observations of the disk from 2 to 4 μm (Russell and Puetter, November 1975, unpublished) and from 7.5 to 9 μm (Gillett and Forrest, 1974). The filled circle represents the 5 μm point from Rieke (1975).

spheric constituents, allowing radiation from deep in the atmosphere to escape. Additional support for this interpretation was given by Westphal (1969) and Keay *et al.* (1973), who showed that the high 5 μm brightness temperatures were localized to the equatorial zone, and could be explained as possible holes in the visible cloud layer.

Beyond 5.2 μm the sharp decrease in surface brightness was attributed by GLS to absorption by gaseous NH_3. For $\lambda > 5.3$ μm the observed flux falls below that for a perfect diffuse reflector at the distance of Jupiter; it is possible that scattered sunlight is responsible for some of the observed flux. This is particularly true at ~ 6 μm, where an effective albedo of ~ 0.02 would account for the observed flux.

If the observed flux at ~ 6 μm is, instead, thermal emission, then the brightness temperature observed at 6.2 μm would be explained as due to opacity of NH_3 deeper in the Jovian atmosphere than that produring the stronger 10 μm ammonia band (France and Williams, 1966).

We have noted in Fig. 1 the wavelength range over which NH_3 should be a dominant source of atmospheric opacity. The brightness temperature of Jupiter shows a sharp increase for $\lambda > 6.3$ μm, indicative of some source of emission above the thermal inversion layer in this wavelength range.

GLS showed that CH_4 emission in a temperature inversion in the upper Jovian atmosphere dominated the emission for $\lambda > 7.5$ μm, producing a peak intensity at $\lambda \sim 7.7$ μm that is observed in this spectrum. While methane does not have significant opacity for $\lambda < 7.3$ μm, several molecules related to methane could provide the needed opacity. Ethane (C_2H_6), acetylene (C_2H_2), and ethylene (C_2H_4) should all be present as photolysis products of methane in the upper Jovian atmosphere (Strobel, 1973). These molecules all have relatively strong bands between 6.5 and 7.8 μm and should be at the same level in the atmosphere as methane. Ridgeway (1974) has identified the presence of ethane and acetylene in the Jovian spectrum from high-resolution spectra for $\lambda > 11.7$ μm. Ethane appears to be responsible for a large portion of the observed intensity, since the sharp rise in intensity at 6.5 μm corresponds to the short-wavelength edge of the ethane band. This is qualitatively in accord with the relative strengths of the 6.8 and 12 μm ethane bands.

Quantitatively, the observed fluxes from the 6.8 and 12 μm bands are consistent with emission from C_2H_6 at 150–155°K. The 12 μm band is optically thin, since the brightness temperature is about 135°K (Ridgeway, 1974) and the 6.8 μm band is

becoming opti
data of Thornd
6.8 μm band is
than the 12 μ
depth of ~ 1 in
with the obser
if the temperat
about 155°K.

It is probable
also provide son
and could cont
from 6.7 to 7.5 μ
change of slope
indication of em

Beyond 7.4 μn
viously seen fr
tions by GLS. T
thick if the CH_4 c
in the atmosph
temperatures of

Saturn

The broadban
Saturn are show
ground-based obs
groups. The bro
converted to inte
intensity over t
Saturn (disk plus
30 arcsec observi
spectral data (R
published) are for
well with previous
Armstrong (1971)
observation is fro
7.5–9 μm data are
(1974), and again
Most, if not all,
flux can be account
5 and 7.5–8 μm d
disk. This suggests
ness temperature of
5.5 to 7.5 μm is quit
spectrophotometry
would be quite usef

becoming optically thick in this layer. The data of Thorndike (1947) indicates that the 6.8 μm band is about three times stronger than the 12 μm band, so that an optical depth of ~1 in the 6.8 μm band is consistent with the observed strengths of both bands if the temperature of the emitting layers is about 155°K.

It is probable that ethylene and acetylene also provide some opacity at the same level and could contribute to the observed flux from 6.7 to 7.5 μm. In particular, the slight change of slope near 6.7 μm may be an indication of emission from ethylene.

Beyond 7.4 μm we see the CH_4 band previously seen from ground-based observations by GLS. This band must be optically thick if the CH_4 emission is at the same level in the atmosphere as the C_2H_6 (i.e., at temperatures of 150–155°K).

Saturn

The broadband KAO observations of Saturn are shown in Fig. 2, along with ground-based observations by several other groups. The broadband KAO fluxes were converted to intensities assuming uniform intensity over the entire solid angle of Saturn (disk plus rings) subtended by the 30 arcsec observing aperture. The 2–4 μm spectral data (Russell and Puetter, unpublished) are for the disk alone and agree well with previous observations reported by Armstrong (1971). The 5 μm broadband observation is from Rieke (1975), and the 7.5–9 μm data are from Gillett and Forrest (1974), and again refer to the disk alone. Most, if not all, of the observed 5–8 μm flux can be accounted for by integrating the 5 and 7.5–8 μm data over the planetary disk. This suggests that the actual brightness temperature of the planetary disk from 5.5 to 7.5 μm is quite low. Higher-resolution spectrophotometry in this wavelength range would be quite useful.

ACKNOWLEDGMENTS

We thank R. Cameron, C. Gillespie, and the entire staff of the KAO for their invaluable assistance in obtaining these observations. The programming efforts of T. Mathieson and D. Wilson were far above and beyond the call of duty. We thank F. Gillett for a critical reading of a draft of this manuscript and G. Rieke for making several helpful suggestions regarding the interpretation of the Saturn data. Airborne infrared astronomy at UCSD is supported through NASA Grant NGR 05-005-055.

REFERENCES

Armstrong, K. R. (1971). Infrared photometry and radiometry of the planets. Ph.D. Thesis, Rice University.

Cameron, R. M., Bader, M., and Mobley, R. E. (1971). Design and operation of the NASA 91.5 cm airborne telescope. *Appl. Opt.* **10**, 2011–2015.

France, W. L., and Williams, D. (1966). Total absorptance of ammonia in the infrared. *J. Opt. Soc. Amer.* **56**, 70–71.

Gillett, F. C., and Forrest, W. J. (1973). Spectra of the Becklin-Neugebauer point source and the Kleinmann-Low nebula from 7.5 to 13.5 microns. *Astrophys. J.* **179**, 483–493.

Gillett, F. C., and Forrest, W. J. (1974). The 7.5–13.5 μ spectrum of Saturn. *Astrophys. J.* **187**, L37–L39.

Gillett, F. C., Low, F. J., and Stein, W. A. (1968). The 2.8–14 micron spectrum of Jupiter. *Astrophys. J.* **157**, 925–934.

Keay, C. S. L., Low, F. J., Rieke, G. H., and Minton, R. B. (1973). High resolution maps of Jupiter at 5 microns. *Astrophys. J.* **183**, 1063–1074.

Ridgeway, S. T. (1974). Jupiter: Identification of ethane and acetylene. *Astrophys. J.* **187**, L41–L43.

Rieke, G. H. (1975). The thermal radiation of Saturn and its rings. *Icarus* **26**, 37–44.

Russell, R. W., Soifer, B. T., and Forrest, W. J. (1975). Spectrophotometric observations of μ Cephei and the Moon from 4 μ to 8 μ. *Astrophys. J.* **198**, L41–L43.

Strobel, D. F. (1973). The photochemistry of hydrocarbons in the Jovian atmosphere. *J. Atmos. Sci.* **30**, 489–498.

Thorndike, A. M. (1947). The experimental determination of the intensities of infrared absorption bands. III. Carbon dioxide, methane, and ethane. *J. Chem. Phys.* **15**, 868–874.

Westphal, J. A. (1969). Observations of localized 5 micron radiation from Jupiter. *Astrophys. J.* **157**, L63–L64.

REPRINT

SPECTRA OF LATE-TYPE STARS FROM 4–8μ

RICHARD C. PUETTER, RAY W. RUSSELL, KRISTEN SELLGREN, AND BARUCH T. SOIFER

Reprinted from the *Publications of the Astronomical Society of the Pacific*
(Vol. 89, No. 529, June 1977)

PUBLICATIONS OF THE ASTRONOMICAL SOCIETY OF THE PACIFIC
89:320–322, June 1977

SPECTRA OF LATE-TYPE STARS FROM 4–8μ

RICHARD C. PUETTER, RAY W. RUSSELL, KRISTEN SELLGREN,* AND BARUCH T. SOIFER
Department of Physics, University of California, San Diego

Received 1977 January 10

The 4–8μ spectra ($\Delta\lambda/\lambda \simeq 0.015$) of three late-type stars, obtained in October 1975 from the Kuiper Airborne Observatory, are reported. These spectra exhibit mainly stellar photospheric blackbody emission in the case of the M stars and thermal circumstellar dust emission in the C star. The only signficant feature seen in this region is that attributed to CO from ~4.5μ to 5.2μ. This feature is observed in both types of stars.

Key words: late-type stars—infrared spectra

Introduction

Infrared wavelengths have become an extremely useful region to study the photospheres of late-type stars because the molecular constituents have strong infrared vibration-rotation bands and these stars emit the majority of their energy at infrared wavelengths. Additionally, many late-type stars are ejecting material in the form of gas and dust, and the ejected dust effectively converts stellar luminosity into infrared radiation.

In this paper we report 4–8μ spectroscopy, with a resolution $\Delta\lambda/\lambda \sim 0.015$, of the late-type stars α Orionis, R Cassiopeiae, and V Cygni obtained on three flights of the Kuiper Airborne Observatory (KAO) in October 1975. The 4–8μ portion of the spectrum is useful for analyzing the molecular constituents of the stellar atmospheres and studying the infrared properties of the circumstellar dust associated with these stars. Because of very strong telluric water vapor absorption, observations in this wavelength region are possible only from aircraft altitudes or above. The observations reported here were obtained using the 0.9-m telescope of the KAO flying at 13 km.

The Observations

The observations were obtained in October 1975 using a circular variable filter wheel spectrophotometer at the bent Cassegrain focus of the KAO. The filter wheel has a spectral resolution $\Delta\lambda/\lambda \sim 0.015$ and spans the range 4.1–8.0μ; however, due to strong telluric CO_2 absorption centered at 4.3μ observations were made only from 4.5–8μ. Data were obtained using the chopping secondary of the telescope for standard infrared beam switching. After synchronous detection of the infrared signal, the signal was sampled by the onboard computer for further processing and recording. The spectrum was obtained by selecting a position on the filter wheel and integrating for a specified length of time, then moving to a new position. The data taking was entirely controlled by the onboard computer system (under interactive control by the observers).

The instrumental response was determined by observing a bright star, α Tauri, on each flight. The spectrum of this star was assumed to be a blackbody of temperature 3800° K except for a 15% depression at ~4.5–5.2μ due to CO absorption in the stellar atmosphere. The strength of this absorption was determined from ground-based photometry in the 5μ atmospheric window (Forrest 1974). Besides the narrow-band spectra from 4.5–8μ, photometry of these stars at 2.3μ, 3.2μ, and 8.5μ was obtained to allow comparison with ground-based observations.

The 2–13μ spectra of the stars are shown in Figure 1. The 2–4μ spectra of R Cas and V Cyg were obtained at the UCSD-University of Minnesota 1.5-m telescope on Mount Lemmon in November 1975, while the 8–13μ spectra (also obtained at Mount Lemmon) were taken from Forrest (1974) and Merrill (1976) and normalized to the 8.0μ flux level observed on the KAO. The 2–4μ and 8–13μ spectra of α Ori were taken from Merrill (1976). The only prominent feature in the 4–8μ portion of the spectra of these stars is the depression from 4.5–5μ present in the spectra of all three stars, and identified as absorption by CO in the stellar atmosphere. Although no other departures from blackbody spectra have sufficient statistical significance to be positively identified in these spectra, molecular features between 7μ and 8μ could explain the complicated shape of the spectra in this region.

Discussion

All of these stars have infrared excesses, indicative of mass loss in the late stage of stellar evolution. Alpha Ori is classified as M1–M2 Ia–Ib, while R Cas and V Cyg are both Mira variables, R Cas being classified as M6e–M8e and V Cyg classified as C7,4e. Since R Cas and α Ori are both oxygen-rich stars, while V Cyg is

*Current address: Department of Physics, California Institute of Technology, Pasadena, CA 91125.

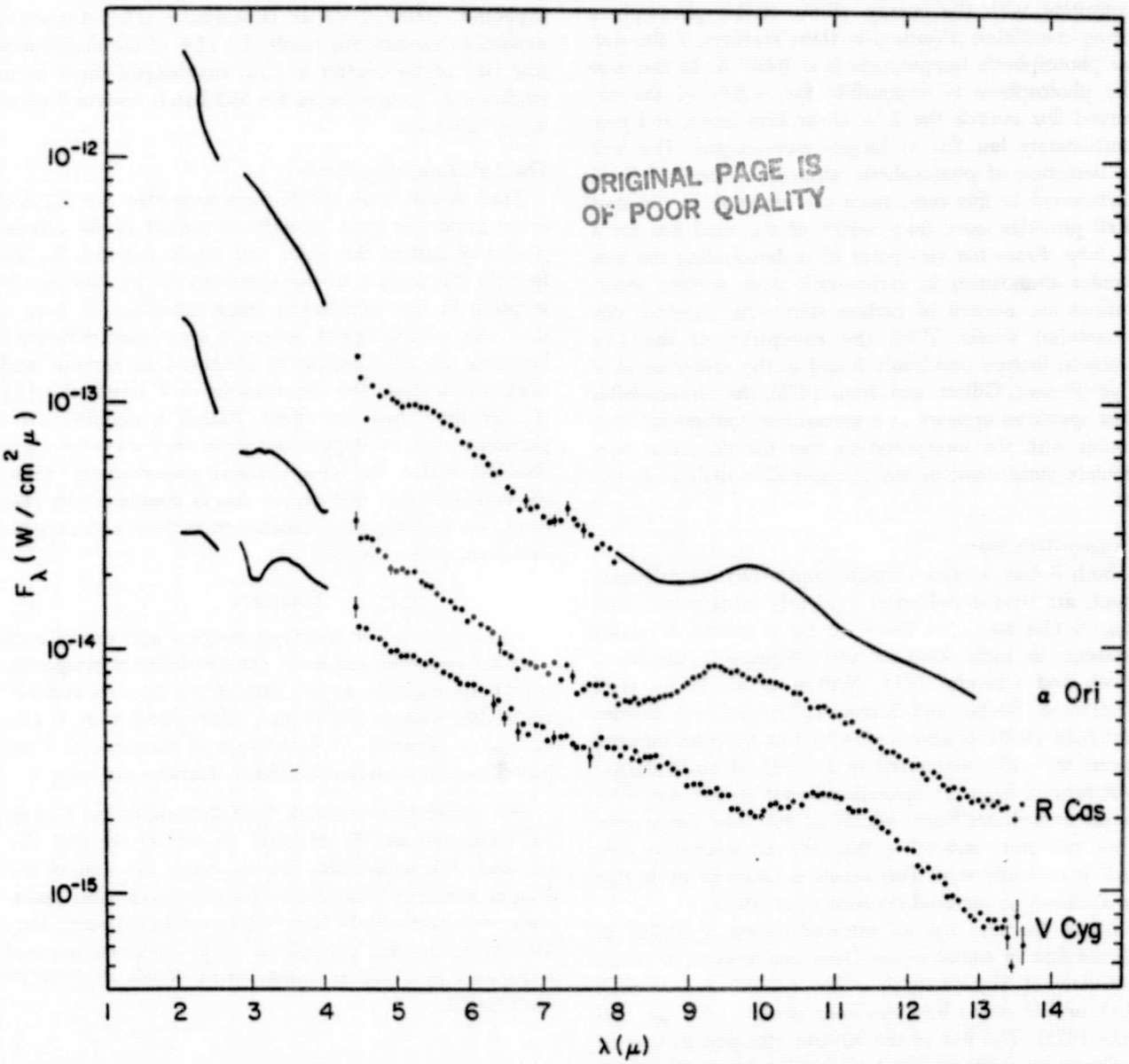

FIG. 1—The 2—13μ spectra of α Ori, R Cas, and V Cyg plotted versus wavelength. The 2–4μ ($\Delta\lambda/\lambda \simeq 0.02$) and 8–13μ ($\Delta\lambda/\lambda \simeq 0.015$) portions are ground-based data. The 4–8μ portions are the new KAO data ($\Delta\lambda/\lambda \approx 0.015$). Error bars are shown if statistical fluctuations exceed 5% of the measured flux.

carbon rich, the two classes of stars will be discussed separately.

V Cygni

The 2–4μ spectra of carbon stars have been discussed most recently by Merrill and Stein (1976) and this portion of the V Cyg spectrum will be mentioned here only briefly. The depression at 2.3μ is well identified as the first overtone band of CO in the stellar atmosphere (McCammon, Münch, and Neugebauer 1967). The origin of the deep absorption at 3.05μ and the shallow depression at 3.9μ have been discussed by Merrill and Stein (1976). At the spectral resolution of this observation, several plausible molecular species could be responsible for the absorptions. The 5μ absorption is probably dominated by CO absorption in the fundamental vibration-rotation band.

Forrest (1974) has analyzed the broad-band energy distribution of V Cyg and found that it could be fit if 80% of the energy emitted by the star were absorbed and reemitted by the circumstellar dust shell. The apparent weakness of the photospheric molecular absorption bands is readily explained by this model. The apparent depth of the 3.1μ and 5μ absorptions are

consistent with the energy of the stellar photosphere being completely absorbed in these features, if the stellar photospheric temperature is $\lesssim 2000°$ K. In this case the photosphere is responsible for ~20% of the observed flux outside the 3.1μ absorption band, and proportionately less flux at longer wavelengths. The lack of detection of photospheric absorptions beyond 5μ is understood in this case, since the emission in the dust shell provides more than ~90% of the total flux for $\lambda > 5.5\mu$. From the viewpoint of understanding the molecular abundances in carbon-rich stars, further observations are needed of carbon stars with minimal circumstellar shells. With the exception of the 11μ emission feature previously found in the spectrum of V Cyg (Forrest, Gillett, and Stein 1975), the circumstellar dust spectrum appears as a featureless continuum, consistent with the interpretation that the dominant particulate constituent of the circumstellar shell is graphite.

Oxygen-Rich Stars

Both R Cas, a Mira variable, and α Ori, an M supergiant, are oxygen-rich stars evidently undergoing mass loss. R Cas has been found to be a source of maser emission in radio lines of OH (Nguyen-Quang-Riew, Fillet, and Gheudin 1971; Wilson et al. 1972). H_2O (Dickinson, Bechis, and Barrett 1973), and SiO (Snyder and Buhl 1975). It also is observed to have an infrared excess at ~10μ, attributed to a cloud of circumstellar dust formed from the ejected material of this star. This excess contributes only ~2.5% of the total luminosity from this star, indicating that the circumstellar dust shell is optically thin. This excess is believed to be due to silicate-type material (Forrest et al. 1975).

Alpha Ori also has an infrared excess identified as silicate dust in emission (see Dyck and Simon (1975) for a review of observations), while no emission in SiO, H_2O, or OH maser lines has been detected (Snyder and Buhl 1975). The flux in the silicate emission feature of α Ori is $< 0.3\%$ of the total stellar luminosity from this star.

In both cases the 4–8μ spectrum is clearly dominated by stellar photospheric flux, although in the case of R Cas there is a suggestion of an excess at $\lambda > 7\mu$. Both spectra show the 5μ depression of CO, and no other obvious features. The 2.3μ and 5μ CO bands appear to be of comparable strength in the spectrum of α Ori, while the 5μ band in R Cas is much weaker than the 2.3μ band.

A puzzling aspect of the 4–8μ spectrum of R Cas is the absence of any evidence of water vapor opacity, which one might expect on the basis of the water vapor absorption seen from 2.5–3.3μ. Since the opacity of hot water vapor is comparable at 2.8μ and 7–8μ, some depression in the photosphere spectrum might be expected. Detailed stellar atmosphere calculations are needed to explain this result. To 15% of the continuum (the size of the scatter at this wavelength) there is no evidence of absorption in the SiO bands around 7.8μ in either spectrum.

The 5μ Absorption Band

Treffers and Gilra (1975) have suggested that C_3 and other molecules may be quite abundant in the atmospheres of carbon-rich stars, and might considerably affect the 5μ portion of the spectrum (C_3 has strong absorption in the wavelength range 4.9–5.9μ). In such a case one would expect to see a significant difference between the 5μ absorptions observed in carbon- and oxygen-rich stars. The observations of V Cyg and α Ori do not show such an effect. Rather a detailed comparison of the 5μ depressions show that they are identical to within the observational uncertainties. Thus, we conclude that this depresssion is dominated by features due to molecules common to carbon- and oxygen-rich stars, primarily CO.

Summary

Spectra (4–8μ) of late-type oxygen- and carbon-rich stars are reported and show mainly stellar photospheric blackbody emission in the case of the M stars and circumstellar dust in the C star. Absorption from ~4.5μ to 5.2μ is observed in both types of stars and is attributed to CO; no other significant features are seen.

We would like to thank Paul Brissenden for technical assistance and K. Michael Merrill for helpful discussions. We would also like to thank the staff of the Kuiper Airborne Observatory for their invaluable assistance, and particularly Don Wilson of Informatics, Inc., for efforts beyond the call of duty. Airborne infrared astronomy at UCSD is supported by NASA grant NGR 05-005-055.

REFERENCES

Dickinson, D. F., Bechis, K. P., and Barrett, A. H. 1973, *Ap. J.* **180**, 831.
Dyck, H. M., and Simon, T. 1975, *Ap. J.* **195**, 689.
Forrest, W. J. 1974, Dissertation, University of California, San Diego
Forrest, W. J. Gillett, F. C., and Stein, W. A. 1975, *Ap. J.* **195**, 423.
McCammon, D., Münch, G., and Neugebauer, G. 1967, *Ap. J.* **147**, 575.
Merrill, K. M. 1976, Dissertation, University of California, San Diego.
Merrill, K. M., and Stein, W. A. 1976, *Pub. A.S.P.* **88**, 285.
Nguyen-Quang-Riew, Fillit, R., and Gheudin, M. 1971, *Astr. and Ap.* **14**, 154.
Snyder, L. E., and Buhl, D. 1975, *Ap. J.* **197**, 329.
Treffers, R. R., and Gilra, D. P. 1975, *Ap. J.* **202**, 839.
Wilson, W. J., Schwartz, P. R., Neugebauer, G., Harvey, P. M., and Becklin, E. E. 1972, *Ap. J.* **177**, 523.

Astron. Astrophys. 54, 959—960 (1977)

ASTRONOMY
AND
ASTROPHYSICS

Research Note

The 4–8 μm Spectrum of the BNKL Source in Orion

R. W. Russell, B. T. Soifer and R. C. Puetter
Department of Physics C-011, University of California, San Diego, La Jolla, California 92093, USA

Received September 27, 1976

Summary. Observations of the 4.5–8 μm spectrum with a resolution $\Delta\lambda/\lambda \sim 0.015$ of the BNKL source in Orion are reported. No obvious spectral features are found. An upper limit on the abundance of carbonate grains in the line of sight to BNKL is determined.

Key words: infrared sources — Orion Nebula

This note reports spectrophotometric observations from 4.5–8 μm of the infrared source in Orion known as BNKL. Previous ground-based observations (summarized by Wynn-Williams and Becklin, 1974) have shown this complex to be a cluster of several point sources. The hottest and brightest is known as the BN source, while the other point sources, and the cool extended source on which they are superimposed are collectively referred to as the KL source.

These observations, using a cryogenically cooled filter-wheel with spectral resolution $\Delta\lambda/\lambda \sim 0.015$, were made using the 0.9 m telescope of the Kuiper Airborne Observatory in October 1975. The details of the equipment and the observing technique are given elsewhere (Russell et al., 1976). Briefly, the observations were obtained using a 30″ focal plane aperture to minimize signal fluctuations due to seeing and drifts in the automatic tracker. The beam separation was 2′ in cross elevation (nearly right ascension at the time of the observations). The observations were made while the airplane was flying at an altitude of 12.5 km. Instrumental response and residual atmospheric opacity due to the small amount (12.5–14.5 μm) of precipitable water vapor along the line of sight were calibrated by observing the standard star α Tau, whose spectrum was taken to be a blackbody at a temperature of 3800 K, except for a depression of 20% from 4.5–5.2 μm due to CO absorption.

The observed 4.5–8 μm spectrum of the BNKL source is shown in Figure 1, while the composite spectrum of BNKL from 2–25 μm is shown in Figure 2. The spectra of Figure 2 were obtained with different focal plane apertures, the effects of which are shown clearly in the 8–13 μm spectrum.

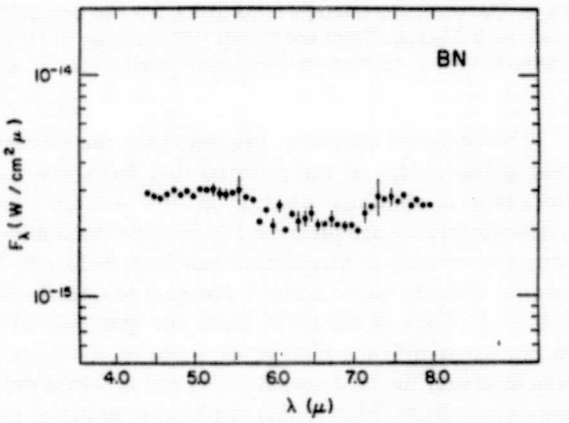

Fig. 1. The 4.5–8 μm spectrum of the infrared (BNKL) cluster in Orion, obtained with a 30″ aperture

The 4.5–8 μ spectrum, obtained with a 30″ aperture, is apparently at a slightly (13%) higher flux level than the overlapping spectra obtained from ground-based observations [Gillett and Forrest (1973), hereafter GF]. This is probably caused by the larger aperture and chopper amplitude employed in the 4.5–8 μm observations.

Discussion

The apparent depression from 6–7 μm in the spectrum of Figure 1 is not fit well by any of the absorptions expected in this wavelength region. From the spectra in Figure 2 it appears that the spectrum for $\lambda < 7$ μm is dominated by the hot BN source, while from 7–8 μm a significant contribution is made by the cooler sources (Rieke et al., 1973) included in the 30″ observing aperture, and the combination of the spectra of these sources causes the apparent depression from 6–7 μm.

Send offprint requests to: R. W. Russell

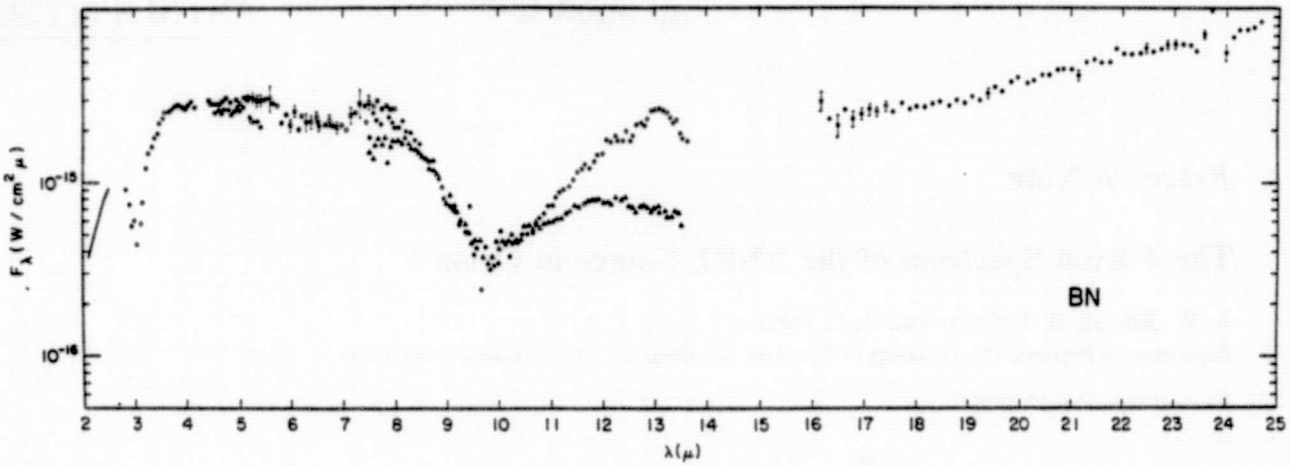

Fig. 2. The composite spectrum of the BNKL complex from 2–25 μm. The measurements and apertures are — 2.1–2.5 μm Gillett et al. (1975b), 17″ aperture; ● 2.8–5 μm Gillett and Forrest (1973), average of 11″ and 22″ aperture; □ 4.5–8 μm this paper, 30″ aperture; △ 7.5–13.5 μm Gillett and Forrest (1973), 11″ aperture; ● Gillett and Forrest (1973), 22″ aperture; ● 16–25 μm Forrest and Soifer (1976), 17″ aperture

The observed spectrum suggests that the dust shell that is the source of the infrared flux from BN has a smoothly continuous opacity in the 4–8 μm range. Silicate materials are presumed to provide the dominant source of opacity of interstellar dust from 8–13 μm. Terrestrial silicates show a rapid decrease in opacity for $\lambda < 8$ μm (Pollack et al., 1973). Since the spectrum of BN shows no significant change of slope at $\lambda < 8$ μm, we conclude that the dust opacity does not decrease drastically at $\lambda < 8$ μm. Thus, either the silicate material has a significantly larger opacity than terrestrial silicates from 5–8 μm, perhaps due to impurities in the grains, or another material provides opacity in this wavelength range. Because the absorption spectrum of the KL source (GF) has a rapidly decreasing opacity for $\lambda < 9$ μm that is characteristic of silicates, we consider the more likely explanation of the continuous spectrum to be that another dust component provides opacity at $\lambda < 8$ μm. Graphite, with no spectral features at infrared wavelengths, is one likely candidate to provide additional opacity.

There is no evidence for any spectral features in the 4.5–8 μm spectrum of BNKL, other than that introduced by the superposition of spectra of different sources within the 30″ observing aperture. In particular, we can use the observed smooth continuum to place upper limits on the column density of carbonate materials in the line of sight to the BN source. Mineral carbonates, which have a strong resonance absorption that peaks at 7 μm, have been tentatively identified by Gillett et al. (1973) in the 8–13 μm spectrum of planetary nebulae. From the lack of any evidence of carbonate absorption, we obtain an upper limit of $\tau_{7\mu}^{abs} < 0.2$. From the 7 μm mass opacity coefficient of carbonates (Hunt et al., 1950) the upper limit on the column density of carbonates is $\varrho dl \leqq 2.5\,10^{-5}$ gm/cm^2 in the line of sight to the BNKL source. Comparing this to the optical depth to BN at 9.7 μm derived by Gillett et al. (1975a), we derive an upper limit of 0.05 on the ratio by mass of carbonate to silicate grains in this line of sight.

Acknowledgements. We would like to thank the staff of the Kuiper Airborne Observatory for their invaluable assistance, and particularly Don Wilson of Informatics, Inc., for efforts beyond the call of duty. K. Sellgren assisted in the data reduction. Airborne infrared astronomy at UCSD is supported by NASA grant NGR 05-005-055.

References

Forrest, W.J., Soifer, B.T.: 1976, *Astrophys. J. Letters* **208**, L129
Gillett, F.C., Forrest, W.J.: 1973, *Astrophys. J.* **179**, 483
Gillett, F.C., Forrest, W.J., Merrill, K.M.: 1973, *Astrophys. J.* **183**, 87
Gillett, F.C., Forrest, W.J., Merrill, K.M., Capps, R.W., Soifer, B.T.: 1975a, *Astrophys. J.* **200**, 609
Gillett, F.C., Jones, T.W., Merrill, K.M., Stein, W.A.: 1975b, *Astron. Astrophys.* **45**, 77
Hunt, J.M., Wisherd, M.P., Bonham, L.C.: 1950, *Anal. Chem.* **22**, 1478
Pollack, J.B., Toon, O.B., Khare, B.N.: 1973, *Icarus* **19**, 372
Rieke, G.H., Low, F.J., Kleinmann, D.E.: 1973, *Astrophys. J. Letters* **186**, L7
Russell, R.W., Puetter, R.C., Sellgren, K., Soifer, B.T.: 1976, in preparation
Wynn-Williams, G.C., Becklin, E.E.: 1974, *Publ. Astron. Soc. Pacific* **86**, 5

BULLETIN

OF THE

AMERICAN ASTRONOMICAL SOCIETY

PUBLISHED BY THE AMERICAN INSTITUTE OF PHYSICS INC.

VOLUME 9, NUMBER 4, PART II Page 571 *1977*

08.05.05 Infrared Spectra of Protostars R. C. PUETTER, R. W. RUSSELL, B. T. SOIFER, and S. P. WILLNER, Univ. of Calif., San Diego -- The 2 to 13 μm spectra of 5 compact infrared sources associated with molecular clouds have been measured with the Kuiper Airborne Observatory and ground-based telescopes. The sources -- OMC 2-IRS3, GL 989 = DAA 6, GL 2591 = UA 27, GL 2884, and NGC 7538E -- are spatially isolated from other sources of comparable strength. The spectra all show broad absorption features near 3.1 and 9.7 μm; the features are attributed to ice and silicates, respectively. Two new absorption features, shallower than the ice and silicate absorptions, are seen near 6.0 and 6.8 μm. The ratios of the depths of the various features are different from object to object. This research was supported by NASA grant NGR 05-005-055 and NSF grant AST 76-82890.

08.06.05 Water in the 2μ Infrared Spectrum of Miras. K. H. HINKLE, McD. Obs. and Dept. of Astron., U.T.--Ten high resolution ($\Delta\sigma$=.15cm^{-1}) 4000-6700 cm^{-1} infrared spectra of the bright M-type Mira variable R Leonis obtained at a variety of phases have been searched for stellar water bands. Three bands are readily identified in the spectra, two at 5300cm^{-1} and another at 6900cm^{-1}. Two bands

#11

BULLETIN
OF THE
AMERICAN ASTRONOMICAL SOCIETY
PUBLISHED BY THE AMERICAN INSTITUTE OF PHYSICS INC.

VOLUME 9, NUMBER 4, PART II Page 582 *1977*

15.05.07 The Infrared Spectrum of BD +30° 3639 and Possible Celestial Grain Constituents R. W. RUSSELL, R. C. PUETTER, B. T. SOIFER, and S. P. WILLNER, Univ. of Calif., San Diego -- Broad emission features at 6.2 and 7.7 μm, first seen in the spectrum of NGC 7027, characterize the 4-8 μm spectrum of the low excitation planetary nebula BD +30° 3639. These features, which are broader than the instrumental resolution ($\Delta\lambda/\lambda \sim 0.015$), have been attributed to peaks in the emissivity of the dust grains that produce the bulk of the infrared flux at these wavelengths. A comparison of the astronomical spectra with laboratory emissivity data for small (~ 2-5 μm) particles of $CaCO_3$ and $MgCO_3$ suggests that neither of these materials can be responsible for the peaks seen in the astronomical data. Alternative materials exhibiting some features similar to those seen in the planetary nebulae spectra have also been studied. However, these materials exhibit features that are not observed in the astronomical data. In addition to the broad features, BD +30° 3639 also possesses a strong [Ar II] line at 6.98 μm. From the strength of this line, argon is found to be over-abundant compared to cosmic abundances. Combined with the earlier report of an over-abundance of neon, this is evidence for significant nuclear processing and mixing in the central star. This research was supported by NASA under grant no. NGR 05-005-055.

THE ASTROPHYSICAL JOURNAL, 217:L121–L124, 1977 November 1

2 TO 8 MICRON SPECTROPHOTOMETRY OF M82

S. P. WILLNER, B. T. SOIFER, AND RAY W. RUSSELL
Department of Physics, University of California at San Diego
AND
R. R. JOYCE AND F. C. GILLETT
Kitt Peak National Observatory*
Received 1977 June 13; accepted 1977 August 2

ABSTRACT

Observations of the central 30″ of the galaxy M82 with 1.5% spectral resolution from 2 to 8 μm are reported. Three emission features broader than the instrumental resolution are observed. Hydrogen recombination lines are also observed; they indicate an amount of thermal bremsstrahlung emission equivalent to 0.8 Jy of radio flux at 3.5 mm and provide an estimate of ~25 magnitudes for the extinction to the H II region. An upper limit on the 8.99 μm [Ar III] line intensity together with the measured [Ar II] intensity implies that the excitation of the H II region is extremely low. Comparison of fine-structure lines, including the 8 to 13 μm 1973 data of Gillett *et al.*, with the hydrogen lines shows that argon and neon have approximately their cosmic abundance.

Subject headings: infrared: spectra — galaxies: individual — abundances

I. INTRODUCTION

The galaxy M82 (NGC 3034) was originally found to be a bright extended infrared source by Kleinmann and Low (1970). Gillett *et al.* (1975*b*, hereafter Paper I) reported 8–13 μm spectrophotometric observations of the nucleus of M82; these observations showed that the nucleus, like the two galactic planetary nebulae NGC 7027 and BD +30°3639 (Gillett, Forrest, and Merrill 1973), has emission features at 8.7 and 11.3 μm. The similarity of the spectrum to those of the planetary nebulae was interpreted as indicating that the emission from M82 is thermal radiation from heated dust. The nucleus of M82 is viewed through a large column density of cold dust, as evidenced by the apparently deep silicate absorption in the 10 μm spectrum.

In this letter, we report new spectrophotometric observations of M82 from 2 to 8 μm. These observations show further similarities with infrared sources in our Galaxy. The observed hydrogen recombination lines are used to derive properties of the ionized gas, extinction to the H II region, and an improved Ne abundance estimate, while a measured [Ar II] line gives the argon abundance.

II. OBSERVATIONS

The observations from 2 to 4 μm were obtained using the Kitt Peak National Observatory 1.3 m telescope, a circular variable filter, and an InSb detector (Gillett and Joyce 1975). Observations were obtained using 15″, 22″, and 30″ apertures centered on the infrared source. The spectral resolution was $\Delta\lambda/\lambda \approx 0.015$ from 1.9 to 2.5 μm and ≈0.02 from 2.8 to 4.2 μm. The spectral shape of the source is nearly independent of aperture size, with the flux nearly proportional to the linear size of the observing aperture over this aperture range. The 30″ aperture spectrum is plotted in Figure 1, along with broad-band photometric points at 1.65 and 4.65 μm.

The observations from 4 to 8 μm were obtained using the 90 cm telescope of the Kuiper Airborne Observatory, flying at ~12.5 km, in 1976 May and November. The basic system is described by Russell and Soifer (1977), except that the detector used for these observations was a Si:As photoconductor cooled with liquid helium. A 28″ focal-plane aperture was used, and the observed spectrum is shown in Figure 1. The spectral resolution was $\Delta\lambda/\lambda \approx 0.015$. Figure 1 also shows the 8–14 μm spectrum from Paper I renormalized by the ratio of the aperture sizes of the airborne and ground-based (Paper I) systems (28″/7″).

III. DISCUSSION

a) *Diffuse Emission Features*

The 2–8 μm spectrum of M82 shows several diffuse emission features in common with those of the planetary nebula NGC 7027 (Russell, Soifer, and Willner 1977*a*). These are the strong emission band at 3.3 μm (Merrill, Soifer, and Russell 1975; Grasdalen and Joyce 1976), a strong emission feature at 6.2 μm, and a broad peak in the emission spectrum at ~7.6 μm. The emission peaks at 8.7 and 11.3 μm have been noted previously in Paper I. The emission features mentioned above are also seen in the spectrum of HD 44179 = CRL 915 (Russell, Soifer, and Willner 1977*b*), and the 3.3, 8.7, 11.3 μm emission peaks are common to other galactic infrared sources such as BD +30°3639 (Russell, Soifer, and Merrill 1977) and CRL 437 (Kleinmann *et al.* 1977).

* Operated by the Association of Universities for Research in Astronomy, Inc., under contract with the National Science Foundation.

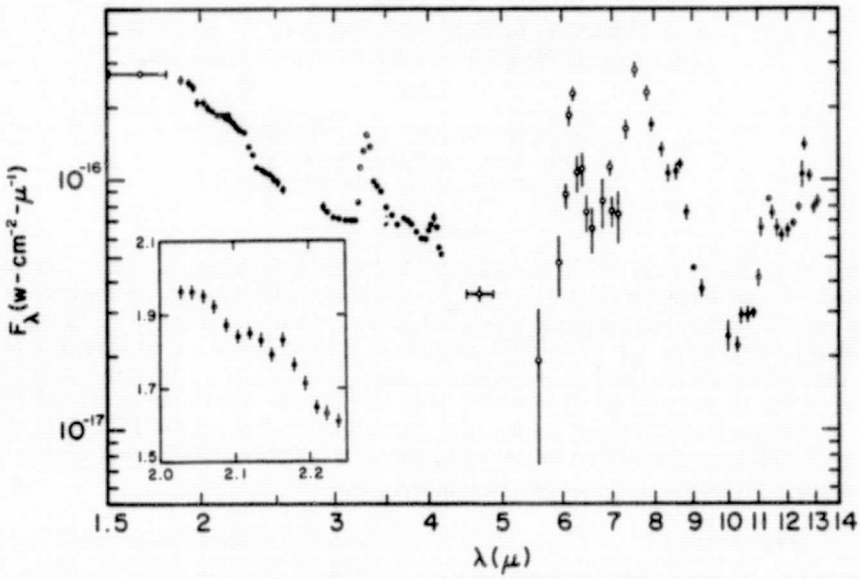

FIG. 1.—The 2–13 μm spectrum of M82. *Filled circles*, data obtained at KPNO; *open circles*, data obtained on the KAO. The filled circles at wavelengths larger than 8 μm represent data from Paper I scaled from their 7″ to the airborne system's 28″ aperture. The 2 to 4 μm data were obtained through a 30″ aperture. Also shown are the photometric fluxes obtained through filters centered at 1.65 μm ($\Delta\lambda \approx 0.29\mu$m) and 4.64 μm ($\Delta\lambda \approx 0.34$ μm). The insert shows details of the spectrum near the Bγ wavelength (2.17 μm).

All these spectral features are broader than the instrumental resolution; the 3.3 μm feature has been found to be a continuum at a resolution $\lambda/\Delta\lambda \approx 3000$ (Smith *et al.* 1976, as discussed in Russell, Soifer, and Merrill 1977).

A likely explanation is that all these features are resonance bands of one or more solids; however, no positive identification of the radiating solid(s) has been made. Gillett, Forrest, and Merrill (1973) suggested that the 11.3 μm emission feature in NGC 7027 could be emission in the ν_2 fundamental of $MgCO_3$, and Bregman and Rank (1975) observed this feature at higher spectral resolution and found it to be a continuum and consistent with the carbonate signature. This identification predicts a much stronger feature (the ν_3 fundamental) near 7.0 μm. The lack of any evidence for this 7 μm peak here or in NGC 7027 (Russell, Soifer, and Willner 1977*a*) must call the carbonate identification into question.

The broad peak at 7.6 μm has the character of a fundamental solid-particle resonance. The full width at half-maximum of this band is typical of solid-state bands ($\Delta\lambda/\lambda \sim 0.1$), and the wavelength of the peak is certainly well within the range expected from solids composed of cosmically abundant elements. However, no specific mineral known to us has a strong resonance at this exact wavelength; in particular, no known carbonate exhibits a strong absorption centered near 7.6 μm.

Although the 6.2 μm and 3.3 μm bands could be identified through wavelength coincidence with water of hydration resonance bands (White 1971; Johan, Povondra, and Slansky 1969), the properties of hydrated minerals seem to make this an unlikely identification. At temperatures necessary to thermally excite these bands, water of hydration rapidly evaporates from most minerals. We therefore regard the 6.2 μm and 3.3 μm bands as having no satisfactory identification at this time.

b) Hydrogen Recombination Lines

Hydrogen recombination lines are extremely important in analyzing the properties of ionized gas. The 4.05 μm Bα line is clearly present in the spectrum of M82 (observed strength 1.6×10^{-18} W cm^{-2} in a 30″ beam). The spectrum also shows a possible detection of Bγ at 2.17 μm, with a strength of $(1.5 \pm 0.7) \times 10^{-19}$ W cm^{-2}. Taking an intrinsic Bα/Bγ ratio of 2.7 (Petrosian 1970; Brocklehurst 1971) and van de Hulst's extinction curve 15 (Johnson 1968), the observed Bα/Bγ ratio yields $A_V \approx 25$ mag to the nucleus of M82. Although there is considerable uncertainty in this value, it is in reasonable agreement with the extinction derived from the best fit to the 10 μm silicate absorption depth (Paper I) and $A_V/\tau_{9.7} \approx 14$ (Gillett *et al.* 1975*a*). This extinction is substantially in excess of that which would be derived from the J(1.25 μm), H(1.65 μm), and K(2.22 μm) broad-band colors, indicating that the radiation short of 3 μm is dominated by foreground stars in the galaxy along the line of sight. Preliminary analysis of higher resolution ($\lambda/\Delta\lambda \approx 400$) observations of Bα and Bγ in an 11″ beam (Simon, Simon, and Joyce 1977) are also consistent with A_V in the neighborhood of 20 mag.

The observed strength of the 4.05 μm Bα line, with *no* correction for extinction at 4 μm, implies an optically thin radio flux of 0.5 Jy at 3.5 mm. If a correction of 0.5 mag is made for 4 μm extinction, based on the strength of the 10 μm absorption, the predicted free-free flux at 3.5 mm is ~0.8 Jy. Within the uncertainties in the electron temperature and the extinction correction,

this predicted free-free flux is equal to the measured radio flux from M82 of ~0.6 Jy at 3.5 mm in a 72″ beam (Kellermann and Pauliny-Toth 1971). The measured flux is also consistent with a power law smoothly extrapolated from lower frequencies. Thus, either the hydrogen recombination line is emitted in very clumpy regions of high enough emission measure to be optically thick at 3.5 mm, or the extrapolation of the low-frequency radio spectrum by Kellermann and Pauliny-Toth represents a chance summation of a steeper power-law spectrum and a free-free continuum at exactly the right levels to mimic the apparently less steep spectrum.

If the H II region in the nucleus of M82 is relatively uniform, the formulae of Schraml and Mezger (1969) can be used to derive the electron density, the emission measure, and the mass of ionized hydrogen. The number of ionizing photons can also be derived and is discussed later. The results are $N_e = 30$ cm^{-3}, $E_m = 5.7 \times 10^5$ pc cm^{-6}, and M (H II) $= 7 \times 10^7\ M_\odot$; all were calculated for a distance of 3.2 Mpc (Sandage 1962), an equivalent free-free radio flux of 0.8 Jy at 3.5 mm, and a gas temperature of 10^4 K. The emission measure is comparable to that derived by Peimbert and Spinrad (1970). They used a 10″ aperture, so it is not surprising that the ionized mass derived here is 20 times larger; the electron density is half their value. Evidently, our observations include the same region, but if the average visual extinction to the H II region is as large as that implied by the silicate absorption (Paper I) and the Bα/Bγ ratio, the extinction must be patchy on a scale of ~10″, and Peimbert and Spinrad observed an area with much less extinction than the average.

The detection of Bα also allows one to estimate the total number of ionizing photons emitted by the energy source in the nucleus of M82. Using the relation developed by Rubin (1968) and the equivalent optically thin radio free-free continuum (including the correction for extinction at 4 μm), we find the energy source emits at least 6×10^{53} Lyman continuum photons per second. On the basis of the excitation of the central region in M82, Peimbert and Spinrad (1970) estimated the temperature of the central ionizing source to be 30,000 K, which leads to a total luminosity of the ionizing source of $L \approx 8 \times 10^{43}$ ergs s^{-1}. This can be compared with the total infrared luminosity of M82 of $L_{IR} \approx 10^{44}$ ergs s^{-1} (Harper and Low 1973). When an aperture correction is applied to our data to estimate the total Bα nuclear flux, it appears that if the temperature of the ionizing source is 30,000 K, the entire infrared luminosity of M82 could be produced by the ionizing source. As in many galactic H II regions, the total bolometric luminosity of the ionizing source can account for the infrared luminosity, but the Lyman continuum luminosity alone is not sufficient (Wynn-Williams and Becklin 1974). In the case of M82, for $T = 30{,}000$ K, the Lyman continuum luminosity is only one-fifth of the total infrared luminosity observed.

c) *Fine-Structure Emission Lines*

The narrow emission feature near 7 μm shown in Figure 1 is identified as the 6.98 μm fine-structure line of [Ar II]. The total flux in the line is about $4 \pm 1 \times 10^{-18}$ W cm^{-2}; the instrumental bandwidth was assumed to be 0.10 μm. From the calculations of Simpson (1975), the observed ratio of [Ar II] line flux to Bα line flux implies n(Ar II)/n(H$^+$) ≈ 5×10^{-6}. No differential reddening correction has been applied in calculating this number; any such correction would tend to decrease the Ar/H ratio, because Bα is more heavily attenuated. [Ar III] emission at 8.99 μm is not apparent [I([Ar III]) < 2.4×10^{-18} W cm^{-2}; Paper I], so Ar II is probably the principal ionization state. Cameron (1973) gives n(Ar)/n(H) ≈ 3.7×10^{-6} as the normal solar abundance, so there is apparently a normal or slightly enhanced Ar abundance in M82.

From the observed [Ne II] line flux at 12.8 μm and the relations derived by Simpson (1975), the apparent n(Ar II)/n(Ne II) ratio is ~0.037, again suggesting a normal cosmic abundance of neon (Cameron 1973). Differential extinction due to silicate absorption should not change this result by more than 50%.

The lack of 8.99 μm emission from [Ar III] places an upper limit n(Ar III)/n(Ar II) < 0.7, if τ_{abs} (9 μm) = 2/3 τ_{abs} (9.7 μm) = 1. Since the ionization potentials of Ar II and He I are nearly the same (27.6 eV versus 24.6 eV), this is reasonably consistent with the ratio n(He II)/n(He I) ≈ 1 determined by Peimbert and Spinrad (1970) and provides additional support for an ionizing source temperature $T \lesssim 30{,}000$ K.

The upper limit on the temperature of the ionizing source suggested by the [Ar III]/[Ar II] ratio implies that the ionization is likely to be due to a thermal source. One possible model for the ionizing source is B0 main-sequence stars; 2×10^6 (Panagia 1973) such stars would radiate the required Lyman continuum flux, their mass would be $2 \times 10^7\ M_\odot$ (Cester 1965), and their luminosity (Panagia 1973) would equal the far-infrared luminosity of M82 (Harper and Low 1973). With this model, cooler stars cannot dominate the infrared luminosity (because the B0 stars already provide sufficient luminosity), nor can there be significant numbers of hotter stars, because they would ionize [Ar II].

d) *The 2 μm Stellar Content*

That cooler stars are present in the nucleus of M82 is evidenced by the presence of the CO overtone absorption band near 2.3 μm. The strength of the 2.3 μm CO absorption is luminosity-dependent and can be used to estimate the stellar component responsible for the 2 μm radiation. Following Frogel *et al.* (1975), we used the CO index [2.4 μm]–[2.2 μm] to quantify the CO band strength. For M82, reddening must also be taken into account, and this is done by comparing the observed [1.65 μm]–[2.2 μm] color of M82 with that of typical galaxies (Frogel *et al.* 1975) and extrapolating the color excess to [2.4 μm]–[2.2 μm] using the van de Hulst curve 15. The resulting "intrinsic" CO index for M82 is ~0.16, which is in the range observed for normal galactic nuclei and corresponds to that of late K, early M giant stars (Frogel *et al.* 1975).

The total luminosity of the stars responsible for the 2 μm radiation can be estimated if the average extinc-

tion at 2 μm and the effective stellar temperature are known. The stellar temperature is taken to be 3000 K, and the 2 μm extinction, estimated from the [1.65 μm]–[2.2 μm] color and van de Hulst curve 15, is about 0.5 mag. As pointed out earlier, this estimate is substantially less than that derived from the Bα/Bγ ratio, indicating that the bulk of stars is less attenuated than the H II region and 10 μm source. The resulting stellar luminosity is $\sim 2 \times 10^{43}$ ergs s^{-1}, which is only one-fifth of the total infrared luminosity and consistent with the idea that B stars provide the bulk of the infrared luminosity.

IV. SUMMARY

1. The nucleus of M82 exhibits several diffuse emission features in common with an increasing number of galactic sources. These features are similar in appearance to resonance bands of solids, but there are at present no convincing identifications for any of them. Understanding the origin and excitation of these features is a major problem in infrared astronomy.

2. The observed Bα and (possibly) Bγ recombination lines indicate the presence of an H II region in the nuclear region of M82 larger than expected from radio continuum observations.

3. The observed upper limit n(Ar III)/n(Ar II) $<$ 0.7 is consistent with n(He II)/n(He I) $\approx$ 1 (Peimbert and Spinrad 1970), and implies that if the ionizing source is thermal, $T \lesssim 30{,}000$ K. For $T = 30{,}000$ K, the total luminosity of an ionizing source sufficient to produce the observed H II region is $L \approx 10^{44}$ ergs s^{-1}, which is essentially the total infrared luminosity of the nucleus of M82 (Harper and Low 1973).

4. The strength of the 2.3 μm CO overtone absorption band indicates that the 2 μm spectrum is dominated by late K and early M giant stars. The luminosity associated with these stars is approximately one-fifth of the total infrared luminosity.

REFERENCES

Bregman, J. D., and Rank, D. M. 1975, *Ap. J.* (*Letters*), **195**, L125.
Brocklehurst, M. 1971, *M.N.R.A.S.*, **153**, 471.
Cameron, A. G. W. 1973, in *Explosive Nucleosynthesis*, ed. D. N. Schramm and W. D. Arnett (Austin: University of Texas Press), p. 3.
Cester, B. 1965, *Zs. f. Ap.*, **62**, 191.
Frogel, J. A., Persson, S. E., Aaronson, M., Becklin, E. E., Matthews, K., and Neugebauer, G. 1975, *Ap. J.* (*Letters*), **195**, L15.
Gillett, F. C., Forrest, W. J., and Merrill, K. M. 1973, *Ap. J.*, **183**, 87.
Gillett, F. C., Jones, T. W., Merrill, K. M., and Stein, W. A. 1975*a*, *Astr. Ap.*, **45**, 77.
Gillett, F. C., and Joyce, R. R. 1975, *Bull. AAS*, **7**, 409.
Gillett, F. C., Kleinmann, D. E., Wright, E. L., and Capps, R. W. 1975*b*, *Ap. J.* (*Letters*), **198**, L65 (Paper I).
Grasdalen, G. L., and Joyce, R. R. 1976, *Ap. J.* (*Letters*), **205**, L11.
Harper, D. A., Jr., and Low, F. J. 1973, *Ap. J.* (*Letters*), **182**, L89.
Johan, Z., Povondra, P., and Slansky, E. 1969, *Amer. Mineralogist*, **54**, 1.
Johnson, H. M. 1968, in *Nebulae and Interstellar Matter*, ed. B. M. Middlehurst and L. A. Aller (Chicago: University of Chicago Press), p. 65.
Kellermann, K. I., and Pauliny-Toth, I. I. K. 1971, *Ap. Letters*, **8**, 153.
Kleinmann, D. E., and Low, F. J. 1970, *Ap. J.* (*Letters*), **161**, L203.
Kleinmann, S. G., Sargent, D. G., Gillett, F. C., Grasdalen, G L., and Joyce, R. R. 1977, *Ap. J.* (*Letters*), **215**, L79.
Merrill, K. M., Soifer, B. T., and Russell, R. W. 1975, *Ap. J.* (*Letters*), **200**, L37.
Panagia, N. 1973, *A.J.*, **78**, 929.
Peimbert, M., and Spinrad, H. 1970, *Ap. J.*, **160**, 429.
Petrosian, V. 1970, *Ap. J.*, **159**, 833.
Rubin, R. H. 1968, *Ap. J.*, **154**, 391.
Russell, R. W., and Soifer, B. T. 1977, *Icarus*, **30**, in press.
Russell, R. W., Soifer, B. T., and Merrill, K. M. 1977, *Ap. J.*, **213**, 66.
Russell, R. W., Soifer, B. T., and Willner, S. P. 1977*a*, in preparation.
———. 1977*b*, in preparation.
Sandage, A. R. 1962, *IAU Symposium No. 15, Problems of Extragalactic Research*, ed. G. C. McVittie (New York: MacMillan), p. 359.
Schraml, J., and Mezger, P. G. 1969, *Ap. J.*, **156**, 269.
Simon, M., Simon, T., and Joyce, R. R. 1977, in preparation.
Simpson, J. P. 1975, *Astr. Ap.*, **39**, 43.
Smith, H., Wollman, E., Lacy, J., Townes, C., and Rank, D. 1976, private communication.
White, W. B. 1971, *Amer. Mineralogist*, **56**, 46.
Wynn-Williams, C. G., and Becklin, E. E. 1974, *Pub. A.S.P.*, **86**, 5.

F. C. GILLETT and R. R. JOYCE: Kitt Peak National Observatory, P.O. Box 26732, Tucson, AZ 85726

RAY W. RUSSELL, B. T. SOIFER, and S. P. WILLNER: Dept. of Physics, C-011, University of California, San Diego, La Jolla, CA 92093

THE ASTROPHYSICAL JOURNAL, 217:L149–L153, 1977 November 1

THE 4 TO 8 MICRON SPECTRUM OF NGC 7027

RAY W. RUSSELL, B. T. SOIFER, AND S. P. WILLNER
Department of Physics, University of California, San Diego
Received 1977 May 26; accepted 1977 August 3

ABSTRACT

Spectrophotometric observations of NGC 7027 with $\Delta\lambda/\lambda \approx 0.015$ are reported. The continuum shows a strong, broad peak near 7.7 μm, but little or no evidence for the strong peak near 7.0 μm expected from previously postulated carbonate grains. A spectrally resolved feature at 6.2 μm is found and attributed to an increase in the emissivity of some as yet unidentified dust material.

Unresolved emission features are seen at 4.49 and 5.60 μm. These are attributed to [Mg IV] λ4.49, [Ar VI] λ4.52, and [Mg V] λ5.61. The flux in the [Mg V] line is used to derive a lower limit on the temperature of the central star of 1.3×10^5 K; a better estimate might be $T_* \approx 2 \times 10^5$ K. It is suggested that magnesium is overabundant.

Subject headings: infrared: spectra — nebulae: planetary

I. INTRODUCTION

Infrared observations of the planetary nebula NGC 7027 (Gillett, Low, and Stein 1967) revealed an infrared excess above the expected free-free continuum extrapolated from the radio observations. This excess is attributed (e.g., Krishna Swamy and O'Dell 1968) to thermal radiation by dust mixed with the nebular gas.

NGC 7027 has an extremely rich infrared spectrum (Merrill, Soifer, and Russell 1975, hereafter Paper I; Gillett, Forrest, and Merrill 1973, hereafter GFM) displaying broad peaks, atomic fine-structure lines, and recombination lines of hydrogen and helium. The broad peaks have, at best, been only tentatively identified as solid state emission bands. We report here airborne 4–8 μm spectroscopy of NGC 7027. The spectrum exhibits considerable structure. Two new broad emission peaks were found; these complicate the interpretation of the dust emission spectrum. In addition, at least two emission lines were observed.

II. OBSERVATIONS

The data were obtained with the UCSD spectrophotometer mounted at the bent Cassegrain focus of the 90 cm telescope on the Kuiper Airborne Observatory (KAO). The system utilized an arsenic-doped silicon detector, but otherwise remains as described by Russell and Soifer (1977). The beam size was 28″ and the two chopped beams were separated by ∼2′.

The 4–8 μm spectrum of NGC 7027 is displayed in Figure 1. The data were obtained in 110 minutes of flight time on 1976 May 26 (U.T.), 50 minutes on 1976 May 28, and 15 minutes on 1976 November 5. Data reduction was accomplished by comparison with a standard star (α Boo or α Tau) also observed during each flight.

Figure 2 shows the 2–14 μm spectrum of NGC 7027; the 2–4 μm data are from Paper I. New data between 7.5 and 13.7 μm were obtained with the UCSD–University of Minnesota 1.5 m telescope on Mount Lemmon using a 17″ beam and standard techniques (Gillett and Forrest 1973). These data, obtained by A. Knutson, K. M. Merrill, and the authors and plotted in Figure 2, have more complete wavelength coverage and a better signal-to-noise ratio than the data of GFM. For Figure 2 no adjustment of the absolute levels of the three spectral regions was made; the slight difference in level is smaller than the uncertainty in the flux densities of the various standard stars used to calibrate the data.

III. RESOLVED FEATURES

a) *Feature at 7.7 μm*

The continuum flux, as shown in Figure 2, rises to a strong peak near 7.7 μm. This peak is significantly broader than the instrumental resolution, yet narrower than a blackbody distribution. If the infrared continuum is due to thermal emission from dust, as is generally accepted, the dominant character of this feature links it implicitly with the dust. If the temperature of the dust $T_D > 250$ K, as indicated by color-temperature estimates based on the data in Figure 2, the dust must have an optical depth $\tau < 10^{-2}$. Because the dust is optically thin, broad emission peaks may be attributed to peaks in the grain emissivity. Other resolved features are seen at 3.3/3.4, 6.2, 8.6, and 11.3 μm; neither these nor the 7.7 μm feature can reasonably be attributed to any blend of atomic lines.

The features are not likely to be molecular bands, because they have all been observed at the same wavelengths in the low-excitation objects HD 44179 (Russell, Soifer, and Willner 1978) and M82 (Willner *et al.* 1977), and molecular bands are usually quite temperature-dependent in their shape and wavelength of peak flux (Russell, Soifer, and Merrill 1977). However, only higher resolution observations can absolutely rule out molecular bands or atomic line combinations. The interpretation that appears most reasonable is that the

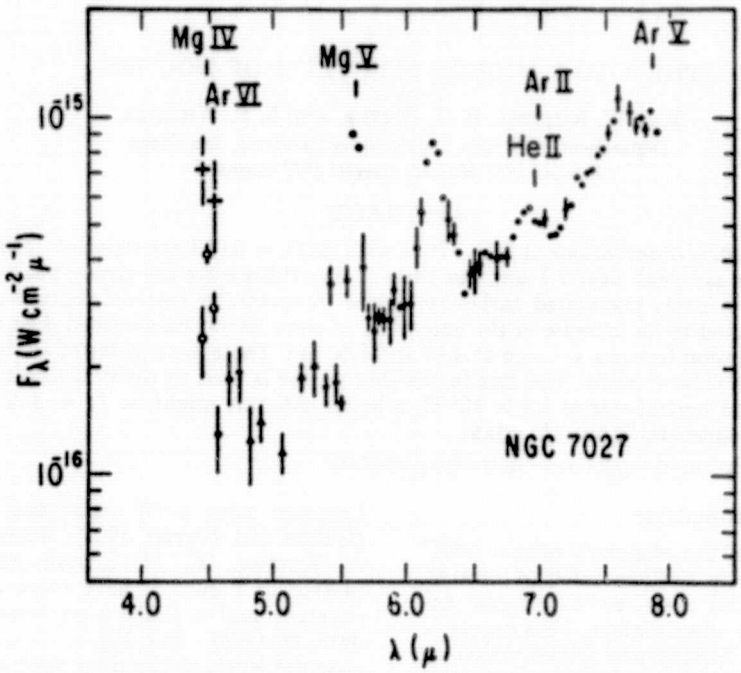

FIG. 1.—The 4–8 μm spectrum of NGC 7027. Wavelengths of fine structure lines are noted, along with the wavelength of the He II line discussed in the text. Open circles represent data obtained on 1976 November 4/5 only. Filled triangles are averages of adjacent wavelengths and have a resolution of 3%. Pluses are 1976 May data at the wavelength of [Mg IV] and [Ar VI]. Significant variations in the observed intensity were seen at these wavelengths, as discussed in the text. Statistical errors $\geq 5\%$ are shown.

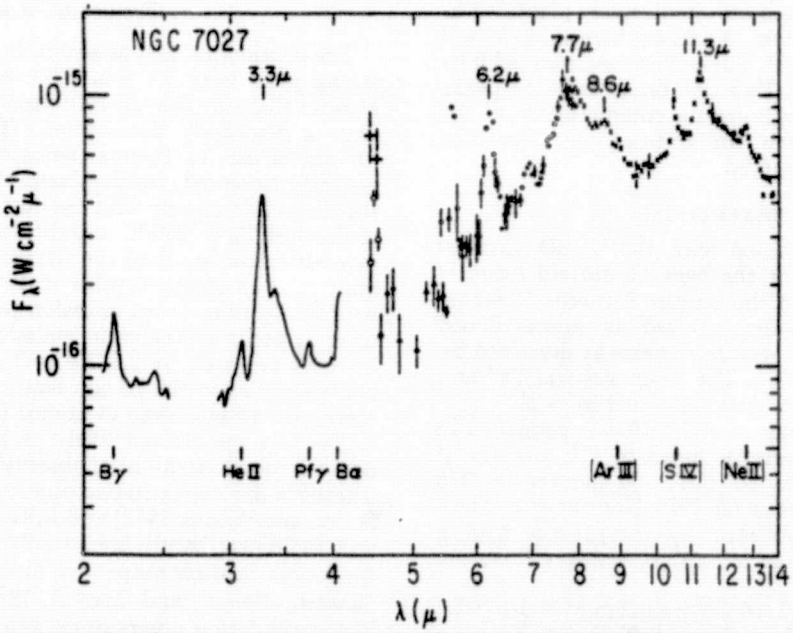

FIG. 2.—The 2–14 μm spectrum of NGC 7027. Symbols for airborne data are the same as for Fig. 1, and crosses represent ground-based data. Data for $\lambda \leq 4.0$ μm are from Paper I. Possible dust emission features and additional atomic transitions are noted.

peaks represent the structure in the emissivity curve of the grains.

b) Nondetection of Carbonates

GFM proposed mineral carbonates as a possible constituent of the dust, based on the wavelength and shape of the 11.3 μm feature. Higher resolution observations (Bregman and Rank 1975) supported this identification. However, terrestrial carbonates studied in absorption (e.g., Hunt, Wisherd, and Bonham 1950) and recently in emission in our laboratory show a peak in their emissivity near 7 μm even larger than that at 11.3 μm. When only the ground-based data were available, it was reasonable to suppose (GFM) that the flux level would peak at 7 μm. The airborne data show that this does not happen; rather, the major peak lies near 7.7 μm.

Four reasons why the 7.0 μm feature is not observed at the expected strength are considered here. First, carbonates may not be present. Second, the wavelength of peak emission may be shifted from 7.0 to 7.7 μm, where NGC 7027 has a feature close in relative strength and half-width to that expected for the 7 μm carbonate feature. The idea of such a large wavelength shift is barely tenable, because the feature can only appear within the wavelength range where the real part of the dielectric constant is negative (Huffman 1977). For terrestrial $MgCO_3$, which exhibits an 11.3 μm feature most like that seen in NGC 7027, the peak emission cannot be shifted to a wavelength longer than 7.05 μm (Huffman 1977).

A third explanation for the smaller peak at 7.0 μm relative to that at 11.3 μm is that the intrinsic strength of the 7 μm feature is weaker in astrophysical grains than in terrestrial samples. This is unlikely because both of these peaks are due to molecular resonances in the CO_3 radical, and the relative strength should be moderately insensitive to the composition or size of the particles. The 11.3 μm feature could possibly be enhanced if it is excited by fluorescence, the mechanism suggested by Gillett (1977) for exciting the strong feature at 3.3 μm.

The fourth alternative is that the carbonate grains have a temperature sufficiently low that the ratio of the strengths of the 7 and 11.3 μm features is reduced. There is a small rise above the adjacent continuum at 7.0 μm. The strength of this rise cannot be completely explained by a blend of He II and [Ar II] atomic lines expected at this wavelength, and the rise is broader than would be expected even for a blend of two lines. If one assumes that carbonates are responsible for the 7 μm rise and the 11.3 μm feature, the relative flux levels place an upper limit of ~150 K on the temperature of the carbonate dust. On the other hand, Penman (1976) found a peak in carbonate spectra near 25 μm. No such peak was observed in NGC 7027 by McCarthy, Forrest, and Houck (1977). Their upper limit, combined with the flux in the 11.3 μm feature, places a lower limit on the temperature of 325 K. The absence of a 25 μm feature might be due to the disruption of long-range order in the carbonate crystal by radiation damage, which would be expected to leave the shorter wavelength carbonate features intact (Day 1977). This explanation still requires that the carbonate grain temperature be very low. Until some explanation for the absence of the 7 and 25 μm features is substantiated, the identification of carbonates in NGC 7027 must be regarded as doubtful.

c) Feature at 6.2 μm

The 6.2 μm feature is characterized both by its strength and comparatively narrow width. The band is slightly broader than the instrumental resolution, having an apparent full width at half-maximum intensity of $\Delta\lambda \approx 0.15$ μm. No atomic fine-structure lines of reasonably abundant elements are known to occur at this wavelength. Moreover, the observation of this band in the low-excitation nebulae M82 (Willner *et al.* 1977) and HD 44179 (Russell, Soifer, and Willner 1977) makes the identification of this band with a combination of several atomic fine-structure lines highly doubtful. The wide variety of excitation conditions under which this band is observed also makes it extremely unlikely that this band is due to a collisionally excited molecular band.

A possible mechanism for producing this feature is emission in a resonance band of the dust associated with this region. If the emission is strictly thermal and the 7.7 μm and 6.2 μm bands are in the same material and have intrinsically equal strengths, the required dust temperature is ~340 K. Water of hydration in a variety of host materials has a strong narrow resonance at ~6.2 μm (Nyquist and Kagel 1971); however, for temperatures $\gtrsim$300 K, most hydrates would lose several, if not all, of their water molecules. Thus, this identification must be regarded as extremely doubtful, and this band must be regarded as unidentified.

IV. UNRESOLVED FEATURES—ATOMIC LINES

No hydrogen or helium recombination lines were clearly detected from 4 to 8 μm, but the upper limits are consistent with observed recombination line strengths (Paper I; Brocklehurst 1971).

Several ions have forbidden lines between 4 and 8 μm. Possible forbidden-line identifications, based on the wavelengths of the observed narrow features and on the observations of related lines in the optical (Kaler *et al.* 1976, hereafter KACE), are indicated in the figures. These include [Mg V] at 5.61 μm and a blend (if both are present) of [Mg IV] at 4.49 μm and [Ar VI] at 4.52 μm. [Ar II] at 6.98 μm and [Ar V] at 7.89 μm might also be present.

The line at 5.60 ± 0.02 μm, identified with [Mg V], is an important one because of the high (109.3 eV) ionization potential of Mg IV. At the same time, this high ionization potential, compared to the more prevalent states of ionization indicated by other ionic species (discussed originally by Aller and Menzel 1945), casts some doubt upon the identification.

A strong, narrow band at 5.6 μm has been seen in several minerals studied in our laboratory. These all have an XYO_3 composition, suggesting that the feature

may be associated with the O_3 structure. While the 5.60 μm feature might be attributed to such minerals in NGC 7027, we regard this as unlikely for two reasons. First, stronger, broader bands at other wavelengths observed in the laboratory spectra remain inconsistent with the astronomical data. Second, if the material that produces the 5.60 μm feature is responsible for other resonances that appear in the NGC 7027 spectrum, the feature should appear in the spectra of M82 and HD 44179, where all the broad spectral features are seen in common. Because the feature at 5.60 μm is not present in the other two sources, we regard it as more likely that this feature is an atomic line uniquely associated with the high excitation in NGC 7027. Higher spectral resolution observations are clearly needed to confirm this assumption.

The line wavelength derived from our observations is in excellent agreement with that tabulated for [Mg v] (Johannesson, Lundstrom, and Minnhagen 1972), and we were unable to find any other atom or ion through iron which had a likely transition near this wavelength. The Mg v ion has two additional forbidden transitions at 2783 Å and 13.54 μm (Johannesson, Lundstrom, and Minnhagen 1972), neither of which has been observed (Bohlin, Marionni, and Stecher 1975; Fig. 2). However, the upper limits are consistent with the expected fluxes of 1.7×10^{-12} ergs cm^{-2} s^{-1} for the UV line and 5.2×10^{-11} ergs cm^{-2} s^{-1} for the IR line; atomic and nebular parameters used to calculate these expected line fluxes were taken from KACE; Bohlin, Marionni, and Stecher (1975); Saraph, Seaton, and Shemming (1969); and Wiese, Smith, and Miles (1969). Observations of both of these lines should be possible with higher resolution in the IR and with the improved sensitivity in the UV reported by Bohlin, Marionni, and Stecher (1975).

If the [Mg IV] line at 4.488 μm (Johannesson, Lundstrom, and Minnhagen 1972) is present, it might be considered a confirmation of the identification of the 5.60 μm feature with the [Mg v] line. Although there is an emission feature at 4.49 μm, it may be partly due to [Ar VI]; furthermore, the total observed strength of this feature is weaker than would be expected for the [Mg IV] line alone, based on the 5.60 μm line strength and a reasonable ionic abundance distribution (Aller and Menzel 1945). One possible explanation for the apparent weakness of the [Mg IV] line is a wavelength coincidence with, and thus absorption by, a telluric line. Both N_2O and $^{13}CO_2$ have lines in this general part of the spectrum, but only an N_2O line is both close enough in wavelength and a strong enough absorber to reduce the strength of the line to that observed (Greenberg 1977). Observational support for at least some telluric absorption is provided by the fact that the observed 4.49 μm flux varied by a factor of 2 between the spring and fall, as shown in Figure 1. This variation was presumably due to the changing relative wavelengths of the celestial and telluric lines caused by the Earth's motion. Depending on the exact wavelengths and on the strength of the telluric line, the total absorption could easily be a factor of 3 (Greenberg 1977). Observations with higher spectral resolution are necessary to confirm the identification and to determine the exact amount of absorption.

The Mg v abundance can be estimated by a comparison of the intensity of the 5.60 μm line with the radio flux (Higgs 1971), provided the identification of the 5.60 μm line is correct. The observed ratio n(Mg v)/n(H II) is $\sim 1.7 \times 10^{-5}$, or about one-half the solar Mg abundance of 2.6×10^{-5} (Allen 1973); the collision strengths were taken from Saraph, Seaton, and Shemming (1969) and the electron temperature from KACE. As indicated by Aller and Menzel (1945), there should be more Mg IV than Mg v; thus magnesium appears to be overabundant in NGC 7027. If the deduced fractional abundance of magnesium in the gas phase of NGC 7027 is typical of planetary nebulae, then either the observed depletion of magnesium in the interstellar medium (Field 1974) is due to processes occurring at a later stage than that evidenced by NGC 7027, or else planetary nebulae produce no more than 10% of interstellar matter.

The flux of the [Mg v] line sets a lower limit on the rate of emission by the central star of photons capable of ionizing Mg IV. This emission rate sets a lower limit on the temperature T_* of the central star, provided the luminosity can be determined. If the infrared luminosity of the nebula (Telesco and Harper 1977) represents the total luminosity of the central star and if all photons capable of ionizing Mg IV do so, then $T_* > 1.3 \times 10^5$ K. The limit is independent of the distance to NGC 7027 but is based on the assumption that the central star radiates like a blackbody. Probably other ions, notably oxygen ions, are important competitors for the UV photons. If the fraction of UV photons absorbed by Mg IV ions is really 1/25, the solar abundance ratio by number of Mg to O (Allen 1973), then $T_* \approx 2 \times 10^5$ K.

V. SUMMARY

Spectroscopy of NGC 7027 from 4 to 8 μm has revealed two resolved features at 6.2 and 7.7 μm, assumed to be due to characteristics of the dust grains responsible for the infrared continuum emission. A large peak near 7.0 μm, expected on the basis of the previous identification of the 11.3 μm feature with mineral carbonates, does not exist in NGC 7027. The emission peak at 6.2 μm is probably due to another resonance band of the dust associated with the nebula.

Two unresolved emission features at 4.49 and 5.60 μm have been observed. The feature at 5.60 μm is best identified as a fine-structure line of [Mg v]. The line intensity implies a lower limit on the temperature of the central star of NGC 7027 of $T_* > 1.3 \times 10^5$ K; a better estimate might be $T_* \approx 2 \times 10^5$ K. Also, the Mg abundance is probably greater than the solar value.

We acknowledge helpful discussions with J. Arnold, J. D. Bregman, F. C. Gillett, D. Gilra, L. Greenberg,

and M. Jura. K. Sellgren assisted with some of the airborne observations and R. C. Puetter with some of the data reduction. We particularly appreciate P. Brissenden's technical assistance, and the superb support of the KAO staff. Airborne astronomy at UCSD is supported by NASA through grant NGR 05-005-055.

REFERENCES

Allen, C. W. 1973, *Astrophysical Quantities* (3d ed.; London: Athlone), p. 31.
Aller, L. H., and Menzel, D. H. 1945, *Ap. J.*, **102**, 239.
Bohlin, R. C., Marionni, P. A., and Stecher, T. P. 1975, *Ap. J.*, **202**, 415.
Bregman, J. D., and Rank, D. M. 1975, *Ap. J.* (*Letters*), **195**, L125.
Brocklehurst, M. 1971, *M.N.R.A.S.*, **153**, 471.
Day, K. L. 1977, *M.N.R.A.S.*, **178**, 49P.
Field, G. B. 1974, *Ap. J.*, **187**, 453.
Gillett, F. C. 1977, private communication.
Gillett, F. C., and Forrest, W. J. 1973, *Ap. J.*, **179**, 483.
Gillett, F. C., Forrest, W. J., and Merrill, K. M. 1973, *Ap. J.*, **183**, 87 (GFM).
Gillett, F. C., Low, F. J., and Stein, W. A. 1967, *Ap. J.* (*Letters*), **149**, L97.
Greenberg, L. 1977, private communication.
Higgs, L. A. 1971, *Catalog of Radio Observations of Planetary Nebulae and Related Optical Data* (Ottawa: National Research Council of Canada), p. 177.
Huffman, D. R. 1977, *Adv. Phys.*, in press.
Hunt, J. M., Wisherd, M. P., and Bonham, L. C. 1950, *Anal. Chem.*, **22**, 1478.
Johannesson, G.-A., Lundstrom, T., and Minnhagen, L. 1972, *Phys. Scripta*, **6**, 129.
Kaler, J. B., Aller, L. H., Czyzak, S. J., and Epps, H. W. 1976, *Ap. J. Suppl.*, **31**, 163 (KACE).
Krishna Swamy, K. S., and O'Dell, C. R. 1968, *Ap. J.* (*Letters*), **151**, L61.
McCarthy, J., Forrest, W., and Houck, J. R. 1977, in *Symposium on Recent Results in Infrared Astrophysics*, NASA TMX-73-190, p. 57.
Merrill, K. M., Soifer, B. T., and Russell, R. W. 1975, *Ap. J.* (*Letters*), **200**, L37 (Paper I).
Nyquist, R. A., and Kagel, R. O. 1971, *Infrared Spectra of Inorganic Compounds* (New York: Academic Press).
Penman, J. M. 1976, *M.N.R.A.S.*, **176**, 539.
Russell, R. W., and Soifer, B. T. 1977, *Icarus*, **30**, 282.
Russell, R. W., Soifer, B. T., and Merrill, K. M. 1977, *Ap. J.*, **213**, 66.
Russell, R. W., Soifer, B. T., and Willner, S. P. 1978, *Ap. J.*, Vol. **220**, in press.
Saraph, H. E., Seaton, M. J., and Shemming, J. 1969, *Phil. Trans. Roy. Soc. London*, **264**, 77.
Telesco, C. M., and Harper, D. A. 1977, *Ap. J.*, **211**, 475.
Wiese, W. L., Smith, M. W., and Miles, B. M. 1969, *Atomic Transition Probabilities—Sodium Through Calcium*, Vol. **2**, NSRDS-NBS 22.
Willner, S. P., Soifer, B. T., Russell, R. W., Joyce, R. R., and Gillett, F. C. 1977, *Ap. J.* (*Letters*), **217**, L121.

Note added in proof.—There is a wavelength coincidence between the $v = 0$, $J = 7 \rightarrow 5$ line (6.91 μm) of H_2 and the 7 μm rise in our data. However, if the H_2 is in thermal equilibrium at a temperature comparable to the excitation temperature of the observed $v = 1$, $J = 3 \rightarrow 1$ line at 2.12 μm (Treffers, Fink, Larson, and Gautier, *Ap. J.*, **209**, 793 [1976]), molecular hydrogen emission should not contribute significantly to the flux (1×10^{-17} W cm^{-2}) in the 7 μm rise in our data. (These calculations are based on the molecular data of Fink, Wiggins, and Rank [*J. Molec. Spectrosc.*, **18**, 384 (1965)]; Gautier, Fink, Treffers, and Larson [*Ap. J.* (*Letters*), **207**, L129 (1976)]; Aannestad [*Ap. J. Suppl.*, **25**, 223 (1973)].) Nonthermal excitation mechanisms are still possible; higher resolution observations are necessary to clarify the identification of the 7 μm feature.

R. W. Russell, B. T. Soifer, and S. P. Willner: Department of Physics, C-011, University of California, San Diego, La Jolla, CA 92093

THE ASTROPHYSICAL JOURNAL, 219:114–120, 1978 January 1

SPECTROPHOTOMETRY OF OH 26.5+0.6 FROM 2 TO 40 MICRONS

W. J. FORREST,* F. C. GILLETT,† J. R. HOUCK,* J. F. MCCARTHY,* K. M. MERRILL,‡
J. L. PIPHER,§ R. C. PUETTER,‖ R. W. RUSSELL,‖ B. T. SOIFER,‖ AND S. P. WILLNER‖

Received 1977 April 22; accepted 1977 June 17

ABSTRACT

Airborne and ground-based observations show that OH 26.5+0.6 has strong 10 μm and weak 18 μm silicate absorptions superposed on an overall energy distribution much like a blackbody. The flux level, color temperature, and depth of the 10 μm absorption have varied during 2 years of observations. A model of the source as a late-type variable star that has ejected an optically thick dust shell is suggested; the mass-loss rate implied is greater than $\sim 10^{-5}\ M_\odot\ \text{year}^{-1}$. The fact that significant flux from the source is observed between 4 and 7 μm is evidence that oxygen-rich dust has significant opacity in that wavelength range.

Subject headings: infrared: sources — stars: circumstellar shells — stars: late-type — stars: mass loss

I. INTRODUCTION

The source OH 26.5+0.6 was first discovered by Andersson *et al.* (1974) to be a bright 1612 MHz OH maser source and was classified by them as a type II OH source. Quite independently, OH 26.5+0.6 was found to be a bright 10 μm infrared source, designated as CRL 2205 (Walker and Price 1975). Workers at the University of Arizona (Low *et al.* 1976) obtained an accurate position and listed the source as UOA 19, and it was one of the sources studied by Evans and Beckwith (1977). This paper reports infrared spectrophotometric observations from 2 to 40 μm of this interesting infrared/OH maser source, obtained over a 2 year period. The source is variable on time scales of months in both flux density and spectral shape.

* Cornell University.
† Kitt Peak National Observatory.
‡ University of Minnesota.
§ University of Rochester.
‖ University of California, San Diego.

II. OBSERVATIONS

The observations reported here were obtained between 1974 May 3 and 1976 June 25; a variety of telescopes and spectrometer systems have been used. The observing log is given in Table 1 and lists the observer, wavelength range, and telescope employed. The 2–4 μm, 4–8 μm, and 8–13 μm observations were all obtained with filter wheel spectrophotometers of basically the same design (Gillett and Forrest 1973), while the 16–40 μm observations were obtained with a cooled grating spectrophotometer (Forrest, Houck, and Reed 1976). All the observations were obtained with resolution $\Delta\lambda/\lambda \approx 0.01$–$0.02$ except for the 25–40 μm observations, for which $\Delta\lambda/\lambda \approx 0.08$. The telescopes used were the UCSD–University of Minnesota 1.5 m infrared telescope on Mount Lemmon, the 1.3 and 2.1 m telescopes at Kitt Peak National Observatory, and the 90 cm telescope of the Kuiper Airborne Observatory flying at an altitude of 12.5 km (41,000 feet).

The 2–40 μm spectrum of OH 26.5+0.6 obtained between 1976 May 21 and 1976 June 25 is shown in

TABLE 1

OBSERVING LOG

Date (UT)	Wavelength Range (μm)	Telescope	Aperture (arcsec)	Observer
1974 May 3.....	8–13	Mount Lemmon 1.5 m	22	K. M. M.
1974 May 21.....	8–13	Mount Lemmon 1.5 m	22	B. T. S., R. W. R.
1974 October 2.....	8–13	KPNO 2.1 m	7	F. C. G.
1975 March 24.....	2–4	Mount Lemmon 1.5 m	17	B. T. S., R. W. R.
1975 April 28.....	2–4	Mount Lemmon 1.5 m	17	B. T. S., R. W. R.
1975 May 1.....	8–13	KPNO 1.3 m	11	F. C. G.
1975 May 27.....	8–13	KPNO 2.1 m	10	J. L. P., B. T. S.
1976 May 6.....	2–4	Mount Lemmon 1.5 m	17	B. T. S., R. C. P.
1976 May 21.....	16–40	KAO 90 cm	30	J. R. H., W. J. F., J. F. McC.
1976 May 28.....	4–8	KAO 90 cm	30	B. T. S., R. W. R., S. P. W.
1976 June 20, 24.....	2–4	Mount Lemmon 1.5 m	17	K. M. M., R. W. R.
1976 June 25.....	8–13	Mount Lemmon 1.5 m	17	K. M. M., R. W. R.

Figure 1. The broad-band 8.4 μm photometry obtained on 1976 May 28 from the KAO and on 1976 June 25 from Mount Lemmon indicate that the flux at this wavelength agreed to 0.01 mag, so no normalization corrections were applied to the plotted data.

The spectrum shows several distinct features superposed on a smooth continuum that, from 2 to 4 μm, approximates a blackbody at a temperature of about 375 K, as shown in Figure 2. The most significant deviations from a smooth continuum are a deep absorption feature at 10 μm and a weaker feature near 18 μm; such features are characteristic of silicate materials. In position and shape, the 18 μm feature is similar to the emission feature seen in the Trapezium by Forrest and Soifer (1976) and Forrest, Houck, and Reed (1976). The 18 μm absorption in OH 26.5+0.6 was first detected by Simon and Dyck (1975).

There are also some very weak features that appear to be absorptions near 2.4 and 3.1 μm, although the location of the continuum is uncertain. The upper portion of Figure 2 most clearly illustrates the presence of these features. The wavelengths of the features suggest identification as gaseous CO and H_2O absorption, respectively, in a stellar photosphere (Merrill and Stein 1976). The feature near 3 μm is unlikely to be the 3.1 μm ice band absorption, because, within the dense region of the circumstellar envelope, the grain temperature is almost certainly higher than 100 K, at which temperature ice will rapidly sublime. Interstellar grains apparently cannot produce appreciable ice absorption outside the protection of dense molecular clouds (Merrill, Russell, and Soifer 1976), which are not present here.

If the 2.4 and 3.1 μm depressions are photospheric absorptions, the flux removed by these bands is a lower limit on the "unabsorbed" photospheric flux at these wavelengths. This lower limit at 2.5 μm, combined with a 3 σ upper limit (obtained 1976 May 13) of 1.7×10^{-19} W cm^{-2} μm^{-1} on the 1.65 μm flux, places a lower limit on the reddening between 1.65 and 2.5 μm of about 5.8 mag. To derive this limit, it was assumed that the temperature of the photosphere is 2000 K and that there is no photospheric absorption at 1.65 μm. A [1.65 μm] − [2.5 μm] color excess of 5.8 mag corresponds to a visual extinction of about 70 mag; a similar result is obtained from the 3.1 μm feature.

The spectra of OH 26.5+0.6 show that the source is variable both in amplitude and spectral shape. The lower spectrum in Figure 1 was obtained in late April and early May of 1975. The upper spectrum was obtained in 1976 May when the source was in a relatively bright phase; the 8 μm flux was about a factor of 2 higher than in 1975 April–May. During this period the 2–4 μm flux increased more than did the 8 μm flux, and the 2–4 μm color temperature increased from about 350 to 375 K. Also, when the flux and temperature were lower, the depth of the 10 μm silicate feature was greater by roughly 0.4 optical depths. This behavior is consistent with a model consisting of a variable star surrounded by an optically thick dust shell, as discussed below.

The observations that cover the longest time interval and best show the variability are those of the 8–13 μm spectrum. Figure 3 shows the 8–13 μm spectra obtained over 2 years. The decreasing depth of the 10 μm absorption with increasing flux is readily seen in these spectra.[1]

III. DISCUSSION

The major characteristics of OH 26.5+0.6 are the presence of a type II OH/IR source, an overall energy distribution within a factor of 3 of being like that of a blackbody, and a deep silicate absorption. These characteristics suggest a model of this object as a central star surrounded by a localized cloud of gas and dust that is optically thick at visual wavelengths and is reradiating the stellar luminosity at infrared wavelengths. The type II OH classification and luminosity variability suggest that we are observing a star in the late stages of stellar evolution that is undergoing large mass loss. That OH 26.5+0.6 is in a late stage of evolution is consistent with the absence of nearby H II regions, large molecular clouds, or young stellar objects.

a) The 10 and 18 μm Absorption Features

The 10 and 18 μm absorption bands, which are identified with the stretching and bending modes, respectively, of silicate minerals, provide useful information concerning the environment within the opaque circumstellar envelope. These absorptions are produced in a cloud of material that is colder than that producing the underlying emission. The fact that the depth of the 10 μm absorption decreases as the infrared luminosity increases is evidence that the absorbing dust is local to the energy source. It is our interpretation that the varying luminosity of the central source within the cloud modulates the dust temperature, causing the apparent change in the 10 μm absorption depth.

The 18 μm absorption is much weaker than that at 10 μm (Fig. 1), even though the absorptivities of the two features are comparable (Forrest, Houck, and Reed 1976). The weakness of the 18 μm feature probably indicates that the dust that is absorbing at 10 μm is warm enough to radiate significantly at 18 μm (Kwan and Scoville 1976). The formulation of Jones and Merrill (1976) suggests that the relative apparent depths of the features are consistent with the presence

[1] Observations obtained 1977 April 21 from Mount Lemmon give the following narrow-band flux densities: 8.00 μm, 6.0×10^{-15}; 10.0 μm, 7.1×10^{-16}; 12.5 μm, 2.6×10^{-15} W cm^{-2} μm^{-1}. Observations obtained 1977 June 22 from the KAO have a better signal-to-noise ratio than those presented in Fig. 1 and give the following flux densities: 16.0 μm, 1.45×10^{-15}; 18.5 μm, 1.10×10^{-15}; 21.0 μm, 1.05×10^{-15}; 30 μm, 5.3×10^{-16}; 38 μm, 2.6×10^{-16} W cm^{-2} μm^{-1}. These flux densities are the brightest yet observed for this object and indicate that the period, if any, is longer than 3 years. The spectral shape is similar to that shown in Fig. 2, but the 9.5 and 18.5 μm absorptions are the shallowest yet seen. The change in absorption depth is in qualitative agreement with the model suggested in § III.

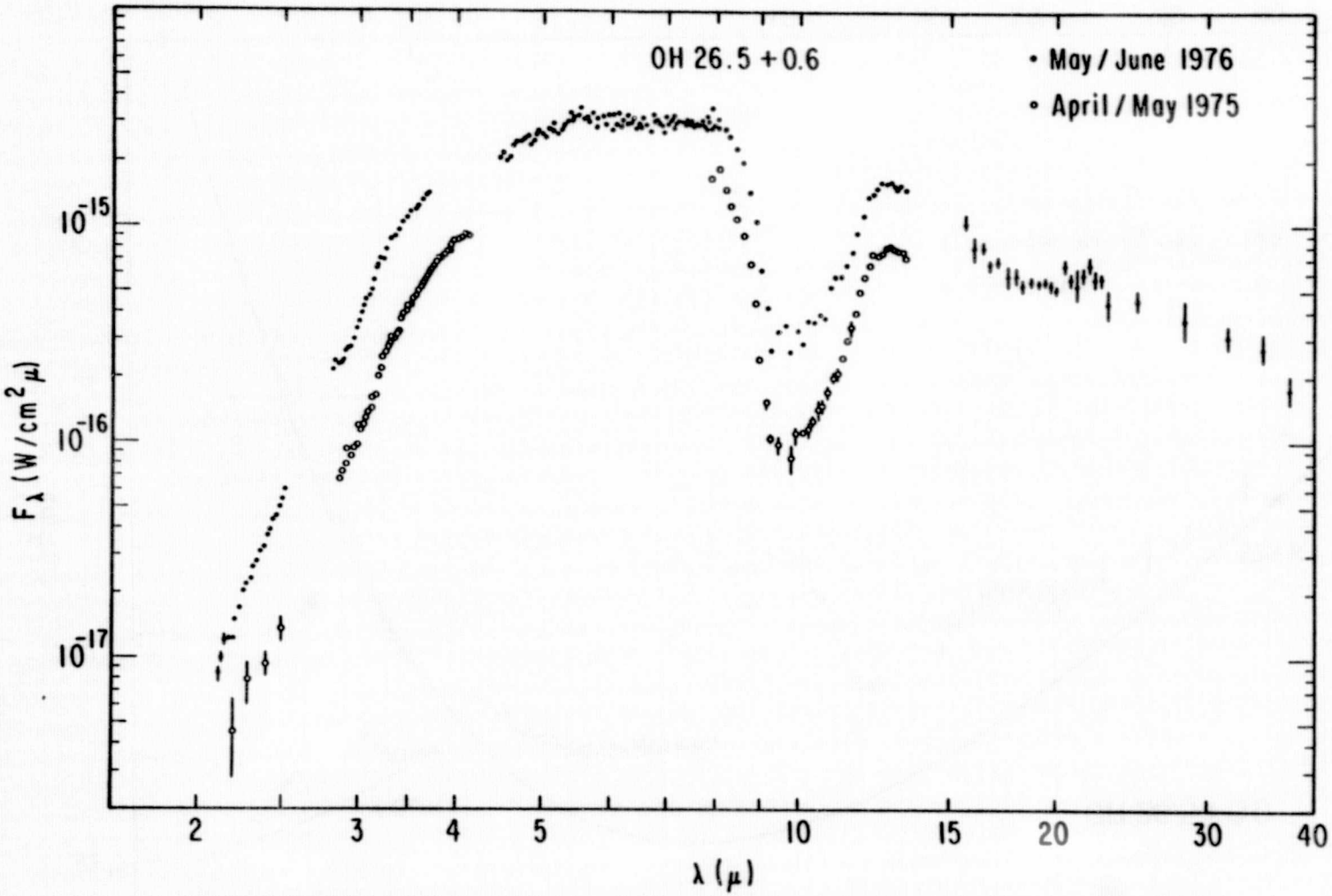

FIG. 1.—Two to 40 μm spectra of OH 26.5+0.6. Error bars are shown for points whose statistical uncertainties exceed 5%.

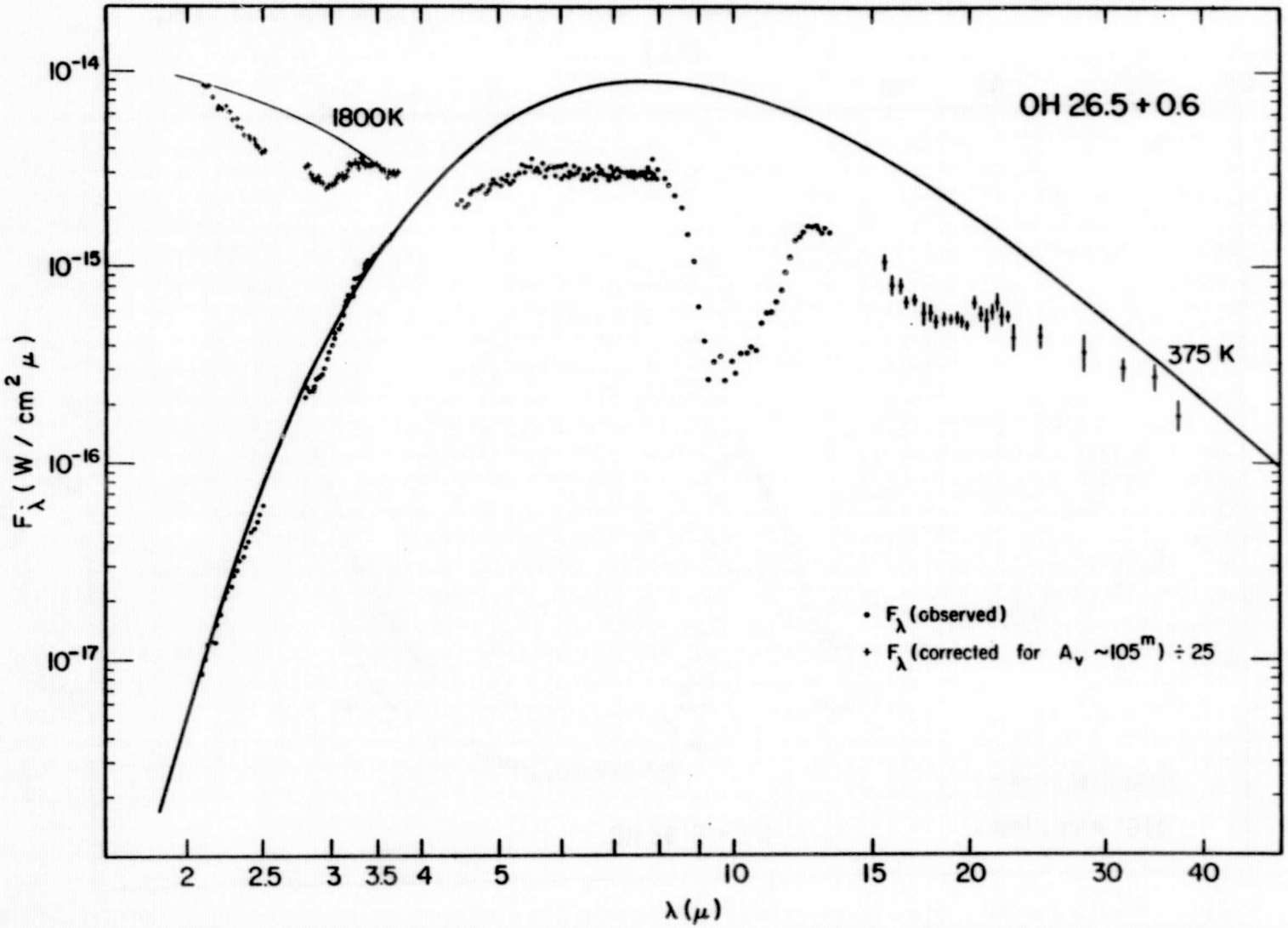

FIG. 2.—Spectrum of OH 26.5+0.6 obtained in 1976 May–June. The solid line represents a 375 K blackbody fit to the 2–4 μm data only. The pluses in the upper portion of the figure are the 2–4 μm data, corrected for an amount of reddening corresponding to $A_V = 105$ mag. The thin line represents a blackbody fit through the corrected 2.0 and 4.0 μm points. This portion of the figure is meant only to illustrate the 2.4 and 3.1 μm features; the amount of reddening was chosen arbitrarily.

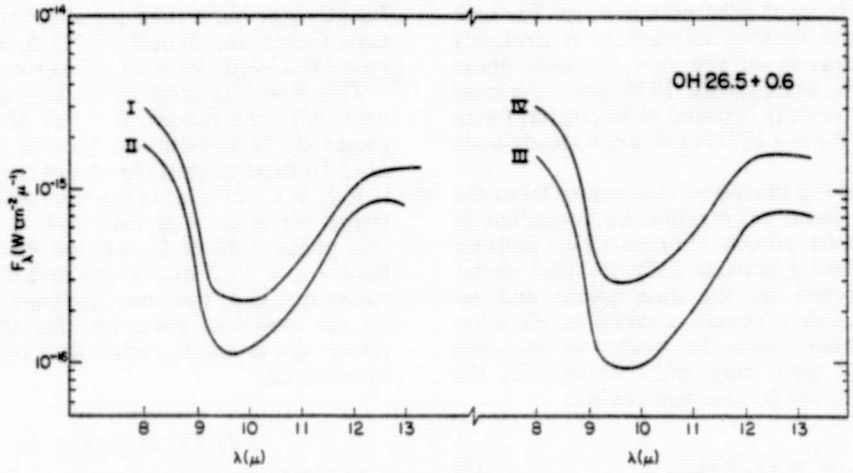

FIG. 3.—Eight to 13 μm spectra obtained at four different times. The larger apparent depth of the absorption when the source is fainter is seen. The dates of the spectra are I: 1974 May 3 and 21, II: 1974 October 2, III: 1975 May 1 and 27, and IV: 1976 June 25.

in the circumstellar envelope of substantial optical depth due to dust at $T \gtrsim 160$ K (the Wien-law temperature for an energy distribution having a maximum at 18 μm) and comparatively smaller optical depth due to colder dust.

Because the dust producing the 10 μm absorption is apparently warm enough to emit at 18 μm, it is physically unrealistic to describe the emergent spectrum from the circumstellar dust envelope as an "underlying continuum" suffering absorption from relatively cold dust. Although such a description may be useful in a qualitative or even semiquantitative sense, a complete radiative-transfer calculation (Jones and Merrill 1976; Kwan and Scoville 1976; Finn and Simon 1977) is needed. Detailed knowledge of the wavelength-dependent dust emissivity is a prerequisite for such a calculation. The spectra presented here will restrict the range of possible solutions.

Preliminary models, based on the formulation of Jones and Merrill (1976), for dust shells with 10 μm optical depths greater than 6 surrounding M-type stars produce reasonable agreement with the observed spectrum (Jones, private communication). The relative 10 and 18 μm absorption depths, the variation of apparent 10 μm optical depth with luminosity, and the weak absorption features near 2.4 and 3.1 μm can be reproduced. The agreement of the model with the observations indicates that the picture of an optically thick dust envelope surrounding a cool variable star is reasonable.

b) *Optical Depth in the Shell*

The amount of extinction A_λ through the shell at short wavelengths can be estimated from the ratio of the observed flux density F_λ to that expected from the central star alone; that is,

$$A_\lambda \geq 2.5 \log [\Omega_* B_\lambda(T_*)/F_\lambda] , \qquad (1)$$

where Ω_* is the solid angle subtended by the star and B_λ is the Planck function. T_* is the central star temperature, which is taken to be 2000 K; the result is insensitive to the temperature assumed. Equation (1) gives only a lower limit on A_λ, because circumstellar dust may contribute to the emission. The solid angle subtended by the central star may be estimated from the requirement that energy be conserved in the radiation-transfer process, so

$$\Omega_* \frac{\sigma}{\pi} T_*^4 = \int_0^\infty F_\lambda d\lambda . \qquad (2)$$

It is found that at least 7 mag of extinction are required at 2.2 μm, indicating a visual extinction $A_V \geq 80$ mag. If $A_V \geq 80$ mag, the 10 μm optical depth through the shell is $\tau_{10\,\mu m} \geq 6$ if the dust materials are similar to those in the line of sight to VI Cyg No. 12 (Gillett *et al.* 1975). The model calculations of Jones and Merrill (1976) indicate that an optical depth $\tau_{10\,\mu m} > 6$ would indeed be required to fit the observed spectrum of this source.

The very large optical depth inferred here indicates that most of the extinction must be local to the source, in agreement with the previous discussion of the 10 and 18 μm absorption features. The extinction appears to be large enough to be consistent with the identification of the 2.4 and 3.1 μm absorption features as photospheric features of a late-type star. Finally, the large optical depth implies that the mass-loss rate from this star must be quite large, as discussed below.

c) *The Mass Loss from* OH *26.5+0.6*

The strong radiation pressure exerted on the dust grains surrounding a very luminous star will accelerate the grains and associated gas and result in mass loss from the circumstellar envelope (Gehrz and Woolf 1971; Gilman 1972; Salpeter 1974). The rate at which mass is lost can be estimated from the outflow

velocity and the observed infrared spectrum. For type II OH sources, the velocity of outflow is probably one-half the separation of the two emission peaks (Elitzur, Goldreich, and Scoville 1976, and references therein); that this velocity is found to be constant with time (Wilson and Barrett 1972) indicates a steady-state mass loss.

One estimate of the mass-loss rate comes from the requirement that linear momentum be conserved in the radiation-transfer process (Forrest 1974; Salpeter 1974). The observed spectrum indicates that stellar radiation is absorbed by the dust grains and reradiated; this process produces a radial acceleration of the circumstellar shell. In order to conserve momentum in the shell, mass must be entering the shell at a rate $\dot{M}$, given by (Salpeter 1974):

$$\dot{M} \approx (\tau_s/Vc)\mathscr{L}_* , \tag{3}$$

where V is the observed final velocity, c the speed of light, $\mathscr{L}_*$ the stellar luminosity, and τ_s the effective radiation-pressure optical depth through the shell. This is part (2) of equation (11) of Salpeter (1974), with a factor of 2 correction (Salpeter, private communication) and with gravitational force ignored in comparison with the force from radiation pressure. A reasonable estimate is that $0.4\tau_{2.2\,\mu m} \leqslant \tau_s < \tau_{2.2\,\mu m}$, because the optical depth at 2.2 μm is greater than that at any longer wavelength, except for wavelengths within the 9.7 μm silicate band. For an observed outflow velocity $V \approx 13$ km s^{-1} (Andersson *et al.* 1974), a lower limit $\tau_{2.2\,\mu m} \gtrsim 7$, and a luminosity $\mathscr{L}_* \approx 10^4\,\mathscr{L}_\odot$ typical of Mira variables (Smak 1966; Lee 1970; Evans and Beckwith 1977), the mass-loss rate $\dot{M} \gtrsim 4.5 \times 10^{-5}\,M_\odot$ year^{-1}.

A second estimate of the mass-loss rate arises from the requirement that $\tau_{10\,\mu m} \geq 6$ in silicate dust through the circumstellar cloud. For radiation-pressure–driven mass loss, with all the dust condensing at a distance $R_0/r_* > 1$, the approximate mass-loss rate will be given by part (1) of equation (11) of Salpeter (1974):

$$\dot{M} = 2\pi(\tau_\lambda/f\kappa_\lambda)R_0 V , \tag{4}$$

where κ_λ is the mass opacity coefficient of the dust and f is the fraction of mass in dust. Equation (4) expresses the column density in terms of the optical depth and mass opacity at a particular wavelength, rather than in terms of wavelength-averaged quantities as in Salpeter (1974). For silicate dust, $f \leq 1/300$ for cosmic abundances, $\kappa_{9.7\,\mu m} \approx 3 \times 10^3$ cm^2 g^{-1} (Gillett and Forrest 1973), and $\tau_{9.7\,\mu m} \gtrsim 6$. Theory (Jones and Merrill 1976) and observation (Zappala *et al.* 1974) indicate that $R_0/r_* \gtrsim 3$ for stars of this type, which for $r_* = 6.5 \times 10^{13}$ cm—corresponding to $\mathscr{L}_* = 10^4\,\mathscr{L}_\odot$ and $T_* = 2000$ K—gives an estimated mass-loss rate of $\dot{M} \geq 1.5 \times 10^{-5}\,M_\odot$ year^{-1}. Within the uncertainties, this is in agreement with the previous estimate of mass loss; both estimates indicate a mass-loss rate for this star more than an order of magnitude larger than Gehrz and Woolf (1971) found for typical M-type Mira variables with thinner circumstellar shells.

The mass-loss rates found here are in good agreement with the models for type II OH/IR stars discussed by Goldreich and Scoville (1976) and Elitzur *et al.* In these models the size of the OH maser source is $R \approx 3 \times 10^{16}$ cm, so the time scale for this phase of stellar evolution is at least $R/V \approx 10^3$ years. During this phase, OH 26.5+0.6 has ejected a total of at least $\sim 2 \times 10^{-2}\,M_\odot$ in gas and dust into the interstellar medium; this mass estimate depends primarily on the model of mass loss for the source and the luminosity estimate, rather than on the details of the observations.

d) The Nature of the Dust

If OH 26.5+0.6 is a star in the process of shedding mass, then the circumstellar dust is manufactured in the shell of ejected material. The presence of silicates and OH indicates that the material is oxygen rich; presumably this material is typical of oxygen-rich material ejected into the interstellar medium. Terrestrial silicates have very little opacity shortward of 7 μm; this fact makes it difficult to fit silicates into the framework of interstellar dust, because some additional source of opacity is needed to provide the known opacity of interstellar dust for $\lambda < 7$ μm. The spectrum of OH 26.5+0.6 shows substantial emission at $\lambda < 7$ μm and indeed is within a factor of 3 of a blackbody curve from 4 to 7 μm. If the emission at these wavelengths were from the photosphere, the central star would be radiating more energy than is observed. Most of the emission must therefore come from the dust; this shows that the oxygen-rich material produced in OH 26.5+0.6 has significant opacity at these wavelengths.

e) Summary

It appears that OH 26.5+0.6 is a late-type variable star which is losing mass. The extreme thickness of the dust shell implies that the rate of mass loss is greater than $\sim 10^{-5}\,M_\odot$ year^{-1}; this rate is one of the largest known for such stars.

We thank T. Jones for discussion of radiative-transfer models and for communicating his preliminary results. The UCSD group thanks P. Brissenden and D. Pedersen for their assistance. Infrared astronomy is supported at Cornell University by NASA grant NGR 33-010-081; at the University of California, San Diego, by NASA grant NGR 05-005-055 and NSF grant AST 74-19239; at the University of Minnesota by NSF grant AST 76-21458 and NASA grant NSG-2014; and at the University of Rochester by NSF grant AST 75-22901 and NASA grant NGR 33-019-127. Kitt Peak National Observatory is operated by Associated Universities, Inc., under contract with the National Science Foundation.

REFERENCES

Andersson, C., Johansson, L. E. B., Goss, W. M., Winnberg, A., and Nguyen-Quang-Rieu. 1974, *Astr. Ap.*, **30**, 475.
Elitzur, M., Goldreich, P., and Scoville, N. 1976, *Ap. J.*, **205**, 384.
Evans, N. J., and Beckwith, S. 1977, *Ap. J.*, **217**, 729.
Finn, G. D., and Simon, T. 1977, *Ap. J.*, **212**, 472.
Forrest, W. J. 1974, Ph.D. thesis, University of California, San Diego.
Forrest, W. J., Houck, J. R., and Reed, R. A. 1976, *Ap. J. (Letters)*, **208**, L133.
Forrest, W. J., and Soifer, B. T. 1976, *Ap. J. (Letters)*, **208**, L129.
Gehrz, R. D., and Woolf, N. J. 1971, *Ap. J.*, **165**, 285.
Gillett, F. C., and Forrest, W. J. 1973, *Ap. J.*, **179**, 483.
Gillett, F. C., Jones, T. W., Merrill, K. M., and Stein, W. A. 1975, *Astr. Ap.*, **45**, 77.
Gilman, R. C. 1972, *Ap. J.*, **178**, 423.
Goldreich, P., and Scoville, N. 1976, *Ap. J.*, **205**, 144.
Jones, T. W., and Merrill, K. M. 1976, *Ap. J.*, **209**, 509.
Kwan, J., and Scoville, N. 1976, *Ap. J.*, **209**, 102.
Lee, T. A. 1970, *Ap. J.*, **162**, 217.
Low, F. J., Kurtz, R. F., Vrba, F. J., and Rieke, G. H. 1976, *Ap. J. (Letters)*, **206**, L153.
Merrill, K. M., Russell, R. W., and Soifer, B. T. 1976, *Ap. J.*, **207**, 763.
Merrill, K. M., and Stein, W. A. 1976, *Pub. A.S.P.*, **88**, 285.
Salpeter, E. E. 1974, *Ap. J.*, **193**, 585.
Simon, T., and Dyck, H. M. 1975, *Nature*, **253**, 101.
Smak, J. I. 1966, *Ann. Rev. Astr. Ap.*, **4**, 19.
Walker, R. G., and Price, S. D. 1975, "AFCRL Infrared Sky Survey," AFCRL-TR-75-0373.
Wilson, W. J., and Barrett, A. H. 1972, *Astr. Ap.*, **17**, 385.
Zappala, R. R., Becklin, E. E., Matthews, K., and Neugebauer, G. 1974, *Ap. J.*, **192**, 109.

W. J. FORREST, J. R. HOUCK, and J. F. MCCARTHY: Center for Radiophysics and Space Research, Space Sciences Building, Cornell University, Ithaca, NY 14853

F. C. GILLETT: Kitt Peak National Observatory, P.O. Box 26732, Tucson, AZ 85726

K. M. MERRILL: School of Physics and Astronomy, University of Minnesota, Minneapolis, MN 55455

J. L. PIPHER: Physics and Astronomy Department, University of Rochester, Rochester, NY 14627

R. C. PUETTER, R. W. RUSSELL, B. T. SOIFER, and S. P. WILLNER: Department of Physics, C-011, University of California, San Diego, La Jolla, CA 92093

THE ASTROPHYSICAL JOURNAL, 220:568–572, 1978 March 1

THE INFRARED SPECTRA OF CRL 618 AND HD 44179 (CRL 915)

R. W. RUSSELL, B. T. SOIFER, AND S. P. WILLNER
Department of Physics, University of California, San Diego
Received 1977 August 15; accepted 1977 August 31

ABSTRACT

Spectrophotometry from 4 to 8 μm is reported for the infrared sources CRL 618 and HD 44179 (CRL 915). In addition, 2–4 μm spectrophotometry of CRL 618 is reported. Except for marginal detection of emission lines at 2.1 and 2.45 μm, the spectrum of CRL 618 is featureless, consistent with graphite being the major constituent of the circumstellar dust cloud. Strong emission bands at 6.2 μm and 7.7 μm are found in the spectrum of HD 44179. These bands have been observed previously in NGC 7027 and M82. No positive identification of these bands is made.

While both objects probably represent advanced stages of stellar evolution, the substantial differences between CRL 618 and HD 44179 suggest that they are members of different evolutionary sequences.

Subject headings: infrared: sources — infrared: spectra — stars: individual

I. INTRODUCTION

Recent infrared, optical, and radio observations (see Zuckerman *et al.* 1976 for a review) have suggested that many bright infrared sources are at intermediate stages of stellar evolution between red giants and planetary nebulae. The distinguishing feature of these sources is their association with a visible reflection nebula. The usual model for such objects consists of a central evolved star surrounded by a disk of gas and dust that often obscures the star from view. Scattering of light from an extensive halo of circumstellar material produces the reflection nebula. If correct, this model has interesting applications for this stage of stellar evolution and for the resulting chemical abundances of interstellar matter. We report here infrared spectroscopy of two of these sources, CRL 618 and CRL 915 = HD 44179. Both were originally discovered in the AFCRL sky survey (Walker and Price 1975) and may belong to the evolutionary sequence suggested by Zuckerman *et al.* (1976).

CRL 618 was observed in detail by Westbrook *et al.* (1976), who found the infrared source to be located between two optical nebulosities. The spectra of the optical nebulae indicated that they are reflection nebulae; the central illuminating star was estimated (Westbrook *et al.*) to be of spectral type ~B0. The infrared source was interpreted as a dust cloud that obscures the exciting star from direct view. From the size of the infrared source and the apparent color temperature, Westbrook *et al.* estimated the 10 μm optical depth to be ~0.3; however, the errors in the source size allow $\tau \geqslant 1$. The 8–13 μm spectrum of CRL 618 was found to be featureless and to fit a 275 K blackbody comparatively well.

CRL 915/HD 44179 was investigated in detail by Cohen *et al.* (1975, hereafter CAZ), who named it the "Red Rectangle." Further optical observations of this object were reported by Greenstein and Oke (1977). Morphologically, this is extremely similar to CRL 618—an infrared source centrally located in a biconical reflection nebula. CAZ suggest that the spectrum of the nebulosity indicates that the spectral type of the central star is B9–A0. However, Greenstein and Oke point out that the spectral type is not easily evaluated and could range from late B to F. The color temperature of the infrared source is ~500 K, and there is no size information on the infrared source except that the diameter $\theta \leqslant 4''$. The appearance in the infrared spectra of several strong emission bands, interpreted by CAZ as being due to resonance bands in dust particles, suggests that the emission is not optically thick. Greenstein and Oke report a remarkably strong emission band at 0.658 μm in the spectrum of the reflection nebula. They interpret this as being due to a strong peak in the reflectivity of the dust in the nebula.

The data reported here are spectrophotometric observations from 4 to 8 μm of these two interesting infrared sources. These observations were made in 1976 November using the 0.9 m telescope of the Kuiper Airborne Observatory flying at ~12.5 km altitude. In addition, we report a 2–4 μm spectrum of CRL 618 obtained at the Mount Lemmon Observatory.

II. THE OBSERVATIONS

The 4–8 μm observations used the filter-wheel system described by Russell and Soifer (1977) with a Si:As detector. The spectral resolution was $\Delta\lambda/\lambda \approx 0.015$, the observing aperture for these observations was 28″, and the chopper amplitude was ~42″. The star α Tau, observed as a calibration standard, was assumed to have a blackbody spectrum at the temperature of 3800 K, except that allowance was made for CO absorption near 5 μm determined from broadband measurements (Forrest 1974).

The 2–4 μm observations of CRL 618 were obtained in 1976 March and September with the system described by Merrill, Soifer, and Russell (1975). The spectral resolution was $\Delta\lambda/\lambda \approx 0.02$. A 17″ focal plane aperture and a 30″ chopper amplitude were used.

a) CRL 618

The 2–13 μm spectrum of CRL 618 is shown in Figure 1. The spectrum of CRL 618 is remarkably featureless, following quite closely the 275 K blackbody curve estimated by Westbrook *et al.* (1975) from their spectral and broad-band observations. There is an excess over the blackbody emission at shorter wavelengths, suggesting that a range of temperatures is present.

The only spectral features of apparent significance are possible emission lines at 2.12 and 2.45 μm. Both lines appear as roughly 3 σ deviations from the continuum and cannot be claimed to be positive detections. Further observations to confirm these lines are essential. If these are real lines, the best identifications are with vibration-rotation lines of H_2 that have been previously detected in the BN source (Gautier *et al.* 1976) and NGC 7027 (Treffers *et al.* 1976). A molecular cloud is known to be associated with this source (Lo and Bechis 1976). No discussion of H_2 is warranted, pending confirmation of its detection.

b) HD 44179

The 2–13 μm spectrum of HD 44179 is shown in Figure 2. The 8–13 μm data are taken from CAZ and

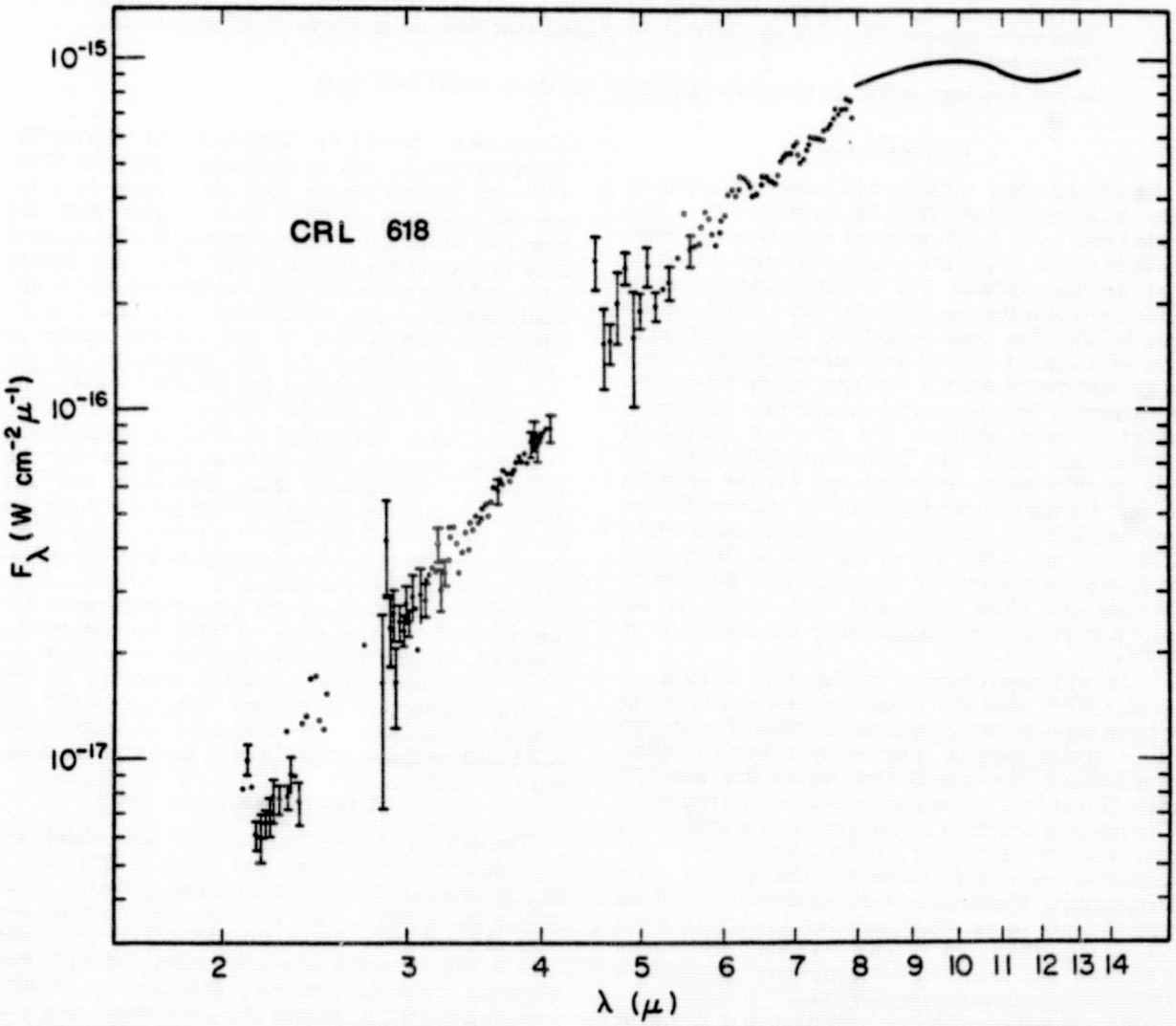

FIG. 1.—The 2–13 μm spectrum of CRL 618. The 2–4 μm data were obtained from Mount Lemmon and the 4–8 μm data from the KAO. Data from 8–13 μm were taken from Westbrook *et al.* (1975), who used a 22″ aperture for their observations. Statistical uncertainties ($\geq$ 8%) are plotted in the figure.

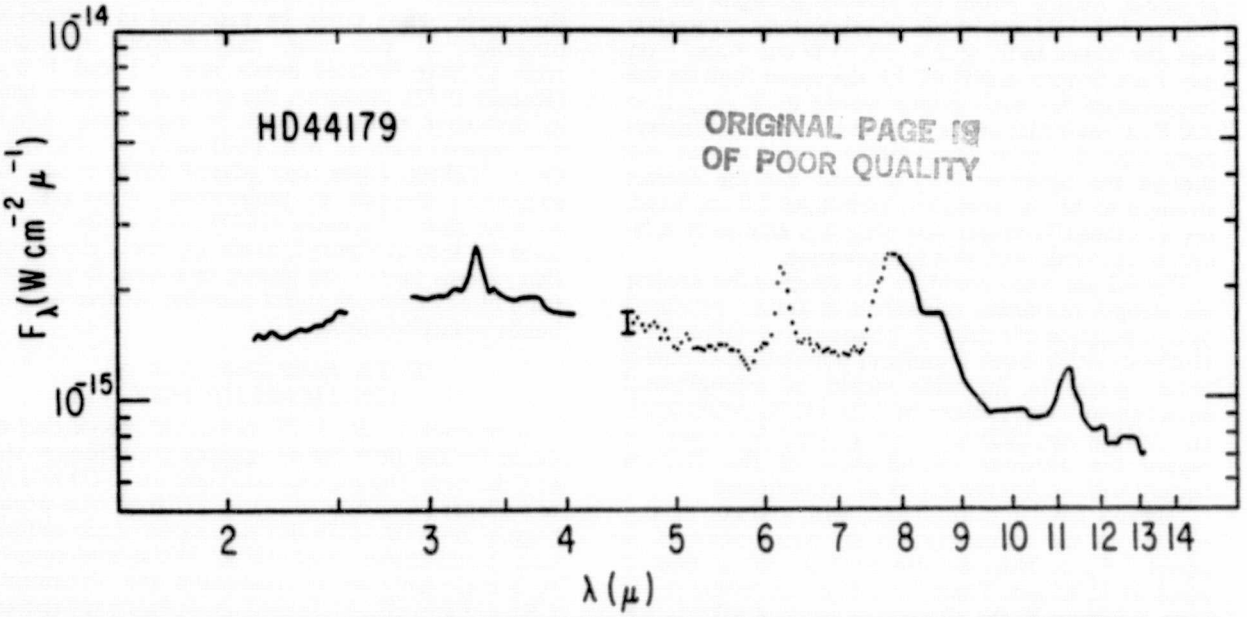

FIG. 2.—The 2–13 μm spectrum of HD 44179 (CRL 915). The 4–8 μm data were smoothed by averaging adjacent points—a typical statistical error is shown on the first data point. The shape of the 2–4 μm data, obtained with a 17″ aperture, was taken from Russell, Soifer, and Merrill (1977), and the level was normalized to the 2.28 μm broad-band flux level measured from the KAO. The ~20% lower level of the airborne data compared with the ground-based data may have been due to the presence of a faint star in one reference beam during the airborne observations. The 8–13 μm data, obtained with a 22″ aperture, were taken from Cohen *et al.* (1975), with no adjustment of the level.

the 2–4 μm spectrum is taken from Russell, Soifer, and Merrill (1977). The 4–8 μm portion of the spectrum shows a very strong continuum and two emission features that are well above the continuum at 6.2 and 7.7 μm. Both of these bands have been observed in the 4–8 μm spectra of NGC 7027 (Russell, Soifer, and Willner 1977) and M82 (Willner *et al.* 1977). The origin of these bands is discussed below.

The strong continuum emission of HD 44179 is most easily interpreted as thermal emission by circumstellar dust (CAZ). This emission is broader than that from a single temperature blackbody and suggests a significant range of temperatures in the dust cloud. The fact that this range of temperatures is detectable requires either that the dust cloud be optically thin throughout the infrared, or that an optically thick disk be viewed nearly face-on. CAZ interpret the polarization observations as requiring that the dust disk be viewed nearly edge-on, which seems to rule out the optically thick cloud. Further support for the optically thin estimate comes from the appearance of the spectral features. The line-to-continuum ratio for these bands is much less in HD 44179 than in M82 or NGC 7027, and yet the shapes are so similar as to be indistinguishable at our resolution. This is most easily understood if the emission in HD 44179 is optically thin.

The angular size of the cloud can be estimated from the assumption that the brightness temperature is no higher than the color temperature $T_c \approx 500$ K. This requires that the angular diameter be greater than 0.1″. The diameter of the cloud should be larger than this, because the geometry is highly nonspherical and the cloud appears to be optically thin. Indeed, the size of the infrared source should be extremely wavelength-dependent, because the heat source is the central star. Angular size measurements of HD 44179 at 2 μm and 10 μm with spatial resolution less than 1″ would be extremely valuable in determining the characteristics of the dust cloud.

III. DISCUSSION

a) Spectral Features

The spectral features found in HD 44179 at 6.2 μm and 7.7 μm have previously been found in the spectra of NGC 7027 and M82. These bands, along with those at 3.3, 8.7, and 11.3 μm are common to all three objects. Many other sources, such as CRL 437 (Kleinmann *et al.* 1977), NGC 253 (Gillett *et al.* 1975), and CRL 3053 (Gillett, Joyce, and Merrill 1978), have been found to possess the 3.3 μm, 8.7 μm, and 11.3 μm bands and a spectrum sharply rising to short wavelengths at 8 μm, suggestive of the peak at 7.7 μm. It is therefore likely that the 6.2 μm and 7.7 μm bands are common to these objects as well.

Russell, Soifer, and Willner (1977) and Willner *et al.* (1977) have suggested that the wide range of temperature, density, and excitation conditions under which these bands are observed argue for resonances of some sort in the dust that is present in these objects. The hypothesis of solid-state bands has the drawback that the materials that produce the bands are unknown. Gillett, Forrest, and Merrill (1973) suggested that the 11.3 μm band is produced by thermal

emission from small carbonate dust grains. This identification predicts a much stronger band centered at about 7.0 μm. From the relative strengths of the 7.0 μm and 11.3 μm bands in laboratory carbonates and the upper limit of 2×10^{-16} W cm^{-2} μm^{-1} on any 7 μm feature in HD 44179, the upper limit on the temperature for such grains would be $T_{\text{carbonates}} < 200$ K, a result that seems to be in substantial disagreement with the color temperature of this source. Although the observed 7.7 μm band has the correct strength to be the predicted carbonate 7.0 μm band, the substantially longer wavelength is extremely difficult to reconcile with this identification.

The 6.2 μm band could be the sought-after shorter wavelength resonance of carbonate grains, produced by a population of extremely oblate grains (Gilra 1977; Huffman 1977). Such a uniform population of purely oblate grains in the wide variety of astrophysical environments represented by HD 44179, NGC 7027, and M82 is very difficult to understand. We therefore regard the previous identification of the 11.3 μm feature with carbonate grains as unconfirmed.

Nitrates have a strong band, with a shape similar to that of the carbonate 7.0 μm band, centered at about 7.5 μm. Nitrates also have a strong, narrow band at 11.95 μm. There is little or no evidence for such a feature in the 10 μm spectrum of HD 44179, and no evidence for such a band in NGC 7027. We therefore regard the identification of the 7.7 μm feature with nitrates as unlikely.

The 6.2 μm feature is another strong, partially resolved band that appears in the spectrum of HD 44179, NGC 7027, and M82. The agreement in wavelength of this feature among the three sources is better than 1%. The variety of physical conditions under which it is found argues for a solid-state resonance. There is wavelength agreement with a narrow water-of-hydration band (Hunt, Wisherd, and Bonham 1950; Nyquist and Kagel 1971); however, we regard this as an unlikely identification because thermal dust temperatures in HD 44179 are high enough that hydrated material should not exist. The 6.2 μm feature must therefore join the other bands heretofore discussed as being currently unidentified.

There are now five infrared bands at 3.3 μm, 6.2 μm, 7.7 μm, 8.7 μm, and 11.3 μm that appear in emission in a variety of celestial sources, but are not identified with bands of terrestrial minerals. In addition, the strong band at 0.658 μm in HD 44179 (CAZ; Greenstein and Oke 1977) is probably associated with the dust and further complicates the understanding of the material. Current work in our laboratory (Russell 1978) indicates that the emissivities of small particles are reasonably represented by previous laboratory data on larger particles. Thus particle size effects alone appear not to be responsible for the lack of identification to date.

The infrared bands seem to appear together in sources where an ultraviolet radiation field is present. Tests of fluorescence emission, suggested by Gillett (1977) as a possible explanation of some of these bands, are under way and may permit a more positive statement about whether this effect can produce bands at the observed wavelengths.

Knacke (1977) and Field (1977) have suggested that these bands might be produced in carbon-rich materials; in particular, carbonaceous chondrites seem to have infrared bands near 3.3 and 11.3 μm (Knacke 1977). However, the presence of these bands as dominant emission bands in apparently oxygen-rich regions such as M82 (Willner *et al.* 1977) and Orion (Gillett, Joyce, and Merrill 1978) makes this suggestion difficult to understand. Moreover, the 4–14 μm data of Knacke (1977) show additional features not seen in Figure 2, in the spectra of the oxygen-rich regions mentioned above, or indeed in the spectrum of any celestial object showing the five emission bands discussed earlier.

b) The Evolutionary State of CRL 618 and HD 44179

Westbrook *et al.* (1975) presented convincing evidence for the post–main-sequence evolutionary stage of CRL 618. The high galactic latitude (12°) and lack of evidence of associated young stellar objects strongly suggest that HD 44179 also is in a post–main-sequence state (Zuckerman *et al.* 1976). While this seems to be a reasonably secure conclusion, the placement of CRL 618 and HD 44179 into an evolutionary sequence is far more difficult.

CRL 618 is probably near the end point of the carbon-rich sequence of stellar evolution into planetary nebulae. The lack of spectral features in the thermal emission argues for graphite's being the dominant dust component in the circumstellar shell. The continuous spectrum is common in post–main-sequence carbon-rich objects such as IRC +10216, CRL 2688, etc. The end point of this evolutionary sequence could be represented by a planetary nebula, such as IC 418, that has evidence for SiC emission from 10 to 12 μm (Willner *et al.* 1978) and lacks the strong unidentified bands found in HD 44179 (except possibly for the 3.3 μm band [Russell, Soifer, and Merrill 1977]).

HD 44179 is difficult to fit into an evolutionary sequence that includes CRL 618. The later spectral type of the star and higher infrared color temperature imply that HD 44179 is less evolved than CRL 618, but the infrared spectral features present in HD 44179 suggest that the dust cloud is optically thin and therefore at a later evolutionary stage than CRL 618, if the compositions are the same. Alternatively, the distinct differences in the infrared spectra of CRL 618 and HD 44179 could suggest real compositional differences in the circumstellar shells. The ratio of ^{12}CO antenna temperature (Lo and Bechis 1976) to infrared flux is substantially less for HD 44179 compared with CRL 618, again suggesting a compositional difference (Zuckerman *et al.* 1977).

Since the infrared spectra of HD 44179 and NGC 7027 are so similar, we would expect that these objects have similar dust compositions, and they might therefore be part of an evolutionary sequence distinct from the carbon-rich sequence. Whether this is the case, or whether we are seeing different forms of

carbon-rich material in these two different objects, will ultimately be decided with the identification of the many strong infrared bands in the spectra of objects such as HD 44179.

We gratefully acknowledge the excellent support of the entire Kuiper Airborne Observatory staff. We thank J. D. Bregman, F. C. Gillett, and K. M. Merrill for several helpful discussions. Infrared astronomy at UCSD is supported by NASA grant NGR 05-005-055 and NSF grant AST 74-19239. The UCSD–UM observing facility at Mount Lemmon is supported by the National Science Foundation.

REFERENCES

Cohen, M., *et al.* 1975, *Ap. J.*, **196**, 179 (CAZ).
Field, G. B. 1977, IAU Symposium 76, Concluding Summary, to be published.
Forrest, W. J. 1974, Ph.D. thesis, University of California, San Diego.
Gautier, T. N., III, Fink, U., Treffers, R. R., and Larson, H. P. 1976, *Ap. J.* (*Letters*), **207**, L129.
Gillett, F. C. 1977, private communication.
Gillett, F. C., Forrest, W. J., and Merrill, K. M. 1973, *Ap. J.*, **183**, 87.
Gillett, F. C., Joyce, R. R., and Merrill, K. M. 1978, in preparation.
Gillett, F. C., Kleinmann, D. E., Wright, E. L., and Capps, R. W. 1975, *Ap. J.* (*Letters*), **198**, L65.
Gilra, D. P. 1977, private communication.
Greenstein, J. L., and Oke, J. B. 1977, *Pub. A.S.P.*, **89**, 131.
Huffman, D. R. 1977, *Advances in Physics*, in press.
Hunt, J. M., Wisherd, M. P., and Bonham, L. C. 1950, *Anal. Chem.*, **22**, 1478.
Kleinmann, S. G., Sargent, D. G., Gillett, F. C., Grasdalen, G. L., and Joyce, R. R. 1977, *Ap. J.* (*Letters*), **215**, L79.
Knacke, R. F. 1977, preprint.
Lo, K. Y., and Bechis, K. P. 1976, *Ap. J.* (*Letters*), **205**, L21.
Merrill, K. M., Soifer, B. T., and Russell, R. W. 1975, *Ap. J.* (*Letters*), **200**, L37.
Nyquist, R. A., and Kagel, R. O. 1971, *Infrared Spectra of Inorganic Compounds* (New York: Academic Press).
Russell, R. W. 1978, in preparation.
Russell, R. W., and Soifer, B. T. 1977, *Icarus*, **30**, 282.
Russell, R. W., Soifer, B. T., and Merrill, K. M. 1977, *Ap. J.*, **213**, 66.
Russell, R. W., Soifer, B. T., and Willner, S. P. 1977, *Ap. J.* (*Letters*), **217**, L149.
Treffers, R. R., Fink, U., Larson, H. P., and Gautier, T. N., III. 1976, *Ap. J.*, **209**, 793.
Walker, R., and Price, S. D. 1975, *AFCRL Infrared Sky Survey*, Report No. AFCRL-TR-75-0373.
Westbrook, W. E., Becklin, E. E., Merrill, K. M., Neugebauer, G., Schmidt, M., Willner, S. P., and Wynn-Williams, C. G. 1975, *Ap. J.*, **202**, 407.
Willner, S. P., Jones, B., Russell, R. W., and Soifer, B. T. 1978, in preparation.
Willner, S. P., Soifer, B. T., Russell, R. W., Joyce, R. R., and Gillett, F. C. 1977, *Ap. J.* (*Letters*), **217**, L121.
Zuckerman, B., Gilra, D. P., Turner, B. E., Morris, M., and Palmer, P. 1976, *Ap. J.* (*Letters*), **205**, L15.
Zuckerman, B., Palmer, P., Morris, M., Turner, B. E., Gilra, D. P., Bowers, P. F., and Gilmore, W. 1977, *Ap. J.* (*Letters*), **211**, L97.

Note added in proof.—Recent ground-based observations at 2.28 μm ($\Delta\lambda = 0.5\ \mu$m) of the field near HD 44179 failed to reveal any source strong enough to account for the level difference noted in Fig. 2. Short-wavelength variability of the source may account for the difference in levels.

R. W. Russell, B. T. Soifer, and S. P. Willner: Department of Physics, C-011, University of California, San Diego, La Jolla, CA 92093

THE ASTROPHYSICAL JOURNAL, 223:L93–L95, 1978 July 15

INFRARED SPECTRA OF HM SAGITTAE AND V1016 CYGNI

R. C. PUETTER, R. W. RUSSELL, B. T. SOIFER, AND S. P. WILLNER
Department of Physics, University of California, San Diego
Received 1978 February 27; accepted 1978 April 21

ABSTRACT

Spectrophotometry of HM Sge from 2 to 13 μm is presented along with 2 to 4 μm spectrophotometry of V1016 Cyg. From 2.5 to 8 μm, the spectrum of HM Sge can be represented by a 950 K blackbody, and a strong silicate emission feature is seen from 8 to 13 μm. Both HM Sge and V1016 Cyg show evidence for CO absorption at 2.3 μm. It is suggested that the infrared radiation from these objects arises from a combination of emission by optically thin dust and by the reddened photosphere of a cool star.

Subject headings: infrared: spectra — stars: circumstellar shells

I. INTRODUCTION

The object known as HM Sge was originally reported by Dokuchaeva (1976) to have undergone a remarkable brightening from $V \sim 16$ mag to $V \sim 12$ mag in less than 6 months. Optical spectroscopy (Stover and Sivertsen 1977) of this object revealed its remarkable emission-line nature and pointed out its spectroscopic similarity to planetary nebulae. Davidson, Humphreys, and Merrill (1978, hereafter DHM), Ciatti, Mammano, and Vittone (1977), and Wallerstein (1978) obtained further optical spectroscopy of HM Sge, as well as photometric observations from 0.3 to 20 μm (DHM). The analysis of DHM and Ciatti *et al.* showed that the emission lines were produced in a region of moderately high ($n_e \sim 10^6$–10^8) density at a relatively high excitation level. DHM also found that HM Sge was a very strong infrared source, consisting of a ~1000 K blackbody spectrum with a 10μm emission band superposed. They suggested that the infrared spectrum and photometric history of HM Sge are similar to those of the symbiotic star V1016 Cyg. The optical spectrum of HM Sge is also similar to that of V1016 Cyg (Ciatti, Mammano, and Vittone 1977; FitzGerald and Pilavaki 1974). In this *Letter* we report observations of the 2–13 μm spectrum of HM Sge and the 2–4 μm spectrum of V1016 Cyg. These data also suggest a symbiotic nature for these stars.

II. OBSERVATIONS

All of the observations reported here were obtained with circular variable filter spectrometers. In all cases the spectral resolution was $\Delta\lambda/\lambda \sim 0.015$–$0.02$. The 2–4 μm spectra were obtained with the UCSD–University of Minnesota 1.5 m telescope at Mount Lemmon and a beam size of 17″. The spectrum of HM Sge was obtained on 1977 September 30 and that of V1016 Cyg on 1975 May 2. The 4–8 μm spectrum of HM Sge was obtained by using the 0.9 m telescope on board the Kuiper Airborne Observatory on a flight on 1977 July 2. Except for the use of a PbSnTe photovoltaic detector, the system was as described by Russell, Soifer, and Willner (1977). The beam size was 28″. The 8–14 μm spectrum was obtained on 1977 October 1 at Mount Lemmon with a 17″ beam size. There is no evidence that either star is extended on the scale of the beam sizes used.

The 2–13 μm spectrum of HM Sge is shown in Figure 1. The 4–8 μm spectrum was normalized by adjusting the 8.4 μm broad-band data obtained on the KAO to the same level as obtained at Mount Lemmon. This required a 20% increase in the 4–8 μm fluxes. The spectrum is continuous, showing no evidence for atomic line emission and none of the unidentified spectral features seen in NGC 7027 (Russell, Soifer, and Willner 1977). The 10 μm emission band (DHM) has the same shape as the silicate emission feature seen in the spectra of many late-type stars (Forrest, Gillett, and Stein 1975). Possible absorption features are seen near 2.3, 3.1, and 4.7 μm. Figure 1 also shows the 2–4 μm spectrum of V1016 Cyg. The only significant feature is a weak absorption near 2.3 μm.

The data on HM Sge are well fitted from 2.5 to 8 μm by a blackbody at a temperature $T_d \approx 950$ K, with an excess at shorter wavelengths. The photosphere of the star seen in visible light cannot contribute significantly to this spectrum because the observed flux density is much greater than an extrapolation of the level attributed to the stellar continuum by DHM. Also, the inferred visual extinction would be $A_V \gtrsim 11$ mag if $T_* \gtrsim 2500$ K, much greater than the $E_{B-V} \approx 0.8$ suggested by DHM.

For $\lambda > 7.8$ μm there is a clear excess over the best-fit blackbody spectrum. The observed flux at the peak (9.5 μm) is a factor of ~4 greater than expected from the blackbody spectrum, in agreement with the measurement of DHM. The shape of the excess suggests that the emission is due to silicate dust that is not optically thick. The peak flux occurs at a slightly shorter wavelength than that seen in the spectra of most late-type stars or the Orion Trapezium (Forrest, Gillett, and Stein 1975). The difference is consistent with the dust

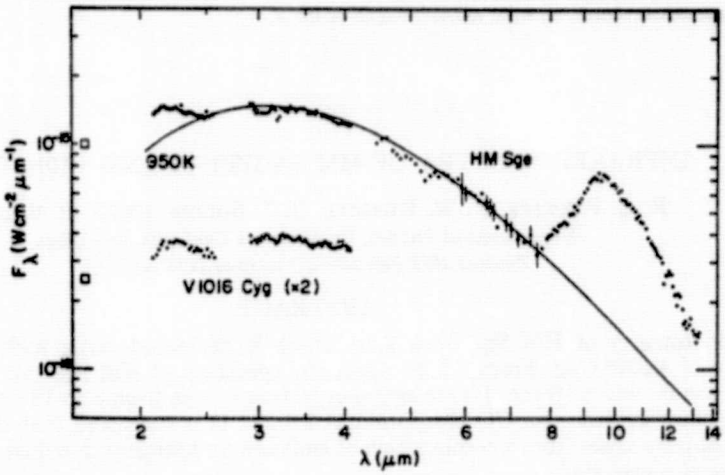

FIG. 1.—The 2 to 13 μm spectrum of HM Sge and the 2 to 4 μm spectrum of V1016 Cyg. The squares represent broad-band measurements at 1.65 μm. The solid line represents a 950 K blackbody. Error bars are shown for points whose statistical uncertainties exceed 5%.

particles having a temperature higher than the sources observed by Forrest *et al.*

III. DISCUSSION

It has been proposed (e.g., Stover and Sivertsen 1977; Kwok, Purton, and FitzGerald 1978) that HM Sge and V1016 Cyg are single stars in the process of becoming planetary nebulae. The infrared emission would then arise from dust surrounding the hot star whose presence is inferred from the optical forbidden lines and continuum. It has also been suggested that HM Sge (DHM), like V1016 Cyg (Harvey 1974), is a symbiotic binary containing a late-type star that is losing mass. The infrared data appear inconsistent with the model of HM Sge as a single hot star, for the following reasons.

Dust emission alone is probably not sufficient to account for the entire infrared energy distribution of HM Sge. If the infrared emission arises solely from heated dust having an emissivity which is proportional to a negative power of the wavelength, either the wrong slope is obtained between 4 and 8 μm, or the observed flux is significantly above the predicted value for wavelengths shorter than 3.5 μm. Dust with a gray emissivity would not explain the 1.65 to 2.5 μm emission (see Fig. 1) unless $T_d > 1000$K, at which temperature the grains are in danger of evaporating. An optically thick ($\tau \gtrsim 1$ at all wavelengths) dust shell is ruled out by the strength of the silicate emission (Jones and Merrill 1976) and by the estimate of the visual reddening of $E_{B-V} \approx 0.8$ (DHM).

The depression of the spectrum near 2.3 μm and possible depressions near 3.1 and 4.8 μm provide direct evidence for the presence of a late-type star. These features are attributed to photospheric absorption by CO (2.3 and 4.8 μm) and H_2O (3.1 μm). The 2.3 μm feature is also seen in the spectrum of V1016 Cyg. These features would not be expected to occur in a dust shell surrounding a hot star, such as is required to produce the optical spectrum.

The infrared flux of V1016 Cyg varies regularly with a period near 450 days; this behavior was also cited as evidence that the major portion of the infrared luminosity arises from an M star (Harvey 1974). Our observations, in combination with those of DHM, suggest that HM Sge may also be variable at infrared wavelengths. Table 1 indicates the broad-band photometry reported by DHM and our data. The strongest evidence for a slight 15%–20% variation is the comparison of the 1977 June 9 and October 1 data which were obtained with the same system and by using the same calibration source. Long-term monitoring of HM Sge is desirable to determine whether the variations are periodic.

A model of HM Sge as a binary containing a dust-embedded cool star as well as the optically observed

TABLE 1

BROAD-BAND MAGNITUDES OF HM SAGITTAE

	77/6/9 (DHM)	77/7/1 (KAO)	77/10/1
2.3 μm.....	+3.83±0.03 typ.	...	+3.61±0.05
3.5 μm.....	+1.94	...	+1.74
4.9 μm.....	+1.00	...	+0.85
8.4 μm.....	−0.65	−0.53±0.1	−0.73
11.2 μm.....	−1.59	...	−1.74

hot star is consistent with the infrared observations. In such a model, the infrared flux is due to a combination of dust emission and emission from the reddened photosphere of the cool star. The model of Jones and Merrill (1976) having $\tau(10\ \mu m) = 1$, $\alpha = 2$ qualitatively fits the observed data; the fit would be greatly improved if they had assumed a higher emissivity for "dirty silicates" near 2 μm. In this model, much of the flux from 1 to 3 μm comes from the photosphere of the late-type star. If the infrared luminosity of HM Sge is $10^4\ L_\odot$, typical of late-type variable stars (Smak 1966), the observed flux of 10^{-7} ergs s^{-1} cm^{-2} (DHM) implies a distance of the order of 2 kpc.

Mass loss from the cool star could provide some of the material that is ionized by the hot star. A constant mass-loss rate of $10^{-5}\ M_\odot$ yr^{-1} at a velocity of 20 km s^{-1} (Wallerstein 1978) implies a density of 10^5 cm^{-3} at a radius from the cool star of 10^{16} cm, the suggested size of the ionized region in HM Sge (DHM). The density would rapidly increase nearer the cool star, giving rise to the density gradient implied by the radio observations (Feldman *et al.* 1977). The infrared and radio observations alone thus do not appear to require that any material have been ejected from the hot star. The observations of the widths of the emission lines in HM Sge (Wallerstein 1978) and the blueshifted component of the optical emission lines in V1016 Cyg (FitzGerald and Pilavaki 1974) probably imply mass loss from the hot star, but such mass loss is required to contribute only a small fraction of the total amount of material surrounding the two stars.

In contrast to the strong optical forbidden emission-line spectrum, the infrared spectrum of HM Sge shows no evidence for any atomic fine-structure lines as observed in planetary nebulae and H II regions. Table 2 indicates upper limits to lines that might be expected. Also given in Table 2 are the electron densities at which each line is significantly decreased in strength relative to the free-free continuum due to collisional de-excitation. For the range of densities discussed for HM Sge, i.e., $n_e \approx 10^6$–10^8 cm^{-3} (DHM; Ciatti *et al.*), the nondetection of these lines is consistent with cosmic abundances of these elements.

One of the unique features of HM Sge and V1016 Cygni is their sudden increase in optical brightness and the fact that they have managed to stay bright ever since. Because the infrared flux appears to arise primarily from a cool companion to the hot ionizing star, our observations do not address this intriguing question.

TABLE 2

UPPER LIMITS ON FORBIDDEN LINES IN HM SAGITTAE

Ion	λ	Flux (ergs cm^{-2} s^{-1})	n_e (crit)* (cm^{-3})
Ar^+	6.98	$<10^{-10}$	2.2×10^6
Ar^{++}	8.99	$<6\times10^{-11}$	5.0×10^5
S^{+++}	10.52	$<6\times10^{-11}$	3.9×10^5
Ne^+	12.81	$<6\times10^{-11}$	7.6×10^5

* At $T_e = 20{,}000$ K.

IV. CONCLUSIONS

The infrared spectrum of HM Sge appears to arise from a combination of emission from heated dust and from a reddened, cool stellar photosphere. Evidence for the presence of a cool star comes from the shape of the continuum, the presence of features at 2.3 and possibly 3.1 and 4.8 μm, and the possible infrared variability. HM Sge is remarkably similar to the symbiotic variable V1016 Cyg. Both stars should be monitored to determine the nature of future changes.

We thank P. A. Feldman and S. Kwok for discussions of the radio observations and of the single-star model of HM Sge, and T. R. Gosnell for assisting with the reduction of the ground-based data. We also thank the entire staff of the KAO for their many varied and vital roles in the task of obtaining the airborne observations, including an extra effort by T. Mathieson (without which the data-acquisition system would not have been functional). Finally, we thank F. C. Gillett of Kitt Peak National Observatory for the loan of the PbSnTe detector. The airborne observations were supported by NASA under grant NGR 05-005-055 and the ground-based observations by the National Science Foundation under grant AST 76-82890.

REFERENCES

Ciatti, F., Mammano, A., and Vittone, A. 1977, *Astr. Ap.*, **61**, 459.
Davidson, K., Humphreys, R. M., and Merrill, K. M. 1978, *Ap. J.*, **220**, [illegible] (DHM).
Dokuchaeva, O. D. 1976, *Infor. Bull. Variable Stars*, No. 1189.
Feldman, P. A., Purton, C. R., Ryle, M., and Seaquist, E. R. 1977, *Bull. AAS*, **9**, 600.
FitzGerald, M. P., and Pilavaki, A. 1974, *Ap. J. Suppl.*, **28**, 147.
Forrest, W. J., Gillett, F. C., and Stein, W. A. 1975, *Ap. J.*, **195**, 423.
Harvey, P. M. 1974, *Ap. J.*, **188**, 95.
Jones, T. W., and Merrill, K. M. 1976, *Ap. J.*, **209**, 509.
Kwok, S., Purton, C. R., and FitzGerald, P. M. 1978, *Ap. J. (Letters)*, **219**, L125.
Russell, R. W., Soifer, B. T., and Willner, S. P. 1977, *Ap. J. (Letters)*, **217**, L149.
Smak, J. I. 1966, *Ann. Rev. Astr. Ap.*, **4**, 19.
Stover, R. J., and Sivertsen, S. 1977, *Ap. J. (Letters)*, **214**, L33.
Wallerstein, G. 1978, *Pub. A.S.P.*, **90**, in press.

R. C. PUETTER, R. W. RUSSELL, and S. P. WILLNER: Department of Physics, C-011, University of California, San Diego, La Jolla, CA 92093

B. T. SOIFER: Downes Laboratory, Physics Department, California Institute of Technology, Pasadena, CA 91125

#17

Ann. Rev. Astron. Astrophys. 1978. 16:335–69

INSTRUMENTATION FOR INFRARED ASTRONOMY

*2134

B. T. Soifer[1]
Department of Physics, University of California, San Diego, La Jolla, California 92093 and California Institute of Technology, Pasadena, California 91125

Judith L. Pipher
Department of Physics and Astronomy, University of Rochester, Rochester, New York 14627

INTRODUCTION

Over the last 10 years infrared astronomy from 2 μm to 1000 μm has blossomed into a major field of observational astrophysics. This development would have been impossible without two major technical advances. First, extremely sensitive detectors have been developed and become available for astronomical applications. As detector sensitivity increased, the new astrophysical problems that could be explored as a consequence spurred on concomitant instrument sophistication. Secondly, and also motivated by the first development, major groups have expended much effort in building and operating telescopes above most or all of the earth's atmosphere, in order to circumvent its opacity and emission throughout the range. As wavelengths longer than 30 μm became available to observers, it became clear (cf the review article by Neugebauer, Becklin & Hyland 1971) that many sources are unexpectedly bright in that previously inaccessible wavelength region. This also provided impetus to improve the selection of available instrumentation.

Many excellent papers describe specific aspects of infrared instrumentation in substantially more detail than is possible here. We name only a few; for example, Low & Rieke (1974) have given an excellent description of the techniques and equipment development of infrared photometry.

[1] Present Address: Department of Physics, California Institute of Technology, Pasadena, California 91125.

0066-4146/78/0915-0335$01.00

Gillett, Dereniak & Joyce (1977) have given a comprehensive review of the current state of infrared detector development. Other detailed discussions of infrared astronomical instrumentation appear in the same volume as Gillett et al. In addition, several conferences have been devoted solely or partly to infrared instrumentation (e.g. Manno & Ring 1971, Rowan-Robinson 1976, Swift, Witteborn & Shipley 1974).

This review is an overview of the variety of the very sensitive instrumentation now or soon to be available to the infrared observer. We make no attempt to be comprehensive, and have, in fact, left out descriptions of the (now) more conventional instruments. Because efforts have been made in contemporary instrument development to minimize the effects of thermal backgrounds on observations, present instruments are generally limited in sensitivity by such fundamental factors as telescope/atmospheric emission and the solid angle of an observation. Of course each instrument has trade-offs as compared with a competing instrument, and we have attempted to provide enough detail (or appropriate references) to make these trade-offs apparent. Because the choice of the observing platform and the detectors plays as important a role as does the choice of instrument, we have preferred to describe each of the above categories under the broad heading of infrared astronomical instrumentation.

INFRARED DETECTORS

The major impetus to the advancement of infrared astronomy has been the tremendous improvement in detectors at infrared wavelengths. Much of this improvement can be attributed either directly or indirectly to the large research effort in infrared technology sponsored by the US Department of Defense. As newly developed high-performance infrared detectors have become commercially available, they have been incorporated into astronomical instruments, usually with vast improvements in instrumental sensitivity. Additionally, the existence of excellent detectors has made possible the design of new instrumentation to fully utilize capabilities of these detectors. Our discussion closely follows the excellent review of detectors for infrared astronomy by Gillett et al. (1977). We have omitted from this discussion CCD and CID arrays, which are still experimental, and upconversion techniques, which have been reviewed by Boyd (1977).

A perfect detector that yields a single unit of charge flow per incident photon will require an incident power

$$P_{\rm inc} = \left(2\,\bar{P}_B \frac{hc}{\lambda}\Delta f\right)^{1/2} \Big/ (1-e^{-hc/\lambda kT})^{1/2} \qquad (1)$$

(where $\bar{P}_B$ is the total radiation power assumed to be blackbody emission at a temperature T on the detector, which is assumed to be at wavelength λ equal to the measuring wavelength) to produce a signal voltage equal to the rms noise voltage of the detector in an electrical bandwidth Δf (Keys & Quist 1970). This relation simply reflects the statistical fluctuations in the background power $\bar{P}_B$.

The most common figure of merit for astronomical applications, the Noise Equivalent Power (NEP) is the amount of incident signal power that will produce an rms voltage (or current) response equal to the rms noise (the NEP is normally calculated from Equation 1 by setting $\Delta f =$ 1 Hz). Of course, in the limit $\bar{P}_B \to 0$ the detector/preamplifier will have some other noise source dominating, and this will determine the ultimate performance of a particular infrared detector. For an otherwise perfect detector of quantum efficienty $\eta(<1)$ the NEP becomes

$$\mathrm{NEP}_\lambda = A\left(2\,\bar{P}_B \frac{hc}{\eta\lambda}\right)^{1/2} \Big/ (1-e^{-hc/\lambda kT})^{1/2}. \qquad (2)$$

For photovoltaic or bolometer detectors the constant A is 1, and for photoconductors A is $\sqrt{2}$ (Keys & Quist 1970).

For conditions common to astronomical observations, photons from the celestial source can be neglected in comparison with local sources (telescope, atmosphere, etc) of thermal background radiation. In this case $\bar{P}_B$ can be estimated for the observing system and is equal to $\varepsilon B_\lambda(T)\Delta\lambda t A\Omega_{\rm obs}$, where $B_\lambda(T)$ is the Planck function (appropriate to the telescope environment), ε is the emissivity of the telescope environment, $\Delta\lambda$ is the optical bandwidth of photons incident on the detector defined by the cold (nonemissive) filtering, t is the net transmission of the cold filter, and $A\Omega_{\rm obs}$ is the throughput of the observation. If we take $A\Omega \sim 4\lambda^2$ cm^2 sr (for diffraction limited observations), the ultimate performance of an infrared detector becomes (from Equation 2)

$$\mathrm{NEP} = A\left[8\varepsilon B_\lambda(T)\Delta\lambda t\lambda\frac{hc}{\eta}\right]^{1/2} \Big/ (1-e^{-hc/\lambda kT})^{1/2}, \qquad (3)$$

$$= 1.2\times10^{-13} A\lambda\left(\frac{B_\lambda \varepsilon t}{\eta R}\right)^{1/2} \Big/ (1-e^{-hc/\lambda kT})^{1/2}\ \mathrm{W\ Hz^{-1/2}}, \qquad (4)$$

where λ is given in microns, $B_\lambda(T)$ is in W cm^{-2} sr^{-1} μm^{-1}, and $R = \lambda/\Delta\lambda$ is the spectral resolving power (or optical band width) of the instrument.

For ground-based photometric observations the quantity $\varepsilon t/\eta R \sim 0.1$, while the same quantity is $\lesssim 10^{-3}$ for a typical ground-based spectro-

scopic observation. The performance of a photovoltaic or bolometer detector under these conditions is plotted in Figure 1 (curves 1 and 2).

Conventional germanium bolometers were first developed for astronomical observations by Low (1961). An excellent review of these detectors is given in Low & Rieke (1974). The best reported NEP of such a detector is $\sim 7 \times 10^{-15}$ W Hz$^{-1/2}$. From Figure 1 it can be seen that such detectors (curve 3) are ideally suited for photometric measurements throughout the region of strong thermal emission produced by the surrounding environment. It is also clear that once the bandwidth of the observation is decreased to a resolving power of $R \gtrsim 100$, or where thermal emission is not strong, such bolometers do not take full advantage of the lower thermal background.

It is under the conditions of low thermal backgrounds that the newly developed photoconductors and photovoltaic detectors can be used to maximum advantage. InSb is an intrinsic photovoltaic detector with a band gap of 0.23 eV at 77 K, corresponding to a long-wavelength response limit of ~ 5.5 μm. This detector is now the most widely used

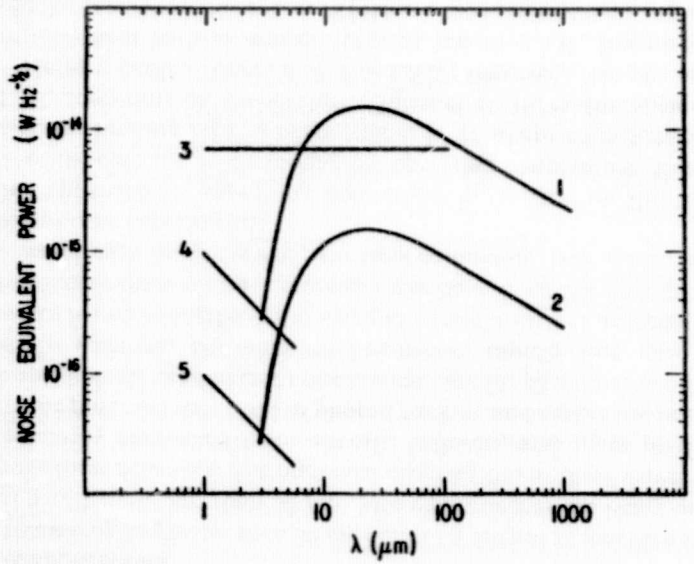

Figure 1 The Noise Equivalent Power plotted vs wavelength for infrared detectors. Curve 1 indicates the performance expected in a good ground-based photometric system using a diffraction-limited observing aperture. Curve 2 indicates the expected performance in a good ground-based spectroscopic system of low spectral resolution ($\lambda/\Delta\lambda \sim 100$). Curve 3 shows the NEP of the best conventional bolometer. Curves 4 and 5 show the equivalent NEP of InSb detectors having impedances of 10^{10} ohms and 10^{12} ohms (the NEP is limited here by the detector impedance).

infrared detector in the 1–5.5 μm band. These detectors have high quantum efficiencies ($\eta > 0.6$ are common) and are limited in ultimate sensitivity by the "Johnson noise" of the zero-bias resistance of the detector. Typical diodes have resistances at 77 K of $\gtrsim 10^8$ Ω for element sizes common for astronomical application ($\sim$1/2–1 mm). Further increase in detector impedance is achieved by further cooling these detectors and by using a technique (called "flashing"), discovered by K. Matthews, of shining near-infrared light onto a diode for $\sim$1 min. Although the physics of this process is not completely understood, it is commonly used to significantly improve the performance of these detectors. Increases of detector impedance by factors greater than 10^4 have been reported by cooling the diode to $\sim$55 K and "flashing" the detector. The theoretical NEP as a function of wavelength for a photovoltaic detector of impedance R (limited by the Johnson noise) is given by

$$\text{NEP} = (9 \times 10^{-12}) T^{1/2} \eta^{-1} R^{-1/2} \lambda^{-1} \text{ W Hz}^{-1/2}$$

(with R in ohms, λ in microns, and T in K). For InSb, this is plotted in Figure 1 for two values of achieved detector impedance at 60 K (curves 4, 5). Further increase in detector impedance is possible by cooling the detector further; however, the quantum efficiency of these detectors decreases at longer wavelengths as the detector is cooled (F. Gillett and R. Joyce, private communication). For InSb detectors, the product of the detector area times the resistance is a constant, so increases in detector impedance at a given temperature are possible by decreasing the detector area. Detector sizes as small as 0.1 mm are readily achieved. At the present time the ultimate performance of InSb detectors appears to be limited more by the technical difficulties of building low-noise preamplifiers than by the detectors themselves.

In the classical "thermal infrared" spectral region of 5–30 μm extrinsic silicon photoconductive detectors have become the most commonly used detectors under low-background conditions. Arsenic-doped silicon, with a quantum efficiency of 0.3–0.5 (Gillett et al. 1977) and an excellent response over the 5–24-μm band, is most commonly used for ground-based astronomy applications. Other extrinsic silicon detectors such as Si:Sb extend the performance of this class of detectors to ~ 30 μm. These detectors must be operated at T < 10 K. Under virtually all background conditions encountered from ground-based astronomy, these detectors remain background limited. Indeed, even under the low-background conditions expected for the Infrared Astronomical Satellite (IRAS) (van Duinen 1976) these detectors have been shown to remain background limited. Ternary compounds such as HgCdTe and PbSnTe have been developed as intrinsic photoconductors and photodiodes and have been

made to operate at wavelengths >14 μm (Moss 1976). Little astronomical work has been done with such detectors; however, the work that has been done with PbSnTe (Russell et al. 1978) has shown that this detector surpasses Si:As. The higher quantum efficiency achievable ($\eta \gtrsim 0.5$) and photovoltaic mode of operation give this detector great potential for future applications.

At wavelengths greater than 30 μm detectors are not as sensitive as they are at wavelengths less than 30 μm. Many approaches are being used to improve these detectors. Astronomical observations at these wavelengths are primarily conducted from aircraft, balloons, and space platforms, where the potential reduction in photon background makes the best conventional bolometers detector noise limited even for photometric observations. In addition, conventional bolometers rapidly lose absorption efficiency for wavelengths >100 μm, and so suffer further degradation of performance. Even so, until recently these have been the best available long wavelength detectors and have been commonly used in aircraft and balloon-borne experiments.

One approach to improving bolometers is to decrease the limiting NEP of the detector by decreasing the operating temperature. For bolometers, the limiting NEP is proportional to T^{α} where α lies between 3/2 and 5/2, depending on temperature (Gillett et al. 1977). Bolometers that use ^{4}He as a coolant operate at $T \sim 1.5$ K; however, ^{3}He provides an alternative heat bath at temperatures as low as 0.3 K. Several groups (Nishioka et al. 1977, Nolt et al. 1974) have used such systems to improve bolometer performance. P. Richards (private communication) reports a measured improvement of a factor of 10 for a bolometer operated at 0.3 K over operation at 1.2 K.

Another technique that has been used effectively and can be coupled to other techniques is the use of light concentrators or heat traps (Harper et al. 1976). This is a light pipe that has an effective focal ratio of $f/0.5$. Use of this device instead of a Fabry lens allows a smaller (hence more sensitive) bolometer to be used in a particular application.

For wavelengths longer than 100 μm, the loss of absorption efficiency of conventional bolometers has led several groups to develop a "composite" bolometer, where the energy absorption and temperature-measuring functions are separated. This approach improves the absorption efficiency while minimizing the heat capacity (and hence the NEP) of the detector. Different groups have attempted various approaches to optimizing the absorber, thermometer combination (Nishioka et al. 1977, Hauser & Notarys 1975, Coron et al. 1971, Clarke et al. 1975). For composite bolometers, the best electrical NEP quoted at 1.2 K for a 4 × 4 mm bolometer is 1.7×10^{-15} W Hz$^{-1/2}$ (Nishioka et al), while at 0.3 K the best quoted NEP is 6×10^{-16} W Hz$^{-1/2}$ (Nishioka et al.).

Photoconductors have not been developed extensively beyond 30 μm, largely because of a lack of interest from the military. The most commonly used long-wavelength photoconductor is gallium-doped germanium. This detector normally responds at $\lambda \lesssim 120$ μm; however, recently Kazanskii et al. (1977) have reported extending the response of Ge:Ga to ~200 μm by stressing the crystal.

As a result of a development study for the IRAS project, Ge:Ga has been shown to be an excellent detector under low background conditions. Detectors made for this study have been tested at NEP's of less than 10^{-16} W Hz$^{-1/2}$ (for elements of ~1 mm area) and appear to be background limited at this level (Moore 1976). The quantum efficiency of these detectors are excellent ($\eta \sim 0.5$), and they should prove to be excellent detectors for low background observations such as in balloon-borne and space experiments. For wavelengths beyond 120 μm, no really good photoconductors presently exist. Despite a fairly extensive development effort (G. E. Stillman, C. M. Wolfe, J. O. Dimmock, 1973, unpublished report) GaAs photoconductors have not proven to have adequate sensitivity for astronomical observations. Similarly, InSb hot-electron bolometers have not surpassed bolometers in sensitivity for $\lambda > 300$ μm (Pipher 1971).

Infrared heterodyne receivers have been developed by several groups for use in spatial interferometry and high-resolution spectroscopic studies. These receivers are quite analogous to microwave and radiowave heterodyne receivers. The basic principles of operation have been described by Keys & Quist (1970) and Johnson (1974). An infrared detector with good high (electrical) frequency response (typically Ge:Cu or HgCdTe at 10 μm) is used as the mixer. For 10-μm applications a laser (either solid state or CO_2 10.6 μm) provides the local oscillator source that is combined with the signal beam in the mixer.

InSb has been used as a mixer at 870 μm by Phillips et al. (1977) in detecting the $J = 3$-2 transition of CO using the Palomar 5-m telescope. This instrument is described in the review article on millimeter wave astronomy instrumentation by Penzias & Burrus (1973).

PLATFORMS FOR INFRARED ASTRONOMY

Infrared astronomy differs most strongly from optical astronomy in its requirements for a wide variety of platforms for different observations. This is a consequence of two major effects, the thermal emission associated

with the telescope environment (and the atmosphere), and the transmission of the earth's atmosphere. The first problem has led to many techniques to maximize the sensitivity of telescopes for infrared observations. The second problem leads to the use, by infrared astronomers, of telescopes on airplanes, balloons, and in space, as well as at ground-based observatories.

Ground-Based Telescopes

The two primary requirements for ground-based infrared telescopes are the selection of a dry high-altitude site and the minimization of the telescope contribution to the background power incident on the focal plane. Since the scale height for water vapor in the atmosphere is about 2 km (Allen 1973), the dryness of a site is primarily determined by its altitude. This is crucial to a good infrared site since H_2O provides a substantial amount of atmospheric opacity. Seeing is also an important consideration. For a 3-m telescope the diameter of the Airy disk (to the first null) is $0''.18\ \lambda$ with λ in microns, so good seeing (i.e. $<1''$) can imply diffraction-limited telescope operation at $\lambda \gtrsim 5\ \mu$m. Sky noise, i.e. the excess noise over background photon fluctuations, introduced by fluctuations in the sky emission, is another consideration, although a difficult one to quantify. After an extensive site survey (Westphal 1974) two major new infrared projects, the U.K. infrared telescope and the NASA Infrared Telescope Facility, have selected Mauna Kea, at an altitude of 4200 m on the island of Hawaii, as the best combined site for these considerations.

The design considerations relevant to building a telescope for ultra-high-sensitivity infrared observations have been described by Low & Rieke (1974). The fundamental guiding principle is to reduce thermal emission by the telescope to an absolute minimum. A further consideration for maximum-sensitivity infrared observations on any telescope is the use of a "chopping" secondary mirror (Low & Rieke 1974) to provide the rapid beam switching necessary to cancel most effectively the thermal emission from the telescope and atmosphere without adding extra noise. (Conventional telescopes have of course been used quite successfully for infrared observations; however, the sensitivity of these instruments is often limited by telescope emission.)

The NASA Infrared Telescope Facility (Neugebauer 1975, Dyck 1975, G. Smith, private communication) is a 3-m telescope constructed primarily for infrared observations, and it conforms closely to the design requirements described by Low & Rieke (1974) for infrared telescopes. This telescope will provide prime, Cassegrain, bent Cassegrain, and coudé foci for a wide variety of infrared investigations. A chopping secondary mirror for the Cassegrain and coudé foci is provided for cancellation of sky emission. To take advantage of the excellent seeing at Mauna Kea the optics is specified to focus 80% of the light (at 5000 Å) from a star into an image $0''.8$ in diameter. In order to locate invisible sources accurately, the offsetting pointing of this telescope will be accurate to $\pm 2''$ up to 15° from a known object. To allow accurate measurement of very faint objects, the tracking error of the telescope is to be less than $\pm 0.1''$ (rms) for periods of several hours.

The U.K. is building a 3.8-m telescope, similar to the NASA telescope and also situated on Mauna Kea (Lee 1977). The U.K. instrument should be completed in 1978, while the NASA instrument will be completed in 1979. The University of Wyoming is building a 2.3-m Cassegrain infrared telescope (R. Gehrz, private communication) at an altitude of ~10,000 ft near Laramie. The image quality, pointing, and tracking specifications for this telescope are somewhat less severe than for the NASA 3-m telescope; however, the performance of this telescope should be excellent. The site of this telescope implies that it will not be as dry on average as Mauna Kea. However, during the extremely cold winter months the Wyoming site could be substantially dryer than Mauna Kea.

One further new project of interest to infrared astronomy is the planned construction by Leighton (private communication) of a 10-m telescope for observations at $\lambda \geqq 350\ \mu$m. Although appropriately classified as a "light-bucket" in the optical astronomy sense, this instrument should be diffraction limited at $\lambda \geqq 350\ \mu$m, and will provide an excellent instrument for submillimeter observations of far infrared sources.

High Altitude Infrared Telescopes

The atmospheric windows that are used from ground-based telescopes for infrared observations are shown in Figure 2. As can be seen from this figure, a substantial fraction of the infrared is not accessible to ground-based telescopes, and for $\lambda > 15\ \mu$m, atmospheric conditions are such that useful photometric observations can be made only on the driest nights. From 15 μm to 1000 μm very little ground-based spectroscopic work has been done, because the windows are very poor for spectroscopic observations, and the atmosphere is effectively opaque from 40 μm to 350 μm. It is for these reasons that substantial efforts have been devoted to developing telescopes carried above much or all of the atmosphere.

AIRCRAFT TELESCOPES The first telescope used regularly in an aircraft environment for infrared astronomical observations was a 30-cm Cassegrain telescope developed by Low, Aumann & Gillespie (1970). This telescope was installed in the side of a Lear Jet 24B for open-port observa-

tions and provided typically 70 min of observations at altitudes of 45–50,000 ft. The telescope was gyrostabilized to allow inertial tracking of celestial sources. The necessary sky chopping was provided by means of a chopping secondary mirror. A highly evolved version of this telescope continues to be operated by NASA as a national facility at the Ames Research Center.

A 32-cm telescope has been designed and built for aircraft observation by the Groupe Infrarouge Spatial of the Observatoire de Meudon (Vanhabost et al. 1976). The telescope is an open-port instrument mounted at a special emergency door that can be installed in a variety of aircraft. Thus far it has flown in a French Caravelle and the NASA Convair 990. This telescope is gyrostabilized and is able to point to an accuracy of $\pm 15''$ (rms) under control of a star tracker.

By far the most extensive effort in aircraft-mounted telescopes has gone into the development and operation of the NASA 0.9-m telescope installed in a modified military transport jet, a C-141 (Cameron, Bader & Mobley 1971, Gillespie 1977). This facility, the Kuiper Airborne Observatory (KAO), is operated by NASA as an international observatory.

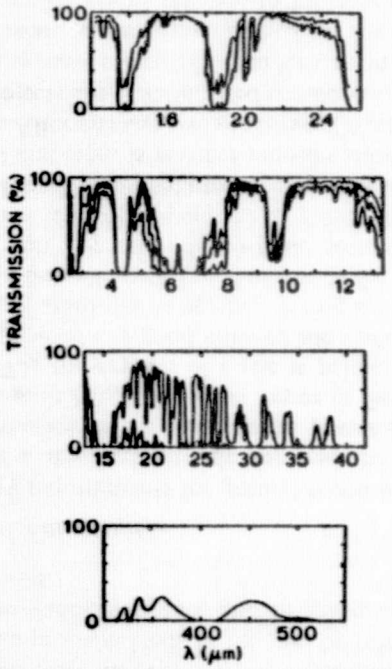

Figure 2 The atmospheric transmission as a function of wavelength in the ground-based infrared atmospheric windows. Transmission is plotted for various atmospheric conditions.

Figure 3 shows the important aspects of this telescope. The telescope is mounted in a specially constructed cavity and is supported on a spherical airbearing. The telescope is gyrostabilized about three axes and field acquisition and tracking use auxillary telescopes boresighted to the main telescope. The tracking performance of the telescope is quite impressive, with peak-to-peak tracking errors of 1″ being common in smooth air. A chopping secondary mirror provides beam-switching for background cancellation.

The sensitivity of observations on the KAO is highly dependent on the wavelength and band pass of the observation. For near infrared observations, the sensitivity is limited by the thermal background for narrow-band ($\Delta\lambda/\lambda \sim 0.01$) observations, or excess sky noise for broad-band ($\Delta\lambda/\lambda \sim 1/2$) observations at wavelengths where sky emission is significant (B. Soifer, unpublished data). In the far-infrared, the limiting sensitivity for diffraction-limited broad-band photometry remains the sensitivity of the detectors (I. Gatley, private communication).

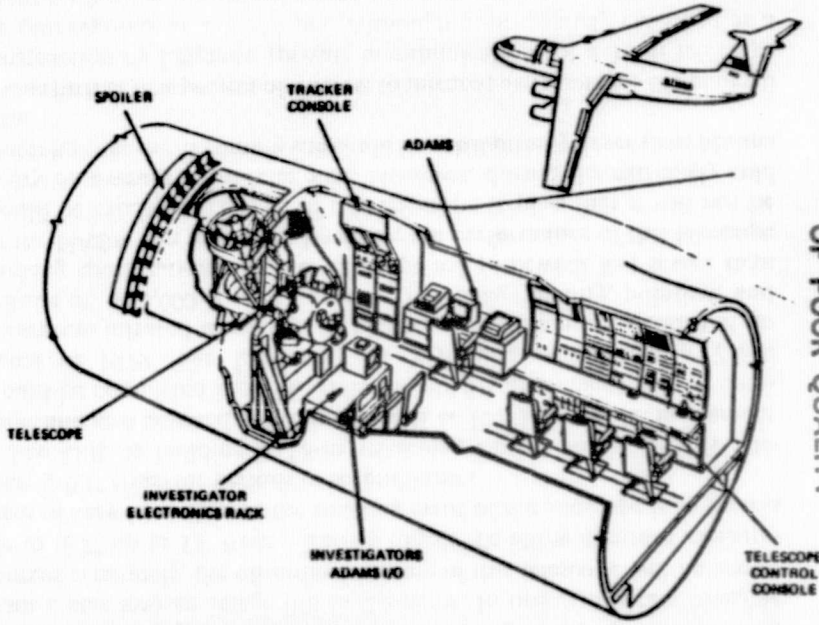

Figure 3 A side view of the Kuiper Airborne Observatory, showing the major elements of the system. The ADAMS (Airborne Data Acquisition and Management System) is the computer system that operates the telescope.

BALLOON TELESCOPES Beginning with the pioneering observations of the galactic center at 100 μm by Hoffmann & Frederick (1969) using a 2.5-cm refractive telescope on a balloon platform, balloon-borne astronomy has been one of the most actively pursued areas in infrared astronomy. Early instrumentation (Hoffmann, Frederick & Emery 1971, Furniss, Jennings & Moorwood 1972) used moderately small telescopes ($\sim$30–40 cm) with large beams (5′–12′) and appropriate pointing capabilities (1′–6′ pointing accuracy). These early programs emphasized photometric surveys of a limited area of the sky (Hoffmann et al.) and relatively coarse resolution maps of specific H-II regions (Furness et al.) at far-infrared wavelengths.

As can be seen from the payloads described in Table 1, the current generation of balloon telescopes has found many groups developing instruments for a wide variety of astronomical observations. Several groups have developed moderately large aperture telescopes (60 cm–1 m) that have excellent pointing capabilities and thus can provide platforms for many observations.

Thus far, most of these telescopes have been used to make high spatial resolution observations of limited regions of the sky. With the excellent pointing capabilities available on several of these telescopes, spectroscopic observations that require substantial integration times should soon become more common on the accurately pointable payloads of the 1-m class.

The low emissivity of the residual atmosphere at balloon altitudes allows large solid-angle observations to be made with balloon-borne telescopes. To exploit this capability several groups have begun programs to survey substantial fractions of the sky at far-infrared wavelengths. Several quite diverse approaches have been taken to building instruments for these surveys. The Berkeley and Goddard Space Flight Center groups have selected 1-m telescopes with multiple detectors in the focal plane for their surveys. These instruments are designed to operate at ambient temperature and emphasize wavelengths longward of 100 μm. In both cases the detectors used are composite bolometers developed by these groups. Low et al. (1977) have developed a unique instrument to survey the galactic plane at 60 μm–300 μm. This instrument uses a single-mirror (20-cm) off-axis Herschelian telescope as part of an ultra-low emissivity optical system in order to take full advantage of the cold, transparent balloon environment. Another approach, taken by Campbell et al. (1977) is to build a cooled telescope to reduce the telescope emission to an insignificant fraction of the atmospheric emission at the operating wavelengths. To prevent atmospheric gases from condensing on the cooled telescope mirrors, a thin polyethylene membrane is stretched across the cylindrical telescope tube (Frederick et al. 1974). Venting helium gas prevents condensation of atmospheric gases on the membrane.

Table 1 Modern infrared balloon payloads

Group	Diameter	Pointing	Purpose	References
SAO/HAO/U. of Arizona	1 m	Gyrostabilized absolute pointing <0.1°, tracking stability <0.5′ rms	Photometric mapping of infrared sources at far infrared wavelengths	Fazio et al. (1976) Hazen et al. (1974)
Imperial College London	1.04 m	Gyrostabilized, pointing <1′, tracking <10″ rms	Photometry, mapping of far infrared sources	R. Joseph et al. (1977)
GSFC	1.2 m	Gyrostabilized, tracking <2″ rms	High-sensitivity galactic plane survey at far infrared	M. Hauser (private communication)
Max Planck, Garching	1 m	3-axis gyrostabilized, pointing <0.5′	Far infrared line spectroscopy	Hofmann, Drapatz & Michel (1977)
UCL	60 cm	Gyrostabilized, tracking <10″	Multi-purpose, far infrared spectroscopy	Furniss et al. (1976b)
Tata Institute	30 cm	Servo-controlled magnetometer sensor. Pointing ~6′	Photometric observations in far infrared	Damle et al. (1976)
ROG	60 cm	Servo-controlled star tracker. Pointing 1′ RSS	Multi-purpose	Greeb & True (1974)
U. of Arizona	20 cm	Magnetometer sensor servo-controlled, pointing ~0.1°, stability 0.1°	High FOV, high-sensitivity far infrared survey of galactic plane	Low et al. (1977)
U. of Arizona/ Cornell Univ.	40 cm	Magnetometer stabilized, pointing ~5′	High-sensitivity far infrared survey of sky*	Campbell et al. (1977), Frederick et al. (1974)
U. of California, Berkeley	97 cm	Fixed elevation, scanning in azimuth	High-sensitivity all-sky far infrared survey	P. Richards (private communication)
Kyoto University	20 cm	Commanded elevation, magnetometer azimuth sensing	Near IR 2.4 μm large-FOV mapping of galactic bulge	H. Okuda et al. (1977)
Max Planck	15 cm	Fixed elevation, azimuth scanning	Near IR (2.4/3.4 μm) large FOV mapping of galactic bulge	Hofmann, Lemke & Thum (1977)

*Telescope cooled to L He temperature.

Two groups have used the low thermal backgrounds of balloon environments to make very large beam (1°) measurements of the galactic disk at 2.4 μm (Hofmann, Lemke & Thum 1977; Okuda et al. 1977).

Most of the modern-generation balloon payloads are just now entering regular use, so the next several years should see these observations making major contributions to infrared astronomy.

Rocket and Space Telescopes

It has long been recognized that space experiments provide the ultimate platforms for high-sensitivity infrared experiments. The space environment allows telescopes to be cooled to temperatures low enough to totally eliminate thermal emission from the telescope itself as a source of background noise (for $\lambda < 120$ μm). Harwit (1964) pointed out that with negligible telescope emission infrared space experiments would ultimately be limited by thermal background radiation from the zodiacal light. Since this emission approximates a blackbody spectrum at $T \sim 300$ K, with an effective emissivity of 10^{-8}–10^{-7} (Soifer, Houck & Harwit 1971), space observations can be as much as $\sim 10^4$ times more sensitive than ground-based observations at the same wavelength.

The first infrared astronomical observations from space were designed primarily to measure diffuse background radiation. Groups at Cornell (Harwit, Houck & Fuhrmann 1969) and NRL (McNutt et al. 1969) flew cryogenically cooled telescopes of ~16 cm diameters on sounding rockets to make absolute flux measurements from 5–1000 μm in relatively broad bands. Modulation of the infrared signal was achieved by chopping the celestial signal against a source at a low enough temperature to produce no significant emission. The most recent flight of the Cornell payload (Briotta & Houck 1977) has incorporated simple spectrometers for obtaining coarse-resolution spectra of the infrared background from 7–15 μm ($\lambda/\Delta\lambda \sim 25$) and 30–125 μm ($\lambda/\Delta\lambda \sim 5$).

The power of space observations at infrared wavelengths was illustrated by the Air Force Geophysical Laboratory all-sky survey at 4, 11, 20, and (partially) 27 μm (Price & Walker 1976). This survey covered 90% of the sky at least once and 60% of the sky at least twice at 11 μm and is statistically complete to a limiting flux density of ~100 Jansky at 11 μm. The telescope was 16.5 cm in diameter, cooled by supercritical helium, and used multiple detectors in the focal plane to scan the sky. Eleven rocket flights, each with ~300 sec of observing time, were required to complete this survey. By comparison a similar survey from the ground with a 1.5-m telescope would take roughly 1 year of *observing* time.

In the last several years several space missions have been studied by groups sponsored by various European and US government agencies.

The only approved projects are the Infrared Astronomical Satellite, a joint project sponsored by the US, the Netherlands, and the U.K. (van Duinen 1976, Aumann & Walker 1977) and a small infrared telescope to be flown on Spacelab 2 (G. Fazio, private communication). The IRAS satellite will perform an all-sky survey at 11, 22, 40, and 90 μm using a 0.5-m telescope cooled to less than 4 K. The typical noise equivalent flux will be $\sim 10^{-19}$ W cm^{-2} at all survey wavelengths. The satellite has a design lifetime of one year and will be launched in 1981.

The Spacelab 2 experiment (G. Fazio, private communication) will consist of a small (15-cm) off-axis Herschelian telescope, cooled to 4 K, and rapidly rocked ~90° in elevation to scan most of the sky approximately thirty times in the nominal 100–200 hours of observing. Detectors will cover a band of five wavelengths from 4–120 μm, both to survey the sky and to determine the effects of the space-shuttle environment on sensitive infrared observations.

Other space infrared telescopes studied thus far are a 3-m warm telescope (LIRTS) used primarily at wavelengths $\lambda > 30$ μm (Moorwood 1977), a 1-m telescope (SIRTF) cooled to ~10 K and used throughout the infrared (Gillett 1977), and a 0.4-m telescope (GIRL) cooled to <10 K (Lemke et al. 1977). These telescopes would be flown on sortie missions of the space shuttle.

FOCAL PLANE INSTRUMENTS

Spectroscopic Instruments

Infrared astronomical spectroscopic instrumentation in current use ranges from low resolving power $R = \lambda/\Delta\lambda \sim 10$ spectrometers incorporating prisms for wavelength separation to $R \sim 6 \times 10^6$ heterodyne spectrometers. Because astronomical spectrometers encounter a varied environment, they must be more rugged than their laboratory analogues. Where detectors are limited by thermal background photon noise, a major consideration in designing infrared instrumentation is the minimizing of local thermal backgrounds. Where detector noise limits the performance, multiplexing instruments are advantageous.

FILTER WHEELS/GRATINGS At wavelengths where the sensitivity of detectors is limited by thermal background radiation, the NEP of a detector is, from Equation 2, $\propto$ (background power)$^{1/2}$. By cooling a spectrometer so that its self-emission becomes negligible, the detector sensitivity is proportional to $R^{-1/2}$, where $R = \lambda/\Delta\lambda$ is the resolving power of the spectrometer. Then the noise equivalent flux density (NEFD) for a cooled spectrometer is $\propto R^{1/2}$. This relatively slow increase of NEFD with

resolving power is the sensitivity premium for cooling the spectrometer, and this has motivated a large number of groups to build such instruments.

The first infrared observations made with cooled spectrometers of resolving power $R \sim 100$ were reported by Gillett & Forrest (1973). These instruments operated from 7.5 μm to 13.5 μm and from 2.8 to 5.6 μm and used a circular variable interference filter as the wavelength selection device. In this device the wavelength transmitted is continuously variable at fixed resolving power over the appropriate range and is a function of angular position on the filter disk. The filter wheel was cooled to 77 K, while the detector, a Ge:Cu photoconductor, operated at 4 K in the same dewar. While achieving the improved sensitivity that is expected, the filter wheel technique is limited to observing a single spectral element at a single position on the sky at one time. Thus, no "multiplex" advantage is possible in this instrument. While the total time required to obtain a spectrum in a particular wavelength band is rather long, these instruments are relatively simple to construct and operate, and many groups have utilized such instruments over the entire 1–14-μm spectral region both in ground-based and airborne applications (Merrill et al. 1975, Russell & Soifer 1977, Gillett & Joyce 1975, Scargle et al. 1977, Witteborn et al. 1977, Willner 1976, Neugebauer et al. 1976). These instruments have become limited by thermal background noise for $\lambda > 2.5$ μm. Little work has been done with such instruments beyond 14 μm.

Because the resolving power of circular variable interference filters is limited to $\leqq 100$, and because sequential observations of spectral elements is required, further improvement of sensitivity in spectroscopic instrumentation has involved multiplexing instruments of various sorts. The simplest type of such an instrument is a dispersing instrument, where many spectral elements are observed simultaneously. Several groups have built cryogenically cooled prism and grating spectrometers having a wide range of resolving powers. Alternatively, the multichannel system can be used to map an extended source simultaneously in many wavelengths. Gehrz, Hackwell & Smith (1976) have constructed a helium-cooled six-channel Czerny Turner spectrometer using a prism as the dispersing element. This instrument has a resolving power $R \sim 10$, and spans the entire 8–13 μm window simultaneously.

At higher resolving power ($R \sim 50$–100) cryogenically cooled grating spectrometers have been built. Schaack (1975) describes a two-channel Ebert-Fastie system operating simultaneously in first and second order to span the 16–14-μm range. This instrument has been operated on the NASA 30- and 90-cm airborne telescopes. Recently this group has operated a 10-element array (J. Houck, private communication) spanning the

16–30-μm wavelength range in an identical spectrograph. D. Aitken and B. Jones (Jones, private communication) have developed a spectrometer cooled to 4 K, which operates at a resolving power $R \sim 100$–200 in the 10-μm and 20-μm atmospheric windows. Currently an array of six detectors is used in this instrument.

Higher resolution grating spectrometers have been built at Kitt Peak (Joyce 1977) and Lick Observatory (Rank & Bregmann 1975). The KPNO instrument is a Littrow mode grating system, cooled to ~77 K, and operates in atmospheric windows from 1–4 μm, at a resolving power $R \sim 500$. The Lick Observatory system is completely cooled to 4 K, and usually operates in the 10-μm atmospheric window at a resolving power of 2000. This instrument has about 30 detectors operating simultaneously.

One of the problems of operating multichannel instruments is the electronic data processing required by the high data rates. Since the thermal backgrounds still dominate the source flux, spatial chopping is necessary, and the processing of many channels of analog signals has initiated the use of minicomputers. A preamplifier and band-limiting amplifier are provided for each detector channel, and the output of this amplifier is sampled and converted to a digital signal, then phase detected in the computer. This technique has shown no significant loss in signal to noise when compared to the classical analog phase sensitive amplifier (Gehrz et al. 1976, D. Rank, private communication) and is much less expensive.

FOURIER TRANSFORM SPECTROMETERS (FTS)

Introduction Fourier transform spectrometers have played an increasingly important role in astronomical spectroscopy since the pioneering work at wavelengths ~2 μm in the early 1960's, which is discussed at length in a review article by P. Connes (1970). These instruments were adapted for astronomical use initially because the available detectors were sufficiently poor that there is an advantage to observing all spectral elements simultaneously with a single detector. As long as the dominant noise is independent of the signal level, or the system is not background limited over the whole spectral range $\Delta\nu$, the signal to noise obtained in an FTS exceeds that obtained in a scanning spectrometer (where individual spectral elements are observed sequentially) by a factor proportional to $\sqrt{N}$ where N is the number of spectral elements. This advantage [called the multiplex advantage (Fellgett 1958)] occurs because the FTS receives information over the entire spectral range during the time of a scan, and the entire spectral range is essentially coded in the interferogram. Subsequent detector improvements, coupled with low background telescopes, have reduced this advantage in some parts of the spectrum.

Since the basic concepts of Fourier transform instruments are well

documented [e.g. J. Connes (1961), Mertz (1965), Bell (1972), and the review article by Schnopper & Thompson (1974)], we only briefly discuss the fundamental principles of operation.

FTS instruments in astronomical use include Michelson interferometers. Lamellar grating interferometers, and Martin-Puplett interferometers in both ground-based and airborne applications. Any attempt to discuss the properties of all current astronomical Fourier transform instrumentation would undoubtedly suffer from repetition, undue length, and inadvertent omission [e.g. Hanel & Kunde (1975) report some 50 planetary oriented FTS instruments in 1973]. In this review we describe in detail a few specific examples of a given genre of instruments that represent advances in the decade since Connes' review article.

A Fourier transform spectrometer operates by separating the incoming radiation into two beams (e.g. in wavefront division, lamellar grating LG and amplitude division, Martin-Puplett MP and Michelson interferometers MI), varying the optical path of one of the beams, then recombining the beams that interfere with one another. The resultant output is called an interferogram: the interference pattern (modulation) is proportional to $\cos 2\pi\nu x$ for all of the above instruments, where ν (cm^{-1}) is the frequency and x (cm) the path difference of the separated beams. The output intensity, or interferogram, $I(x)$, can be expressed for an ideal interferometer as

$$I(x) = \int_0^\infty T(\nu)S(\nu)\,d\nu + \int_0^\infty T(\nu)S(\nu)\cos(2\pi\nu x)\,d\nu$$

$$= I(0) + \int_0^\infty T(\nu)S(\nu)\cos(2\pi\nu x)\,d\nu,$$

where $T(\nu)$ is the transmission efficiency of the spectrometer and $S(\nu)$ is the spectral intensity that can be recovered by Fourier transform techniques. (See any of the review references or texts cited for a discussion of the reduction techniques). Discrete sampling of $I(x)$ over a finite interval introduces some limitations in recovering $S(\nu)$ [see Bell (1972), for example]. The maximum spectral frequency at which data can be obtained is $\nu_{max} = 1/(2\Delta x)$, where Δx is the path difference between sampling. This limitation arises because discrete sampling causes a replication in the resultant Fourier transformed spectrum; the sampling interval must be chosen in terms of the desired cut-off ν_{max} to avoid overlap of the desired spectrum and a replicated spectrum (aliasing). If N samples are taken past the zeroth path difference, the best resolution possible is related to the maximum path difference D_{max} by $\delta\nu_{min} = 1/(2N\Delta x) = 1/D_{max}$.

Advantages of FTS instruments have been discussed at length in the

references cited. When not limited by source noise, the multiplex advantage, previously discussed, prevails. Order-sorting problems associated with dispersive spectrometers are absent, and it is only necessary to filter frequencies above ν_{max} and to limit the total spectral band pass in order to reduce background radiation falling on the detector. A large throughput ($A\Omega$) can be accommodated by an FTS instrument without strongly compromising the instrument resolution: this is called the throughput or Jacquinot advantage. Limitation in physical size of the optics limits the ultimate resolving power of dispersive instruments, but FTS instruments need only increase the interference path difference of the beams to increase resolving power. Intrinsic accuracy of wave-number measurement results from the interference phenomena inherent in FTS instruments. Because the moveable optic can be accurately controlled, the resultant precise changes in the displacement of the mirror are transformed into high wave-number accuracy.

A disadvantage of the single-input, single-output FTS instruments described so far is the presence of the term $I(0)$ in the interferogram, an offset subject to spurious fluctuations. This can be eliminated by a variety of schemes in different instruments. For example, a dual-input, dual-output Michelson interferometer can make use of the fact that the two outputs are complementary, i.e. that the beam passed through the interferometer in the opposite direction has an interferogram

$$I(x) = I(0) - \int_0^\infty T(\nu)S(\nu)\cos(2\pi\nu x)\,d\nu$$

so that the difference between these outputs cancels the DC offset $I(0)$ and doubles the modulation. If such a Michelson is operated in a rapid scan mode, in which the moving optic is moved at constant velocity at high speed (Mertz 1967), spurious effects are efficiently eliminated. Another FTS device that eliminates the $I(0)$ term is the polarizing (Martin-Puplett) Michelson interferometer. In this device the interferogram is proportional to either $1 - \cos\Delta$ or $1 + \cos\Delta$ [where Δ is $(2\pi\nu x)$], depending on whether the analysing (exit) polarizer is perpendicular or parallel to the entrance polarizer. The entrance or exit polarizer is used as a chopper, eliminating the DC term (Martin & Puplett 1970).

Michelson interferometers Two classes of near and intermediate infrared Michelson interferometers are in use today on ground-based telescopes, namely compact moderate resolution spectrometers (initially introduced by Mertz 1967) that operate at the Cassegrain focus and more complex and sophisticated high resolution interferometers that operate at the coudé focus.

Several common problems beset designers of ground-based Michelson interferometers. Weak signals and high thermal background levels most strongly influence design. Scintillation and seeing noise due to atmospheric turbulence (spuriously interpreted as interferometric fringes) can be eliminated by rapidly scanning the moving mirror at constant velocity so that fringe frequencies exceed scintillation frequencies (see Mertz 1967): in addition, the rapid scanning of the fringes themselves "chops" the radiation, eliminating the necessity for an articulating secondary. As a consequence of the scan speeds chosen, individual interferograms are quickly generated but often at low signal-to-noise ratio, so that repeated scans (sometimes up to tens of thousands) are co-added to improve the signal-to-noise ratio. Digital processing of the data is thus required, and most contemporary instruments depend on a reference signal (derived from the sinusoid interferogram of a monochromatic laser beam that also passes through the interferometer) to control the sampling. A white light beam is passed through the interferometer close to the source beam: the white light fringe is used as a fiducial mark so that successive individual interferograms may be co-added in phase. A particularly complete description of the data processing involved is given by Larson & Fink (1975): earlier descriptions follow Johnson et al. (1973).

Michelson interferometers mounted at the Cassegrain focus allow minimization of the telescope thermal background radiation because there

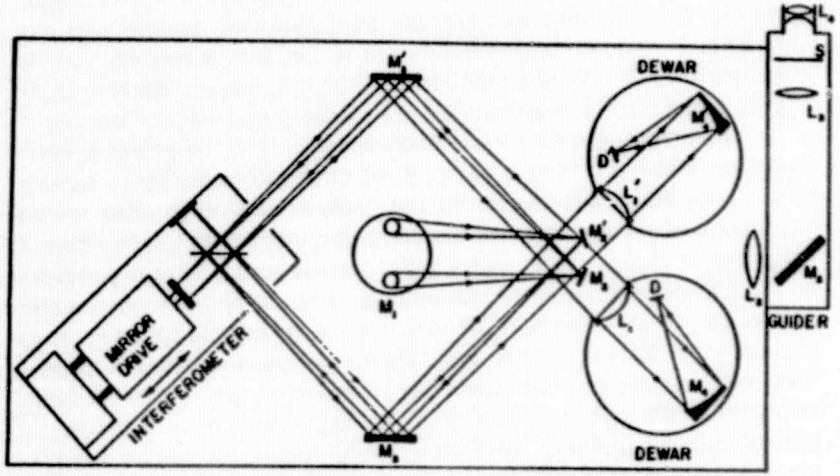

Figure 4 Schematic illustration of the internal optical configuration of Larson and Fink's Michelson interferometer. The ray diagram beginning at bending mirror M_1 (which deflects radiation into the spectrometer) illustrates the two-beam input/two-beam output geometry using on-axis but diverging beams.

are only two reflections at that focus and no moving telescope parts in the beam. Figure 4 illustrates the optical design of a typical device (Larson & Fink 1975). In this device, mirrors M_1 divert light from the telescope into the plane of the interferometer, while injection mirrors M_2, M'_2 define the field to be diverted into the interferometer via bending mirrors M_3, M'_3. The dual beams then are transmitted and reflected by the beam splitter to the stationary and moving mirrors in the interferometer. One of the dual beams is transmitted, and the other is reflected to the moving mirror. Recombination on the beam splitter then takes place, and the beams exit via M_3 and M'_3 (in this scheme still diverging as $f/45$ so that the injection mirrors only slightly obscure the exit beams) and matched detectors are provided for each output. For a Michelson interferometer to be useful beyond 3 μm where the thermal background is high, the two complementary inputs of such a two-beam interferometer are used for thermal background compensation: adjacent beams on the sky (one includes the source) are fed into the two inputs, and the background radiation (sky + telescope) fringe is cancelled to first order at each output because of the complementary nature of the two beams (as noted earlier). To reduce residual imbalance due to asymmetric optics, nonuniform background and lossy beam splitters, the source is switched from one beam to the other between successive scans or groups of scans.

The dual-beam input, dual-beam output is also typical of designs of Thompson & Reed (1975), Ridgway & Capps (1974), and Treffers (1975). With the exception of Thompson and Reed, all of the above instruments have adapted the commercial rapid-scanning Idealab 1F-3 interferometers for astronomical use and all employ dielectric beam splitters. Thompson and Reed successfully incorporated a printed circuit motor and tachometer rather than a magnetic coil driver (typical of the Idealab Units) to drive their moving mirror. Because of the high background conditions, the Ridgway and Capps and the Treffers instruments (built for the 10- and 20-μ atmospheric windows) must have very well balanced dual beams in order to effect thermal background compensation. In order to achieve this end Ridgway and Capps mounted their instrument on the unobscured aperture of the McMath 150-cm solar telescope and utilized variable focal plane apertures to define the two beams precisely. All of these instruments are aligned in the lab, and input mirror and dewar adjustments are done on the telescope. Most observing groups take one-sided interferograms: a phase-corrected (Forman et al. 1966) interferogram is co-added, then cosine transformed.

D. Hall and S. Ridgway (1977, preprint) have achieved success with a prototype 10-cm FTS at the coudé focus of the KPNO 4-m telescope and are constructing a rapid-scanning FTS optimized for high-resolution

visible and infrared spectroscopy (0.4–20 μm) of planetary and galactic sources. The instrument will employ thermally compensated, preadjusted components [e.g. beam-splitter and cats-eye retroreflectors (Beer 1968)], accurate to interferometric tolerances. A massive table supports the instrument, and no folding flats are planned. The moving cats-eye will be mounted on a screw drive and hydrodynamic bearing: Path differences up to 2 m will be possible. The instrument will be computer controlled, so that beam-splitter changes and dewar servicing will represent the only hands-on operation. Entrance apertures up to 30″ will ultimately allow panoramic detectors to sample spectra simultaneously across an extended source. Conventional rapid scanning, co-adding of interferograms, and full dual-beam utilization are planned. The authors estimate, on the basis of their prototype, that use of symmetric matched inputs cancels background radiation to $\leqq 1\%$ at 5 μm, and beam switching reduces this to 10^{-4}–10^{-5}. A chopping secondary is not required.

Daehler & Ade (1975) report the construction, theory, and use of a submillimeter Michelson interferometer that employs an unusual beam splitter, consisting of a pair of solid prisms separated by a narrow gap, and that utilizes frustrated total internal reflection. Because the beam splitter operates effectively over two octaves of frequency, it is an attractive choice. Actual use of the interferometer on the Queen Mary College 1.5-m far-infrared telescope employed phase modulation (Chamberlain & Gebbie 1971) rather than radiant-flux chopping, and was tested in measurements of the daytime sky at 0.5 cm^{-1} resolution.

A substantial number of experimenters have successfully flown Michelson interferometers on airplane, balloon, rocket, and satellite telescopes in order to exploit freedom from atmospheric constraints. For example, Larson and Fink's instrument has been flown on the KAO C-141 facility many times. They have recently updated their instrument (H. Larson 1977, preprint) to a substantially higher-resolution (0.02 cm^{-1}) system operative from 0.8–5.6 μm. It also is a dual-input, dual-output interferometer, employs rapid stepping, and utilizes cats-eye retroreflectors in place of the moving and stationary interferometer mirror in Figure 3. Although designed for KAO observations, it can be adapted to ground-based use.

Hilgeman & Smith (1976) have achieved excellent results on the NASA Lear Jet in the 1.5–3.5 μm region of the spectrum at 2 cm^{-1} with their Michelson interferometer, which is unusual in the sense that the telescope employed, a 30-cm $f/23$ folded Dahl-Kirkham, is hard-mounted to the interferometer assembly. The NASA heliostat is then used in conjunction with the interferometer/telescope.

Two far-infrared Michelson interferometers have been flown on KAO.

Erickson et al. (1977) have flown a single-beam interferometer, sensitive from 30–125 μm, housed in the vacuum space of their helium dewar so that acoustic vibration of the mylar beam splitter is prevented. The articulating secondary of the telescope is used in this case, and zero path difference is found by computer-peaking up a bright source.

The most elaborate Michelson interferometer currently in use on the KAO is described in a pair of articles (Baluteau et al. 1977, Langlet et al. 1977). A high-resolution (0.02 cm^{-1}) rapid-scan Michelson for use from 10 to 300 μm, more analogous to previously described instruments, was constructed. The instrument contains a built-in alignment laser and a variable temperature blackbody source that can be rotated into place. A cold $\Delta\lambda/\lambda \sim 0.1$ band-pass filter limits the background from the warm telescope/interferometer so that detector noise dominates. The interferometer can be evacuated during flight, and the dewar (mounted on a table with six adjustment degrees of freedom), reference laser, and drive motor are at cabin altitude. The whole system mounts on a massive plate that serves as an optical bench. Sky chopping is not employed. This instrument, with a different choice of beam splitters, has also been used in ground-based application (e.g. Anderegg et al. 1976).

Two balloon experiments utilizing Michelson interferometers have conventional design: Furniss et al. (1976a) report far infrared measurements from 60 to 220 cm^{-1} from the University College London 40-cm balloon-borne telescope. Traub (1976) is planning moderate resolution (0.1 cm^{-1}) 25–150-μm spectroscopy on the SAO balloon-borne 1-m telescope. The main input beam will alternately view the source and blank sky with the second beam viewing a cold surface. Thus the sky emission spectrum can be calculated, and subtracted from the source spectrum, eliminating need for a balanced output with a chopping secondary.

Although the Air Force Geophysical Laboratory HIRIS experiment (A. T. Stair, J. W. Rogers, W. R. Williamson, 1977, preprint) is not in astronomical use, it is interesting for potential astronomical use because of its 10 K operating temperature. It incorporates a rapid-scan helium-cooled Michelson interferometer and is carried on a Sergeant rocket. The system, built by Honeywell Radiation Center, incorporates a specially developed Idealab Inc. interferometer slide assembly, and it obtained 2 cm^{-1} resolution data on the atmosphere in the 4–22 μm region of the spectrum. The instrument is doubly unique in that the system aperture is 2.54 cm and the optics is $f/1$.

The infrared investigation on the Voyager mission uses a pair of Michelson interferometers in conjunction with a boresighted single-channel radiometer (Hanel et al. 1977). The MIRIS interferometers, one a far infrared device (60–600 cm^{-1}) and the other near infrared (1000–

7000 cm^{-1}), share the telescope aperture. A tuning fork chopper allows radiation to alternately fall on one interferometer or the other. Both interferometers depend on a common linear motor to drive the moving mirrors. Mariner 9 also carried an infrared interferometer experiment (Hanel et al. 1972), IRIS M, which was similar in design to the atmospheric Nimbus interferometers. IRIS M operated from 20–2000 cm^{-1} at 2.4 cm^{-1} resolution. Like the Nimbus interferometers, this system was a dual-detector double-beam device, employing the constant velocity mode of driving the moving mirror. Hanel et al. first proposed preserving the dual-beam nature without employing a beam-splitter size twice the size of the beam cross section. They use the technique of solid-angle splitting of the interfering beams instead.

Lamellar grating interferometers There have been several airborne lamellar grating experiments in the far infrared. The lamellar grating employs wavefront rather than amplitude division of the input beam, with nearly 100% beam-splitter efficiency for $\lambda \gtrsim 100$ μm. Since only the zeroth order of diffracted radiation from the lamella is used in this mode of spectroscopy, higher (odd) orders are irretrievably lost. Interferograms are generated as a function of the path difference between the beams reflected from the fixed and moving lamella. These systems are single-input, single-output devices, employ an articulating secondary (or some sort of chopping), and cannot dispose of the offset term $I(0)$. Pipher, Savedoff & Duthie (1977) have employed a lamellar grating interferometer with lamella fabricated on a brass sphere matched to the f ratio of the KAO telescope: collimating optics are not required. They have made observations from 28 to 500 μm at resolutions to 1.7 cm^{-1}; at much higher resolutions shadowing would be a problem, and waveguide effects diminish efficiency of the device at long wavelengths. A step and integrate mode was utilized for data acquisition in this device.

Hofmann, Drapatz & Michel (1977) are constructing an experimental balloon-borne 20–200-μm lamellar grating cooled by liquid nitrogen, to achieve a maximum resolution of 0.05 cm^{-1}. An off-axis mirror provides a collimated beam of radiation that is parallel to the travel of the moving lamella and driven by a stepping motor attached to a micrometer screw. The reflected beams are focused on the detector by a second off-axis mirror. The lamella in this experiment are cut from a low thermal expansion ceramic, ZERODUR, lapped to optical tolerance, and the moving lamella glides on a ZERODUR plane.

Mercer et al. (1976) have designed a balloon-borne lamellar grating interferometer, cooled by liquid helium, for cosmic-background spectral measurements from 3–12 cm^{-1}. Entrance and exit apertures consisting of

light pipes feed the collimating off-axis paraboloid with an 8° × 30° beam. Lamella are constructed of Dural, and 0.1 cm^{-1} is the maximum resolution. A disc chopper modulates the radiation.

Martin Puplett interferometers Two balloon-borne submillimeter cosmic background experiments (Woody et al. 1975, Robson 1976) have utilized liquid-helium-cooled polarizing Michelson interferometers as developed by Martin & Puplett (1970). These interferometers modulate the polarization of the radiation rather than the intensity as in a conventional Michelson interferometer. The input radiation is linearly polarized by an entrance polarizer before reaching the wire grid polarizer, oriented at 45° to the entrance polarizer (see Figure 5). The radiation is split into two orthogonally polarized beams by the beam splitter. Dihedral mirrors (one moving, one stationary) rotate the polarization plane by 90° so that the beam originally transmitted by the polarizing beam splitter is now reflected and vice versa. The output beam is analyzed by the polarizing chopper before detection. Beam-splitter efficiencies are very high over a wide spectral interval in this interferometer, making it an ideal choice for space astronomy. Details of experiments differ: for example, Woody et al. use a single detector scheme, collect radiation from a reflecting horn and cone antenna, and immerse their interferometer in cryogen. Robson uses a dual detector system and passes incident radiation through a low-emissivity window on the cryostat vacuum jacket.

The Cosmic Background Explorer Satellite will include three instruments covering the 8-μm–13-mm spectral range, to determine the spectrum and angular distribution of the large-scale background radiation

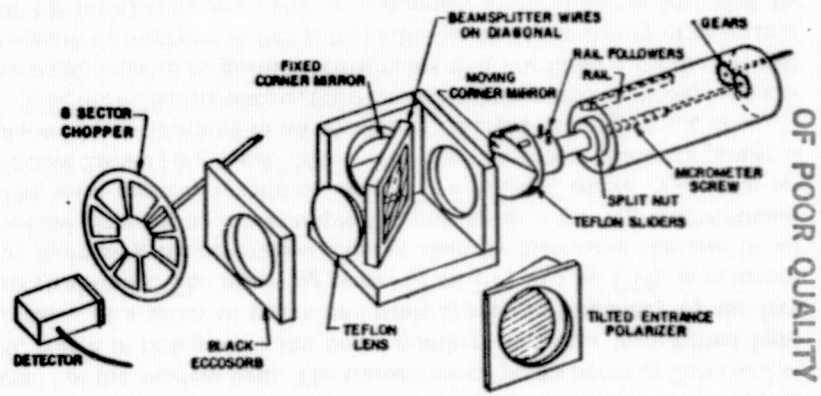

Figure 5 An exploded view of the Martin-Puplett interferometer flown by the University of California, Berkeley (D. P. Woody, 1975, PhD thesis).

fields (Mather 1977). The spectrometer is a cryogenic Martin-Puplett interferometer to measure the 3 K background. It will cover a range of 3.3–33 cm^{-1}, have at least 1 cm^{-1} resolution, and have a 7° beam. The critical aspects of the experiment will be its flux collector and calibration techniques (not yet finalized). The spectrometer will operate at 3 K as a null tester; this will allow unprecedented sensitivity in detecting deviations from blackbody form.

HADAMARD TRANSFORM SPECTROMETERS (HTS) Both FTS and HTS systems record the entire spectrum in encoded form and image it onto a single detector. Hadamard transform spectrometers are dispersive spectrometers with either the entrance or exit aperture or both encoded by multislit masks. The encoding pattern is represented by the rows or columns of the Hadamard matrices, which are binary digital in which one digit represents an open slit and the other digit represents a closed slit so that the spectrum can be recovered by matrix inversion (Sloane et al. 1969, Decker & Harwit 1969, Philips & Harwit 1971). There have been somewhat controversial comparisons of the relative merits of FTS and HTS techniques in the literature, and most recently Tai & Harwit (1976) conclude that the Hadamard encoding process has a $\sqrt{N}/2$ multiplex advantage while the single detector FTS has a $\sqrt{N}/8$ multiplex advantage system (Treffers 1977). In practice, however, the HTS has not been used extensively in astronomy, with a few notable exceptions. For example, Houck et al. (1973) successfully employed a single Hadamard mask at the exit aperture of a 1/4-m modified Ebert Fastie spectrometer, which was flown on the Convair 990, to make observations of bound water on Mars. The observations were made from 2.2 μm to 3.8 μm at 0.1-μm resolution. Phillips & Briotta (1974) made the first measurements of the ν_2 band of NH_3 absorption (11.5–13 μm) in the Jovian atmosphere using an HTS. In this case the HTS was doubly multiplexed, and a $f/1.2$ Littrow mode spectrometer was utilized: the resolution obtained was $\Delta\lambda/\lambda \sim 0.004$.

FABRY-PEROT SPECTROMETERS (FP) For very high resolving power, and large throughput astronomical observations of a single-line profile (with the potential of velocity resolution), scanning Fabry-Perot spectrometers are unsurpassed. For example, very little multiplex advantage could be obtained with an FTS in the study of a single line, and the FP is a much simpler system. An ideal FP consists of a pair of semi-transparent flats (at the wavelength of interest) with reflecting surfaces facing each other, and accurately parallel. If the reflectance of the facing surfaces is $\mathscr{R}$, the system transmission T is

$$T = \{1 + 4\mathscr{R}(1-\mathscr{R})^{-2} \times \sin^2[2\pi nlv\cos\theta]\}^{-1},$$

where n is the refractive index of the inter-flat material, l is the etalon plate separation, θ is the angle of incidence, and v is the frequency in cm^{-1} of the incident light. The transmittance peaks occur at $2nlv\cos\theta = m$, where m (integral) is the order number, and thus transmitted light consists of a series of peaks uniformly spaced in frequency by the free spectral range. The resolving power of an FP, like an FTS, is achieved by increasing the separation l rather than by increasing the size of an optical element, as for example the grating in a grating spectrometer. The wave-number resolution $\delta v(cm^{-1}) = 1/2N_{\mathscr{R}}l$, where $N_{\mathscr{R}}$ is the reflective finesse $[N_{\mathscr{R}} = \pi\mathscr{R}^{1/2}/(1-\mathscr{R})]$. The theoretical resolving power is $R_T = 2N_{\mathscr{R}}vl$. Scanning in wavelength is achieved by varying n, l, or θ.

Like the FTS instruments, the FP enjoys a luminosity or throughput advantage, relative to grating instruments that are limited by the slit size to small throughput. A fine general discussion of the theory of operation of FP interferometers (with astronomical application) is provided by Roesler (1974): earlier reviews by Vaughan (1967) and Meaburn (1970) are also useful.

Townes and collaborators at the University of California, Berkeley (Geballe 1974, Holtz 1971, Greenberg et al. 1977, Brandshaft et al. 1975, L. T. Greenberg and P. Dyal, private communication) have developed a variety of FP spectrometers for both ground-based and airborne application using both ambient temperature and cooled etalons. One example of a ground-based instrument, developed by this group, consists of ambient tandem FP etalons and filters. The series placement of the etalons was predicated by the unavailability of filters for satisfactory blocking of unwanted orders at the desired resolving power, finesse, and transmission. Unwanted orders of the first etalon are blocked by using the second etalon in a different order. Spacings are varied by driving one mirror of each pair piezo-electrically. Mirrors of finesse 15 used with filters of 20 cm^{-1} bandwidth result in a resolution at 5 μm of 0.1 cm^{-1}. The sweep range is between 1 cm^{-1} and 2.5 cm^{-1}. A 20-μm adaptation of this system has also been used at Mauna Kea.

Another instrument developed by this group consists of a cooled FP (77 K) and grating (10 K) that limits thermal background radiation on the detector to the 0.1–0.2 cm^{-1} width of the instrument (at 12.8 μm). This cooled instrument yields a 10–20 factor improvement in sensitivity at 10-μm over a warm system.

Another FP system for the 50 μm–1 mm region was developed and used on the Lear Jet telescope (Brandshaft et al. 1975), and recently on KAO by the same group. Quartz plates coated with aluminum grids were used initially for the FP etalon. Free standing Ni grids replaced the quartz plates for subsequent flights on the KAO. The resolution of this instrument is 1.6 cm^{-1} at 100 μm.

Michel, Nishimura & Olthof (1977) plan to use the angle-scan Fabry-Perot technique for a satellite survey of molecular hydrogen (28 μm). The FP filter is tilted to wavelength scan in this technique (Roche & Title 1975). They propose multidetector arrays so that mechanical tilts of the FP filter become superfluous. Light passing through the FP at different angles and then focussed at different detectors allows each to receive light from an adjacent wavelength. They have tested a $N_R \simeq 60$, $R \sim 3000$ FP consisting of a Si wafer (200 μm) coated with $\lambda/4$ alternate layers of CsI and Ge, and use it in the $m = 50$ order of dispersion.

HETERODYNE SPECTROSCOPY Many groups are involved in heterodyne spectroscopy including Peterson et al. (1974), Mumma et al. (1975), de Graauw & Van de Staadt (1973), and de Batz et al. (1973). They utilize heterodyne spectroscopy in the infrared to achieve resolving powers in excess of 10^6; by converting infrared frequencies to microwave frequencies spectral analysis can be performed electronically. To exemplify the method, Betz et al. (1976) utilized the system developed by Peterson et al. on one of the KPNO 81-cm solar telescopes to measure emission lines on Venus. The infrared signal at 10.6 μm is combined with a few milliwatts of output power of a stabilized CO_2 laser and focused onto a cooled HgCdTe mixer; the difference frequency is amplified; and a 200-MHz segment of the 0–1500-MHz spectrum is converted by a single side-band mixer to 50–250 MHz and directed into a multichannel RF filter bank, where the spectrum is analyzed into 40 independent 5 MHz channels. Synchronous demodulation at the chopping frequency of the 40 channels, then multiplexing into the computer is performed, leading to $R = 6 \times 10^6$ at 3×10^{13} Hz. At this resolving power velocity resolution of the order of 50 m sec^{-1} is possible, underlining the significance of this type of spectroscopy.

High Spatial Resolution Instrumentation

Diffraction-limited observations on a single telescope can yield useful information on spatial structure of a wide variety of infrared sources from molecular clouds to galaxies. When seeing permits, diffraction-limited spatial resolution is achievable at 10 μm. Source sizes of 0.″5–1″ have been measured using the 5-m Hale reflector (Becklin et al. 1973, Wynn-Williams et al. 1977). At 100 μm, the angular resolution of the 0.9-m KAO telescope, about 20″, is much larger than the seeing disk. Several groups (Werner et al. 1977, Harvey et al. 1976) fly far-infrared photometers on the KAO and make diffraction-limited observations of molecular cloud/H II region complexes.

From the ground, infrared lunar-occultation measurements of infrared point-like sources [e.g. IRC+10216, Toombs et al. (1972)] provide the

only single-aperture method of improving spatial resolution above diffraction-limited operation. Several groups routinely monitor occultations of all appropriate objects. Sizes of ~0.″1 have been measured using this technique (Zappala et al. 1974).

The University of Arizona infrared spatial interferometer (McCarthy & Low 1975, McCarthy et al. 1977) is now being used for measurements of the sizes and shapes of circumstellar shells at 5 μm–11.1 μm. The instrument as operated at the Cassegrain foci of various telescopes is shown in Figure 6. Two circular apertures mounted symmetrically across the telescope diameter admit the interfering beams: each beam is reflected by mirrors mounted on piezoelectric stacks, then by a roof mirror to a dichroic beam splitter. The infrared beam is admitted to the detector through a slotted mask (width and separation equal that of the fringes, i.e. ~0.5 mm). Observations at different baselines are made by using various diameter telescopes (1.5–4 m). Accurate positioning of the roof mirror equalizes path lengths of the beams, and modulation of the fringes is achieved by "sawtooth" chopping of one of the mirrors mounted on a piezoelectric stack. Fringe visibility functions can be measured at 5 μm, 8.3 μm, 10.2 μm, and 11.1 μm, and angular sizes as small as 0.″4 have been measured at 10 μm.

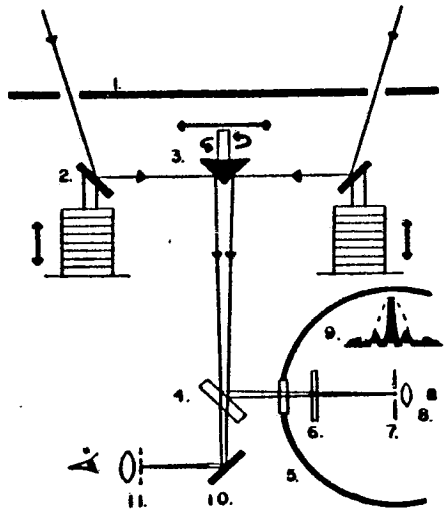

Figure 6 Schematic diagram of McCarthy and Low's spatial interferometer. The mask over the telescope aperture is (1), the plane mirror on the piezoelectric stack is (2), the roof mirror is (3), the dichroic mirror allowing light to pass to the dewar is (5) and the eyepiece (11) is numbered (4). Interference fringes (9) on the slotted mask (7) are focussed on the detector by the field lens (8), while the prefilter is (6).

Johnson (1974, see also Johnson et al. 1976) has reported the successful development of a two-element stellar infrared interferometer. The Berkeley interferometer mimics the microwave VLBI, in which heterodyne detection at each telescope is used. Phase and amplitude information of the original infrared signal is preserved at the difference microwave frequency, and direct radio-frequency interference of the output is employed. The two telescopes used for the interferometer are the McMath Solar Observatory auxiliary telescopes, which each have a 4000-cm^2 collecting area and are separated by 5.5 m on an east-west baseline. Angular resolution of the instruments is 0".2 for sources on the meridian.

De Batz et al. (1977) have applied an innovative multiplex technique using Hadamard coding to astronomical infrared imaging at 2 μm. The multiplex advantage of FTS and HTS was discussed above. A similar multiplex advantage obtains when N image elements are observed at one time by superposing an appropriate code sequentially on the image. In this experiment the incident beam is diffracted by a holographic grating at the coudé focus of the CERGA 1-m telescope, and the zeroth-order radiation is modulated, then imaged onto a Hadamard grid of opaque/transparent squares. An angular resolution $\leqq 1''$ was achieved, with a multiplex advantage of half the theoretical value of 23.

Polarimetry

Infrared polarization measurements provide important additional information about the emission mechanisms of astronomical objects. For example, polarization studies of galactic nuclei (Knacke et al. 1976, Capps & Knacke 1976) yield information on the predominance of thermal or nonthermal processes. In the presence of scattering (as for example in a planetary atmosphere or circumstellar shell) radiation fields become polarized. In those cases spectral variations of the observed radiation intensity and polarization state, particularly in line profiles, yield structure and composition information. Both photometric and spectroscopic polarimeters have been constructed.

Photometric instrumentation at both far-infrared and near-infrared wavelengths generally employs a rotating analyzer. For example, Dall'Oglio et al. (1973) describe a far-infrared polarimeter which is also discussed by Coletti et al. (1976). The balloon-borne instrument consists of an $f/4$ 20-cm telescope, a rotating analyzer that modulates the polarized component of infrared radiation (300–3000 μm), a bolometer, and two lock-in amplifiers 90° apart to measure intensity and plane of the polarized radiation.

Dennison (1976) reports on 100-μm polarization measurements of M42 and Venus carried out on the NASA Lear Jet Airborne Observatory, using a rotating wire-grid analyser with their photometer system. A modification of this instrument has been used on the KAO (M. Harwit, private communication).

Kemp et al. (1977) have utilized a new type of infrared polarimeter employing photoelastic modulators. In contrast to the conventional near-infrared polarimeter (Dyck et al. 1973, Blanco et al. 1976), in which a rotating analyzer is used, the instrumental polarization is 0.01 %±0.03 % at 1.6 μm and 0.03%±0.04% at 2.2 μm. The photoelastic modulators are constructed of CaF_2, and the instrument uses a beat frequency arrangement involving two modulators, yielding polarization chopping at 15–20 Hz, appropriate for detector response times.

Astronomical Fourier spectropolarimetry has been discussed in depth by Forbes & Fymat (1974). They show that the Fourier spectroscopic technique can be adapted to the measurement of all four Stokes parameters with a comparable degree of resolution and over a wide spectral range. In the two-beam Michelson, polarizer(s) are inserted into the beams with transmission axes at angles $\theta = 0$, 45, 90°. These interferograms, with different configurations of the polarizers, are needed to extract the Stokes parameters. This technique was successfully used to obtain spectropolarimetry of Venus from 0.8–2.7 μm with 0.5 cm^{-1} resolution.

SUMMARY AND FUTURE DIRECTIONS

The expansion of infrared astronomy over the last five to ten years has been as vigorous as any field of astrophysics. To a great extent this growth has been generated through applications of technological advances to astronomy. Much of this new technology has come in the form of high-sensitivity infrared detectors becoming commercially available. Furthermore, the development of various platforms optimized for infrared observations has opened the entire 1 μm–1 mm wavelength range to astronomical investigations.

With currently available detectors, instruments limited in sensitivity only by fundamental constraints of fluctuations in thermal background radiation are coming increasingly into operation. One major example of this increasingly sophisticated instrumentation is high spectral resolution devices. Excellent sensitivity is now being achieved at high spectral resolution, and the trend towards high-resolution spectroscopy in the infrared should continue.

Two major new advances in technology should drastically affect infrared astronomy in the years to come. The first of these is the introduction of one- and two-dimensional detector arrays. Such devices should provide a major increment in the sensitivity of infrared observations. A major

challenge to infrared astronomers will be to adapt these devices to fully exploit their capabilities.

The second major advance in technology is the feasibility of long-life infrared space missions. These missions will increase the sensitivity of infrared observations by several orders of magnitude, and should revolutionize our picture of the infrared sky. With the beginning infrared space missions, Spacelab 2 and IRAS, scheduled for launch in early 1981, the next decade should see infrared astronomy grow even more rapidly than in the past.

ACKNOWLEDGMENTS

It is a pleasure to thank our many colleagues who provided us with descriptions of their instrumentation and those who provided figures used in this article. F. Gillett, M. Harwit, J. Houck, H. Larson, K. Matthews, G. Neugebauer, M. Werner, and S. Willner were kind enough to read and comment on a draft of the manuscript. Special thanks go to Dawn Pedersen, Linda Van Vliet, Sharon Hage, and Alice Pruett for typing various stages of the manuscript. Infrared astronomy at the University of California, San Diego, California Institute of Technology, and the University of Rochester is funded by grants from the NSF and NASA.

Literature Cited

Allen, C. W. 1973. *Astrophysical Quantities*, p. 120. London: Athlone. 3rd ed.
Aumann, H. H., Walker, R. G. 1977. *Opt. Eng.* 16:537
Anderegg, M., Moorwood, A. F. M., Hippelein, H. H., Baluteau, J. P., Bussoletti, E., Coron, N. 1976. *Far Infrared Astronomy*, ed. M. Rowan-Robinson, p. 171. Oxford: Pergamon
Baluteau, J. P., Anderegg, M., Moorwood, A. F. M., Coron, N., Beckman, J. E., Bussoletti, E., Hippelein, H. 1977. *Appl. Opt.* 16:1834
Becklin, E. E., Matthews, K., Neugebauer, G., Wynn-Williams, C. G. 1973. *Ap. J. (Lett.)* 186:L69
Beer, R. 1968. *The Physics Teacher* 6, no. 4
Bell, R. J. 1972. *Introductory Fourier Transform Spectroscopy*. New York: Academic
Betz, A. L., Johnson, M. A., McLaren, R. A., Sutton, E. C. 1976. *Ap. J. (Lett.)* 208:L141
Blanco, A., Bussoletti, E., Melchiorri, B., Melchiorri, F., Natale, V. 1976. *Infrared Phys.* 16:569
Boyd, R. 1977. *Opt. Eng.* 16:563
Brandshaft, D., McLaren, R. A., Werner, M. W. 1975. *Ap. J. (Lett.)* 199:L115
Briotta, D. A., Houck, J. R. 1977. In *Proc. Symp. Recent Results in Infrared Astrophys., NASA Tech. Memo. X-73*, 190, ed. P. Dyal, p. 12. Ames Res. Cen.
Cameron, R. M., Bader, M., Mobley, R. E. 1971. *App. Opt.* 10:2011
Campbell, M. F., Harvey, P. M., Hoffmann, W. F., Jacobson, M. R., Ward, D. B., Harwit, M. O., Aannestad, P. A. 1977. See Briotta & Houck 1977, p. 52
Capps, R. W., Knacke, R. F. 1976. *Ap. J.* 210:76
Chamberlain, J., Gebbie, H. A. 1971. *Infrared Phys.* 11:57
Clarke, J., Hoffer, G. I., Richards, P. L., Yeh, N. H. 1975. In *Low Temperature Physics—LT1-4*, eds. M. Krusius, M. Vuorio, 4:226. New York: American Elsevier
Coletti, A., Melchiorri, F., Natale, V. 1976. See Anderegg et al. 1976, p. 125
Connes, J. 1961. *Rev. Opt.* 40:45, 116, 171, 231
Connes, P. 1970. *Ann. Rev. Astron. Astrophys.* 8:209
Coron, N., Danbier, G., Leblanc, J. 1971. In *Infrared Detection Techniques for Space Research*, eds. V. Manno, J. Ring, p. 121. Dordrecht: Reidel
Daehler, M., Ade, P. A. R. 1975. *J. Opt. Soc. Am.* 65:124
Dall'Oglio, G., Melchioni, B., Melchioni, F., Natale, V., Gandolfi, F. 1973. *Infrared Phys.* 13:1
Damle, S. V., Daniel, R. R., Iyengar, K. V. K., Rengarajan, T. N., Tandon, S. N., Verma, R. P. 1976. *COSPAR Symp. Infrared and Submillimeter Astron.*, p. 23
de Batz, B., Bensammar, S., Delavand, J., Gay, J., Journet, A. 1977. *Infrared Phys.* 17:305
de Batz, B., Granes, P., Gay, J., Journet, A. 1973. *Nature Phys. Sci.* 245:89
Decker, J. A., Harwit, M. 1969. *Appl. Opt.* 8:2552
de Graauw, Th., Van de Staadt, H. 1973. *Nature Phys. Sci.* 246:73
Dennison, B. K. 1976. See Damle et al. 1976, p. 17
Dyck, H. M. 1975. *Bull. Am. Astron. Soc.* 7:408
Dyck, H. M., Capps, R. W., Forrest, W. J., Gillett, F. C. 1973. *Ap. J. Lett.* 183:L99
Erickson, E. F., Strecker, D. W., Simpson, J. P., Goorvitch, D., Augason, G. C., Scargle, J. D., Caroff, L. J., Witteborn, F. C. 1977. *Ap. J.* 212:696
Fazio, G. G., Wright, E. L., Low, F. J. 1976. See Anderegg et al. 1976, p. 21
Fellgett, P. B. 1958. *J. Phys.* 19:187, 237
Forbes, F. F., Fymat, A. L. 1974. *Planets, Stars and Nebulae Studied with Photopolarimetry*, ed. T. Gehrels. Tucson: University of Arizona. p. 637
Forman, M. L., Steel, W. H., Vanesse, G. A. 1966. *J. Opt. Soc. Am.* 56:59
Frederick, C., Jacobson, M. R., Harwit, M. 1974. In *Symp. Telesc. Syst. for Balloon Borne Res., NASA Tech. Memo. X62, 397*, eds. C. Swift, F. C. Witteborn, A. Shipley. p. 81
Furniss, I., Jennings, R. E., King, K. J. 1976a. See Anderegg et al. 1976, p. 71.
Furniss, I., Jennings, R. E., Towlson, W. A., Venis, T. E., Welsh, B. U. 1976b. See Anderegg et al. 1976, p. 15
Furniss, I., Jennings, R. E., Moorwood, A. F. M. 1972. *Ap. J. Lett.* 176:L105
Geballe, T. 1974. PhD thesis. Univ. Calif., Berkeley.
Gehrz, R. D., Hackwell, J. A., Smith, J. R. 1976. *Publ. Astron. Soc. Pac.* 88:971
Gillespie, C. 1977. In *Proc. SPIE Sem. on Modern Utilization of Infrared Technol., II, Vol. 95*, ed. I. J. Shapiro. San Diego, CA.
Gillett, F. C. 1977. In *Infrared and Submillimeter Astronomy*, ed. G. Fazio, p. 195. Dordrecht: Reidel
Gillett, F. C., Dereniak, E. L., Joyce, R. R. 1977. *Opt. Eng.*, 16:544
Gillett, F. C., Forrest, W. J. 1973. *Ap. J.* 179:483
Gillett, F. C., Joyce, R. R. 1975. *Bull. Am. Astron. Soc.* 7:409
Greeb, M. E., True, G. A. 1974. See Frederick et al. 1974, p. 268
Greenberg, L. T., Dyal, P., Geballe, T. R. 1977. *Ap. J. Lett.* 213:L71
Hanel, R., Conrath, B., Gautier, D., Gierasch, P., Kumar, S., Kunde, V., Lowman, P., Maguire, W., Pearl, J., Pirraglia, J., Ponnamperuma, C., Samuelson, R. 1977. *Space Sci. Rev.* 21:129
Hanel, R., Schlachman, B., Breihan, E., Bywaters, R., Chapman, F., Rhodes, M., Rodgers, D., Vanous, D. 1972. *Appl. Opt.* 11:2625
Hanel, R. A., Kunde, V. G. 1975. *Space Sci. Rev.* 18:201
Harper, D. A., Hildebrand, R. H., Stiening, R., Winston, R. 1976. *Appl. Opt.* 15:53
Harvey, P. M., Campbell, M. F., Hoffmann, W. F. 1976. *Ap. J. Lett.* 205:L69
Harwit, M. 1964. *Liege Symp.* 26:506
Harwit, M., Houck, J. R., Fuhrmann, K. 1969. *Appl. Opt.* 8:473
Hauser, M. G., Notarys, H. A. 1975. *Bull. Am. Astron. Soc.* 7:409
Hazen, N. L., Coyle, L. M., Diamond, S. M. 1974. See Frederick et al. 1974, p. 202
Hilgeman, T., Smith, L. L. 1976. *Grumman Res. Dept. Rep. RE-531*
Hoffmann, W. F., Frederick, C. L. 1969. *Ap. J. Lett.* 155:L9
Hoffmann, W. F., Frederick, C. L., Emery, R. J. 1971. *Ap. J. Lett.* 164:L23
Hofmann, W., Drapatz, S., Michel, K. W. 1977. *Infrared Phys.* 17:451
Hofmann, W., Lemke, D., Thum, C. 1977. *Astron. Astrophys.* 57:111
Holtz, J. Z. 1971. PhD thesis. Univ. Calif., Berkeley
Houck, J. R., Pollack, J. B., Sagan, C., Schaack, D., Decker, J. A. Jr. 1973. *Icarus* 18:470
Johnson, H. L., Forbes, F. F., Thompson, R. I., Steinmetz, D. L., Harris, O. 1973. *Publ. Astron. Soc. Pac.* 85:458
Johnson, M. A. 1974 PhD thesis. Univ. Calif., Berkeley
Johnson, M. A., Betz, A. L., McLaren, R. A., Sutton, E. C., Townes, C. H. 1976. *Ap. J. Lett.* 208:L145
Joseph, R. D., Allen, J., Meikle, W. P. S., Sugden, K. C., Kessler, M. F., Rosen, D. L., Masson, G. 1977. *Opt. Eng.* 16:558
Joyce, R. R. 1977. *KPNO Users Manual.*
Kazanskii, A. G., Richards, P. L., Haller, E. E. 1977. *Appl. Phys. Lett.* 31:496

Kemp, J. C., Ricke, G. H., Lebofsky, M. J., Coyne, G. V. 1977. *Ap. J. Lett.* 215: L107
Keys, R. J., Quist, T. M. 1970. In *Semiconductors and Semi Metals*, eds. R. K. Willardson, A. C. Beer, 5: 321. New York: Academic
Knacke, R. F., Capps, R. W., Johns, M. 1976. *Ap. J. Lett.* 210: L69
Langlet, A., Delagi, C., Stefanovitch, D., Talureau, B., Tualy, J., Vervier, J., Fischer, W. P., Gills, J. M., Scheper, R., Leblanc, J., Dambier, G. 1977. *Appl. Opt.* 16: 1841
Larson, H. P., Fink, U. 1975. *Appl. Opt.* 14: 2085
Lee, T. J. 1977. *Infrared Phys.* 17: 485
Lemke, D., Klipping, G., Romisch, N. 1977. In *Cryogenic Eng. Conf.*, Boulder, CO.
Low, F. J. 1961. *J. Opt. Soc. Am.* 51: 1300
Low, F. J., Aumann, H. H., Gillespie, C. M. 1970. *Astronaut. Aeronaut.*, July 1970, p. 26
Low, F. J., Kurtz, R. F., Poteet, W. M., Nishimura, T. 1977. *Ap. J. Lett.* 214: L115
Low, F. J., Ricke, G. H. 1974. In *Methods of Experimental Physics*, ed. N. Carleton, 12: 415. New York: Academic
Manno, V., Ring, J. (eds.) 1971. *Infrared Detection Techniques for Space Research.* Dordrecht: Reidel
Martin, D. H., Puplett, E. 1970. *Infrared Phys.* 10: 105
Mather, J. 1977. In *Proc. SPIE Sem. Far Infrared/Submillimeter Wave Techn./ Appl.*, Vol. 105, ed. T. S. Hartwick, D. T. Hodges
McCarthy, D. W., Low, F. J. 1975. *Ap. J. Lett.* 202: L37
McCarthy, D. W., Low, F. J., Howell, R. 1977. *Opt. Eng.* 16: 569
McNutt, D. P., Shivananden, K., Feldman, P. D. 1969. *Appl. Opt.* 8: 2199
Meaburn, J. 1970. *Astrophys. Space Sci.* 9: 206
Mercer, J. B., Wilson, S., Chaloupka, P., Griffiths, W. K., Marchant, P., Marsden, P. L., Morath, C. C. 1976. See Anderegg et al. 1976, p. 103
Merrill, K. M., Soifer, B. T., Russell, R. W. 1975. *Ap. J. Lett.* 200: L37
Mertz, L. 1965. *Transformations in Optics.* New York: Wiley
Mertz, L. 1967. *J. Phys. Paris*, Collog. C2, Suppl. 3–4, Tome 28, C2-87
Michel, K. W., Nishimura, T. S., Oithof, H. 1977. *Space Sci. Instrum.* In press
Moore, W. J. 1976. *Final Rep. NASA Contract NAS 2-8706*
Moorwood, A. F. M. 1977. See Gillett 1977, p. 207.
Moss, T. S. 1976. *Infrared Phys.* 16: 29.
Mumma, M., Kostiuk, T., Cohen, S., Buhl, D., von Thum, P. C. 1975. *Space Sci. Rev.* 17: 661
Neugebauer, G. 1975. *Bull. Am. Astron. Soc.* 7: 408
Neugebauer, G., Becklin, E. E., Beckwith, S., Matthews, K., Wynn-Williams, G. C. 1976. *Ap. J. Lett.* 205: L139
Neugebauer, G., Becklin, E., Hyland, A. R. 1971. *Ann. Rev. Astron. Astrophys.* 9: 67
Nishioka, N. S., Richards, P. L., Woody, D. P. 1977. *Lawrence Berkeley Lab., Rep. No. 6085*
Nolt, I. G., Radostitz, J. V., Donnelley, R. J., Murphy, R. E., Ford, H. C. 1974. *Nature* 248: 659
Okuda, H., Marhoru, T., Oda, N., Sugiyama, T. 1977. *Nature* 265: 515
Penzias, A. A., Burrus, C. A. 1973. *Ann. Rev. Astron. Astrophys.* 11: 51
Peterson, D. W., Johnson, M. A., Betz, A. L. 1974. *Nature* 250: 128
Phillips, P. G., Briotta, D. A. 1974. *Appl. Opt.* 13: 2233
Phillips, P. G., Harwit, M. 1971. *Appl. Opt.* 10: 2780
Phillips, T. G., Huggins, P. J., Neugebauer, G., Werner, M. W. 1977. *Ap. J.* 217: L161
Pipher, J. L. 1971. PhD thesis. Cornell Univ. CRSR Rep. 461
Pipher, J. L., Savedoff, M. P., Duthie, J. G. 1977. *Appl. Opt.* 16: 233
Price, S. D., Walker, R. G. 1976. *AFGL Rep. No. AFGL-TR-76-0208*
Rank, D. M., Bregmann, J. D. 1975. *Bull. Am. Astron. Soc.* 7: 409
Ridgway, S. T., Capps, R. W. 1974. *Rev. Sci. Instrum.* 45: 676
Robson, E. I. 1976. See Anderegg et al. 1976, p. 115
Roche, A. E., Title, A. M. 1975. *Appl. Opt.* 14: 765
Roesler, F. C. 1974. See Low & Rieke 1974, p. 531
Rowan-Robinson, M., ed. 1976. *Far Infrared Astronomy.* Oxford: Pergamon
Russell, R. W., Soifer, B. T. 1977. *Icarus* 30: 282
Russell, R. W., Puetter, R. C., Soifer, B. T., Willner, S. P. 1978. *Bull. Am. Astron. Soc.* 9: 582
Scargle, J. D., Witteborn, F. C., Strecker, D. W., Erickson, E. F. 1977. See Briotta & Houck 1977, p. 15
Schaack, D. F. 1975. PhD thesis. Cornell Univ.
Schnopper, H. W., Thompson, R. I. 1974. See Low & Rieke 1974, p. 491
Sloane, N. J. A., Fine, T., Phillips, P. G., Harwit, M. 1969. *Appl. Opt.* 8: 2103
Soifer, B. T., Houck, J. R., Harwit, M. O. 1971. *Ap. J. Lett*, 168: L73
Swift, C., Witteborn, F., Shipley, A. (eds.) 1974. *Symp. Telescope Syst. Balloon Borne Res., NASA Tech. Memo. X62*, 397. Ames Res. Cent.
Tai, M. H., Harwit, M. 1976. *Appl. Opt.* 15: 2664
Thompson, R. I., Reed, M. A. 1975. *Publ. Astron. Soc. Pac.* 87: 929
Toombs, R. I., Becklin, E. E., Frogel, J. A., Law, S. K., Porter, F. C., Westphal, J. A. 1972. *Ap. J. Lett.* 173: L71
Traub, W. A. 1976. See Anderegg et al. 1976, p. 1
Treffers, R. R. 1975. *Astron. Astrophys.* 38: 345
Treffers, R. R. 1977. *Applied Optics* 16: 3103
van Duinen, R. 1976. See Damle et al. 1976, p. 25
Vanhabost, G., Gigan, P., Hammal, K., Mondellini, J., Darpentigny, C., Michel, J. P., Lux, D. 1976. *Space Sci. Instrumen.* Preprint
Vaughan, A. H. 1967. *Ann. Rev. Astron. Astrophys.* 5: 139
Werner, M. W., Becklin, E. E., Gatley, I., Neugebauer, G. 1977. See Briotta & Houck 1977, p. 55
Westphal, J. 1974. Final Report NASA Grant NGR 05-002-185
Willner, S. P. 1976. *Ap. J.* 206: 728
Witteborn, F. C., Strecker, D. W., Erickson, E. F., Smith, S. M., Goebel, J. M. 1977. See Briotta & Houck 1977, p. 35
Woody, D. P., Mather, J. C., Nishioka, N. S., Richards, P. L. 1975. *Phys. Rev. Lett.* 34: 1036
Wynn-Williams, C. G., Becklin, E. E., Forster, J. R., Matthews, K., Neugebauer, G., Welch, W. J., Wright, M. C. H. 1977. *Ap. J. Lett.* 211: L89
Zappala, R. R., Becklin, E. E., Matthews, K., Neugebauer, G. 1974. *Ap. J.* 192: 109

UNIVERSITY OF CALIFORNIA

San Diego

An Analysis of Infrared Spectra of Some Gaseous Nebulae, with Emphasis on the Planetary Nebula NGC 7027

A dissertation submitted in partial satisfaction of the

requirements for the degree Doctor of Philosophy

in Physics

by

Ray William Russell

Committee in charge:

Professor Baruch T. Soifer, Chairman
Professor James R. Arnold
Professor E. Margaret Burbidge
Professor Robert J. Gould
Professor Barnaby J. Rickett

1978

ABSTRACT OF THE DISSERTATION

An Analysis of Infrared Spectra of Some Gaseous Nebulae,

with Emphasis on the Planetary Nebula NGC 7027

by

Ray William Russell

Doctor of Philosophy in Physics

University of California, San Diego, 1978

Professor Baruch T. Soifer, Chairman

Infrared spectra from 2 to 13 μm (with resolution $\Delta\lambda/\lambda \sim 0.015$-$0.02$) of a variety of objects (including the planetary nebulae NGC 7027, BD +30°3639, and IC 418; the galaxy M82; and CRL 915/HD 44179) are discussed. The inclusion of 4 to 8 μm spectrophotometry obtained from the Kuiper Airborne Observatory is stressed, although the entire 2 to 13 μm region is shown to be very useful in understanding the physical conditions and radiation mechanisms in these and other sources.

A basic summary of collisionally excited forbidden-line analysis is presented, and the equations and parameters developed to

permit the identification of such lines in the astronomical data and their subsequent use in ion abundance calculations. For both NGC 7027 and BD + 30°3639 evidence is found for enhancement of several products of the α process, indicating substantial nuclear processing and mixing has occurred in the central stars of these planetary nebulae.

A possible identification of [Mg V] at 5.6 μm in the spectrum of NGC 7027 is discussed. Assuming the identification is correct, one can argue not only that magnesium is overabundant, but also calculate a lower limit on the temperature of the central star of $1.3 \cdot 10^5$ K. When the absorption of ultraviolet photons by oxygen ions is considered, this limit is raised to $\sim 2 \cdot 10^5$ K.

The Br γ line in BD + 30°3639 is used in conjunction with existing optical observations to calculate the reddening to the source, which can be expressed as $\sim 1\overset{m}{.}5$ extinction at Hβ. When previous radio observations are also considered, this leads to the suggestion that a very compact (< 0.1"), or equivalently, a very high density ($n_e > 1 \cdot 10^6$ cm^{-3}) radio component exists in the BD + 30°3639 field.

Broad strong emission features at 6.2 μm and 7.7 μm are seen for the first time in the spectrum of NGC 7027. This brings to five the number of such features discovered in the spectrum of NGC 7027 and subsequently found in common in the other spectra discussed here. These features, unidentified at present, are seen at 3.28/3.4 μm, 6.2 μm, 7.7-7.8 μm, 8.6 μm, and 11.3 μm. Various possible emission

mechanisms for producing these features are considered, and that of structure in the emissivity curve of the material(s) emitting thermally at these wavelengths explored in some detail.

In line with that approach to the problem, emissivity measurements on collections of small (2-5 μm), isolated particles have been obtained and are presented for a number of materials either suggested in the literature or considered reasonable candidates based on abundance arguments and characteristic frequencies of vibration of molecular groups found in such materials. Although carbonates, sulfates, and nitrates all have spectral features similar in some respects to the astronomical data, they are sufficiently different that no identification can be made at this time. The 6.2 μm feature may be due to water of hydration in some host material, as an amorphous silicate with water of hydration exhibits a 6.2 μm feature quite similar to that seen in the data for NGC 7027. However, until the host material can also be identified, this must be considered a tentative identification. Other materials whose spectra disagree with the celestial data are discussed.

Some avenues of future research in trying to understand the emission mechanism which produces these features include variations on the method of sample preparation to more closely approximate the astrophysical grain condensation process, consideration of molecular forbidden transitions, emission from organic species associated with the celestial grains, and fluorescence mechanisms.

The ubiquity of the emitting material (evidenced by the presence of the features in the spectrum of the galaxy M82, as well as in the spectra of a large variety of galactic objects) and the importance of the emission mechanism (indicated by the relatively large amount of energy radiated in the features compared to that in the continuum at these wavelengths) point out the crucial nature of this problem.

THE ASTROPHYSICAL JOURNAL, 228:118–122, 1979 February 15

SPECTROPHOTOMETRY OF COMPACT H II REGIONS FROM 4 TO 8 MICRONS

R. C. PUETTER, R. W. RUSSELL, B. T. SOIFER,* AND S. P. WILLNER
Department of Physics, University of California, San Diego
Received 1978 June 5; accepted 1978 August 21

ABSTRACT

Spectrophotometric observations from 4 to 8 μm of the compact H II regions W51–IRS 2 and K3-50 are reported. Two broad absorption features at $\sim$6.0 μm and 6.8 μm are observed in the spectra of W51–IRS 2, and the 6.0 μm feature is seen in K3-50. These features may be due to absorption by silicate grains. A more speculative identification is absorption by hydrocarbon molecules. The continuum flux from 2 to 13 μm is broader than emission from a single-temperature blackbody; this suggests a distribution of dust temperatures within the H II regions. Failure to detect hydrogen Pfund α in W51–IRS 2 indicates significant 7.5 μm extinction. Upper limits are placed on the abundance of Ar^+.

Subject headings: infrared: sources — infrared: spectra — nebulae: general

I. INTRODUCTION

H II regions have long been known to be strong emitters of infrared radiation (see Wynn-Williams and Becklin 1974 for a review). Since the early observations, it has been accepted that the mechanism for producing the infrared emission is predominantly thermal emission by dust associated with the ionized gas. Among the brightest galactic infrared sources are the compact ratio H II regions that have no optical counterparts. Through 2–4 μm and 8–13 μm spectroscopy of these regions (Soifer, Russell, and Merrill 1976, hereafter SRM; Gillett *et al.* 1975, hereafter GFMCS), identifications of major constituents of the warm emitting dust and cold absorbing dust have been obtained. Furthermore, a quantitative estimate of the near-infrared extinction to these regions has been obtained from measurements of hydrogen recombination lines.

In an effort to expand our understanding of these H II regions, we report here 4–8 μm spectrophotometric observations of two compact H II regions, W51–IRS 2 and K3-50. W51 is a large complex of H II regions (Martin 1972) associated with a dense molecular cloud having a CO column density on the order of 10^{19} cm^{-2} (Scoville and Solomon 1973). Wynn-Williams, Becklin, and Neugebauer (1974) mapped the W51 region at 2 μm and 20 μm and found a bright compact infrared source, IRS 2, to be coincident with the radio source G49.5d (Martin 1972). Deep absorptions at 3 μm and 10 μm indicate the presence of ice and a large column density of cold silicate dust, respectively (SRM, GFMCS), in the line of sight to the infrared source. In addition, there is considerable extinction at near-infrared wavelengths. SRM suggest the flux at Bγ is down by a factor of about 10 from that expected on the basis of optically thin radio observations.

K3-50 is also a bright infrared source associated with a compact thermal radio source (Neugebauer and Garmire 1970). This object shows 10 μm silicate absorption (GFMCS) and significant near-infrared extinction, but only marginal evidence for 3 μm ice absorption (SRM). Wynn-Williams *et al.* (1977) have shown that the previously assumed association of the infrared source with an optical H II region in K3-50 was, in fact, incorrect. The radio and infrared sources, however, are apparently coincident. A molecular cloud with CO column density $N_{CO} \approx 4 \times 10^{18}$ cm^{-2} is associated with K3-50 (Wilson *et al.* 1974).

II. OBSERVATIONS

K3-50 was observed on two flights and W51–IRS 2 on one flight aboard the Kuiper Airborne Observatory in 1977 July. The observations were obtained with a variable filter wheel spectrophotometer having a spectral resolution $\lambda/\Delta\lambda \approx 65$ and spanning the spectral range 4.1 to 8.0 μm. The chopping secondary of the telescope permitted standard infrared beam switching with a separation of approximately 45″. The instrument and observing procedure were as described by Russell, Soifer, and Willner (1977), except that the detector was a PbSnTe photovoltaic cell. The beam diameter was 28″ for both sources. The combined instrumental response and atmospheric transmission were determined by observing α Boo on each flight. The spectrum of α Boo was measured with respect to that of α Lyrae on one flight and is well fitted by a 4000 K blackbody with a 15% depression at $\sim$4.5 to 5.2 μm due to CO absorption in the atmosphere of α Boo. The star α Lyr was assumed to have a blackbody spectrum of temperature 9700 K with an absolute flux density level of 4.07×10^{-14} W cm^{-2} μm^{-1} at 2.2 μm. The strength of the CO absorption in α Boo, as determined by comparison with ρ Lyr, is consistent with that measured by Forrest

* Also California Institute of Technology.

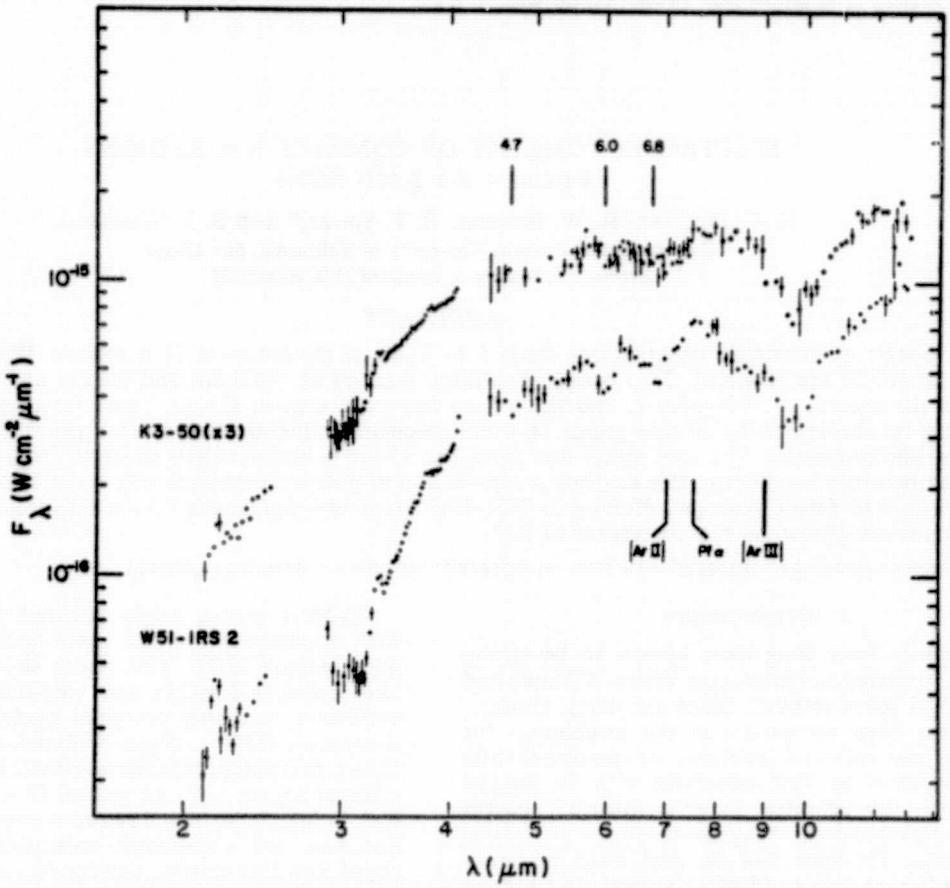

FIG. 1.—The 2 to 13 μm spectra of W51–IRS 2 and K3-50. The 4–8 μm spectra are from the present work. The 2–4 μm data are from SRM, and the 8–14 μm data are from GFMCS. The spectral resolution for all the data is $\lambda/\Delta\lambda \sim 65$, and error bars are shown for points whose statistical uncertainties are greater than 5%. For K3-50 from 5.45 to 7.41 μm, alternate points were obtained on different flights in most cases.

(1974) from ground-based photometry in the 5 μm atmospheric window. In addition to narrow-band spectrophotometric observations, broad-band photometry at 8.4 μm was obtained to allow direct comparison with ground-based observations. The data are summarized in Figure 1, which displays the 2–13 μm spectra. The 2–4 μm data are from SRM, while the 8–13 μm spectra are from GFMCS.

III. DISCUSSION

a) The Absorption Features

The spectra of W51–IRS 2 and K3-50 show a relatively flat continuum between 4 and 8 μm with several apparent absorption features. The 6.0 μm feature occurs in both objects, while the 6.8 μm feature is apparent in W51–IRS 2 and is possibly present in K3-50. Both features are seen in the spectra of several protostellar objects (Puetter *et al.* 1978). These absorptions might be attributed to silicate features, although this identification cannot be made definitive at this time. Some protosilicates produced in the laboratory show two absorptions between 5.8 and 7.0 μm (Duley and McCullough 1977). Although no single sample correctly reproduces both observed features, this class of material must be regarded as a relatively likely identification for these bands due to the close wavelength agreements of these bands and the associated strong featureless 10 μm absorption known to be present in the materials.

The 6.0 μm feature could be attributed to water of hydration in silicate grains. It is well known that hydrated silicates constitute a considerable fraction of the mass of some meteorites (Mason 1962); thus it might not be surprising to find hydrated grains in interstellar space. Hydrated minerals show a vibration band associated with the bound water at about 6.1 μm, with the exact wavelength being dependent on the host material.

One difficulty with the above identification is that hydrated silicates show an absorption at $\sim$2.9–3.0 μm typically stronger than that shown at 6.1 μm (Saksena 1961). The evidence for such an absorption in the 3 μm spectra of these objects is weak or inconclusive. The absorption feature at 3.08 μm in W51–IRS 2 appears to be strongest at a wavelength longer than that expected for bound water and has been identified with interstellar ice absorption (SRM). Furthermore, the relatively constant shape of this absorption (Merrill

Russell, and Soifer 1976) as seen in various objects would require a remarkably constant ratio of hydrated material to ice among these different clouds. This seems unlikely, since the ratio of ices to silicates appears to vary widely within these same clouds. We therefore regard this identification as quite tentative.

Carbonate minerals have a strong resonance band near 6.8 μm which might be identified with this absorption. We regard this identification as unlikely, because an expected carbonate band of comparable strength does not appear at $\lambda > 25$ μm (McCarthy, Forrest, and Houck 1978). A weaker carbonate feature at 11.3 μm that might be expected to appear is not seen (GFMCS), but the presence of the silicate absorption makes the absence of this feature a weaker constraint. In addition, the presence of carbonates in interstellar material is doubtful, on the basis of infrared spectra where the 11.3 μm band had previously been seen in emission (Russell, Soifer, and Willner 1977).

Because none of the above identifications of the absorptions at 6.0 and 6.8 μm are completely satisfactory and because the H II regions are viewed through large column densities of cold molecular cloud material, more exotic identifications associated with this material might be considered. Both the 6.0 and 6.8 μm bands coincide with frequencies common to hydrocarbon bonds. The 6.0 μm absorption may be due to aliphatic carbonyl groups (C=O, not associated with ring structures) that arise from the oxidation of hydrocarbons, and the 6.8 μm band may be caused by the bending vibration of CH_2 or CH_3. The structural group C=C also has a feature at 6.0 μm, but the integrated band intensity is probably too small for this to be a correct identification. It has been shown that complicated hydrocarbons exist in molecular clouds (Zuckerman and Palmer 1974), so perhaps this wavelength coincidence is more than random chance. Hydrocarbons would also be expected to show a feature near 3.3–3.4 μm due to C—H stretching. In fact, the "ice" band at 3.1 μm has a longer-wavelength wing that cannot easily be attributed to H_2O absorption or scattering (Merrill *et al.*).

The column densities of functional groups required to explain the absorption features as hydrocarbons can be calculated from the observed equivalent widths. The integrated band intensities, A, of these functional groups are well known and are found to be essentially independent of the nature of the molecule in which they are contained (Wexler 1967). The column density

$$N = 2.62 \times 10^{20} W A^{-1} \lambda^{-2} \text{ cm}^{-2}, \qquad (1)$$

where A is in units of 10^4 liters cm^{-2} mole^{-1} and W and λ are in microns.

For the aliphatic carbonyl group A is approximately 1 (Wexler 1967); thus the required column density of this group for both K3-50 and W51–IRS 2 is roughly 1/20 the observed radio CO column density. For CH_2 and CH_3, the value of A is roughly 0.07 for the absorption band at 6.8 μm. The inferred column density of CH_2 and/or CH_3 is ~one-half to ~one-quarter that of the observed radio CO. These column densities are most probably too high for the molecules to be in the gas phase, on the basis of molecular abundances inferred from radio observations (Allen and Robinson 1977, and references therein). Molecules adsorbed on dust grains, however, would not generally be detected by radio observations and might provide the necessary column densities to produce the observed infrared features. It must be emphasized that the presence of hydrocarbons in such large abundances has not been demonstrated. This possibility should be considered speculative, unless silicates can be shown to be incompatible with the observations or some other evidence for large quantities of hydrocarbons can be found.

There is an apparent absorption at 4.7 μm in the spectrum of W51–IRS 2. A similar feature appears in the spectra of two protostellar objects (Puetter *et al.* 1978) and possibly BN (Russell, Soifer, and Puetter 1977). If real, the most obvious identification of this feature is with absorption in the fundamental vibration-rotation band of CO. High-spectral-resolution observations (Hall *et al.* 1978) have revealed the presence of CO absorption at 4.7 μm in BN. The equivalent width of the absorption in W51–IRS 2 (0.01–0.03 μm) is comparable to that derived from the observations of Hall *et al.* for BN.

b) The Continuum

The overall continuum from 2 to 13 μm in W51–IRS 2 and K3-50, like that in many other H II regions, is quite flat, much broader than expected from any single-temperature blackbody. The emission from small dust grains at a single temperature and possessing a λ^{-n} emissivity dependence would be even narrower. Thus simple models incorporating only a single temperature for the emitting dust in the H II region (e.g., GFMCS) are not sufficient to explain all the observations. More detailed models of H II regions, such as those described by Panagia (1975) and Natta and Panagia (1976), predict that a relatively small fraction (less than 50%) of the dust heating within the H II region is produced by the trapped Lα emission. These models suggest substantial gradients in the dust temperature within the H II regions and would be consistent with our observations.

Another possible explanation of the observations is that several distinct objects dominate the observed flux at different wavelengths. If, for example, the Orion Nebula were observed from 10 times farther away (as in W51), the BN source, the KL nebula, and the Trapezium region would all be included in the observed spectrum, and the result would be very difficult to unravel.

Both of these possibilities are amenable to observational tests. Both predict a wavelength-dependent size of the infrared source, with the source size increasing as the wavelength increases. Indeed, just such a behavior has been found for W51–IRS 2 by Wynn-Williams, Becklin, and Neugebauer (1974). They found that the source diameter changes from

TABLE 1

EMISSION LINES

Parameter	W51–IRS 2	K3-50	Unit
Radio flux*	14.7	5.2	Jy
Pfα 7.46 μm flux	< 9	< 11.5	10^{-18} W cm^{-2}
[Ar II] 6.98 μm flux	< 14	5 ± 3	10^{-18} W cm^{-2}
$n(Ar^+)/n(Ar)$	< 0.3	0.3 ± 0.2	...
[Ar III] 8.99 μm flux†	< 6.5	< 6.5	10^{-18} W cm^{-2}
$n(Ar^{++})/n(Ar)$	< 0.4	< 1.2	...

* 10.6 GHz radio flux density from Felli *et al.*
† 8.99 μm line flux upper limit from GFMCS.

less than 2″ at 4.8 μm to 5″ at 20 μm. However, the single H II region model would require the position of the center of the infrared source to remain the same, while this position might change as a function of wavelength if the multiple-source model is valid. Such observations have been made for K3-50 by Wynn-Williams *et al.* (1977). To within 1″, or 0.05 pc, the radio, 2 μm, and 10 μm positions agree.

As previously suggested (Natta and Panagia 1976, and references therein; Willner 1977, and references therein), if the infrared emission raises from dust interior to the H II region, this region may have a normal dust-to-gas ratio. Previous estimates of large dust depletion in H II regions (e.g., GFMCS; Soifer and Pipher 1975) refer only to the dust hot enough to emit substantially near 10 μm and thus neglect the larger mass of colder material that should exist within the H II region.

c) *Hydrogen Recombination Line Pfund α*

The hydrogen (6–5) recombination line at 7.46 μm (Pfund α) was not observed in either source. Three sigma upper limits are given in Table 1. The expected line flux was calculated on the basis of 10.6 GHz radio observations (Felli, Tofani, and D'Addario 1974) and unpublished $b(n, l)$ values calculated by Brocklehurst (1971). In W51–IRS 2 the expected flux is 30% greater than the upper limit, consistent with the 0.7 mag of extinction estimated by extrapolating the extinction at Bγ (SRM) to 7.46 μm with a λ^{-1} law. In K3-50, the upper limit is larger than the predicted flux and places no bound on the extinction. In the following section, 0.7 mag of extinction will be assumed to apply at 6.98 μm for both W51 and K3-50.

d) *The Argon Fine-Structure Lines*

Emission lines from fine-structure transitions in heavy elements have been predicted to be quite strong from regions such as W51–IRS 2 and K3-50 (Petrosian 1970; Simpson 1973). The strongest such line in the 4–8 μm region is the 6.98 μm line of [Ar II]. This line is only marginally present in K3-50 and is not seen in W51–IRS 2, as shown in Table 1. The ionic abundances were calculated from the collision strength of Krueger and Czyzak (1970) and the transition probability given by Wiese, Smith, and Miles (1969) for an assumed electron density of 10^4 cm^{-3} and temperature of 10^4 K. These abundances, corrected for extinction, are given relative to the cosmic abundance of argon (Allen 1973) in Table 1. Similar upper limits are given for the line flux and abundance of Ar^{++}, based on the data of GFMCS. In W51–IRS 2, argon either is underabundant or is in higher ionization states. In K3-50, the limits are weaker, but probably most of the argon is more than singly ionized. The nondetection of the [Ne II] 12.8 μm fine-structure line in the same regions (GFMCS) suggests that most of the argon should be at least triply ionized.

IV. SUMMARY

The present observations of the compact H II regions K3-50 and W51–IRS 2, combined with other infrared spectroscopic observations of these regions, lead us to the following conclusions:

1. Two broad absorption features at 6.0 μm and 6.8 μm are observed in W51–IRS 2, and the 6.0 μm feature is seen in K3-50. The most plausible explanation of these bands is absorptions by silicate minerals; however, a unique identification does not appear to exist at this time. Hydrocarbon absorptions could also explain both features, but must be regarded as a much more speculative identification.
2. There is evidence for absorption due to the fundamental band of CO in W51–IRS 2.
3. The continuum flux distribution in these sources is broader than a single-temperature blackbody and is consistent with a distribution of dust temperatures within the H II regions.
4. The absence of Pfund α in W51–IRS 2 implies a finite extinction at 7.46 μm. The amount of extinction is consistent with a λ^{-1} extrapolation from 2.17 μm.
5. Most of the argon is probably more than singly ionized in both sources and more than doubly ionized in W51–IRS 2.

We would like to thank C. M. Gillespie and the entire staff of the Kuiper Airborne Observatory for their help in making the observations. We also thank F. C. Gillett and Kitt Peak National Observatory for the loan of the PbSnTe detector and D. N. B. Hall and W. J. Forrest for discussions of their observations in advance of publication. This research was supported by NASA under grant NGR 05-005-055.

C-2

REFERENCES

Allen, C. W. 1973, *Astrophysical Quantities* (3d ed.; London: Athlone Press).
Allen, M., and Robinson, G. M. 1977, *Ap. J.*, **212**, 396.
Brocklehurst, M. 1971, *M.N.R.A.S.*, **153**, 471.
Duley, W. W., and McCullough, J. D. 1977, *Ap. J.* (*Letters*), **211**, L145.
Felli, M., Tofani, G., and D'Addario, L. R. 1974, *Astr. Ap.*, **31**, 431.
Forrest, W. J. 1974, Ph.D. thesis, University of California, San Diego.
Gillett, F. C., Forrest, W. J., Merrill, K. M., Capps, R. W., and Soifer, B. T. 1975, *Ap. J.*, **200**, 609 (GFMCS).
Hall, D. N. B., Kleinmann, S. G., Ridgway, S. T., and Gillett, F. C. 1978, *Ap. J.* (*Letters*), **223**, L47.
Krueger, T. K., and Czyzak, S. J. 1970, *Proc. Roy. Soc. London*, *A*, **318**, 531.
Martin, A. H. M. 1972, *M.N.R.A.S.*, **157**, 31.
Mason, B. 1962, *Meteorites* (New York: Wiley).
McCarthy, J., Forrest, W. J., and Houck, J. R. 1978, private communication.
Merrill, K. M., Russell, R. W., and Soifer, B. T. 1976, *Ap. J.*, **207**, 763.
Natta, A., and Panagia, N. 1976, *Astr. Ap.*, **50**, 191.
Neugebauer, G., and Garmire, G. 1970, *Ap. J.* (*Letters*), **161**, L91.
Panagia, N. 1975, *Astr. Ap.*, **42**, 139.
Petrosian, V. 1970, *Ap. J.*, **159**, 833.
Puetter, R. C., Russell, R. W., Soifer, B. T., and Willner, S. P. 1978, *Bul. AAS*, **9**, 571.
Russell, R. W., Soifer, B. T., and Puetter, R. C. 1977, *Astr. Ap.*, **54**, 959.
Russell, R. W., Soifer, B. T., and Willner, S. P. 1977, *Ap. J.* (*Letters*), **217**, L149.
Saksena, B. D. 1961, *Trans. Faraday Soc.*, **57**, 242.
Scoville, N. Z., and Solomon, P. M. 1973, *Ap. J.*, **180**, 31.
Simpson, J. P. 1973, *Astr. Ap.*, **39**, 43.
Soifer, B. T., and Pipher, J. L. 1975, *Ap. J.*, **199**, 663.
Soifer, B. T., Russell, R. W., and Merrill, K. M. 1976, *Ap. J.*, **210**, 334 (SRM).
Wexler, A. S. 1967, *Appl. Spectrosc. Rev.*, **1**, 29.
Wiese, W. L., Smith, M. W., and Miles, B. M. 1969, *Atomic Transition Probabilities*, Vol. 2 (Washington: NSRDS-NBS22).
Willner, S. P. 1977, *Ap. J.*, **214**, 706.
Wilson, W. J., Schwartz, P. R., Epstein, E. E., Johnson, W. A., Etcheverry, R. C., Mori, T. T., Berry, G. G., and Dyson, H. B. 1974, *Ap. J.*, **191**, 357.
Wynn-Williams, G. C., and Becklin, E. E. 1974, *Pub. A.S.P.*, **86**, 5.
Wynn-Williams, G. C., Becklin, E. E., Matthews, K., Neugebauer, G., and Werner, M. W. 1977, *M.N.R.A.S.*, **179**, 255.
Wynn-Williams, G. C., Becklin, E. E., and Neugebauer, G. 1974, *Ap. J.*, **187**, 473.
Zuckerman, B., and Palmer, P. 1974, *Ann. Rev. Astr. Ap.*, **12**, 279.

R. C. PUETTER and S. P. WILLNER: Department of Physics, C-011, University of California, San Diego, La Jolla, CA 92093

R. W. RUSSELL: Astronomy Department, Cornell University, Space Science Building, Ithaca, NY 14853

B. T. SOIFER: Department of Physics, Downes Lab, 320-47, California Institute of Technology, Pasadena, CA 91125

THE ASTROPHYSICAL JOURNAL, 229:L65–L68, 1979 April 15

THE 4 TO 8 MICRON SPECTRUM OF THE GALACTIC CENTER

S. P. WILLNER, R. W. RUSSELL, AND R. C. PUETTER
Department of Physics, University of California, San Diego
B. T. SOIFER
California Institute of Technology
AND
P. M. HARVEY
Steward Observatory, University of Arizona
Received 1978 November 20; accepted 1979 January 16

ABSTRACT

Observations of the complex Sgr A W(N) with a 28″ beam and 1.5% spectral resolution are reported. Neither unidentified absorption features at 6.0 and 6.8 μm nor emission features at 6.2 and 7.7 μm were detected. The absence of the absorption features demonstrates that they are not characteristic of general interstellar extinction. The absence of emission features suggests that there is considerable distance between the ionized gas and the molecular clouds. The absence of 6.2 and 7.7 μm emission features also suggests that a feature previously seen at 3.3–3.4 μm is an absorption at 3.4 μm, and this absorption is apparently characteristic of interstellar extinction. The strength of the [Ar II] emission indicates an overabundance of argon. CO absorption seen at 4.67 μm indicates that saturation effects are not large, and there is evidently a large velocity dispersion in the line of sight to the infrared sources.

Subject headings: galaxies: Milky Way — galaxies: nuclei — infrared: spectra

I. INTRODUCTION

The galactic center contains a complex of infrared sources discussed most recently by Becklin *et al.* (1978*a*) and Rieke, Telesco, and Harper (1978). The sources are embedded in an H II region, as demonstrated by radio observations (see, e.g., Ekers *et al.* 1975). The infrared radiation from the sources can also act as a probe of interstellar extinction, because the total extinction to the various sources is essentially uniform, although there are probably variations at the 20% level (Becklin *et al.* 1978*b*; Rieke *et al.* 1978; Knacke and Capps 1977). The extinction to the galactic center is thought to be general interstellar extinction, rather than associated with particular molecular clouds (Soifer, Russell, and Merrill 1976; Becklin *et al.* 1978*b*).

The wavelength range of 4 to 8 μm contains many important spectral features: unidentified emission features at 6.2 and 7.7 μm that have usually been seen whenever dust, molecules, and ultraviolet radiation are present (Russell, Soifer, and Willner 1978, and references therein); the fundamental CO band at 4.7 μm; unidentified absorption features at 6.0 and 6.8 μm; and an [Ar II] fine-structure line at 6.99 μm. This *Letter* reports exploratory observations in this spectral range to see which features are present. The spatial resolution of 28″ is too low to permit observations of individual sources, but the general nature of the source complex and some properties of the extinction are discussed.

II. OBSERVATIONS

Observations were obtained aboard the Kuiper Airborne Observatory on a flight from Moffett Field to Honolulu (1978 May 16 UT) and on a flight based in Honolulu (May 18). The beam size was 28″, the reference beam was 1′ separated in azimuth, and the spectral resolution $\lambda/\Delta\lambda$ was ~65. The position of largest 6.5 μm surface brightness was observed, corresponding to the complex of sources called Sgr A W(N) (Rieke *et al.*). A standard was observed on each flight, but the on-board water-vapor measurements (Kuhn, Magaziner, and Stearns 1976) showed somewhat lower water vapor during most of the galactic center observations than during the standard observations. The data taken with lower water vapor were compared with observations of α Boo obtained on a subsequent flight from Honolulu (May 20). Every fourth point in the spectrum was measured consecutively, followed by a broad-band measurement and then a measurement of a different set of points. The results are presented in Figure 1, which shows that excellent agreement was obtained among the various passes through the spectrum. All of the data in Figure 1 from 5.6 to 8.0 μm were in fact obtained on the May 18 flight; the earlier data had a somewhat poorer signal-to-noise ratio. Clouds were encountered during parts of both flights. The presence of clouds could be determined by large values and rapid fluctuations of the indicated water vapor, by their visibility in the wide-field acquisition camera, or by visual observations by the aircraft pilots. All data that were in any way questionable have been omitted from Figure 1, although inclusion of the omitted data would not have changed the spectrum significantly.

Figure 1 also displays 2 to 4 μm data obtained with a 17″ beam (Soifer, Russell, and Merrill 1976) and a smoothed version of 8 to 13 μm data obtained by Gillett

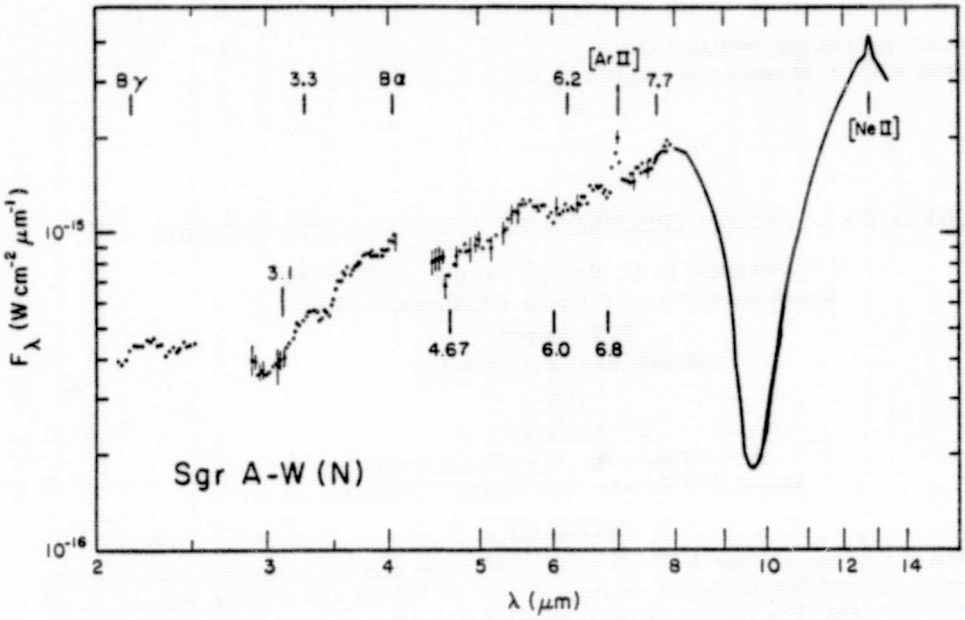

FIG. 1.—The 2–13 μm spectrum of the galactic center. The 2–4 μm portion is from Soifer, Russell, and Merrill (1976) and the 8–13 μm portion from Woolf (1973). Both were multiplied by 1.72 to normalize to the 4–8 μm data, and the 8–13 μm data were smoothed. Error bars are shown on the 2–8 μm data whenever the statistical uncertainty exceeds 5%.

and Woolf (Woolf 1973) with a 22″ beam. The latter data show a deeper 9.7 μm silicate absorption than the data of Becklin *et al.* (1978*a*) obtained with a 5″ beam. The ground-based data have been multiplied by 1.72 to normalize them to the airborne measurements. The factor of 1.72 for both the 2 to 4 and 8 to 13 μm. data was determined from the 16″ beam observations of Becklin and Neugebauer (1969) and from broad-band measurements with the KAO. Also marked in Figure 1 are the wavelengths or identifications of various spectral features. The only features plainly seen in the new data are an absorption at 4.7 μm, the wavelength of the fundamental band of CO, and the [Ar II] emission line at 6.99 μm.

The continuum shown in Figure 1 is much broader than a blackbody. Most of the emission beyond 3 μm is thought to be due to heated dust (Becklin and Neugebauer 1969), and the width implies that there is a distribution of dust temperatures. In this respect, the galactic center is similar to H II regions rather than to compact "protostellar" sources.

III. BROAD FEATURES

One of the most remarkable aspects of the spectrum in Figure 1 is the absence of any of the unidentified emission features seen in many planetary nebulae and H II regions. Two of the most prominent features should occur at 6.2 and 7.7 μm, but there is no evidence for them in the observed spectrum. These emission features generally are seen whenever heated dust, molecules, and ultraviolet radiation occur together. Although there may be a few instances where the features would be expected but are absent, such as the evolved object GL 618 (Russell *et al.*), the presence of the emission features seems to be independent of the spectrum of the ultraviolet source. The evidence for the association of heated dust and ultraviolet radiation in the galactic center is clear (Rieke, Telesco, and Harper 1978; Becklin *et al.* 1978*a*; Lacy *et al.* 1979). Molecules are also present, but their location relative to the heated dust and ionized gas is not well established (Oort 1977). Though no conclusion can be definite until the emission features are identified, we tentatively suggest that the interface between the ionized and molecular gas contains relatively little mass. In other words, the H II regions appear to be density-bounded and separated from the molecular clouds, and there is no prominent ionization front.

One absorption feature is seen near 4.67 μm, the wavelength of the fundamental vibration-rotation band of CO. The CO toward the galactic center has a large velocity dispersion (Oort 1977) permitting efficient absorption to occur. To produce the observed equivalent width of 4.8 cm^{-1} (=0.010 μm), a minimum column density of CO molecules of 5×10^{17} cm^{-2} (Burch and Williams 1962) is required.[1] A larger column density would be needed if the lines in the band are saturated. The depth of the silicate absorption and the near-infrared extinction (Becklin *et al.* 1978*b*) compared with the visual extinction of ζ Oph imply a total

[1] The measurements of Burch and Williams refer to a temperature of 273 K. If the CO is colder, fewer rotational levels will be populated. The transition probability is proportional to the angular momentum J, and J^2 is approximately proportional to T (see, e.g., Kovacs 1969). Thus at a temperature near 70 K, the integrated band intensity will be halved, and the implied column density will be doubled. The temperature is uncertain but is likely to be less than 273 K, so the value for that temperature is used to give a lower limit on the column density.

hydrogen column density of about (0.3 to 3) $\times 10^{23}$ cm^{-2}. At least 2% of the cosmic abundance of carbon is thus in the form of CO, comparable to the value found for ζ Oph (Morton 1975). The usual estimate for this fraction in molecular clouds is 10%, but, as discussed by Oort (1977), that value may be too low for the galactic center. Nevertheless, the saturation of the CO band does not appear to be larger than an order of magnitude, and thus a wide velocity dispersion is probably required in the CO directly in front of the infrared sources in order to produce the observed absorption. The velocity dispersion seen in the radio is therefore likely to occur along the line of sight, rather than only in separate clouds included in the larger radio beam.

The absence of 6.2 and 7.7 μm emission features suggests that there should be no 3.3 μm emission, because the features normally occur together (Russell *et al.*). It therefore appears likely that the structure in the spectrum at 3.3–3.4 μm (Soifer, Russell, and Merrill 1976) is an absorption at 3.4 rather than emission at 3.3 μm. The feature appears with approximately the same strength in both 17″ and 8″.5 beams and in the difference spectrum, so it is more likely to be associated with interstellar absorption than with any particular source. No ice absorption was seen in any of the three spectra (Soifer, Russell, and Merrill 1976).

An absorption at 3.4 μm has also been seen in the spectrum of the heavily reddened star VI Cygni No. 12 (Merrill, private communication). Such a feature may also be present in the spectrum of the infrared source W33 A (Capps, Gillett, and Knacke 1978), but if so it is relatively weak compared with the extremely strong ice absorption seen in that source. The 3.4 μm feature is thus probably characteristic of interstellar absorption. In the galactic center, it has a peak optical depth of about 3% of the 9.7 μm silicate optical depth.

A molecular identification of the 3.4 μm absorption might be possible, because the existence of molecules along the line of sight is demonstrated by the CO absorption. The best candidates are probably the stretching vibrations of methyl and/or methylene groups, occurring between 3.35 and 3.50 μm. These bands are the strongest exhibited by these groups, so no other features would be expected to appear in the data. The integrated band intensities (Wexler 1967), together with the measured equivalent width of 0.014 μm, imply a minimum column density of functional groups of 9×10^{17} cm^{-2} (Puetter *et al.* 1979). Molecules in the required abundance are very unlikely to exist in the gas phase (Morton 1975), but observations do not rule out the inferred column density of molecules or radicals as mantles on grains. Acceptance of this identification must, however, be reserved until further observational evidence for the existence of molecular mantles is found.

Two other features which might be expected to appear in the galactic center spectrum are absorptions at 6.0 and 6.8 μm seen in compact H II regions (Puetter *et al.* 1979) and several "protostars" (Puetter *et al.* 1977), including most prominently W33 A (Soifer *et al.* 1979). Figure 1 shows neither absorption feature, although there is an inflection near 5.6 μm that could possibly be interpreted as due to a very broad, shallow absorption centered at 6.0 μm. The 6.0 and 6.8 μm absorptions were suggested to be due to silicates; as can be seen from Figure 1, the galactic center suffers as much silicate extinction near 10 μm as many of the sources in which 6.0 and 6.8 μm absorptions were seen. The only difference that we can ascribe to the galactic center is that the absorption toward the galactic center is not due to cold, high-density molecular cloud material, as evidenced by the absence of ice absorption at 3.1 μm (Soifer, Russell, and Merrill 1976) and by the uniform amount of absorption (Becklin *et al.* 1978*b*). Perhaps only silicates that have been hydrated or otherwise processed in molecular clouds are capable of absorbing selectively at 6.0 and 6.8 μm. Another possibility is the speculative identification of the absorption features as due to hydrocarbon molecules (Puetter *et al.* 1979), which would occur only within molecular clouds. This identification may be somewhat strengthened if the 3.4 μm feature is identified with CH_3 and CH_2. Depending upon the exact molecule, the 6.8 μm feature would be weaker than the one at 3.4 μm (Wexler 1967), consistent with the absence of a 6.8 μm absorption in the observed spectrum. If this identification of the 6.0 and 6.8 μm features is correct, the small absorption at 3.4 μm would arise from those hydrocarbons that are sufficiently stable to exist in relatively unshielded interstellar space.

IV. EMISSION LINES

The most prominent feature in the 4 to 8 μm spectrum is the emission feature at 6.99 μm identified as a fine-structure line of [Ar II]. A number of other emission lines have been seen from approximately the same region, and these are listed in Table 1. The interpretation of the emission lines and their identification with individual sources within the galactic center complex is complicated, because the lines are broad and consist of many velocity components (Lacy *et al.* 1979). Nevertheless, large beams probably take similar sums over the emitting regions for all lines, and it is reasonable to compare the results. Comparison with radio observations is more difficult. Ekers *et al.* (1975) find 26 Jy at 5 GHz in a 0′.6 $\times$ 1′ beam, implying a brightness temperature of 800 K. Their map, on the other hand, shows a peak brightness temperature of 660 K. In order to predict the fluxes of infrared lines, we adopt the larger brightness temperature. Table 1 shows the predicted fluxes in various emission lines, based on the extinction curve adopted by Becklin *et al.* (1978*b*) and a constant radio surface brightness. The predicted fine-structure line fluxes are based on the assumption that each ionic abundance equals the cosmic abundance of the element (Allen 1973). Also shown in Table 1 are the measured line fluxes through various beam sizes; in each case, the beam size of the observation was used to calculate the predicted flux. Collision strengths and transition probabilities were taken from Osterbrock (1974), and a temperature of 10^4 K and electron density of 10^4 cm^{-3} were assumed.

Comparison of the predicted and measured fluxes in Table 1 suggests a factor of 2 overabundance of argon

TABLE 1

LINE FLUXES

Line	λ (μm)	Extinction (magnitudes)	Predicted Flux* (10^{-14} W m^{-2})	Measured Flux (10^{-14} W m^{-2})	Beam Size (arcsec)	Reference
Bγ	2.17	2.70	0.90	1.1±0.1	32	1
[Ar II]	6.99	0.70	31	64±12	28	2
[Ar III]	8.99	2.96	0.5	0.3	7	3
[Ne II]	12.81	1.14	62	78±7	25	4

* Including effect of extinction.

REFERENCES.—[1] Becklin *et al.* 1978*c*; [2] this *Letter*; [3] Lacy *et al.* 1979; [4] Aitken *et al.* 1976.

and a slight overabundance of neon. If the correct radio flux density is found to be lower, these overabundances will increase. Such large abundances of singly ionized species suggest that the H II regions in the galactic center are ionized by relatively cool stars, as also suggested by Aitken *et al.* (1976) and Lacy *et al.* (1979).

V. CONCLUSIONS

The absence of strong 6.0 and 6.8 μm absorption features in the spectrum of the galactic center implies that they are not characteristic of normal interstellar extinction, but rather that only material in molecular clouds produces these absorptions. Whether they come from hydration or other processing of silicate grains or from the formation of molecular mantles is not known. At 3.4 μm, there is absorption that is apparently characteristic of normal interstellar material, and which may be due to CH_2 and/or CH_3 groups.

The 6.2 and 7.7 μm unidentified emission features are not seen. The lack of detection of these bands, probably characteristic of interface regions between molecular clouds and H II regions, suggests that the galactic center H II regions may be density-bounded.

The large absorption found in the fundamental vibration-rotation band of CO requires substantial velocity dispersion in the material in a column in front of the infrared sources.

The observed [Ar II] flux implies that argon is overabundant in the galactic center compared with the vicinity of the Sun. A relatively low excitation level is also probable.

We thank the entire crew of the Kuiper Airborne Observatory for their efforts under the difficult conditions of operation away from base. We particularly thank J. W. Kroupa and P. M. Kuhn for obtaining the latest weather reports and modifying the flight plan to avoid most of the clouds. We also thank F. C. Gillett of Kitt Peak National Observatory for the loan of the PbSnTe detector. Airborne astronomy at UCSD is supported by NASA grant NGR 05-005-055 and at the University of Arizona by grant NGR 03-002-390. B. T. S. is also partially supported by NSF grant AST 77-20516 to the California Institute of Technology.

REFERENCES

Aitken, D. K., Griffiths, J., Jones, B., and Penman, J. M. 1976, *M.N.R.A.S.*, **174**, 41P.
Allen, C. W. 1973, *Astrophysical Quantities* (3d ed.; London: Athlone Press).
Becklin, E. E., Matthews, K., Neugebauer, G., and Willner, S. P. 1978*a*, *Ap. J.*, **219**, 121.
———. 1978*b*, *Ap. J.*, **220**, 831.
Becklin, E. E., Matthews, K., Neugebauer, G., and Wynn-Williams, C. G. 1978*c*, *Ap. J.*, **220**, 149.
Becklin, E. E., and Neugebauer, G. 1969, *Ap. J.* (*Letters*), **157**, L31.
Burch, D. E., and Williams, D. 1962, *Appl. Optics*, **1**, 587.
Capps, R. W., Gillett, F. C., and Knacke, R. F. 1978, *Ap. J.*, **226**, 863.
Ekers, R. D., Goss, W. M., Schwarz, U. J., Downes, D., and Rogstad, D. H. 1975, *Astr. Ap.*, **43**, 159.
Knacke, R. F., and Capps, R. W. 1977, *Ap. J.*, **216**, 271.
Kovacs, I. 1969, *Rotational Structure in the Spectra of Diatomic Molecules* (New York: American Elsevier), p. 121.
Kuhn, P. M., Magaziner, E., and Stearns, L. P. 1976, *Geophys. Res Letters*, **3**, 529.
Lacy, J. H., Baas, F., Townes, C. H., and Geballe, T. R. 1979, *Ap. J.* (*Letters*), **227**, L17.
Morton, D. C. 1975, *Ap. J.*, **197**, 85.
Oort, J. H. 1977, *Ann. Rev. Astr. Ap.*, **15**, 295.
Osterbrock, D. E. 1974, *Astrophysics of Gaseous Nebulae* (San Francisco: Freeman).
Puetter, R. C., Russell, R. W., Soifer, B. T., and Willner, S. P. 1977, *Bull. AAS*, **9**, 571.
———. 1979, *Ap. J.*, in press.
Rieke, G. H., Telesco, C. M., and Harper, D. A. 1978, *Ap. J.*, **220**, 556.
Russell, R. W., Soifer, B. T., and Willner, S. P. 1978, *Ap. J.*, **220**, 568.
Soifer, B. T., Puetter, R. C., Russell, R. W., Willner, S. P., and Harvey, P. M. 1979, in preparation.
Soifer, B. T., Russell, R. W., and Merrill, K. M. 1976, *Ap. J.* (*Letters*), **207**, L83.
Wexler, A. A. 1967, *Appl. Spectrosc. Rev.*, **1**, 29.
Woolf, N. J. 1973, in *IAU Symposium No. 52, Interstellar Dust and Related Topics*, ed. J. M. Greenberg and H. C. van de Hulst (Dordrecht: Reidel), p. 485.

P. M. HARVEY: Steward Observatory, University of Arizona, Tucson, AZ 85721

R. C. PUETTER and S. P. WILLNER: Department of Physics, C-011, University of California, San Diego, La Jolla, CA 92093

R. W. RUSSELL: Astronomy Department, Space Sciences Bldg., Cornell University, Ithaca, NY 14853

B. T. SOIFER: Downes Lab, 320-47, California Institute of Technology, Pasadena, CA 91125

UNIDENTIFIED INFRARED SPECTRAL FEATURES*

S. P. WILLNER, R. C. PUETTER and R. W. RUSSELL
University of California, San Diego, U.S.A.

and

B. T. SOIFER
California Institute of Technology, Pasadena, California, U.S.A.

Abstract. The infrared spectra between 2 and 13 μm of a variety of objects have become available in the past few years. These spectra have shown many objects to have up to six emission features that are still unidentified. Other objects show absorptions due to ice, carbon monoxide, silicates, and two unidentified features. The observational characteristics of the unidentified features are discussed here, together with several possible identifications.

1. Emission Features

The emission features were all discovered in NGC 7027, but at different times and by different observers. The infrared spectrum of this high-excitation planetary nebula is shown in Figure 1 (Russell *et al.*, 1977). From 2 to 3 μm the emission is due to recombination processes, while the general rise from 4 to 13 μm is thought to be due to thermal dust emission. The five features whose wavelengths are marked in the figure, as well as the 3.4 μm wing of the 3.3 μm feature, are the unidentified features under discussion. These features occur together in many objects, including the low-excitation planetary nebula BD +30°3639, several optical H II regions such as NGC 7538, the central H II regions in the galaxy M82, and a star surrounded by dust (HD 44179). In these objects, the relative strengths and shapes of the features are much the same, although the equivalent widths vary.

The earliest explanation for the emission features was that of emissivity peaks in inorganic material constituents of the dust. For example, Gillett *et al.* (1973) proposed that the 11.3 μm feature, the first to be discovered, was due to mineral carbonates. With wider spectral coverage and with the addition of measurements of inorganic compounds in our laboratory, it now seems that, at most, one of the unidentified bands can be due to thermal emission by inorganic minerals. The single possible candidate is water of hydration, which in most minerals produces a peak near 6.2 μm and no other features that are comparably strong. An example of such an emission peak in a silicate is given by Russell (1978). However, if the observed

* Invited contribution to the Proceedings of a Workshop on *Thermodynamics and Kinetics of Dust Formation in the Space Medium* held at the Lunar and Planetary Institute, Houston, 6–8 September, 1978.

Astrophysics and Space Science 65 (1979) 95–101. 0004–640X/79/0651–0095$01.05

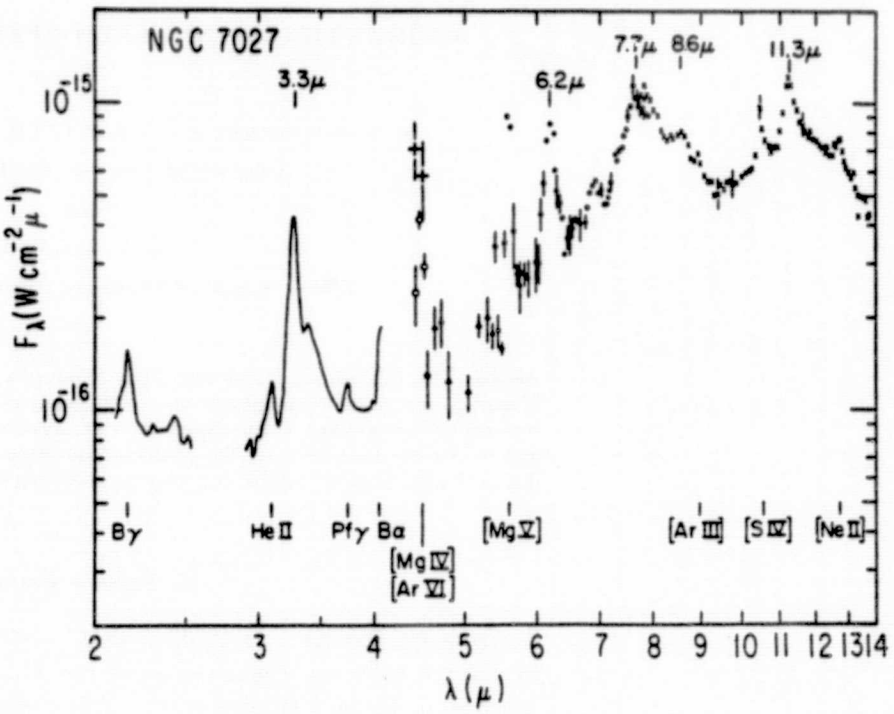

Fig. 1. The 2 to 13 μm spectrum of NGC 7027. Filled triangles have a resolution of 3%, and other points have a resolution of about 2%. Statistical uncertainties greater than 5% are shown. Unidentified emission features are marked, as are the wavelengths of various atomic transitions.

6.2 μm feature is due to water of hydration, the difficulty of identifying the underlying mineral and the rest of the features remains. All minerals suggested as identifications for the other emission bands have at least one additional emissivity peak at a wavelength where no peak is observed in the celestial sources.

There is still one possible way that inorganic minerals could contribute to the observed features. Gillett has suggested that the features may be excited by fluorescence, in which case it might be possible for only one infrared mode to be excited. A theoretical investigation of this possibility is certainly needed. Observationally the features have been seen only from regions where ultraviolet radiation is known to be present. Further observations to test this association are clearly required.

Thermal emission by carbonaceous minerals was proposed by Knacke (1977) to contribute to some of the unidentified features. Such minerals are known to be present in the interplanetary medium. The CH stretching at 3.3–3.4 μm is particularly promising, but it is difficult to see how the 6.2, 7.7, 8.6 and 11.3 μm features could be produced.

A very different possibility for the origin of the emission features is that they are due to molecules, either in the gas phase or attached to the grains. Grasdalen and

Joyce (1976) proposed that CH^+ excited by electron collision is responsible for the 3.3 μm feature. Herzberg (as quoted by Black) and Black (1978) have suggested that HeH^+ and OH excited by ultraviolet radiation might produce the 3.3 μm feature. All these molecules have relatively large rotational constants, and if such gas-phase molecules are responsible for the 3.3 μm emission, observations with 10 cm^{-1} or better spectral resolution should separate the rotational lines. Allamandola and Norman (1978) have proposed various molecules in ice mantles on grains for all the features. A possible difficulty with such proposals has been that for the estimated molecular abundances and excitation cross-sections, the efficiencies required are very high. In NGC 7027, for example, if the infrared bands are produced by ultraviolet fluorescence, each ultraviolet photon emitted by the central star must produce about three infrared photons in the emission bands. Such efficiencies require every ultraviolet photon to be absorbed by molecules, perhaps after conversion to Lyman-α (Black, 1978). The most promising single molecule is perhaps CH_4, which has fundamental bands at 3.3, 3.4 and 7.7 μm. Another promising candidate molecule, H_2O, has bands at 6.2 and 11.3 μm, although the wavelength agreement for the latter is not entirely satisfactory (Allamandola and Norman, 1978).

There are two additional observations that may bear on the origin of the emission features. In the region of the Orion nebula, the 6.2 and 7.7 μm features are strongest near the edge of the H II region and decrease in equivalent width nearer the center, where the silicate emission feature becomes prominent. Higher spatial resolution observations (Aitken *et al.*, 1979) have shown that the 11.3 μm feature arises just outside the ionized region. Thus, it seems that the material responsible for the features may originate in the molecular cloud and either does not penetrate to or is destroyed within the H II region.

The second observation bears on the question of whether the emission features are characteristic of carbon- or oxygen-rich chemistry. It has been found that at least the 3.3 μm feature occurs in IC 418, a planetary nebula that apparently shows silicon carbide emission (Willner *et al.*, 1979a) and thus can be considered to be carbon rich. The shape of this 3.3 μm feature is different from that in most other objects, however, in that it lacks the 3.4 μm wing. The presence of the other emission features is also doubtful. This observation suggests that at least one 3.3 μm feature is associated with a chemical mixture where carbon is more abundant than oxygen. On the other hand, the emission features are seen in the Orion Nebula and the galaxy M82 (Willner *et al.*, 1977), where oxygen is thought to be more abundant than carbon.

2. Absorption Features

A typical spectrum having absorption features is shown in Figure 2. NGC 7538–IRS 9 is a compact infrared source associated with a large H II region, molecular cloud complex (Werner *et al.*, 1979). The absorptions at 3.1, 4.7 and 9.7 μm are attributed to ice, gaseous carbon monoxide, and silicates, respectively. The features

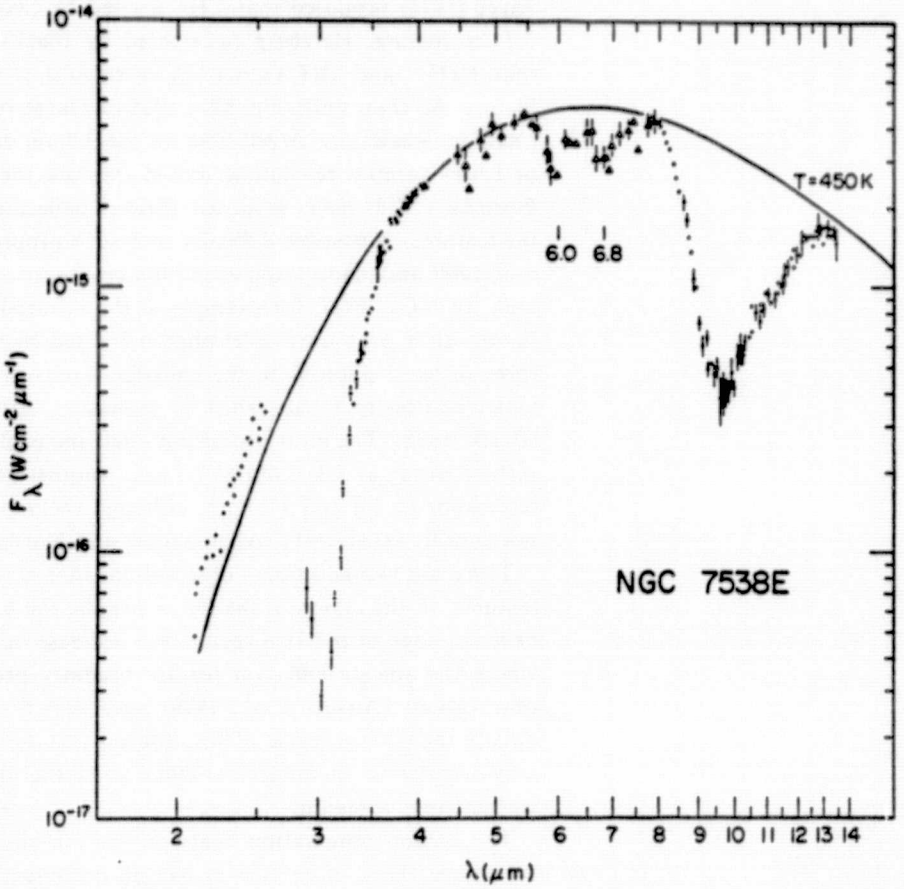

Fig. 2. The 2 to 13 μm spectrum of NGC 7538*E*. The infrared emission is dominated by the compact source IRS 9 (Werner *et al.*, 1979). The spectral resolution is about 2%, and statistical uncertainties greater than 5% are indicated. The line representing a 450 K blackbody radiation is intended to show the general shape of the spectrum rather than necessarily to represent a continuum. The unidentified features at 6.0 and 6.8 μm are marked.

at 6.0 and 6.8 μm are unidentified. These features are seen in at least six sources, mostly associated with molecular cloud complexes. The depths of the 6.0 and 6.8 μm features are not correlated with the depth of the silicate feature but do appear to increase when the ice absorption is strong. In particular, the strongest features occur in the OH source W33A (Soifer *et al.*, 1979), which has the strongest known ice absorption (Capps *et al.*, 1978). On the other hand, the features are weak or absent in the spectrum of the galactic center (Willner *et al.*, 1979b), which has no ice absorption and which is thought to be subject to interstellar rather than to molecular cloud type extinction (Soifer *et al.*, 1976; Becklin *et al.*, 1978). The lack of correlation with the 9.7 μm feature and the fact that the unidentified features are present only when

ice absorption is present suggest that the unidentified features, like the 3.1 μm ice feature (Gillett *et al.*, 1975), are characteristic of molecular cloud material rather than general interstellar material.

One plausible identification of the 6.0 and 6.8 μm features is absorption by amorphous silicate grains. Some laboratory protosilicates (Duley and McCullough, 1977) have two features between 5.8 and 7.0 μm, although no sample matches the wavelengths of the astronomical features. K. L. Day has informed us that features between 5.8 and 7 μm normally appear in amorphous silicates produced in aqueous solution. Silicates produced by condensation from vapor also have such features (Stephens and Russell, 1979), but again do not match the wavelengths of the astronomical features. We do not know the molecular or solid state mode that produces the features, and it is therefore difficult to assess the importance of the wavelength disagreement. Also, the large depth of the absorption features relative to the 9.7 μm feature seen in W 33A has not been seen in laboratory samples. More laboratory work to attempt to produce a silicate with sufficiently deep features at the correct wavelengths is needed.

One additional difficulty with the identification of the 6.0 and 6.8 μm features as silicate absorption is the apparent absence of these features in general interstellar material, while the 9.7 μm silicate feature is present (Gillett *et al.*, 1975; Merrill *et al.*, 1976). If a silicate identification is correct, the silicates must somehow be processed in molecular clouds to give them absorption bands near 6.0 and 6.8 μm.

A second, perhaps more speculative, identification is molecular absorption features. The 6.0 μm absorption could be due to stretching of a carbonyl (C=O) group in a hydrocarbon molecule. The exact wavelength of the C=O stretching is sensitive to the environment of the functional group and is at the observed wavelength if the molecules are adsorbed on certain surfaces (Little, 1966), if the group is subject to hydrogen bonding as in a carboxyl (Rao, 1963), and under various other conditions. The 6.8 μm feature would be primarily due to bending of CH_2, possibly with some contribution from CH_3. C=C might also contribute to the 6.0 μm feature, but the bond intensity is too small compared to that of the CH_2 group for C=C to be the major absorber (Wexler, 1967). One attractive feature of explaining the 6.0 and 6.8 μm features as hydrocarbon absorptions is that the CH stretching absorption would occur between 3.3 and 3.5 μm, where there is apparent absorption that cannot easily be attributed to ice. The major problem with these molecular identifications is that the required abundances of hydrocarbons are very large: towards two compact H II regions, for example, for every twenty CO molecules indicated by the radio observations, one C=O group and five to ten CH_2 or CH_3 groups in hydrocarbon molecules are required (Puetter *et al.*, 1979). These abundances are far too large for the molecules to be present in the gas phase, but molecules could be present as coatings on dust grains. Recent observations (Wooten *et al.*, 1978) have shown that the gas-phase abundance of simple molecules actually is lower in the densest molecular clouds than in less dense ones. If large abundances of hydrocarbons are present, it will necessarily

alter our understanding of the composition of dust grains and the chemistry of molecular clouds.

3. Summary

If the various emission and absorption features can be definitely identified, they will provide new information on the composition and physical state of interstellar dust. Better laboratory data, particularly with regard to UV fluorescence for the emission features, are needed. It should be emphasized that in laboratory experiments it is necessary to measure separately the emissivities and scattering efficiencies of potential dust components, rather than only their sum. Future astronomical observations should be made of regions having a variety of temperatures, densities, and radiation fields so as to better define the conditions under which the various features occur. Better theoretical understanding of UV fluorescence and of hydrocarbon surface chemistry under astrophysical conditions is also needed.

Acknowledgement

The authors thank E. E. Becklin and K. M. Merrill for valuable comments on the manuscript. This research was supported by NASA Grant NGR 05-005-055 and NSF Grant AST 76-82890.

References

Aitken, D. K., Roche, P. F., Spenser, P. M. and Jones, B.: 1979, *Astron. Astrophys.* (in press).
Allamandola, L. J. and Norman, C. A.: 1978, *Astron. Astrophys.* **63**, L23.
Becklin, E. E., Matthews, K., Neugebauer, G. and Willner, S. P.: 1978, *Astrophys. J.* **220**, 831.
Black, J. H.: 1978, *Astrophys. J.* **222**, 125.
Capps, R. W., Gillett, F. C. and Knacke, R. F.: 1978, *Astrophys. J.* **226**, 863.
Duley, W. W. and McCullough, J. D.: 1977, *Astrophys. J.* **211**, L145.
Gillett, F. C., Forrest, W. J. and Merrill, K. M.: 1973, *Astrophys. J.* **183**, 87.
Gillett, F. C., Jones, T. W., Merrill, K. M. and Stein, W. A.: 1975, *Astron. Astrophys.* **45**, 77.
Grasdalen, G. L. and Joyce, R. R.: 1976, *Astrophys. J.* **205**, L11.
Knacke, R. F.: 1977, *Nature* **269**, 132.
Little, L. H.: 1966, *Infrared Spectra of Adsorbed Species*, Academic Press, London, p. 350.
Merrill, K. M., Russell, R. W. and Soifer, B. T.: 1976, *Astrophys. J.* **207**, 763.
Puetter, R. C., Russell, R. W., Soifer, B. T. and Willner, S. P.: 1979, *Astrophys. J.* **228**, 118.
Rao, C. N. R.: 1963, *Chemical Applications of Infrared Spectroscopy*, Academic Press, New York, p. 192.
Russell, R. W.: 1978, Ph.D. Thesis, University of California, San Diego.
Russell, R. W., Soifer, B. T. and Willner, S. P.: 1977, *Astrophys. J.* **217**, L149.
Soifer, B. T., Russell, R. W. and Merrill, K. M.: 1976, *Astrophys. J.* **207**, L83.
Soifer, B. T., Puetter, R. C., Russell, R. W., Willner, S. P., Harvey, P. M. and Gillett, F. C.: 1979, *Astrophys. J.* **232** (in press).
Stephens, J. R. and Russell, R. W.: 1979, *Astrophys. J.* **228**, 780.
Werner, M. W., Becklin, E. E., Gatley, I., Matthews, K., Neugebauer, G. and Wynn-Williams, C. G.: 1979, *Monthly Notices Roy. Astron. Soc.* (in press).

Wexler, A. S.: 1967, *Applied Spect. Rev.* **1**, 29.
Willner, S. P., Soifer, B. T., Russell, R. W., Puetter, R. C., Joyce, R. R. and Gillett, F. C.: 1977, *Astrophys. J.* **217**, L121.
Willner, S. P., Jones, B., Puetter, R. C., Russell, R. W. and Soifer, B. T.: 1979a, *Astrophys. J.* **234** (in press).
Willner, S. P., Puetter, R. C., Russell, R. W., Soifer, B. T. and Harvey, P. M.: 1979b, *Astrophys. J.* **229**, L65.
Wooten, A., Evans, N. J. II, Snell, R. and vanden Bout, P.: 1978, *Astrophys. J.* **225**, L143.

THE ASTROPHYSICAL JOURNAL, 232:L53–L57, 1979 August 15

THE 4–8 MICRON SPECTRUM OF THE INFRARED SOURCE W33 A

B. T. SOIFER,[1] R. C. PUETTER,[2] R. W. RUSSELL,[2] S. P. WILLNER,[2] P. M. HARVEY,[3] AND F. C. GILLETT[4]

Received 1979 April 2; accepted 1979 May 15

ABSTRACT

Spectrophotometry with a resolution $\Delta\lambda/\lambda \sim 0.015$ of the highly obscured infrared source W33 A IR from 4.5 μm to 8 μm is reported. Three deep absorption bands, centered at 4.61 μm, 5.99 μm, and 6.78 μm, are observed. The band at 4.61 μm is most likely predominantly due to absorption in the fundamental vibration-rotation band of CO, although the wavelength of maximum absorption occurs slightly shortward of that expected for gaseous CO and could be affected by other absorbers. If no other absorber contributes to this band, then the minimum column density is 10% of the expected column density of carbon inferred from observed strength of the silicate absorption at 10 μm.

The absorption bands at 5.99 μm and 6.78 μm are extremely strong. Absorption processes in grains are needed to produce these bands, due to the large half-widths and equivalent widths of the absorptions. Observations of these bands in molecular cloud material, but not in the line of sight to the galactic center, strongly suggest that the formation process for these bands occurs within the molecular clouds. Arguments based on absorption strengths of these and the 10 μm silicate absorption require the 6.0 μm and 6.8 μm bands be caused by materials formed from cosmically abundant elements. The preponderance of available evidence suggests that these absorptions are due to hydrocarbon materials associated with interstellar dust. If this is the case, a substantial fraction of the carbon in the line of sight to W33 A IR is in the form of hydrocarbons.

Subject headings: infrared: sources — interstellar: matter

I. INTRODUCTION

Observations of infrared sources associated with the molecular clouds and OH sources have shown that the energy distributions of these objects can be described crudely as blackbody radiators obscured by large column densities of cold intervening material. The study of the spectral absorbance of the intervening matter permits analyses of the composition and column density of the intervening absorbing material.

W33 A IR is an infrared source that is particularly well suited as a background source for the detailed study of cold, dense interstellar material. The infrared source was originally discovered to be coincident with the OH source W33 A by Capps and Gillett (see Capps, Gillett, and Knacke 1978, hereafter CGK). Spectrophotometry of W33 A IR reported by CGK, and infrared photometry (Dyck and Simon 1977), have shown an extremely deep absorption band at 10 μm, indicating a large column density of cold silicate material in the line of sight. Both the silicate absorption at 10 μm and an extremely strong absorption at 3.1 μm (CGK), attributed in part to absorption by H_2O ice, were found by CGK to be much deeper than in any other previously reported infrared source.

In this *Letter* new spectrophotometric observations of W33 A IR from 4.5 μm to 8 μm are reported. These observations show that the absorption properties of the obscuring material are far more complex than had been previously thought. Some rather speculative compositional analyses of interstellar "dust" are consistent with the observations and are now more plausible.

[1] California Institute of Technology, Pasadena, CA 91125.
[2] Physics Department, University of California, San Diego, La Jolla, CA 92093.
[3] Steward Observatory, University of Arizona, Tucson, AZ 85721.
[4] Kitt Peak National Observatory, Tucson, AZ 85726.

II. OBSERVATIONS

The observations reported here were made with the UCSD 4–8 μm filter wheel spectrometer (Russell, Soifer, and Willner 1977; Puetter *et al.* 1979) on two flights of the Kuiper Airborne Observatory on 1978 May 16 and 1978 May 18 UT. The focal plane aperture for the observations was 27″ with a spacing between chopped beams of ~50″ in azimuth (nearly right ascension). The spectral resolution of the instrument is $\Delta\lambda/\lambda \sim 0.015$. For $4.5\ \mu m \leq \lambda \leq 4.9\ \mu m$ the spectrum was sampled at approximately half-resolution element intervals, while for $\lambda > 4.9\ \mu m$ the sampling was at approximately full-resolution element intervals. A total of 3 hours of observing were obtained on the source W33 A IR. Correction for telluric absorption and calibration of the spectrum was derived through observations of the K2 III star α Boo, whose spectrum was assumed to be a blackbody, except for a 15% absorption from 4.5 to 5.2 μm due to absorption by CO in the stellar atmosphere.

The observed spectrum of W33 A IR from 4.5 μm to 8 μm is shown in Figure 1. The spectrum of W33 A IR shows three strong absorption features centered at $4.61 \pm 0.02\ \mu m$, $5.99 \pm 0.08\ \mu m$, and $6.78 \pm 0.08\ \mu m$. The uncertainty in the center wavelength of each band reflects both the sampling of the spectrum and the

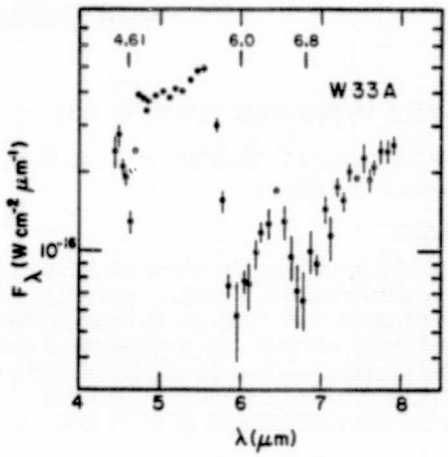

FIG. 1.—The 4.5–8 μm spectrum of W33 A IR. Statistical uncertainties are shown when they exceed 5% of the observed flux. The absorption features at 4.61 μm, 6.0 μm, and 6.8 μm are marked.

breadths of the bands. All three of the bands are resolved at the spectrometer resolution of $\Delta\lambda/\lambda \sim 0.015$.

The observed properties of these absorption bands are listed in Table 1. It is assumed that the bands centered at 5.99 μm and 6.78 μm are distinct bands, although we have no direct evidence that this is the case. The parameters were derived assuming that the apparent continuum can be smoothly interpolated between the absorption bands, and that the absorptions at the edges of the bands are zero (except at 6.4 μm). The values of the wavelengths of half-maximum absorption and the equivalent widths for the 6.0 μm and 6.8 μm bands are uncertain due to the difficulty in evaluating the effects of overlapping absorptions.

While absorptions at the wavelengths of 4.67 μm, 6.0 μm, and 6.8 μm have been reported previously in the spectra of the infrared sources W51 IRS 2, K3-50 (Puetter *et al.* 1979), and NGC 7538 E (Willner *et al.* 1979*a*), the bands observed in W33 A IR are by far the strongest yet observed. This is not surprising, in view of the fact that the 3.1 μm and 9.7 μm bands in W33 A IR are also the deepest examples of these bands yet observed (CGK).

The full 2–13 μm spectrum of W33 A IR is shown in Figure 2. The data for $\lambda < 4$ μm and $\lambda > 8$ μm were taken from CGK. The agreement between the flux determined from ground-based and that from airborne observations is excellent. Because the data were obtained with substantially different aperture sizes (5″–12″ for the ground-based data, 27″ for the airborne data), these data show that there is little or no extended emission in the wavelength interval $3 < \lambda < 8$ μm associated with the compact source.

III. DISCUSSION

The nature of the infrared source W33 A IR, as deduced from infrared observations, was discussed by CGK. We shall not expand on this discussion except to note that the present observations are completely consistent with the interpretation of W33 A IR as a highly compact object in the early stages of stellar formation (CGK).

The more interesting implication of the new observation regards the material responsible for the strong absorptions found in the 4.5–8 μm region. From this point of view, the infrared source is a convenient background source seen through a large column density of cold, interstellar matter. In fact, the cold material is most likely associated with the W33 molecular cloud and the infrared source.

a) The 4.61 Micron Band

The absorption band centered at 4.61 μm is very close in wavelength to the fundamental vibration band of the CO molecule, and it is most likely that CO is in some way responsible for this absorption. However, the central wavelength of the CO fundamental band is 4.67 μm (2143 cm^{-1}), while the center wavelength of the observed absorption is at 4.61 μm (2169 cm^{-1}). This band was observed 3 separate times in the two flights, and the minimum flux occurred at the same wavelength in each scan. Furthermore, there are no telluric spectral features at this wavelength (to <5% of the continuum) in evidence in spectra of stars that could contribute to a wavelength discrepancy. While this discrepancy is not large, we believe it to be real, since observations of the galactic center with the same instrument on the same flights showed a CO absorption band centered at the correct wavelength.

Several possible forms of CO might contribute to this absorption. The vibration fundamental of CO with differing isotopic composition (e.g., $^{13}C^{16}O$, $^{12}C^{18}O$, etc.) would occur at a longer wavelength than 4.67 μm. The CO band center shifts to shorter wavelengths as the gas temperature increases; however, the shift is only 0.02 μm from 20 to 250 K.

TABLE 1

ABSORPTIONS IN W33 A

λ_{max}(μm)	τ_{max}	λ(1/2 τ_{max})		Equivalent Widths	
3.08[a]	>7	...	~3.3 μm	...	...
4.61±0.02	0.9	4.56 μm	4.67 μm	0.092 μm	43 cm^{-1}
5.99±0.08	2.0	5.77 μm	(6.40) μm	0.58 μm	176 cm^{-1}
6.78±0.08	1.7	(6.45) μm	7.16 μm	0.67 μm	145 cm^{-1}
9.7[a]	~6	8.70 μm	11.35 μm	3.70 μm	380 cm^{-1}

[a] Data from CGK.

The fundamental vibration band of CO^+ is centered at 4.58 μm; however, neither radio observations (Hollis *et al.* 1978) nor theoretical abundance analyses (Mitchell, Ginsburg, and Kuntz 1978) have suggested that this molecule is at all abundant in molecular clouds.

Carbon monoxide absorbed on a variety of metals and metal oxides produces an absorption band near 4.61 μm (Little 1966). This band generally disappears at low pressures; however, the physics of this wavelength shift is unknown, and absorption on grains cannot be ruled out as the mechanism responsible for the observed band.

It would be remarkable that a material that produces a greater absorption than CO would be present at a wavelength so near the CO vibration fundamental, and yet would not be a sufficiently common material to be readily identifiable. We therefore regard the CO identification as the most likely explanation of this band. The lack of a ready explanation for the discrepancy between the observed central wavelength of the band and that of gaseous CO must leave open the possibility that the main absorber is another material.

If the CO identification is correct and the CO is in the gas phase, the observed equivalent width of 43 cm^{-1} can be used to estimate some properties of the CO in the line of sight. Taking $T \sim 150$ K as an estimate of the gas temperature, then the number of significant absorption lines in the fundamental vibration-rotation band would be $\lesssim 25$. The equivalent width per line then must be $\gtrsim 1.7$ cm^{-1}. This requires a minimum velocity width per line of at least 250 km s^{-1}. At this time there is no direct evidence for such extraordinary velocities in W33 A IR. The observed width of the $J = 1$–0 line of CO in W33 A is ~15 km s^{-1} (Wilson *et al.* 1974), although this was not measured at the exact position of W33 A IR. On the other hand, velocity widths of ~100 km s^{-1} are known to exist in other similar objects. The plateau source in Orion is known to have a velocity width of order ~50–100 km s^{-1} (e.g., Phillips *et al.* 1977; Kwan and Scoville 1976; Nadeau and Geballe 1979). Observations of the CO fundamental in CRL 2591 (Kleinmann *et al.*, private communication) show heavily saturated CO lines of width ~100 km s^{-1}. Thus CO lines of the required width are not totally unprecedented. If, however, the absorption is due to CO absorbed on grains, the large widths of the lines could be caused by varying degrees of CO–host interactions.

If we assume that the absorption is due to gaseous CO, a lower limit to the line-of-sight concentration of CO can be estimated. Assuming the individual lines are optically thin, using the band constants from Mantz

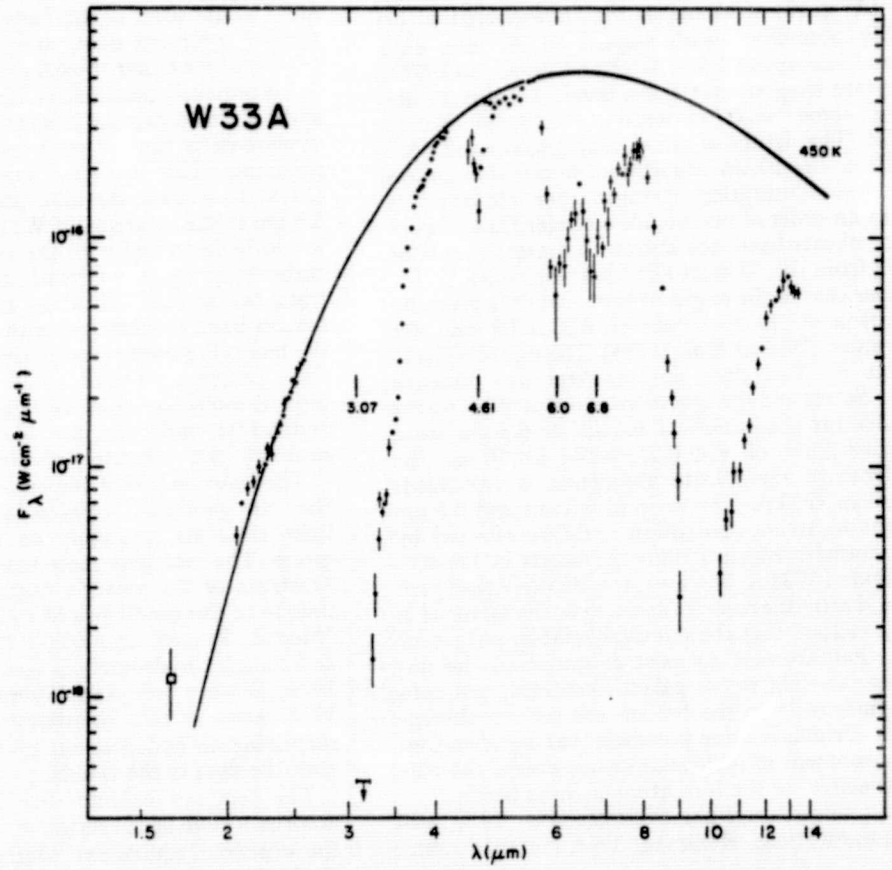

FIG. 2.—The 2–13 μm spectrum of W33 A IR. The data from 2–4 μm and 8–13 μm are taken from CGK. A blackbody curve fitted through the observations at 2–2.5 μm and 4–5 μm is shown for comparison.

et al. (1975), and taking $T \sim 150\ K$, an equivalent width of 43 cm^{-1} requires a column density of $N_{CO} \sim 10^{19}\ cm^{-2}$. This can be compared with the total column density of carbon inferred from the silicate absorption in the same line of sight. Taking the optical depth of silicates to be 6 at 10 μm (CGK), the mass opacity coefficient of silicates to be $\sim 3 \times 10^3\ cm^2\ g^{-1}$, and a C/Si ratio of 10 for cosmic abundances, the total column density of carbon is $N(C) \sim 10^{20}\ cm^{-2}$ if all the Si is bound in the silicate dust. Thus we would conclude that a significant fraction of all the carbon in the line of sight to W33 A IR is in the form of gaseous CO. If the CO in the line of sight is not in the gas phase, being, for example, absorbed on grains, the above estimate of the CO concentration will be correct only if the integrated band intensity is the same as for gas-phase CO. Clearly, high spectral resolution observations of the 4.61 μm band are critically important to understanding its origin and implications.

b) The Bands at 6.0 and 6.8 Microns

The strengths of the bands at 6.0 μm and 6.8 μm are striking in comparison to those previously observed in H II regions and "protostars." The widths of these bands are too large to be identified with absorption from the ground vibration state of any cold ($T \lesssim 100$ K) gas-phase molecule comprised of a relatively small number ($N \lesssim 10$) of atoms or that is expected to be reasonably abundant (with respect to H_2, see, e.g., Herbst and Klemperer 1973; Allen and Robinson 1977). We therefore suggest that these bands are due to absorption in some "solid" material in the line of sight to W33 A IR. The depths of these bands, compared with the depth of the 10 μm absorption, imply that unless their intrinsic absorption strength (per absorber) is more than an order of magnitude stronger than that of the 10 μm silicate band, the absorbing material must be composed from the 10 most abundant elements.

A further clue to the origin of these bands is given by a comparison of the spectrum of W33 A IR and the galactic center (Willner *et al.* 1979*b*). The line of sight to Sagittarius A West does not intersect any massive molecular clouds and the spectrum of Sgr A West shows no evidence for absorption at 6.0 μm or 6.8 μm (to a conservative limit of $\tau < 0.2$), while at 10 μm the optical depth of the silicate absorption is two-thirds that found in W33 A. The ratio of 6.0 μm and 6.8 μm absorptions to 10 μm absorption could be affected by radiative transfer effects within the bands in the molecular cloud of W33 A; however, it is unlikely that such effects could alter the ratio by as much as the factor of 2. Thus we conclude that the relatively stable, refractory materials that are able to exist as grains in the unshielded line of sight to the galactic center do not contribute significantly to the 6.0 μm and 6.8 μm absorption bands. Evidently some processes that are enhanced in the environment of molecular clouds create the material responsible for the formation of these bands.

Hydrated silicates and protosilicates (Day 1978, private communication; Rossman 1978, private communication; Duley and McCullough 1977) could be responsible for these bands. Such materials show absorption bands generally between 6 and 7 μm. In this case the band at 6.0 μm must be identified with the water of hydration band in the hydrated materials. There are several difficulties with this identification. First, the relative strengths of the 6.0 μm and 6.8 μm bands are usually much less than that of the 10 μm band, rather than the ratio 1/3 found in W33 A IR. Second, the formation of the hydrated grains must occur within the molecular clouds where the cold temperatures characteristic of the W33 molecular cloud are more appropriate to the formation of ice mantles than of hydrated materials. Third, the center wavelength of the 6.0 μm band in hydrated minerals is usually at 6.1–6.2 μm with a FWHM of 0.2–0.3 μm (Day 1978, private communication; Russell 1978, private communication), depending on the material. The observed center wavelength in W33 A occurs at 6.0 μm, and the apparent FWHM is approximately twice the value found in hydrated terrestrial minerals. A final, and perhaps most serious, difficulty comes from the observation of the 4–8 μm spectrum of the OH maser source OH 26.5+0.6 (Forrest *et al.* 1978). This is an oxygen-rich, heavily dust-enshrouded late-type star which shows a strong 10 μm silicate absorption band ($\tau_{10\ \mu m} \gtrsim 3$) in its spectrum. The circumstellar environment would seem particularly conducive to the formation of hydrated dust, and yet there is no evidence ($\tau < 0.2$) for either the 6.0 μm or the 6.8 μm band.

A previously speculative identification of the 6.0 μm and 6.8 μm absorption bands that must now be seriously considered is that of resonance bands of hydrocarbon materials. This was first suggested by Puetter *et al.* (1979) to explain the absorption bands at 6.0 μm and 6.8 μm in the spectrum of W51 IRS 2. The 6.0 μm band would be identified with the stretching vibration of the carbonyl group (C=O) and possibly some contribution from the stretch vibration of the C=C group. The 6.8 μm band is identified with the scissors vibration in the methyl or methylene group. The molecules in which these groups are found would form volatile mantles of organic molecules on more stable refractory core grains. Individual molecules are likely to be complex and probably not separately identifiable.

The wavelengths of the observed bands indicate that they are produced by molecules containing relatively light elements, probably no heavier than the CNO group. The fact that these bands do not appear in the spectrum of the galactic center implies that they are unique to the conditions of molecular clouds. Both ices (Merrill, Russell, and Soifer 1976; Gillett *et al.* 1975) and complex hydrocarbons (see Zuckerman and Palmer 1974; Winnewisser and Walmsley 1978; Kroto *et al.* 1978) exist in this environment, so it should not be surprising if hydrocarbon molecules were associated with the dust in the clouds.

The required column densities of the appropriate absorbers have been crudely estimated in Table 2, using the observed equivalent widths and laboratory inte-

TABLE 2

ABUNDANCES OF ORGANIC BONDS TOWARD W33 A

λ (μm)	Band Intensity A[a] (10^4 liter cm^{-2} mole^{-1})	Bond	Equivalent Width (μm)	N_{Bond}[b] (cm^{-2})
6.0.....	1	C=O	0.62	4×10^{18}
	0.06	(C=C)	...	(6×10^{19})
6.8.....	0.04	CH_3, CH_2	0.67	5×10^{19}
3.3.....	0.3	CH_2, CH, CH_3	0.3	3×10^{19}

[a] From Wexler 1967.

[b] The conversion from equivalent width to column density is through the relation $N = 2.6 \times 10^{20}\, W/A\lambda^2$ cm^{-2} (Puetter *et al.* 1979), where W is the equivalent width of the band (in μm), λ is the wavelength (in μm), and A is the band intensity (in 10^4 liter cm^{-2} mole^{-1}).

grated band intensities (Wexler 1967; Puetter *et al.* 1979). These column densities can be compared with the total column density of silicon calculated above. The column density of silicon to W33 A IR is $N_{Si} \sim 10^{19}$ cm^{-2}. From Table 2 the ratio of carbon bonds to silicon atoms is then ~5 (assuming the C=O identification of the 6.0 μm band), consistent with cosmic abundances of carbon if a substantial fraction of the carbon is in the form of the suggested functional groups. While these estimates are subject to large errors, they show that this identification cannot be ruled out on the basis of elemental abundance arguments, and they at least show a consistent column density for the CH groups in the stretching and scissors vibration modes.

An identification of the 6.0 μm and 6.8 μm bands as due to organic molecules suggests a solution to a difficulty with the identification of the 3.1 μm absorption band as H_2O ice. Merrill *et al.* showed that, while the peak absorption of this band occurs at a wavelength that agrees well with water-ice absorption, the shape of the absorption, in particular the wing at longer wavelengths, did not fit the expected ice absorption. CGK showed that this problem was particularly acute in the case of W33 A IR and suggested that the stretching mode of C—H molecules could contribute to absorption in the wing of the ice band. The stretching vibration of the C—H band occurs at 3.3–3.5 μm, depending on the specific group being observed, and would naturally account for the long-wavelength wing of the 3.1 μm absorption. The relative strength is expected to be somewhat greater than that of the 6.8 μm band, consistent with the present observations.

While the above identifications suggest which functional groups are present in large abundances, they do not define the specific molecules, since the wavelengths of the resonances of the functional groups are usually only weakly sensitive to the specific host molecules. It is doubtful that any single molecule would be responsible for the observed absorptions, but rather a large variety of molecules on grain surfaces would contribute to the absorption bands. This is consistent with the broad absorptions that are observed, while the characteristic signatures of the functional groups in specific molecules are lost.

It is a pleasure to thank the entire staff of the Kuiper Airborne Observatory for their assistance in obtaining these observations. We especially thank Allan Meyer for his expert assistance in acquisition of the infrared targets and in operating the KAO tracking system. We also thank Don Hall for providing calculations of CO line strengths, Kendrick Day for providing unpublished laboratory spectra of silicates, and Ken Day, George Rossman, and Mike Werner for helpful discussions. Airborne astronomy at UCSD and CIT is supported by NASA grant NGR 05-005-055. P. M. H. is supported by NASA grant NGR 03-002-390. B. T. S. is also partially supported by NSF grant AST77-20516 to CIT. Kitt Peak National Observatory is operated by AURA, Inc., under contract with the national Science Foundation.

REFERENCES

Allen, M., and Robinson, G. W. 1977, *Ap. J.*, **212**, 396.
Capps, R. W., Gillett, F. C., and Knacke, R. 1978, *Ap. J.*, **226**, 863 (CGK).
Duley, W. W., and McCullough, J. D. 1977, *Ap. J.* (*Letters*), **211**, L145.
Dyck, H. M., and Simon, T. 1977, *Ap. J.*, **211**, 421.
Forrest, W. J., *et al.* 1978, *Ap. J.*, **219**, 114.
Gillett, F. C., Jones, T. W., Merrill, K. M., and Stein, W. A. 1975, *Astr. Ap.*, **45**, 77.
Herbst, E., and Klemperer, W. 1973, *Ap. J.*, **185**, 505.
Hollis, J. M., Ulich, B. L., Snyder, L. E., Buhl, D., and Lovas, F. J. 1978, *Ap. J.*, **219**, 74.
Kroto, H. W., Kirby, C., Walton, D. R. M., Avery, L. W., Broten, N. W., MacLeod, J. M., and Oka, T. 1978, *Ap. J.* (*Letters*), **219**, L133.
Kwan, J., and Scoville, N. 1976, *Ap. J.* (*Letters*), **210**, L39.
Little, L. H. 1966, *Infrared Spectra of Adsorbed Species* (London: Academic Press).
Mantz, A. W., Maillard, J. P., Roh, W. R., and Rao, K. N. 1975, *J. Molec. Spectrosc.*, **57**, 155.
Merrill, K. Y., Russell, R. W., and Soifer, B. T. 1976, *Ap. J.*, **207**, 763.
Mitchell, G. F., Ginsburg, J. L., and Kuntz, P. J. 1978, *Ap. J. Suppl.*, **38**, 39.
Nadeau, D., and Geballe, T. R. 1979, *Ap. J.* (*Letters*), **230**, L169.
Phillips, T. G., Huggins, P. J., Neugebauer, G., and Werner, M. W. 1977, *Ap. J.* (*Letters*), **217**, L161.
Puetter, R. C., Russell, R. W., Soifer, B. T., and Willner, S. P. 1979, *Ap. J.*, **228**, 118.
Russell, R. W., Soifer, B. T., and Willner, S. P. 1977, *Ap. J.* (*Letters*), **217**, L149.
Wexler, A. S. 1967, *Appl. Spectrosc. Rev.*, **1**, 29.
Willner, S. P., Puetter, R. C., Russell, R. W., and Soifer, B. T. 1979*a*, *Ap. Space Sci.*, in press.
Willner, S. P., Puetter, R. C., Russell, R. W., Soifer, B. T., and Harvey, P. M. 1979*b*, *Ap. J.* (*Letters*), **229**, L65.
Wilson, W. J., Schwartz, P. R., Epstein, E. E., Johnson, W. A., Etcheverry, R. D., Mori, T. T., Berry, G. G., and Dyson, H. B. 1974, *Ap. J.* **191**, 357.
Winnewisser, G., and Walmsley, C. M. 1978, *Astr. Ap.*, **70**, L37.
Zuckerman, B., and Palmer, P. 1974, *Ann. Rev. Astr. Ap.*, **12**, 279.

THE ASTROPHYSICAL JOURNAL, 234:496–502, 1979 December 1

INFRARED SPECTRA OF IC 418 AND NGC 6572

S. P. WILLNER,[1] B. JONES,[2] R. C. PUETTER,[1] R. W. RUSSELL,[1] AND B. T. SOIFER[1,3]
Received 1978 October 13; accepted 1979 May 21

ABSTRACT

Spectrophotometric observations from 2 to 4 and 8 to 13 μm of NGC 6572 and from 4 to 13 μm of IC 418 are reported. Also reported are observations of the size of IC 418 in the optical and at 1.65 and 2.2 μm. Both planetary nebulae emit more radiation than expected from recombination at wavelengths longer than ~ 4 μm; this radiation is attributed to heated dust. The spectra show a plateau from 10.5 to 13 μm, and this peak is tentatively attributed to emission from large silicon carbide particles. Fine-structure emission lines are also discussed; the presence of [Ar III] but not [Ne II] in NGC 6572 suggests that ions having the same ionization potential can nevertheless have different fractional abundances.

Subject headings: infrared: spectra — nebulae: planetary

I. INTRODUCTION

Infrared emission from planetary nebulae is usually attributed to a combination of recombination[4] and radiation from heated dust. At wavelengths near 10 μm, the dust emission often greatly exceeds the recombination contribution, often by two orders of magnitude (for a summary of observations, see Cohen and Barlow 1974). The dust emission decreases toward shorter wavelengths, and near 2 μm recombination alone can account for the observed emission for most planetaries (Khromov and Moroz 1972; Willner, Becklin, and Visvanathan 1972; Persson and Frogel 1973*b*). A few nebulae, including IC 418, are brighter than expected from recombination even at wavelengths as short as 1.6 μm; the excess radiation has been attributed to thermal radiation from very hot dust grains.

Infrared spectra are available for only a few planetary nebulae (Gillett, Forrest, and Merrill 1973; Merrill, Soifer, and Russell 1975; Treffers *et al.* 1976; Russell, Soifer, and Merrill 1977, hereafter RSM; Russell, Soifer, and Willner 1977, hereafter RSW; Russell *et al.* 1977; Aitken *et al.* 1979; Grasdalen 1979), although individual spectral lines and features have been measured in several more (see, e.g., Gillett, Merrill, and Stein 1972). The two best-studied planetaries, NGC 7027 and BD +30°3639, show emission features at 3.3/3.4 μm, 6.2 μm, 7.7 μm, 8.6 μm, and 11.3 μm. These features, or at least some of them, are common to a variety of other objects (Russell, Soifer, and Willner 1978 and references therein) and have been attributed to emissivity peaks in the dust that produces most of the infrared radiation. The 3.3 μm peak is especially intriguing, because it seems to appear with at least two different shapes (RSM). In most objects, including NGC 7027 and BD +30°3639, the 3.3 μm feature includes a wing at longer wavelengths, but in IC 418 the longer wavelength wing is not present.

The present observations of IC 418 were intended to test whether the other emission features are associated with the 3.3 μm feature alone or only with the 3.3 μm feature that includes a 3.4 μm wing. In fact, weak features at 6.2 and 7.7 μm appear to be present. The 8.6 and 11.3 μm features were not detected and are much weaker relative to the 3.3 μm feature than in other objects. Instead, a broad feature, tentatively attributed to solid silicon carbide particles, was seen near 11 μm.

NGC 6572 is a planetary nebula that is relatively bright in the radio, but, unlike IC 418, NGC 6572 emits only recombination radiation near 2 μm. Both 2–4 μm and 8–13 μm spectra were obtained, and a peak near 11 μm similar to that in IC 418 was seen. The observations and a description of the spectra are presented in § II, while § III discusses the results for the dust features, for the atomic emission lines, and for measurements of the angular size of IC 418. An attempt is made to relate IC 418 and NGC 6572 to the carbon-rich evolutionary sequence suggested by Zuckerman *et al.* (1976, 1978).

II. OBSERVATIONS

a) Spectroscopy

Observations were made with the Mount Lemmon 1.5 m telescope in 1976 December and 1977 January, March, May, and October. The focal plane diaphragm was 17″ in diameter, and the spectral resolving power ($\lambda/\Delta\lambda$) was approximately 65. Airborne observations of IC 418 were made in 1978 February and of NGC 6572 in 1977 July from the Kuiper Airborne Observatory. The instrument has been described by RSW, and the present observations were made with a focal plane diaphragm 28″ in diameter. The results, converted to

[1] University of California, San Diego.
[2] School of Physics and Astronomy, University of Minnesota.
[3] California Institute of Technology.
[4] As used here, recombination includes free-bound, free-free, bound-bound, and two-photon processes.

flux density outside the Earth's atmosphere through observations of standard stars (Puetter *et al.* 1979), are shown in Figure 1. Data on IC 418 between 2 and 4 μm were taken from RSM. No effort was made to correct for the different beam sizes; the 4–8 μm observations of IC 418 should probably be lowered by between 20 and 40% to be compared with the ground-based observations. The data points for NGC 6572 shown as open circles represent averages of data at three wavelengths; the spectral resolution of these points is thus only 0.06 μm. The observations presented here have better signal-to-noise ratio and wavelength coverage but are in good agreement with those obtained earlier by Gillett, Forrest, and Merrill (1973), Gillett and Stein (1969), and Geballe and Rank (1973).

From 2 to 4 μm, the spectrum of NGC 6572 is in agreement with that predicted from recombination theory and radio observations (Higgs 1971 and references therein) to within the statistical uncertainties of the observations. The Brackett γ and α and Pfund δ recombination lines are prominent. No evidence for a broad feature at 3.3 μm is seen, although the data of Table 1 permit a weak feature to be present. The absence of Pfγ is not explained, but the noise in that part of the spectrum is relatively high.

At 8 μm, the flux density of NGC 6572 is well above the predicted level from recombination and appears to increase to longer and possibly to shorter wavelengths. There is some indication that the 7.7 μm emission feature found in other objects might be present, but further observations are needed to confirm this. There is no evidence of a peak at 11.3 μm. Fine-structure lines of [Ar III] and [S IV] are present (Gillett, Merrill, and Stein 1972; Gillett, Forrest, and Merrill 1973), but the [Ne II] line at 12.8 μm was not detected. Fluxes of various lines and other features are given in Table 1. The shape of the spectrum between 8 and 13 μm is similar to that of IC 418 and is discussed below. The data presented here are in agreement with those of Grasdalen (1979) if allowance is made for his smaller beam size (11″).

IC 418 is about a factor of 2 brighter between

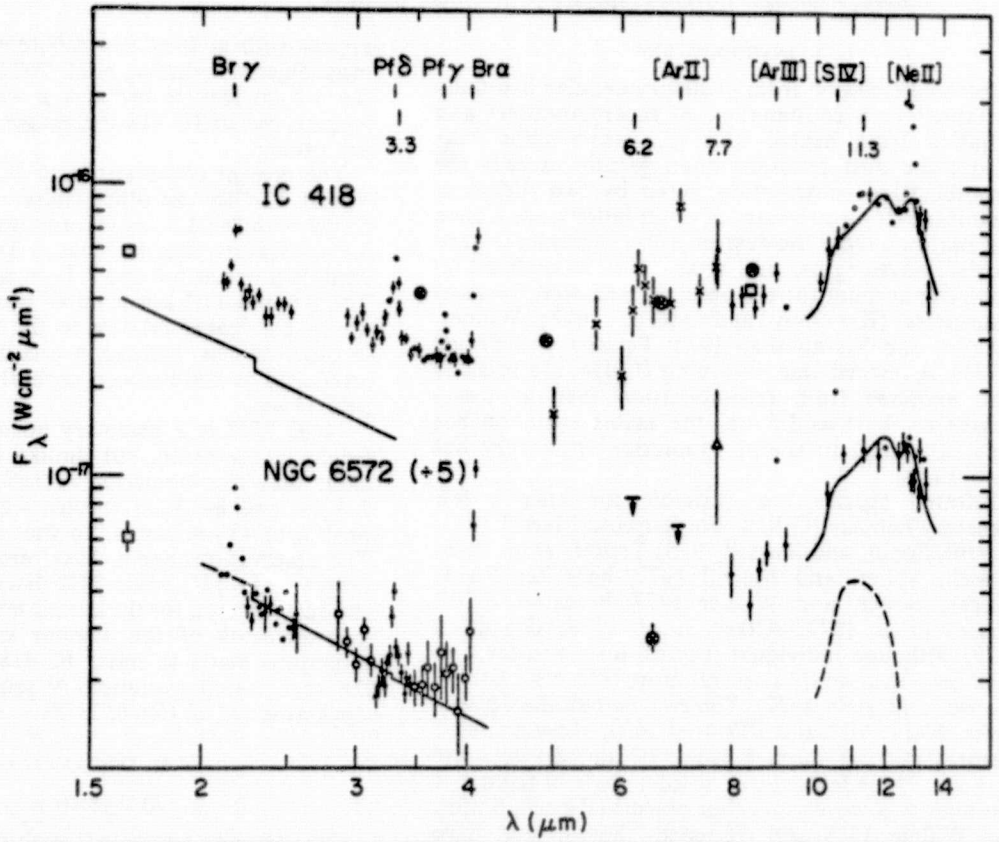

FIG. 1.—The 2–14 μm spectra of IC 418 and NGC 6572. Error bars are shown when the statistical uncertainty exceeds 5%. The 2–4 μm data on IC 418 are from RSM. The open circles represent averages of adjacent data points giving a resolution of 0.06 μm. The squares represent broad-band observations with the 17″ beam used for all of the ground-based observations. The circled x's represent broad-band observations obtained from the KAO with the 28″ beam used for all the airborne observations. No corrections for beam size have been applied to the observations. Wavelengths of various emission lines and features are marked. The solid lines from 2 to 4 μm show the recombination flux density predicted from radio observations. The solid lines near 11 μm show the emissivity of large silicon carbide particles plus a constant emissivity of 40% of the peak value. The dashed line shows the shape of the silicon carbide emission seen in IRC +10216 (Forrest 1974) plus a constant emission equal to 22% of the peak.

TABLE 1

FLUXES IN SPECTRAL FEATURES

λ (μ)		NGC 6572 (10^{-14} W m^{-2})	IC 418 (10^{-14} W m^{-2})
2.17.....	Bγ	1.15 ± 0.15	1.22 ± 0.18
3.27.....	Unidentified + Pfδ	0.47 ± 0.10	1.8 ± 0.2
3.30*....	Pfδ	0.35	0.44
3.74.....	Pfγ	< 0.7	0.62 ± 0.11
4.05.....	Bα	3.7 ± 0.2	2.8 ± 0.2
7.00.....	[Ar II]	< 3.8	4.9 ± 0.6
8.99.....	[Ar III]	5.7 ± 0.7	2.0 ± 0.9
10.52.....	[S IV]	10.6 ± 1.3	< 2.4
12.81.....	[Ne II]	< 2.9	28 ± 2

* Fluxes predicted from radio observations.

2 and 4 μm than predicted from radio observations (Higgs 1971 and references therein). The existence of an excess was known from previous measurements of the equivalent width of Bγ (Hilgeman 1969) and from broad-band observations (Willner, Becklin, and Visvanathan 1972); the latter also show an excess at 1.65 μm. The flux density of the excess is a slowly increasing function of wavelength. Bγ and α and Pfγ recombination lines are present with reduced equivalent width, confirming the continuum excess. The 3.3 μm feature is broader than the Pfδ line seen in NGC 6572 but lacks the 3.4 μm wing (RSM) seen, for example, in NGC 7027. The continuum rises slowly from 8 to 13 μm and is at a level much above that expected from recombination. Superposed on this rise is a broad peak between 10.5 and 12.5 μm, similar in shape to an emission feature seen in late-type carbon stars; the carbon star emission feature is attributed to silicon carbide (Forrest 1974). Weak 6.2 and 7.7 μm features appear to be present. The [Ne II] and [Ar II] fine-structure lines are strong. The [Ne II] line has the same equivalent width as measured by Gillett and Stein (1969); [Ar III] and [S IV] are weak or absent. IC 418 is the second planetary nebula, after BD +30°3639 (Russell *et al.* 1977), in which [Ar II] has been detected.

b) Size of IC 418

Broad-band photometric observations of IC 418 were made with a series of circular focal plane diaphragms in order to compare the spatial extent of the 2–4 μm excess emission to the extent of the emission from ionized gas. Such observations are useful because the nebula is highly symmetric. Previous observations (Willner, Becklin, and Visvanathan 1972) showed that the 2.2 μm excess was not confined to the region of the central star. The present observations extend to larger diaphragm sizes, include some color information, and include direct measurements of the Hα size.

Infrared observations were obtained in 1972 February, October, and December with the 1.5 m and 60 cm telescopes at Mount Wilson. The results are given in Table 2, together with the Hα + [N II] observations

TABLE 2

FLUX DENSITY FROM IC 418 AS A FUNCTION OF BEAM SIZE

Diaphragm Diameter (arcsec)	Telescope*	Flux Density (10^{-12} W m^{-2} μm^{-1}) 1.65 μm	2.2 μm	Line Flux (arbitrary units) Hα + [N II]
5.0.....	C	...	0.07	
8.0.....	B	0.26	0.18	0.30
9.7.....	C	...	0.23	
11.....	B	...	...	0.58
15.....	B	0.53	0.45	0.84
17.....	D	0.59	0.47	
18.....	A	...	0.46	
20.....	C	...	0.52	
22.....	B	0.68	0.58	0.97
24.....	B	...	0.59	0.98
31.....	B	0.77	0.67	0.98
36.....	A	...	0.66	
44.....	B	0.79	0.72	1.00
56.....	A	...	0.70	
101.....	A	...	0.75	
Total predicted from radio flux density.....		0.48	0.34	

* Key to telescope: A = Mt. Wilson 60 cm; B = Mt. Wilson 1.5 m; C = Mt. Wilson 2.5 m (Willner *et al.* 1972 corrected to present flux density calibration); D = Mt. Lemmon 1.5 m (λ_{eff} = 2.3 μm corrected to 2.2 μm).

obtained in 1973 January with the Mount Wilson 1.5 m telescope. These were obtained with the same optical arrangement as the infrared observations, except that the chopper was turned off; a photomultiplier with an S-20 photocathode and an interference filter that isolated the Hα and [N II] λ6583 emission lines were used. The optical observations were uncalibrated and have been arbitrarily normalized. The size of the Hα emission appears to be the same as expected on the basis of high-resolution radio observations (Terzian, Balick, and Bignell 1974). Table 2 also gives the total recombination flux density as predicted (Willner, Becklin, and Visvanathan 1972) from radio observations that include the entire nebula (Higgs 1971).

Figure 2 shows the measurements of Table 2 normalized to the measurement through the largest diaphragm. The data indicate that the infrared emission is coming from a region at least as large as the optical emission. Furthermore, the infrared surface brightness is relatively larger near the outside of the nebula than is the Hα + [N II] surface brightness. The excess radiation is not enhanced near the central star; it is even possible that up to half the 2.2 μm excess comes from outside the ionized region. The 1.65–2.2 μm color becomes bluer closer to the central star.

III. DISCUSSION

a) Feature at 3.3 μm

The feature at 3.3 μm has been attributed to a peak in the emissivity of dust (RSM); molecular bands, as suggested by Grasdalen and Joyce (1976), for example, are also possible. In IC 418, the Pfδ line contributes about ¼ of the flux observed for the 3.3 μm feature,

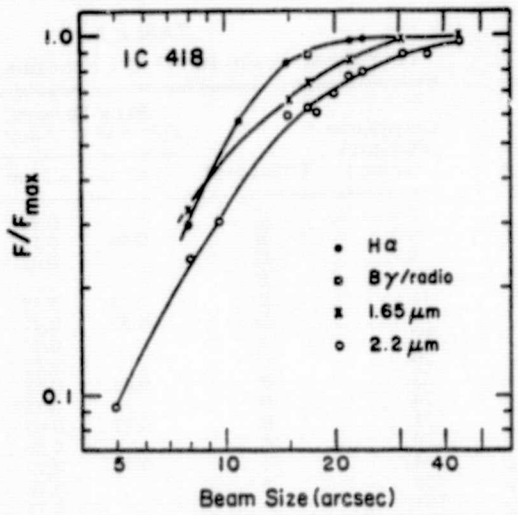

FIG. 2.—Flux from IC 418 as a function of beam size. The measurements at each wavelength are normalized to the measurement with the largest beam size. The square represents the ratio of the Bγ flux measured with a 17″ beam to the Bγ flux predicted from radio observations of the whole nebula (Higgs 1971). The points labeled Hα represent the sum of Hα and [N II] λ6583 with the latter actually contributing about ⅓ of the measured flux. G. Righini-Cohen and M. Simon (private communication) have measured Bα and Bγ with an 11″ beam; their measurements fall below the curve in the figure, near $F/F_{max} = 0.45$.

while the relative line contribution is much smaller for other objects in which a broad 3.3 μm feature has been observed.

In other sources that show a 3.3 μm feature, a 3.4 μm wing and features at 6.2, 7.7, and 11.3 μm have always been seen. Compared with NGC 7027, the 6.2 and 7.7 μm features in the spectrum of IC 418 are a factor of 2 or more weaker relative to the 3.3 μm feature. It is difficult to assess the strength of an 11.3 μm feature in IC 418 because of the uncertainty in the continuum shape. The local maximum observed at 11.3 μm is much broader than the 11.3 μm features seen in NGC 7027 and other objects and could be entirely due to silicon carbide, as discussed below. On the other hand, if a lower continuum level is adopted, an 11.3 μm feature as strong as that in NGC 7027 could be present. We emphasize that the apparent weakness of the various emission features in IC 418 is not due to their being veiled by a strong continuum, for the continuum is redder in NGC 7027 than in IC 418. It thus appears that different relative feature strengths may be associated with different shapes of the 3.3 μm feature, and in particular the lack of a 3.4 μm wing may be associated with weak 6.2, 7.7, and possibly 11.3 μm features.

The two shapes observed for the 3.3 μm feature do not appear to be correlated with the excitation of the object. A molecular band might vary in shape as a function of temperature; unfortunately the present data are not sufficient to indicate a correlation of shape with temperature. Allamandola and Norman (1978) have suggested that the 3.3 μm band may be due to methane adsorbed on dust grains. If this identification is correct, the 3.4 and 7.7 μm bands ought always to accompany the 3.3 μm feature (Allamandola, Greenberg, and Norman 1979). The weakness of these features in IC 418 thus appears to cast doubt on an identification of the 3.3 μm feature as methane in this object.

b) Other Dust Features

One of the most striking features in the spectra of these two planetaries is the rise in flux density between 9 and 11 μm. Both planetaries show the rise and a plateau from 11 to 13 μm. The spectrum of IC 418 appears to decline at longer wavelengths; such a decline may also be present in NGC 6572. The shape of the feature is suggestive of that of silicon carbide, which has been observed in emission in many late-type carbon stars (Forrest 1974) but never before in a nebula. The emissivity, as measured in our laboratory (Russell and Stephens 1979), of silicon carbide particles about 5 μm in diameter is shown in Figure 1 for comparison. Figure 3 shows the 8–13 μm data alone, so that the shape and strength of the 11–13 μm feature can be judged without any prejudice from the laboratory measurements. Particles larger than about 0.5 μm (Treffers 1973) have a different emissivity than is typical for the small particles seen around carbon stars (Forrest 1974) in that there is a second emissivity peak near 13 μm. The presence of this peak, and thus of relatively large particles, is probably required if silicon carbide is to fit the observed data. If such large

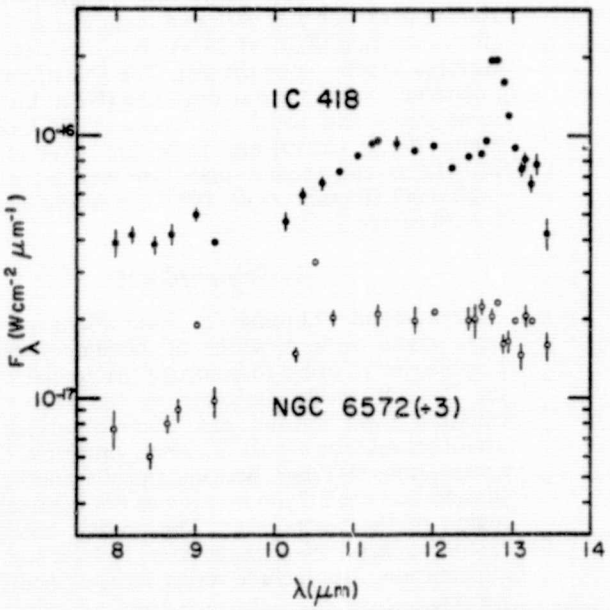

FIG. 3.—The 8–14 μm spectra of IC 418 and NGC 6572. The same data as in Fig. 1 are shown without any lines representing laboratory measurements so that the reader can form a better idea of the shape of the feature suggested to be silicon carbide.

particles are really present, their origin in these planetary nebulae and their absence in carbon star dust shells must be explained. The shape of the plateau between 11 and 12 μm depends on the shape mixture of particles (Treffers and Cohen 1974), and a distribution having more prolate particles would have higher emissivity near 11 μm than near 13 μm and thus better fit the observed spectra. However, better spectra of these faint objects are required before the silicon carbide identification can be considered definite.

If the identification of silicon carbide is correct, the dust particles evidently condensed in an environment having more carbon than oxygen, and planetary nebulae such as IC 418 and NGC 6572 might be the end point of the evolutionary sequence that includes carbon stars (Zuckerman *et al.* 1976, 1978). Additional evidence that planetary nebulae may be carbon-rich comes from recent ultraviolet observations (Bohlin, Marionni, and Stecher 1975; Bohlin, Harrington, and Stecher 1978). Although derivation of carbon abundances is model dependent, Bohlin, Harrington, and Stecher (1978) and Shields (1978) conclude that carbon is more abundant than oxygen in a number of nebulae. Unfortunately, IC 418 and NGC 6572 were not studied, but if the former nebula is indeed carbon-rich, it lends support to the identification of the 3.3 μm feature as a resonance of a CH bond, either in a molecule in the gas phase (Grasdalen and Joyce 1976; Black 1978) or in a solid particle (Knacke 1977; Allamandola and Norman 1978; Allamandola, Greenberg, and Norman 1979).

c) *Excess Continuum in IC 418*

The excess continuum radiation from 2 to 4 μm from IC 418 has been attributed to thermal emission from very hot dust grains (Willner, Becklin, and Visvanathan 1972). The color temperature of the excess can be estimated from the data in Table 2, if the expected recombination flux density is subtracted. Figure 2 shows that about half the Hα flux originates inside a 10″ beam. The grain temperatures are 1350 K for a 10″ beam and 950 K for a 44″ beam, if the grain emissivity $\epsilon \propto \lambda^{-2}$, or hotter if a less steep emissivity law applies. The decrease in temperature suggests that most of the grain heating is due to direct radiation from the central star, as is the case for most planetary nebulae (Ferch and Salpeter 1975).

The temperature of a grain is determined by the balance between incident and emitted radiation. For temperatures in the range of interest, the grains may be considered as being in thermal equilibrium; non-equilibrium processes, which may be important in the interstellar medium, are significant only at low grain temperatures (Purcell 1976). For IC 418, the grain temperature

$$T_g = 61(U/I)^{1/4}(r/1'')^{-1/2}(T_*/3 \times 10^4\ \mathrm{K}), \quad (1)$$

where U and I are the effective ultraviolet and infrared emissivities, r is the apparent angular distance of a grain from the central star, and T_* is the effective temperature of the central star. In deriving equation (1), it was assumed that the central star radiates like a blackbody, and the apparent visual magnitude was taken from Liller and Shao (1968). To estimate U/I, we assume that $\epsilon \propto \lambda^{-2}$ and take the ultraviolet wavelength to be 912 Å and the infrared wavelength 3 μm. Then $U/I \approx 10^3$, and

$$T_g = 350(r/1'')^{-1/2}(T_*/3 \times 10^4\ \mathrm{K}). \quad (2)$$

The central star of IC 418 is not much hotter than 3×10^4 (Kaler 1978*a*), and certainly the applicable angular radius is larger than 1″ (Fig. 2), so there is a serious difficulty in accounting for the high grain temperatures observed. One possibility is that the emissivity is a steeper function of wavelength ($\propto \lambda^{-2}$) than would be appropriate for small graphite particles. Even if T_* is as large as 5×10^4 K, U/I would have to be greater than 2×10^5, and if $\epsilon \propto \lambda^{-\alpha}$, then $\alpha \gtrsim 3.5$. We do not know whether grains with such properties exist. Moreover, if the actual grain temperatures are as high as the color temperatures, the grains might evaporate unless they are composed of highly refractory materials.

In view of the difficulty of heating grains to the high temperatures required, it is worthwhile to examine other possible mechanisms for producing the continuum radiation. Free-free radiation from interactions between hydrogen atoms and electrons ("H^- free-free") or hydrogen molecules and electrons ("H_2^- free-free") has been suggested as a mechanism for producing infrared radiation from certain stars (Milkey and Dyck 1973). The former process would not produce the correct wavelength dependence because of the presence of a bound state of H^-, but the latter process might be possible. Molecular hydrogen might be present in a region between expanding shock and ionization fronts in IC 418, perhaps in the same region where CO is found (Mufson, Lyon, and Marionni 1975; Black 1978). The H_2 would be heated, and free electrons would be available from the ionization of elements with lower ionization potentials than hydrogen by radiation from the central star. The absorption coefficients of H_2^- tabulated by Somerville (1964) were multiplied by a Planck function at various temperatures to find the appropriate temperature for IC 418. A temperature of 2500 K, reasonable for shock heating, produces an energy distribution in reasonable agreement with that of the excess radiation from IC 418. In order to estimate the densities required, it is necessary to determine the volume from which the radiation is emitted. One difficulty is that the region must be optically thick at radio wavelengths; otherwise 1.9 Jy of radio flux density would arise from the H_2^- alone. For unit optical depth to be reached in a distance equal to the nebular radius of 7×10^{16} cm (the distance of IC 418 is from Cudworth 1974), the required density product is $N_e N(H_2) \approx 10^{13}\ \mathrm{cm}^{-6}$, which seems too high to be consistent with the CO measurement (Mufson, Lyon, and Marionni 1975) and is much higher than the density calculated by Black (1978). Thus any form of

thermal bremsstrahlung radiation seems unlikely to account for the excess 2 μm emission.

The excess continuum might be produced near the central star and scattered in the outer part of the nebula or in the surrounding neutral material. Scattering of visible light by particles has probably been detected in the nebula BD +30°3639 (Persson and Frogel 1973*a*), and large particles, as suggested by the shape of the silicon carbide feature in IC 418, would scatter efficiently at 2 μm. A serious difficulty with the scattering hypothesis is that the lack of detection of excess radiation from the vicinity of the central star (Willner, Becklin, and Visvanathan 1972) requires that the scattering optical depth be larger than unity. For this to be achieved within the radius of the nebula and without the grain mass exceeding the limit set by cosmic abundances requires the grain diameter to be less than 0.1 μm, even if the scattering efficiency is one. Such small grains would, however, have much smaller scattering efficiencies, and a highly nonuniform geometry is required. In particular, a concentration of scattering particles must be directly in our line of sight to the central star. This seems unlikely because of the observed brightness of the central star at optical wavelengths.

The excess 1.6–2.3 μm radiation from IC 418 is thus not satisfactorily explained. The previous suggestion of thermal emission requires grains with a very high ratio of ultraviolet to infrared emissivity, and no other acceptable suggestion has been made.

d) Fine-Structure Lines

The observed fluxes in the fine-structure lines of [Ne II], [S IV], [Ar II], and [Ar III] are given in Table 1. The observed fluxes of [S IV] and [Ar III] in NGC 6572 agree well with those reported by Gillett, Merrill, and Stein (1972) and Gillett, Forrest, and Merrill (1973); the [Ne II] flux from IC 418 agrees with that reported by Gillett and Stein (1969) if account is taken of the different absolute calibration.

The fluxes in the fine-structure lines can be used to derive ionic abundances. These ionic abundances are given in Table 3 and are almost independent of temperature and density. Calculations similar to those of Simpson (1975) were used with collision strengths from Osterbrock (1974), and the line fluxes were compared with radio fluxes listed by Higgs (1971); the adopted value for the optically thin 10 GHz radio flux from the entire nebula is shown in Table 3. Table 3 also gives the fractional abundance of each ion compared with the cosmic abundance of the element (Allen 1973), the ionization potential range for each ion, and similar information for Ne III from optical observations (Peimbert and Torres-Peimbert 1971).

The absence of S IV and low abundance of Ar III show that IC 418 is of very low excitation. The Ar III–to–Ar II ratio and the Ne III–to–Ne II ratio suggest that even lower excitation is present than in the model of Buerger (1973); only $\sim$0.1 of these species appear to be doubly ionized.

NGC 6572 is of higher excitation than IC 418, as shown by the presence of [Ar III] and [S IV] and expected from the temperature of its central star (Kaler 1976*b*, 1978*a*). One surprising fact is that there is no detectable [Ne II] emission, although that ion occurs in a range of ionization potentials that includes Ar III, which is seen (Table 3). Optical observations tabulated by Kaler (1976*a*) together with atomic parameters (Osterbrock 1974) suggest that the dominant ionization states are in fact Ne III and Ar III, even though these ions have different ranges of ionization potential. Such an effect was found in a model of IC 4593 by Buerger (1973), but this nebula has a considerably cooler central star than NGC 6572 (Kaler 1976*b*). Kaler (1978*b*) has found that only about half of the argon in planetary nebulae can be in either the Ar II or Ar III state, contrary to the behavior of oxygen and neon. R. J. Gould (private communication) has pointed out to us that it is the photoionization and recombination rates, rather than simply the ionization potentials, that determine the ionization balance. Evidently the relative rates for argon and neon are different, and it appears that abundances of unobserved argon ions derived solely on the basis of abundances of other ions having similar ionization potentials must be considered questionable.

IV. SUMMARY

The spectra of IC 418 and NGC 6572 show an emission plateau from 10.5 to 13 μm. We suggest that this feature is due to large silicon carbide grains. It is therefore suggested that the grains are carbon-rich,

TABLE 3

DERIVED IONIC ABUNDANCES

LINE	IONIZATION POTENTIAL RANGE	NGC 6572		IC 418	
		N(ion)/N(H II)	N(ion)/N(cosmic)	N(ion)/N(H II)	N(ion)/N(cosmic)
[Ar II] λ6.99	16–28 eV	$< 2.9 \times 10^{-6}$	< 0.46	3.0×10^{-6}	0.48
[Ar III] λ8.99	28–41 eV	2.2×10^{-6}	0.35	6.1×10^{-7}	0.10
[Ne II] λ12.81	22–41 eV	$< 8 \times 10^{-6}$	< 0.10	6.1×10^{-5}	0.74
[S IV] λ10.51	35–47 eV	3.4×10^{-6}	0.16	$< 6 \times 10^{-7}$	< 0.03
[Ne III][a]	41–64 eV	1.4×10^{-4}	1.7	4.8×10^{-6}	0.06
Adopted 10 GHz radio flux		1.29 Jy		1.62 Jy	

[a] Peimbert and Torres-Peimbert 1971.

and the emission feature observed at 3.3 μm is due to a grain species or molecular constituent containing C–H bonds. Other emission features previously associated with that at 3.3 μm are weak or absent, and it appears that these features should be associated with the 3.4 μm wing rather than with the 3.3 μm feature itself.

The short wavelength excess emission in IC 418 appears to form a true continuum between 2 and 4 μm. This emission has too high a color temperature to be easily understood as direct thermal emission from grains, but no other plausible mechanism has been suggested.

The Ar^{++} to Ne^{+} abundance ratio is extraordinarily high in NGC 6572, although the ionization potential range of Ne^{+} includes that of Ar^{++}. The low excitation of IC 418 is confirmed by the large ratio of singly to doubly ionized argon and neon.

The authors thank J. H. Black and K. M. Merrill for valuable discussions and the entire staff of the Kuiper Airborne Observatory for their assistance with the airborne observations. We also thank F. C. Gillett of Kitt Peak National Observatory for the loan of the PbSnTe detector with which the 4–8 μm observations of IC 418 were made and for helpful comments on the manuscript. The observations of the size of IC 418 were made at Hale Observatories by S. P. Willner, who thanks H. C. Arp for the loan of the Hα filter and P. M. Harvey and S. J. Loer for help with some of the observations. Airborne astronomy at UCSD is supported by NASA grant NGR 05-005-055. This research was also supported by NSF grants AST 76-82890 and AST 76-21458.

REFERENCES

Aitken, D., Roche, P., Spenser, P. M., and Jones, B. 1979, *Ap. J.*, in press.
Allamandola, L. J., Greenberg, J. M., and Norman, C. A. 1979, *Astr. Ap.*, in press.
Allamandola, L. J., and Norman, C. A. 1978, *Astr. Ap.*, **63**, L23.
Allen, C. W. 1973, *Astrophysical Quantities* (3d ed.; London: Athlone Press).
Black, J. H. 1978, *Ap. J.*, **222**, 125.
Bohlin, R. C., Harrington, J. P., and Stecher, T. P. 1978, *Ap. J.*, **219**, 575.
Bohlin, R. C., Marionni, P. A., and Stecher, T. P. 1975, *Ap. J.*, **202**, 415.
Buerger, E. G. 1973, *Ap. J.*, **180**, 817.
Cohen, M., and Barlow, M. J. 1974, *Ap. J.*, **193**, 401.
Cudworth, K. M. 1974, *A.J.*, **78**, 1384.
Ferch, R. L., and Salpeter, E. E. 1975, *Ap. J.*, **202**, 195.
Forrest, W. J. 1974, Ph.D. thesis, University of California, San Diego.
Geballe, T. R., and Rank, D. M. 1973, *Ap. J.* (*Letters*), **182**, L113.
Gillett, F. C., Forrest, W. J., and Merrill, K. M. 1973, *Ap. J.*, **183**, 87.
Gillett, F. C., Merrill, K. M., and Stein, W. A. 1972, *Ap. J.*, **172**, 367.
Gillett, F. C., and Stein, W. A. 1969, *Ap. J.* (*Letters*), **155**, L97.
Grasdalen, G. L. 1979, *Ap. J.*, **229**, 587.
Grasdalen, G. L., and Joyce, R. R. 1976, *Ap. J.* (*Letters*), **205**, L11.
Higgs, L. A. 1971, *Catalog of Radio Observations of Planetary Nebulae and Related Optical Data* (Ottawa: National Research Council of Canada).
Hilgeman, T. 1969, Ph.D. thesis, California Institute of Technology.
Kaler, J. B. 1976*a*, *Ap. J. Suppl.*, **31**, 517.
———. 1976*b*, *Ap. J.*, **210**, 843.
———. 1978*a*, *Ap. J.*, **220**, 887.
———. 1978*b*, *Ap. J.*, **225**, 527.
Khromov, G. S., and Moroz, V. I. 1972, *Soviet Astr.—AJ*, **15**, 892.
Knacke, R. F. 1977, *Nature*, **269**, 132.
Liller, W., and Shao, C. Y. 1968, in *IAU Symposium No. 34, Planetary Nebulae*, ed. D. E. Osterbrock and C. R. O'Dell (Dordrecht: Reidel), p. 320.
Merrill, K. M., Soifer, B. T., and Russell, R. W. 1975, *Ap. J.* (*Letters*), **200**, L37.
Milkey, R. W., and Dyck, H. M. 1973, *Ap. J.*, **181**, 833.
Mufson, S. L., Lyon, J., and Marionni, P. A. 1975, *Ap. J.* (*Letters*), **201**, L85.
Osterbrock, D. E. 1974, *Astrophysics of Gaseous Nebulae* (1st ed.; San Francisco: Freeman).
Peimbert, M., and Torres-Peimbert, S. 1971, *Ap. J.*, **168**, 413.
Persson, S. E., and Frogel, J. A. 1973*a*, *Ap. J.*, **182**, 177.
Persson, S. E., and Frogel, J. A. 1973*b*, *Ap. J.*, **182**, 503.
Puetter, R. C., Russell, R. W., Soifer, B. T., and Willner, S. P. 1979, *Ap. J.*, **228**, 118.
Purcell, E. M. 1976, *Ap. J.*, **206**, 685.
Russell, R. W., Puetter, R. C., Soifer, B. T., and Willner, S. P. 1977, *Bull. AAS*, **9**, 582.
Russell, R. W., Soifer, B. T., and Merrill, K. M. 1977, *Ap. J.*, **213**, 66 (RSM).
Russell, R. W., Soifer, B. T., and Willner, S. P. 1977, *Ap. J.* (*Letters*), **217**, L149 (RSW).
———. 1978, *Ap. J.*, **220**, 568.
Russell, R. W., and Stephens, J. R. 1979, in preparation.
Shields, G. A. 1978, *Ap. J.*, **219**, 559.
Simpson, J. P. 1975, *Astr. Ap.*, **39**, 43.
Somerville, W. B. 1964, *Ap. J.*, **139**, 192.
Terzian, Y., Balick, B., and Bignell, C. 1974, *Ap. J.*, **188**, 257.
Treffers, R. R. 1973, Ph.D. thesis, University of California, Berkeley, pp. 31–32.
Treffers, R., and Cohen, M. 1974, *Ap. J.*, **188**, 545.
Treffers, R. R., Fink, U., Larson, H. P., and Gautier, T. N., III. 1976, *Ap. J.*, **209**, 793.
Willner, S. P., Becklin, E. E., and Visvanathan, N. 1972, *Ap. J.*, **175**, 699.
Zuckerman, B., Gilra, D. P., Turner, B. T., Morris, M., and Palmer, P. 1976, *Ap. J.* (*Letters*), **205**, L15.
Zuckerman, B., Palmer, P., Gilra, D. P., Turner, B. E., and Morris, M. 1978, *Ap. J.* (*Letters*), **220**, L53.

B. JONES: School of Physics and Astronomy, University of Minnesota, Minneapolis, MN 55455

R. C. PUETTER and S. P. WILLNER: Department of Physics, C-011, University of California, San Diego, La Jolla, CA 92093

R. W. RUSSELL: Astronomy Department, Cornell University, Space Science Building, Ithaca, NY 14853

B. T. SOIFER: Downes Laboratory, 320-47, California Institute of Technology, Pasadena, CA 91125

INFRARED MOLECULAR ABSORPTION FEATURES

S.P. Willner and R.C. Puetter
University of California, San Diego

Ray W. Russell
Cornell University

B.T. Soifer
California Institute of Technology

Spectra of infrared sources associated with molecular clouds have shown absorption features at wavelengths of 6.0 and 6.8 μm. We suggest that the 6.0 μm feature can be identified with the stretching vibration of C=O and the 6.8 μm feature with the bending vibrations of CH_2 and CH_3. The amount of carbon in the form of hydrocarbon molecules may be comparable to the amount in CO. This abundance of hydrocarbons is probably too large to be consistent with radio observations if the molecules are gaseous, but large abundances of hydrocarbons on the surfaces of grains may explain the infrared features, yet be unobservable in the radio.

OBSERVATIONS

Infrared sources associated with molecular clouds include compact HII regions and sources with much smaller or nonexistent thermal radio emission, often called "protostars". Spectra (typically with resolution $\lambda/\Delta\lambda \gtrsim 60$) in the ground-based 2-4 μm and 8-13 μm windows of many examples of both classes of objects are available in the literature. The 8-13 μm spectra show evidence of silicate dust grains. The silicate feature is seen in emission in the Orion Trapezium, but most objects exhibit various amounts of silicate absorption, believed due to extensive overlying cold dust. In the 2-4 μm spectrum there is often an absorption feature having maximum depth at 3.1 μm; this feature is usually attributed to water ice. The shape of the feature is, however, not entirely consistent with water ice absorption, in that there is significant optical depth between 3.3 and 3.5 μm (Merrill et al. 1976). Neither water nor ammonia ices would be expected to absorb sufficiently at these wavelengths to explain the observed shape of the feature. There is no correlation between the ice and silicate optical depths, except that if ice absorption is present, there is also finite silicate absorption present.

B. H. Andrew (ed.), Interstellar Molecules, 381–386.

The Kuiper Airborne Observatory has recently made possible observations in the 4.5 to 8 μm spectral region. A total of 11 sources obscured by molecular cloud material have now been observed spectroscopically at these wavelengths (Russell et al. 1977, Puetter et al. 1979, Soifer et al. 1979, Puetter et al. 1980). All have depressions in the spectrum between 6 and 7 μm, and in most cases it can clearly be seen that there are two dips, centered near 6.0 and 6.8 μm. By far the strongest features were observed in the source W33A (Soifer et al. 1979), which also has the strongest silicate and 3.1 μm absorptions known (Capps et al. 1978). The spectrum of this source is shown in Figure 1. The 6.0 and 6.8 μm features are spectrally resolved and have

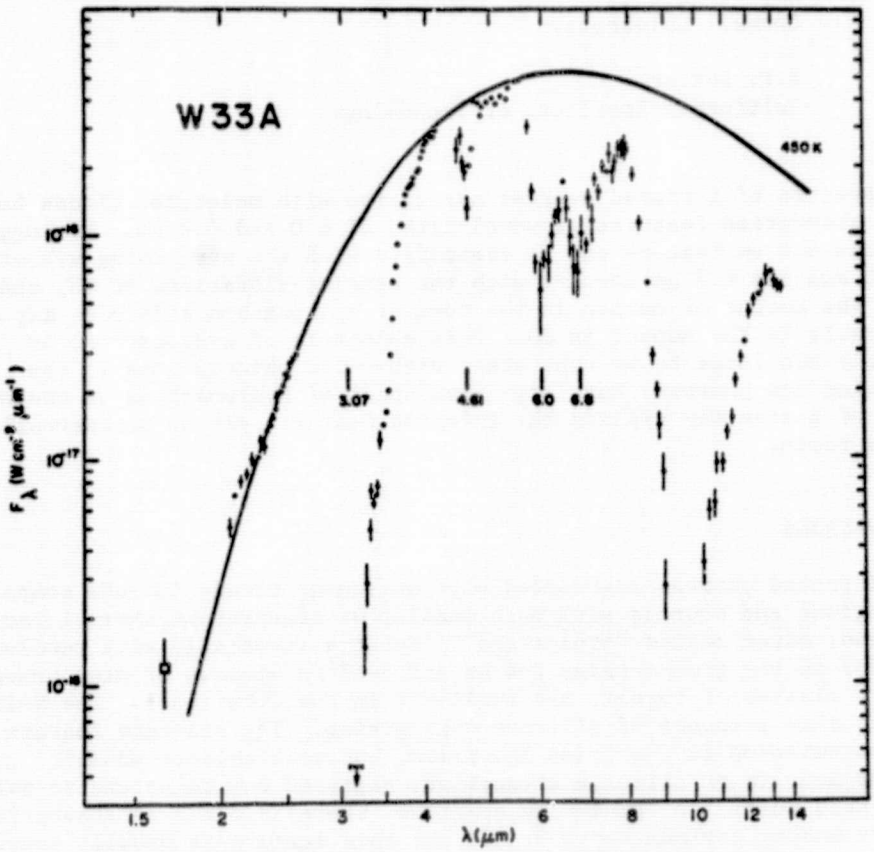

Fig. 1. The 2 to 13 μm spectrum of W33A. The 1.6-4 and 8-13 μm data are from Capps et al. (1978), and the 4-8 μm data are from Soifer et al. (1979). Error bars are shown when the statistical uncertainty exceeds 5%. The solid line represents the spectrum of a 450 K blackbody. Central wavelengths of 4 absorption features are marked.

widths of about 0.6 and 0.7 μm, respectively. The widths and positions of similar features are less easily determined in the spectra of other sources, but they are consistent with those in W33A. Table 1 gives the approximate peak optical depths of the features measured in 11 sources; the observations will be reported in more detail elsewhere. These numbers are, of course, strongly dependent on the choice of continuum level, which has generally been chosen as a blackbody fit through the spectrum at 4.5-5.5 μm and at 8.0 μm.

TABLE 1

PEAK ABSORPTION OPTICAL DEPTHS

Object	6.0 μm	6.8 μm
Becklin-Neugebauer	0.3	0.3
Sharpless 255	0.2	0.2
AFGL 989	0.3	0.4
W33A	1.9	1.5
AFGL 2136	0.3	0.3
AFGL 2591	0.2	0.2
AFGL 2884	0.5	0.3
NGC7538/IRS1	0.5	0.4
NGC7538/IRS9	0.6	0.4
W51/IRS2	0.5	0.5
K3-50	0.3	0.3

The 6.0 and 6.8 μm features were not seen in the line of sight to the galactic center (Willner et al. 1979). The features must therefore be characteristic of material in molecular clouds, rather than low-density interstellar material. The strengths of the features are not correlated with the strength of the silicate absorption and are only weakly correlated with the strength of the ice absorption.

DISCUSSION

It was first proposed that the 6.0 and 6.8 μm features were characteristic of hydrated or otherwise processed silicate minerals. Such features have been seen between 6 and 7 μm in the laboratory (Duley and McCullough 1977, Stephens and Russell 1979, Day 1978), although not at the exact wavelengths of the astronomical features. However, the features have not been seen to be as deep relative to the 10 μm band as in W33A. Moreover, the water of hydration band in silicates is usually at 6.1-6.2 μm rather than 6.0 μm and is only about half as wide as the astronomical absorption bands (Stephens and Russell 1979, Day 1978). Finally, the low temperatures of molecular clouds would seem more con-

ducive to the formation of ice mantles than hydrated grains, whereas in the envelope of an OH-IR star, where hydrated grains might be expected, no 6.0 or 6.8 μm features were found (Forrest et al. 1978). These arguments suggest that silicates are unlikely to be responsible for the 6.0 and 6.8 μm features.

Hydrocarbon bonds presently appear to be the most likely candidates for explaining the 6.0 and 6.8 μm features. The 6.0 μm band would be identified with the stretching vibration of the carbonyl group (C=O) with possibly some contribution from the stretch vibration of the C=C group. The 6.8 μm band would be identified with the scissors vibration in the methyl (CH_3) or methylene (CH_2) group. It is doubtful that any single molecule would be responsible for the observed absorptions, but rather, a large variety of molecules containing these groups would contribute to the observed bands. This is consistent with the broad absorptions that are observed, with the characteristic signatures of the functional groups in specific molecules being lost.

The column densities of the appropriate absorbers can be crudely estimated using observed equivalent widths and laboratory integrated band intensities (Puetter et al. 1979, Wexler 1967). These column densities, compared either to silicate or to radio CO column densities, generally indicate an amount of carbon comparable to but less than that in the form of CO.

The stretching vibration of the C-H bond is centered at 3.1-3.4 μm, depending on the specific group involved. The absorption is expected to be somewhat greater than that of the 6.8 μm band, and it could even be strong enough to explain all of the observed absorption between 2.9 and 3.5 μm. It is possible that some of the absorption is actually due to ice, but a major portion must be due to hydrocarbons. There will probably be no difficulty explaining the observed shape of the absorption with an appropriate mixture of molecules, either with or without ice.

Radio observations have shown the presence of quite complex hydrocarbons in molecular clouds (e.g., Kroto et al. 1978, Winnewisser and Walmsley 1978), but the derived abundance of known hydrocarbons is considerably smaller than that indicated here (Allen and Robinson 1977 and references therein). The lack of radio detection of such large abundances of hydrocarbons could be explained if most of the molecules are coated onto grains, where the lack of freedom to rotate would prevent radio emission. Such a situation would not be surprising at the low temperatures characteristic of molecular clouds (Watson and Salpeter 1972).

If large abundances of hydrocarbons in molecular clouds can be confirmed, it will probably require that their formation rates be higher than presently believed. Most of the available calculations include only gas-phase reactions, but for a full understanding of molecular clouds, it may be necessary to consider the far more complex subject of surface reactions.

This work was supported by NASA grant NGR 05-005-055 and by NSF grant AST 76-82890.

REFERENCES

Allen, M., and Robinson, G.W.: 1977, Astrophys. J. 212, pp. 396-415.
Capps, R.W., Gillett, F.C., and Knacke, R.F.: 1978, Astrophys. J. 226, pp. 863-868.
Day, K.L.: 1978, private communication.
Duley, W.W., and McCullough, J.D.: 1977, Astrophys. J. (Letters) 211, pp. L145-L148.
Forrest, W.J., Gillett, F.C., Houck, J.R., McCarthy, J.F., Merrill, K.M., Pipher, J.L., Puetter, R.C., Russell, R.W., Soifer, B.T., and Willner, S.P.: 1978, Astrophys. J. 219, pp. 114-120.
Kroto, H.W., Kirby, C., Walton, D.R.M., Avery, L.W., Broten, N.W., MacLeod, J.M., and Oka, T.: 1978, Astrophys. J. (Letters) 219, pp. L133-L137.
Merrill, K.M., Russell, R.W., and Soifer, B.T.: 1976, Astrophys. J. 207, pp. 763-769.
Puetter, R.C., Russell, R.W., Soifer, B.T., and Willner, S.P.: 1979, Astrophys. J. 228, pp. 118-122.
Puetter, R.C., Russell, R.W., Soifer, B.T., Willner, S.P.: 1980, in preparation. For partial abstract see Bull. Amer. Astron. Soc. 9, p. 571.
Russell, R.W., Soifer, B.T., and Puetter, R.C.: 1977, Astron. Astrophys. 54, pp. 959-960.
Soifer, B.T., Puetter, R.C., Russell, R.W., Willner, S.P., Harvey, P.M., and Gillett, F.C.: 1979, Astrophys. J. (Letters) 232, pp. 53-57.
Stephens, J.R., and Russell, R.W.: 1979, Astrophys. J. 228, pp. 780-786.
Watson, W.D., and Salpeter, E.E.: 1972, Astrophys. J. 174, pp. 321-340.
Wexler, A.S.: 1967, Appl. Spectrosc. Rev. 1, pp. 29-98.
Willner, S.P., Russell, R.W., Puetter, R.C., Soifer, B.T., and Harvey, P.M.: 1979, Astrophys. J. (Letters) 229, pp. L65-L68.
Winnewisser, G., and Walmsley, C.M.: 1978, Astron. Astrophys. 70, pp. L37-L39.

DISCUSSION FOLLOWING WILLNER

Thaddeus: It does not seem to me that you are talking about an unreasonable amount of carbon in C=O bonds. We only see a fraction of the total carbon in molecules like CO, and the rest has to be somewhere.

Willner: Yes. There must be a family of molecules with C=O bonds because the spectral features are resolved even with our low resolution, and no one particular molecule would make features as broad as that. If ~10% of the carbon is in the form of CO, another 10% in the form of hydrocarbons would be more than enough to account for the observations. The implied abundance is, however, much higher than suggested for individual hydrocarbons in the radio.

Greenberg: Earlier the point was made that there is as much oxygen

in H_2O as in CO, as if this were an awful lot of H_2O. I figured out that this would mean that at most 10% of all the oxygen is in H_2O. If what you say is true about CO relative to H_2O, then there is a further reduction by a factor of 4, so there is not such a large amount of H_2O compared to what we find in dust.

Willner: The data show considerable scatter, but the 3.1 μm absorption is roughly 10 times as strong as the 6.0 μm absorption. If the absorption efficiency per bond for OH stretch is as great as for C=O stretch, half as much oxygen in OH bonds as in CO would account for the 3.1 μm feature. If I have interpreted them correctly, Hagen's data suggest that OH stretch is a more efficient absorber than C=O, so an even smaller number of OH bonds would suffice.

Allamandola: I will take the bait early. What are your reasons for attributing the 6.0 μm feature to hydrocarbons and not, say, water of hydration or the H-O-H bend or H-N-H bend in the classic dirty ice? This vibration shifts considerably from its uncomplexed position at 1600 cm^{-1} toward 1700 cm^{-1} (6.0-6.2 μm), and undergoes substantial broadening when it complexes.

Willner: We are not aware of the possible shift in wavelength or the suppression of the 11.3 μm ice feature. There are a few sources, such as OH 0739-14, where the 3.1 μm absorption has returned to the continuum level by 3.3 μm, and the 11.3 μm absorption is present, and we felt that these characteristics indicated the presence of ice. Most sources do not look like this, and it seemed natural to suggest something other than ice. Also, the 3.1, 6.0, and 6.8 μm features occur together, and would probably be the strongest absorptions for hydrocarbon molecules.

NAL, 235: 104–113, 1980 January 1

RED SPECTRUM OF THE CARBON STAR Y CANUM VENATICORUM BETWEEN 1.2 AND 30 MICRONS

J. H. GOEBEL,[1] J. D. BREGMAN,[1] D. GOORVITCH,[2] D. W. STRECKER,[3]
R. C. PUETTER,[4] R. W. RUSSELL,[4] B. T. SOIFER,[5] S. P. WILLNER,[4]
W. J. FORREST,[6] J. R. HOUCK,[6] AND J. F. MCCARTHY[6]

Received 1979 February 20; accepted 1979 July 19

ABSTRACT

The infrared spectrum of Y CVn (N3; C4, 5; SR*b* variable) is presented with essentially complete wavelength coverage from 1.2 to 30 μm and mostly at a resolution $\Delta\lambda/\lambda$ of 0.02. The previous identification of C_3 at 5.2 μm by Goebel *et al.* is confirmed. There is no clear evidence for the SiC_2 ν_3 fundamental absorption band at 5.7 μm; but the 11.5 μm SiC particulate emission band is seen. The 11.5 μm band shape is consistent with the laboratory measurements of crystalline SiC made by Dorschner *et al.* Thus both C_3 in the stellar photosphere and circumstellar SiC contribute to the violet opacity in Y CVn, although C_3 is dominant. The power radiated in the circumstellar SiC band is shown to be inadequate to account for the violet opacity in Y CVn, a result which supports the conclusion of Bregman and Bregman. A 7.5 μm absorption band is observed for the first time and attributed to a mixture of HCN and C_2H_2. Opacity between 2.4 and 2.7 μm is observed for the first time and is consistent with the $\Delta v = -1$ C_2 band. The molecules present in the infrared spectrum—CO, CN, C_2, C_3, HCN, and C_2H_2—are generally in agreement with the models of Tsuji, Scalo, Johnson, Beebe, and Sneden, and Querci and Querci. A possible emission feature is observed at 22.5 μm. Its significance and possible origin are discussed. The 1.6 μm H^- opacity minimum is seen, a requirement for detection of the photosphere. With the exception of the 11.5 μm SiC band and the emission feature at 22.5 μm, the photosphere is dominant over circumstellar emission out to 30 μm. This result should limit the amount of carbon-rich material (graphite) which early N type carbon stars similar to Y CVn could be capable of injecting into the interstellar medium.

Subject headings: infrared: spectra — line identifications — stars: carbon — stars: individual

I. INTRODUCTION

The N type carbon star Y CVn (N3; C5, 4; SR*b* variable) is the first star in which the 5.2 μm band of C_3 has been identified (Goebel *et al.* 1978*a*). This molecule is probably the source of the well known violet opacity in many carbon stars (Bregman and Bregman 1978), although particulate SiC may be important in others. The original infrared observations of C_3 used an InSb detector, restricting spectral coverage to wavelengths less than 5.6 μm. Consequently, the presence of the 5.7 μm band of SiC_2, the molecule responsible for the Merrill-Sanford bands and from which SiC particles may condense, could not be addressed.

This paper reports spectrophotometric observations covering the essentially complete wavelength interval 1.2–30 μm. Two new sets of observations were made, the first within a 1 month interval. Previous observations of another carbon star, V Cyg (N; C7, 4e; Mira variable), suggested that dust emission was responsible for most of the flux beyond 4 μm (Forrest, Gillett, and Stein 1975; Puetter *et al.* 1977). In contrast, the flux of Y CVn is apparently dominated by the photosphere out to 30 μm. Our wide spectral coverage also allows the H^- continuum to be examined. These are the first observations from 2.4 to 3.0 μm, 5.5 to 8.0 μm, and 16 to 30 μm of such an unveiled carbon star. The data from 1.2 to 30 μm indicate that the photospheric continuum dominates over any featureless circumstellar radiation out to 30 μm. A newly discovered emission feature at 22.5 μm is interpreted as arising from circumstellar material.

The present observations confirm the identification of the C_3 band at 5.2 μm; and show that if SiC_2 is present, the SiC_2 absorption band at 5.7 μm would be obscured by C_3 at 1% spectral resolution. Silicon carbide (SiC) emission at 11.5 μm exists simultaneously with C_3 absorption at 5.2 μm, requiring a contribution of both species to the violet opacity in Y CVn. The polyatomic molecules HCN and C_2H_2 are expected to have absorption bands of observable strength between 4 and 8 μm, and a band centered near 7.5 μm is attributed to a mixture of HCN and C_2H_2, with a possible contribution from CS allowed.

[1] Ames Associate, NASA Ames Research Center.
[2] NASA Ames Research Center.
[3] Ball Aerospace Systems Division.
[4] University of California, San Diego, Department of Physics.
[5] Department of Physics, California Institute of Technology.
[6] CRSR, Cornell University.

II. OBSERVATIONS

The data discussed here represent the combined observations of the Ames group (1.2–4.0 μm, 1.2–5.5 μm, and 8.0–13.5 μm), the San Diego group (2.1–4.0 μm, 4.3–8.0 μm, and 8.0–13.5 μm), and the Cornell group (16–30 μm), and are displayed in Figure 1 as Spectra II and III. The data set of 1976 December 14 (Spectrum I) was discussed by Goebel *et al.* (1978*a*). Table 1 lists the pertinent observational parameters. The method of data reduction to absolute spectrophotometry of the Ames group is discussed in detail by Strecker, Erickson, and Witteborn 1979. The San Diego group's method is discussed by Puetter *et al.* (1979). Both techniques produce calibrated spectrophotometry through reference to established secondary standards, which in turn are calibrated against an α Lyrae flux curve. The Cornell group's method is discussed by Forrest, McCarthy, and Houck (1979).

The observations taken between 1978 January 4 and February 18 are combined into Spectrum II, Figure 2. The vertical scale of Figure 2 may be called normalized deviations from the Planck function. Since Y CVn is an SR*b* variable, it is necessary to observe the different wavelength intervals nearly simultaneously. The calibrated spectrophotometry can be recovered from Figure 2 by multiplication of each point by a function

$$F_\lambda = N_F^{-1} B(T_{BB}, \lambda),$$

where $B(T_{BB}, \lambda)$ is the Planck function of temperature T_{BB} at the wavelength λ, and N_F is a normalization constant. N_F and T_{BB} are listed in Table 1 for all the observations. T_{BB} will be considered an infrared color temperature $T_{IR} = T_{BB}$. The data in Figure 2 are plotted with a logarithmic vertical axis. This allows the data from the three spectral regions to be shifted vertically to normalize them, while preserving the spectral shape. The vertical shifts are only a few percent. The logarithmic horizontal axis transforms constant resolving power (50) into a constant linear measurement on the page across the entire range of wavelengths.

The observations taken between 1978 April 5 and June 26 were combined into Spectrum III. The 16–30 μm flux was calibrated by comparison with several standard stars, which were observed during the same flight series, and is believed to be accurate to approximately ±15%. The shape of the spectrum and the air mass corrections necessary shortward of 17 μm due to terrestrial CO_2 were derived using our unpublished spectrum of Mars, the spectrum of IRC +10420 (Forrest, McCarthy, and Houck 1979), and laboratory blackbody spectra obtained before and after the flight series. Because of the low signal-to-noise in the original 0.2 μm resolution spectrum, the data have been binned into 1 μm (from 18.5 to 25.4 μm) and 2 μm (at 17 μm, 27 μm, and 29 μm) bandpasses and averaged. There were from 40 to 100 individual measurements in each bin. The data shown in Figure 1 have $\pm 1\,\sigma_{mean}$ error bars. Within the errors, the 16–30 μm flux is a smooth continuation of the shorter wavelength data.

There is an important difference between the data reproduced here and that of Goebel *et al.* (1978*a*). That work approximated the standard star (β Gem, K0 III) flux curve by a 4700 K blackbody. The procedure was justified because no spurious molecular features were introduced, and spectroscopy of molecular constituents was the subject of discussion. But that method is inadequate for the determination of any continuous opacity sources unless the standard is free of H^- opacity (β Gem is not). The standards have now been referenced to α Lyr, permitting the nature of any continuous opacity to be examined.

III. INTERPRETATION

a) The Photospheric Continuum

There are a variety of opacity sources which might form the continuum level which is observed here (Querci, Querci, and Tsuji [QQT] 1974), e.g., molecular lines, H^-, and photospheric or circumstellar dust. We argue that H^- dominates the continuous photospheric opacity in Y CVn. A direct comparison should be made of Spectrum II (Fig. 2) and Spectrum I

TABLE 1

INFRARED OBSERVATIONS OF Y CANUM VENATICORUM

Date of Observation	Wavelength Range (μm)	Composite Spectrum Number	Observatory	Detector Type	T_{BB} (°K)	N_F	Standard Star	Observers
1976 Dec 14....	1.2–2.4, 2.9–5.6	I	KAO	InSb	2900	2.67×10^{19}	β Gem	Ames
1978 Jan 4.....	1.2–4.0	II	Learjet	InSb	2750	2.50×10^{18}	β And	Ames
1978 Feb 2.....	4.3–8.0	II	KAO	PbSnTe	2750	2.50×10^{18}	α Tau	UCSD
1978 Feb 18.....	8.0–13.5	II	NASA–UA Mt. Lemmon	Si:As	2750	3.05×10^{18}	3000 K (α Boo)	Ames
1978 May 23....	4.3–8.0	III	KAO	PbSnTe	2800	2.50×10^{18}	α Boo	UCSD
1978 Jun 26.....	2.1–4.0	III	UCSD–UM Mt. Lemmon	InSb	2800	2.3×10^{19}	η UMa	UCSD
1978 Apr 5.....	8.0–13.5	III	UCSD–UM Mt. Lemmon	Si:As	2800	2.50×10^{18}	α Boo (4000 K)	UCSD
1978 May 6.....	16–30	III	KAO	Si:Sb	2800	2.25×10^{18}	IRC +10420	Cornell

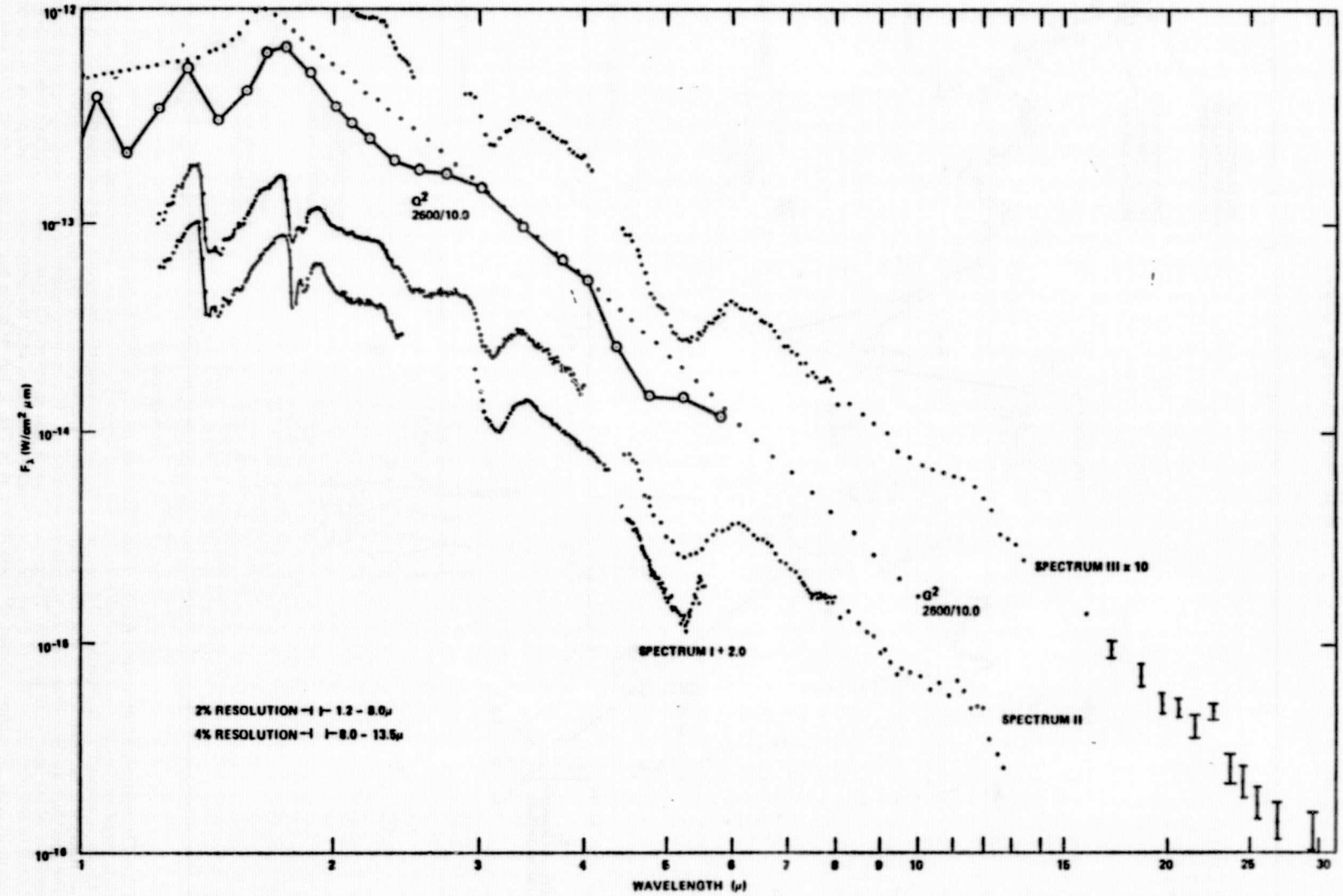

FIG. 1.—The absolute spectrophotometry of Y CVn taken on the dates listed in Table 1 and combined into three composite spectra. Although Spectrum III has been shifted vertically by a factor of 10, it does not overlie Spectrum II, but is slightly higher across the entire spectrum. The variability can be attributed to a combination of temperature and size changes. From 16 to 30 μm the data has been spectrally averaged to obtain a higher S/N. Below 16 μm the resolution is oversampled, so differences between adjacent datum points is a measure of noise. The curve labeled Q^2 2600/10.0 is a model carbon star of $T_{\rm eff}$ = 2600 K and g = 10.0 cm s^{-2} from Querci and Querci (1974). The curve G^2 2600/10.0 is explained in the text.

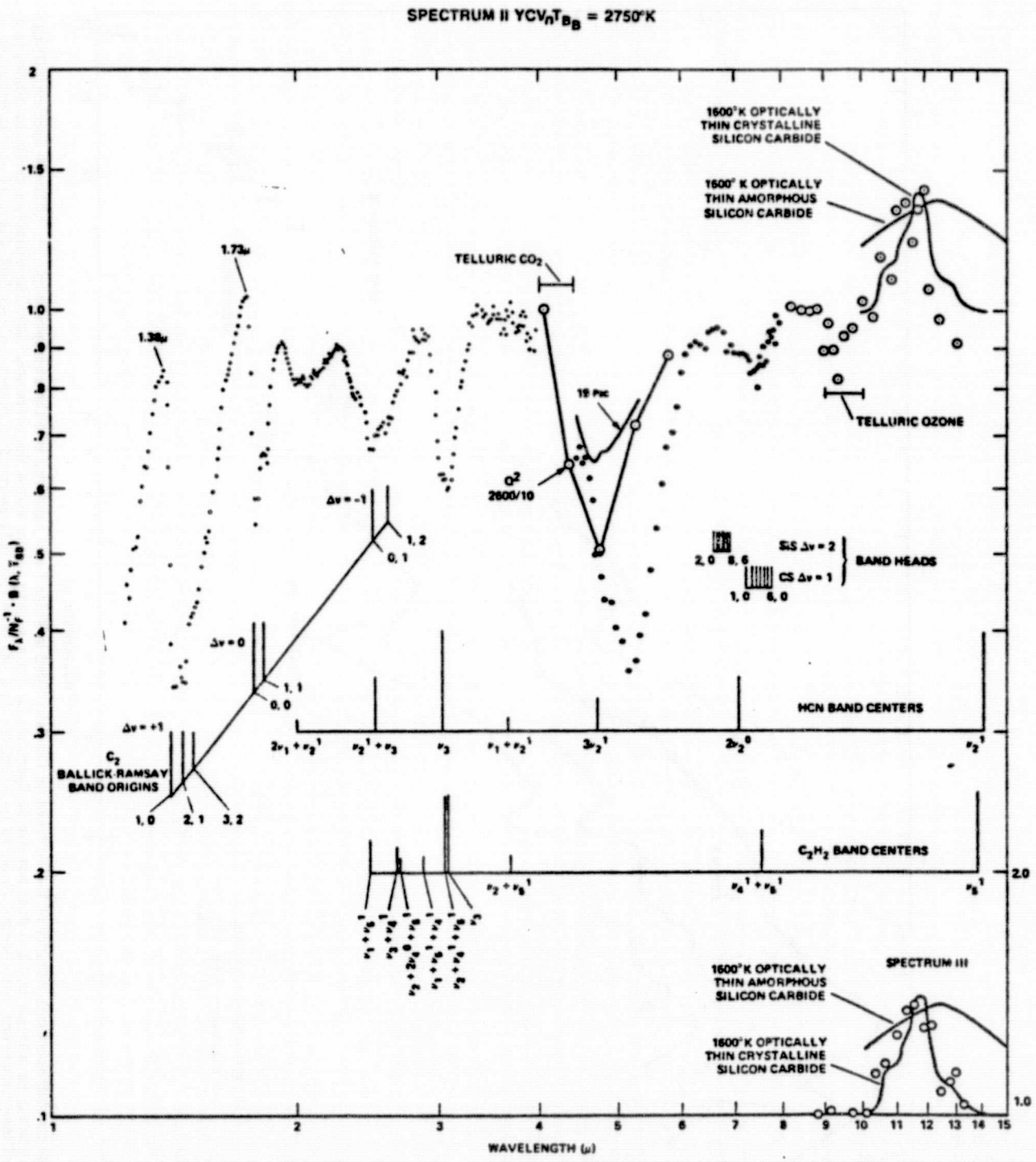

FIG. 2.—The normalized deviations from a Planck function of T_{BB} = 2750 K for the carbon star Y CVn. The three wavelength intervals covered by the observers are: *small dots*, 1.2–4.0 μm; *large dots*, 4.3–8.0 μm; *circled small dots*, 8.0–13.5 μm. The resolution out to 8.0 μm is about 2%; from 8.0 to 13.5 μm, it is 4%. The fundamental absorption band as observed in 19 Psc is indicated by a smooth heavy line between 5 and 6 μm. The band heads, origins, and centers of various species discussed in the text are positioned below the spectrum at their measured or computed wavelength. The relative height of HCN and C_2H_2 band indicators gives a crude measure of intrinsic band strength. The gap at 4.2 μm is due to telluric CO_2 interference. The apparent absorption at 9.5 μm is attributed to telluric ozone. The 11.5 μm emission band is compared with the properties of amorphous and crystalline SiC, as discussed in the text. The curve labeled Q^2 2600/10.0 is as in Fig. 1, but with the continuum removed by G^2 2600/10.0.

(Figure I of Goebel *et al.* 1978*a*). The point to note is that in Spectrum I, the 1.38 μm level of Y CVn is not depressed relative to the 1.73 μm level. The H^- present in β Gem (K0 III) causes a depression of its own 1.38 μm level relative to its 1.73 μm level when comparison is made directly with a blackbody of temperature (4700 K) appropriate to wavelengths longward of 1.6 μm. Thus one can conclude that there is H^- opacity present in Y CVn in an amount nearly equal to that observed in β Gem, if the effect in question cannot be attributed to other opacity sources.

Photospheric dust could cause opacity throughout the entire 1.0–2.5 μm range but is not expected in an atmosphere with a T_{eff} of 2500 K. Circumstellar extinction, which produces absorption of the 1.38 μm radiation relative to the 1.73 μm radiation, also causes unacceptably large extinction in the visible. Dust can contribute very little to the effect being considered.

Cyanogen (CN) is the only abundant molecule which has absorption bands at 1.38 and 1.73 μm. In order to check the effect of weak CN lines at 1.38 and 1.73 μm when large column densities are present, we computed the opacity at 1% spectral resolution for column densities of up to 10^{26} CN molecules per cm^2 (a typical model atmosphere will have less than 10^{25} molecules per cm^2 of H_2 and less than 10^{19} of CN [Johnson, Beebe, and Sneden 1975]). *All* known weak lines were included (Augason and Bailey 1978, private communication); between 1.35 and 1.75 μm there are over 12,000 lines. Only column densities greater than 10^{24} depressed the 1.38 and 1.73 μm levels significantly. A relative depression of only 9% could be produced with 10^{26} molecules/cm^2, less than half the observed depression.

Querci, Querci, and Tsuji (1974) and Querci and Querci (1974, hereafter Q^2) have produced carbon star models with T_{eff} as low as 2200 K. A depression shortwards of 1.6 μm similar to that being discussed here is characteristic of the models. A synthesis of their spectra using continuum sources only for comparison with a variety of carbon stars (Goorvitch and Geobel 1980, hereafter G^2) shows that H^- bound-free opacity dominates the continuous opacity sources at wavelengths less than 1.6 μm in the models. Addition of CN red system opacity using the band model of Johnson, Marenin, and Price (1972) did not change this conclusion, even though this band model produces CN bands much stronger than those in real stars, principally because of their use of the straight mean band model (Carbon 1974).

The flux curve of the 2600 K/10.0 cm s^{-2} model of Q^2 has been reproduced in Figure 1. Although it is not exactly appropriate to Y CVn, it does illustrate the H^- opacity effect under discussion. Even though the CN bands are strong, the underlying continuum sources are evident, specifically the H^- peak. The H^- peak has been shifted to a longer wavelength because of the presence of the CN and CO bands, a fact noted by F. Querci in his thesis (1969). A T_{eff} of 2500 K might be more appropriate to Y CVn and might produce stronger C_2 bands than are apparent in the 2600 K model. It would be very valuable to create a denser grid of models of the Querci type for carbon stars in terms of T_{eff}, N_C/N_O, and perhaps g than is presently available, as well as extending them to lower temperatures.

In Figure 3 we make a direct comparison between Spectrum I and the Q^2 band model with T_{eff} = 2600 K and g = 10.0 cgs units along with the continuum only calculation of G^2 for the same values of T_{eff} and g. Except for the C_2 Ballik-Ramsay $\Delta V = 0$ band at 1.8 μm, the polyatomic band at 3.1 μm, and the C_3 band at 5.2 μm, the Q^2 flux curve comes quite close to the measured curve. (In fact, the angular diameter θ determined from the ratio of stellar flux F^* and model flux F^M at 3.7 μm is $\theta = [(4/\pi)(F^*/F^M)]^{1/2} = 13.1$ milli-arcsec, a very reasonable value.) The bands weaken the H^- peak, but have little effect on the 1.35 μm continuum level. It is the H^- opacity minimum which gives rise to the depression of the 1.35 μm level in Figure 2 compared to the 1.73 μm level. If, in Figure 2, we had chosen to divide the flux by a blackbody passing through 1.35 μm and 3.6 μm, then the 1.73 μm level would have been greater than 1.0, and therefore would have been an apparent emission feature.

Thus H^- is the dominant source of the observed relative depression of the 1.35 and 1.73 μm levels in Spectrum II. Since the H^- opacity effects can be seen, we can conclude that we are observing the photospheric continuum in Y CVn.

From Spectrum III, there is no featureless infrared excess above what we are interpreting to be the photospheric continuum of Y CVn, at least out to 30 μm. Broad-band photometry (Jones and Merrill 1976) of early N type stars and N type spectra at our disposal indicate the lack of large featureless excesses in the early N type carbon stars, at least to N3. Thus it appears that photospheric continuum with superposed molecular absorptions dominate the spectra of early N type carbon stars to N3, i.e., those with T_{IR} greater than 2800 K.

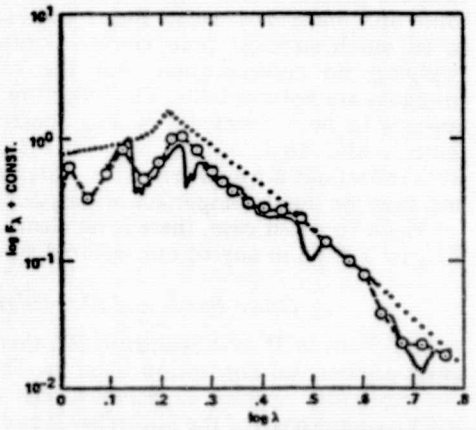

FIG. 3.—A direct comparison of the observed Spectrum I of Y CVn (*solid line*) with the flux spectra of the Q^2 2600 K/10.0 cm s^{-2} model atmosphere (*circled dots* connected with *dashes*) and the G^2 2600 K/10.0 cm s^{-2} model (*dots*). The lack of agreement in certain bands is discussed in the text.

b) CO, C_3, *and* SiC_2

With extension of spectral coverage out to 8 μm in Spectrum II, we confirm the upturn, in Spectrum I, of the 5.2 μm absorption band at wavelengths greater than 5.2 μm. In fact, the upturn proceeds to essentially a continuum level at 6.6 μm. In Figure 2, the CO fundamental of 19 (TX) Psc (N0; C6, 4) has been superposed. The star 19 Psc has a higher T_{IR} (4000 K) than Y CVn (2800 K). Hence the CO fundamental of 19 Psc should extend to longer wavelengths than that of Y CVn. The extraordinary difference in band profiles between the two stars requires another source of opacity in Y CVn. The observational indications of C_3 are confirmed by the Q^2 model discussed above. In Figure 2 are plotted the CO fundamental values of Q^2 2600/10.0. Again the differences require some other molecule than CO. The C_3 molecule quite adequately accounts for the difference (Treffers and Gilra 1975). On the basis of temperature alone (Tsuji 1964), C_3 is expected to be abundant in Y CVn and not in 19 Psc. A 5.2 μm band profile similar to Y CVn has also been observed in UU Aur and RY Dra (Goebel, unpublished data). The C_3 molecule is expected to be abundant in the latter stars, because of their temperatures.

On the long-wavelength side of the 5.2 μm band there is a small inflection between 5.8 and 6.0 μm. From the preliminary high-temperature laboratory data of Treffers and Gilra (Treffers, private communication), the SiC_2 ν_3 fundamental is expected between 5.6 and 6.0 μm. But on the basis of a dissociation equilibrium model (Scalo 1973) appropriate to Y CVn ($N_C/N_O = 1.66$ [Gow 1977]) with $N_C/N_O = 1.5$, $\log P_g = 2$, and 2700 K (the choice of 2700 K will become apparent in the next section), the ratio of partial pressures of C_3 and SiC_2 is expected to be $P_{C_3}/P_{SiC_2} \sim 100$. If the C_3 5.2 μm band and SiC_2 5.7 μm band are of equal strength per molecule, then Scalo's model does not predict a strong SiC_2 band. However, the Merrill-Sanford electronic bands of SiC_2 are present in the visible spectrum of Y CVn, so some SiC_2 must be present. Electronic bands do tend to be much stronger than vibration-rotation bands, implying no contradiction, but the relative band strengths are not available. The inflection near 5.7 μm appears in both Spectrum II and Spectrum III, but there is also an inflection between 6.3 and 6.5 μm. Both inflections are near terrestrial water vapor bands, and may be due to imperfect atmospheric correction for H_2O. In either case, there is no clear indication of SiC_2 in Y CVn in any of our infrared spectra.

c) *Other Bands and Molecules*

At 7.5 μm in II and Spectrum III, there is a previously unobserved absorption band. In Table 2 we list the molecular species expected to be abundant in Y CVn on the basis of the Scalo (1973) and Tsuji (1964) models, and which have absorption bands between 4 and 8 μm. Consideration of temperature, relative abundance, and band center wavelength leaves only HCN, C_2H_2, and CS as real possibilities. Pierson, Fletcher, and Guntz (1956) show the 7.1 μm band of HCN and 7.5 μm band of C_2H_2 to be roughly equal in strength at room temperature. By combining the bands of both molecules, it appears that qualitative agreement is possible with Spectrum II. An overlapping of HCN *P*-branch and C_2H_2 *R*-branch, with the HCN absorption somewhat stronger, would reproduce the 7.45 μm minimum, while the HCN *R*-branch (7.0 μm) would be stronger than the C_2H_2 *P*-branch (7.8 μm). An additional contribution to the 7.45 μm minimum could come from a temperature-sensitive *Q*-branch of C_2H_2 (Bell and Nielsen 1950), which is centered at 1328.5 cm^{-1} (7.5 μm). The *Q*-branch becomes stronger as temperature increases. A contribution from CS is allowed in the 7.5 μm band, but cannot account for the band shape or the band center wavelength. It would be useful to test these conclusions at high resolution in the 7.5 μm band.

From Table 2, Tsuji's models show HCN to be about an order of magnitude more abundant than C_2H_2 at 2000 K, and the model is included for comparison. While trends in molecular abundances of Tsuji's model appear to be consistent with our data, none of them are exactly appropriate for Y CVn. In contrast, Scalo's models may be more consistent with our analysis. For $N_C/N_O = 1.5$, and $\log P_g = 2.0$, he finds $P_{HCN}/P_{C_2H_2} \approx 10$ at 2800 K, ≈ 1 at 2700 K, and $\approx \frac{1}{3}$ at 2600 K.

Since the bands at 7.5 and 3.1 μm involve both HCN and C_2H_2, their shapes should be sensitive to temperature changes on the order of 100 K at both high and medium resolution. Spectra I, II, and III Y CVn show band shape changes not attributable to noise, while the infrared continuum temperature changes on the order of 100 K. This change in the 3.1 μm band shape is displayed in Figure 4. Band variability at 3.1 μm also occurs in other carbon stars that we have observed more than once from the Kuiper Airborne Observatory or Learjet (Goebel *et al.* 1978*b*).

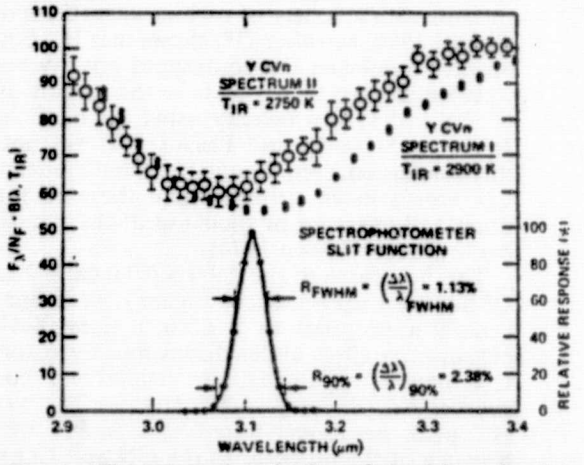

FIG. 4.—The temporal variability of the 3.1 μm band in Y CVn. Variation also occurs in other carbon stars as well, such as TX Psc and R Lep. 1 σ error bars deduced from multiple scans of the band are indicated vertically. The spectrophotometer slit function evaluated near 3.1 μm is also included.

TABLE 2

A. Tsuji's Model[a] ($N_C/N_O = 5$, $\log P_g = 3.0$, $T_e = 2000$ K)

Molecule	Band Center[b] at 300 K (μm) or Band Head	Temperature Range of Maximum Partial Pressure ÷1000 K	P_{molec}/P_{HCN}
HCN	7.1, 4.8, 3.1	1.0–2.5	1.0
C_2H_2	7.5, 3.1	1.0–2.5	0.06
C_3	5.2 (3000 K)	2.1–3.2	4×10^{-5}
CH_4	7.7	< 1.2	4×10^{-5}
C_2H_4	6.9	< 1.2	6×10^{-7}
C_2N_2	3.9, 4.8	1.7–3.0	2×10^{-3}
C_6H_6	6.7	1.25	$< 10^{-16}$
Si > S (Solar)			
CS	7.3	2.0–3.0	5×10^{-3}
SiS	6.6	< 2.0	2×10^{-3}
SiO	8.1	< 1.8	4×10^{-5}
SiC_2	5.7 (3000 K)	1.5–2.5	3×10^{-4}
H_2S	7.8	< 1.2	6×10^{-6}
Si < S			
CS	7.3	< 3.5	3×10^{-2}
SiS	6.6	1.2–2.0	8×10^{-3}
SiO	8.1	> 1.8	3×10^{-6}
SiC_2	5.7 (3000 K)	1.8–2.8	2×10^{-4}
H_2S	7.8	< 1.2	6×10^{-6}

B. Scalo's Models[c] ($N_C/N_O = 1.5$)

Molecule	$\log P_{mol} - \log P_H$	P_{mol}/P_{HCN}
$\log P_g = 2.0$, $T_e = 2650$ K		
HCN	−6.6	1.0
C_2H_2	−6.6	1.0
C_3	−6.3	2.0
SiC_2	−8.0	0.04
CS	−4.8	63
SiS	−7.7	0.08
CO	−3.0	4000
CN	−4.5	130
C_2	−5.7	7.9
$\log P_g = 0.0$, $T_e = 2300$ K		
HCN	−7.3	1.0
C_2H_2	−7.3	1.0
C_3	−6.3	10
SiC_2	−8.0	0.16
CS	−4.8	250
SiS	...	...
CO	−3.0	16,000
CN	−4.6	50
C_2	−5.9	25

[a] From Tsuji 1964, 1973.

[b] C_3 from Treffers and Gilra 1975, SiC from Treffers (private communication), polyatomics from Pierson *et al.* 1956, diatomics from Bailey (unpublished).

[c] From Scalo 1973.

The star Y CVn is not the most dramatic example. These band changes are also accompanied by temperature changes on the order of 100 K.

An interesting feature of Scalo's models is that, in principle, luminosity class can be determined from a knowledge of $P_{HCN}/P_{C_2H_2}$, N_C/N_O, and stellar temperature. In the case of Y CVn, if $P_{HCN}/P_{C_2H_2} = 1$, $N_C/N_O = 1.5$, and $T_e \simeq 2650$ K, then $\log P_H = 2$. If $T_e = 2300$ K, then $\log P_H = 0$. All the other molecules listed in Table 2 from his models—CO, CN, C_2, C_3, SiS, *and* SiC_2—have the same ratios P_{mol}/P_H in either case.

Beyond the CO first overtone minimum at 2.35 μm there is additional opacity. The likely possibilities are C_2 Ballik-Ramsay $\Delta V = -1$ (Ballik and Ramsay 1963), HCN $\nu_2 + \nu_3$ and $2\nu_2 + \nu_3$ Q-branches (Rank *et al.* 1960), C_2H ν_3 (Jacox 1975), and C_2H_2 $\nu_3 + \nu_4^1$, $\nu_1 + 2\nu_4^{2,0} + \nu_5^1$, $\nu_1 + \nu_4^1 + \nu_5^1$, and $\nu^1 + \nu_5^1$ combination bands (Bell and Nielsen 1950). Ridgway *et al.* (1976) have observed a line of the $\nu^1 + \nu_5^1$ C_2H_2 band in IRC +10216. Goebel *et al.* 1978*b* have identified the C_2H_2 bands in other carbon stars mainly of infrared temperature less than 2000 K. In Y CVn, $T_{IR} \approx$ 2800 K. For this higher temperature C_2 and perhaps HCN are the most likely candidates. Ab initio band shape calculations by D. Cooper (private communication) of C_2 at 2000 K and viewed by a 1% resolution slit function give good agreement with the two observed minima at 2.48 and 2.58 μm (see Fig. 5). High-resolution observations are needed from the Kuiper Airborne Observatory (KAO) to clarify the 2.5–2.9 μm region in Y CVn. Any unaccounted for lines may well come from C_2H, an abundant radical.

None of our spectra of Y CVn reveal significant CS at 3.9 μm or SiS at 6.6 μm. The CS molecule has been observed by Ridgway, Hall, and Carbon (1978) and Bregman, Goebel, and Strecker (1978) in other carbon stars, and may contribute to the 7.5 μm band observed here. The two molecules CS and SiS are among the most abundant of species; but their abundances are two orders of magnitude less than CO. Their lack of strong absorption bands is easily accounted for because they are diatomics; their fundamental and overtone bands should be considerably weaker than those due to CO. An instrumental spectral resolution of 2% further dilutes their strongest band heads. At high resolution, CS and SiS may be apparent in Y CVn at 7.3 and 6.6 μm. The relative strength of CS at 7.3 μm and SiS at 6.6 μm could provide a determination of the Si/S ratio based on Tsuji's models. Alternatively the CS and SiS measurements could choose whether Tsuji's models or Scalo's models in Table 2 are appropriate in carbon stars. Tsuji obtains a much lower partial pressure of CS than Scalo, even with a much greater N_C/N_O.

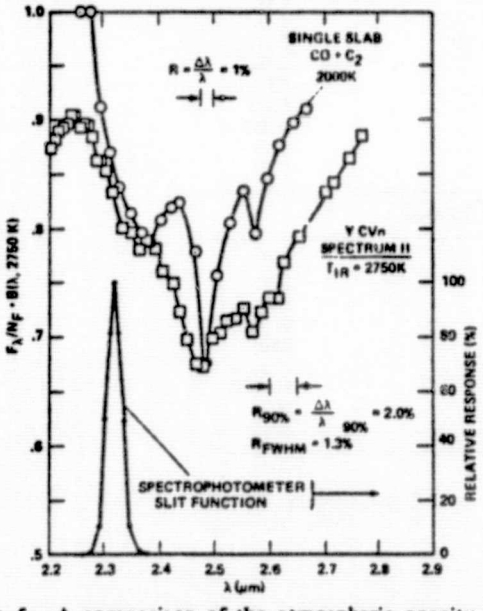

FIG. 5.—A comparison of the atmospheric opacity in the 2.5 μm region of Y CVn Spectrum II with a single slab opacity of 2000 K. CN opacity at 2.2 μm is not included in the computation, even though present in the star. The spectrophotometer slit function near 2.3 μm is also included.

d) Dust Grains

The well known particulate emission band of SiC at 11.5 μm is present in the spectrum of Y CVn. The band shape is similar to that observed in other carbon stars by Hackwell (1973), Treffers and Cohen (1974), and Forrest, Gillett, and Stein (1975). The usual interpretation is that SiC grains are injected into a circumstellar cloud by mass loss from the stellar photosphere (Gilra 1972; and Treffers and Cohen 1974). We have computed how the 11.5 μm band would appear if it were due to amorphous SiC based on the absorption coefficient given by Fagan (1973), and how it would appear if the band were due to the mixture of SiC crystalline forms measured by Dorschner, Friedemann, and Gürtler (1977). The crystalline material provides a reasonable fit to the 11.5 μm band in Y CVn, while the amorphous material does not (see Fig. 2). This confirms the conclusion of Treffers and Cohen (1974) that crystalline SiC is responsible for the 11.5 μm emission band.

The C_3 molecule is the principal vaporization product of graphite. The presence of C_3 in the photosphere and SiC in the circumstellar shell implies that both are capable of contributing to the violet opacity observed in Y CVn. Bregman and Bregman (1978) have shown that photospheric C_3 apparently dominates the violet opacity in this star. The presence of C_3 in the photosphere implies that graphite is a likely constituent of the circumstellar cloud. Graphite is not as easily identified as SiC due to a lack of distinct spectral features in the infrared. In principle, limits on the amount of graphite can be set by the depth of photospheric absorption features, principally the strong C_3 feature at 5.2 μm. The dust shell temperature is probably less than 1700 K, since SiC is expected to condense at 1700 K (Gilman 1969). This is a calculation beyond the scope of the present paper (Lucy 1976). But from the data of Figure 1, it appears there is little or no graphite in the circumstellar shell about Y CVn.

In spectrum III of Y CVn, there is an apparent emission feature at 22.5 μm (444 cm^{-1}). Although the

signal-to-noise ratio (S/N) of the individual spectral points is only modest (about 12), still the feature appears 4 σ above the continuum level defined by the adjacent spectral elements. The 16–30 μm data were obtained at higher spectral resolution than is presented here. In the original data, the feature is apparent in several adjacent spectral elements. Spectrum III is a spectral average of 1 μm wide intervals between 18 and 25 μm, as discussed earlier, for the purpose of presenting a higher S/N ratio. Since these are the first observations of a spectral feature in this wavelength region in a carbon star, confirmation of the observations are necessary in Y CVn and other similar N type stars like RY Dra, X Cnc, or UU Aur. However, a brief discussion of the feature's nature and possible origin is warranted by the present data.

The 22.5 μm feature rises above the photospheric Rayleigh-Jeans continuum by about 40%, roughly the same amount as the 11.5 μm feature, which is attributable to crystalline SiC. The fractional half-width of the 22.5 μm band is no more than 4%, while that of the 11.5 μm band is 16%. The circumstance that these are the only two emission features in the infrared spectrum of Y CVn, naturally leads to their association with the circumstellar shell. Other carbon stars which have been observed in the 22.5 μm region do not show the feature. However, they are only a few in number, and their continua at these wavelengths are dominated by emission from thick circumstellar shells, presumably composed of graphite grains (Treffers and Cohen 1974). In contrast, Y CVn is dominated by photospheric continuum, and components other than graphite may be apparent. Treffers and Cohen (1974) do not see the feature in CIT 6 or IRC +10216, nor do Forrest, McCarthy, and Houck (1979) see it in V Cyg or CIT 6. The known optical properties of SiC or graphite have no outstanding features in this wavelength range.

None of the atomic or molecular species known or suspected to be abundant in Y CVn or its circumstellar shell provide a satisfactory identification. We suggest that the feature arises from a circumstellar condensate. In searching for a possible species, we have restricted ourselves to condensates of the most abundant heavy elements in a carbon star as adopted by QQT (1974): C, O, N, Fe, Si, S, and Mg. All of the O and N and most of the S should reside in some gaseous form—e.g., CO, N_2, CN, HCN, SiS, and H_2S. That leaves graphite, metallic iron, and possibly sulfur, along with the carbides, sulfides, and silicides, as the simplest possibilities.

The silicides are not well studied, but the few which have been measured by Nyquist and Kagel (1971) are featureless in this region. Further study is warranted. For example, Birkholz *et al.* (1968) have shown that β–$FeSi_2$ is a semiconductor, and has a lattice absorption at 22.5 μm. However, it has a stronger 27 μm band and can be ruled out.

Excepting SiC, the knowledge of carbide spectra is also very limited. Pure SiC shows no bands at these wavelengths of consequence (Tanzilli, Gebhardt, and Ulrich 1975). A weakly bound impurity species could produce a narrow absorption band in the acoustic phonon continuum (Sievers 1964) at wavelengths greater than the transverse optical phonon. Since these modes do not require conservation of lattice momentum during absorption, relatively high absorption cross sections may be possible.

Sulfur and the sulfides have been studied more than the carbides and silicides. Neither FeS (Kammori, Sato, and Kurosawa 1968) nor MgS (Povarennykh *et al.* 1971) possesses bands at the right places. Neither SiS or SiS_2 has been reported in the indexed literature. Sulfur crystals show a band at 21.6 μm and 11.8 μm (MacNeill 1963). But sulfur is not expected to be stable toward formation of S_2, FeS_2, or MgS in the circumstellar environment around a carbon star (J. Stevens, private communication). Solid FeS_2 is a material which needs further consideration. Verble and Wallis (1969) and Schlegel and Wachter (1976) have shown that FeS_2 has optical phonon modes between 22.5 and 25 μm. Schlegel and Wachter find no other bands between 1.2 and 22.5 μm. Before FeS_2 can be accepted or rejected, a calculation similar to that of Gilra (1972) for SiC or experiments similar to those of Dorschner, Friedemann, and Gürtler (1977) must be performed.

More complex condensates such as cyanides and thiocyanates are spectroscopically interesting. Whether one would expect such condensates is not known at the present time. For example, iron thiocyanate, $Fe(SCN)_2$, has a fairly strong and narrow band near 21.5 μm according to Nyquist and Kagel (1971). With the exception of a much stronger band near 4.7 μm, the 21.5 μm band is the strongest feature in the spectrum of $Fe(SCN)_2$. The 4.7 μm band might be obscured by the stronger photospheric background at the shorter wavelengths.

Unfortunately, we are left without a positive identification of the 22.5 μm emission feature. Further observations in the 20–25 μm region are planned in order to confirm the 22.5 μm feature.

One final point concerns the relation of the SiC emission in the infrared to the well known violet opacity. Although Y CVn is a SR*b* variable, the magnitude of variability is small, about $0.5m_v$. Many of the bands have nearly constant strength, such as the C_3 absorption and SiC emission bands in particular. With these factors in mind, we can compare the amounts of power absorbed, P_A(violet), by the violet bands as measured by Bregman and Bregman (1978) with the power emitted P_E(SiC) in the SiC emission band of Spectrum III. The ratio is $P_A(\text{violet})/P_E(\text{SiC}) = 7.8$. This ratio is too large to be accounted for by the variability of Y CVn. Thus the reradiation by circumstellar SiC is inadequate to account for the violet opacity in Y CVn. This result supports the conclusion of Bregman and Bregman that the violet opacity in early N type carbon stars is primarily due to photospheric C_3.

Dr. G. Augason contributed in computing the synthetic models. Drs. F. C. Witteborn and E. F. Erickson contributed to the observations. Part of the

observations reported here were obtained when J. H. G. and J. D. B. were NRC/NAS Postdoctoral Research Associates at Ames Research Center. The UCSD group thanks Dr. F. C. Gillett of Kitt Peak National Observatory for the loan of a PbSnTe detector. We wish to acknowledge Daniel A. Briotta, Jr., for his help in obtaining these observations and thank the pilots and staff of the NASA Learjet and Gerard P. Kuiper Airborne Observatory for their assistance. Infrared astronomy at UCSD is supported by NASA grant NGR 05-005-055 and NSF grant AST 76-82890. B. T. S. is supported by AST 77-20516. The work at Cornell was supported in part by NASA grant NGR 33-010-081. R. W. R. and B. T. S. were at UCSD when part of this work was performed.

Note added in manuscript.—On 1979 July 11, additional observations of Y CVn from the KAO between 20 and 25 μm were made which do not confirm the possible emission feature at 22.5 μm discussed in the text. These new data resulted in approximately a factor of 2 increase in the signal-to-noise ratio over that displayed in Figure 1. Within the errors, the shape of the spectrum is Rayleigh-Jeans and the flux level is the same as that seen in 1978 May. We must conclude that either the 22.5 μm feature is variable in time, or it is not real. The latter possibility seems most likely.—W. J. F.

REFERENCES

Ballik, E. A., and Ramsay, D. A. 1963, *Ap. J.*, **137**, 61.
Bell, E. E., and Nielsen, H. H. 1950, *J. Chem. Phys.*, **18**, 1382.
Bikholz, V., Finkenrath, H., Naegele, J., and Uhle, N. 1968, *Phys. Stat. Sol.*, 30, K81.
Bregman, J. D., and Bregman, J. N. 1978, *Ap. J. (Letters)*, **222**, L41.
Bregman, J. D., Goebel, J. H., and Strecker, D. W. 1978, *Ap. J. (Letters)*, **223**, L45.
Carbon, D. 1974, *Ap. J.*, **187**, 135.
Dorschner, J., Friedemann, C., and Gürtler, J. 1977, *Astr. Nach.*, 298, 279.
Fagan, E. A. 1973, in *Proceedings of the Third International Conference on* SiC, ed. R. C. Marshall, J. W. Faust, Jr., and C. E. Ryan (Columbia: University of South Carolina Press), p. 542.
Forrest, W. J., Gillett, F. C., and Stein, W. A. 1975, *Ap. J.*, **195**, 423.
Forrest, W. J., McCarthy, J. F., and Houck, J. R. 1979, in preparation.
Gilman, R. C. 1969, *Ap. J. (Letters)*, **155**, L185.
Gilra, D. P. 1972, in *The Scientific Results from the Orbiting Astronomical Observatory (OAO 2)*, ed. A. D. Code (NASA SP-310), p. 310.
Goebel, J. H., Bregman, J. D., Strecker, D. W., Witterborn, F. C., and Erickson, E. F. 1978*a*, *Ap. J. (Letters)*, **222**, L129.
Goebel, J. H., Strecker, D. W., Bregman, J. D., Witteborn, F. C., and Erickson, E. F. 1978*b*, *Bull. AAS*, **10**, 406.
Goorvitch, D., and Goebel, J. H. 1980, in preparation (G^2).
Gow, C. E. 1977, *Pub. A.S.P.*, **89**, 510.
Hackwell, J. A. 1973, *Astr. Ap.*, **21**, 239.
Jacox, M. E. 1975, *Chem. Phys.*, **7**, 424.
Johnson, H. R., Beebe, R. F., and Sneden, C. 1975, *Ap. J. Suppl.*, **29**, 123.
Johnson, H. R., Marenin, I. R., and Price, S. D. 1972, *J. Quant. Spectrosc. Rad. Transf.*, **12**, 189.
Jones, T., and Merrill, K. M. 1976, *Ap. J.*, **209**, 509.
Kammori, O., Sato, K., and Kurosawa, R. 1968, *Bunseki Kagadu*, **17**, 1270.
Lucy, L. B. 1976, *Ap. J.*, **205**, 482.
MacNeill, C. 1963, *J. Opt. Soc. Am.*, **53**, 398.
Nyquist, R. A., and Kagel, R. O. 1971, *Infrared Spectra of Inorganic Compounds* (New York: Academic Press), p. 87.
Pierson, R. H., Fletcher, A. N., and Guntz, E. St. C. 1956, *Analy. Chem.*, **28**, 1218.
Povarennykh, A. A., Sidorenko, G. A., Solntseva, L. S., and Solnstev, B. P. 1971, *Mineal. Sb. L'vov*, **25**, 306.
Puetter, R. C., Russell, R. W., Sellgren, K., and Soifer, B. T. 1977, *Pub. A.S.P.*, **89**, 320.
Puetter, R. C., Russell, R. W., Soifer, B. T., and Willner, S. P. 1979, *Ap. J.*, in press.
Querci, F. 1969, Thèse de doctorate de specialité, Faculté des Sciences, Université de Toulouse.
Querci, F., and Querci, M. 1974, in *Highlights of Astronomy*, Volume 3, ed. G. Contopoulos (Dordrecht: Reidel), p. 341 (Q^2).
Querci, F., Querci, M., and Tsuji, T. 1974, *Astr. Ap.*, **31**, 265 (QQT).
Rank, D. H., Skorinko, G., Eastman, D. P., and Wiggins, T. A. 1960, *J. Opt. Soc. Am.*, 50, 421.
Ridgway, S. T., Hall, D. N. B., and Carbon, D. F. 1978, *Bull. AAS*, **9**, 636.
Ridgway, S. T., Hall, D. N. B., Kleinmann, S. G., Weinberger, D. A., and Wojslaw, R. S. 1976, *Nature*, **264**, 345.
Scalo, J. M. 1973, *Ap. J.*, **184**, 809.
Schlegel, A., and Wachter, P. 1976, *J. Phys. C*, **9**, 3363.
Sievers, A. J. 1964, *Phys. Rev. Letters*, **13**, 310.
Strecker, D. W., Erickson, E. F., and Witteborn, F. C. 1979, *Ap. J. Suppl.*, in press.
Tanzilli, R. A., Gebhardt, J. J., and Ulrich, D. R. 1975, unclassified portion of a confidential report: Development of Infrared Materials, A. F. Project 7360 by General Electric Co., Philadephia, Pa. (Re-entry and environmental Systems Division).
Treffers, R. R., and Cohen, M. 1974, *Ap. J.*, **188**, 545.
Treffers, R. R., and Gilra, D. P. 1975, *Ap. J.*, **202**, 839.
Tsuji, T. 1964, *Ann. Tokyo Astr. Obs.*, **9**, 1.
———. 1973, *Astr. Ap.*, **23**, 411.
Verble, J. L., and Wallis, R. F. 1969, *Phys. Rev.*, **182**, 783.
Wing, R. F., and Spinrad, H. 1970, *Ap. J.*, **159**, 973.

J. D. Bregman, J. H. Goebel, and D. Goorvitch: Mail Stop 245-6 NASA Ames Research Center, Moffett Field, CA 94035

W. J. Forrest, J. R. Houck, J. F. McCarthy, and R. W. Russell: CRSR, Cornell University, Ithaca, NY 14853

R. C. Puetter and S. P. Willner: C-011, Physics Department, University of California, San Diego, La Jolla, CA 92093

B. T. Soifer: 320-47, Downs Laboratory, Department of Physics, California Institute of Technology, Pasadena, CA 91125

D. W. Strecker: Ball Aerospace Systems Division, MP-4, P.O. Box 1062, Boulder, CO 80306

THE ASTROPHYSICAL JOURNAL, 244: 511–516, 1981 March 1

MEASUREMENTS OF FORBIDDEN LINE RADIATION OF Ar II (6.99 μm) IN W3 IRS 1

T. HERTER,[1] J. L. PIPHER, AND H. L. HELFER
Department of Physics and Astronomy, University of Rochester
S. P. WILLNER, R. C. PUETTER, AND R. J. RUDY
Center for Astrophysics and Space Sciences, University of California, San Diego
AND
B. T. SOIFER
Department of Physics, California Institute of Technology
Received 1980 June 23; accepted 1980 September 10

ABSTRACT

Observations of the [Ar II] (6.99 μm) line flux in W3 IRS 1 are combined with previously obtained measurements of the [Ar III] (8.99 μm) line flux. The observed ratio of [Ar II]/[Ar III] is inconsistent with the calculated ratio for an H II region with the densities required by radio observations and with a central 40,000–45,000 K star with atmosphere as described by a Mihalas model. A softer effective UV radiation field is required; a dusty model we had previously invoked fits the observations. In addition we determine that the argon abundance is $n(\mathrm{Ar})/n(\mathrm{H}) \approx 8 \times 10^{-6}$, a value about twice that usually adopted for normal solar abundance; however, there are uncertainties in the extinction and the model which do not allow us to preclude solar abundance.

Subject headings: infrared: spectra — nebulae: abundances — nebulae: individual

I. INTRODUCTION

We present in this paper observations of the [Ar II] (6.99 μm) line flux in the compact H II region W3 IRS 1, which complement previously obtained measurements of [Ar III] (8.99 μm). The [Ar II]/[Ar III] ratio is of importance in assessing not only the argon abundance but also the excitation conditions in the nebula.

W3 is one of the few compact H II regions, such as G75.84+0.4 (Pipher, Soifer, and Krassner 1979), G298.2−0.3 (Rank *et al.* 1978), and G45.1+0.1 (Hefele and Schulte in dem Bäumen 1978), studied thus far which exhibit all three fine structure lines in the 8–13 μm atmospheric window, namely Ar III (8.99 μm), S IV (10.52 μm) and Ne II (12.78 μm) (Willner 1977; Lacasse *et al.* 1980, hereafter Paper 1). The presence of S IV (which requires 35 eV photons to produce) *and* the presence of a significant fraction of Ar II (with a relatively low ionization potential of 27.6 eV) is not expected for most theoretical models to date. Direct measurements of the dominant ionizing star (IRS 2) of W3 IRS 1 by Beetz, Elsasser, and Weinberger (1974) and Wynn-Williams, Becklin, and Neugebauer (1972) imply an effective temperature ~ 45,000 K (Harris and Wynn-Williams 1976), which is also required to explain the radio strength of IRS 1. However, models of dust-free H II regions (Paper 1) indicate Ar II to be present in an appreciable fraction only for exciting stars with effective temperatures less than 35,000 K.

Because of the presence of a strong [S IV] line, the strong detection of the 6.99 μm [Ar II] line reported here was unexpected on the basis of simple dust-free H II region models. We interpret the observations below using a dusty H II region model; other interpretations may be possible, as discussed in § III.

II. OBSERVATIONS

Observations of the [Ar II] line and adjacent continuum were made with the UCSD 4–8 μm filterwheel spectrometer (Russell, Soifer, and Willner 1977; Puetter *et al.* 1979) on a flight of the Kuiper Airborne Observatory 1979 June 27. The focal plane aperture for the observations was 27″ with a spacing between chopped beams of ~ 50″ in azimuth (nearly north-south). Data points were taken at 6.83 μm, 6.99 μm (line center), and 7.11 μm with a spectral resolution of $\Delta\lambda/\lambda = 0.015$. Measurements were made at three positions: centered on IRS 2 (the dominant exciting star of IRS 1) and with offsets of one-half the beamwidth to the east and to the north of IRS 2. Accurate pointing was assured by offsetting to IRS 2 from IRS 5. A broad-band observation at 6.57 μm was also obtained at the central position. Correction for telluric absorption and calibration of the spectrum was derived through observations of the K2 III star α Boo, whose spectrum was assumed to be a 4000 K blackbody over the spectral region of interest. The [Ar II] line and adjacent continuum measurements at the central position are shown in Figure 1. Data for all three spatial positions are tabulated in Table 1 along with the [Ar II] line flux, both uncorrected and corrected for extinction by

[1] Fannie and John Hertz Foundation Fellow.

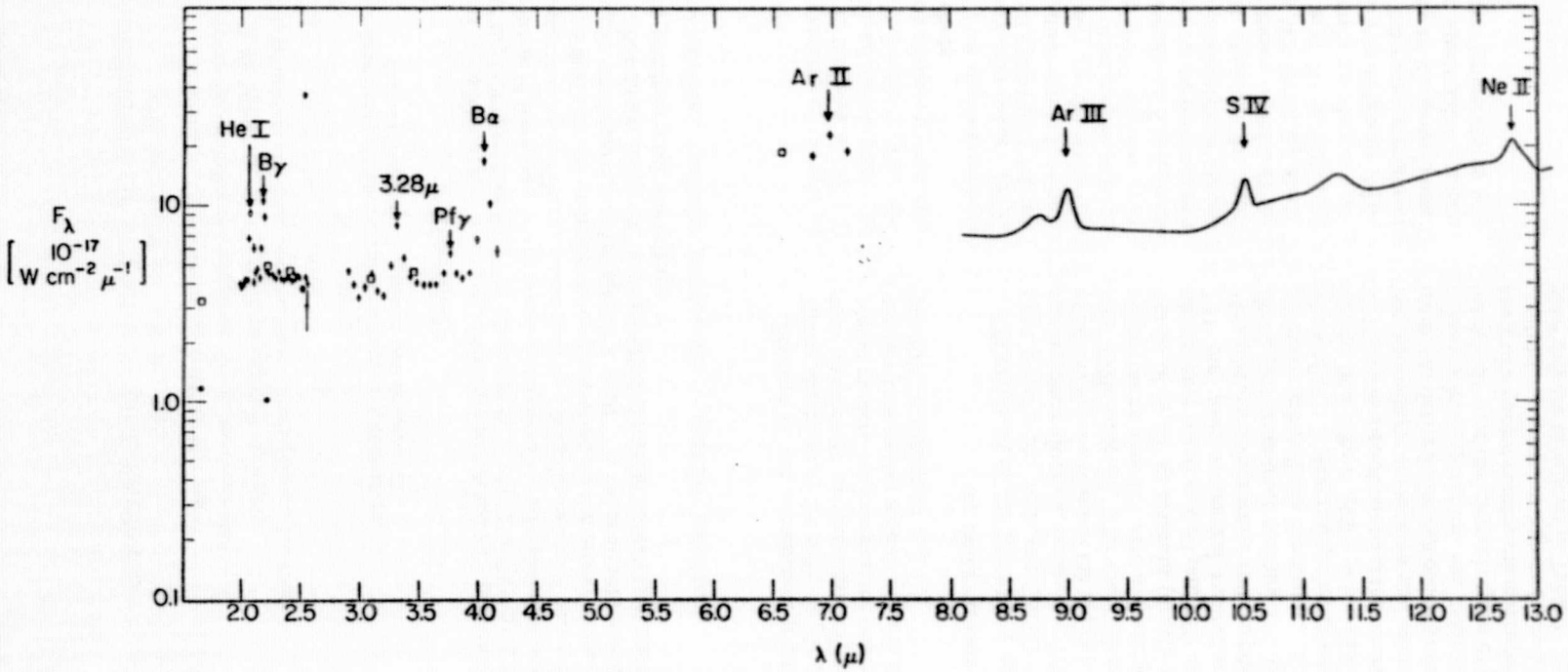

FIG. 1.—The 2–8 μm spectrum of W3 IRS 1 and a schematic representation of the 8–13 μm spectrum of W3 IRS 1. The 2–4 μm spectrum was obtained with a 22″ beam, the 4–8 μm with a 28″ beam, and the 8–13 μm with an 11″ beam. The open squares represent photometry, while the open circles are photometry (Wynn-Williams *et al.*) centered on IRS 2 obtained with a 10″ beam.

TABLE 1

Ar II LINE FLUX

Position Relative to IRS 2	Observed Flux Densities (10^{-16} W cm^{-2} μm^{-1})			Ar II Line Flux (10^{-17} W cm^{-2})	
	6.83 μm	6.97 μm	7.11 μm	Uncorrected for Extinction	Corrected[a] for Extinction
Center	1.84 ± 0.09	2.34 ± 0.09	1.95 ± 0.09	0.47 ± 0.19	0.77 ± 0.30
13″ east	1.42 ± 0.12	2.16 ± 0.13	1.50 ± 0.13	0.74 ± 0.27	1.63 ± 0.60
13″ north	1.67 ± 0.13	2.17 ± 0.15	1.78 ± 0.10	0.47 ± 0.28	0.83 ± 0.47

[a] Error bars include uncertainty in the absorption optical depth used to correct for extinction.

cool material in the line of sight, as discussed in the next section.

Included in Figure 1 is a 2–4 μm spectrum centered on IRS 2 which was obtained at Kitt Peak National Observatory using the 1.3 m telescope with a 22″ beam size (Krassner and Pipher, in preparation). The spectral resolution for these observations is $\Delta\lambda/\lambda = 0.013$–$0.021$. Also displayed in Figure 1 are photometric points at H band (1.66 μm), K band (2.22 μm), L band (3.45 μm), CO band (2.4 μm), and the ice band (3.08 μm). The hydrogen recombination lines, a recombination line of helium (2.05 μm) and the unidentified 3.28 μm feature are present in the 2–4 μm spectrum.

In addition, we reproduce schematically in Figure 1 an 8–13 μm spectrum (from Paper 1) taken with a 10″ beam diameter. The fine-structure lines of [Ar III], [S IV], and [Ne II] are evident. Simple scaling of the 8–13 μm spectrum by beam sizes is not an appropriate way to estimate line strengths because there is nebular ionization structure, that is, the ionic distributions do not mimic the dust continuum distribution measured by Hackwell *et al.* (1978); see Paper 1 for ionic distributions.

III. DISCUSSION

a) *The Extinction*

In some cases, the largest source of error in infrared abundance analyses derives from uncertainty in estimation of the extinction, in spite of the fact that the extinction is much smaller than at visual wavelengths. Hence we have computed the extinction in several independent ways.

An estimate of the extinction to the H II region can be obtained from the observed hydrogen recombination lines, Bα (4.05 μm) and Bγ (2.17 μm). From the 5 GHz map of Harris and Wynn Williams (1976), the estimated optically thin radio flux at 5 GHz in a 22″ beam is 8 Jy. At an assumed electron temperature of 10^4 K, the predicted ratio of $F(\mathrm{B}\alpha)/S_{5\,\mathrm{GHz}}$ is 2.5×10^{12} Hz and $F(\mathrm{B}\gamma)/S_{5\,\mathrm{GHz}}$ is 0.88×10^{12} Hz (Brocklehurst 1971; Giles 1977) so that the predicted line fluxes are 2.0×10^{-17} W cm^{-2} in Bα and 7.0×10^{-18} W cm^{-2} in Bγ. Comparing these with the measured flux densities of 11.5×10^{-17} and 5.8×10^{-17} W cm^{-2} μm^{-1}, and assigning instrumental resolutions of $\Delta\lambda/\lambda = 0.021$ and 0.013 at Bα and Bγ respectively, we find that $\tau_{4.05\,\mu\mathrm{m}} = 0.71$ and $\tau_{2.2\,\mu\mathrm{m}} = 1.46$. From $\tau_{2.2\,\mu\mathrm{m}}$ and using a λ^{-1} extinction curve, we derive the optical depth at 7 μm to be 0.45; with the same extinction law $\tau_{4.05\,\mu\mathrm{m}} = 0.71$ yields $\tau_{7\,\mu\mathrm{m}} = 0.41$. Using just the ratio of Bγ and Bα line strengths, and a λ^{-1} extinction curve, we deduce that $\tau_{7\,\mu\mathrm{m}} = 0.50$.

We now estimate $\tau_{7\,\mu\mathrm{m}}$ using the 8–13 μm spectrum. In Paper 1, the optical depth at 9.7 μm was estimated to be 2.1 from the 8–13 μm spectrum by assuming hot, optically thin, silicate dust emission attenuated by cool, absorbing silicate dust. Assuming that the emissivity of the cool absorbing dust in W3 has the same spectral characteristics as the emitting dust in the Trapezium (Gillett *et al.* 1975), we find that $\tau_{8\,\mu\mathrm{m}} = 0.54$. It is not clear what technique best interfaces the extinction at shorter wavelengths with that from 8–13 μm. If we assume a λ^{-1} extinction curve from 8 to 7 μm, this implies $\tau_{7\,\mu\mathrm{m}} \sim 0.6$, in reasonable agreement with the above estimates, in spite of our having ignored beamsize effects and despite the fact that it is difficult to center on IRS 2 at 8–13 μm.

We adopt a mean value of $\tau_{7\,\mu\mathrm{m}} = 0.49 \pm 0.08$[2] to correct the observed [Ar II] line flux when the measurement is centered on IRS 2. The optical depth corrections for the positions 13″ to the east and north can be different from that estimated above since there is differential extinction across IRS 1 (Hackwell *et al.* 1978). We estimate (from Hackwell *et al.* and Paper 1) that $\tau_{9.7\,\mu\mathrm{m}} = 3.0$ and 2.1 for the positions east and north of IRS 2, respectively. This leads to $\tau_{7.0\,\mu\mathrm{m}} \sim 0.64$ for the eastern position and $\tau_{7.0\,\mu\mathrm{m}} \sim 0.45$ for the northern position. The corrected fluxes for all three observed spatial positions are listed in Table 1, and we adopt the same uncertainty in $\tau_{7\,\mu\mathrm{m}}$ for all positions. In this case, the uncertainty in optical depth (which translates to 8% uncertainty in the corrected fluxes) is less than the measurement uncertainty.

b) *The* [Ar II] *Line Flux*

In Paper 1, model ionization structures of Ne II, Ar III, and S IV were calculated for a number of situations (including both dusty and dust-free H II regions) in an attempt to understand the observed forbidden line fluxes and ionic distributions. The shell models employed used the "on the spot" approximation to treat the diffuse radiation from hydrogen and helium and ignored charge-exchange and dielectronic recombination. A uniform

[2] The error quoted is the standard deviation.

TABLE 2

COMPARISON OF MEASURED AND PREDICTED FLUX

Position (1)	Observed Corrected Line Flux (10^{-17} W cm^{-2}) (2)	[a]Predicted Flux (10^{-17} W cm^{-2}) No Dust (3)	INI[b] (4)	Step[c] (5)	Power Law[d] (6)
Center	0.77 ± 0.30	0.02	0.44	1.6	1.1

[a] The predicted fluxes for the center and 13″ offset positions were the same.
[b] Opacity law shown in figure 2a.
[c] Opacity law shown in figure 2b; we note that an error crept into Paper 1, so that the step in those calculations occurred at 330 Å instead of 504 Å as intended.
[d] Opacity law with $\kappa(\nu) \propto \nu^2$.

electron temperature was assumed for the H II region, and for W3 IRS 1 we assumed an exciting star temperature of 42,000–45,000 K (as suggested by both the photometry of the star and the radio structure), and employed the non-LTE stellar atmospheres of Mihalas (1972). From the dust-free model, we calculate line fluxes for the appropriate beam size and in Table 2 compare the corrected line flux of Ar II to that predicted. As can be seen, the observed line flux without any extinction correction is at least 20 times larger than predicted by the dust-free models (column [3]). A *softer* UV spectrum than our model 42,000 K star or an alternative reason for an increased fraction of low-excitation ions is required to reproduce these observations. The ratio of [Ar II]/[Ar III] also requires lower excitation, as did the previous observations of [Ar III], [Ne II], and [S IV] line strengths reported in Paper 1.

Several mechanisms have been suggested for lowering the observed excitation. These include clumping, shadowing, charge exchange, and the presence of internal absorbing dust. It has been suggested by Panagia and Smith (1978) that selectively absorbing dust (e.g., $\bar{\tau}_{He}/\bar{\tau}_H \approx 5$ where $\bar{\tau}_{He}$ and $\bar{\tau}_H$ represent the average dust opacity to helium ionizing photons and hydrogen ionizing photons, respectively, and $\bar{\tau}_H \sim 1$) may account for the observed $n(He^+)/n(H^+)$ ratio for a number of H II regions. Only this possibility will be considered below.[3]

As in Paper 1, we have constructed models with internal dust with four different forms for the frequency dependence of the UV dust absorption cross section. These included power-law behavior (with the absorption proportional to ν and ν^2) and two different shapes (shown in Figs. 2*a* and 2*b*) which reflect the cross section ratios proposed by Panagia and Smith (1978). Scattering by the dust has been neglected. (For further details of the models and a discussion of the assumptions see Paper 1.) We assume as standard number abundances

$$(H:Ne:S:Ar) = (1.0:1.5 \times 10^{-4}:1.6 \times 10^{-5}:4.7 \times 10^{-6}),$$

deduced from planetary nebula observations by Kaler (1978) and from O/H and S/H as given by Cameron (1973). It was found in Paper 1 that a model with an exciting star with $T_{eff} = 45{,}000$ K, an optical depth of ~ 1 at 912 Å[4] for the H II region, and the frequency behavior of the UV dust optical depth shown in Figure 2*a* reproduced the observed line fluxes of Ar III (8.99 μm), S IV (10.52 μm), Ne II (12.79 μm), S III (18.7 μm), and O III (88.35 μm). The agreement between the observed and model fluxes was within 10–20% except for Ar III for which the calculated flux was a factor of 2 *lower* than that observed. This factor of 2 may not be significant because of large uncertainty in the extinction at 8.99 μm as well as uncertainties in the model. This factor of 2, if real, means that the argon abundance is a factor of 2 higher than assumed. Since the extinction is much more severe at 8.99 μm (Ar III) than at 6.99 μm (Ar II), and since most of the argon is in the form of Ar III, the argon abundance is the most difficult one to estimate from the infrared fine-structure lines. By employing similar models here, we find that the calculated Ar II line flux is moderately sensitive (by as much as a factor of 10) to the assumed frequency dependence of the UV opacity for the dust. A more general statement (which is not model-specific) is that the Ar II line flux is a sensitive indicator of the degree of UV softening of the radiation field of a central 45,000 K star.

The predicted [Ar II] line flux in a 27″ beam for three of the different opacity laws (with $\tau_{912\,Å} \sim 1$) is given in Table 2 (in addition to the dust-free case). The predicted fluxes are the same for the central position and the positions offset 13″ to the east and north. The opacity law "INI" (initial) (Fig. 2*a*) that allowed the best fit in Paper 1 also yields a calculated flux which is a factor of 1.2 to 3.9 *lower* than the observed [Ar II] flux, depending on which spatial position is considered. Equally important, however, is the fact that the *ratio* of [Ar II]/[Ar III] calculated from our model agrees fairly well with the observed ratio centered on IRS 2, as well as at the other two positions. (The models in Table 3 were constrained to produce the correct radio flux.) If no dust is present, a 42,000 K central star will support the radio strength, *but does not yield an appropriate ratio of* [Ar II]/[Ar III]. However, models with central stellar temperatures of 45,000 K and the dust models and optical depths shown give reasonable agreement with the observed argon line

[3] We are presently considering the effects of clumping, shadowing, and charge exchange on excitation conditions, and these results will be presented in a separate paper.

[4] Because the OTS (on the spot) approximation was used, rather than the modified OTS approximation, this represents an overestimate of the dust optical depth by $\sim$ 15–25%.

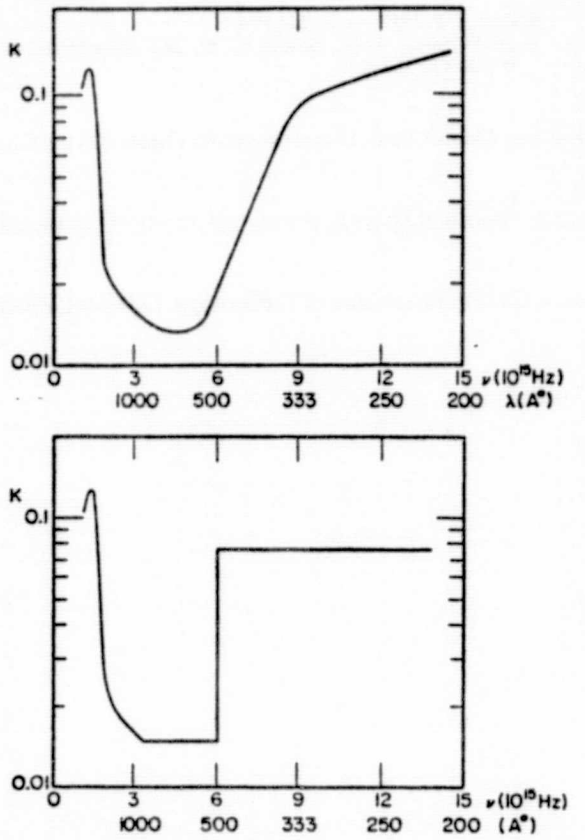

FIG. 2*a*. (*top*)—The assumed absorptivity of the dust for the INI opacity model. 2*b*. (*bottom*)—Step function absorptivity of the dust.

TABLE 3

PREDICTED FLUX RATIOS FOR VARIOUS DUST MODELS

Stellar Temperature (10^4 K)	Dust Model	Dust Optical Depth	Ar II[a] / Ar III
42	...	0	0.06
45	INI	1.1	0.4
45	step	1.1	4.3
45	ν^2	0.6	0.8

[a] Predicted flux ratios for appropriate beam sizes; observed ratio is 0.3.

ratio and the radio strength. Not only does the INI dust model best fit the observed [Ar II]/[Ar III] ratio, it also fits our observed [S III]/[S IV] ratio (see Paper 1). The other opacity laws (ν^2 and step) predict the observed [Ar II] flux but do not reproduce the ratio of [Ar II]/[Ar III] as well as the INI opacity law. Furthermore, the other infrared line flux densities reported in Paper 1 are best represented by the INI opacity law.

IV. CONCLUSIONS

The observed [Ar II] line flux at 6.99 μm is too large to be consistent with dust-free models of H II regions of appropriate density and with an exciting star of 42,000–45,000 K. However, we find that the observed [Ar II] line flux is consistent with a model incorporating internal dust. This model has been successful in reproducing the observed [Ar III], [S IV], [Ne II], [S III] (18.71 μm), and [O III] (88.35 μm) line strengths in W3, and requires the optical depth of dust internal to the H II region to be ~ 1 at 912 Å. Further, the dust is assumed to be selectively absorbing in the ultraviolet with an opacity law increasing to shorter wavelengths. On the basis of this model and the combined [Ar II] and [Ar III] measurements, we deduce that the argon abundance is $n(\mathrm{Ar})/n(\mathrm{H}) \approx 8 \times 10^{-6}$ in W3 IRS 1, higher than Kaler's average determination of 4.7×10^{-6}. Uncertainties in the extinction correction at 8.99 μm for Ar III, and in the model, reduce the significance of the higher abundance, however. But these uncertainties do not affect our major conclusion concerning the large [Ar II] line flux, and the direct inference that the UV radiation field in the nebula must be softened by some mechanism. Any alternate model which softens the UV radiation field in a similar way to our dusty model should be capable of predicting the observed line strengths: a constraint on such models is that the volume of the H II region must remain sufficiently large to supply the observed line and radio continuum flux. Other mechanisms such as the effects of clumping, shadowing, and charge exchange should clearly be investigated.

We wish to thank the support staff of the Kuiper Airborne Observatory for their excellent performance during flight operations. All of the authors are supported by grants from NASA and the NSF.

REFERENCES

Beetz, M., Elsasser, H., and Weinberger, R. 1974, *Astr. Ap.*, **34**, 335.
Brocklehurst, M. 1971, *M.N.R.A.S.*, **153**, 471.
Cameron, A. G. W. 1973, *Space Sci. Rev.*, **15**, 121.
Giles, K. 1977, *M.N.R.A.S.*, **180**, 57P.
Gillett, F. C., Jones, T. W., Merrill, K. M., and Stein, W. A. 1975, *Astr. Ap.*, **45**, 77.
Hackwell, J. A., Gehrz, R. D., Smith, J. R., and Briotta, D. A. 1978, *Ap. J.*, **221**, 797.
Harris, S., and Wynn-Williams, G. G. 1976, *M.N.R.A.S.*, **174**, 649.
Hefele, H., and Schulte in den Bäumen, J. 1978, *Astr. Ap.*, **66**, 465.
Kaler, J. B. 1978, *Ap. J.*, **225**, 527.
Lacasse, M., Herter, T., Krassner, J., Helfer, H. L., and Pipher, J. L. 1980, *Astr. Ap.*, **86**, 231 (Paper 1).
Mihalas, D. 1972, NCAR-TN/STR-76.
Panagia, N., and Smith, L. F. 1978, *Astr. Ap.*, **62**, 277.
Pipher, J. L., Soifer, B. T., and Krassner, J. 1979, *Astr. Ap.*, **74**, 302.
Puetter, R. C., Russell, R. W., Soifer, B. T., and Willner, S. P. 1979, *Ap. J.*, **228**, 118.

Rank, D. M., Dinerstein, H. L., Lester, D. F., Bregman, J. K., Aitken, D. K., and Jones, B. 1978, *M.N.R.A.S.*, **185**, 179.
Russell, R. W., Soifer, B. T., and Willner, S. P. 1977, *Ap. J.*, **213**, 66.
Willner, S. P. 1977, *Ap. J.*, **214**, 706.
Wynn-Williams, G. G., Becklin, E. E., and Neugebauer, G. 1972, *M.N.R.A.S.*, **160**, 1.

H. L. HELFER, T. HERTER, and J. L. PIPHER: Physics and Astronomy Department, University of Rochester, River Campus Station, Rochester, NY 14627

R. C. PUETTER, R. J. RUDY, and S. P. WILLNER: Center for Astrophysics and Space Sciences, University of California, San Diego, La Jolla, CA 92093

B. T. SOIFER: Division of Physics, Mathematics, and Astronomy, California Institute of Technology, Downes Laboratory C-011, Pasadena, CA 91125

ICARUS 45, 653–660 (1981)

Observations of Saturn in the 5- to 8-μm Spectral Region

F. C. WITTEBORN, J. B. POLLACK, J. D. BREGMAN,[1] AND J. H. GOEBEL

Ames Research Center, NASA, Moffett Field, California 94035

B. T. SOIFER

California Institute of Technology, Pasadena, California 91109

AND

R. C. PUETTER, R. J. RUDY, AND S. P. WILLNER

University of California, San Diego, La Jolla, California 92037

Received August 18, 1980; revised January 29, 1981

A spectrum of Saturn obtained from the Kuiper Airborne Observatory exhibits an emission peak at 6.8 μm attributed to ethane, but is otherwise dominated by absorption from 5.3 to 7.2 μm. While the large absorption in this spectral region is consistent with the presence of ammonia gas or ammonia ice, or both, such an explanation is inconsistent with the lack of a major absorption near 3.0 μm.

INTRODUCTION

Infrared spectral observations of the outer planets can provide information on their gaseous composition, cloud material, and temperature structure. Prior observations of Saturn have been made in parts of the 0.3- to 5.6-μm and 8- to 300-μm spectral domains. The former wavelength domain is dominated by reflected sunlight and is characterized by numerous strong absorption features due to gaseous methane as well as by features due to the pressure-induced vibrational fundamental of hydrogen and permitted transitions of ammonia vapor (Trafton, 1977). The latter wavelength region is dominated by thermal emission and exhibits structure due to the pressure-induced rotational transition of hydrogen as well as permitted transitions of methane, ethane, and phosphine (Trafton, 1977). In addition, measurements have been obtained at a few discrete wavelengths in the 4- to 8-μm interval (Russell and Soifer, 1977; Rieke, 1975).

In this paper, we present spectral observations of Saturn in the hitherto poorly characterized region 5–8 μm. These observations were obtained from NASA's Kuiper Airborne Observatory, which flies at altitudes above almost all the obscuring water vapor. We find that the Saturn spectrum exhibits a very deep minimum at 6.3 μm, a minimum near 7.1 μm, and a peak near 6.8 μm. After describing our observational protocol, we present a preliminary analysis of these features based on comparisons with the spectrum of Jupiter, the spectrum of Saturn at shorter wavelengths, and the absorption characteristics of materials that are known or suspected to be abundant in Saturn's atmosphere.

OBSERVATIONS

The 5- to 8-μm spectra were obtained with the 4- to 8-μm circular variable filter (CVF) spectrometer (Univ. of California,

[1] Ames Associate.

0019-1035/81/030653-08$02.00/0

San Diego) discussed previously by Puetter *et al.* (1979). This system employs a PbSnTe detector cooled to 4.2°K and a CVF cooled to 77°K. The spectral resolution $\Delta\lambda/\lambda$ is about 1.6%. The focal plane aperture is 2 mm, which limits the field of view to 27 arcsec. Whole-disk spectra were obtained. The portion of the rings in the field of view constituted 14% of the area of the disk.

Observations were made on April 20 UT, 1979, and June 21 UT, 1979, from the Kuiper Airborne Observatory at an altitude of about 12.2 km (40,000 ft). Absolute flux calibrations were obtained by taking spectra of α Lyrae and α Boötis with the same instrument through the same air mass. The Saturn spectra were divided by the α-Lyrae spectra and multiplied by absolute flux spectra determined by Schild *et al.* (1971) from a stellar model that gives agreement with absolute visible light photometry of α Lyrae. The resulting flux spectrum (Fig. 1) is thereby corrected for instrumental effects and the small amount of terrestrial water absorption (about 20% near 6 μm) still present above 12.2 km (40,000 ft).

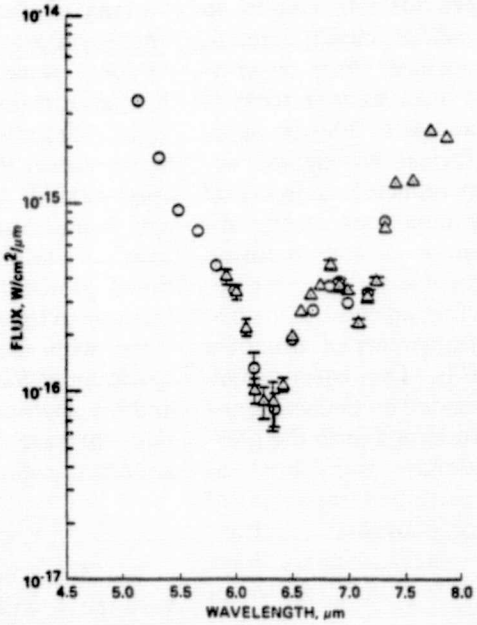

FIG. 1. Saturn spectrum, 5–8 μm. Error bars represent one standard deviation of the mean. Circles are data taken on 4/20/79; triangles are data taken on 6/19/79 multiplied by 1.23 to raise the flux to the value it would have had if Saturn were viewed from its distance on 4/20/79.

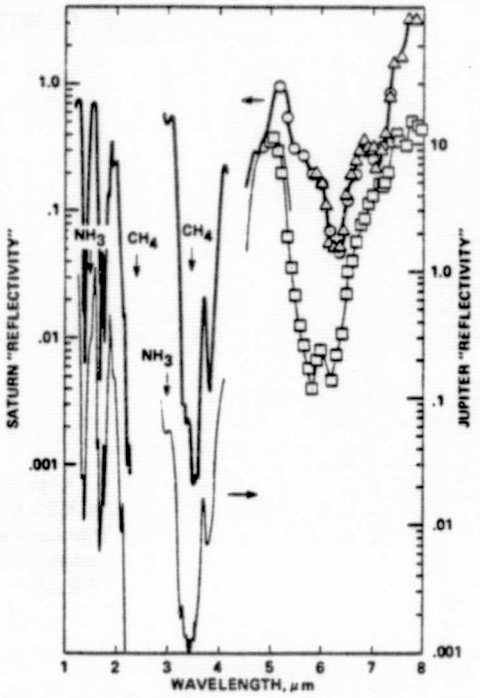

FIG. 2. Upper curve: Saturn "reflectivity" spectrum. Saturn spectra from KAO (5.1–7.9 μm) and Mt. Lemmon are divided by the solar flux of Smith and Gottlieb (1974). Thermal emission contributes in varying amounts at the longer wavelengths. The spectrum in the range 1–5 μm was obtained with rings edge on in March 1980. The reflectivity from 1.25–5.4 μm (solid curve) is normalized to agree with the 4/20/79 data at 5.14 μm. The circles and triangles are absolute reflectivities to the extent that thermal emission is negligible. Lower curve: Jupiter "reflectivity" spectrum. This spectrum was obtained in the same way as that of Saturn so that features may be compared. Note that the scale for Jupiter reflectivity is displayed and on the right.

The measurement errors in relative flux are indicated by 1σ error bars in Fig. 1. These range from about 20% in regions of highest absorption to 2% in the brightest parts of Saturn's spectrum. The wavelength uncertainty is less than 0.03 μm.

In Fig. 2 Saturn's flux has been di-

vided by the incident solar flux determined from the values of Smith and Gottlieb (1974). Such a plot permits direct comparisons of the depths of absorption features. Unit reflection corresponds to reflection by a perfectly diffuse ellipse of Saturn's angular dimensions placed at the distances from the Sun appropriate to the observing dates. No correction was made for the contribution of and obscuration by the rings. The 1- to 5-μm portion of the spectrum is made up of data taken with 1.5% resolution at the Mt. Lemmon 60-in. telescope (NASA and Univ. of Arizona) in March, 1980, when the rings were edge on. These data also were taken with circular variable filter spectrometers and were corrected for terrestrial absorption by comparison with spectra of α Lyrae taken with the same instrument and corrected for air mass differences; they are shown primarily to illustrate the relative depths of absorption at 3 and 6.3 μm. The emission features have not been subtracted out, so that the values are only an upper limit to the reflectivity. Since the upper limits are well below unity from 5.3 to 7.2 μm, Saturn's atmosphere is strongly absorbing in this spectral range.

For comparison, a 1- to 8-μm spectrum of Jupiter divided by the solar spectrum is also shown in Fig. 2. This was obtained from a composite of Russell and Soifer's (1977) 4- to 8-μm Jupiter spectrum and a 1- to 5-μm CVF spectrum of the central 18 arcsec of Jupiter obtained at Mt. Lemmon on the same night as the 1- to 5-μm portion of the Saturn spectrum. Much of the 4- to 8-μm portion is actually an emission spectrum, as is part of Saturn's spectrum in that range.

DISCUSSION

We first review the known spectral features in the 1- to 8-μm reflectivity spectrum of Saturn and then discuss possible sources for the new features seen at 6.3, 6.8, and 7.1 μm in Fig. 2. Almost all the absorption features in the region 1–4 μm can be attributed to gaseous methane, including the feature in the region 3–4 μm that is due to the 3.3-μm vibration fundamental of methane. Notable exceptions include the region near 2.2 μm, which is strongly influenced by the pressure-induced vibrational fundamental of hydrogen and the feature at 2.9 μm that may be due to phosphine (Larson *et al.*, 1980). Recent data and discussion of the 0.8- to 2.4-μm spectrum are presented by Clark and McCord (1979) and of the 2.5- to 5.6-μm spectrum by Larson *et al.* (1980).

Although gaseous ammonia has been detected at 0.645 μm (e.g., Woodman *et al.*, 1977), its bands at longer wavelengths are not evident. This difference in the detectability of ammonia is due in part to the wavelength dependence of the line formation process, which is strongly influenced by scattering within the upper cloud layer. Thus, using a reflecting-layer model, Woodman *et al.* (1977) derive a vertical column abundance for NH_3 of 2.0 ± 0.5 m-am from their analysis of the 0.645-μm feature, and Owen *et al.* (1977) and Larson *et al.* (1980) set upper limits of 0.15 and 0.001 m-am from their measurements covering the 1.56- and 3.0-μm bands of NH_3, respectively. These results indicate the limitations of reflecting-layer models of line formation; they might be understood by postulating a lower single-scattering albedo in the scattering layers of the atmosphere at the longer wavelengths due to the combined effects of the particulate absorption properties and the tails of nearby methane bands. The greatest difference between the spectra of Jupiter and Saturn (e.g., Fig. 2) arises from the absence of gaseous ammonia features in the case of Saturn (e.g., the region 2.75–3.0 μm).

At wavelengths longer than 7.35 μm the apparent reflectivity of Saturn exceeds unity; hence, thermal emission is the dominant source of the observed radiation in this spectral interval. The thermal radiation is believed to originate chiefly in the temperature inversion region of the stratosphere, with the 7.7-μm vibrational fundamental of methane providing the opacity (Gillett and Forrest, 1974). In the case of Jupiter, the

"reflectivity" values in excess of unity near 5 μm can be attributed to thermal emission that arises deep in the atmosphere in very localized "hot spot" regions that lack the usual high-level clouds. Because the 5-μm flux from Saturn is roughly comparable to that from a perfect diffuse reflector, it is difficult to assess whether "hot spots" are also present in Saturn's atmosphere. Spatial scans of the 5-μm flux with a 3-arcsec beam size showed no structure (Rieke, 1975). Observations with high spatial resolution are needed to settle this question.

Before relating our new data to constituents in Saturn's atmosphere, it is important to assess the possible contributions of the rings in the 5- to 8-μm spectral domain. The near-infrared reflectivity spectrum of the rings is dominated by water-ice bands (e.g., Pilcher *et al.*, 1972; Puetter and Russell, 1977). At wavelengths longer than 4 μm, the reflectivity of water-ice frosts is very low, a few percent (Smythe, 1975). Furthermore, at the low temperature of the rings (~80°K), thermal emission from them will not be important at wavelengths shorter than 8 μm. Since the solid angle subtended by the rings in our field of view was about 14% of that of Saturn, we conclude that the influence of the rings in the 5- to 8-μm spectral domain is very small and can be neglected.

The spectrum of Saturn shown in Fig. 1 exhibits two new flux minima centered near 6.3 and 7.1 μm. We first consider the origin of the 7.1-μm feature. In principle, this feature could be due either to the occurrence of a maximum absorption in the reflectivity spectrum of Saturn or to a minimum opacity in the thermal emission spectrum. At abundances that are consistent with those inferred from its visible and near-infrared bands, ammonia is transparent near 7 μm (France and Williams, 1974). Certain forms of ammonia ice exhibit a weak absorption feature centered near 7.2 μm (Staats and Morgan, 1959). By itself, gaseous methane appears to be unable to account for the 7-μm feature. Its opacity declines sharply from 7.4 to 7.1 μm and then more gradually from 7.1 to 6.6 μm (Burch *et al.*, 1962). Superimposed on this overall trend, there is a very weak local opacity maximum centered at 6.94 μm (Burch *et al.*, 1962) and a local opacity minimum at 7.09 μm. This might account for the observed minimum near 7.1 μm, but not for the 6.7- to 6.8-μm peak.

We propose that the most likely explanation for the 7.1-μm feature is that it is a thermal emission minimum situated between the ethane ν_8 band located at 6.8 μm (Thorndike, 1947; Pierson *et al.*, 1956) and the tail of the 7.7-μm methane ν_4 band. If this explanation is correct, we can obtain a crude estimate of the ethane mixing ratio in Saturn's stratosphere by using the observed enhancement of the flux at 6.8 μm, $\Delta F(6.8\ \mu\text{m})$ above the continuum value that was estimated as the average of the fluxes at 7.07 and 6.57 μm. We define $\tau(6.8\ \mu\text{m})$ as the broadband opacity due to ethane in the emitting region of the stratosphere. It is related to $\Delta F(6.8\ \mu\text{m})$ and the properties of the 7.7-μm methane band by

$$\tau(6.8\ \mu\text{m}) = [\Delta F(6.8\ \mu\text{m})\, B(7.7\ \mu\text{m})/ \Delta F(7.7\ \mu\text{m})\, B(6.8\ \mu\text{m})], \quad (1)$$

where B is the Planck function at the characteristic emitting temperature of the stratosphere (~130°K) (Gillett and Forrest, 1974), and $\Delta F(7.7\ \mu\text{m})$ is the emitted flux at the center of the methane 7.7-μm feature. In deriving (1) we assume that the emitting region of the stratosphere is optically thick at the center of the methane band and optically thin at the center of the ethane band. Using (1), the observed value of ΔF, and computed values of B, we find that $\tau(6.8\ \mu\text{m}) \cong 0.2$.

We next use the inferred value of $\tau(6.8\ \mu\text{m})$ and laboratory measurements of the 6.8-μm ethane band to infer a mixing ratio for ethane. Assuming that the transmission of ethane is in the strong-line limit for the path lengths of interest, $\tau(6.8\ \mu\text{m})$ is related to the average pressure P, ethane column

density W, slant path factor μ, and ratio of foreign (H_2) to self-broadening f, by

$$\tau(6.8\ \mu\text{m}) = K(WPf/\mu)^{1/2}. \quad (2)$$

With $\mu = 0.5$, $\tau = 0.2$, $f = 0.64$ (Burch *et al.*, 1962) and $K = 1.2$ determined by the laboratory measurements of Pierson *et al.* (1956), we find that $W_{C_2H_6} \cong 21$ cm atm/P(mbar). Finally, the ratio of the column density of ethane to the total column density or the mixing ratio of ethane, α, is given by

$$\alpha = \frac{W}{H2P(T_0/T)} \cong \frac{1 \times 10^{-3}}{P^2(\text{mbar})}, \quad (3)$$

where H is the atmospheric scale height, T is the atmospheric temperature, and T_0 is the standard value of temperature (273°K). The value of P may be derived from the atmospheric level at which T equals the brightness temperature at the center of the methane band (~130°K). We use the Curtiss–Godsend approximation to deduce $2P$ as the pressure at the bottom of the column contributing to the ethane opacity. On the basis of Voyager I/Saturn data (Eschelman, 1980), we set $P = 3$–10 mbar and hence find that $\alpha = 10^{-4}$ to 10^{-5}. These values are roughly consistent with values of 10^{-5} to 10^{-8} that have been derived from photochemical models (Strobel, 1977). Our value can only be approximate for several reasons: (1) We do not know the shape of the continuum. (2) We did not do a full integration of the equation of radiative transfer. (3) We used a crude pressure scaling ($P^{1/2}$) in comparing laboratory measurements with measurements in Saturn's atmosphere. The presence of ethane in the stratosphere would also require a 12-μm emission feature. Such a feature was observed by Gillett and Forrest (1974), and its identity with the ν_9 band of ethane was clearly established by Tokunaga *et al.* (1975). The ν_9 band has about one-third the absolute intensity of the ν_8 band which, in turn, is one-half as strong as the ν_4 band of methane (Thorndike, 1947). Using the data of Gillett and Forrest (1974) for Saturn's ethane emission at 12 μm and the laboratory ethane spectra of Pierson *et al.* (1956) we can estimate the mixing ratio of ethane from the 12-μm band just as we did from the 6.8-μm band. In this case we find $\alpha = 2.4 \times 10^{-5}$ to 2.7×10^{-4}, again an approximate value in fair agreement with that inferred from the 6.8-μm band.

We next consider the source of the 6.3-μm feature. One possibility is that it is a reflectivity feature of an optically thick ammonia cloud, whose presence has been postulated on the basis of cosmochemical and vapor pressure considerations (Lewis, 1969). However, there is a very serious difficulty associated with such an identification. Although ammonia ice does exhibit a strong feature from 6.1 to 6.4 μm (Bromberg *et al.*, 1977), it has a stronger band whose center is close to 3 μm. The high reflectivity of Saturn at 3.0 and 3.1 μm places strong constraints on the contribution of ammonia ice at these wavelengths and hence on its influence in the 6-μm region. Slobodkin *et al.* (1978) have reported that the spectral location of the 3-μm band of ammonia-ice is sensitive to the manner in which it is formed. They have suggested that the band center could be located at 3.29 μm for conditions relevant to Saturn's atmosphere, in which case the band center could be obscured by the strong methane 3.3-μm band. However, the reflectivity of this shifted band is quite low at 3.1 and 3.0 μm; hence, it is incompatible with the spectra shown in Fig. 2.

It is highly unlikely that the 6.3-μm band can be attributed to gaseous methane. The transmission spectrum of methane has a local *maximum* close to 6.3 μm (Burch *et al.*, 1962). Further, the spectrum of Saturn fails to reveal any indication of a narrow, strong methane band centered at 6.45 μm (Burch *et al.*, 1962).

We note that phosphine which is present in the atmosphere of Saturn (Bregman *et al.*, 1975) does not have appreciable absorption in the 5.3- to 7.3-μm range (Robertson and Fox, 1928).

We cannot help noticing the strong resemblance between the 6.3-μm feature in Saturn's reflectivity spectrum and a similarly located feature in Jupiter's spectrum (e.g., Fig. 2). Economy of hypotheses and other similarities between the two giant planets would suggest that these two features have a common explanation. In the case of Jupiter, fine structure can be discerned in its 6.2-μm band that can be readily attributed to gaseous ammonia (Hanel *et al.*, 1979). We propose that absorption by gaseous ammonia is chiefly responsible for the 6.3-μm feature of Saturn's spectrum.

To pursue our proposed explanation further, we compared the laboratory transmission spectrum obtained by France and Williams (1964) with our reflectivity spectrum of Saturn and found a crude overall agreement. The wings of the ammonia vapor band extend to wavelengths as small as about 5.4 μm, and there is a sharp increase in absorption beginning near 6.0 μm and extending to the band center at 6.14 μm. However, the band center of ammonia vapor is at somewhat too short a wavelength. Using the laboratory data of France and Williams (1964), the strong-line approximation, a simple reflecting-layer model, and an average pressure of 700 mbar, we find that a vertical column density of about 4-cm-am of ammonia vapor is required to produce the observed reflectivity near the band center.

Aside from the apparent misalignment of the band centers, our explanation of the 6.3-μm feature is not without problems. Although 4 cm-am would depress the reflectivity spectrum by less than 30% at 3 μm, and hence be compatible with the results of Fig. 2, a much more severe upper bound on the ammonia vapor abundance of 0.1 cm-am has been set by high-resolution studies of the 3-μm regions (Larson *et al.*, 1980). Observations at 10 μm by Tokunaga *et al.* (1980) set an upper limit of about the same magnitude. We do not feel that these latter results necessarily rule out our explanation of the 6.3-μm feature. As noted earlier, observations in the visible indicate ammonia gas amounts to 2 m-am. Hence, the effective ammonia abundance is wavelength dependent. Two types of interaction between radiation and particulates may be involved. (1) Near 0.645 μm radiation may be internally reflected in the cloud particles and only weakly absorbed by the particles and surrounding gas, thus allowing a long path before this radiation escapes from Saturn. (2) At wavelengths greater than the particle size the efficiency of interaction decreases as the ratio of wavelength to particle size increases. Thus, due to the presence of small particles in Saturn's upper troposphere and stratosphere, radiation may penetrate more deeply, on the average, at 6 μm than at 3 μm; hence, the upper bound on the ammonia amount obtained by Larson *et al.* (1980) may not be applicable to the 6-μm region. This hypothesis, in conjunction with our postulation of ammonia vapor absorption in the 6-μm region, reopens the possibility that ammonia ice also contributes to the depressed reflection in this wavelength region. The absence of ammonia features at 10 μm is not inconsistent with this hypothesis if the 10-μm continuum arises predominantly from emission in the stratosphere and/or the upper troposphere. For example, the larger mixing ratio of phosphine inferred by Tokunaga *et al.* (1980) for Saturn relative to Jupiter in conjunction with the lower temperature of Saturn's atmosphere at a given pressure level, may make it more difficult to see down to the NH_3 cloud level in Saturn in the 10-μm region. Higher spectral resolution measurements near 6 μm are needed to further explore these possibilities.

CONCLUSIONS

Saturn's 5- to 7.5-μm spectrum is dominated by absorption from 5.3 to 7.2 μm. A peak found at 6.8 μm appears to be ethane in emission. The absorption cannot be attributed to ammonia ice under the laboratory conditions used by Bromberg *et al.*

(1977) or more recently by Sill *et al.* (1980) because of the absence of a deep feature near 3 μm. Whether they can be explained in part by ammonia ice formed under unusual conditions (Slobodkin *et al.*, 1978) is still an open question. Much of the absorption can be explained by 4 cm-am of NH_3 gas, provided that the scattering properties of overlying clouds can account properly for the absence of NH_3 absorption at 3.0 and 10 μm.

ACKNOWLEDGMENTS

We are indebted to the ground and air crews of the Kuiper Airborne Observatory; their efforts were essential to the obtainment of the data. Support for this work from the National Science Foundation is acknowledged by B.T.S., and from the National Aeronautics and Space Administration by B.T.S., P.C.P., R.J.R., and S.P.W. F.C.W. acknowledges helpful discussion with H. P. Larson and U. Fink on the spectra of methane and ammonia. We are grateful to W. J. Forrest for pointing out errors in the manuscript and for other helpful comments.

REFERENCES

Bregman, J. D., Lester, D. F., and Rank, D. M. (1975). Observations of the ν_2 band of PH_3 in the atmosphere of Saturn. *Astrophys. J.* **202**, L55–L56.

Bromberg, A., Kimel, S., and Ron, A. (1977). Infrared spectrum of liquid and crystalline ammonia. *Chem. Phys. Lett.* **46**, 262–266.

Burch, D. E., Gryvnak, D., Singleton, E. E., and Williams, D. (1962). *Infrared Absorption by Carbon Dioxide, Water Vapor, and Minor Atmospheric Constituents*. Air Force Cambridge Research Laboratory Report 62-698.

Clark, R. N., and McCord, T. B. (1979). Jupiter and Saturn: Near-infrared spectral albedos. *Icarus* **40**, 180–188.

Eshleman, V. R. (1980). Paper presented at the December, 1980 meeting of the AGU by G. F. Lindal, J. D. Anderson, T. A. Croft, V. R. Eshleman, G. S. Levy, G. L. Tyler, and G. E. Wood (1980). Radioscience: The atmospheres of Saturn and Titan. *EOS Trans. Amer. Geophys. Union* **61**, Nov. 11, 1980.

France, W. L., and Williams, D. (1964). *Total Absorptance of Ammonia in the Infrared*. Air Force Cambridge Research Laboratory Report 64-652.

Gillett, F. C., and Forrest, W. J. (1974). The 7.5- to 13.5-micron spectrum of Saturn. *Astrophys. J.* **187**, L37–L39.

Hanel, R., Conrath, B., Flasar, M. Herath, L., Kunde, V., Lowman, P., McGuire, W., Pearl, J., Pirraglia, J., Samuelson, R., Gautier, D., Gierasch, P., Horn, L., Kumar, S., and Ponnamperuma, C. (1979). Infrared observations of the Jovian system from Voyager 2. *Science* **206**, 952–956.

Kliore, A., Lindal, G. F., Patel, I. R., Sweetman, D. N., and Hortz, H. B. (1980). Vertical structure of the ionosphere and neutral atmosphere of Saturn from Pioneer radio occultation. *Science* **207**, 446–449.

Larson, H. P., Fink, U., Smith, H. A., and Davis, D. S. (1980). The middle infrared spectrum of Saturn: Evidence for phosphine and upper limits to other trace atmospheric constituents. *Astrophys. J.* **240**, 327–337.

Lewis, J. S. (1969). The clouds of Jupiter and the NH_3–H_2O and HN_3–H_2S systems. *Icarus* **10**, 365–389.

Owen, T., McKellar, A. R. W., Encrenaz, Th., Lecacheux, J., de Bergh, C., and Maillard, J. P. (1977). A study of the 1.56 μ NH_3 band in Jupiter and Saturn. *Astron. Astrophys.* **54**, 291–295.

Pierson, R. H., Fletcher, A. N., and St. Clair-Gantz, E. (1956). Catalog of infrared spectra for qualitative analysis of gases. *Anal. Chem.* **28**, 1218–1239.

Pilcher, C. B., Chapman, C. R., Lebofsky, L. A., and Kieffer, H. (1972). Saturn's rings: Identification of water frost. *Science* **167**, 1372–1373.

Puetter, R. C., and Russell, R. W. (1977). The 2–4-μm spectrum of Saturn's rings. *Icarus* **32**, 37–40.

Puetter, R. C., Russell, R. W., Soifer, B. T., and Willner, S. P. (1979). Spectrophotometry of compact H II regions from 4 to 8 microns. *Astrophys. J.* **228**, 118–122.

Rieke, G. H. (1975). The thermal radiation of Saturn and its rings. *Icarus* **26**, 37–44.

Robertson, R., and Fox, J. J. (1928). Studies in the infra-red region of the spectrum. Part III—Infra-red absorption spectra of ammonia, phosphine and arsine. *Proc. Roy. Soc. London* **120**, 128–169.

Russell, R. W., and Soifer, B. T. (1977). Observation of Jupiter and Saturn at 5-8 μm. *Icarus* **30**, 282–285.

Schild, R., Peterson, D. M., and Oke, J. B. (1971). Effective temperature of B- and A-type stars. *Astrophys. J.* **166**, 95–108.

Sill, G., Fink, U., and Ferraro, J. R. (1980). Absorption coefficients of solid NH_3 from 50 to 700 cm^{-1}. *J. Opt. Soc. Amer.*, **70**, 724–739.

Slobodkin, L. S., Buyakov, I. F., Cess, R. D., and Caldwell, J. (1978). Near infrared reflection spectra of ammonia frost: Interpretation of the upper clouds of Saturn. *J. Quant. Spectrosc. Radiat. Transfer* **20**, 481–490.

Smith, E. V. P., and Gottlieb, D. M. (1974). Solar flux and its variations. *Space Sci. Rev.* **16**, 771–802.

SMYTHE, W. D. (1975). Spectra of hydrate frosts: Their application to the outer solar system. *Icarus* **24**, 421–427.

STAATS, P. A., AND MORGAN, H. W. (1959). Infrared spectra of solid ammonia. *J. Chem. Phys.* **31**, 553.

STROBEL, D. F. (1977). Aeronomy of Saturn and Titan. In *The Saturn System*, pp. 185–193. NASA CP-2068.

THORNDIKE, A. M. (1947). The experimental determination of the intensities of infra-red absorption bands. III. Carbon dioxide, methane and ethane. *J. Chem. Phys.* **15**, 868–874.

TOKUNAGA, A. T. (1977). The thermal structure of Saturn: Inferences from ground-based and airborne infrared observations. In *The Saturn System*, pp. 53–57. NASA CP-2068.

TOKUNAGA, A., KNACKE, R. F., AND OWEN, T. (1975). The detection of ethane on Saturn. *Astrophys. J.* **197**, L77–L78.

TOKUNAGA, A. T., DINERSTEIN, H. L., LESTER, D. F., AND RANK, D. M. (1980). The phosphine abundance on Saturn derived from new i0-micrometer spectra. *Icarus* **42**, 79–85.

TRAFTON, L. M. (1977). Saturn's atmosphere: Results of recent investigation. In *Saturn System*, pp. 31–51. NASA CP-2068.

WOODMAN, J., TRAFTON, L., AND OWEN, T. (1977). The abundances of ammonia in the atmospheres of Jupiter, Saturn, and Titan. *Icarus* **32**, 314–340.

THE ASTROPHYSICAL JOURNAL, 246:455–463, 1981 June 1

IDENTIFICATION OF NEW INFRARED BANDS IN A CARBON-RICH MIRA VARIABLE

J. H. GOEBEL, J. D. BREGMAN,[1] F. C. WITTEBORN, B. J. TAYLOR[1]
Ames Research Center, NASA, Moffett Field, California
AND
S. P. WILLNER
Center for Astrophysics and Space Sciences, University of California, San Diego
Received 1980 May 5; accepted 1980 December 5

ABSTRACT

For the first time, we present complete 0.75–13 μm spectrometry of a carbon-rich, Mira-class variable star. Although the near-infrared is dominated by photospheric absorption bands of the CN red system, the infrared becomes progressively dominated by the bands of the polyatomic molecules HCN and C_2H_2. Since the band at 3.1 μm is known to be due to HCN and C_2H_2, we are able to associate bands at 1.04, 1.53, 1.85, 2.5, 2.7, 3.56, 3.85, 4.8, and 7.1 μm with HCN and C_2H_2. The spectrum indicates that radiative transfer in the carbon Mira class cannot be discussed quantitatively without the inclusion of HCN and C_2H_2 opacity. From a consideration of the carbon star models of Querci and Querci, it is deduced that the abundance ratio of HCN to C_2H_2, $A(\mathrm{HCN})/A(C_2H_2)$, can be used to indicate whether 3α-processed or CNO-processed material is in the outer atmosphere. $A(\mathrm{HCN})/A(C_2H_2) \gg 1 \Rightarrow$ CNO; $A(\mathrm{HCN})/A(C_2H_2) \leq 1 \Rightarrow 3\alpha$. An 11.3 μm SiC dust-emission feature is present, although it is significantly different from the 11.7 μm SiC feature in Y CVn. A featureless emission is present from 4 to 13 μm and can be ascribed to optically thin graphite grains with a temperature of 450 K.

Subject headings: infrared: spectra — line identification — molecular processes — stars: abundances — stars: carbon — stars: long-period variables

I. INTRODUCTION

The star V Coronae Borealis (V CrB; C6, 2) represents a type of carbon star intermediate in its color temperature between the SR*b* variables and the dust-enveloped CW Leo (IRC +10216) class of objects. Previous interpretations of such stars have relied on broad-band photometry (Mendoza and Johnson 1965; Forrest, Gillett, and Stein 1975, hereafter FGS; and Merrill 1977), or on incomplete spectrophotometry (Frogel and Hyland 1972; and Merrill and Stein 1976, hereafter MS) as a data base. Generally, the flux curve of cool carbon stars has appeared too broad for description by a single blackbody; hence, the conclusion may be drawn that photospheric radiation is being redistributed at longer wavelengths (Frogel and Hyland 1972). The above argument must certainly be true for the Mira V Cyg (FGS; Puetter *et al.* 1977), while Merrill (1977) suggests that the radiation we are observing from the Mira R Lep is from its cold photosphere. Apparently all Miras do not behave in the same way.

In this paper we present the 0.75–13 μm infrared spectrum of V CrB. This is the first such complete infrared spectrophotometry of a carbon-rich Mira-type variable. In the near-infrared, V CrB displays strong CN red-system ($\Delta v = 2$, 1, and 0) bands, indicating photospheric-dominated radiation. Beyond 1.2 μm, the spectral characteristics of V CrB change dramatically. We will argue that its spectrum is dominated by bands of HCN and C_2H_2 molecules. The domination is so extensive that radiative transfer calculations (model atmospheres) cannot be attempted for this star, or for any other cold carbon star, without the inclusion of HCN and C_2H_2 opacities. The HCN and C_2H_2 opacities are analogous to H_2O steam opacity in oxygen-rich, cool Mira stars.

The presence of large column densities of HCN and C_2H_2 may lessen the amount of graphite necessary to explain carbon Mira flux curves, as is outlined below. The previously accepted conclusion that the emergent flux of all carbon Miras is redistributed by dust will require modification in light of the present data, as (1) the previous analysis did not include polyatomic opacity, (2) the polyatomics compete with graphite for free carbon, and (3) the opacity effects of the strong CN bands were not considered. We will not provide the model solution to the problem; rather, we will show that these effects can no longer be ignored if further progress in modeling this class of stars is anticipated.

II. OBSERVATIONS

The infrared spectrophotometry of V CrB is presented in Figure 1. The spectrum is a composite of four different spectral regions taken with four different instruments. Each region was reduced independently and the flux density plotted. No attempt has been made to shift regions to attain agreement, as there are no overlapping spectral regions.

Because of its period of 357.8 days, an effort was made

[1] Ames Associate.

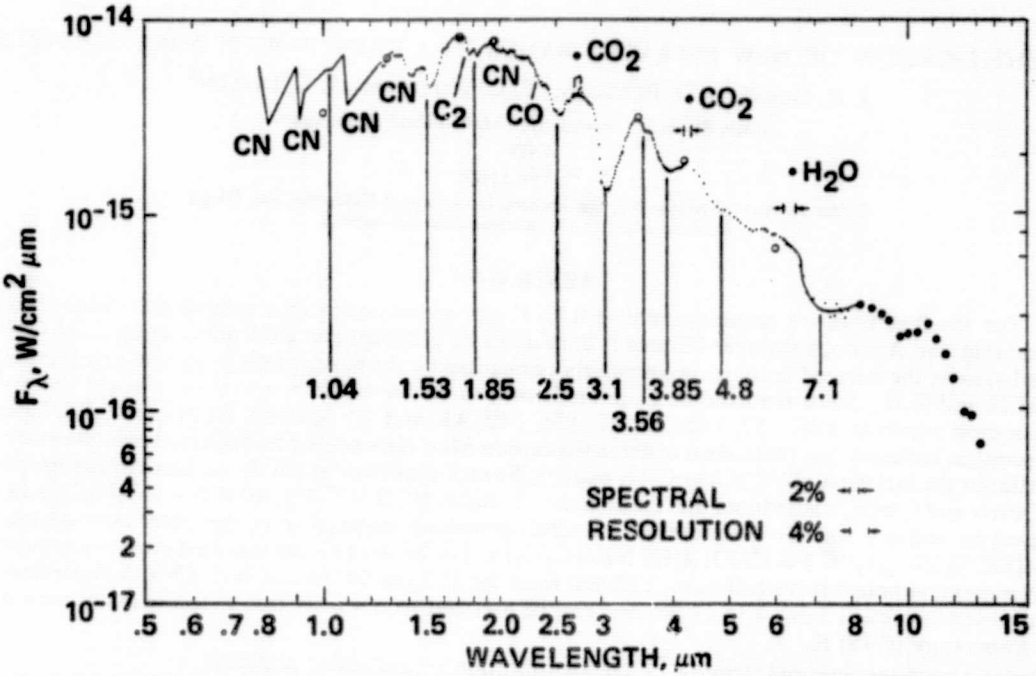

FIG. 1.—Spectrophotometry of the carbon star V CrB (C6, 2e) between 0.75 and 13 μm. Regions of atmospheric interference at 2.7, 4.3, and 6.3 μm are indicated. Data points between 0.75 and 1.1 μm are connected with straight lines. The solid line between 6 and 8 μm is a hand-drawn average of data points done for clarity. The open circles are computed 1675 K blackbody fluxes.

to observe V CrB nearly simultaneously in each of the separate spectral regions. The inherent difficulties in coordinating this effort made this goal impossible. But as can be seen from Table 1, the times are close enough that unification into a single spectrum is reasonable for all but the shortest wavelength region.

The 0.75–1.1 μm spectrum was observed on two nights by B.J.T. using the 0.9 m (36-inch) Crossley telescope of Lick Observatory. Selected Wing bands (Wing 1967) at 7812, 8116, 9044, 9190, 9316, 10104, 10400, 10834, and 10964 Å were used. The spectral resolution was 32 Å. The averaged data from the two nights are given here; their signal-to-noise ratio exceeds 50 at all wavelengths. For one night, atmospheric extinction was determined from two observations each of β Leo and α Ser; for the other, standard extinction was used. The passbands and standards are from Wing (1967); the correction of the latter, from the Oke (1964) to the Hayes and Latham (1975) system, is small and was not applied.

The 1.23–4.2 μm spectrum was taken from the NASA Ames Research Center Kuiper Airborne Observatory (KAO), using the instrument and techniques described by Strecker, Erickson, and Witteborn (1979, hereafter SEW). The secondary standard used was α Boo, assumed to have

TABLE 1

OBSERVATIONS OF V CRB

Wavelength range (μm)	Date (UT)	Telescope	Instrument	Standard Star	Spectral Resolution	Mira Phase[a]
0.75–1.1	1979 June 12 1979 June 13	UCLO Crossley 36 inch (91 cm)	UCLO single channel scanner with trimetal phototube	β Leo α Ser	0.4%	0.74
1.23–4.6	1979 April 19	NASA KAO 36 inch (91 cm)	NASA ARC filter spectrometer with InSb detector	α Boo	2%	0.59
4.0–8.0	1979 April 11	NASA KAO 36 inch (91 cm)	UCSD filter wheel spectrometer with PbSnTe detector	α Lyra α Boo	2%	0.57
8.0–13.0	1979 May 11	NASA Mount Lemmon 60 inch (1.5 m)	NASA ARC filter wheel spectrometer with Si : As detector	α Boo	4%	0.65

[a] Mattei, J. A., private communication.

the flux distribution given by SEW. The spectral resolution is 1.5%. Because we oversample resolution elements, the scatter between adjacent data points is a measure of signal to noise.

The 4.4–8.0 μm segment was taken from the KAO utilizing the University of California at San Diego spectrophotometer (Puetter *et al.* 1981). The methodology of observation and data reduction was the same as that of SEW in the 1.2–4.2 μm region. Both α Lyr and α Boo were observed on another night, so the flux of α Boo could be determined directly on that night from the model of Schild, Peterson, and Oke (1971) for α Lyr. Because of an atmospheric correction problem at 6.3 μm, the data displayed are in two segments. From 4.4 to 6 μm, V CrB is ratioed directly to α Lyr. From 6 to 8 μm, V CrB is ratioed to α Boo, whose flux is known from its ratio to α Lyr as described above. In order to enhance signal-to-noise in the 6–8 μm region, each spectral point has been averaged with a three-point slit function. This causes only a small loss of spectral resolution, since the spectrum is oversampled. The resulting spectral resolution is 2%.

The 8–14 μm spectrum was taken with the NASA Mount Lemmon 1.5 m (60 inch) telescope. The standard star used was α Boo. The observational method is described by Bregman and Witteborn (1980). The spectral resolution is 4%.

The Mira phase in Table 1 has been kindly provided by the American Association of Variable Star Observers (AAVSO) (Mattei, private communication). AAVSO observations dating back to 1967 show visual maxima ranging from 7.5 to 6.9 and the minima from 12.2 to 11.0. No trend toward brighter maxima or fainter minima is indicated by their data, and the average amplitude is 4.9 mag. Our data were taken near visual minimum ($m_v \approx 10.8$), except for the 0.75–1.1 μm portion, which was taken at about three-quarters phase, i.e., at the beginning of the steeply rising portion of the visual light curve. As the shortest wavelength range is nearest the visible, and is therefore the most variable, we have not included it in Figure 2.

III. DISCUSSION

Because of the lack of simultaneity, certain problems cannot be addressed, such as the precise nature of the underlying photospheric continuum or the exact amount of overlying "graphite" dust. In this discussion, we will therefore avoid conclusions which are strongly dependent upon simultaneity. Similarly, since the phase was chosen for temporal convenience, no problems relating to variability can be addressed, such as phase dependence of band strengths or infrared color temperature. This latter type of problem is addressed in detail by Bregman and Witteborn (1980).

The infrared color temperature T_{IR} is defined (see

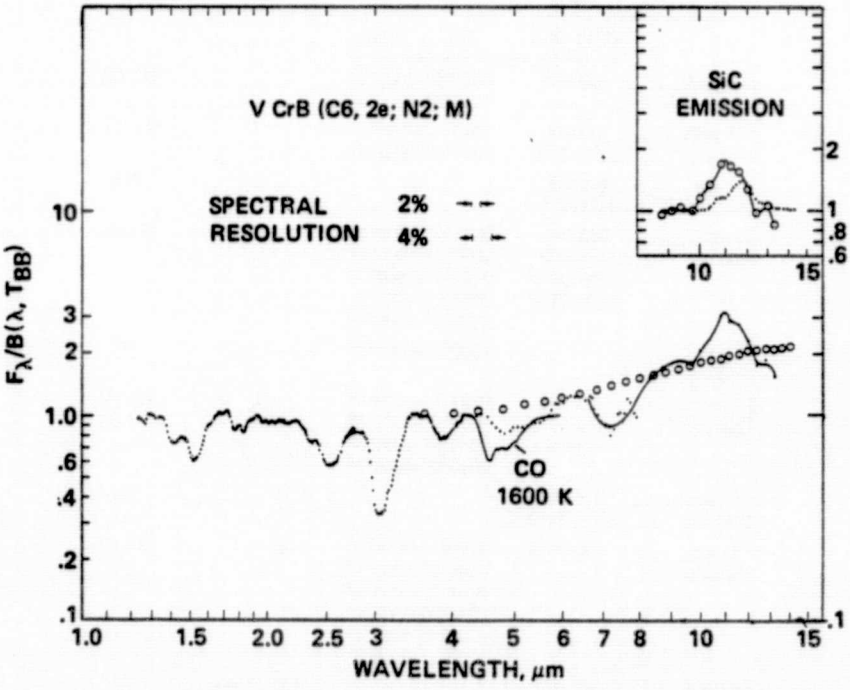

FIG. 2.—The data of Fig. 1 are normalized to a 1675 K blackbody curve between 1.2 and 13 μm. The solid line beyond 6 μm is a hand fit of the data for clarity. The solid line between 4 and 6 μm is the CO fundamental vibration-rotation band opacity of a single slab at 1600 K in absorption against a continuum level of 1.0. The open circles are the graphite excess emission at 450 K as explained in the text. The upper right-hand corner insert is a relative comparison of the present V CrB data (*circled dots*) and the laboratory measurements of Dorschner, Friedemann, and Gürtler (1977) (*dots*) as taken from Goebel *et al.* 1980.

Goebel *et al.* 1978*a*) to be that of the best-fitting blackbody flux curve $B(\lambda, T_{BB})$, $T_{IR} = T_{BB}$, in the wavelength range from 1.2 to 6 μm. For V CrB, $T_{IR} = 1675$ K when our data were obtained. The T_{IR} changes with phase for carbon Miras (Goebel *et al.* 1977). Upon division by $B(\lambda, T_{BB})$, the spectrum is as shown in Figure 2. For purposes of spectroscopy, Figure 2 is the preferred way to present data over such a broad wavelength range. The spectral portion below 1.2 μm has been deleted in Figure 2, as it was the least simultaneous observation, and that region is most sensitive to temperature.

Throughout the infrared spectrum, absorption bands appear which cannot be explained by the most abundant diatomics CN, C_2, and CO. The diatomic band positions and shapes are well known for warmer carbon stars like Y CVn, for which $T_{IR} = 2800$ K (Goebel *et al.* 1978*a* and references therein). Temperature and abundance can modify the CN, C_2, and CO band shapes and centers, but these effects are well understood and are not important to the bands under discussion. We will discuss each band individually. The bands are listed in Table 2 with associated molecules and their vibrational bands in the region of interest.

a) Molecular Bands

i) *The 1.04 Micron Band*

Although CN opacity at 10400 Å is smaller than in the stronger band head regions (Wing 1967), it is not completely negligible in carbon stars. At 10400 Å, some of the carbon stars observed by Wing show a possible opacity other than CN, as he recognized at that time. Our spectrophotometry was at selected bandpasses only, and we cannot say definitively that a polyatomic band is present in V CrB. But it appears, from a comparison of our observations of V CrB with those of other carbon stars observed by Wing, that a polyatomic band is a possible contributor at 10400 Å. Complete scanner spectra are needed in this region (e.g., Faÿ and Honeycutt 1972), preferably at a phase in the V CrB light curve when the polyatomic bands are stronger. It would then be possible to compare the observed spectrum with CN band computations.

TABLE 2

PROPOSED IDENTIFICATION OF BANDS IN V CRB

λ	HCN	C_2H_2	CS	References
	$G'(v)$ $G(v)$	$G(v')$ $G(v)$		
1.04 μm[a]	300–000	0030^00^0–0000^00^0	...	(1), (2)
9620 cm^{-1}	...	1112^00^0–0000^00^0	...	...
1.53 μm	200–000	1010^00^0–0000^00^0	...	(1), (3)
6540 cm^{-1}	21^10–01^10	1011^00^0–0001^10^0	...	...
1.85 μm	101–000	...	...	(1)
5410 cm^{-1}	11^11–01^10	...	...	...
2.5 μm	002–000	0011^00^0–0000^00^0	...	(1), (4)
4000 cm^{-1}	11^10–000	1000^01^1–0000^00^0	...	...
	12^20–01^10	0102^01^1–0000^00^0	...	...
	12^00–01^10	1001^11^1–0001^10	...	...
		0100^03^1–0000^00^0	...	
2.8 μm	...	1000^01^1–0001^10^0	...	(4)
3570 cm^{-1}	...	...	...	...
3.1 μm	100–000	0101^11^1–0000^00^0	...	(1), (4)
3230 cm^{-1}	11^10–01^10	0102^01^1–0001^10^0	...	(5), (6)
	others	0011^00^0–0001^10^0	...	...
		0010^00^0–0000^00^0	...	...
3.56 μm	01^1–000	...	...	(1)
2810 cm^{-1}	02^01–01^10	...	...	...
3.85 μm	100–01^10	0100^01^1–0000^00^0	$\Delta v = 1$	(1), (4)
2600 cm^{-1}	...	0100^02^0–0000^01^1	...	(7)
	...	0101^11^1–0001^10^0	...	...
	...	0010^00^0–0001^10^0	...	...
	...	1000^00^0–0000^01^1	...	...
	...	0003^11^1–0000^00^0	...	...
4.8 μm	001–000[b]	...	CO $\Delta v = 0$	(1)
2100 cm^{-1}	03^10–000	...	(see text)	...
7.1 μm	020–000	0001^11^1–0000^00^0	$\Delta v = 0$	(1), (4)
1410 cm^{-1}	...	...	...	...

[a] Band at 1.04 is an association, not an identification.

[b] Raman band, but weakly infrared active due to Coriolis interaction.

REFERENCES: (1) Rank *et al.* 1960; (2) Ghersetti, Adams, and Rao 1977; (3) Varanasi and Bangaru 1975; (4) Bell and Nielsen 1950; (5) Wiggens, Plyler, and Tidwell 1961; (6) Ridgway, Carbon, and Hall 1978; (7) Bailey, private communication.

Opacity other than CN may also be present elsewhere in 0.75–1.1 μm region (Wing 1967). Possible detections of HCN bands in this region have been reported by Faÿ, Fredrick, and Johnson (1968) and Giguere (1973) in much warmer carbon stars. Additional lines attributed to HCN in the 7900–8600 Å range have been reported by Querci and Querci (1970) in another carbon star, UU Aur.

Nearly all the stars examined previously have been rather warm and without very strong 3.1 μm polyatomic bands. Based upon our spectrum of V CrB and the spectra of cooler carbon stars shown in Wing's thesis (1967), we suggest these bands may be found in cool carbon Miras with scanner spectra and are probably due to HCN and C_2H_2, although, according to Ghersetti, Adams, and Rao (1977), the C_2H_2 band may be weak compared with the bands discussed below.

ii) *The 1.53 Micron Band*

This band is quite distinct, even though it is seen against the CN $\Delta v = -1$ red-system band. It does not appear at our 2% spectral resolution nor at higher spectral resolution (McCammon, Münch, and Neugebauer 1967) in carbon stars of infrared color temperatures (T_{IR}) greater than 2500 K. Connes *et al.* (1968) may have observed individual lines from C_2H_2 and HCN in Y CVn. To date, it has only appeared in the spectra of the cold Mira-type stars such as V CrB, R Lep, S Cep, U Cyg, and SS Vir. At filter wheel resolution, the fully developed band was first noticed by Goebel *et al.* (1977) in S Cep, but could not be identified at that time. Goebel *et al.* (1978*b*) showed that the band increased with decreasing infrared color temperatures. The band is strongest in V CrB, which has the coldest T_{IR} yet measured in a carbon Mira (1675 K). Oddly, it has the same band shape as the CO second overtone but is displaced a full 0.1 μm shortward of the CO band center's position.

Herzberg (1945) lists an HCN band at 1.53 μm ($2\nu_2$) and a C_2H_2 band at 1.54 μm ($\nu_1 + \nu_3$). Other bands of HCN and C_2H_2 also occur near this wavelength and are listed in Table 2 along with literature references. There is no convenient published spectrum of either molecule at our resolution. We have measured C_2H_2 with a Beckman DK2A spectrometer (Fig. 3) and find a band at 1.52 μm with a half-width of 0.25 μm at 300 K. The intensity measurements of the C_2H_2 bands at 1.53 μm by Varanasi and Bangaru (1975) indicate the band is moderately strong.

The most abundant polyatomic species at temperatures below 2500 K are HCN and C_2H_2 according to most dissociation equilibrium models: Tsuji (1964); Johnson, Beebe, and Sneden (1975); Scalo (1973); and Querci and Querci (1974). Furthermore, as listed by Herzberg, none of the other molecules expected to be abundant in carbon stars has bands reasonably nearby 1.53 μm. For another species to give rise to the band, an unusually strong band strength per molecule would be required. We think this to be quite unlikely. Hence, HCN and C_2H_2 are the most plausible contributors to this band.

iii) *The 1.85 Micron Band*

This band is relatively weak. It might have gone unnoticed except for its effect on the (1, 1) band head of the $\Delta v = 0$ Ballik-Ramsay band of C_2. In all other carbon stars observed to date, the (0, 0) band head at 1.78 μm is noticeably stronger than the (1, 1) band head. In V CrB,

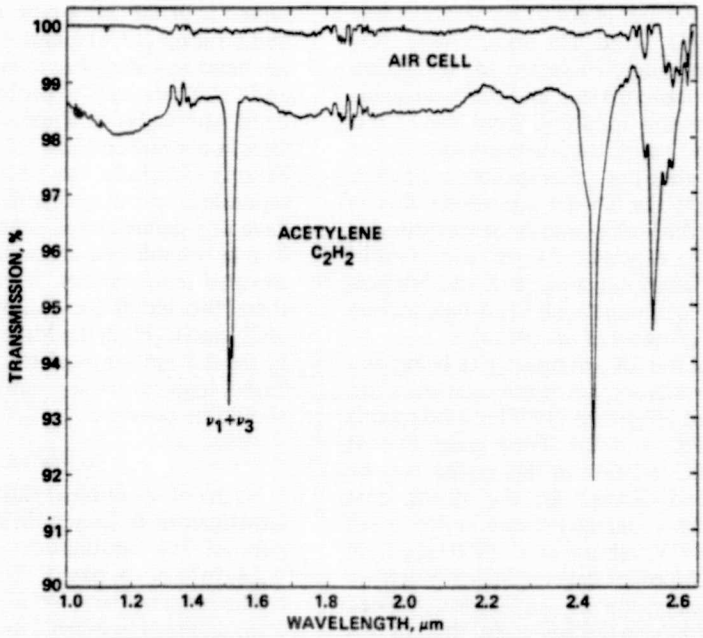

FIG. 3.—A laboratory spectrum of C_2H_2 in absorption at 300 K taken using a Beckman DK2 double-beam spectrometer. The curve labeled "air cell" had the same experimental arrangement but lacked C_2H_2. The 1.5 μm band shows a *P*-branch and *R*-branch but no *Q*-branch. The bands at 2.43 and 2.56 μm contribute to the 2.5 μm absorption discussed in the text.

however, the reverse occurs. Herzberg (1945) lists a medium-strength band $\nu_1 + \nu_3$ at 1.85 μm for the HCN molecule. Even though there is a telluric water-vapor band at 1.85 μm, telluric water cannot be the cause because this spectral region is quite transparent from the KAO, and our calibration procedure does not produce this effect in any of the dozens of stars of various spectral types which we have observed. By itself, this band is insignificant; but coupled with the other polyatomic bands, it serves to strengthen our conclusions concerning the importance of polyatomic opacity.

iv) *The 2.5 Micron Band*

This band was first noticed by Merrill and Stein (1976) as a continued depression of the stellar flux beyond the CO first overtone. The depression could not be clearly observed from the ground because of telluric water beyond 2.5 μm. A 2.5 μm band is not confined to Mira variables only, and this served to confuse identification. Goebel *et al.* (1980) have shown that the 2.5 μm band in SR*b*-type carbon variables is due mostly to C_2 Ballik-Ramsay $\Delta v = 1$ opacity. However, in V CrB, the C_2 Ballik-Ramsay $\Delta v = 0$ band is weak, so the strong 2.5 μm band cannot be due to C_2. Both HCN and C_2H_2 have significant bands in this region. (See, for example, Rank *et al.* 1960; Bell and Nielsen 1950; and Fig. 3.) Ridgway *et al.* (1976) identified the $\nu_1 + \nu_5{}^1$ Q-branch of C_2H_2 in this region in IRC +10216, a carbon star with an extensive circumstellar shell. Therefore, we associate this band with HCN and C_2H_2. No other abundant molecules have bands at this wavelength.

v) *The 2.8 Micron Band*

This region of our spectrum is not exceptionally clear because of the telluric CO_2 band. The atmospheric CO_2 band has not been completely corrected for extinction between V CrB and the standard star, and the band heads at 2.69 and 2.77 μm are still apparent. Since these band heads are no more than 1 resolution-element wide in our spectrum, we can interpolate the stellar spectrum through them. The result is that the 2.6–2.9 μm stellar flux is depressed relative to all the high points in the spectrum by about 20%. This is to be expected if C_2H_2 is present in strength, as the 3.1 μm band indicates (Bell and Nielson 1950). A 2.8 μm opacity is present in all Mira-type carbon stars observed to date (Goebel *et al.* 1978*b*).

The interpretation of the 2.8 μm opacity as being due to C_2H_2 offers an alternative to the recent interpretation by Krassner, Smith, and Hilgeman (1979) regarding this opacity observed in IRC +10216. Their claim is that opacity observed in IRC +10216 in this region may be due to an HN–X bond. Except for the strong dust continuum, the molecular bands present in the 3 μm region of IRC + 10216 (Witteborn *et al.* 1980) are little different from any of the other carbon Miras which we have observed. Specifically, the 2.9 μm flux is depressed relative to other continuum points even though the 3.1 μm band is weaker in IRC +10216 than in Miras. Ridgway, Carbon, and Hall (1978) discuss specifically the 3.1 μm band at very high resolution in IRC +10216 and include a portion of the region shortward of 2.9 μm. Their spectrum shows no outstanding features other than those directly attributable to HCN and C_2H_2. Thus, the 20% depression is explainable without invoking an HN–X bond.

vi) *The 3.1 Micron Band*

The 3.1 μm band is well known and studied at high and low resolution (Ridgway, Carbon, and Hall 1978; MS; and Noguchi *et al.* 1977). The predominant species contributing to the band are known to be HCN and C_2H_2, with the relative abundances varying from star to star. Except for the ν_5 fundamental of C_2H_2 at 13.7 μm, the 3.1 μm band is the strongest band in the infrared both in the laboratory (Varanasi and Bangaru 1975) and in the series of bands we are discussing in the V CrB spectrum. Because of the great depth and width of the band, it is evident that it is formed far out in the colder regions of the atmosphere. In V CrB the band cannot be filled in by thermal reradiation of dust, as is the case in IRC + 10216. The contention that there is little dust reradiation in the 2–3 μm region of V CrB is supported by the presence of the CO first overtone at 2.3 μm, C_2 Ballik-Ramsay at 1.8 μm, and the CN $\Delta v = -2$ red-system opacity in the 2 μm region of V CrB.

vii) *The 3.56 Micron Band*

The presence of the band in carbon star spectra was first pointed out by Goebel *et al.* (1978*a*) and is associated with the HCN molecule ($\nu_1{}^1 + \nu_3$). It appears as a weak band in conjunction with the 3.1 and 3.85 μm bands.

viii) *The 3.85 Micron Band*

The 3.85 μm band was first studied by MS who observed it in the Mira-type variables. Bregman, Goebel, and Strecker (1978) found it to be correlated with the 3.1 μm band and identified it with a complex of C_2H_2 bands and CS. There may be problems associating the 3.85 μm band with C_2H_2 as Ridgway has failed to detect C_2H_2 lines in the carbon Mira S Cep (Wing, private communication). Generally, the 3.85 and 3.56 μm bands are well separated, unconfused with other molecular bands, and have well-defined band shapes. If their relative strengths can be established from laboratory measurements at elevated temperatures, it may prove possible to utilize these two bands for column density measurements of HCN and C_2H_2 in the Mira carbon stars. Both bands are in the 3.5 μm atmospheric window; therefore, ground-based, high-resolution measurements of individual lines should be possible.

ix) *The 4.8 Micron Band*

At the phase of observation, V CrB had no strong CO fundamental at 4.6 μm. In fact, the flux at 4.6 μm forms part of the continuum on which our estimate of $T_{IR} = 1675$ K is based. There is an apparently rising continuum level between 6.0 and 6.7 μm which is different from that seen between 2 and 4 μm. In order to verify the apparent absence of CO, we have computed the CO fundamental band profile in absorption with respect to unity for isothermal 1600 K CO, as shown in Figure 2.

Clearly the band shape in V CrB does not imitate the 1600 K CO fundamental in that the star shows no absorption shortward of 4.6 μm, although it has opacity extending from 4.6 μm out to about 5.8 μm. If the band were dominated by C_3, as in Y CVn (Goebel *et al.* 1978*a*), then the band center should be at about 5.2 μm. Similarly, SiC_2 should be at 5.7 μm (Treffers, private communication), and C_2H should be at 5.4 μm. HCN has bands near 4.7 μm (Herzberg 1945), which are shown by Rank *et al.* (1960). Band intensity measurements by Kim and King (1979) indicate the HCN bands to be about 500 times weaker than the 3.1 μm band, so this band is not likely to be due to HCN.

In spite of the apparent discrepancy in the band shape, CO may cause the observed absorption. Wing (private communication) has suggested that if reemission in the CO fundamental band is present, then the emission intensity is likely to be greatest at the band head near 4.6 μm and decline in strength to longer wavelengths. The CO absorption band head could then be weakened relative to the 5.0 μm wing of the band. This interpretation requires a fairly strong fundamental band, i.e., a large column density of CO, and that is not ruled out by our observations of other carbon stars. This, like all other identifications proposed, is directly subjectable to future verification with observations at high spectral resolution.

Emission near the first CO overtone band head was seen in the Becklin-Neugebauer (BN) object (Scoville *et al.* 1979); the emission was postulated to be caused by a shock. Although the BN object is a very different type of object than V CrB, Mira variables are likely to have shocks in their atmospheres (Cohen 1980). Similar band-head emission has been seen for SiO in oxygen-rich Miras (Ridgway *et al.* 1977). If the CO mechanism is correct, it may not be sufficient to explain the absorption between 5.5 and 5.8 μm.

One of the more abundant polyatomic species (Tsuji 1964) predicted in low-temperature carbon stars is C_2N_2. With strong bands at 3.76, 3.90, and 4.65 μm and a weak band at 4.78 μm (Herzberg 1945), it might also contribute to the 3.85 μm band. We think this unlikely, as the 4.65 μm band should be stronger than the 4.78 μm band. This is not the kind of 4.8 μm band we see in V CrB. Hence, we can say there is no substantial column density of C_2N_2 in V CrB.

x) *The 7.1 Micron Band*

This is the strongest example of the 7.1 μm band we have seen to date in any type of carbon star. The band is more nearly centered on the HCN band center than the C_2H_2 band center. It is difficult to attribute the band to only one of the two species, although HCN may be dominant. As shown by Goebel *et al.* (1980), this region may also be confused by CS, an abundant diatomic. The best that can be done at our resolution is to attribute the band to both HCN and C_2H_2 with possible CS, and leave the quantitative measurements to high-resolution spectroscopy. The long wavelength wing of this band (the C_2H_2 wing) is apparently the cause of the 8 μm turndown noted in the 8–14 μm spectra of carbon-star Miras taken from the ground some years ago (Forrest, Gillett, and Stein 1975).

xi) *The Molecules* HCN *and* C_2H_2

The knowledge that the 3.1 μm band is caused by HCN and C_2H_2, combined with (1) the presence of the 1.53, 1.85, 2.5, 2.7, and 3.56, 3.85, 4.8, and 7.1 μm bands at wavelengths appropriate to HCN and C_2H_2, and (2) the appropriate relative band strengths and bandwidths, leads to the conclusion that HCN and C_2H_2 are the opacity sources of the bands mentioned above. An inspection of the V CrB flux curve shows that, at wavelengths > 1 μm, the flux spectrum becomes increasingly dominated by these polyatomic bands. The effect is so severe that the radiative transfer process in the atmosphere of V CrB becomes dominated by the polyatomic bands. There are no models to date which take this fact into account. We note that the analogous M star models using H_2O steam opacity have been the subject of continued modeling efforts (Auman 1969; Johnson 1974; and Tsuji 1966, to name a few). This lack of previous modeling is a hindrance to the further understanding of both the stellar atmospheric structure in carbon Miras and the question of how much graphite is being produced in the atmosphere.

The best models to date of carbon stars are those of Querci, Querci, and Tsuji (1974) and Querci and Querci (1974) which cover the range of effective temperatures between 2200 K and 4200 K. They point out correctly that the polyatomic opacities need to be included below 2600 K. For effective temperatures above 2600 K, their models provide a good description of both infrared flux curves and angular diameters (Goebel and Goorvitch 1979). In spite of the fact that none is exactly appropriate to V CrB, we intend to discuss the properties of C_2H_2 and HCN in the warmer models insofar as they relate to the 3α and CNO nuclear burning processes.

xii) *Nuclear Processes*

The relative partial pressures of HCN and C_2H_2 may indicate the type of nuclear processing a star has undergone. For the CNO cycle, $[C] \approx [O] \ll [N]$, while for 3α, $[C] \gtrsim [O] \approx [N]$ (Querci 1974). Thus for 3α production and plume-type mixing, HCN and C_2H_2 abundances are about equal, while for equilibrium CNO-cycle abundances and deep envelope mixing, HCN is far more abundant. The abundances can be estimated from detailed models for particular stars, but, because the dissociation energies are similar, relative abundances can probably be determined by comparing individual unsaturated lines at nearby wavelengths from the two molecules. Hence, it should be possible to deduce which nuclear process dominates the stellar interior by observing the outer atmosphere, with spectral resolution sufficient to resolve the individual lines, provided there is efficient mixing.

Under this scheme, the observations of Ridgway, Carbon, and Hall (1978) would imply that TX Psc, UU Aur, and Y Tau are dominated by CNO processing since only HCN was detected without any C_2H_2. On the other

hand, T Lyr, which is dominated by C_2H_2, could be a 3α star.

Querci and Querci (1975) have suggested another method for determination of the dominant nuclear process. They noted that the 3α process preferentially enhanced the carbon abundance, while the CNO process depleted the carbon abundance with respect to the solar value. Thus stars with extensive dust envelopes (e.g., V Cyg) should be 3α dominated; stars without extensive envelopes (e.g., TX Psc) should be CNO dominated. It would be interesting to compare the results of their suggestions with more results of spectroscopy at higher resolution.

b) Circumstellar Dust

We would like to know how much graphite (or other carbon-rich dust or soot) is being expelled from the atmosphere of the star. The discussion above indicates that the presence of the many strong polyatomic absorption bands severely modifies the spectral flux distribution in the infrared. This new interpretation implies that dust reradiation in the infrared, to which had previously been ascribed the role of spectral redistribution, plays a lesser role in many stars. As indicated, a quantitative answer will have to wait for models which take the polyatomic bands into account in the 1–8 μm range. When the photospheric energy distribution is better known, the role of graphite (soot) can be more clearly understood.

From the presence of the 2.5 μm polyatomic band and CN $\Delta v = -2$ red-system band, it is clear that the CO first overtone at 2.3 μm should be weakened by those bands alone. The weakening effect of CN was first explained by Wing and Spinrad (1970). A similar effect occurs in Y CVn, a graphite-free carbon star (Goebel *et al.* 1980). In the past, such weakening has also been attributed to dust alone (Frogel and Hyland 1972). If the CO first overtone were weakened in V CrB because of dust, then the CO fundamental should be absent or nearly absent. This may be the case in V CrB in our spectrum. But we see nearly 20% absorption in the CO fundamental at other phases in V CrB (Bregman and Witteborn 1980). To see that much absorption by the CO fundamental, we cannot be observing through an extensive dust shell which redistributes the radiation at 2.5 μm. Furthermore, the infrared band strengths of the other diatomics CN and C_2 can be adequately interpreted in terms of association into polyatomics, CN into HCN, and C_2 into C_2H_2 (Goebel *et al.* 1978*b*), rather than by dust veiling.

To be sure, there is support for some dust about V CrB, both from our data and elsewhere. In our spectrum, the flux curve never achieves Rayleigh-Jeans slope out to 14 μm, although it does closely fit a 1675 K blackbody between 1.5 and 4 μm. Beyond 4 μm, the flux levels exceed the 1675 K blackbody increasingly as the wavelength increases (Fig. 2). At 11.3 μm, V CrB also displays the SiC dust feature. Interestingly, the SiC band in V CrB is sensibly different from the SiC band in Y CVn (cf. Fig. 2). In Y CVn the peak is at 11.7 μm, rather than 11.3 μm, and the shape of the 11.7 μm band was well described by the polytrope assembly of Dorschner, Friedemann, and Gürtler (1977). A possible interpretation is that the polytrope mixture is sensitive to formation temperature, which may be different in the two stars. Perhaps the polytrope assembly is sensitive to other parameters like pressure or the Si to C abundance ratio, or perhaps the grain size and shape differ in Y CVn and V CrB. This effect could account for a different band shape (Gilra 1972). Most carbon stars appear to have an 11.3 μm like V CrB (FGS; Puetter *et al.* 1977; MS).

Emission by dust composed of SiC cannot explain the rising continuum between 4 and 14 μm because (1) it is confined to the 10–13 μm range in all carbon stars (FGS), (2) it is observed in carbon stars without rising continua (Goebel *et al.* 1980), and (3) no laboratory data exist which show crystalline SiC bulk absorption coefficients to be significant outside the 11.3 μm band (Dorschner, Friedemann, and Gürtler 1977). If one interpolates through the bands at 4.8 and 7.2 μm, then the rising continuum appears to be featureless. For graphite, this is what one expects. In Figure 2, we show an emission shell contribution which we calculated for the optically thin case in excess of the 1675 K blackbody using a graphite optical depth normalized to 10^{-3} at 10 μm and based on the graphite $\tau/\tau_{10\,\mu m}$ given by Jones and Merrill (1976). Using a shell temperature of 450 K, this calculation gives a reasonable description of the interpolated 4–14 μm rising continuum. The value 450 K is not an optimized single slab temperature, nor has there been any endeavor to adjust temperature gradients (nonexistent in our calculation) or particle size distribution (0.1 μm assumed by Jones and Merrill). There is no significant thermal contribution by the shell below 4 μm.

The existence of such a shell has several implications. First, the SiC and graphite are probably in the same spatial region. If so, the SiC temperature is similar to the graphite temperature, as it is also seen in emission in the same spectral region. This is consistent with the theoretical models of Jones and Merrill (1976). A 450 K temperature would cause the SiC emission band to be shifted to longer wavelengths than the 11.75 μm band in Y CVn, which was described by a 1600 K band temperature. Since the SiC band in V CrB is peaked at 11.3 μm, rather than 11.75 μm, we can eliminate temperature as a single cause of the differing SiC band profiles in the two stars. Probably something more fundamental is occurring, as suggested above.

Second, the graphite shell emission should continue to rise to longer wavelengths above the 1675 K blackbody. Potentially, this future observation should provide a test of the material constants assumed by Jones and Merrill (1976) in their analysis of thick circumstellar shells.

Third, the 7.1 μm band is seen in absorption against the 450 K continuum. If the band is formed below the 450 K dust shell and is partly filled in by emission, the intrinsic depth of the band relative to the photosphere must be larger than is apparent. Since CS is a diatomic molecule, it probably needs the entire atmospheric column density to contribute significantly to the band. The CS abundance is down from CO considerably, while the CO fundamental band may be absent. Therefore, we suggest that the CS

contribution is minimal. The most likely carriers of the 7.1 μm band are then HCN and C_2H_2.

Thus, V CrB appears to have very large polyatomic column densities and an optically thin graphite and SiC dust shell. The thinness of the shell may find explanation in the ratio of C to O for V CrB, which is 1.23 according to Kilston (1975). According to Scalo (1973), at temperatures less than 2200 K, C_2H_2 competes very effectively with graphite for free carbon. If most of the carbon in V CrB's outer atmosphere and shell is bound in C_2H_2 and CO, then a small graphite abundance is expected.

We wish to thank the flight and ground crews of the KAO for their cooperation in installing our systems and operating in the short but demanding observing periods required for obtaining the 4–8 μm data. Drs. R. Wing and C. Rinsland provided a critical reading of the manuscript and many helpful comments. B.J.T. again wishes to thank Dr. Donald E. Osterbrock, director of Lick Observatory, for granting him guest observing privileges at the Crossley, and Dr. Sandra M. Faber for scheduling telescope time to fit his peculiar schedule.

REFERENCES

Auman, J. R. 1969, *Ap. J.*, **157**, 799.
Bell, E. E., and Nielsen, H. H. 1950, *J. Chem. Phys.*, **18**, 1382.
Bregman, J. D., Goebel, J. H., and Strecker, D. W. 1978, *Ap. J. (Letters)*, **223**, L45.
Bregman, J. D., and Witteborn, F. C. 1980, preprint.
Cohen, M. 1980, *M.N.R.A.S.*, **186**, 837.
Connes, P., Connes, J., Bouigue, R., Querci, M., Chauville, J., and Querci, F. 1968, *Ann. d'Ap.*, **31**, 485.
Dorschner, J., Friedemann, C., and Gürtler, J. 1977, *Astr. Nach.*, **298**, 279.
Faÿ, T. D., Fredrick, L. W., and Johnson, H. R. 1968, *Ap. J.*, **152**, 151.
Faÿ, T. D., and Honeycutt, R. K. 1972, *Ap. J.*, **77**, 29.
Forrest, W. J., Gillett, F. C., and Stein, W. A. 1975, *Ap. J.*, **195**, 423 (FGS).
Frogel, J. A., and Hyland, A. R. 1972, *Mém. Soc. Roy. Sci. Liège*, **3**, 111.
Ghersetti, S., Adams, J. E., and Rao, K. N. 1977, *J. Molec. Spectrosc.*, **64**, 157.
Giguere, P. T. 1973, *Ap. J.*, **186**, 585.
Gilra, D. P. 1972, The Scientific Results from the *Orbiting Astronomical Observatory (OAO-2)*, ed. A. Code (NASA SP-310), p. 310.
Goebel, J. H., Bregman, J. D., Strecker, D. W., Witteborn, F. C., and Erickson, E. F. 1977, *Bull. AAS*, **9**, 364.
———. 1978*a*, *Ap. J. (Letters)*, **222**, L129.
Goebel, J. H., *et al.* 1980, *Ap. J.*, **235**, 104.
Goebel, J. H., and Goorvitch, D. 1979, *Bull. AAS*, **11**, 470.
Goebel, J. H., Strecker, D. W., Witteborn, F. C., Bregman, J. D., and Erickson, E. F. 1978*b*, *Bull. AAS*, **10**, 407.
Hayes, D. S., and Latham, D. W. 1975, *Ap. J.*, **197**, 593.
Herzberg, G. 1945, *Molecular Spectra and Molecular Structure II. Infrared and Raman Spectra of Polyatomic Molecules* (Princeton: Van Nostrand).
Johnson, H. R. 1974, *NCAR Technical Note #NCAR-TN/STR-95* (Boulder: National Center for Atmospheric Research).
Johnson, H. R., Beebe, R. F., and Sneden, C. 1975, *Ap. J. Suppl.*, **29**, 280, 123.
Jones, T. W., and Merrill, R. M. 1976, *Ap. J.*, **209**, 509.
Kilston, S. 1975, *A.J.*, **87**, 189.
Kim, Y., and King, K. 1979, *J. Chem. Phys.*, **71**, 1967.
Krassner, J., Smith, L. L., and Hilgeman, T. 1979, *Ap. J. (Letters)*, **231**, L31.
McCammon, D., Münch, G., and Neugebauer, G. 1967, *Ap. J.*, **147**, 575.
Mendoza, E. E., and Johnson, H. L. 1965, *Ap. J.*, **141**, 161.
Merrill, K. M. 1977, in *IAU Colloquium 42, The Interaction of Variable Stars with their Environment*, ed. R. Kippenhahn, J. Rehe, and W. Strohmeier (Bamberg: Veroeffentlichungen der Remeis Sternwarte).
Merrill, K. M., and Stein, W. A. 1976, *Pub. A.S.P.*, **88**, 285 (MS).
Noguchi, K., Maihara, T., Haruyuki, O., Sato, S., and Mukai, T. 1977, *Pub. Astr. Soc. Japan*, **29**, 511.
Oke, J. B. 1964, *Ap. J.*, **140**, 689.
Puetter, R. C., Russell, R. W., Sellgren, K., Soifer, B. T. 1977, *Pub. A.S.P.*, **89**, 320.
Puetter, R. C., Russell, R. W., Soifer, B. T., and Willner, S. T. 1981, *Ap. J.*, in press.
Querci, F., and Querci, M. 1974, *Highlights of Astronomy*, vol. 3, ed. G. Contopoulos (Dordrecht: Reidel), p. 341.
———. 1975, *Astr. Ap.*, **39**, 113.
Querci, F., Querci, M., and Tsuji, T. 1974, *Astr. Ap.*, **31**, 265.
Querci, M. 1974, Thésis de Doctoral d'État, Université de Paris.
Querci, M., and Querci, F. 1970, *Astr. Ap.*, **9**, 1.
———. 1976, *Astr. Ap.*, **49**, 443.
Rank, D. H., Skorinko, G., Eastman, D. P., and Wiggins, T. A. 1960, *J. Opt. Soc. Am.*, **50**, 421.
Ridgway, S. T., Carbon, D. F., and Hall, D. N. B. 1978, *Ap. J.*, **225**, 138.
Ridgway, S. T., Hall, D. N. B., and Carbon, D. F. 1977, *Bull. AAS*, **9**, 636.
Ridgway, S. T., Hall, D. N. B., Kleinmann, S. G., Weinberger, D. A., and Wojslaw, R. S. 1976, *Nature*, **264**, 345.
Scalo, J. M. 1973, *Ap. J.*, **184**, 801.
Schild, R., Peterson, D. M., and Oke, J. B. 1971, *Ap. J.*, **166**, 95.
Scoville, N. Z., Hall, D. N. B., Kleinmann, S. G., and Ridgway, S. T. 1979, *Ap. J. (Letters)*, **232**, L121.
Strecker, D. W., Erickson, E. F., and Witteborn, F. C. 1979, *Ap. J. Suppl.*, **41**, 501 (SEW).
Tsuji, T. 1964, *Ann. Tokyo Astr. Obs.*, **9**, 1.
———. 1966, *Pub. Astr. Soc. Japan*, **18**, 127.
Varanasi, P., and Bangaru, B. R. P. 1975, *J. Quant. Spectrose. and Rad. Transf.*, **14**, 839.
Wiggens, T. A., Plyler, E. K., and Tidwell, E. D. 1961, *J. Opt. Soc. Am.*, **51**, 1219.
Wing, R. F. 1967, Ph.D. thesis, University of California, Berkeley.
Wing, R. F., and Spinrad, H. 1970, *Ap. J.*, **159**, 973.
Witteborn, F. C., Strecker, D. W., Erickson, E. E., Smith, S. M., Goebel, J. H., and Taylor, B. J. 1980, *Ap. J.*, **238**, 577.

BREGMAN, J. D., GOEBEL, J. H., TAYLOR, B. J., and WITTEBORN, F. C.: 245-6 NASA Ames Research Center, Moffett Field, CA 94035

WILLNER, S. P.: Smithsonian Astrophysical Observatory, 60 Garden Street, Cambridge, MA 02138

THE ASTROPHYSICAL JOURNAL, 250:186–199, 1981 November 1

ABUNDANCES OF ARGON, SULFUR, AND NEON IN SIX GALACTIC H II REGIONS FROM INFRARED FORBIDDEN LINES

T. HERTER,[1,2] H. L. HELFER, AND J. L. PIPHER[2]
University of Rochester
W. J. FORREST, J. MCCARTHY, AND J. R. HOUCK
Cornell University
S. P. WILLNER, R. C. PUETTER, AND R. J. RUDY
Center for Astrophysics and Space Sciences, University of California at San Diego
AND
B. T. SOIFER
California Institute of Technology
Received 1980 December 12; accepted 1981 May 7

ABSTRACT

Airborne measurements of the [Ar II] (6.99 μm) and [S III] (18.71 μm) lines for six compact H II regions are presented, as well as ground-based 2–4 μm and 8–13 μm spectroscopy if not already published. From these data and radio data, we deduce lower limits to the elemental abundances of Ar, Ne, and S. G29.9−0.0 at 5 kpc from the galactic center is overabundant in all these elements. The other five regions (at distances 6–13 kpc from the center) mainly appear to be consistent with standard abundances, with the exception of G75.84+0.4 at 10 kpc from the galactic center, which is overabundant in S. However, our preliminary results on G12.8−0.2 at 6 kpc from the galactic center suggest a possible underabundance. We feel that a large statistical sample of H II regions is required in order to determine if there is a radial gradient in the heavy element abundances in our Galaxy.

Subject headings: infrared: spectra — nebulae: abundances — nebulae: H II regions

I. INTRODUCTION

We report here ground-based and airborne spectroscopic observations from 2 to 4 μm, 4 to 8 μm, 8 to 13 μm, and 16 to 30 μm for the compact H II regions G29.9–0.0, G45.1+0.1, G75.84+0.4, G12.8−0.2 (W33), NGC 7538 IRS2, and W3 IRS1. When available, the ground-based 2–4 μm and 8–13 μm data were gathered from the literature, and the new data were acquired at the Kitt Peak National Observatory (KPNO) and the Mt. Lemmon Observatory. The airborne 4–8 μm and 16–30 μm data were obtained on the Kuiper Airborne Observatory (KAO). Line fluxes at 6.99 μm [Ar II], 8.99 μm [Ar III], 10.51 μm [S IV], 12.81 μm [Ne II], and 18.71 μm [S III] are reported for these six H II regions, and estimates of the ionic abundances relative to hydrogen are deduced by using radio continuum data to obtain the ionized hydrogen column density.

The infrared fine-structure lines are well suited for abundance analysis for two reasons. First, the infrared line strengths are comparatively insensitive to the electron temperature, so that the temperature correction techniques employed at optical wavelengths (e.g., Peimbert 1975) are not required. Second, infrared lines provide a probe to much larger distances from the Sun than possible with optical lines, although substantial extinction corrections must still be made. The H II regions listed above range in galactocentric radii from 5 kpc to 13 kpc. A goal of this long range program is to search for possible abundance gradients in the Galaxy.

In spite of these advantages, it has become increasingly evident that a moderately complete data set is required to derive elemental abundances from observations of the infrared fine-structure lines. Relatively simple models of the ionization structure employing densities and excitation parameters consistent with radio observations are at variance with ground-based observations of the [Ar III], [S IV], and [Ne II] line strengths (Zeilik 1977; Balick and Sneden 1976; Lacasse *et al.* 1980). In addition, previous airborne observations of the [S III] and [Ar II] lines (McCarthy, Forrest, and Houck 1979; Puetter *et al.* 1979) indicate that S III is more abundant than S IV, and Ar II is also a primary ionization state, contrary to expectations if the ionizing source is a single hot star. Hence, observation of more than one ionization state of sulfur and argon is required for abundance analysis, and this allows an indirect probe of the UV radiation field in the nebula.

[1] Fannie and John Hertz Foundation Fellow.
[2] Visiting Astronomer at Kitt Peak National Observatory, Tucson, Arizona, operated by the Association of Universities for Research in Astronomy, Inc., under contract with the National Science Foundation.

II. OBSERVATIONS

The data described here were obtained with a variety of infrared systems. The 2–4 μm and 8–13 μm data were primarily obtained either at KPNO or the Mt. Lemmon Observatory using circular variable filter wheel (CVF) spectrometers with resolutions $\Delta\lambda/\lambda \sim 0.015$–$0.02$. These data are mainly published results, and new results are noted in Table 1. Sampling densities are typically one to two data points per resolution element.

The 4–8 μm data reported here consist of observations in the [Ar II] line and adjacent continuum using the University of California at San Diego (UCSD) filter wheel spectrometer (Russell, Soifer, and Willner 1977*a*; Puetter *et al.* 1979) on

TABLE 1

LINE FLUXES

Object	Line	τ_λ[a]	Measured Line Flux[b] (10^{-18} W cm^{-2})	Aperture (arc sec)	Reference	Line Flux Corrected for Extinction (10^{-18} W cm^{-2})
G29.9−0.0	Ar III	1.75 ± 0.25	13.0 ± 2.8	22	1	74.8 ± 24.7
	S IV	1.85 ± 0.26	< 6.6[c]	22	1	< 42
	Ne II	0.79 ± 0.11	113.8 ± 14.9	22	1	250 ± 42.9
	S III	1.31 ± 0.18	41.5 ± 4.3	30	2	153.8 ± 32.0
	Ar II	0.66 ± 0.09	22 ± 4	27	2	42.6 ± 8.6
	Brα	...	> 3.8	17	2	...
	Brγ	...	0.76 ± 0.10	17	2	...
G75.84+0.4	Ar III[d]	1.68 ± 0.08	1.53 ± 0.37	11	3	8.2 ± 2.0
	S IV[d]	1.77 ± 0.08	1.98 ± 0.22	11	3	11.6 ± 1.0
	Ne II[d]	0.76 ± 0.04	4.58 ± 0.47	11	3	9.8 ± 1.0
	S III	1.26 ± 0.06	52.2 ± 3.6	30	2	184 ± 11
	Ar II	0.63 ± 0.03	6.0 ± 2.5	27	2	11.3 ± 2.5
	Brα	...	1.56 ± 0.20	11	3	...
	Brγ	...	0.25 ± 0.03	11	3	...
G12.8−0.2	Ar III	3.44	0.69 ± 0.72	11	4	21.5 ± 22.4
	S IV[e]	3.64	0.97 ± 0.33	15	2	36.9 ± 12.3
	Ne II[e]	1.55	20.3 ± 1.7	15	2	95.6 ± 8.0
	S III	2.58	8.84 ± 2.02	30	2	116.7 ± 26.4
	Ar II	1.29	6.8 ± 1.7	27	2	24.7 ± 6.2
	Brα	...	1.1 ± 0.2	11	5	...
	Brγ	...	0.054 ± 0.016	11	5	...
G45.1+0.1	Ar III	1.62 ± 0.27	9.15 ± 2.02	...	6	46.2 ± 16.2
	S IV	1.71 ± 0.29	9.69 ± 2.13	...	6	53.6 ± 19.5
	Ne II	0.73 ± 0.12	30.8 ± 2.9	...	6	63.9 ± 9.8
	S III	1.21 ± 0.20	15.8 ± 1.9	30	2	53.0 ± 12.4
	Ar II	0.61 ± 0.10	5.2 ± 2.6	27	2	9.6 ± 4.9
	Brα	...	5.3 ± 0.4	11	4	...
	Brγ	...	0.89 ± 0.03	11	4	...
NGC 7538 (IRS2)	Ar III	0.96 ± 0.22	1.5 ± 1.3	11	4	3.9 ± 3.5
	S IV	1.01 ± 0.23	< 3.9	11	4	< 10.8
	Ne II	0.43 ± 0.10	20 ± 2.0	11	4	30.8 ± 4.4
	S III	0.72 ± 0.17	5.8 ± 2.8	30	2	11.8 ± 6.0
	Ar II	0.36 ± 0.08	13 ± 13	27	2	18.6 ± 18.6
	Brα	...	< 0.3	17	7	...
	Brγ	...	0.18 ± 0.05	17	7	...
W3 (IRS1)	Ar III	1.50 ± 0.23	5.7 ± 0.98	11	8	25.8 ± 7.4
	S IV	1.59 ± 0.25	5.7 ± 1.06	11	8	28.2 ± 8.8
	Ne II	0.68 ± 0.10	9.79 ± 2.02	11	8	19.3 ± 4.4
	S III	1.13 ± 0.17	95.8 ± 7.5	30	2	297 ± 56
	Ar II	0.56 ± 0.09	4.7 ± 1.9	27	2	8.2 ± 3.4
	Brα	...	9.8 ± 0.2	22	9	...
	Brγ	...	1.6 ± 0.2	22	9	...

[a] From Tables 2 and 3.

[b] For details of line fits see text; two continuum points and a single point at 6.97 μm were used for the Ar II line fits.

[c] Upper limits are 3 σ.

[d] A partial spectrum obtained recently by blind offsetting to the nominal radio peak, rather than "peaking up", yields Ar III and S IV line fluxes similar to those listed here, while the Ne II flux is about a factor of 2 larger. The shape of the spectrum also indicates $\tau_{9.7} > 3$, larger than the value adopted in the present analysis.

[e] Measurements from 15" partial spectrum as noted in text.

REFERENCES.—(1) Soifer and Pipher 1975. (2) Observations presented in this paper. (3) Pipher, Soifer, and Krassner 1979. (4) Provided by F. C. Gillett. (5) Pipher and Willner 1981. (6) Weighted average of Hefele and Schulte in den Bäumen 1978 and Pipher, Soifer, and Krassner 1979; only the latter data are plotted in Fig. 3. (7) Soifer, Russell, and Merrill 1976. (8) Lacasse *et al.* 1980. (9) Krassner and Pipher 1980.

flights of the KAO in 1979 June. For these observations a 27″ focal plane aperture was employed, and the chopped beam spacing and orientation were chosen to avoid beam cancellation.

The 16–30 μm data consist of complete spectra obtained with the Cornell University cooled grating spectrometer (McCarthy, Forrest, and Houck 1979) on flights of the KAO in 1979 June. A focal plane aperture of 30″ and choice of beam throw similar to that used with the UCSD instrument were employed. The spectral resolution over the [S III] line is 0.2 μm, sampled at a density of approximately three points per resolution element.

The observed line fluxes (uncorrected for extinction) are listed in Table 1 along with the beam sizes and references for the observations. The line fluxes for all but [Ar II] have been derived from a detailed fit to each line of the form $F_\lambda = a + b\lambda + c \exp - [(\lambda - \lambda_c)/\sigma_\lambda]^2$; that is, a linear continuum plus line emission at $\lambda = \lambda_c$, and $\sigma_\lambda \sim 0.6\Delta\lambda_{\rm FWHM}$, where $\Delta\lambda_{\rm FWHM}$ was determined from laboratory measurements. We vary a, b, and c to minimize

$$\chi^2 = \Sigma\left(\frac{F_{\rm obs} - F_{\rm model}}{\rm error}\right)^2 .$$

In one case (G29.9 − 0.0), a linear continuum was inadequate, and a quadratic continuum was assumed. For [Ar II] only one point in the line and one on either side in the adjacent continuum were used to estimate the line flux. The complete spectra from 2 to 30 μm are presented in Figures 1–3. In plotting these spectra, when different beam sizes were employed in different wavelength regions, we have *not* attempted to correct for beam size effects, since the ionization structure of the region prohibits simple scaling of the line intensities.

The spectra of Figures 1–3 show a number of emission and absorption features superposed upon the strong continuum primarily generated by dust. Atomic emission lines addressed in this paper include Brγ (2.17 μm), Brα (4.05 μm), and the fine-structure lines of [Ar II], [Ar III], [S IV], [Ne II], and [S III]. In addition, recombination lines of He I (2.06 μm) and Pfγ (3.76 μm) are visible in the spectrum of W3 IRS1. A number of continuum features are also visible. The familiar 9.7 μm silicate feature is clearly in absorption in G29.9 − 0.0, G12.8 − 0.2, and G45.1 + 0.1, and in emission in NGC 7538 IRS2. The associated 18 μm silicate absorption feature is not immediately evident to the eye, but it can be understood in terms of compensating emission and absorption features at 18 μm. Unidentified continuum emission features at 3.3, 6.2, 7.7, 8.6, and 11.3 μm have been detected in a variety of astronomical sources (Russell, Soifer, and Willner 1977*b*) and are seen in several of these spectra. Finally the 2–4 μm spectrum of NGC 7538 which includes both IRS1 and IRS2 shows a strong continuum absorption feature at $\sim$ 3 μm, which is attributed to grain mantle molecules undergoing O–H, N–H, and C–H stretching vibrations. On the basis of the 8–13 μm spectra, and the 2.2 and 3.5 μm photometry, most of the continuum flux and the absorption are probably due to IRS1.

III. DISCUSSION

a) The Extinction

In order to compute the line fluxes from the H II regions, the infrared spectra must be corrected for extinction, which can be substantial. Depending on the wavelength, there are several ways of computing the extinction. At 2.17 μm (Brγ) and 4.05 μm (Brα), hydrogen recombination lines are observed and can be compared with radio continuum measurements of free-free radiation, or the ratio of the Brα and Brγ lines can be employed to compute the extinction. At 8–13 μm, the broad absorption feature seen in spectra is assumed due to cool silicate material in the line of sight. By use of an assumed extinction law, extinction at wavelengths between 4 and 8 μm can be extrapolated from shorter and longer wavelengths. At wavelengths longer than 13 μm, we adopt the value of $\tau_{18}/\tau_{9.7}$ determined by Forrest, McCarthy, and Houck (1979) from circumstellar shell data. This ratio is consistent with the value derived from simple two-component dust models of H II regions (McCarthy, Forrest, and Houck 1980). The adopted extinction law is presented in Table 2 and discussed below.

The 8–13 μm data have been corrected for extinction due to cool silicate material external to the line-emitting region by two simplified models. One of these (model I) assumes that hot grains radiate as blackbodies, and the other (model II) assumes optically thin silicate emission (Gillett *et al.* 1975*a*; Soifer and Pipher 1975). These models were computed by minimizing

$$\chi^2 = \Sigma'\left(\frac{F_{\rm obs} - F_{\rm model}}{\rm error}\right)^2 .$$

Generally the model II better fit the H II region discussed here. Limitations of these models have been discussed by Kwan and Scoville (1976) and Willner (1977). Also Jones *et al.* (1980) have shown that the trough between the unidentified 11.3 and 8.7 μm emission features mimics the silicate absorption feature at 9.7 μm in NGC 7027, and they suggest that the presence of unidentified features in a compact H II region spectrum might lead to an overestimate of the silicate optical depth. In Table 3 we list the computed model II fit of $\tau_{9.7}$ for each H II region studied. The Trapezium spectral shape (Gillett *et al.* 1975*a*) is used to determine $\tau_\lambda/\tau_{9.7}$ from 8 to 13 μm.

The 4–8 μm data have been treated in several ways. First, at 8 μm, there is overlap with the 8–13 μm data, and the extinction at 8 μm can be obtained through fitting the silicate feature from 8–13 μm as described briefly above. Second, the line flux to the radio continuum flux $\mathcal{F}$(Brα)/S_ν(radio) can be used to deduce the extinction at 4.05 μm if the Brα line is

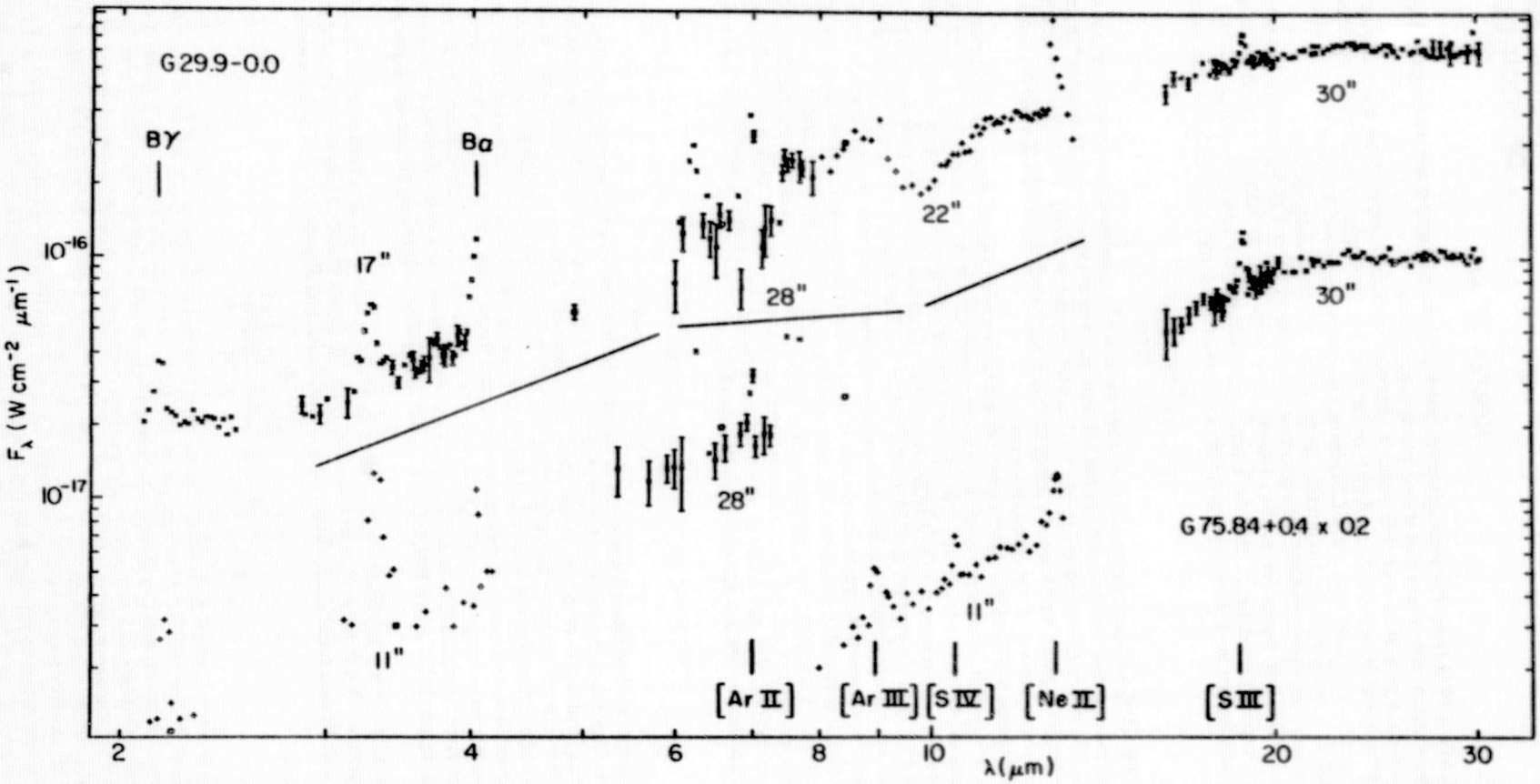

FIG. 1.—The 4–8 μm and the 16–30 μm data for G29.9−0.0 and G75.84+0.4, and the 2–4 μm data for G29.9−0.0 were obtained as described in text. The 8–13 μm data for G29.9−0.0 are from Soifer and Pipher 1975, and for G75.84+0.4 from Pipher, Soifer, and Krassner 1979. The 2–4 μm data are from Pipher, Soifer, and Krassner 1979. Plots from the literature do not include error bars. Apertures for the observations plotted are marked on the figure.

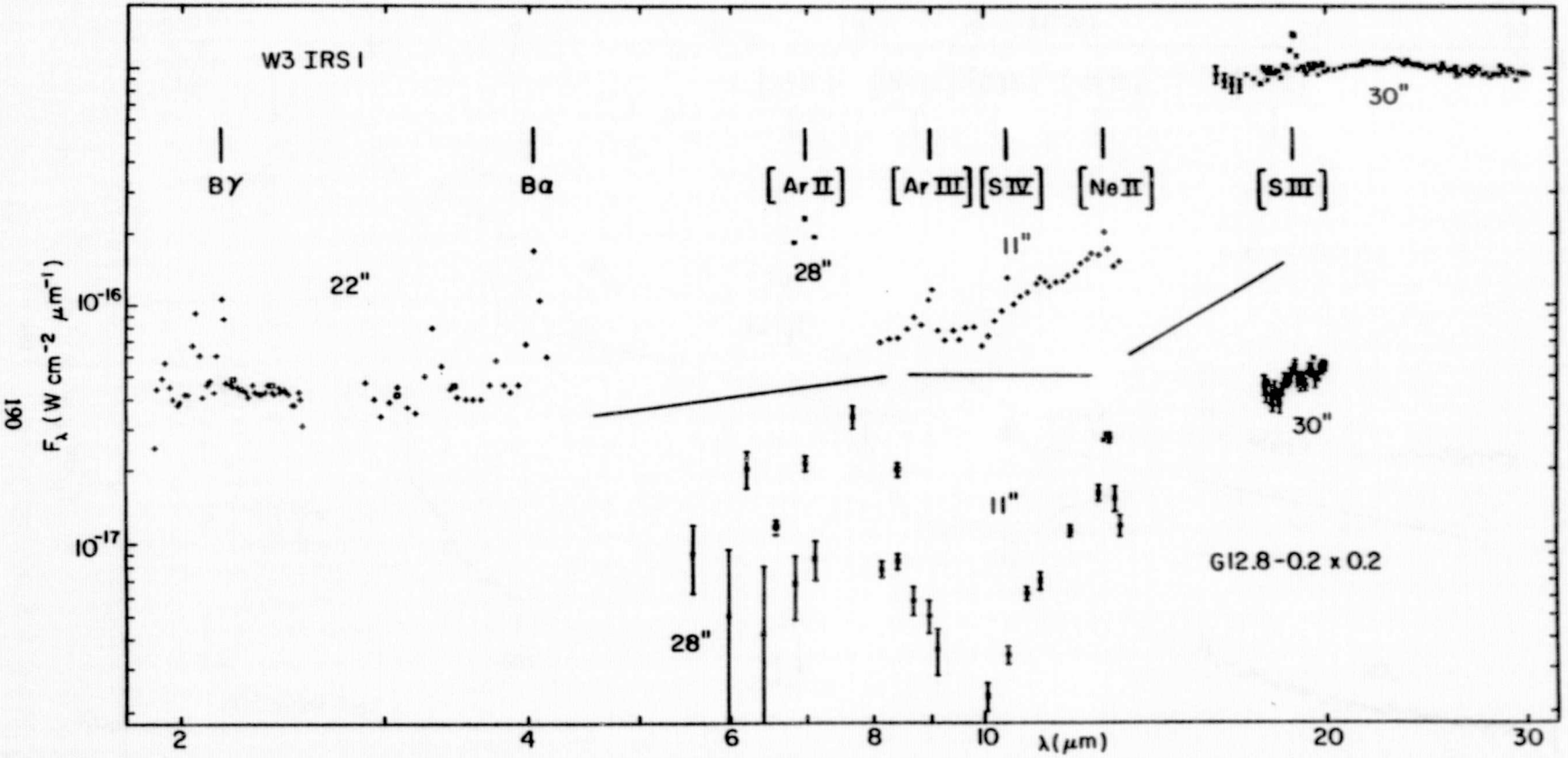

FIG. 2.—The 4–8 μm and 16–30 μm data for W3 IRS1 and G12.8 – 0.2 were obtained as described in text. The 8–13 μm data for W3 IRS1 are from Lacasse *et al.* 1980, and for G12.8 – 0.2 are provided by Gillett. The 2–4 μm data for W3 IRS1 are from Krassner and Pipher 1980. Plots from the literature do not include error bars. Apertures for the observations plotted are marked on the figure.

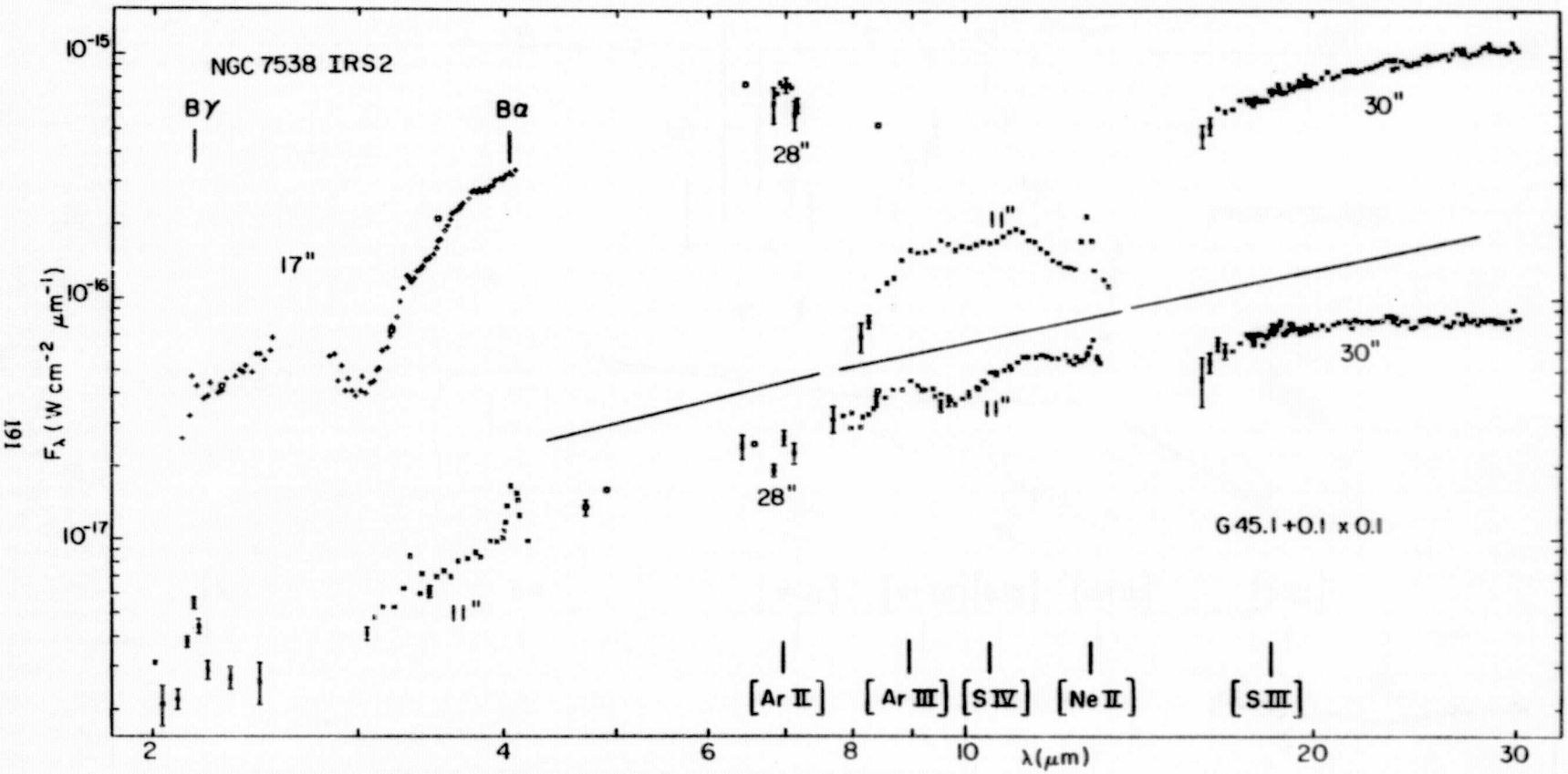

FIG. 3.—The 4–8 μm and 16–30 μm data for NGC 7538 IRS2, and G45.1+0.1 were obtained as described in text. The 8–13 μm data for NGC 7538 IRS2 and G45.1+0.1 are provided by Gillett and with better than 5% accuracy, so error bars are not plotted. The 2–4 μm data for NGC 7538 IRS2 are from Soifer, Russell, and Merrill 1976 and for G45.1+0.1 from Krassner and Pipher 1980. Plots from the literature do not include error bars. Apertures for the observations plotted are marked on the figure. Note that all the apertures except for the 8–13 μm data include IRS1 as well as IRS2 for NGC 7538, so that continuum levels disagree.

TABLE 2

ADOPTED EXTINCTION LAW

λ (μm)	Line	$\tau_\lambda/\tau_{9.7}$
1.25	...	2.21
1.65	...	1.31
2.17	Brγ	0.98
4.05	Brα	0.52
6.99	Ar II	0.30
8.99	Ar III	0.80
10.51	S IV	0.845
12.81	Ne II	0.36
18.71	S III	0.60

TABLE 3

COMPUTATION OF EXTINCTION[a]

Object	$\tau_{2.17}$[b]	$\tau_{4.05}$[c]	$\tau_{2.17}$[c]	$\tau_{9.7}$ (Model II)	$\tau_{1.25}$	$\tau_{1.65}$	$\bar{\tau}_{9.7}$[d]
G29.9−0.0	...	<0.94(<1.8)	1.5(1.5)	2.5	3.8(1.7)	2.3(1.8)	1.9 ± 0.4
G75.84+0.4	2.16(2.2)	...	...	2.0	...	...	2.1 ± 0.1
G45.1+0.1	1.60(1.6)	1.27(2.4)	1.99(2.0)	2.0	...	...	2.0 ± 0.3
NGC 7538 IRS2	...	...	1.15(1.2)	1.0	...	...	1.2 ± 0.3
W3 IRS1	1.8(1.9)	0.94(1.7)	1.7(1.8)	2.3	...	...	1.9 ± 0.3
G12.8−0.2	4.23(4.3)	...	...	4.3	...	...	4.3

[a] Quantities in parenthesis indicate $\tau_{9.7}$ determined from that value of τ_λ.
[b] From $\mathcal{F}$(Brγ)/$\mathcal{F}$(Brα).
[c] From $\mathcal{F}$(Brγ)/S$_\nu$ and $\mathcal{F}$(Brα)/S$_\nu$.
[d] The errors are standard deviations.

detected. Alternately, one can use the Brγ line at 2.17 μm.[3] This technique has been used by a number of authors (e.g., Simon, Simon, and Joyce 1979; Soifer, Russell, and Merrill 1976) to determine the extinction. In some instances we have used the ratio of $\mathcal{F}$(Brα)/$\mathcal{F}$(Brγ) instead. This ratio is not very sensitive to the value of T_e assumed and does not necessitate estimating the radio flux in our beam. Both methods weight regions of lower optical depth if there is differential extinction across the beam. (The adopted Brα and Brγ fluxes are listed in Table 1.) Some assumed or measured value of the extinction law between 4 and 8 μm is then required to correct the data. The Van de Hulst number 15 reddening law approximates observed values from visual wavelengths out to 3–4 μm; beyond 4 μm the data are scarce and controversial. For example, Hackwell and Gehrz (1974) find a law consistent with $A_\lambda \propto \lambda^{-1}$ out to 10 μm (within the error bars), and the ratio $R = A_v/E_{B-V} = 3.4$ (rather than 3.1 for Van de Hulst number 15). The data of Gillett *et al.* (1975*b*) on VI Cygni Star 12 are also consistent with $A_\lambda \propto 1/\lambda$ from 4 to 8 μm; hence, we use this law to extrapolate to 6.99 μm from either 4 or 8 μm. From 16 to 30 μm the only available data are from the paper by Forrest, McCarthy, and Houck (1979) on circumstellar shells. They conclude that $\tau_{18.7} \sim 0.6\tau_{9.7}$. Because extinction corrections are so important in our abundance calculations, we have computed $\tau_{9.7}$ from $\tau_{2.17}$ and/or $\tau_{4.05}$ when the data were available using $\tau_\lambda/\tau_{9.7}$ and have deduced a mean value of the optical depth at 9.7 μm, $\bar{\tau}_{9.7}$, for use in further calculations, which is tabulated in Table 3, along with the standard deviation. This value of $\bar{\tau}_{9.7}$ is then employed with the assumed extinction law $\tau_\lambda/\tau_{9.7}$ to calculate the extinction at the wavelengths of the forbidden lines of Ar III, Ar II, Ne II, S III, and S IV. Table 1 presents line fluxes corrected for the extinction by this method. The corrected fluxes are used later in the abundance analysis. All of the uncertainties quoted for the corrected line fluxes, and ultimately the abundances (see next section), include our estimated uncertainty in the adopted $\bar{\tau}_\lambda$. The remaining uncertainty is the assumption that the extinction law is the same from region to region.

b) Estimating Ionic Abundances

In order to convert corrected line strengths into abundances, we follow the techniques of Petrosian (1970) and compute

$$\left\langle \frac{N_x{}^i}{N_H} \right\rangle = \frac{\int N_x{}^i N_e dV}{\int N_e N_H dV} = \frac{\int (N_x{}^i/N_H) N_e N_H dV}{\int N_p N_e dV}, \quad (1)$$

which gives an average abundance of element x in the ith ionization state with respect to hydrogen, weighted by the electron density N_e. In this expression, $N_x{}^i$ is the ionic number density, and N_H is the hydrogen number density. If N_e is

[3] The assumed values of $\mathcal{F}$(Brα)/S$_\nu$(5 GHz) and $\mathcal{F}$(Brγ)/S$_\nu$(5 GHz) are 3.2×10^{12} Hz and 1.1×10^{12} Hz respectively at an electron temperature of 7500 K and are approximately proportional to $(T_e)^{-0.85}$ and $(T_e)^{-0.75}$, respectively. These ratios are not sensitive to the electron density and were calculated for He/H = 0.15, with no He^{++}.

TABLE 4

ADOPTED COLLISION STRENGTHS (Ω)

Ion	Transition	Ω
Ne II	$^2P_{1/2}$–$^2P_{3/2}$	0.368
S III	$^3P_1$–$^3P_0$	1.17
	$^3P_2$–$^3P_0$	0.56
	$^1D_2$–$^3P_0$	0.55
	$^1S_0$–$^3P_0$	0.11
	$^3P_2$–$^3P_1$	2.72
	$^1D_2$–$^3P_1$	1.64
	$^1S_0$–$^3P_1$	0.33
	$^1D_2$–$^3P_2$	2.74
	$^1S_0$–$^3P_2$	0.54
	$^1S_0$–$^1D_2$	1.29
S IV	$^2P_{3/2}$–$^2P_{1/2}$	1.66
Ar II	$^2P_{1/2}$–$^2P_{3/2}$	0.74
Ar III	$^3P_1$–$^3P_2$	2.21
	$^3P_0$–$^3P_2$	0.51
	$^1D_2$–$^3P_2$	2.55
	$^1S_0$–$^3P_2$	0.37
	$^3P_0$–$^3P_1$	1.12
	$^1D_2$–$^3P_1$	1.53
	$^1S_0$–$^3P_1$	0.22
	$^1D_2$–$^3P_0$	0.51
	$^1S_0$–$^3P_0$	0.074
	$^1S_0$–$^1D_2$	0.83

NOTE.—The preceding list was complied by W. J. Forrest. The Ne II collision strength was computed from calculations of Seaton 1975, while all other collision strengths are calculated from the data of Krueger and Czyzak 1970.

constant, and the integrals are evaluated over the entire H II region, then the above ratio is the actual ionic abundance. For density fluctuations, the abundance is weighted towards regions of higher radio flux. Using the expression for the radio flux S_ν, given by Osterbrock (1974) in the optically thin limit, and the line flux

$$F_l = \frac{1}{D^2}\int \left(\frac{j}{N_x{}^i N_e}\right)\frac{N_x{}^i}{N_H} N_e N_H dV\,, \tag{2}$$

where j is the emissivity in ergs cm^{-3} s^{-1} sr^{-1}, we obtain (assuming $N_e/N_H = 1.15$)

$$\left\langle\frac{N_x{}^i}{N_H}\right\rangle = 3.53\times 10^{-6}\left(\frac{F_l}{10^{-18} W\ \mathrm{cm}^{-2}}\right)\left(\frac{\nu}{5\ \mathrm{GHz}}\right)^{-0.1}\left(\frac{T_e}{7500\ \mathrm{K}}\right)^{-0.35}\left(\frac{S_\nu}{\mathrm{Jy}}\right)^{-1}\left(\frac{j/N_x{}^i N_e}{10^{-22}\ \mathrm{ergs\ cm^3\ s^{-1}\ sr^{-1}}}\right)^{-1}. \tag{3}$$

We assume an average value of $(j/N_x{}^i N_e)$ over the H II region ionization zone. The quantity $j/N_x{}^i N_e$ is obtained by solving the population balance equations (Osterbrock 1974) at the N_e and T_e of interest (obtained from radio continuum data), using the wavelengths and transition probabilities given by Osterbrock (1974). We use the collision strengths listed in Table 4 since the values tabulated by Osterbrock (1974) are in error for ions with $Z > 1$, and $T_e = 7500$ K (Forrest 1980). When employing equation (3) to compute ionic abundances, we use the line flux F_l corrected for extinction. Although use of $F_l/F_{\text{Brackett line}}$ would require a smaller differential extinction correction than F_l/S_ν, we wish to avoid the resulting dependence on electron temperature, which itself is abundance dependent.

In most cases cited here, the beam sizes for the Ar III, S IV, and Ne II measurements are *smaller* than the diameters of the H II regions. Because the ions being measured are not evenly distributed over the nebula, the computed ionic abundance from a small beam measurement (e.g., from only part of the H II region) does not necessarily reflect the *ionic* abundance for the entire H II region.

To illustrate how beam size effects for different ions of the same element are treated when combining ionic abundances, we imagine a situation in which only two ionization states [(1), (2)] of element x dominate the H II region. Then

$$\left\langle\frac{N_x}{N_H}\right\rangle = \frac{\int (N_x{}^{(1)}/N_H) N_e N_H dV + \int (N_x{}^{(2)}/N_H) N_e N_H dV}{\int N_e N_p dV}\,, \tag{4}$$

where the integrals are over any common volume (even if not the volume of the H II region). However, if common volumes are not sampled, we underestimate $\langle N_x/N_H\rangle$. For example, consider measurements of S III and S IV in an H II region with 30″ and 11″ apertures, respectively. These measurements can be combined to yield a lower limit to the

TABLE 5

$\langle N_x^i/N_H\rangle_{corrected}/N_x/N_{H\ standard}$[a]

Source	$\tau_{9.7}$[b]	Ar III	S IV	Ne II	S III	Ar II	Distance from Galactic Center (kpc)
G29.9−0.0	1.9 ± 0.4	1.9 ± 0.7	<0.2	1.8 ± 0.3	1.8 ± 0.7	3.1 ± 0.7	5
G12.8−0.2	4.3	0.46 ± 0.48	0.12 ± 0.04	0.30 ± 0.03	0.34 ± 0.08	0.32 ± 0.08	6
G45.1+0.1	2.0 ± 0.3	0.81 ± 0.28	0.22 ± 0.08	0.27 ± 0.04	0.53 ± 0.12	0.38 ± 0.20	7.5
G75.84+0.4	2.1 ± 0.1	0.63 ± 0.15	0.20 ± 0.02	0.18 ± 0.02	2.2 ± 0.1	0.72 ± 0.16	10
W3 (IRS1)	1.9 ± 0.3	1.7 ± 0.5	0.44 ± 0.14	0.32 ± 0.07	1.1 ± 0.2	0.15 ± 0.06	12
NGC 7538 (IRS2)	1.2 ± 0.3	0.29 ± 0.26	0.03 ± 0.06	0.55 ± 0.08	0.49 ± 0.25	3.2 ± 3.2	13

NOTE.—Adopted standard abundances relative to hydrogen: $N_{argon}/N_H = 4.7 \times 10^{-6}$; $N_{sulfur}/N_H = 1.6 \times 10^{-5}$; and $N_{neon}/N_H = 1.5 \times 10^{-4}$; from Cameron 1973 and Kaler 1978.

[a] Deduced as discussed in text: always referenced to beam sizes for the measurement. Errors include uncertainties from infrared line flux determinations and standard deviation of errors in τ (Table 3) but do *not* include those resulting from uncertainties in estimating radio flux for that volume.

[b] From Table 3.

elemental sulfur abundance by assuming that a minimum estimate of the amount of S IV that would be observed in a 30″ beam is the amount observed in the 11″ beam. If S and L represent the smaller and larger beams respectively, then

$$\left\langle \frac{N_x}{N_H} \right\rangle \geq \frac{\int_S (N_x^{(1)}/N_H) N_e N_H dV}{\int_L N_e N_H dV} + \frac{\int_L (N_x^{(2)}/N_H) N_e N_H dV}{\int_L N_e N_H dV} = \left\langle \frac{N_x^{(1)}}{N_H} \right\rangle_S \frac{V_s}{V_L} + \left\langle \frac{N_x^{(2)}}{N_H} \right\rangle_L . \quad (5)$$

V_S/V_L is the ratio of the radio fluxes in the small and large beams and the inequality is present because all of the S IV (ion number 1) may not be contained within the smaller aperture. If the S IV ion is distributed beyond 11″, the underestimate is substantial. However, if the S IV is completely contained within 11″, the equality holds, and we have a good estimate of the sulfur abundance. A further complication is the neglect of other ionization states, which also leads to an underestimate of the elemental abundance. However, without empirical knowledge of the ionization structure, these abundance estimates are the best possible. Correction factors designed to improve the abundance estimate by including a guess at the ionization structure are model dependent (see, e.g., Lacasse *et al.* 1980) and will not be employed here.[4] If clumping is present, $j/N_e N_x^i$ may decrease due to collisional de-excitation which also leads to an abundance underestimate.

Using the expression for $\langle N_x^i/N_H\rangle$, the line fluxes corrected for extinction from Table 1, and values of S_ν (justified below) for the same beam sizes as used in the IR measurements, we list the computed ionic abundances for the six H II regions studied in Table 5 relative to the standard elemental abundance. For comparison we adopt as our standard abundances (i.e., solar neighborhood) the values of Cameron (1973) for S/H, O/H and Kaler (1978) for Ar/O, Ne/O.

c) Individual Sources

In this section, we discuss computation of the ionic abundances for each of the individual sources and justify the choice of S_ν used in the computation; radio data for each source are given in Table 6. We emphasize at the outset that the choice of S_ν for extended sources is uncertain due to both the difficulties of obtaining integrated fluxes for our beams from radio maps with relatively poor resolution and the lack of knowledge concerning the exact infrared beam positions on the H II regions. We have no satisfactory method of deducing the amount of this uncertainty; hence, it is not included in our error estimates. However, this problem should be kept in mind when interpreting the final results. In what follows, we adopt a value of $T_e = 7500$ K for the electron temperature. Electron temperatures quoted (from radio recombination line studies) in the literature are quite discrepant (e.g., Lichton, Rodriquez, and Chaisson 1979; Churchwell *et al.* 1978) and have large uncertainties. The H II regions closer to the galactic center may have lower temperatures (due to presumed higher abundances); this point is currently under debate (Silvergate and Terzian 1979). Because this study is attempting to assess the existence of abundance gradients in the Galaxy, we do not a priori assume a temperature gradient.

i) G29.9−0.0

Spectrophotometric data from 8 to 13 μm have been previously obtained for G29.9−0.0 by Soifer and Pipher (1975). These investigators found a 12.6 μm half-power diameter of 13″ which agrees with that determined by Felli, Tofani, and D'Addario (1974) and Krassner *et al.* (1980) from radio continuum observations. Thus we can assume that both the airborne measurements of [Ar II] and [S III] line fluxes (27″, 30″ beams) and the ground-based measurements (22″ beam)

[4] As a guide to the reader, the Ar^+/Ar^{++} and/or S^{++}/S^{+++} ratios observed for G29.9−0.0, G12.8−0.2, G75.84+0.4, and NGC 7538 IRS2 suggest that the ionic abundance for Ne^+ should be roughly within a factor of 2 of the total Ne abundance.

TABLE 6

RADIO DATA

Source (1)	θ_s (arc sec) (2)	E (10^6 cm^{-6} pc) (3)	N_e (10^{+4} cm^{-3}) (4)	U (cm^{-2} pc) (5)	Flux (Jys) Total (6)	11" (7)	27" (8)	ν (GHz) (9)	References[d] (10)
G29.9−0.0	13[a]	7.7	0.4	75	2.9	~2.9	2.9	10.7	(1)
G75.84+0.4	22	6.8	0.34	66	3.7 ± 0.4	1.3	3.7	5	(2)
	11.7 × 6.9				2.54			2.7	(3)
G12.8−0.2	~35	34	0.8	100	25 ± 3	5.3	19.3	5	(4), (5)
G45.1+0.1	9.1	57	1.2	110	4.0 ± 0.3	~4.0	4.0 ± 0.3	5	(6)
NGC 7538 (IRS2)	10.9 × 7.8	14	1.1	31	1.4 ± 0.1	~1.4	1.4	5	(7)
	7.6[b]	20	1.3	36	1.3 ± 0.2	1.3	1.3	5	(8)
W3 (IRS1)	40 × 40[c]	...	0.6	92	33 ± 4	1.5	~12–14	5	(9), (10)

[a] Gaussian half-power width.
[b] Cylindrical geometry (diameter-length).
[c] Rough estimate from radio map.
[d] REFERENCES.—(1) 16".1 × 2.50" beam; Felli, Tofani, and D'Addario 1974. (2) Component A, 7".2 × 9".0 beam; Matthews *et al.* 1973. (3) Total flux, 9".4 × 5".5 beam; Turner *et al.* 1974. (4) G12.80−0.20, 5".6 × 30" beam; Goss, Matthews, and Winnberg 1978. (5) VLA measurements of T. Herter and J. Krassner 1980. (6) Component A, 7" × 38" beam; Matthews *et al.* 1977. (7) Component A, 2".0 × 2".3 beam; Martin 1973. (8) Component G2, 7".5 × 8".7 beam; Israel 1977. (9) W3A, 2".0 × 2".3 beam; Harris and Wynn-Williams 1976. (10) Wynn-Williams 1971.

of [Ar III], [S IV], and [Ne II] line fluxes were made with beams which encompassed the entire H II region. This allows direct computation of the ionic abundances. A 2–4 μm spectrum obtained at Mt. Lemmon on three nights from 1977–1979 is shown in Figure 1 along with other spectra noted above.

The radio flux density, S_ν, used in the abundance calculations is that of Felli, Tofani, and D'Addario (1974), who found a total flux of 2.9 Jy at 10.7 GHz. A recent VLA measurement of G29.9−0.0 by Herter and Krassner (1980) yielded 2.8 Jy at 5 GHz.

The extinction to G29.9−0.0 has been computed in a variety of ways. First, the model II fit to the 8–13 μm data of Soifer and Pipher (1975) yields $\tau_{9.7} = 2.5$. Because there is line emission from unidentified features at 3.3 μm, 6.2 μm, and 7.7 μm, one wonders whether a smaller value of $\tau_{9.7}$ might be appropriate. However, there is only marginal evidence for 8.7 and 11.3 μm features in the 8–13 μm spectrum of G29.9−0.0. Because we do not understand the nature of the emission features, and because the 11.3 μm feature is generally strong in H II regions where all features are present (Dwek *et al.* 1980), we consider the model II value of $\tau_{9.7}$ to provide an upper limit to the extinction. We can also compute the extinction from the radio and Brγ fluxes, assuming $T_e = 7500$ K and find that $\tau_{2.17} = 1.5$ which implies $\tau_{9.7} = 1.5$. Because this value is quite different from the model II upper limit, we examine other independent methods of computing the extinction. Photometry at J and H, with a 17" beam, yields value of 3.5×10^{-18} W cm^{-2} μm and 8.3×10^{-18} W cm^{-2} μm, respectively. Using the expressions developed by Willner, Becklin, and Visvanathan (1972) relating the predicted flux density in these bands relative to radio flux density on the assumption that only recombination processes contribute to the infrared flux density, we compute lower limits to the opacity at J and H of $\tau_{1.25} \geq 3.8$ and $\tau_{1.65} \geq 2.3$, respectively. These in turn lead to $\tau_{9.7} \geq 1.7$, 1.8 respectively, where the equality applies if there is no additional source of infrared radiation such as dust emission. We have assumed dust emission to be negligible at J and H and have adopted the average of the four extinction values derived above. The main remaining discrepancy is that we can compute a lower limit to the Brα flux (incomplete wavelength coverage of data) which implies $\tau_{9.7} < 1.8$. This is close to the adopted value of $\bar{\tau}_{9.7} = 1.9 \pm 0.4$, and either a lower electron temperature or a different extinction curve could resolve the remaining discrepancy. Such changes would act in a direction to *increase* the derived abundances.

We now compute the ionic abundances $\langle N_x/N_H \rangle$, using the corrected line fluxes F_i (assuming the average extinction correction $\bar{\tau}_{9.7}$) and the value of S_ν adopted. In Table 4, the ionic abundances are expressed as ratios with respect to the standard elemental abundances. Since the measurement beams encompass the H II region, the *sum* of the Ar II and Ar III abundance ratios represent a lower limit to the measured argon abundance ratio in G29.9−0.0, namely 5.0 ± 1.4 times standard argon abundance. Ar IV is also expected to be present in G29.9−0.0, although the nondetection of S IV suggests this may be a small constituent. We note that even if $\tau_{6.99\,\mu m} = 0$, Ar II alone is 1.6 times standard argon abundance, and thus argon is clearly overabundant in this source. The total sulfur abundance ≈ the S III abundance, and is 1.8 ± 0.7 times standard. Finally, the Ne II abundance is 1.8 ± 0.3 times the standard *elemental* neon abundance, indicating that neon is also overabundant. Furthermore, much of the neon is expected to be in the form of Ne III, based on the excitation parameter (Table 6). We note that if there is clumping, all of these abundance ratios would be even larger.

ii) *G75.84+0.4*

Spectrophotometric measurements of this source have been obtained by Pipher, Soifer, and Krassner (1979) in the spectral ranges from 2 to 4 μm and 8 to 13 μm (see Table 1, note e). A map at 12.6 μm by these authors and radio continuum mapping by Matthews *et al.* (1973) at 5 GHz (7".2 × 9" beam size) and Turner *et al.* (1974) at 2.7 GHz

(9".4 × 5".5 beam size) confirm the multiple structure of this source and indicate a general coincidence between the infrared and radio emission. Both radio measurements indicate two main components of comparable total flux and size. According to Matthews *et al.* (1973), component A is 19" × 12" with a total flux of 3.7 ± 0.4 Jy, while component B, which lies ~ 20" to the east of A, is 20" × 18" and has a total flux of 2.7 ± 0.3 Jy. Turner *et al.* (1974) find a total flux of 1.6 Jy for component A and a total flux for all components added together of 2.5 Jy and note that G75.84+0.4 is probably optically thick at 2.7 GHz. Line flux measurements were taken with beams centered on component A; hence, this component will be the dominant contributor to the radio flux for the beam sizes of interest here ($\leq 30''$). We assume that for [Ar II] and [S III] line flux measurements the beam encompassed the entire H II region associated with component A. For computation of the [Ar III], [S IV], and [Ne II] abundances we estimate from the parameters for the H II region given by Matthews *et al.* (1973) that ~ 1.3 Jy at 5 GHz would be contained in a radio beam centered on component A with a beam size comparable to the infrared measurements (11"). (See, however, discussion by Turner *et al.* (1974) who find the physical parameters derived by Matthews *et al.* (1973) to be uncertain, because the complex may have multiple components. Hence the adopted values of S_ν in our beam size may be in error by as much as a factor of 2.)

According to Pipher, Soifer, and Krassner (1979) the value of $\tau_{9.7}$ is 0.5 or 2.1 depending whether a model I and model II fit is chosen (see § III*a*). Typically, the model II fit is the "best fit." But since neither χ^2 model fit was unambiguously better, we consider other extinction estimates. Because we are uncertain about the radio flux in our beam, we use the ratio of the Brγ and Brα line fluxes, coupled with the assumed extinction law, to deduce $\tau_{2.17} = 2.2$, which would imply $\tau_{9.7} = 2.2$. The 2–4 μm spectrum may have been obtained at a somewhat different spatial position, and variable extinction across the nebula is possible; hence, there may be some uncertainty in comparing these estimates of $\tau_{9.7}$. Despite the excellent agreement of the model II value with that determined from the Brackett lines, we adopt $\bar{\tau}_{9.7} = 2.15 \pm 0.3$. Here the error is not the formal standard deviation but a *typical* uncertainty in $\bar{\tau}_{9.7}$. Ionic abundances relative to the standards are listed in Table 4 for this mean value of $\tau_{9.7}$. Combining ionic abundances according to the prescription outlined in § III*b*, we find the following *lower* limits to the elemental abundances for argon and sulphur (relative to standard abundance), of 0.94 ± 0.21 and 2.3 ± 0.1 respectively. We can conclude that the *lower* limit to the abundance for Ar is consistent with the adopted standard abundance, within the errors, and S is a factor of 2 overabundant. Since other stages of ionization have not been observed (notably Ar IV and Ne III) and since not *all* of the H II region was sampled for *all* ions measured (see § III*b*), the resultant Ne and Ar abundances may even exceed standard values.

iii) *G45.1+0.1*

Spectrophotometric observations of G45.1+0.1 have been obtained by Krassner and Pipher (1980) and by F. C. Gillett from 2 to 4 μm with an 11" beam and from 8 to 13 μm by Hefele and Schulte in den Bäumen (1978) and a 22" beam. New observations from 8 to 13 μm are presented here (Fig. 3) with a 7".5 beam (observations with an 11" beam are identical in spectral shape and flux density). A radio continuum map of G45.1+0.1 at 5 GHz by Matthews *et al.* (1977) with a 7" × 38" beam size reveals two dominant components separated by ~ 50". Component A is found to be ~6".5 in size with a total flux of 4.0 ± 0.3 Jy,[5] whereas component B is 25" in size with a total flux of 2.1 ± 0.3 Jy. All infrared line flux measurements were taken centered on component A; thus, due to the small source size, we expect *all* infrared beams to include all of component A, but none of B. The multiplicity of beam sizes for 8–13 μm measurements, which show no appreciable differences in forbidden line flux, also support this contention.

The ionic abundances are computed using a flux of 6.0 Jy at 5 GHz (see note 5) for component A and the corrected line fluxes for G45.1+0.1. An average (weighted by errors determined by the χ^2 line fits) of the line fluxes of Hefele and Schulte in den Bäumen (1978) and the present data has been adopted. Although the present data (11" beam) show no apparent detection of [S IV] and [Ar III], Hefele and Schulte in den Bäumen (1978) detected these lines in a 22" beam. The mean extinction correction ($\bar{\tau}_{9.7} = 2.0 \pm 0.3$) is listed in Table 3: it was deduced from the ratio of the Brγ and Brα line fluxes to the radio flux, the model II fit to the 8–13 μm measurements presented here, $\tau_{9.7} = 2.0$, and the assumed $\tau_\lambda/\tau_{9.7}$ extinction law. The corrected ionic abundances relative to hydrogen are listed in Table 5. Since all infrared beams are assumed to encompass the entire H II region, these ionic abundances can be combined to yield the elemental abundance (see § III*b*). This gives elemental abundance ratios for argon and sulphur (relative to standard) of 1.2 ± 0.5 and 0.75 ± 0.2, respectively. We conclude that the abundances for Ar, S, and Ne in G45.1+0.1 are consistent with the adopted standard abundances. If Ar IV and Ne III are present in any quantity, as is expected on the basis of the high excitation parameter (Table 6) and/or if there is clumping, the actual elemental abundances may very well exceed standard abundances.

NGC7538 IRS2

Southwest of the optical H II region NGC 7538 = S158 is a compact radio source which high resolution continuum measurements resolve into three distinct components. Martin (1973) has mapped this source at 5 GHz with 2" resolution and finds component A (which is 8".9 × 8".0) with a total flux of 1.4 ± 0.1 Jy dominates components B and C which have total fluxes of only 0.12 ± 0.02 and 0.02 ± 0.01 Jy respectively. Israel (1977) finds similar results with lower resolution

[5] Matthews *et al.* (1977) find $\tau_{5\ \mathrm{GHz}} \approx 0.87$, thus equation (3), which assumes that S_ν is optically thin, is not directly applicable. Since the radio flux in the optically thin limit $= S_0\tau$, we can deduce an "equivalent" S_ν in this case, by multiplying the measured 4 Jy by $\tau/(1 - e^{-\tau})$. The "equivalent" S_ν is 6 Jy for use in equation (3).

(~7″) 5 GHz measurements. Wynn-Williams, Becklin, and Neugebauer (1974) have mapped this region at 20 μm with a 5″ beam and find infrared sources coincident with each of the radio sources found by Martin. Willner (1976) has obtained spectra from 8 to 13 μm of all three components with a 7″.5 beam and finds IRS2 to be the only source in the complex showing evidence of infrared forbidden line emission. A new 8–13 μm spectrum of IRS2 (provided by F. C. Gillett) was obtained with an 11″ beam. All of the other measurements were obtained with an observing aperture sufficiently large to encompass both IRS1 and IRS2. Thus there is a large discrepancy among the continuum levels plotted in Figure 3.

The line fluxes for IRS2 are listed in Table 1. [Ne II] is the only line unambiguously detected; formal fitting procedures give upper limits to the strengths of other lines. An extinction correction of $\tau_{9.7} = 1.0$ was determined from a model II fit to our 8–13 μm spectrum. Soifer, Russell, and Merrill (1976) observed the Brγ flux and using the appropriate value of $\mathcal{F}_{2.17}/S_{5\ GHz}$ we find $\tau_{2.17} = 1.2$. From the adopted extinction law (Table 2), we deduce $\bar{\tau}_{9.7} = 1.2 \pm 0.3$. After correcting the [Ne II] line flux for extinction, we compute the Ne II abundance relative to standard for NGC 7538 IRS2, namely 0.55 ± 0.08. Because other stages of ionization may be present for neon (e.g., Ne III), we can only conclude that the measured ionic abundance of Ne II is consistent with the adopted standard abundance. For other ions (with the marginal exception of S III below), the signal-to-noise ratio is sufficiently poor to prohibit any conclusions.

The nearby optical H II region NGC 7538 has been observed for [S III] flux using the Lear Jet telescope with a 2′.7 beam (Forrest, Briotta, and Gull 1979). The beam was centered on the optical nebulosity and a flux of $19 \pm 3 \times 10^{-17}$ W cm^{-2} was observed in the 18.7 μm line. Using the 15 GHz radio data of Schraml and Mezger (1969), we estimate a radio flux of approximately 11.9 Jy from this region. As this region is optically visible, the extinction at 18.7 μm should be quite small. Then the above fluxes imply a S III abundance (relative to standard elemental sulfur abundance) of 0.82; our determination of the relative S III abundance from IRS2, where an extinction correction *was* employed, is 0.49 ± 0.25 (see Table 5). For comparison, Talent and Dufour (1979) derive a [S III] abundance of 0.46 standard from optical observations in two small regions and also derive a S II abundance of only 0.07 standard. As some of the sulfur may be in the form of S IV in this region, we conclude the [S III] measurements in NGC 7538 are compatible with the standard S abundance.

v) *W3 IRS1*

Spectrophotometric observations of W3 IRS1 have been obtained by Willner (1977) from 8 to 13 μm with an 11″ beam and by Krassner and Pipher (1980) from 2 to 4 μm and 8 to 13 μm with 22″ and 11″ observing apertures, respectively. The [Ar II] and [S III] data reported here were obtained with 27″ and 30″ apertures, respectively. A radio continuum map at 5 GHz with 2″ resolution by Harris and Wynn-Williams (1976) reveals a shell structure in the emitting gas approximately 40″ in diameter roughly centered in IRS2, the dominant exciting star (Harris and Wynn-Williams 1976). Due to the extended nature of this source, *none* of the infrared apertures include all of IRS1. The 2–4 μm and 8–13 μm spectra of Krassner and Pipher (1980), adopted here, and the [Ar II] measurement of this paper were acquired with the beams approximately centered on IRS2; we estimate from the radio map of Harris and Wynn-Williams (1976) that 5 GHz radio fluxes of 0, 1.5, and 13 Jy respectively would be contained in 22″, 11″, and 27″ apertures. The peak [S III] line flux was found to occur at the 5 GHz ridge to the northwest of IRS2. We estimate ~ 13 Jy at 5 GHz will be contained in this observing aperture.

The measured line fluxes for W3 IRS1 are presented in Table 1. A model II fit to the 8–13 μm spectrum of Krassner and Pipher (1980) yields an extinction correction of $\tau_{9.7} = 2.3$. The ratios of the Brγ and Brα line fluxes to the radio flux in the same beam size imply $\tau_{2.17} = 1.7$ and $\tau_{4.05} = 0.9$. The ratio of the Brackett fluxes leads to $\tau_{2.17} = 1.8$. Because there is differential extinction across W3, these values all underestimate the optical depth. Nonetheless, we use these and the adopted extinction law, $\tau_\lambda/\tau_{9.7}$, to deduce $\bar{\tau}_{9.7} = 1.9 \pm 0.3$. Using the correct line fluxes (Table 1) and the appropriate value of S_ν, we derive the corrected ionic abundances relative to the adopted standard elemental abundances; these values are listed in Table 5.

If the ionic abundances are combined according to the prescription given in § III*b*, we find that the lower limit for sulphur relative to standard abundance is 1.2 ± 0.2. The observed ionic abundance of [Ar II] in a 28″ beam shows that this ion is neligible compared to [Ar III]. Thus the argon abundance is $\geq 1.7 \pm 0.5$ standard, suggesting the argon may be overabundant. We conclude that the abundances in W3 IRS1 of S and Ne are consistent with the adopted standard abundances, noting that models of W3 IRS1 suggest that the argon measurement is indeed a lower limit (Herter *et al.* 1981). A large aperture (2′.7) measurement by McCarthy (1980) yields S III abundance of 0.22 standard sulfur abundance (uncorrected for extinction). After correcting for extinction, this is in reasonable agreement with the value found here.

vi) *G12.8 − 0.2*

We present a new 8–13 μm spectrum (with an 11″ beam) of the strong thermal radio source G12.8 − 0.2 in the W33 complex as well as a 4–8 μm and 16–30 μm spectrum in Figure 2. A partial 8–13 μm spectrum using a 15″ beam was also obtained; the spectrum is not plotted in Figure 2, but the [Ne II] and [S IV] measurements are reported in Table 1. Goss, Matthews, and Winnberg (1978) find that this source dominates the complex with a radio flux at 5 GHz of 25 Jy and a radio size of ~ 14″ × 27″. The other weaker compact sources in the complex (~ 12′ in diameter) contribute less than 2 Jy radio flux, although diffuse flux of ~ 30 Jy spread over the 12′ diameter is indicated. Unfortunately, the highest resolution radio map available had a resolution of 5.6″ × 30″.[6]

[6] Our VLA data (resolution ~ 2″) on G12.8 − 0.2 are not yet complete. Preliminary analysis suggests that the source is larger than 30″ arc in diameter, and that 15%, 21%, 33%, and 76% of the total flux is contained in beams of 9″, 11″, 15″, and 30″ respectively.

The measured line fluxes are given in Table 1. A 2–4.3 μm spectrum of G12.8 − 0.2 has been obtained by Pipher and Willner (1981), and they estimate $\tau_{2.7} = 4.2$ from the ratio of $\mathcal{F}(\mathrm{Br}\alpha)/\mathcal{F}(\mathrm{Br}\gamma)$. From a model II fit to the 8–13 μm spectrum we find $\tau_{9.7} = 4.3$, in excellent agreement with the Brackett line estimate. A mean value of $\bar{\tau}_{9.7} = 4.3 \pm 0.1$ is assumed to correct the line fluxes. Using the adopted radio fluxes, and the corrected line fluxes, we deduce the corrected ionic abundances relative to elemental standard abundances (Table 5). Combining these according to the prescription in § III*b*, we find that the elemental abundances are 0.3 ± 0.1 times standard for Ar II, 0.4 ± 0.1 times standard for sulfur and 0.3 ± 0.03 times standard for neon. Because we have no information on other ionization states or clumping, we quote these abundances as lower limits. However, as noted below, a rather enigmatic situation exists for this source.

Though the above calculations indicate a possible underabundance of S III in G12.8 − 0.2, measurements of the same area with a 2'.7 beam gave a much larger [S III] flux than was found with the 28" beam reported here. McCarthy (1980) reports $13 \pm 2 \times 10^{-17}$ W cm^{-2} for the [S III] 18.7 μm flux. This is about 16 times larger than the 28" measurements. However, radio observations of this region indicate that most of the radio flux in a 2'.7 beam (Schraml and Mezger 1969; Altenhoff *et al.* 1978) which we estimate at about 25 Jy at 10 GHz, originates from the ~ 20" diameter compact H II region (Felli, Tofani, and D'Addario 1974; Goss, Matthews, and Winnberg 1978). Since the radio emission should be a good tracer for the ionized gas in this region, it is not clear where the large S III flux observed in the 2'.7 beam is coming from. This property is similar to that found for W51, where the S III fluxes from the compact components IRS1 and IRS2 (Forrest 1980) provide only a small fraction of the flux seen in a 2'.7 beam (McCarthy, Forrest, and Houck 1979), even though the radio maps indicate that they dominate the thermal emission from that region.

The possibility that the small aperture observations somehow missed the compact H II region has been considered but does not seem likely. The position in the sky which was observed was determined by first offsetting from a nearby guide star to the nominal position of the H II region (Goss, Matthews, and Winnberg 1978) and then peaking up in the continuum around 19 μm. The final position gave a continuum 20 μm flux of about 2.8×10^{-16} W cm^{-2} μm^{-1} which, considering the beam sizes, is consistent with the flux of 2×10^{-16} W cm^{-2} μm^{-1} found by Dyck and Simon (1977) for their brightest component in this region (IRS3). In the process of peaking up, data on the strength of the 18.71 μm line in the immediate vicinity of the compact H II region were gathered. Though the peak up signal-to-noise ratio was not large ($S/N \sim 2/1$), within ± 15" of the final peak the line flux was not significantly larger than at the final position. We conclude that we were pointed at the compact H II region.

The question of what is responsible for the relatively large [S III] line flux observed in the larger beam is an intriguing one. Because of the difficulty of separating a low surface brightness radio component from the very bright compact component with the data currently available, it is possible that the region viewed in the large beam had some thermal radio emission in addition to the 25 Jy from the compact component. The amount could not be large compared to the emission from the compact H II region. If we estimate an upper limit to its radio emission as $\lesssim 10$ Jy, then we estimate a S III abundance relative to standard sulfur abundance of $\geq 0.6 \times [\exp(\tau_{18.7})]$, where $\tau_{18.7}$ is the extinction to the region. *Thus even with no extinction assumed, the abundance of* S III *in the extended component appears to be at least a factor of 2 higher than in the compact* H II *region and is comparable to the standard abundance.* The source of this disparity is not understood at present. Some possible explanations are: (1) severe clumping in the compact H II region suppressing the S III flux; (2) a much larger optical depth to the compact H II region than has been assumed here—if the extinction is patchy across our beam size, we seriously underestimate $\tau_{9.7}$ by all the methods used; (3) an actual difference in the gaseous sulfur abundances between the compact H II region and the diffuse H II region. There is some controversy on the relative distances to the different components and we may be sampling two separated regions (Goss, Matthews, and Winnberg 1978). The [S IV] and Brackett measurements rule out substantially higher or lower excitation. We plan spatial observations of the complex in the Brα and [Ne II] lines and abjacent continua to attempt to resolve the disparity.

IV. CONCLUSIONS

We have gathered infrared line fluxes for [Ar II] (6.99 μm), [Ar III] (8.99 μm), [Ne II] (12.81 μm), [S III] (18.71 μm), and [S IV] (10.51 μm) in six compact H II regions well distributed in distance from the galactic center. Extinction to these regions was estimated by a variety of methods in order to arrive at a realistic value of the correction factor to apply to these measured line fluxes. The Ne, Ar, and S abundance for these regions are calculated by combining these data with radio data on the same objects; quoted errors in the calculated abundances include uncertainties in estimating the extinction. The two H II regions sampled close to the galactic center (G29.9 − 0.0 and G12.8 − 0.2) give quite different results. G29.9 − 0.0 appears to be overabundant in Ne, Ar, and S, while G12.8 − 0.2 appears to be roughly standard or underabundant in these elements. We believe that errors in the extinction have been carefully taken into consideration, and that this is not the cause of the abundance difference. However, it is possible that the radio fluxes used in these calculations do not exactly correspond to the radio flux contained in the infrared beam size. We are attempting to overcome this possible source of error through an extensive series of measurements on the VLA. Other regions with possible overabundance include G75.84 + 0.4 (in S) and W3 (in Ar), both at ≥ 10 kpc from the galactic center. Our limited data suggests region to region abundance variations. Abundance gradients determined optically (Peimbert, Torres-Peimbert, and Rayo 1978 and references therein) often show scatter of the same order of magnitude as the derived abundance gradients. Because of the small number of regions sampled and the uncertainties in interpreting the infrared line data (such as importance of clumping, neglect of other stages of ionization, and nature of the extinction law), we do

not propose to attempt an estimate of the alleged gradient. However, it is important to obtain more measurements of the type outlined here in greater detail (e.g., better spatial coverage and similar beam sizes) so that *total* abundances can be reliably estimated. We require a sufficiently large sample of such observations to assess statistically the abundance pattern in our Galaxy. The present results seem to indicate that the abundances of Ar, S, and Ne vary substantially from H II region to H II region, whatever the underlying reason.

We wish to thank the support staff of the Kuiper Observatory for their excellent performance during flight operations. We thank Dr. F. C. Gillett for providing unpublished data, and for his helpful comments on the manuscript. All of the authors are supported by grants from NASA and the NSF.

REFERENCES

Altenhoff, W. J., Downes, D., Pauls, T., and Schraml. J. 1978, *Astr. Ap. Suppl.*, **35**, 23.
Balick, B., and Sneden, C. 1976, *Ap. J.*, **208**, 336.
Cameron, A. G. W. 1973, *Space Sci. Rev.*, **15**, 121.
Churchwell, E., Smith, L. F., Mathis, J., Mezger, P. G., and Huchtmeier, W. 1978, *Astr. Ap.*, **70**, 719.
Dwek, E., Sellgren, K., Soifer, B. T., and Werner, W. M. 1980, *Ap. J.*, **238**, 140.
Dyck, H. M., and Simon, T. 1977, *Ap. J.*, **211**, 421.
Felli, M., Tofani, G., and D'Addario, L. R. 1974, *Astr. Ap.*, **31**, 431.
Forrest, W. J. 1980, private communication.
Forrest, W. J., Briotta, D. A., and Gull, G. E. 1979, private communication.
Forrest, W. J., McCarthy, J. F., and Houck, J. R. 1979, *Ap. J.*, **233**, 611.
Gillett, F. C., Forrest, W. F., Merrill, K. M., Capps, R. W., and Soifer, B. T. 1975*a*, *Ap. J.*, **200**, 609.
Gillett, F. C., Jones, T. W., Merrill, K. M., and Stein, W. A. 1975*b*, *Astr. Ap.*, **45**, 77.
Goss, W. M., Matthews, H. E., and Winnberg, A. 1978, *Astr. Ap.*, **65**, 307.
Hackwell, J. A., and Gehrz, R. P. 1974, *Ap. J.*, **194**, 49.
Harris, S., and Wynn-Williams, C. G. 1976, *M.N.R.A.S.*, **174**, 649.
Hefele, H., and Schulte in den Bäumen, J. 1978, *Astr. Ap.*, **66**, 465.
Herter, T., and Krassner, J. 1980, private communication.
Herter, T., Pipher, J., Helfer, H. L., Willner, S. P., Puetter, R. C., and Rudy, R. 1981, *Ap. J.*, **244**, 511.
Israel, F. P. 1977, *Astr. Ap.*, **59**, 27.
Jones, B., *et al.* 1980, preprint.
Kaler, J. B. 1978, *Ap. J.*, **225**, 527.
Krassner, J., and Pipher, J. L. 1980, in preparation.
Krassner, J., Pipher, J. L., Savedoff, M. P., and Soifer, B. T. 1980, in preparation.
Krueger, T. K., and Czyak, F. J. 1970, *Proc. Roy. Soc. London, A*, **318**, 531.
Kwan, J., and Scoville, N. 1976, *Ap. J.*, **209**, 102.
Lacasse, M., Herter, T., Krassner, J., Helfer, H. L., and Pipher, J. L. 1980, *Astr. Ap.*, **86**, 231.
Lichton, S. M., Rodriguez, L. F., and Chaisson, E. J. 1979, *Ap. J.*, **229**, 524.
Martin, A. H. M. 1973, *M.N.R.A.S.*, **163**, 141.
Matthews, H. E., Goss, W. M., Winnberg, A., and Habing, H. J. 1973, *Astr. Ap.*, **29**, 309.
Matthews, H. E., Goss, W. M., Winnberg, A., and Habing, H. J. 1977, *Astr. Ap.*, **61**, 261.
McCarthy, J. F., Ph.D. thesis, Cornell University.
McCarthy, J. F., Forrest, W. J., and Houck, J. R. 1979, *Ap. J.*, **231**, 711.
Osterbrock, P. E. 1974, *Astrophysics and Gaseous Nebulae* (San Francisco: Freeman).
Peimbert, M. 1975, *Ann. Rev. Astr. Ap.*, **13**, 113.
Peimbert, M., Torres-Peimbert, S., and Rayo, J. F. 1978, *Ap. J.*, **220**, 516.
Petrosian, V. 1970, *Ap. J.*, **159**, 883.
Pipher, J. L., Soifer, B. T., and Krassner, J. 1979, *Astr. Ap.*, **74**, 302.
Pipher, J. L., and Willner, S. P. 1981, in preparation.
Puetter, R. C., Russell, R. W., Soifer, B. T., and Willner, S. P. 1979, *Ap. J.*, **228**, 118.
Russell, R. W., Soifer, B. T., and Willner, S. P. 1979*a*, *Ap. J.*, **213**, 66.
———. 1977*b*, *Ap. J (Letters)*, **217**, L149.
Seaton, M. J. 1975, *M.N.R.A.S.*, **170**, 475.
Schraml, J., and Mezger, P. G. 1969, *Ap. J.*, **156**, 269.
Silvergate, P. R., and Terzian, Y. I. 1979, *Ap. J. Suppl.*, **39**, 157.
Simon, T., Simon, M., and Joyce, R. R. 1979, *Ap. J.*, **230**, 127.
Soifer, B. T., and Pipher, J. L. 1975, *Ap. J.*, **199**, 663.
Soifer, B. T., Russell, R. W., and Merrill, K. M. 1976, *Ap. J.*, **210**, 334.
Talent, D. L., and Dufour, R. J. 1979, *Ap. J.*, **233**, 888.
Turner, B. E., Balick, B., Cudaback, D. D., Heiles, C., and Boyle, R. J. 1974, *Ap. J.*, **194**, 279.
Willner, S. P. 1976, *Ap. J.*, **206**, 728.
———. 1977, *Ap. J.*, **214**, 706.
Willner, S. P., Becklin, E. E., and Visvanathan, N. 1972, *Ap. J.*, **175**, 699.
Wynn-Williams, C. G. 1971, *M.N.R.A.S.*, **151**, 397.
Wynn-Williams, C. G., Becklin, E. E., and Neugebauer, G. 1974, *Ap. J.*, **187**, 473.
Zeilik, M. 1977, *Ap. J.*, **218**, 118.

H. L. HELFER, W. J. FORREST, and J. L. PIPHER: Department of Physics and Astronomy, University of Rochester, Rochester, NY 14627

T. HERTER, J. R. HOUCK, and J. MCCARTHY: Astronomy Department, Cornell University, Space Sciences Building, Ithaca NY 14853

R. C. PUETTER, R. J. RUDY, and S. P. WILLNER: Center for Astrophysics and Space Sciences, University of California at San Diego, C-011, La Jolla, CA 92093

B. T. SOIFER: Division of Physics, California Institute of Technology, Downes Lab 320-47, Pasadena, CA 91125

THE ASTROPHYSICAL JOURNAL, 250:631–635, 1981 November 15

4–8 MICRON SPECTROPHOTOMETRY OF OH 0739−14

B. T. SOIFER[1], S. P. WILLNER[2], R. W. CAPPS[3], AND R. J. RUDY[2]
Received 1981 April 2; accepted 1981 May 19

ABSTRACT

Spectrophotometry of the dust-embedded late-type star OH 0739−14 shows an absorption feature at 6.0 μm characteristic of H_2O ice at temperatures significantly lower than 150 K, confirming the identification of H_2O ice in the circumstellar shell in this source. The differences in the infrared spectra of OH 0739−14 and embedded molecular cloud sources are attributed to the different cloud lifetimes and temperature regimes in which the molecules are formed. A lower limit to the mass loss rate of $10^{-4}\ M_\odot/\mathrm{yr}^{-1}$ is derived, based on the column density of ice and the size and the expansion velocity of the circumstellar cloud.

Subject headings: infrared: sources — infrared: spectra — masers — stars: individual

I. INTRODUCTION

The star OH 0739−14 (OH 231.8+4.2) is one of the most intriguing OH maser/infrared sources known. Two recent works at infrared (Allen *et al.* 1980) and radio wavelengths (Morris and Bowers 1980) have summarized the known properties of OH 0739−14. Briefly, the properties of this source are an unusual OH spectrum with strong 1667 and absent 1665 MHz lines, OH emission over a very broad velocity width, weak H_2O maser emission, no detected thermal emission from abundant gaseous species such as CO, spatially extended infrared emission at 2.2 and 3.8 μm, high (~30%) linear polarization at 2.2 μm, an infrared spectrum showing absorption by both H_2O ice at 3.1 μm and silicates at 10 μm, and large amplitude infrared variability. The infrared spectrum is unusual in that the shapes of the ice and silicate features are different from those of sources associated with molecular clouds (Gillett and Soifer 1976, hereafter GS). Several authors have interpreted these observations as evidence of a late-type, oxygen-rich star undergoing significant mass loss. In this paper, we report spectrophotometric observations in the wavelength range from 4 to 8 μm of OH 0739−14 that elucidate the chemistry of the circumstellar dust shell and have significant implications for understanding the composition of interstellar solids in a wide variety of environments.

II. OBSERVATIONS

The observations reported here are spectrophotometric observations of OH 0739−14 with spectral resolution $\Delta\lambda/\lambda \approx 0.03$. The observations were obtained with a 27″ aperture on flights of the Kuiper Airborne Observatory on 1979 December 5 and 7 (UT). The instrument and observing procedures have been described previously by Puetter *et al.* (1979). Observations were obtained at a wavelength spacing of ~0.08 μm, corresponding roughly to a full spectral resolution element of the circular variable filter. In addition to the narrow-band spectrophotometry, broad-band observations were obtained at 3.5, 4.9, 6.5, and 8.4 μm to allow comparison with ground-based observations. The spectrum obtained from 4 to 8 μm is shown in Figure 1, along with spectra of OH 0739−14 from 2 to 4 μm and 8 to 13 μm obtained within a period of 1½ months of the airborne observations.

III. DISCUSSION

a) Identification of Spectral Features

We interpret the spectrum shown in Figure 1 as a combination of photospheric emission both directly observed from a late-type star and scattered in the circumstellar shell (Kobayashi *et al.* 1978) and thermal emission from a dust shell surrounding the central star (GS; Allen *et al.* 1980). The strong H_2O absorption below 2.16 μm and CO absorption from 2.2 to 2.5 μm indicate that, for wavelengths less than 2.5 μm, the flux is dominated by photospheric emission. Beyond 3 μm, the spectrum is dominated by thermal dust radiation, with prominent absorptions at 3.1 μm and 10 μm as previously noted by GS. Between 4 and 8 μm, the spectrum rises slightly, with a significant absorption centered near 5.9 μm. Within the statistical uncertainties, the shape and central wavelength of the absorption feature (derived by assuming the underlying continuum is a smooth interpolation between the flux observed at 5 and 8 μm) is indistinguishable from absorptions near

[1]Division of Physics, Mathematics, and Astronomy, California Institute of Technology.
[2]Center for Astrophysics and Space Science, University of California, San Diego.
[3]Institute for Astronomy, University of Hawaii.

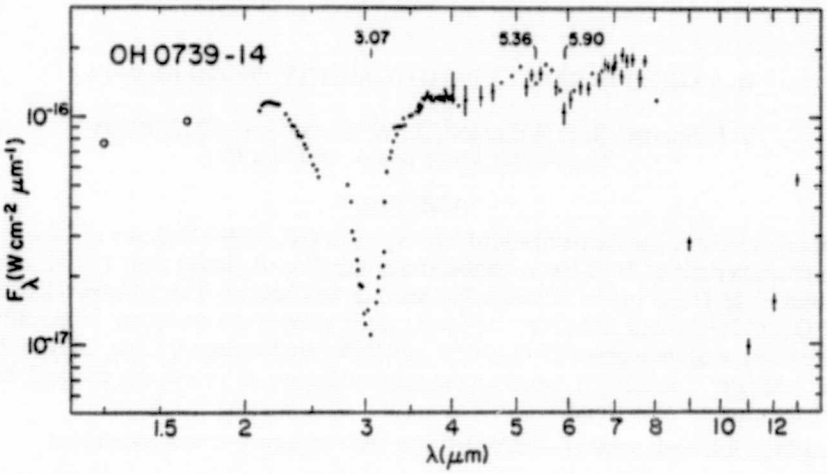

FIG. 1.—The spectrum of OH 0739−14 from 2 to 13 μm. The data from 2 to 4 μm were obtained at the Mount Lemmon Observatory with a 17″ aperture on 1979 November 1 (UT) and 1980 January 24 (UT). The observations from 8 to 13 μm were obtained with an 8.″5 aperture on 1979 November 4 (UT). The data from 4 to 8 μm were obtained with a 27″ aperture on flights of the KAO on 1979 December 5 and 7 (UT). The open circles indicate broad-band photometric data. Because the source is variable, the overall continuum levels have all been adjusted to agree with those measured from the KAO.

6.0 μm seen in sources viewed through molecular clouds (Puetter *et al.* 1979; Soifer *et al.* 1979). This absorption will subsequently be referred to as "the 6.0 μm absorption." There is also an apparent dip near 5.36 μm; if it is real, this dip has no obvious identification. However, because the existence of the feature is based on a single data point obtained on one flight, we cannot be assured of its reality and will not discuss it further.

Because H_2O ice is most likely present in the circumstellar shell of OH 0739−14, an identification of the 6.0 μm absorption with this material is plausible. Previously published infrared spectra of solids have shown that H_2O ice has an absorption at about 6.0 μm (e.g., Bertie, Labbé, and Whalley 1969). This band is potentially an excellent candidate for an identification of the 6.0 μm absorption. Bertie, Labbé, and Whalley find the 6.0 μm ice band extends from 5.7 to 7.1 μm at half strength, substantially broader than the width of 5.7 to 6.3 μm observed in OH 0739−14. Recently, however, laboratory experiments that more closely simulate the interstellar environment (Hagen, Allamandola, and Greenberg 1980) have shown that the width of the ice band is strongly dependent on the temperature. They find that, at ~10 K, this absorption band is significantly narrower than that reported by Bertie, Labbé, and Whalley. Hagen, Tielens, and Greenberg (1981) have observed a 6 μm absorption in the spectrum of H_2O ice formed at 10 K that is remarkably similar to that observed in OH 0739−14. The laboratory sample shows a sharp increase in absorbance at 5.8 μm, a peak absorbance at 6.0 μm, and a gradual decrease in the absorbance to longer wavelengths. This is quite similar to that seen in OH 0739−14 in Figure 1.

Given the observed size (Allen *et al.* 1980) and total flux of OH 0739−14 (Kleinmann *et al.* 1978), there should be dust present at temperatures of ~50 K. If, as seems likely, the ice is in the form of mantles on this cold dust, this temperature is sufficiently low to ensure narrow absorption in the 6.0 μm ice feature. Thus, we conclude that the 6.0 μm absorption is due to H_2O ice which is probably in the form of mantles on the dust grains surrounding the central star in OH 0739−14. This identification is consistent with the previous identification of pure H_2O ice mantles in the absorbing dust surrounding OH 0739−14 that was based on the observed profile of the 3.08 μm absorption (GS).

Considering the 3.1 μm and 6.0 μm features and the presence of H_2O maser emission, the identification of H_2O ice must be regarded as strong. The question then must be raised as to what other ice absorption features might be expected to be present. It is known that H_2O ice shows another absorption at ~11.5 μm (Bertie, Labbé, and Whalley 1969); however, the work of Hagen, Allamandola, and Greenberg (1980) shows that this feature is characteristic of pure H_2O ice and need not be present in mixtures of ices. The 8–13 μm spectrum of OH 0739−14 shows evidence for such a feature, as can be seen in Figure 2. The solid and dashed lines show the best fit to the observed spectrum (from GS) using the silicate absorption profile found to be common in modeling many galactic sources. The solid line beyond 10 μm shows the effect of adding to the calculated profile ice absorption with a central optical depth of 0.55 using the Bertie, Labbé, and Whalley optical constants for H_2O ice at 100 K. The qualitative agreement between the latter profile and the observations is excellent. The

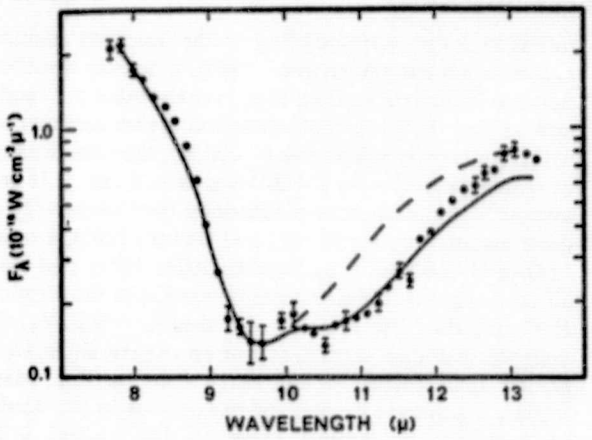

FIG. 2.—The 8–13 μm spectrum of OH 0739−14 from GS fitted with two different models. The solid and dashed lines indicate the best fit of the data to a model where a central blackbody source is viewed through cold silicate grains. The solid line beyond 10 μm adds to this model absorption by H_2O ice with a maximum optical depth of 0.55 at 11.5 μm.

discrepancy is that the wing of the observed absorption does not extend to wavelengths as long as expected. A similar discrepancy between the observed 6 μm feature and that predicted by the 100 K ice optical constants has been noted above. While additional absorption due to ice is not the only possible interpretation of the breadth of the 10 μm absorption, (e.g., GS), it is supported by the identification of the absorptions at 3.08 μm and 6.0 μm as due to H_2O ice. If these identifications are made, then the total band strengths of the three ice absorptions, proportional to the equivalent widths of the features, are in the ratio 1:0.16:0.16 for the 3.08 μm: 6.0 μm: 11.5 μm bands. This compares to 1:0.05:0.13 for the equivalent widths of these bands measured by Bertie, Labbé, and Whalley for H_2O ice Ih at 100 K and 1:0.05:0.09 for cold amorphorous ice (Leger *et al.* 1979; Hagen, Tielens, and Greenberg 1981). Considering the widely different conditions under which the ices were found, the agreement between the observed and laboratory band strengths is satisfactory.

b) *Implications for the Chemistry of the Circumstellar Environment*

Many other highly obscured infrared sources have been observed in the 2–13 μm wavelength region and show significant qualitative differences with the spectra of OH 0739−14. The most interesting comparison comes between the spectra of OH 0739−14 and those sources viewed through molecular cloud material. In Figure 3, we have plotted the absorption in the 3–8 μm wavelength range of such a source, W33A (Capps, Gillett, and Knacke 1978; Soifer *et al.* 1979), in addition to that of OH 0739−14 over the same wavelength range. The absorptions are normalized to agree roughly at 6.0 μm. Both the similarities and differences between the spectra are striking. The shapes of the absorptions at ~6.0 μm in the two sources are so similar as to be indistinguishable to within the experimental errors. Soifer *et al.* suggested that the cause of the band at 6.0 μm in W33A was absorption by the carbonyl (C=0) group in complex organic molecules. However, the similarity between the bands in OH 0379−14 and W33A strongly argues that the same material must be responsible in both sources. The identification of ice in OH 0739−14 is strong, and thus H_2O probably produces the 6.0 μm absorption in molecular cloud sources, as suggested by Hagen, Allamandola, and Greenberg (1980).

The strengths of the absorptions at 3.08 μm in W33A and OH 0739−14 are quite similar, relative to the 6.0 μm absorption. This similarity is perhaps surprisingly good, considering that the strength of the 3 μm ice band is strongly dependent on the nature of the solid in which the H_2O is embedded (Allamandola, private communication), while the 6.0 μm band is much less sensitive to this effect. It thus appears likely that, in the molecular cloud sources, the absorption near 3.08 μm is predominately due to H_2O ice.

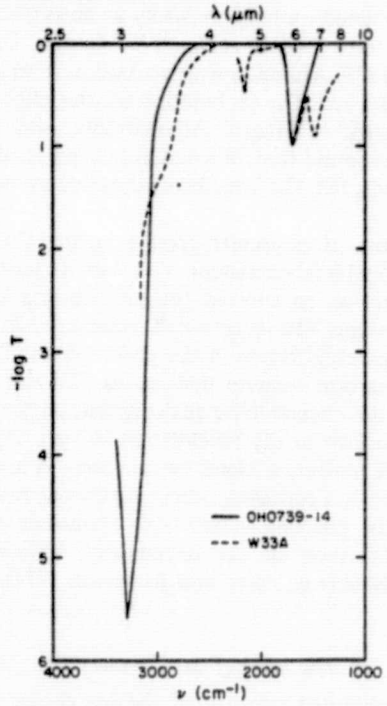

FIG. 3.—The effective transmittance from 3 to 8 μm of the absorbing material observed in OH 0739−14 and W33A. The dashed line is W33A, while the solid line is OH 0739−14. The transmittance of each spectrum has been normalized to agree at 6.0 μm to that observed in W33A. From 4 to 5 μm, the transmittance in OH 0739−14 is consistent with log T=0. From 5.5 to 6.5 μm, the profiles of the absorption in the two objects are indistinguishable.

There are spectral regions that show absorption in W33A without counterparts in OH 0739−14. Two of these are the long wavelength wing of the 3 μm absorption and the strong absorption centered at 6.8 μm. The observations at 4.6 μm, where a strong absorption is seen in the W33A spectrum, are inconclusive as to whether a similar feature is present in OH 0739−14.

Capps, Gillett, and Knacke (1978) recognized that the absorption at 3.1 μm in W33A was incompatible with pure H_2O ice absorption and suggested that the C–H stretch band in organic molecules could provide the long wavelength wing to this band. Soifer *et al.* (1979) identified the 6.8 μm band with scissors vibrations in methyl (CH_3) or methylene (CH_2) groups. The column densities inferred for these bands from the absorption strengths probably require that these molecules be in the solid state, i.e., associated with the grains, in the form of complex mantles on core grains. The work of Hagen, Allamandola, and Greenberg (1980) has shown that cosmic mixtures of photolyzed ices produce both the 3.3–3.5 and 6.8 μm bands with roughly the correct relative strengths.

The 10 μm absorption in molecular cloud sources has been explained quite successfully as absorption by pure silicates (e.g., Gillett *et al.* 1975; Capps, Gillett, and Knacke 1978) without any contribution from ice absorption at 11.5 μm. The explanation for this might be found in the work of Hagen, Allamandola, and Greenberg 1980, who found that, in ice mixtures expected in molecular clouds, the 11.5 μm absorption feature need not be present.

The lack of molecular groups having CH bands in OH 0739−14 is consistent with our understanding of this object as an evolved oxygen-rich star ejecting its own envelope. The oxygen-rich chemistry has proceeded to thermal equilibrium in the photosphere (Tsuji 1964), leaving carbon entirely tied up in CO and unable to react in the circumstellar environment on the time scale of the outflow of the envelope ($\sim 10^3$ yr). On the other hand, the molecular cloud environment is a much more long-lived environment, where statistical reactions will eventually produce substantial quantities of organic molecules, even in the oxygen-rich environment expected there (e.g., Allen and Robinson 1977).

c) *The Mass of the Circumstellar Shell*

The observed strength of the ice absorption can be used to estimate the mass of the circumstellar shell. If we assume the mass opacity coefficient of the 3.08 μm ice feature is $\sim 10^4$ cm^2 gm^{-1} (Bertie, Labbé, and Whalley 1969; Hagen, Tielens, and Greenberg 1981), the column density of water molecules in the line of sight to the central source is 7×10^{18} cm^{-2}. Further, if we assume the radius of the shell is $\sim 2\times10^{17}$ cm, a linear radius at 3 kpc corresponding to the observed angular radius at 3.8 μm (Allen *et al.* 1980), a density distribution $\rho \propto r^{-2}$ (corresponding to a constant mass loss rate), and an inner radius corresponding to the temperature at which ice rapidly sublimates ($\sim$120 K), then the density of water molecules at 2×10^{17} cm is ~ 2 cm^{-3}. If we assume a spherical mass distribution (not necessarily a good assumption, see Morris and Bowers 1980), a ratio of O to H of 6×10^{-4} by number (Allen 1973), and that all the oxygen in the circumstellar shell is in the form of H_2O ice, then the mass of the shell is $\sim 0.2\ M_\odot$. A nonspherical mass distribution or an oxygen abundance greater than cosmic would likely decrease this mass, while a significant fraction of oxygen not in ice would increase the circumstellar mass. In this context, it is worth noting that the strength of the 10 μm absorption (GS) suggests that roughly equal masses of oxygen are in H_2O ice and silicate grains. Taking 0.1 $M_\odot$ as a minimum mass in the circumstellar shell, then a minimum mass loss rate for OH 0739−14 is $10^{-4}\ M_\odot$ yr^{-1}, if, as suggested by the velocity width of the OH line (Morris and Bowers), the lifetime of the shell is $\sim 10^3$ yr. This mass loss rate is consistent with the upper end of the range of mass loss quoted for OH infrared stars by Zuckerman (1980).

IV. CONCLUSIONS

Infrared spectroscopy from 4 to 8 μm of the source OH 0739−14 reveals a moderately strong absorption centered at 6.0 μm and an otherwise flat continuum. This feature is identified with a corresponding absorption in H_2O ice. Other ice absorptions are observed at 3.08 μm and probably 11.5 μm. The mass inferred for the circumstellar shell of OH 0739−14 requires a mass loss rate $\gtrsim 10^{-4}\ M_\odot$ yr^{-1}.

Based on a comparison of the spectra of OH 0739−14 and infrared sources viewed through molecular clouds, we conclude that the 3.08 μm and 6.0 μm features seen in molecular clouds are probably due to H_2O ice, while the 3.4 μm and 6.8 μm features observed in molecular cloud sources are due to constituents not present in OH 0739−14. The most plausible constituents responsible for the 3.4 μm and 6.8 μm features are C–H bonds.

It is a pleasure to thank the staff of the Kuiper Airborne Observatory for their assistance in obtaining the airborne observations reported here. We thank F. Gillett of KPNO for the loan of the detector used to make the airborne observations. We also thank F. Williamson and B. Jones for assistance in obtaining the observations at Mount Lemmon. B. T. S. would like to thank Mark Allen for helpful discussions. This research was supported by grants from NASA and the NSF.

REFERENCES

Allen, C. W. 1973, *Astrophysical Quantities* (3rd ed.; London: Athlone), p. 31.
Allen, D. A., Barton, J. R., Gillingham, P. R., and Phillips, B. A. 1980, *M.N.R.A.S.*, **190**, 531.
Allen, M., and Robinson, G. W. 1977, *Ap. J.*, **212**, 396.
Bertie, J. E., Labbé, H. J., and Whalley, E. 1969, *J. Chem. Phys.*, **50**, 4501.
Capps, R. W., Gillett, F. C., and Knacke, R. F. 1978, *Ap. J.*, **226**, 863.
Gillett, F. C., and Soifer, B. T. 1976, *Ap. J.*, **207**, 780 (GS).
Gillett, F. C., Forrest, W. J., Merrill, K. M., Capps, R. W., and Soifer, B. T. 1975, *Ap. J.*, **200**, 609.
Hagen, W., Allamandola, L. J., and Greenberg, J. M. 1980, *Astr. Ap.*, **86**, L3.
Hagen, W., Tielens, A. G. G. M., and Greenberg, J. M. 1981, *Chem. Phys.*, (in press).
Kleinmann, S. G., Sargent, D. G., Moseley, H., Harper, D. A., Loewenstein, R. F., Telesco. C. M., and Thronson, H. A. 1978, *Astr. Ap.*, **65**, 139.
Kobayashi, Y., Nawara, K., Maihara, T., Okuda, H., and Sato, S. 1978, *Pub. Astr. Soc. Japan*, **30**, 377.
Leger, A., Klein, J., DeChevigne, S., Guinet, C., Detourneau, D., and Belin, M. 1979, *Astr. Ap.*, **79**, 256.
Morris, M., and Bowers P. F. 1980, *A.J.*, **85**, 724.
Puetter, R. C., Russell, R. W., Soifer, B. T., and Willner, S. P. 1979, *Ap. J.*, **228**, 118.
Soifer, B. T., Puetter, K. C., Russell, R. W., Willner, S. P., Harvey, P. M., and Gillett, F. C. 1979, *Ap. J.* (*Letters*), **232**, L53.
Tsuji, T. 1964, *Ann. Tokyo Astr. Obs.*, 2d ser., **9**, 1.
Zuckerman, B. 1980, *Ann. Rev. Astr. Ap.*, **18**, 263.

R. W. CAPPS: Institute for Astronomy, 2680 Woodlawn Drive, Honolulu, HI 96822

R. J. RUDY: Center for Astrophysics and Space Science, University of California, La Jolla, CA 92093

B. T. SOIFER: Downs Laboratory of Physics, 320-47, California Institute of Technology, Pasadena, CA 91125

S. P. WILNER: Smithsonian Astrophysical Observatory, 60 Garden Street, Cambridge, MA 02138

THE ASTROPHYSICAL JOURNAL, 253:174–187, 1982 February 1

INFRARED SPECTRA OF PROTOSTARS: COMPOSITION OF THE DUST SHELLS

S. P. WILLNER,[1,2] F. C. GILLETT,[3] T. L. HERTER,[4,5] B. JONES,[1] J. KRASSNER,[4,5] K. M. MERRILL,[3,6] J. L. PIPHER,[4,5] R. C. PUETTER,[1] R. J. RUDY,[1] R. W. RUSSELL,[1] AND B. T. SOIFER[1,7]

Received 1981 July 17; accepted 1981 August 10

ABSTRACT

Nearly complete 2 to 13 μm spectra are presented for 13 compact infrared sources associated with molecular clouds, as well as partial spectra of six additional objects. The spectra resemble blackbodies with superposed absorption features from 2.8 to 3.5 μm, at 6.0 and 6.8 μm, and in the silicate band centered near 9.7 μm. Correlations among the features are studied in an attempt to confirm possible identifications. A good correlation between the deepest part of the absorption at 3.1 μm, its long wavelength wing, and the 6.0 μm features suggests that all may be due to large amorphous water ice particles. The relatively poor correlation between the 3.4 and 6.8 μm optical depths adds no evidence to support the suggestion that these bands may be due to CH bonds.

Subject headings: infrared: spectra — interstellar: matter — molecular processes — stars: pre-main-sequence

I. INTRODUCTION

From the time of its discovery the Becklin-Neugebauer infrared source (BN object) was thought to represent a very early stage of stellar evolution (Becklin and Neugebauer 1968). It is now apparent that the BN object is one example of a large class of objects sharing similar properties, and the members of this class are often referred to as "protostars." These may be defined observationally as infrared sources, having roughly blackbody energy distributions from 2 to 20 μm with color temperatures of 400 to 600 K, having little or no thermal radio emission, and not known to have angular sizes large enough to indicate that the emission is optically thin. These sources are distinct from "compact H II regions," which have broader infrared energy distributions, generally have larger angular diameters and thus small emission optical depths, and considerable thermal radio emission from ionized gas. Both types of sources are associated with molecular clouds (Wynn-Williams and Becklin 1974; Wynn-Williams 1977; Willner 1977; Puetter *et al.* 1979). Werner, Becklin, and Neugebauer (1977) have reviewed the properties and probable evolutionary status of both types of objects. The distinction between the two classes is, however, probably sharper than those authors indicated, and if protostars as defined above indeed evolve into compact H II regions, a relatively short period of time must be required for the transition from protostar to compact H II region.

The first low resolution [$30 < (\lambda/\Delta\lambda) < 150$] spectra of protostars (see references in Table 1) found broad absorption features near 3.1 and 9.7 μm. The latter is identified as due to relatively cold silicate particles (Woolf and Ney 1969; Gillett and Forrest 1973), and its shape closely matches that of dust particles seen in emission in the Orion Trapezium and around cool oxygen-rich stars. The 3.1 μm feature has usually been attributed to amorphous water ice particles (e.g., Gillett and Forrest 1973) on the basis of its central wavelength and shape (Leger *et al.* 1979), the lack of other sufficiently abundant candidates, and the occurrence of other absorption features consistent with water ice in an oxygen-rich star undergoing rapid mass loss (Soifer *et al.* 1981). Ammonia ice may also contribute to the short wavelength side of the 3.1 μm absorption (Merrill, Russell, and Soifer 1976) but is not necessarily required (Leger *et al.* 1979). In the protostar spectra, there is also significant absorption between 3.3 and 3.5 μm (Merrill, Russell, and Soifer 1976). This attenuation cannot be due to absorption by pure water ice, but it may be due to scattering if the particles are unexpectedly large ($\gtrsim 1$ μm) and thus scatter efficiently. Another candidate for the 3.3 to 3.5 μm absorber is a molecule containing CH bonds (e.g., Hagen, Allemandola, and Greenberg 1980).

Spectra of two compact H II regions (Puetter *et al.* 1979) and two protostars (BN object—Russell, Soifer and Puetter 1977, and W33 A—Soifer *et al.* 1979) from 4 to 8 μm have shown additional broad absorption features at 6.0 and 6.8 μm. While the identification is uncertain, these features have been attributed to solid state hydrocarbon molecules. Absorption near 4.6 μm has also been seen and is attributed to the CO fundamental (e.g., Hall *et al.* 1978; Soifer *et al.* 1979).

This paper reports new low resolution 4.5 to 8 μm

[1] Center for Astrophysics and Space Sciences, University of California, San Diego.
[2] Harvard-Smithsonian Center for Astrophysics.
[3] Kitt Peak National Observatory, which is operated by the Association of Universities for Research in Astronomy, Inc. under contract with the National Science Foundation.
[4] University of Rochester.
[5] Visiting Astronomer, Kitt Peak National Observatory.
[6] University of Minnesota.
[7] California Institute of Technology.

spectra of 11 protostars; new spectra of seven protostars from 2 to 4 μm and ten from 8 to 13 μm are also reported. Together with previously published spectra, the data provide essentially complete 2 to 13 μm spectra for 13 protostars and partial spectra for six more. In this paper, the data are examined for possible correlations among the strengths of the various spectral features, and possible identifications of the features are discussed. The properties and nature of individual sources will be discussed in a later paper.

II. OBSERVATIONS

All of the observations reported here were made with spectrometers using circular variable filters as the wavelength selective element. The spectral resolution ($\lambda/\Delta\lambda$) is about 60, and the beam sizes are shown in Table 1. The 2 to 4 μm and 8 to 13 μm portions of the spectra were obtained using the UCSD-U.Minn. 1.5 m telescope at Mount Lemmon or the 1.3 or 2.1 m telescopes at KPNO. The 4.5 to 8 μm spectra were obtained using the Kuiper Airborne Observatory. Most of the sources are known to be considerably smaller than the beam sizes used, and most are isolated from other objects bright enough to contribute to the observed fluxes. The exceptions to this are the BN object (see Downes *et al.* 1981) and NGC 7538/IRS 1, for which IRS 2 and IRS 3 may contribute most of the flux in the deepest part of the 3.1 μm absorption and at 1.65 μm (see Wynn-Williams, Becklin, and Neugebauer 1974).

Table 1 gives the dates on which the spectra reported here were obtained; in addition, references to previously published spectra are given. Table 1 also lists the spectral range covered, the beam size, references to published spectra, and the observers for the new spectra. Observations of single spectral features, e.g., Brackett α, are not included in Table 1. We believe that Table 1 is a complete list of objects classified as protostars for which continuum spectra between 2 and 13 μm exist in the literature.

Figure 1 presents the new observations. In a few cases, the overall levels of the spectra were adjusted based on broad-band observations made along with the spectra and on the overlap of spectra near 8 μm. The normalization factors applied appear in the last column of Table 1, along with any notes concerning the figures. This column also serves to indicate which data are included in Figure 1; whenever possible we have presented new data, even if data in the literature are of equal or superior quality. In all cases, the new data agree well with previous data. Where Table 1 indicates that several spectra covering the same range are included in Figure 1, the various spectra have been combined with points at the same wavelengths being averaged according to their respective statistical uncertainties.

III. ABSORPTION FEATURES

a) Shapes

The silicate feature appears to have the same shape in all objects. Such differences as exist can be attributed to different optical depths and different underlying dust temperatures, although different emissivity spectra cannot be ruled out. In particular, there is no apparent change in the shape of the silicate feature with varying 3.1 μm optical depths, even though ice has an absorption feature near 12 μm (Bertie *et al.* 1969). The spectra of AFGL 2591 and NGC 7538/IRS 9, for example, have nearly identical silicate shapes in spite of very different 3.1 μm optical depths. The similarity of silicate shapes for these two objects implies that any 12 μm ice absorption has a peak optical depth no more than 1/15 as large as that of the 3.08 μm feature, whereas the laboratory ratio is nearer 1/8. The 12 μm feature is due to a librational mode rather than a fundamental mode of the water molecule, and its absence does not necessarily imply that ice is absent. Hagen, Allamandola, and Greenberg (1980), for example, have shown that a laboratory mixture of H_2O, CH_4, NH_3, and CO ices may have strong 3.1 μm absorption due to water ice but no detectable absorption near 12 μm.

The detailed shape of the 3.08 μm feature is harder to define because the continuum slopes show more dispersion. A normalized profile of the observed 3.08 μm feature was given by Merrill and Stein (1976*a*). In general, the shape of the feature agrees well with that expected for H_2O ice (Cohen 1976), but there is certainly considerable absorption beyond 3.3 μm, where water ice is transparent provided the particle sizes are smaller than about 1 μm (Mukai, Mukai, and Noguchi 1978). Figure 1 appears to show some differences in the short wavelength sides of the 3.1 μm minimum, but except for S255/IRS 1, the differences are due to different wavelength coverage. In that one object, the wavelength coverage extends to as short a wavelength as for any source, yet the flux density still appears to be considerably below the interpolated continuum level. Definite statements about the shape of the short wavelength wing are, however, impossible because of the large telluric absorption at those wavelengths.

The long wavelength wing is not present in all objects that show 3.1 μm absorption. For example, OH 0739 − 14 (Gillett and Soifer 1976), a dust-enshrouded late-type variable star, shows strong absorption at 3.1 μm, but the flux density is nearly back to the continuum level by 3.3 μm. This star also shows considerable 6.0 μm and silicate absorption, but it shows no absorption at 6.8 μm (Soifer *et al.* 1981). One possibility (Soifer *et al.* 1981) is that the 3.3–3.5 μm wing and the 6.8 μm absorption are due to a constituent of the dust shell other than water ice and this constituent is absent in OH 0739–14 but present in the protostars. Hydrocarbon molecules are the leading candidate for such a constituent. A second possibility is that the ice forms larger particles around protostars than around OH 0739 − 14, and the 3.3–3.5 μm wing is due to scattering from the large particles. This hypothesis would not suggest any identification for the 6.8 μm feature, and its absence in OH 0739 − 14 would be coincidental.

One piece of evidence that there may be two constituents contributing to the 2.8–3.5 μm absorption is the existence of a small inflection in many spectra at a wavelength of 3.30 μm. The inflection appears at the same wavelengths in all objects where it is seen to within the

TABLE 1

OBSERVING LOG AND REFERENCES

Observing Log and References	Spectral Range (microns)	Beam Size (arcsec)	Date (UT)	Ref.[a] and Tel.[b]	Observers	Norm. Factor [c]
W 3 /IRS 5	2.0- 2.5	11	80/ 9/23	C	TLH	1.0 D
	2.9- 4.1	18	77/ 3/ 2	B	JK	1.0 D
	2.9- 4.2	11	77/ 2/ 7	sB		1.0 H
	3.2- 4.0	11	80/ 9/23	C	TLH	1.0 B
	4.4- 5.0	27	79/12/11		RJR,BTS,SPW	1.0
	4.4- 7.9	27	79/12/ 5		RJR,BTS,SPW	1.0
	7.6-13.2	7.5	79/11/ 1	C	FCG	
	7.7-13.3	11	75/11/16	C	FCG	1.06
	7.7-13.5	7.5	75/ 1/22-26	n		
	7.8-13.4	11	76/11/ 2	C	FCG	1.0
	8.0-13.2	9	72/11/29	@		
AFGL 490 (UOA 1)	2.0- 2.4	7	78/ 8/10,12	a		
	2.1- 4.0	22	74/10/25,11/26	&1A		
	7.7-13.3	11	75/11/14	C	FCG	
	8.0-13.3	22	73/11/22,24,74/11/27,29	&1A		
BN	0.8- 2.7	7.3	75/10/23,76/ 1/15,16	b		
	1.5- 5.0	2.8	78	c		
	2.0- 2.4	<=5	70-71 (?)	o		
	2.0- 2.5	3.8	77/11/ 8,79/ 2/7,10	q		
	2.1- 4.0	17	74/10/25,12/6,12	g1&A		0.79 H
	2.8- 4.0	3.4	79/10	t		
	2.8- 5.1	11	72/ 3/10	fA		
	2.8- 5.1	22	72/ 3/15	fA		
	2.9- 4.2	14	79/10/30	sC		
	3.1- 5.0	11	78/ 2/21-23	y		
	3.3- 5.5	11	76/12/14,15	y		
	4.4- 8.0	30	75/10	e		0.71 H
	7.5-13.5	11	72/ 1/11,13	fA		
	7.5-13.5	22	72/ 3/ 8,9	fA		
	7.7-13.3	7.5	75/11/11-13	C	FCG	1.0
	8.0-13.3	3.4	77/ 8	t		
Orion IRc2	2.8- 4.0	3.4	79/10	t		
	8.0-13.3	3.4	77/ 8	t		
Orion IRc4	8.0-13.3	3.4	77/ 8,78/ 7	t		
	8.2- 9.3	3.4	79/12	t		
OMC-2 /IRS 3	1.9- 4.2	11	78/11/ 9	sB		
	1.9- 4.2	11	79/ 3/ 8	sB		
	2.1- 4.0	17	75/11/24,25	A	RWR,BTS	1.0
	8.0-13.3	17	76/12/13	A	RWR,BTS,SPW	1.0
NGC 2170 /IRS 3	1.9- 4.2	11	78/11/ 9	sB		
	2.0- 2.5	7	77/10/27	z		

TABLE 1—*Continued*

Observing Log and References	Spectral Range (microns)	Beam Size (arcsec)	Date (UT)	Ref.[a] and Tel.[b]	Observers	Norm. Factor[c]
	2.1- 4.0	17	80/ 1/24	A	BJ,SPW	1.0
	4.4- 7.9	27	79/12/11		LH,JLP,RJR,SPW	1.0 F
	7.9-13.3	7.5	76/ 1/12	C	FCG	
	7.9-13.3	5	76/10/31	C	FCG	
	7.9-13.3	7.5	77/10/24	C	FCG	
	8.0-13.4	11	76-77	C	JLP	1.0
S 255 /IRS 1	1.9- 4.2	11	79/ 3/12,13	sB		
	2.1- 3.7	17	79/11/ 2	A	FOW,SPW	1.0
	2.8- 4.0	17	74/11	pA		
	2.8- 4.0	17	77/ 3/18,19	A	BJ,SPW	1.0
	2.9- 4.2	11	79/ 4/ 6	sB		
	4.4- 7.9	27	78/ 2/ 3		RCP,RWR,BTS,SPW	0.85
	4.4- 4.7	27	79/12/11		LH,JLP,RJR,SPW	1.0
	8.0-13.1	8.5	74/11	pA		
	8.0-13.3	8.5	77/ 3/16	A	BJ,SPW	1.15 G
	8.1-13.4	11	77/10/26	C	FCG	
AFGL 961	2.1- 2.5	17	75/ 4/24,26	rA		1.0
	2.8- 4.0	17	75/ 4/24,26	rA		
		11	79/ 3/12	sB		
	2.8- 4.0	17	80/ 1/26	A	BJ,SPW	1.0
	4.5- 7.4	27	79/12/ 7		RJR,BTS,SPW	1.0
	4.5- 7.9	27	79/12/12		RJR,BTS,SPW	1.0
	7.6-13.3	10	77/10/25	C	FCG	1.0
	8.5-13.1	11	80/ 9/22	C	TLH	
AFGL 989 (DAA 6)	1.9- 4.2		78/10/17	C	FCG	
	1.9- 4.2	11	79/ 3/13	sB		
	2.0- 2.5	7	77?	v		
	2.1- 4.0	22	74/12/6,12,75/1/5	lA		
	2.9- 4.1	22	73/10/24,25	A	KMM	
	4.4- 7.9	27	76/11/ 5		RCP,RWR,BTS,SPW	1.10
	7.8-13.4	11	72/1/10,12	A	FCG,WJF	
	7.8-13.4	11	77/10/23	C	FCG	1.0
	8.0-13.3	22	73/ 9/29	lA		
	8.0-13.4	11	78/12/13	C	JK,JLP	1.0
AFGL 2046 [W 28 A(2)]	2.9- 4.1	5.4	75/ 8/13	y		
	7.7-13.3	11	75/ 5/30,31	C	FCG	
AFGL 2059 (M 8 E)	2.1- 4.0	17	77/ 5/15	A	BJ,SPW	0.70
	2.9- 4.1	32	76/ 5/28- 6/ 1	uB		
	4.4- 7.9	27	78/ 5/20		RCP,RWR,BTS,SPW,PMH	1.0
	8.0-13.3	8.5	77/ 6/ 9,10	A	KMM,RCP	1.20
W 33 A	2.0- 4.1	5-12	74/ 5, 75/ 5,7	h		
	4.4- 7.9	27	78/ 5	i		
	7.4-10.1			w		
	8.0-13.5	5-12	74/ 4-5, 75/ 5	h		
AFGL 2136	1.9- 4.2	11	78/ 6/15	xB		
	2.1- 4.0	17	78/ 4/28	A	KMM	1.0
	4.4- 7.9	27	79/ 6/20,27		RCP,RJR,BTS,SPW	1.0
	8.0-13.2	8.5	77/ 4/29	A	KMM,SPW	1.0 E

TABLE 1—*Continued*

Observing Log and References	Spectral Range (microns)	Beam Size (arcsec)	Date (UT)	Ref.[a] and Tel.[b]	Observers	Norm. Factor[c]
G45.07+0.13 /IRS	7.6-13.3	11	75/ 5/ 1	B	FCG,RCC	1.0 E
	8.2-10.9	11	75/ 5/22	C	FCG,RCC	1.0 E
AFGL 2591 (CRL 809 -2992, UOA 27)	2.0- 2.4	7	78/ 8/10	s		
	2.1- 4.0	22	74/11/16,12/7	l&A		
	2.1- 4.0	17	77/ 9/30	A	RCP,SPW	1.0 G
	2.8- 4.0	22	73/10/24,25	jA		
	4.4- 7.9	27	77/ 7/13		RCP,RWR,BTS,SPW	1.0
	7.8-13.2	11	75/ 5/31	C	FCG,RCC	1.0 E
	7.7-13.3	11	75/10/23	B	FCG	
	7.8-13.4	11	77/10/24	C	FCG	
	8.0-13.5	22	73/10/ 1, 2, 6	jA		
AFGL 2884 (S 140 IR)	1.9- 4.2	11	77/11/18	sB		
	1.9- 4.2	15	78/12/10	sB		1.0
	2.0- 2.5	7	77/10/25,11/25,26	z		
	4.4- 7.9	27	76/11/ 3		RCP,RWR,BTS,SPW	0.80
	7.7-13.3	11	75/11/14	C	FCG	1.0
	7.8-13.3	11	76/11/ 2	C	FCG	1.0
	7.8-13.4	11	77/10/23	C	FCG	1.0
	7.9-13.4	8	76-77	d		
	8.0-13.3	11	79/ 5/11	C	TLH	1.0
		11	79/10/27	xC		
NGC 7538 /IRS 1	1.9- 4.2	11	79/10/10	sB		
	2.1- 2.4	5	77?	%		
	2.1- 4.0	17	75/11/24,25	mA		1.0
	4.4- 7.9	27	79/ 6/20		RCP,RJR,BTS,SPW	0.90
	7.7-13.3	7.5	76/11/ 1	C	FCG	
	7.8-13.5	5,7.5	74/ 9	k		1.0
	9.0-10.4	7.5	76/11/ 6	C	FCG	1.0
NGC 7538 /IRS 9	1.9- 4.2	14	78/12/10	xB		
	1.9- 4.2	11	79/11/ 1	sC		
	2.1- 2.4	5	77?	%		
	2.1- 3.6	17	77/10/24	A	BJ,KMM,RCP,SPW	1..
	2.9- 4.0	17	77/10/ 1	A	RCP,SPW	1.10
	4.4- 7.9	27	77/ 7/13		RCP,RWR,BTS,SPW	1.0
	4.5- 7.9	27	77/ 7/ 8		RCP,RWR,BTS,SPW	1.0
	8.0-13.3	17	76/12/15	A	BTS,SPW	1.0

[a] REFERENCES.—(a) Thompson and Tokunaga 1979*b*. (b) Gautier *et al.* 1976 and unpublished. (c) Hall *et al.* 1978 and unpublished. (d) Blair *et al.* 1978. (e) Russell, Soifer, and Puetter 1977. (f) Gillett and Forrest 1973. (g) Gillett *et al.* 1975*b*. (h) Capps, Gillett, and Knacke 1978. (i) Soifer *et al.* 1979. (j) Merrill and Soifer 1974. (k) Willner 1976. (l) Merrill, Russell, and Soifer 1976. (m) Soifer, Russell, and Merrill 1976. (n) Willner 1977. (o) Penston, Allen, and Hyland 1971. (p) Pipher and Soifer 1976. (q) Scoville *et al.* 1979 and unpublished. (r) Cohen 1976. (s) Joyce and Simon 1982. (t) Aitken *et al.* 1981. (u) Wright *et al.* 1977. (v) Thompson and Tokunaga 1978. (w) R. C. Capps, unpublished. (x) R. R. Joyce, unpublished. (y) Smith, Larson, and Fink 1979. (z) Thompson and Tokunaga 1979*a*. (@) Aitken and Jones 1973. (%) Werner *et al.* 1979. (&) Merrill and Stein 1976*b*.

[b] TELESCOPE.—(A) Mount Lemmon 1.5 m. (B) Kitt Peak 1.3 m. (C) Kitt Peak 2.1 m.

[c] NORMALIZATION FACTOR.—(D) Filled symbols in Fig. 1. (E) Open symbols in Fig. 1. (F) Data smoothed by 3 point triangle function. (G) Open circles denote average of three adjacent data points. (H) Not plotted; normalization used for measuring optical depths.

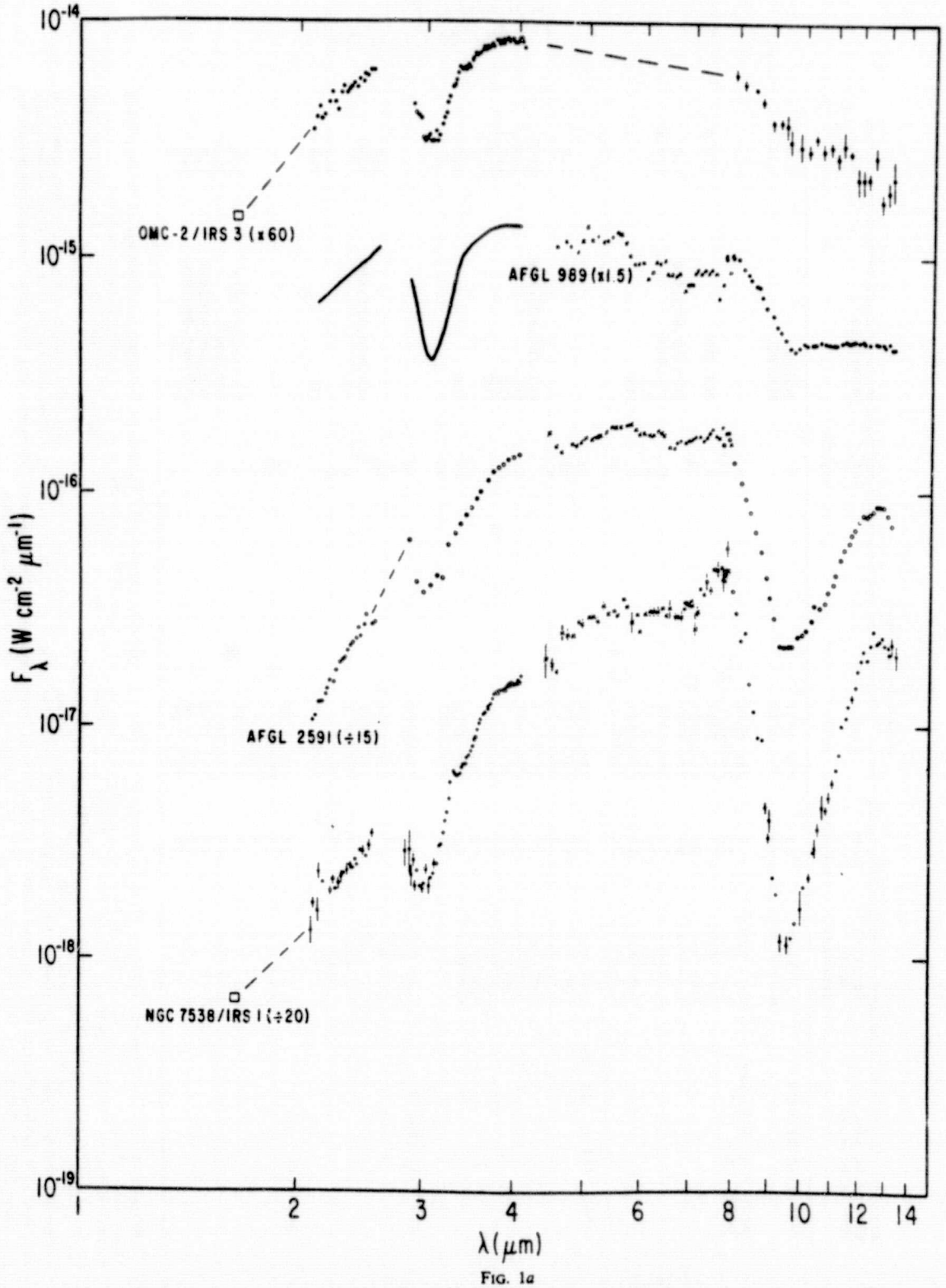

FIG. 1a

FIG. 1.—New 2–13 μm spectra of protostars. Normalization and significance of open and closed symbols are indicated in Table 1. Airborne observations are shown by X's. Solid lines represent data taken from the literature. The thin dashed lines serve only to connect points for clarity. Large squares represent broad band observations. Statistical uncertainties are less than 5% unless indicated.

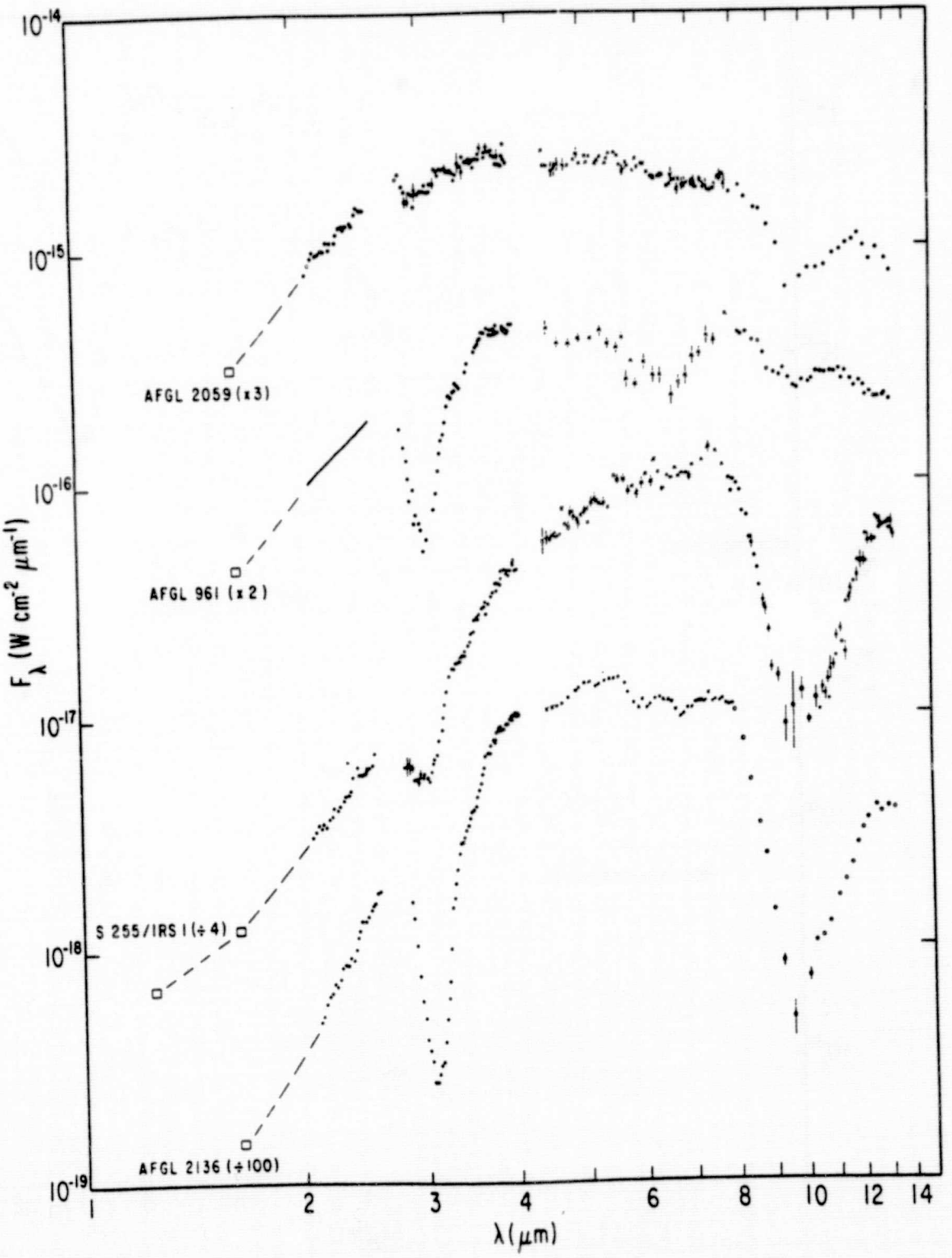

FIG. 1b

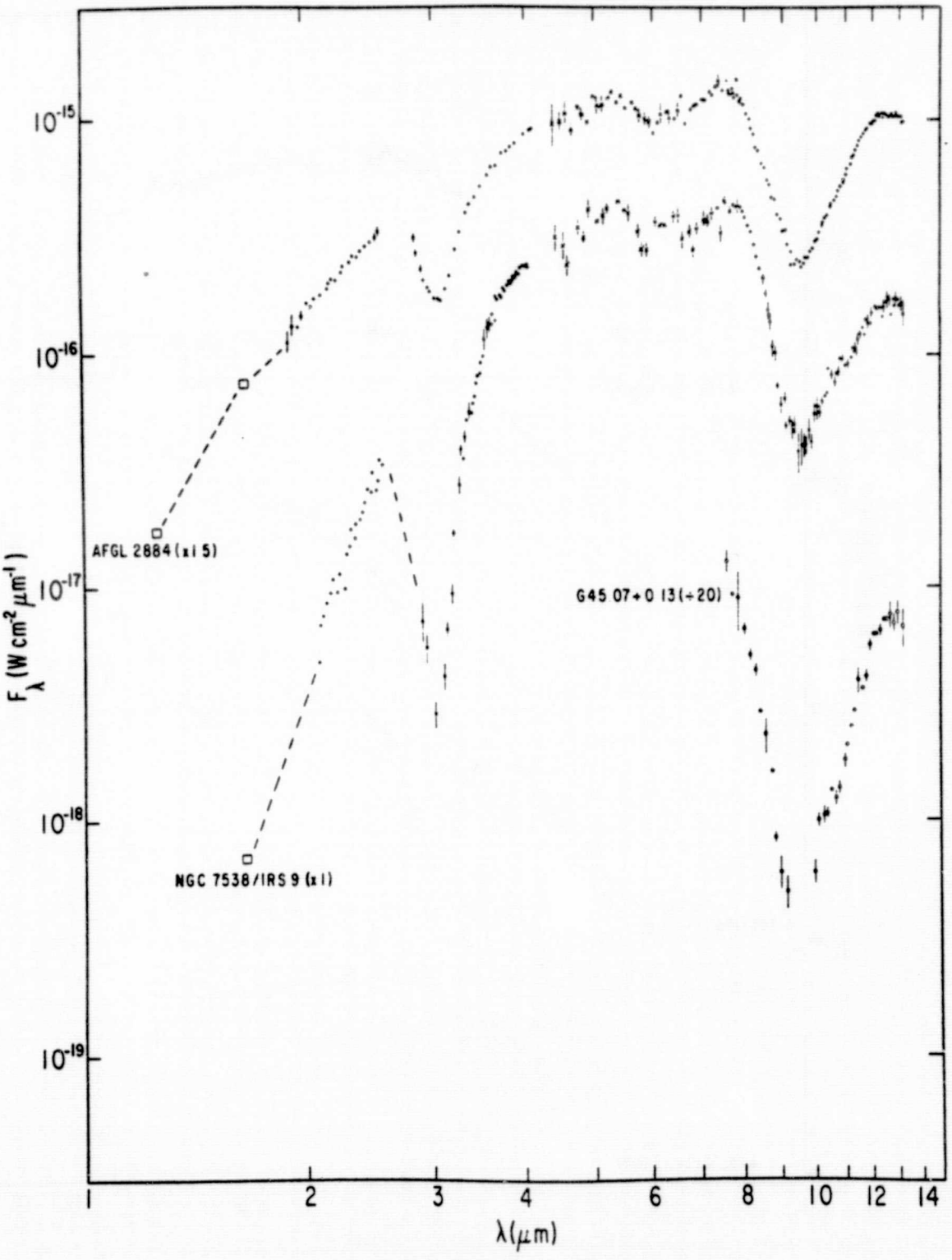

FIG. 1c

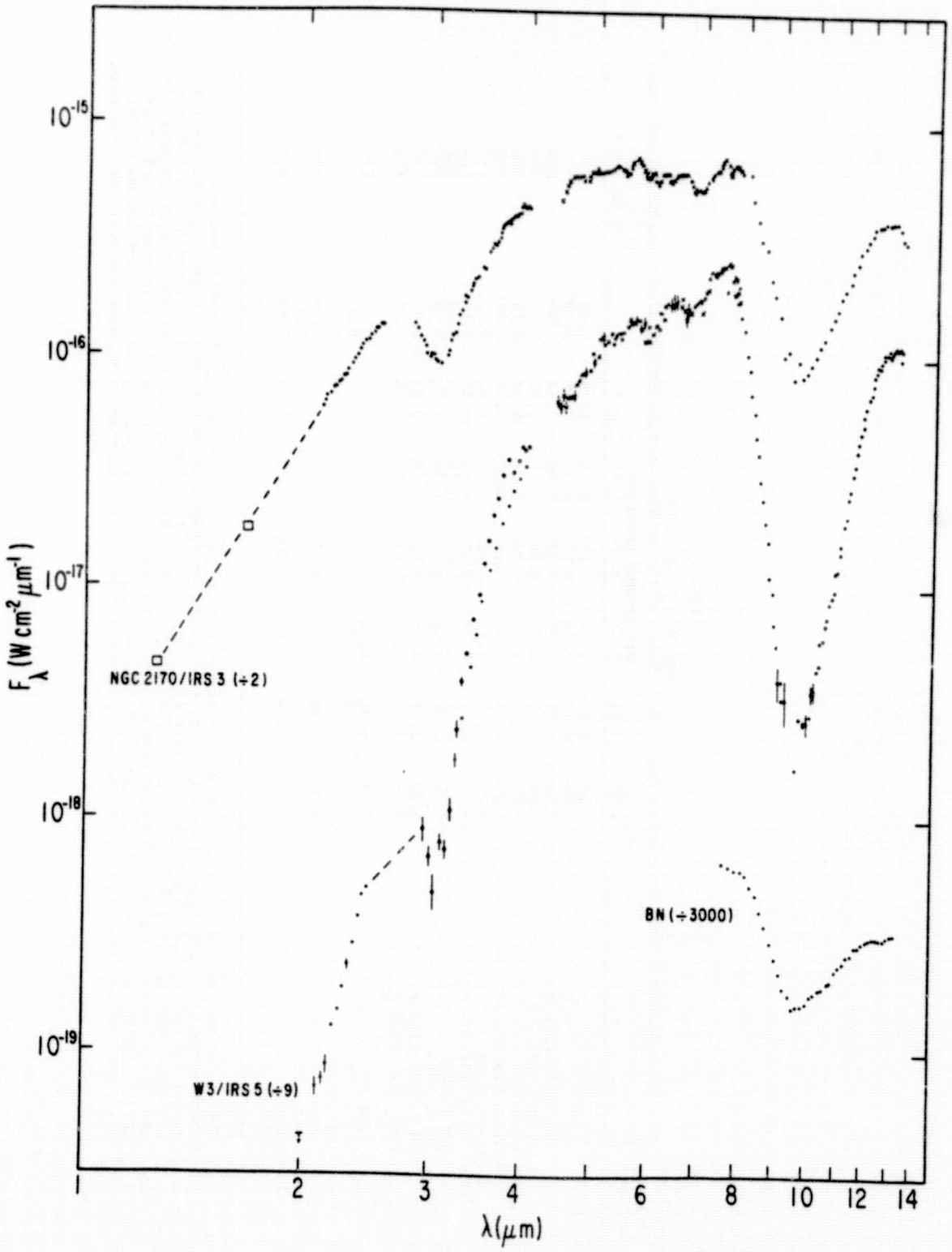

FIG. 1d

TABLE 2

MEASURED OPTICAL DEPTHS

Object	Wavelength (Microns)							
	2.92	3.08	3.35	3.47	6.0	6.8	9.7	T (2.5-4.0)
W 3 /IRS 5	1.87	3.00	1.30	0.84	0.33	0.28	7.64	370
BN	1.04	1.47	0.25	0.15	0.36	0.38	3.28	680
NGC 2170 /IRS 3	0.84	1.04	0.55	0.40	0.26	0.34	4.30	620
S 255 /IRS 1	1.05	1.13	0.47	0.40	0.20	0.18	5.11	520
AFGL 961	1.31	1.62	0.45	0.29	0.51	0.52	2.11	660
AFGL 989	0.79	1.24	0.32	0.24	0.35	0.46	2.46	825
AFGL 2059	0.16	0.18	0.07	0.06	0.00	0.12	2.6	750
AFGL 2136	1.48	2.72	0.77	0.57	0.26	0.27	5.07	510
AFGL 2591	0.45	0.69	0.21	0.13	0.12	0.17	4.14	540
AFGL 2884	0.92	1.28	0.58	0.46	0.46	0.29	3.97	650
NGC 7538 /IRS 1	1.08	1.29	0.54	0.42	0.37	0.43	6.38	550
NGC 7538 /IRS 9	2.34	3.28	1.00	0.64	0.45	0.36	4.46	480
AFGL 490	0.30	0.33	0.09	0.07			2.77	875
Orion IRc2		2.20	0.12				6.2	
Orion IRc4							5.1	
OMC-2 /IRS 3	0.65	0.89	0.28	0.19			1.93	820
AFGL 2046							5.0	
W 33 A		>5.4	3.02	2.53	1.75	1.49	7.84	450
G45.07+0.13 /IRS							5.15:	

NOTE - For the smaller optical depths, the major uncertainty is in estimating the continuum; such uncertainty generally amounts to 0.1. The statistical uncertainties in the data are usually much smaller except for the 6.0 and 6.8 micron features in a few objects (see figure 1). The wavelength calibration may introduce uncertainties up to 0.2 in the 2.92 micron optical depth, especially for the reddest objects. For the larger optical depths, the major uncertainty is the applicability of the simple technique used to make the estimates; a quantitative assessment of this uncertainty is not possible, but the conclusions of the paper will be unaffected provided the measured optical depths at least scale in some way with the true ones.

observational uncertainty of ± 0.02 μm. The inflection appears in spectra taken at Kitt Peak, Mount Lemmon, and Mauna Kea (Capps, Gillett, and Knacke 1978) with different instruments. Moreover, the shape of the absorption is different in different objects; AFGL 961, for example, shows more absorption at 3.1 μm than AFGL 2884 but less beyond 3.3 μm. The possibility of two or more absorbers is also suggested by a laboratory spectrum of a mixture of water and methane ices that is a good match to the protostar spectra (Hagen, Allamandola, and Greenberg 1980). The lab spectrum has a local absorption minimum at 3.30 μm, between the water ice (OH stretching) and methanol ice (CH stretching) maxima at 3.08 and 3.35 μm respectively.

b) Correlations between Features

In order to assess correlations between the various absorption features, optical depths at several wavelengths within the spectral features have been estimated in a consistent way for all of the sources. A blackbody was fitted to the assumed continuum fluxes on either side of each feature, and the logarithm of the ratio of the blackbody flux to the measured flux at the appropriate wavelength was taken to represent the optical depth, except for the 9.7 μm silicate feature. For this feature, the tabulated value is $\tau \equiv 1.4\tau' + 1.6$, where τ' is the value measured as above. This value of τ is nearly equal to the value obtained by more elaborate model-fitting techniques (e.g., Gillett *et al.* 1975*a*) if the underlying emission is also due to silicate dust.[8] The chosen continuum wavelengths were 2.0–2.5 and 3.8–4.0 μm for 2.92, 3.08, 3.35, and 3.47 μm; 5.0–5.5 and 7.5–8.0 μm for 6.0 and 6.8 μm; and 8.0 and 12.5–13.3 μm for 9.7 μm. While there is no guarantee that the derived optical depths accurately represent the true absorption optical depths, they should at least be consistent from object to object. Table 2 lists the optical depths measured for each object.

Measurements were made at four wavelengths near 3 μm in order to provide a quantitative representation of the shape of the 3.1 μm absorption feature. The optical depth measurements at 2.92 μm should be sensitive to molecules with NH bonds, those at 3.08 μm to OH bonds, and those at 3.35 μm to CH bonds. The wavelength 3.47 μm was chosen simply as the longest wavelength where the wing of the 3.1 μm absorption produces an easily measurable deviation from the assumed continuum.

In order to determine whether the strengths of the features are correlated with each other, the linear correlation coefficient was calculated for each pair of wavelengths in Table 2. The statistical sample consists of the 12 sources having complete spectra, and the results are shown in Table 3.

The high correlations between the optical depths of nearby features should be interpreted with caution. The 6.0 and 6.8 μm feature optical depths, and similarly the set of optical depths near 3 μm, were measured with respect to the same continuum level, and any errors in the choice of continuum level would cause each set of optical depths to be highly correlated.

TABLE 3

OPTICAL DEPTH CORRELATION COEFFICIENTS[a]

	2.92	3.08	3.35	3.47	6.0	6.8
3.08	0.96	...	...	...	...	...
3.35	0.87	0.89	...	...	...	...
3.47	0.83	0.85	[b]	...	...	...
6.0	0.63	0.53	0.44	0.43	...	...
6.8	0.36	0.28	0.13	0.11	[b]	...
9.7	0.47	0.49	0.72	0.76	0.01	−0.20

[a] For 12 measurements, 98% significance requires a coefficient of 0.658, 99% requires 0.708, and 99.9% requires 0.823.

[b] These values are high but meaningless because the measured optical depths depend so strongly on the choice of continuum level.

The silicate and 3.08 μm features are only weakly correlated. This conclusion has been stated many times before (e.g., Merrill, Russell, and Soifer 1976; Gillett *et al.* 1975*b*) and is obvious from inspection of the data. (Compare, for example, AFGL 961 or AFGL 989 with AFGL 2591 or AFGL 2059.) The significant but weak correlation between these features is not surprising if the 3.08 μm feature is due to ice mantles formed within molecular clouds so that the physical conditions and age of the molecular cloud control the thickness of the mantles (e.g., Allen and Robinson 1977).

The large correlation between the 3.08 μm optical depth and the 2.92, 3.35, and 3.47 μm optical depths is probably significant, even considering the caution stated above. If a second constituent contributes to any of these absorptions, its abundance must be correlated with the water ice abundance.

A weak but significant correlation exists between the silicate absorption and the 3.35 and 3.47 μm optical depths. This is probably the result of a contribution to the optical depths at the latter wavelengths from the weak absorption near 3.4 μm observed towards the galactic center (Willner *et al.* 1979). This absorption may occur everywhere in the interstellar medium rather than strictly in molecular clouds; towards the galactic center, it has an optical depth of about 3% of that of the silicate absorption.

In order to search for additional composition or abundance differences among the sources, it is desirable to remove the effect of differences in the total column density of material. Since silicate grains are not easily destroyed, the silicate optical depth should be proportional to the total dust column density. The optical depth of each feature was therefore divided by the silicate optical depth for that source, and the linear correlation coefficient of the ratios was calculated. The results are shown in Table 4.

Some of the positive correlations shown in Table 3 are shown to be statistically significant in Table 4. The most

[8] Underlying silicate emission was chosen because of the better fit of such models to the observed data. If τ' had been used instead of τ, Table 3 would be unchanged, but all of the correlations in Table 4 would be much higher because of the contribution of AFGL 961 and 989, which have relatively small silicate optical depths.

TABLE 4

NORMALIZED OPTICAL DEPTH[a] CORRELATION COEFFICIENTS

	2.92	3.08	3.35	3.47	6.0
3.08	0.96	...	...	...	...
3.35	0.84	0.86	...	...	...
3.47	0.77	0.79	[b]	...	...
6.0	0.84	0.77	0.63	0.60	...
6.8	0.72	0.65	0.43	0.39	[b]

[a] Each optical depth is normalized by the 9.7 μm optical depth.

[b] These values are high but meaningless because the measured optical depths depend so strongly on the choice of continuum level.

striking results are the good correlations between the 6.0 and 6.8 μm depths and among all four depths related to the 3 μm feature. Such correlations must be viewed with some caution, however, as noted above. The correlation between 6.0 μm depth and the depth of the ice band, particularly at 3.08 μm, is more likely to be real, and its interpretation is discussed below.

Several possible identifications for the 6.0 and 6.8 μm features have been suggested. These include hydrated or otherwise processed silicates (Puetter *et al.* 1979), icy grain molecules (Hagen, Allamandola, and Greenberg 1980), and hydrocarbon molecules (Puetter *et al.* 1979). Previous evidence for these identifications has been discussed by Soifer *et al.* (1979) and Willner *et al.* (1980), who consider hydrated silicates improbable. The complete lack of correlation between silicate optical depth and either 6.0 or 6.8 μm optical depth (Table 3) is further evidence against such an identification.

The 6.0 μm feature has been identified as the bending mode of H_2O or NH_3 ice (Hagen, Allamandola, and Greenberg 1980; Hagen, Tielens, and Greenberg 1981; Knacke and Krätschmer 1980; Soifer *et al.* 1981) in OH 0739−14, a late-type star surrounded by an extensive circumstellar shell. The shape and central wavelength of the 6.0 μm feature in that source are indistinguishable from those observed in the protostar spectra discussed here, so the same identification must be considered the most likely. One would then expect the good correlation between the normalized depth at 6.0 μm and the 3.1 μm ice absorption. The good correlation found (Table 4) must be considered additional evidence in favor of the identification of both the 3.08 and 6.0 μm absorptions as water ice, perhaps with some contribution from ammonia.

The 6.8 μm feature has been suggested to be the bending mode of CH_2 or CH_3 groups (Puetter *et al.* 1979; Hagen *et al.* 1980). If this is correct, the stretching mode from 3.3–3.5 μm (Hagen, Allamandola, and Greenberg 1980) should also be present and correlated with the 6.8 μm optical depth. Table 4 shows no such correlation, but there is a significant correlation between the 6.8 and 2.92 μm optical depths. The physical significance of this correlation is unclear, because we know of no abundant functional groups with bands at these two wavelengths.[9] The statistical evidence is thus of little help in identifying the 6.8 μm feature.

IV. CONTINUUM ENERGY DISTRIBUTIONS

The overall 1.5 to 13 μm energy distributions of the protostars are remarkably similar to blackbody distributions. A blackbody fit between 2.5 and 4 μm, for example, also closely fits the local slopes just shortward of those wavelengths. A single blackbody curve can often be fitted at 4, 8, and 13 μm, although some objects (e.g., AFGL 2884) have slightly broader energy distributions. All of the protostars have convex energy distributions as displayed in Figure 1; the energy distributions of compact H II regions, by contrast, resemble power laws and would be much straighter (e.g., Puetter *et al.* 1979).

The observed blackbody-like energy distributions suggest an optically thick dust cloud. While a blackbody energy distribution could also be produced by optically thin emission from grey dust grains, such a situation is unlikely because the required brightness temperatures of many sources are nearly equal to the color temperatures (Dyck 1980 and references therein). Furthermore, grey grains would have to be larger than the applicable wavelengths, and there is no evidence that such large grains exist.

Dust cooler than the observed color temperatures is needed to produce the observed absorption features, but most objects must have relatively little unobscured hotter dust. If such hot dust were present, emission well above the blackbody curve would be expected at the shortest wavelengths, and the overall energy distribution would be broader than a blackbody. Such emission is seen for AFGL 961 and 989 but not for most of the other sources.

The overall energy distribution of the protostars is probably determined by the radial density distribution of the dust and by possible departures from spherical symmetry (Yorke and Shustov 1981 and references therein). The dust radiative transfer models of Jones and Merrill (1976), for example, imply that in order to produce most of the observed energy distributions, the dust density must decrease at least as steeply with distance from the central heat source as r^{-2}. Both more detailed radiative transfer models and angular diameter measurements at different wavelengths would be valuable for defining the dust emissivity and density distribution.

The evolutionary state of the protostars cannot be specified but is generally consistent with star formation models (Larson 1977 and references therein). In particular, models with blackbody-like energy distributions in the middle infrared and the observed color temperatures have been produced.

[9] Ammonia adsorbed on a silicate clay has bands at slightly longer wavelengths than 2.9 and 6.8 μm (Little 1966), but further investigation is needed to see whether the observed bands can be produced by ammonia in appropriate conditions.

V. CONCLUSIONS

1. Protostars commonly have blackbody-like energy distributions from 2 to 13 μm. Superposed on this continuum are strong absorptions centered at 3.1, 6.0, 6.8, and 9.7 μm.

2. Only weak correlation between the strength of the 3.1 μm (ice) and 9.7 μm (silicate) absorptions is present. Silicate optical depth is relatively large whenever ice absorption is strong, but the reverse is not always true.

3. There is no correlation between the 6.0 or 6.8 μm optical depth and the 9.7 μm optical depth. It is therefore unlikely that the 6.0 or 6.8 μm features can be identified with silicates.

4. The strong correlation between the depths of the 3.1 and 6.0 μm features provides additional evidence that both are primarily due to water ice, possibly with a small amount of ammonia.

5. The optical depth in the long wavelength wing of the ice absorption appears to correlate with the optical depth at the center. This correlation may be partially due to the choice of continuum level, but it tends to imply that large (~ 1 μm), efficiently scattering ice particles are present and contribute at least part of the absorption out to 3.5 μm.

6. There is a correlation between the silicate optical depth and the optical depths near 3.4 μm. This probably implies that the weak 3.4 μm absorption previously seen towards the galactic center is present towards the protostars as well.

7. There is little correlation between the 6.8 μm feature depth and the depth in the 3.3 to 3.5 μm wing of the ice band, but there is a correlation between the 6.8 μm feature and the short wavelength wing of the ice band. The probable contribution of ice extinction at 3.3 to 3.5 μm makes finding a correlation with the 6.8 μm feature more difficult. Thus, although the statistical evidence provides no support for hydrocarbons being an additional absorber from 3.3–3.5 μm and producing the 6.8 μm feature, this identification, which is plausible on other grounds, cannot be ruled out. Additional possibilities for the identification of the 6.8 μm feature, especially any that might explain the correlation with the 2.9 μm optical depth, should be explored.

The authors thank R. R. Joyce and R. C. Capps for communicating data prior to publication and P. M. Harvey, F. O. Williamson, and R. C. Capps for help with some of the observations. The authors are also grateful for the dedicated support of the Kuiper Airborne Observatory staff. This research was supported by NASA grant NGR 05-005-055 and NSF grants AST 76-82890 and AST 79-16885 to UCSD, and by Kitt Peak National Observatory, which is operated by Associated Universities for Research in Astronomy, Inc. under contract with the National Science Foundation.

REFERENCES

Aitken, D. K., and Jones, B. 1973, *Ap. J.*, **184**, 127.
Aitken, D. K., Roche, P. F., Spenser, P. M., and Jones, B. 1981, *M.N.R.A.S.*, **195**, 921.
Allen, M., and Robinson, G. W. 1977, *Ap. J.*, **212**, 396.
Becklin, E. E., and Neugebauer, G. 1968, *Ap. J.*, **147**, 799.
Bertie, J. E., Labbé, H. J., and Whalley, E. 1969, *J. Chem. Phys.*, **50**, 4501.
Blair, G. N., Evans, N. J., II, Vanden Bout, P. A., and Peters, W. L., III. 1978, *Ap. J.*, **219**, 896.
Capps, R. W., Gillett, F. C., and Knacke, R. F. 1978, *Ap. J.*, **226**, 863.
Cohen, M. 1976, *Ap. J.*, **203**, 169.
Downes, D., Genzel, R., Becklin, E. E., and Wynn-Williams, C. G. 1981, *Ap. J.*, **244**, 869.
Dyck, H. M. 1980, *A.J.*, **85**, 891.
Gautier, T. N., III, Fink, U., Treffers, R. R., and Larson, H. P. 1976, *Ap. J. (Letters)*, **207**, L129.
Gillett, F. C., and Forrest, W. J. 1973, *Ap. J.*, **179**, 483.
Gillett, F. C., Forrest, W. J., Merrill, K. M., Capps, R. W., and Soifer, B. T. 1975*a*, *Ap. J.*, **200**, 609.
Gillett, F. C., Jones, T. W., Merrill, K. M., and Stein, W. A. 1975*b*, *Astr. Ap.*, **45**, 77.
Gillett, F. C., and Soifer, B. T. 1976, *Ap. J.*, **207**, 780.
Hagen, W., Allamandola, L. J., and Greenberg, J. M. 1980, *Astr. Ap.*, **86**, L3.
Hagen, W., Tielens, A. G. G. M., and Greenberg, J. M. 1981, *Chem. Phys.*, **56**, 367.
Hall, D. N. B., Kleinmann, S. G., Ridgway, S. T., and Gillett, F. C. 1978, *Ap. J. (Letters)*, **223**, L47.
Jones, T. W., and Merrill, K. M. 1976, *Ap. J.*, **209**, 509.
Joyce, R. R., and Simon, T. 1982, *Ap. J.*, submitted.
Knacke, R. F., and Krätschmer, W. 1980, *Astr. Ap.*, **92**, 281.
Larson, R. B. 1977, *IAU Symposium 75, Star Formation*, ed. T. de Jong and A. Maeder (Dordrecht: Reidel), p. 249.
Leger, A., Klein, J., de Cheveigne, S., Guinet, C., Detourneau, D., and Belin, M. 1979, *Astr. Ap.*, **79**, 256.
Little, L. H. 1966, *Infrared Spectra of Adsorbed Species* (New York: Academic Press), p. 349.
Merrill, K. M., Russell, R. W., and Soifer, B. T. 1976, *Ap. J.*, **207**, 763.
Merrill, K. M., and Soifer, B. T. 1974, *Ap. J. (Letters)*, **189**, L27.
Merrill, K. M., and Stein, W. A. 1976*a*, *Pub. A.S.P.*, **88**, 285.
———. 1976*b*, *Pub. A.S.P.*, **88**, 874.
Mukai, T., Mukai, S., and Noguchi, K. 1978, *Ap. Space Sci.*, **53**, 77.
Penston, M. V., Allen, D. A., and Hyland, A. R. 1971, *Ap. J. (Letters)*, **170**, L33.
Pipher, J. L., and Soifer, B. T. 1976, *Astr. Ap.*, **46**, 153.
Puetter, R. C., Russell, R. W., Soifer, B. T., and Willner, S. P. 1979, *Ap. J.*, **228**, 118.
Russell, R. W., Soifer, B. T., and Puetter, R. C. 1977, *Astr. Ap.*, **54**, 959.
Scoville, N. Z., Hall, D. N. B., Kleinmann, S. G., and Ridgway, S. T. 1979, *Ap. J. (Letters)*, **232**, L121.
Smith, H. A., Larson, H. P., and Fink, U. 1979, *Ap. J.*, **233**, 132.
Soifer, B. T., Puetter, R. C., Russell, R. W., Willner, S. P., Harvey, P. M., and Gillett, F. C. 1979, *Ap. J. (Letters)*, **232**, L53.
Soifer, B. T., Russell, R. W., and Merrill, K. M. 1976, *Ap. J.*, **210**, 334.
Soifer, B. T., Willner, S. P., Capps, R. C., and Rudy, R. J. 1981, *Ap. J.*, **250**, 631.
Thompson, R. I., and Tokunaga, A. T. 1978, *Ap. K.*, **226**, 119.
———. 1979*a*, *Ap. J.*, **229**, 153.
———. 1979*b*, *Ap. J.*, **231**, 736.
Werner, M. W., Becklin, E. E., Gatley, I., Matthews, K., and Wynn-Williams, C. G. 1979, *M.N.R.A.S.*, **188**, 463.
Werner, M. W., Becklin, E. E., and Neugebauer, G. 1977, *Science*, **197**, 723.
Willner, S. P. 1976, *Ap. J.*, **206**, 728.
———. 1977, *Ap. J.*, **214**, 706.

Willner, S. P., Puetter, R. C., Russell, R. W., and Soifer, B. T. 1980, *IAU Symposium 87, Interstellar Molecules*, ed. B. H. Andrew (Dordrecht: Reidel), p. 381.
Willner, S. P., Puetter, R. C., Russell, R. W., Soifer, B. T., and Harvey, P. M. 1979, *Ap. J. (Letters)*, **229**, L65.
Woolf, N. J., and Ney, E. P. 1969, *Ap. J. (Letters)*, **155**, L181.
Wright, E. L., Lada, C. J., Fazio, G. G., and Kleinmann, D. E. 1977, *A.J.*, **82**, 132.
Wynn-Williams, C. G. 1977, *IAU Symposium 75, Star Formation*, ed. T. de Jong and A. Maeder (Dordrecht: Reidel), p. 105.
Wynn-Williams, C. G., and Becklin, E. E. 1974, *Pub. A.S.P.*, **86**, 5.
Wynn-Williams, C. G., Becklin, E. E., and Neugebauer, G. 1974, *Ap. J.*, **187**, 473.
Yorke, H. W., and Shustov, B. M. 1981, *Astr. Ap.*, **98**, 125.

F. C. GILLETT and K. M. MERRILL: Kitt Peak National Observatory, P.O. Box 26732, Tucson, AZ 85726

T. L. HERTER and J. L. PIPHER: Department of Physics and Astronomy, University of Rochester, Rochester, NY 14627

B. JONES and R. C. PUETTER: C-011, University of California, La Jolla, CA 92093

J. KRASSNER: Research Department, M.S. A01-26, Grumman Aerospace Corporation, Bethpage, NY 11714

R. J. RUDY: Steward Observatory, University of Arizona, Tucson, AZ 85721

R. W. RUSSELL: Space Sciences Laboratory, The Aerospace Corporation A6-2617, P.O. Box 92957, Los Angeles, CA 90009

B. T. SOIFER: 320-47, California Institute of Technology, Pasadena, CA 91125

S. P. WILLNER: Harvard-Smithsonian Center for Astrophysics, 60 Garden Street, Cambridge, MA 02138

THE ASTROPHYSICAL JOURNAL, 260:141–146, 1982 September 1

OBSERVATION OF INTERSTELLAR AMMONIA ICE

R. F. KNACKE,[1,2] S. MCCORKLE,[1] R. C. PUETTER,[3] E. F. ERICKSON,[4] AND W. KRÄTSCHMER[2]
Received 1981 December 14; accepted 1982 March 15

ABSTRACT

An absorption band probably due to solid ammonia on interstellar grains has been detected in the infrared spectrum at 2.97 μm of the Becklin-Neugebauer object and probably in NGC 2264-IR. An ammonia-water amorphous ice mixture can explain the structure of the new band and of the 3.07 μm interstellar absorption. Laboratory data suggest that a long wavelength wing extending to 3.5 μm in interstellar dust spectra may be absorption by $NH_3 \cdot H_2O$ complexes in the ices. In the molecular cloud obscuring the BN object, about 20 times as much NH_3 is frozen in grains as exists in the gas phase, suggesting that gas-grain interactions may be important in the ammonia chemistry of molecular clouds. Arguments are given that interstellar features at 6.0 and 6.8 μm are also ammonia-related absorptions.

Subject headings: infrared: spectra — interstellar: matter — interstellar: molecules — line identification — nebulae: Orion Nebula

I. INTRODUCTION

The spectra of most astronomical sources showing the interstellar dust absorption feature near 3.07 μm agree poorly with laboratory spectra of water ice in the wings of the band. It has been proposed that in addition to H_2O ice, another absorber, such as ammonia ice, may be present to account for the short wavelength structure of the observed band (Merrill, Russell, and Soifer 1976) and its long wavelength wing. Several other possibilities are a C–H absorption (Capps, Gillett, and Knacke 1978), a hydrated silicate (Knacke and Krätschmer 1980), or an alcohol (Hagen, Allamandola, and Greenberg 1980). Since fundamental vibration-absorption frequencies of C–H, N–H, and O–H groups all occur between 2.5 and 3.5 μm in various substances, the significance of this wavelength interval to interstellar grain studies is apparent. However, previous observations have been limited by interference of atmospheric water vapor. This closes the 2.5–2.85 μm interval to ground-based observations so that the complete band structure could not be determined. Noise and limited atmospheric transmission also hamper observations between 2.85 and 3.5 μm. To overcome the limitations imposed by the atmosphere, we obtained observations with NASA's Kuiper Airborne Observatory. Above the tropopause, water vapor interference is minimal even in the center of the atmospheric 2.7 μm water band, although there is still appreciable absorption by telluric CO_2. In this paper we present the first complete interstellar absorption spectra between 2.5 and 3.3 μm.

[1] Astronomy Program, Department of Earth and Space Sciences, State University of New York, Stony Brook.
[2] Max-Planck-Institut für Kernphysik, Heidelberg.
[3] Center for Astrophysics and Space Sciences, University of California, San Diego.
[4] NASA Ames Research Center.

II. OBSERVATIONS

Observations were made with a circular variable filter (CVF) spectrometer at the bent Cassegrain focus of the Kuiper telescope. The resolution, including the effects of beam size, was approximately 1.2%. It is noteworthy for the discussion below that this resolution is higher than the 1.5%–2.0% employed in many earlier studies of interstellar ice (cf. Merrill, Russell, and Soifer 1976; Gillett and Forrest 1973). The detector was a nitrogen-cooled InSb cell with a 25″ aperture. Best noise response was found to be at 14 Hz. This is a lower chopper frequency than usually used at the Kuiper telescope and appears to be possible because of the low background conditions at the short wavelengths employed in this experiment.

At an altitude of 12.5 km, atmospheric transmission in the 2.5–3.5 μm range is very high. Figure 1*a* is a spectrum of the star 29 Ori. Since this star has a smooth spectrum in this part of the infrared, the observations show the relative transmission at 12.5 km. The remaining strong atmospheric feature is a band of CO_2 at 2.75 μm.

Several highly reddened sources were observed on the nights of 1981 February 18, 19, and 21. A spectrum of the Becklin-Neugebauer object (BN) is shown in Figure 1*b*. Such spectra taken in the three observing nights were corrected for atmospheric extinction by dividing by the spectrum of the nearby, unreddened calibration star 29 Ori, and summed. The result is shown in Figure 2*a*. The statistical noise is indicated by the error bars; when none are shown, the calculated errors are smaller than the data points. The spectrum is dominated by the interstellar water ice band at $\sim$3.07 μm. This band has a weaker feature in its wing at 2.97 ± 0.10 μm, which is apparently resolved from the water ice feature for the first time here. Apparent structure at 2.63 and 2.72 μm may be noise introduced by incomplete correction of the

C - 3

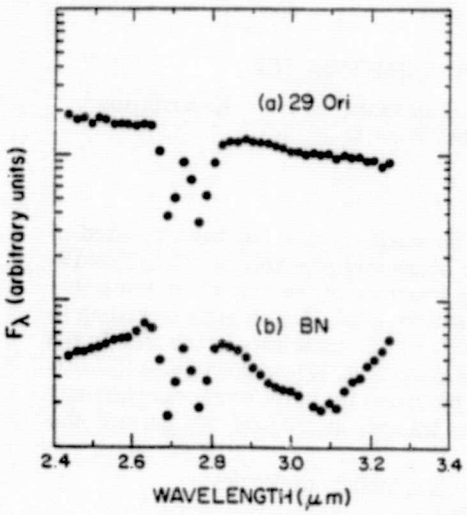

FIG. 1.—Spectra of (*a*) 29 Ori and (*b*) BN, uncorrected for atmospheric absorption. The absorption bands between 2.6 and 2.8 μm are atmospheric CO_2.

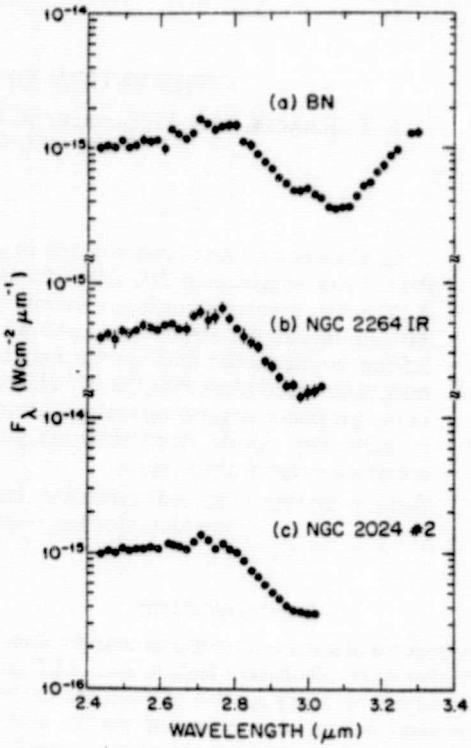

FIG. 2.—Spectra of (*a*) BN, (*b*) NGC 2264-IR, and (*c*) NGC 2024 No. 2, corrected for atmospheric absorption by dividing by a nearby calibration star. Apparent structure between 2.6 and 2.8 μm is probably the result of incomplete correction for the very strong CO_2 band.

strong CO_2 bands, but further observations are needed to check this point. We also obtained spectra of the infrared sources NGC 2264-IR (Allen 1972) and NGC 2024 No. 2 (Grasdalen 1974) (Figs. 2*b* and 2*c*). These spectra cover a smaller part of the ice band, but the feature at 2.97 μm is probably also present in NGC 2264-IR. The source NGC 2024 No. 2 has a smoother spectrum near 2.97 μm, although the shape of the short wavelength wing resembles that in BN. This may reflect a real difference in the composition of the ices in the sources. Unfortunately, time limitations allowed us to observe NGC 2024 No. 2 only once, and we do not have good error estimates for the data.

In earlier observations of BN (Merrill, Russell, and Soifer 1976), there is poorly defined structure near 2.97 μm, but the band is unresolved at lower resolution. A clearer indication of such structure may be present in the spectrum of W51 (Puetter *et al.* 1979), and there are hints in other spectra also (Merrill and Stein 1976). Merrill, Russell, and Soifer (1976), and later Hagen, Allamandola, and Greenberg (1980), proposed that this structure could be ammonia ice in absorption. The higher resolution and greatly improved atmospheric transmission have made the 2.97 μm feature stand out in the present data so that its existence as a separate band is now established.

III. BAND IDENTIFICATION

A band near 3 μm caused by a relatively abundant species (as will be shown in § IV) is strongly suggestive of an O–H or N–H group vibrational absorption. The only other likely candidate known to us is the C–H group absorption. However, absorptions of the C–H group tend to fall in the 3.0–3.4 μm range (Herzberg 1945), well away from the observed band. Therefore we rule C–H out as a possible identification for the 2.97 μm band.

Hydroxyl groups could be present in grains either as water ice or as functional groups in silicates of the hydrated types. We have investigated numerous models of water ice in crystalline and amorphous phases, with grain size distributions, and as mantles on dielectric grains. No feature at all resembling the observed structure at 2.97 μm was found. The ice absorption is at longer wavelengths. We did obtain good fits to the 3.07 μm band with amorphous water ice (see below).

A discussion of the spectra of hydrated silicates with reference to interstellar dust was given by Knacke and Krätschmer (1980). Lattice hydroxyls often have a sharp feature near 2.71 μm due to structural OH and a broader band extending to 3.5 μm due to weakly hydrogen bonded OH groups. None of the three sources observed show convincing sharp structure at 2.71 μm. A plot showing the broad OH and H_2O absorption structure in Murchison, a meteorite containing mainly hydrated mineral, is shown in Figure 3*a*. Although optical constants needed for detailed comparisons are not available, the spectrum shows the typical problems with such an identification. The hydrated silicate band is too broad and is not centered at the observed band. Another difficulty is that the long wavelength wing of the inter-

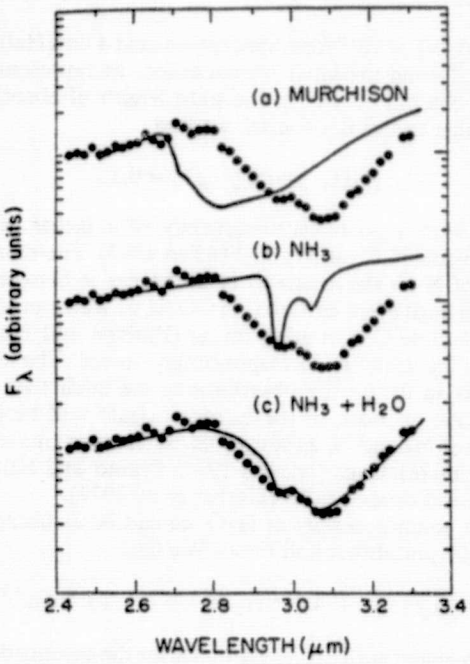

FIG. 3.—Comparison of the BN data (*filled circles*) with spectra (*solid lines*) of (*a*) Murchison meteorite, (*b*) ammonia ice particles (0.2 μm diameter), and (*c*) a water-ammonia ice mixture of 4:1 (1.0 μm diameter).

stellar band (not shown in Fig. 2, see Merrill, Russell, and Soifer 1976) could not be caused by a hydrated silicate band of the strength indicated by the observations. Finally, strong hydrated silicate absorption seems less likely than an absorption by more volatile compounds in view of the weakness of the 3 μm feature in unshielded clouds (Gillett *et al.* 1975; Merriil, Russell, and Soifer 1976). Therefore, we believe that hydroxyl absorptions in a mineral matrix are also an unlikely identification for the 2.97 μm feature.

The position of the interstellar band is highly suggestive of ammonia, probably in the solid phase. In gaseous ammonia, the ν_1 at 2.997 μm and the ν_3 near 2.93 μm fundamental vibrations occur near the observed band (Herzberg 1945). With the optical constants of Robertson *et al.* (1975), we calculate that particles of ammonia ice smaller than 0.5 μm absorb most strongly at 2.97 μm, in better agreement with the observations. A calculated spectrum of NH_3 ice particles 0.2 μm in diameter (Fig. 3*b*) shows the good wavelength coincidence with the interstellar band. A Mie calculation of a model consisting of a 4:1 mixture of ammonia ice particles and amorphous water ice particles (optical constants of Léger *et al.* 1979) is shown in Figure 3*c*. Such models give a quite reasonable fit to the data if large particles with mean sizes in the range 0.6–2.0 μm in diameter are assumed. Large particles are, in fact, indicated by polarization observations of dense cloud regions (Carrasco, Strom, and Strom 1973; Breger 1977; Harris, Woolf, and Rieke 1978). An exact fit is not attempted now because the optical constants of ammonia are temperature and phase dependent. The Robertson *et al.* (1975) constants used were obtained for ammonia ice at approximately 193 K, while the predominant grain temperature of ices in our beam is ≤ 100 K (Erickson *et al.* 1980). Amorphous water ice is necessary to give a good fit; crystalline ice (Bertie, Labbé, and Whalley 1969) gives a decidedly poorer fit.

A more plausible model of icy interstellar grains would consist of ammonia and water ices mixed in the same particles. For this reason, we are studying ammonia hydrates ($NH_3 \cdot H_2O$) in the laboratory. A preliminary spectrum of a mixture in the ratio of approximately 5 to 1 is shown in Figure 4. This spectrum and others (not shown) that we have obtained indicate that a water-ammonia mixture in the ratios of 4 ± 1 to 1 gives reasonable agreement with the interstellar spectra, thus supporting the conclusions of the model calculations. The detailed results of the laboratory investigations will be published in a future paper. Besides the 2.95 μm absorption, there is also absorption near 3.4 μm in Figure 4. It occurs in spectra of ammonia hydrates but *not* in spectra of either ice separately. Waldron and Hornig (1953) proposed vibration of an NH–O bond as the most likely origin of this band. This absorption provides an attractive explanation for at least part of the long wavelength wing of the interstellar band (§ I), without invoking new constituents. Many sources also have an inflection near 3.3 μm similar to the inflection at this wavelength in Figure 4. Note that in this explanation, the wing should always be present when ammonia hydrates occur on grains, but not in the case of a pure water ice mantle.

An interesting object from this point of view is OH 231.8+4.2 (Gillett and Soifer 1976). It has a narrower, sharper feature than most other ice sources and also a weak long wavelength wing. This, in the above interpretation, could be a case where NH_3 ice and the consequent wing are absent. There is evidence that the absorbing material in OH 231.8+4.2 is heated by a changing luminosity of the underlying source.

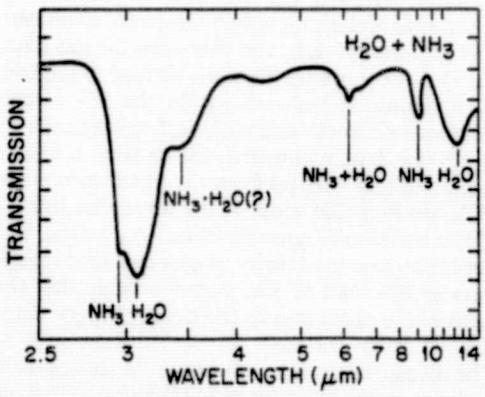

FIG. 4.—A laboratory spectrum of (thin layer) water-ammonia ice mixture (H_2O:$NH_3 \approx 5$:1). The temperature was 70 K.

In summary, an ammonia-water ice mixture gives a satisfactory fit to the interstellar features near 3 μm, including the structure within the band and its long wavelength wing. As a volatile ice, this mixture is consistent with the occurrence of the 3 μm feature solely in dense clouds. We have found no other abundant molecule or solid with a strong band at 2.97 μm. That the observed ammonia is frozen rather than gaseous is suggested by the better wavelength agreement with the solid. In the next section we also show that abundance comparisons with NH_3 detected in the radio rule out a gaseous origin for the 2.97 μm NH_3 band.

IV. DISCUSSION

Using the fit shown in Figure 3c, we infer a column density of ammonia molecules to BN of

$$N(NH_3, 2.95\ \mu m) = 1 \times 10^{18}\ cm^{-2}\ ,$$

where we have used an ammonia density of 0.6 g cm^{-3} (*Handbook of Chemistry and Physics* 1980). We believe that the uncertainty in this estimate is on the order of a factor of 2–3 because (1) the background source continuum in the BN spectrum in the 2.7–3.3 μm region is uncertain; and (2) the optical constants of ammonia are temperature dependent, and the constants measured at 193 K are probably not exactly correct for the lower temperatures characteristic of ices in the Orion molecular cloud.

The column density of ammonia estimated here is much greater than that inferred from radio measurements of ammonia in the gas phase. Ammonia abundances in the KL region have recently been reevaluated by Barrett, Ho, and Myers (1977), Sweitzer (1978), and Sweitzer *et al.* (1979). Barrett *et al.* derive a column density of $N(NH_3, gas) \approx 4 \times 10^{16}\ cm^{-2}$. Sweitzer (1978) modeled several NH_3 lines and found $n(NH_3) \approx 0.5\ cm^{-3}$ in a region 16″ in diameter ($\sim 10^{17}$ cm). This gives $5 \times 10^{16}\ cm^{-2}$, in good agreement with the Barrett *et al.* estimate. BN lies near the edge of the indirectly inferred 16″ diameter dense region centered on KL, and therefore the gas density to BN may not be exactly the same as that to the source of NH_3 emission. It lies well inside the SO distribution centered on KL measured with high resolution by Welch *et al.* (1981). If we assume that the density in front of BN is similar to that derived from the observations centered on KL, we find that most of the ammonia (by a factor ≥ 20) in the clouds must be frozen on grains. This is a lower limit since the density of gaseous ammonia should be less to BN than to KL, and it is likely that the path lengths of the radio measurements are longer than those measured in the infrared.

The measured amount of ammonia ice appears to be consistent with abundance constraints. The column density of gaseous carbon monoxide (CO does not freeze at the temperature believed to be characteristic of the KL region) to BN is estimated to be $N(CO) \approx 2 \times 10^{19}\ cm^{-2}$ from radio measurements (Liszt *et al.* 1974) and $N(CO) \approx 1 \times 10^{19}$ from absorption near 4 μm (Hall *et al.* 1978). Taking the latter measurement as representative of the column density in the path length of absorption by grains to the BN source, we find

$$[NH_3, grains]/[CO] = 0.1\ ,$$

again with a probable uncertainty of a factor of 2–3. The cosmic N/C ratio is 0.32 (Allen 1973). Therefore the ratio of N on the grains to N in the gas is between 0.1 and 1 if most of the carbon is in CO. If, as seems probable, considerable C is in other forms (Phillips and Huggins 1981), the ratio is correspondingly lower. The uncertainties in fitting the observations are such that large amounts, or most, of the nitrogen could still be in the forms of N_2 and N, as suggested by calculations of ion-molecule reactions (Iglesias 1977; Prasad and Huntress 1980) and observations (Herbst *et al.* 1977).

The column density of H_2O ice can be estimated for the 3.07 μm absorption band. We find

$$N(H_2O\ ice) \approx 4N(NH_3\ ice) \approx 4 \times 10^{18}\ cm^{-2}\ ,$$

in agreement with earlier estimates for the column density of H_2O to BN by Gillett and Forrest (1973). Waters *et al.* (1980) estimated $10^{17} < N(H_2O, gas) < 10^{18}\ cm^{-2}$ to KL. This density, while uncertain, suggests abundances higher than those predicted by Herbst and Klemperer (1973), but close to the predictions of Mitchell, Ginsberg, and Kuntz (1978) and Prasad and Huntress (1980). In time-dependent calculations including condensation in grains, all the abundances depend strongly on the cloud age, with time scales on the order of 3×10^5 years (Iglesias 1977). From this initial estimate, the amount of H_2O frozen on the grains appears to be of the same order as the amount in the gas in the BN cloud.

The results of ion-molecule reaction calculations that do not include reactions on grains (except for H_2) give $[NH_3]/[H_2]$ abundances (in the gas phase) of a minimum of $\sim 4 \times 10^{-10}$ (Herbst and Klemperer 1973), a maximum of $\sim 1 \times 10^{-6}$ (Mitchell, Ginsberg, and Kuntz 1978), and other values in between (Prasad and Huntress 1980; Graedel, Langer, and Frerking 1981). With the above column densities we find

$$[NH_3, grains]/[H_2] \approx 1 \times 10^{-5}\ ,$$

compared to the gas abundance in the Orion cloud (Sweitzer 1978) of $[NH_3, gas]/[H_2] \approx 5 \times 10^{-7}$. The large amount of NH_3 on the grains is evidence for gas-grain interactions. Since observed amounts of gaseous and solid ammonia strain the predictions of ion-molecule schemes, it seems that reactions on grains could be an additional source of ammonia.

Sweitzer (1978) suggested that the gas abundance is indicative of ammonia evaporation from grains. His estimated abundance of $[NH_3, ice]/[H_2] \approx (2\text{–}4) \times 10^{-5}$ required for this process is close to the present measured value, but the calculation is strongly temperature dependent, and the H_2 density is also somewhat uncer-

tain. In the ion-molecule calculations, most nitrogen tends to occur as molecular N_2 and atomic N. Although N_2 may not be highly reactive on grain surfaces, it seems that N would be, and that it would react to the saturated form, NH_3, as was proposed by van de Hulst (1949) and by Watson and Salpeter (1972). In any event, the presence of ammonia ice in clouds suggests that gas-grain interactions are a necessary part of reaction sequences of nitrogen-containing molecules.

Corroborating evidence for the presence of ammonia ice could be sought in the detection of the ν_4 ammonia band at 6 μm and the ν_2 band near 9.4 μm in pure, solid ammonia. There is an absorption near 6 μm in several heavily reddened sources (Soifer *et al.* 1979). However, water ice also absorbs near 6 μm, so the presence of this band is only corroboratory evidence for the NH_3 identification. The predicted ν_2 NH_3 interstellar absorption would occur where many sources show substantial infrared emission and where the wing of the 9.8 μm silicate band interferes, but a careful search for this NH_3 band might be productive. In ice mixtures, however, the ν_2 band center shifts. In a 5:1 water-ice mixture, the center is near 9.0 μm (Fig. 4). Observation of this band shift would provide strong support for ammonia hydrates on the grains.

Another unidentified interstellar band in heavily obscured sources is at 6.78 $\pm$ 0.08 μm (Soifer *et al.* 1979). The ammonia identification suggests a possible origin for this band also. Ammonia absorbed into clay minerals forms the ammonium ion (NH_4^+) upon interacting with H_2O in interlayer positions (Little 1966). The ν_4 deformation mode of ammonium absorbs near 6.8 μm. In different montmorillonites, the band lies between 6.85 and 6.97 μm (Mortland *et al.* 1963). Thus this is an attractive possibility for the 6.78 μm band in the context of ammonia-grain interactions, although it should be noted that the wavelength coincides with other possible absorbers also (Soifer *et al.* 1979; Knacke and Krätschmer 1980). The ammonium ion has a stretching mode that lies between 3.0 and 3.05 μm in clays (Mortland *et al.* 1963). This band would be hidden by the water ice. Possible indications of clay minerals in interstellar grains have been discussed by Zaikowski and Knacke (1975) and Knacke and Krätschmer (1980), but the evidence cannot be considered conclusive. Further observations are needed to clarify the nature of the interstellar silicate as well as of the ices.

V. CONCLUSIONS

1. A new interstellar band at 2.97 μm is identified as ammonia ice on interstellar grains.
2. In the molecular cloud associated with the BN/KL complex, there is about 20 times as much ammonia frozen on the grains as is in the gas phase. Evidently gas-grain interactions are important in the nitrogen chemistry of molecular clouds.
3. Bands at 3.4 μm and 6.0 μm, observed in interstellar dust, are probably absorptions of ammonia-water ice mixtures.
4. An interstellar band at 6.8 μm may be absorption by ammonium (NH_4^+) ions in clay minerals.

We would like to thank the staff of the Kuiper Airborne Observatory for their unstinting support and generous cooperation. We thank Dr. K. Kitta for helpful comments. This research was supported by NASA grant NAG 256.

REFERENCES

Allen, C. W. 1973, *Astrophysical Quantities* (London: Athlone).
Allen, D. A. 1972, *Ap. J. (Letters)*, **172**, L55.
Barrett, A. H., Ho, P. T. P., and Myers, P. J. 1977, *Ap. J. (Letters)*, **211**, L39.
Bertie, J. E., Labbé, H. J., and Whalley, E. 1969, *J. Chem. Phys.*, **50**, 4501.
Breger, M. 1977, *Ap. J.*, **215**, 119.
Capps, R. W., Gillett, F. C., and Knacke, R. F. 1978, *Ap. J.*, **226**, 863.
Carrasco, L., Strom, S. E., and Strom, K. M. 1973, *Ap. J.*, **182**, 95.
Erickson, E. F., Knacke, R. F., Tokunaga, A. T., and Haas, M. R. 1980, *Ap. J.*, **245**, 148.
Gillett, F. C., and Forrest, W. J. 1973, *Ap. J.*, **179**, 483.
Gillett, F. C., Jones, T. W., Merrill, K. M., and Stein, W. A. 1975, *Astr. Ap.*, **45**, 77.
Gillett, F. C., and Soifer, B. T. 1976, *Ap. J.*, **207**, 780.
Graedel, T. E., Langer, W. D., and Frerking, M. A. 1981, preprint.
Grasdalen, G. L. 1974, *Ap. J.*, **193**, 373.
Hagen, W., Allamandola, L. J., and Greenberg, J. M. 1980, *Astr. Ap.*, **86**, L3.
Hall, D. N. B., Kleinmann, S. G., Ridgway, S. T., and Gillett, F. C. 1978, *Ap. J.*, **223**, L47.
Harris, D. H., Woolf, N. J., and Rieke, G. H. 1978, *Ap. J.*, **226**, 829.
Herbst, E., Green, S., Thaddeus, P., and Klemperer, W. 1977, *Ap. J.*, **215**, 503.
Herbst, E., and Klemperer, W. 1973, *Ap. J.*, **285**, 505.
Herzberg, G. 1945, *Molecular Spectra and Molecular Structure*, Vol. 2 (New York: Van Nostrand Reinhold).
Iglesias, E. 1977, *Ap. J.*, **218**, 697.
Knacke, R. F., and Krätschmer, W. 1980, *Astr. Ap.*, **92**, 281.
Léger, A., Klein, J., de Cheveigne, S., Guinet, C., Defourneau, D., and Belin, M. 1979, *Astr. Ap.*, **79**, 256.
Liszt, H. S., Wilson, R. W., Penzias, A. A., Jefferts, K. B., Wannier, D. G., and Solomon, P. M. 1974, *Ap. J.*, **190**, 557.
Little, L. H. 1966, in *Infrared Spectra of Absorbed Species* (New York: Academic Press), p. 334.
Merrill, K. M., Russell, R. W., and Soifer, B. T. 1976, *Ap. J.*, **207**, 763.
Merrill, K. M., and Stein, W. A. 1976, *Pub. A.S.P.*, **88**, 294.
Mitchell, G. F., Ginsberg, J. L., and Kuntz, P. J. 1978, *Ap. J. Suppl.*, **38**, 39.
Mortland, M. M., Fripiat, P. J., Chaussidon, J., and Uytterhoeven, J. 1963, *J. Phys. Chem.*, **67**, 248.
Phillips, T. G., and Huggins, P. J. 1981, *Ap. J.*, **251**, 533.
Prasad, S. S., and Huntress, W. T. 1980, *Ap. J.*, **239**, 151.
Puetter, R. C., Russell, R. W., Soifer, B. T., and Willner, S. P. 1979, *Ap. J.*, **228**, 118.
Robertson, C. W., Downing, H. D., Curnutte, B., and Williams, D. 1975, *J. Opt. Soc. Am.*, **65**, 432.
Soifer, B. T., Puetter, R. C., Russell, R. W., Willner, S. P., Harvey, P. M., and Gillett, F. C. 1979, *Ap. J. (Letters)*, **232**, L53.
Sweitzer, J. S. 1978, *Ap. J.*, **225**, 116.
Sweitzer, J. S., Palmer, P., Morris, M., Turner, B. E., and Zuckerman, B. 1979, *Ap. J.*, **227**, 415.
van de Hulst, H. C. 1949, *Rech. Astr. Obs. Utrecht*, Vol. 2, Part 2.

Waldron, R. D., and Hornig, D. F. 1953, *J. Amr. Chem. Soc.*, **75**, 6079.
Waters, J. W., Gustincic, J. J., Kakar, R. K., Kuiper, T. B. H., Roscoe, H. K., Swanson, P. N., Rodriguez Kuiper, E. N., Kerr, A. R., and Thaddeus, P. 1980, *Ap. J.*, **235**, 57.
Watson, W. D., and Salpeter, E. E. 1972, *Ap. J.*, **174**, 321.
Welch, W. J., Wright, M. C. H., Plambeck, R. L., Bieging, J. H., and Baud, B. 1981, *Ap. J. (Letters)*, **245**, L87.
Zaikowski, A., and Knacke, R. F. 1975, *Ap. Space Sci.*, **37**, 3.

E. F. ERICKSON: NASA Ames Research Center, Moffett Field, CA 94035

R. F. KNACKE and S. MCCORKLE: Department of Earth and Space Sciences, SUNY, Stony Brook, NY 11794

W. KRÄTSCHMER: Max Planck Institut für Kernphysik, Postfach 103980, 6900 Heidelberg, West Germany

R. C. PUETTER: C-011, University of California at San Diego, La Jolla CA 92093

THE ASTROPHYSICAL JOURNAL, 262:153–163, 1982 November 1

ABUNDANCES IN FIVE NEARBY GALACTIC H II REGIONS FROM INFRARED FORBIDDEN LINES

T. HERTER,[1] H. L. HELFER, AND J. L. PIPHER[1]
Department of Physics and Astronomy, University of Rochester
D. A. BRIOTTA, JR., W. J. FORREST, AND J. R. HOUCK
Department of Astronomy, Cornell University
AND
R. J. RUDY AND S. P. WILLNER
Center for Astrophysics and Space Sciences, University of California at San Diego
Received 1982 March 1; accepted 1982 May 3

ABSTRACT

Airborne measurements of the [Ar II] (6.99 μm) and [S III] (18.71 μm) lines for five compact H II regions in the solar neighborhood are presented, as well as 2–4 μm and 8–13 μm spectroscopy where available. From these data and radio data we deduce lower limits to the elemental abundances of Ar, Ne, and S. Some of these H II regions suffer substantial nebular extinction, and some are extended. After correcting for beam size effects and extinction, we find that four of the objects are consistent with standard abundances, within the uncertainties of correcting for unobserved ionization states. A Perseus arm object, S156, is apparently overabundant in sulfur.

Subject headings: infrared: spectra — nebulae: abundances — nebulae: H II regions

I. INTRODUCTION

Observations of infrared fine-structure lines in H II regions provide a probe of nebular conditions (Lacy 1980). Optical observations, which are limited by interstellar extinction to H II regions within a few kiloparsecs of the Sun, have yielded information on atomic abundances, excitation, temperature, and density of the gas (e.g., Hawley, 1978). Radio observations, while not suffering extinction, offer abundance determinations only for He^+ and sometimes C^+. Although extinction corrections may be significant, infrared observations are not so severely limited by extinction as those at optical wavelengths (Herter *et al.* 1981, hereafter Paper I). The benefits of probing to large distances from the Sun, or deep within a local molecular cloud, and the lack of severe temperature dependence of the lines make infrared fine-structure lines well suited for abundance analyses in our Galaxy.

In this paper we report ground-based and airborne spectroscopic observations of fine-structure lines from 2 to 30 μm for the compact H II region complexes of S156, S88B, S106, NGC 2170 (Mon R2), and Orion. Since these regions are all relatively nearby (9–13 kpc from the galactic center), and since all have optical counterparts, we have the opportunity to compare available optically determined abundances with the infrared estimates presented here. These observations, in concert with those reported previously (Paper I), will be used to discuss potential abundance and/or excitation gradients in the Galaxy.

The fine-structure lines studied here include [Ar III] (8.99 μm) and [Ar II] (6.99 μm); [S III] (18.7 μm) and [S IV] (10.51 μm); and [Ne II] (12.81 μm). These argon and sulfur ionization states constitute the major ionization states for H II regions with exciting stars of temperature $T_* = 30{,}000$–$45{,}000$ K for sulfur, and $T_* = 25{,}000$–$40{,}000$ K for argon according to simple, dust-free ionization structure models (e.g., Lacasse *et al.* 1980; Lacy 1980). Thus, we can measure total atomic abundances.

To estimate the extinction to the emission line regions we measure the ratio of the Brα/Brγ hydrogen recombination line strengths, the ratio of the Brackett lines to the free-free radio flux, and the depth of the 9.7 μm silicate feature.

II. OBSERVATIONS

The data described here were obtained with a variety of infrared systems. The 2–4 μm and 8–13 μm data were primarily obtained either at Kitt Peak National Observatory (KPNO) or the University of California at San Diego-University of Minnesota Mount Lemmon Observatory using CVF spectrometers with resolutions $\Delta\lambda/\lambda \sim 0.013$–$0.02$. These data, both previously published and new results, are noted in Table 1. Sampling densities are typically one to two data points per resolution element.

The 4–8 μm data reported here consist of observations in the [Ar II] line and adjacent continuum using the UCSD filter wheel spectrometer (Russell,

[1] Visiting Astronomer at Kitt Peak National Observatory, which is operated by the Association of Universities for Research in Astronomy, Inc., under contract with the National Science Foundation.

TABLE 1

LINE FLUXES

Object	Line	$\tau_{9.7}$	Measured Line Flux (10^{-18} W cm^{-2})	Aperture (arcsec)	Reference	Line Flux Corrected for Extinction (10^{-18} W cm^{-2})
S88B	Ar III	3.6 ± 1.0	0.4 ± 0.2	11	1	7 ± 7
	S IV		0.7 ± 0.2	11	1	15 ± 13
	Ne II		7.0 ± 0.9	11	1	26 ± 11
	S III		9.0 ± 1.6	30	2	80 ± 50
	Ar II		12.0 ± 1.0	27	2	37 ± 12
S156	Ar III	0	1.5 ± 0.2	11	2	1.5 ± 0.2
	S IV		...	11	2	...
	Ne II		7.8 ± 0.9	11	2	7.8 ± 0.9
	S III		21 ± 4	30	2	21 ± 4
	Ar II		≤7.5	27	2	≤7.5
S106[a] Source 2	Ar III	1.5	<0.8	11	2	<3
	S IV		<2.0	11	2	<7
	Ne II		14.4 ± 1.9	11	2	25 ± 3
	S III		20.8 ± 3.0	30	2	52 ± 7
	Ar II		12.2 ± 1.2	27	2	19 ± 2
NGC 2170 IRS 1	Ar III	2.1 ± 0.3[b]	<2.0	7	2	<9
	S IV		<0.75	7	2	<4.5
	Ne II		23.0 ± 1.6	7	2	51.0 ± 6.0
	S III		14 ± 3	30	2	51 ± 15
	Ar II		14 ± 4	27	2	26 ± 8
M42 (20″ N θ^1C)	Ar III	0	3.4 ± 0.7	11	2	3.4 ± 0.7
	S IV		7.2 ± 1.0	11	2	7.2 ± 1.0
	Ne II		6.6 ± 0.5	11	2	6.6 ± 0.5
	S III		93 ± 12	30	2	93 ± 12
	Ar II		<12	27	2	<12

[a] S106 source 1, 15″ beam, almost identical line fluxes to S106 source 2.
[b] Adopted uncertainty.
REFERENCES.—(1) Pipher *et al.* 1977. (2) This paper.

Soifer, and Willner 1977; Puetter *et al.* 1979) on flights of the Kuiper Airborne Observatory (KAO) in 1979 June and December. For these observations a 27″ focal plane aperture was employed, and the chopped beam spacing and orientation were chosen to avoid beam cancellation.

The 16–30 μm data consist of spectra obtained with the Cornell University cooled grating spectrometer (McCarthy *et al.* 1979) on flights of the KAO in 1980 March and July. A focal plane aperture of 30″ and choice of beam throw similar to that used with the UCSD instrument were employed. The spectral resolution over the [S III] line is 0.2 μm, sampled at a density of approximately three points per resolution element. The complete spectra from 2–30 μm are presented in Figures 1–3 and 5–6. When different beam sizes were employed in different wavelength regions, we have *not* attempted to correct for beam size effects in plotting these spectra, since the ionization structure of the region prohibits simple scaling of the line intensities.

The observed line fluxes (uncorrected for extinction) are listed in Table 1 along with the beam sizes and references for the observations. The line fluxes for all but [Ar II] have been derived from a detailed line fit to the observations of the form $F_\lambda = a + b\lambda + c\{\exp -[(\lambda - \lambda_c)/\sigma_\lambda]^2\}$; that is, a linear continuum plus unresolved line emission at $\lambda = \lambda_c$, and $\sigma_\lambda \sim 0.6\Delta\lambda_{\rm FWHM}$, where $\Delta\lambda_{\rm FWHM}$ was determined from laboratory measurements. We vary a, b, and c to minimize $\chi^2 = \sum [(F_{\rm obs} - F_{\rm model})/\text{obs error}]^2$. For [Ar II] a single point in the line and one on either side in the adjacent continuum were used to determine the line flux. The spectral resolution determined in the laboratory was 0.10 μm.

III. DISCUSSION

a) *Estimating Extinction*

In Paper I we discussed extensively the nature of the extinction correction, and here we will only briefly review the correction techniques, the general philosophy of extinction correction, and the uncertainties involved. First, there is no guarantee that the extinction law is the same from region to region. Second, although we can accurately compute the extinction at 2.17 and 4.05 μm by (1) comparing observed and predicted Brackett fluxes with the free-free radio flux (assuming constant extinction over a beam size), or (2) by comparing the observed and predicted ratio of the Brackett fluxes, and assuming the form of the extinction law from 2 to 4 μm, we cannot easily extrapolate to the longer wavelengths at which the fine-structure lines appear. The 9.7 μm silicate extinction (Gillett *et al.* 1975*a*) has been determined by fitting the absorption spectrum of the 8–13 μm continuum radiation with an opacity law τ_λ which describes optically thin emission from hot dust in the Trapezium region from 8–13 μm. The underlying emission is assumed to be a

[illegible] (model I) or a Trapezium emission spectrum [illegible] II). Radiative transfer effects may be important (Aitken and Scoville 1976) but are not included. This method of extinction determination is quite uncertain. However, if $\tau_{8\,\mu m}$ derived by this method is approximately [illegible] where $\tau_{4\,\mu m}$ is determined from the Brackett line flux and also assuming a λ^{-1} extinction law to join these wavelengths,[2] then we can "choose" a model I or model II fit. Usually model II better fits the observations (minimizes the χ^2), and it is generally correlated with the measured value of $\tau_{4\,\mu m}$ (see also Lester and Rank 1980). As developed by Aitken *et al.* (1979) and Jones *et al.* (1980), one can perform a multicomponent fit to the 8–13 μm spectrum including contributions from the unidentified 8.6 and 11.3 μm features as well as the 9.7 μm silicate feature. Where these features dominate the spectrum, we use this method to provide a better estimate of $\tau_{9.7}$. From observations of circumstellar shells, Forrest, McCarthy, and Houck (1979) conclude $\tau_{18.7\,\mu m} \sim 0.6\tau_{9.7\,\mu m}$, a relationship which also holds for galactic H II regions (McCarthy, Forrest, and Houck 1982).

In Paper I we have listed the adopted extinction law $\tau_\lambda \tau_{9.7}$ used throughout. Mean values of $\bar{\tau}_{9.7\,\mu m}$ are computed for each region from all extinction techniques available, and $\tau_\lambda/\tau_{9.7}$ is then employed to deduce $\bar{\tau}_\lambda$, for the line fluxes listed in Table 1. All line fluxes, and the abundances calculated from them, reflect the estimated uncertainty in the adopted $\bar{\tau}_{9.7\,\mu m}$.

b) *Estimating Abundances*

Ionic abundances are estimated by comparison of the observed line fluxes with radio fluxes at frequencies where the nebulae are optically thin, using equation (3) of Paper I. In all the H II regions considered here, at 9–13 kpc from the galactic center, an electron temperature of 7500 K is appropriate (Wilson, Bieging, and Wilson 1979). The ratio of electrons to protons is assumed to be 1.15.

The prescription for computing total atomic abundances for argon and sulfur from the [Ar II], [Ar III], [S III], and [S IV] observations was discussed in Paper I. The abundances thus computed are strictly lower limits to the total abundance because (1) other ionization states may be present; (2) clumping may cause us to underestimate ionic abundances; (3) sources extended with respect to measurement beam sizes lead to exclusion of certain ionic contributions, as discussed in Paper I.

Since only one ionization state of neon is observed (Ne II), it is more difficult to comment on the total neon abundance. We will report in a separate paper theoretical predictions of the ratio of [Ne II/Ne] with [S III/S IV]. In most of the cases reported here, Ne II is expected to be the dominant ionization state, because all of the H II regions except M42 are low excitation objects. In the case of M42, optical estimates of [Ne III/H] are available. In this paper, we adopt a standard neon abundance [Ne/H] of 1×10^{-4} rather than 1.5×10^{-4} assumed in Paper I. This new value is deduced by Aller (1978) and Beck *et al.* (1981) from observations of planetary nebulae.

c) *Individual Sources*

S88B = G61.5+0.1.—The Hα knot, S88B, near the diffuse H II region S88 and the Hα knot S88A, has been studied previously by a number of investigators. Infrared maps by Zeilik (1977) and Pipher *et al.* (1977) revealed extended structure at 2.2 μm and 12.6 μm that encompassed the radio compact structure (Felli, Tofani, and D'Addario 1974; Felli and Harten 1981) as well as the more diffuse Hα knot. Maps of S88B at 1.6 μm, 2.2 μm, 3.4 μm, 50 μm, and 100 μm by Evans *et al.* (1981) confirm the extent of the IR source, and the 5 GHz maps of Felli and Harten delineate radio emission in the dark cloud to the east of the Hα knot. The latter authors resolve two components to S88B, namely a high electron density ($\geq 1.9 \times 10^4$ cm^{-3}), high emission measure ($\geq 1.8 \times 10^7$ pc cm^{-6}), unresolved source S88B-2, and a normal compact region source S88B-1 which contributes most of the radio flux. Molecular maps of the region close to S88B by Evans *et al.* extend all the way to S88A where an exciting star has been identified; the distance to this star places S88A at 2 kpc from the Sun. We adopt that distance in what follows.

The radio maps of Felli and Harten correspond to a completely obscured region at the peak position of S88B-1. Since the eastern edge of the Hα knot is very sharp, and since radio emission extends across this edge, there must be differential extinction. This is consistent with the assumption that the compact H II region is embedded in dark cloud material, and the Hα knot is a "blister" model artifact. The infrared maps of Pipher *et al.* (1977) and Evans *et al.* (1981) peak at different spatial positions than the radio peak, in the sense that longer wavelength maps peak closer to the radio center. This might also be interpreted as evidence for differential extinction, but the possibility of additional near-infrared heating sources cannot be discounted.

We have obtained new data centered on S88B-1 at wavelengths in and near the [Ar II] and [S III] lines, and these data as well as previously published data discussed below are plotted in Figure 1.

Extinctions have been estimated at several positions by different techniques. First, 2–4 μm spectroscopy on S88B at the peak 2.2 μm position was reported by Pipher *et al.* (1977). The Brα and Brγ line fluxes quoted by them incorporate an error in the assumed spectral resolution of the spectrometer. New line fits to the data lead to observed fluxes of $4.0 \pm 0.7 \times 10^{-19}$ W cm^{-2} in the 17″ beam at 2.17 μm (Brγ) and $3.1 \pm 0.6 \times 10^{-18}$ W cm^{-2} at 4.05 μm (Brα). The ratio of observed line fluxes compared to the predicted ratio $F(\text{Br}\alpha)/F(\text{Br}\gamma) = 2.84$ (case B, $N_e \sim 10^4$ cm^{-3}, $T_e = 7500$ K), using the extinction law from Paper I, yields an extinction of $\tau_{2.17\,\mu m} = 2.2 \pm 0.8$. This value corresponds to $A_v = 26 \pm 9$ mag and $\tau_{9.7\,\mu m} = 2.3 \pm 0.8$. The extinction to the

[2] Independent observations of obscured stars (Hackwell and Gehrz 1974 and Gillett *et al.* 1975*b*) suggest an extinction law of this form.

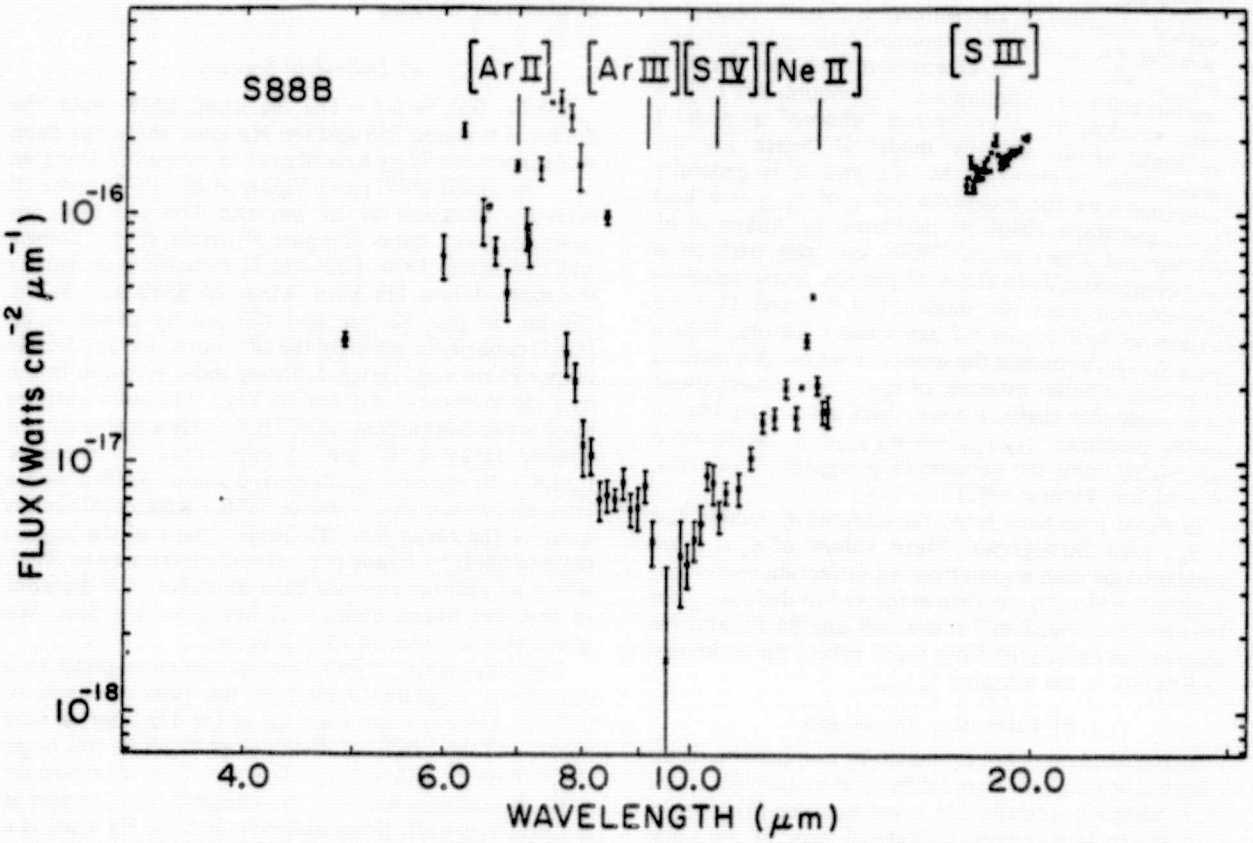

FIG. 1.—The 4–30 μm spectrum of S88B. Squares denote broad-band observations with a 27" beam. The beam sizes were 27" from 4 to 8 μm, 30" from 16 to 30 μm, and 11" from 8 to 13 μm. Error bars are shown for points where statistical uncertainties exceed 5%.

Hα knot of ~4 mag suggests the Hα knot is in the foreground.

Another extinction estimate, at the peak 12.6 μm position, is derived from the 8–13 μm continuum data (Pipher *et al.* 1977). A model II fit to the 9.7 μm silicate absorption feature leads to $T_{dust} = 290$ K and $\tau_{9.7\,\mu m} = 3.6$. The mean extinction is substantially larger than that found at the peak 2.2 μm position. Since the 12.6 μm peak position is closer to the visual eastern "edge" of the Hα knot and to the radio center than the 2.2 μm peak position, a gradient in the extinction is suggested. We assume that the discrepancy in $\tau_{9.7}$ between the two positions is real, and adopt $\tau_{9.7} = 3.6$ for the ionic line fluxes of [Ar III], [Ne II], and [S IV] observed from 8–13 μm. The line fluxes observed with the larger beams used at 16–30 μm and 4–8 μm ([S III] and [Ar II]) probably include both obscuring regions as well as an even more heavily obscured region centered on the radio peak; we adopt $\tau_{9.7} = 3.6$ in interpreting those data. Estimating the uncertainty in $\tau_{9.7}$ is more difficult, but we adopt a value of 1.0.

Line fluxes of [Ar II], [Ar III], [Ne II], [S III], and [S IV] are listed in Table 1, both measured and corrected for extinction. Uncertainties quoted reflect uncertainty in the extinction correction as well as in the line measurement. The radio data of Felli and Harten show that the compact H II region with a half power diameter of 21" provides the bulk of the total flux of 6.1 Jy at 5 GHz. The radio interferometer results of Pipher *et al.* (1977) gave 4.3 Jy at 2.7 GHz in a 15" diameter region, and Felli and Harten show that the object is optically thin at these frequencies. At 2 kpc, a single 35,000 K ZAMS star could supply the ionizing radiation and would give reasonably low excitation. We assume a radio flux of 6.1 Jy for the [Ar II] and [S III] measurements and we adopt 2.3 Jy for the [Ar III], [Ne II], and [S IV] measurements. Using equation (3) of Paper I, we compute the ionic abundances, which are listed in Table 2, relative to standard atomic abundance. The argon and sulfur ionic abundances taken at face value are consistent with S88B having standard atomic abundance. Because S88B is a relatively low excitation region, we expect that roughly 50% of the neon is in the form of Ne II. Within the uncertainty of correcting for other ionization states, we conclude that the neon abundance may be consistent with standard abundance or may be underabundant in S88B ($\geq 0.5 \times$ standard).

S156 = G110.1+0.0.—This compact H II region has been studied optically by Deharveng (1974), Glushkov and Karyagina (1972), and Heydari-Malayeri *et al.*

TABLE 2

IONIC ABUNDANCES RELATIVE TO STANDARD ABUNDANCES[a]

$$\frac{\langle N_x^i/N_H\rangle}{(N_x/N_H)_{\text{standard}}}$$

Object	Ar III	S IV	Ne II	S III	Ar II
S88B	<0.5	<0.2	0.3 ± 0.1	0.7 ± 0.5	1.5 ± 0.5
S156	0.26 ± 0.03	...	0.48 ± 0.04	1.7 ± 0.3	<3
S106	<0.2	<0.1	0.62 ± 0.05	1.0 ± 0.2	1.5 ± 0.2
NGC 2170 IRS 1	<0.3	<0.03	0.50 ± 0.04	0.4 ± 0.1	0.8 ± 0.3
M42 (20″ N θ_1C)	0.6 ± 0.1	0.27 ± 0.04	0.41 ± 0.02	1.0 ± 0.1	<0.8

[a] Assumed standard abundances: S/H = 1.6×10^{-5}; Ar/H = 4.7×10^{-6}; Ne/H = 1.0×10^{-4}.

(1980), and at radio wavelengths by Israel, Habing, and de Jong (1973), Israel (1977), and Birkinshaw (1978). Its optical diameter is ~30″, and the strong compact radio source corresponds to the northern optical condensation. The central star is visible, and the O7 V spectral classification is consistent with the observed optical ionization structure.

Spectrophotometric data from 2 to 4 μm obtained at Mount Lemmon in 1979 November and from 8 to 13 μm at the KPNO 2.1 m telescope in the same month around the [Ar III] and [Ne II] lines, are shown in Figure 2. We present the averaged data from several nights. Radio observations, at 5 GHz (Israel 1977), indicate a dominant 0.59 Jy source, 5″ × 12″ in size with two weaker components positioned ~15″ south of the main source of flux density 0.04 Jy each. For computation of all ionic abundances, 0.59 Jy will be used for comparison with the measured line fluxes.

The extinction to S156 appears to be fairly uniform over the whole nebula and has an average value of $A_v \approx 3.6$ mag with some positions in the central bright part having $A_v = 5$ mag (Israel 1977 and references

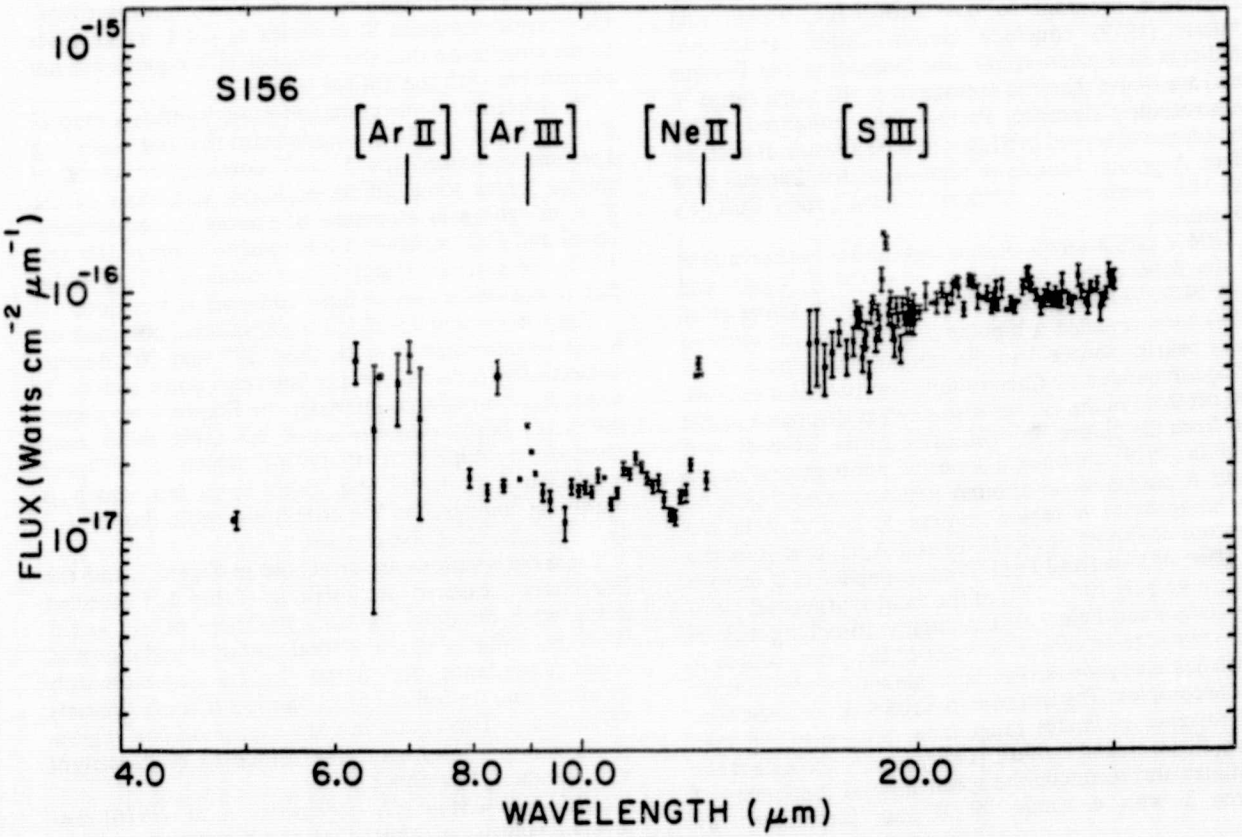

FIG. 2.—The 4–30 μm spectrum of S156

therein). Since this represents $\tau_{9.7} \leq 0.40$ and *at most* a 30% correction to the observed line fluxes, a conservative value of zero will be adopted for $\tau_{9.7}$. This is consistent with the extinction deduced from a ratio of the Brackett fluxes and from the shape of the 8–13 μm spectrum.

The computed ionic abundances relative to the standard elemental abundances are given in Table 2. Ar II was not detected, and S IV was not reliably measured; hence, we cannot combine ionic abundances or estimate the [Ar III/Ar II] or [S IV/S III] ratios; however, [S III] alone is 1.7 times greater than standard. In addition we note that for our calculated emissivities for S156 we adopted an rms value of $N_e^{rms} = 5200$ cm^{-3} as found by Israel, but as Israel points out, [S II] measurements by Glushkov and Karyagina and Deharveng yield electron densities as high as $N_e =$ 19,000 cm^{-3}, indicating massive clumping in the nebula with $\phi \leq 0.1$ (ϕ = filling factor). This high density, if adopted, will have little effect on the ionic abundances of Ne II and Ar III but will increase the estimate above the S III abundance by 60% due to a decrease in the calculated emissivity at the higher density.

In conclusion, S156 exhibits ionic abundances for Ne II and [Ar III] which are consistent with the adopted standard atomic abundances of Ne and Ar, while S III has an ionic abundance approximately two times higher than standard.

Although S156 has not been included in an optical abundance program to our knowledge, Talent and Dufour (1979) conclude certain radial abundance gradients in a given spiral arm (including the Perseus arm) are larger than the average over the same range in galactocentric distance. Perhaps the enhanced sulfur abundance observed in S156 might be a result of such an effect. A greater sample of regions in the Perseus arm will be needed to confirm Talent and Dufour's conclusion.

S106 = G76.4−0.6.—Radio and infrared observations of the S106 complex (Pipher *et al.* 1976; Israel and Felli 1978; Tokunaga and Thompson 1979; Lucas *et al.* 1978) have revealed a bipolar nebula with an infrared point source (source 3 in the notation of Pipher *et al.* 1976) surrounded by three to four compact H II regions. The centroid of the cluster is somewhat displaced to the east from the diffuse Hα nebulosity. Eiroa, Elsässer, and Lahulla (1979) obtained a series of photographs in the *I* and *R* passbands and found nebulous knots close to the compact H II region centers 1, 2, and 4 in the notation of Pipher *et al.* (1976) and A, C, and B in the notation of Israel and Felli. These compact H II regions contribute only 20%–25% of the total synthesized radio flux (Israel and Felli 1978). A highly absorbing disk of dust seen edge-on crosses in front of the point source 3, which has been proposed as the single source of excitation for the complex. The distance to S106 is quite uncertain, and distance estimates range from 500 pc to 3.6 kpc. Eiroa, Elsässer, and Lahulla (1979) discuss these distance estimates and reconcile the spectrum and luminosity of source 3 with a single B0 V star (attenuated by $A_v = 22$ mag) as sole exciting source of the complex at a distance of 500 pc.

Hefele and Hölzle (1980) present 8–13 μm spectroscopy at $\Delta\lambda/\lambda = 0.019$, with a 24″ aperture and a 45″ beam separation in right ascension for sources 1, 2, and 3. Unfortunately, their beam sizes were large enough to include not only the compact H II regions 1 and 2 (diameters 8″ × 8″ and 18″ × 12″, respectively; Israel and Felli 1978) but also the regions beyond the ionization edges where radiation in the 11.3 μm emission feature is strongest (Aitken *et al.* 1979*b*). This complicates interpretation of their deduction of the 9.7 μm absorption optical depth, as discussed in detail by Aitken *et al.* (1979*b*). We present in Figure 3 new 8–13 μm spectra on sources 1 and 2, obtained with an 11″ beam, and an EW beam separation of 50″. As can be seen, a small 11.3 μm feature as well as an 8.6 μm feature are present, but they do not dominate the 8–13 μm spectrum as in the observations of Hefele and Hölzle (1980). The model II silicate absorption depth (model II fit) is $\tau_{9.7} = 2.6$ for both regions when the 8.6 and 11.3 μm features are not allowed for. A multicomponent fit, also incorporating the 8.6 and 11.3 μm features, leads to $\tau_{9.7} = 1.5$ for both sources 1 and 2. This estimate exceeds the Calvet and Cohen (1978) estimate of $A_v = 8$ mag to optical knot 8 and the Eiroa, Elsässer, and Lahulla (1979) estimate of $A_v = 5$ mag and 11 mag to optical-infrared knots *close* to the positions of sources 1 and 2 (corresponding to $\tau_{9.7} = 0.4$ and 0.9, respectively). Our multicomponent fit excludes $\tau_{9.7} < 1$, which leads to the conclusion that the compact H II regions are not identifiable with the optical nebulosity.

By reference to the complete radio synthesis map of S106 by Israel and Felli, we ascertain that our observing aperture contained the 8″ × 8″ compact structure of source 1 plus some diffuse emission and most of the 8″ × 18″ compact structure of source 2, respectively. Israel and Felli measure 5 GHz radio fluxes of 0.8 and 1.3 Jy for sources 1 and 2; we estimate 1.5 Jy radio flux in our beam size for each compact H II region.

The 4–8 μm and 16–30 μm observations, obtained on KAO as described in § II, used 27″ and 30″ beams, respectively, centered on the infrared point source 3, which has no radio counterpart. In Figure 4 we depict the KAO beam position on a 2.7 GHz radio map obtained by Pipher *et al.* (1976), which is of lower resolution than Israel and Felli's map but which is otherwise comparable. We estimate a radio flux of ~3 Jy within the KAO beam sizes.

These observations are presented in Figure 3, and the line fluxes measured are listed in Table 1. Corrected fluxes were obtained for an extinction of $\tau_{9.7} = 1.5$. With this value of $\tau_{9.7}$, the total sulfur abundance and argon abundance are found to be approximately standard, and the ionized neon fraction is approximately 0.6 standard. This region is a low excitation H II region, so we take the total neon abundance to be consistent with standard abundance.

NGC 2170 = Mon R2.—Beckwith *et al.* (1976) discovered a cluster of infrared sources associated with the

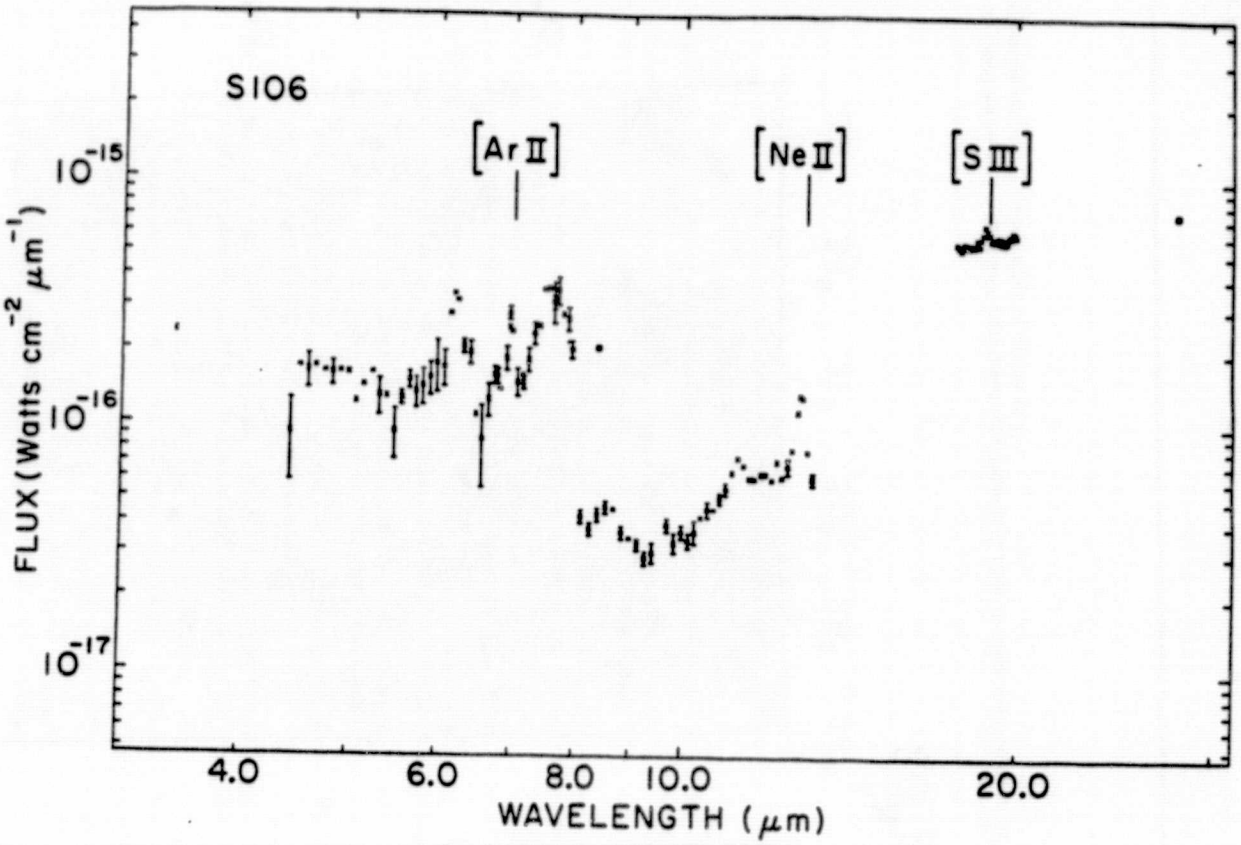

FIG. 3.—The 4–30 μm spectrum of S106

peak of the molecular cloud in Mon R2, which is an association of reflection nebulae. These sources are coincident with a region containing compact H II region(s), a type I OH maser and an H_2O maser (Downes *et al.* 1975; Brown, Knapp, and Kuiper 1976). A high resolution radio continuum map at 5 GHz obtained by Simon, Righini-Cohen, and Fischer (1981) with the VLA reveals a compact H II region approximately 20″ in diameter with the peak radio flux at IRS 1. Little continuum emission appears around the nearby source IRS 2. Since the extinction to IRS 2 at 9.7 μm is about a factor of 2 greater than that to IRS 1 (Beckwith *et al.* 1976; Pipher 1981), IRS 2 may be a background object. For these reasons IRS 1 is taken to be the dominant source of infrared forbidden line emission.

Spectroscopic data from 8–13 μm obtained with a 7″ aperture at KPNO are shown in Figure 5. The extinction was computed using the method of Gillett *et al.* (1975*a*) to obtain the model II value of $\tau_{9.7}$. In addition, 4–8 μm and 16–30 μm measurements were obtained on KAO, and the 27″ and 30″ beam sizes probably encompass the entire H II region. Unfortunately we do not have 2–4 μm data on this source. Only the [Ne II] line was detected from 8–13 μm, and scans across IRS 1 show that [Ne II] fills the H II region. Because [Ar II] and [S III] were the only ions of argon and sulfur detected, we can say that NGC 2170 is a low excitation H II region, and that [Ne II] is the primary ionization state of neon. The line fluxes, both corrected and observed, are listed in Table 1.

The abundances are computed assuming a radio flux of 3.8 Jy for the 7″ aperture measurements and 7.5 Jy for the KAO data. Although the argon abundance is approximately standard, the sulfur abundance (S III + S IV) is somewhat low compared to the other H II regions that have been sampled. A probable explanation for this latter result is the low temperature of the exciting star (see below) which would result in most sulfur being in the [S II] ionization state. For an assumed distance of 0.95 kpc (Beckwith *et al.* 1976), the observed 7.5 Jy radio continuum flux at 5 GHz (Simon *et al.* 1981) implies only a 31,000 K exciting star, although this probably is a lower limit to the stellar temperature due to possibility of absorption of Lyman-continuum photons by dust within the H II region. The ionized neon abundance is ~0.5 standard abundance. Since NGC 2170 IRS 1 is of *very* low excitation, it is possible that neon is somewhat underabundant in this region.

M42: The Orion Nebula.—M42, containing the closest compact H II region to us, is, of course, the best studied. For example, it was because silicate dust in Orion was

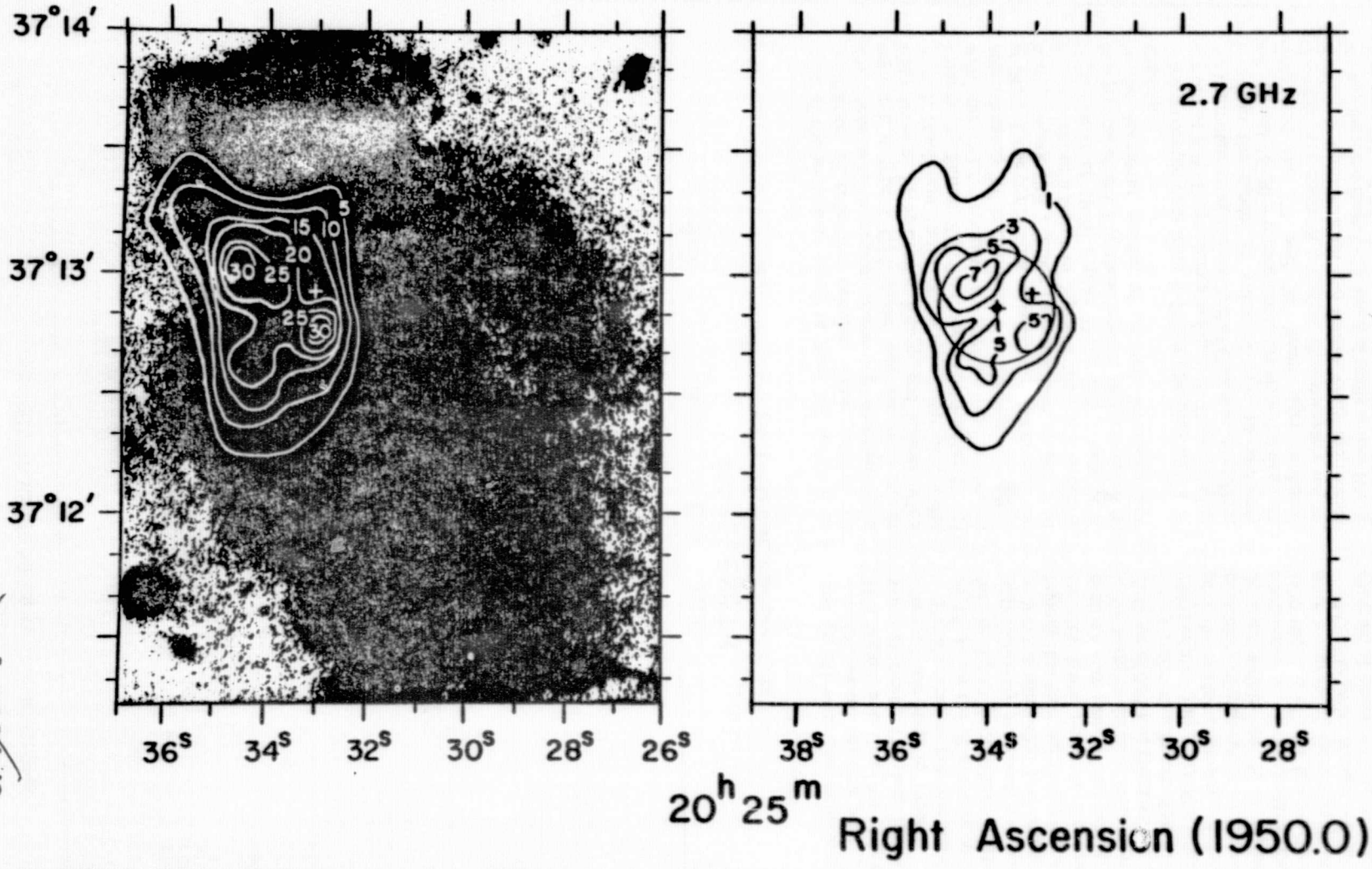

FIG. 4.—*(left)* An infrared map of S106 superposed on a Palomar E plate, showing the location of the infrared sources. *(right)* The 2.7 GHz map of S106 by Pipher *et al.* with the KAO beam location marked by a circle centered on source 3.

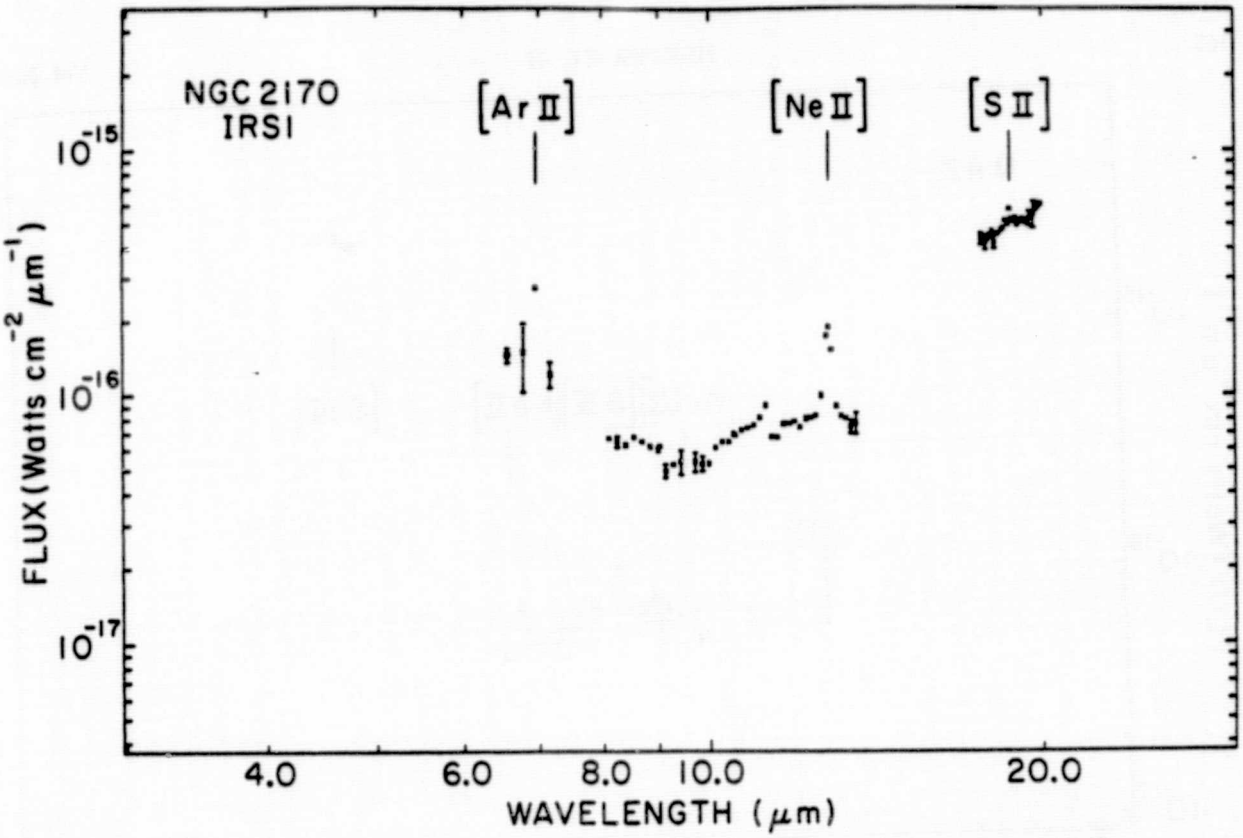

FIG. 5.—The 4–30 μm spectrum of NGC 2170 IRS 1. The 8–13 μm data are multiplied by a factor of 10. The beam sizes employed and chopper throws are discussed in the text, for all sources.

observed in emission at 9.7 μm that the model II fit of Gillett *et al.* (1975*a*) is typically quoted in assessing the extinction, $\tau_{9.7}$. Thus, it is natural to obtain observations of the fine-structure lines at various locations in the compact H II region. Unfortunately, however, the angular extent of the nebula is sufficiently large that we cannot beamswitch off the region, so that there is always some reduction in signal level.

We have obtained observations at several positions in Orion, but report here only observations 20″N of θ^1C, which are shown in Figure 6. The 8–13 μm observations were obtained at KPNO, with an 11″ beam and a 48″ N-S beam throw. The 4–8 μm and 16–30 μm data were obtained on KAO with ~30″ beams, and beam throws of 2.5 E-W, and 2.0 N-S, respectively. Radio fluxes were estimated from the 5 GHz maps of Martin and Gull (1975) and are assumed to be 0.6 Jy in the beam corresponding to the 8–13 μm observations, and 4.4 and 3.6 Jy in the 16–30 μm and 4–8 μm observation beam sizes, respectively. Extinction to this part of Orion is negligibly small. The line fluxes are listed in Table 1 and ionic abundances relative to hydrogen are reported in Table 2.

For the case of sulfur, where more than one ionic state was detected, the ionic abundances can be combined. (See Paper I for the formalism.) If the S IV does not extend beyond the 11″ beam, then the total sulfur abundance is approximately 1.0 ± 0.1 times standard, whereas if the S IV extends to at least the limits of the 30″ beam, then the sulfur abundance would be 1.3 ± 0.2 times standard. The ionic abundances of Ar III and Ne II are 0.6 ± 0.1 and 0.41 ± 0.03 times standard, respectively. These latter ionic abundances will be significant underestimates of the total elemental abundances of Ar and Ne for two reasons. As mentioned previously, due to the extended nature of the source, the 53″ N-S chop employed in the observations is inadequate to prevent cancellation effects which decrease the observed fluxes. Lester, Dinerstein, and Rank (1979), who obtained measurements on the radio continuum peak 1″ W and 10″ S of θ^1C with a 10″ beam and a 26″ N-S chop, find correction factors of 4.8 for their [Ar III] and [Ne II] measurements, and 1.3 for their [S IV] measurements from multiple beam switching techniques (to extend the chop to 100″) and drift scans in Hα. Second, for an O6 exciting star, higher ionization states such as A IV and Ne III can be expected to contribute significantly to abundance estimates. Lester,

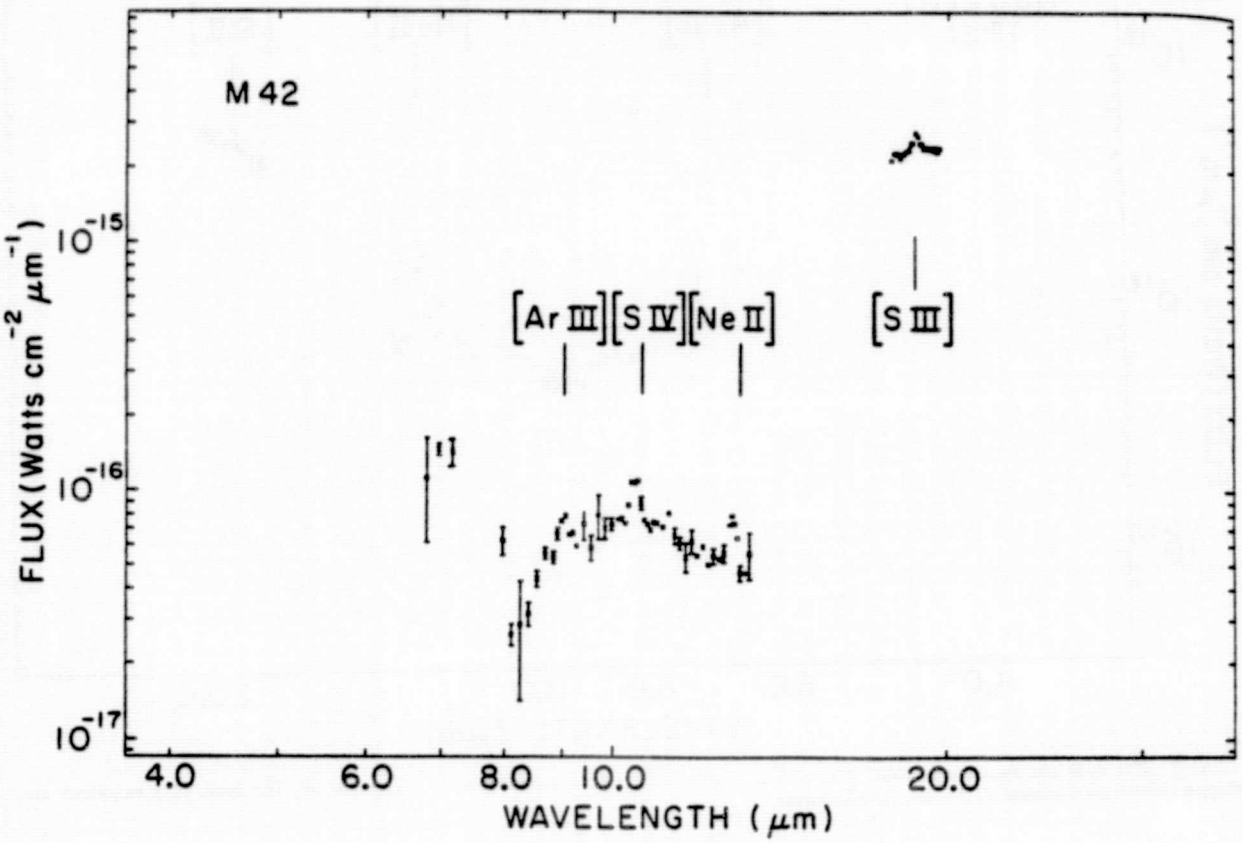

FIG. 6.—The 4–30 μm spectrum of M42, at a position 20″ N of θ^1C

Dinerstein, and Rank (1979) measured [Ne III] optically with a beam size similar to their infrared measurements and find 70% of the neon to be Ne III in the region they sampled. They found ionic abundances of 0.75, 0.60, and 0.26 relative to our adopted standard abundances for S III, S IV, and Ne II, respectively, with S II being negligible. Upon comparison with the results reported here, we find that the spatial position sampled by Lester, Dinerstein, and Rank (1979) appears to be of considerably higher excitation than the position we sampled. The total sulfur abundance deduced by both groups is in agreement.

Optical abundances have been measured for Orion by Peimbert and Torres-Peimbert (1977). They sample a position 45″ N of θ^1C and find ionic abundances of 0.8 standard neon abundance for Ne III, 0.03 standard sulfur abundance for S II, and 0.6 standard sulfur abundance for S III. They deduce, on the basis of their ionization state correction procedures, a total neon abundance of 0.93 standard, and a total sulfur abundance of 1.9 standard. Because of differing beam sizes, it is difficult to make quantitative comparisons. However, our Ne II abundance of 0.4 standard agrees qualitatively with Peimbert and Torres-Peimbert's conclusion that greater than 50% of the neon is Ne III.

IV. CONCLUSIONS

We have gathered infrared line fluxes for [Ar II], [Ar III], [Ne II], [S III], and [S IV] in five compact H II regions in the solar neighborhood. With the exception of M42, the regions are all low excitation objects with temperatures of the exciting stars < 35,000 K. This result is consistent with radio excitation parameters for the objects. We have corrected the line fluxes of these objects for extinction and beam size effects using the techniques developed in Paper I. Since our sample includes one extended object with virtually no extinction and several small and extended objects embedded in molecular cloud material, as well as one small object with negligible extinction and since the abundances calculated are for the most part consistent with standard abundance for the solar neighborhood, we claim that the techniques used in these analyses are thus validated. Thus, when we combine the results of this paper, Paper I, and recently obtained results on a larger sample of objects close to the galactic center in a future paper, we can evaluate whether excitation and abundance gradients exist in the Galaxy. Gradients not only with galactocentric distance but also in a spiral arm will be assessed once a larger sample of H II regions has been observed. It is interesting to note an overabundance of S in the Perseus arm object

S156 in the present paper; we shall compare S156 with other Perseus arm objects in a future paper to assess whether abundance variations in H II regions at a given galactocentric radius are spiral arm dependent.

We wish to thank the staff of KAO and KPNO for their excellent support. In addition, we thank George Gull of Cornell University for his devoted assistance. Infrared Astronomy at Cornell University, University of Rochester, and University of California at San Diego is supported by grants from NASA.

REFERENCES

Aitken, B. K., Roche, P. F., Spenser, P. M., and Jones, B. 1979*a*, *Ap. J.*, **233**, 925.
———. 1979*b*, *Astr. Ap.*, **76**, 60.
Aller, L. H. 1978, in *IAU Symposium 76, Planetary Nebulae, Observations and Theory*, ed. Y. Terzian (Dordrecht: Reidel), p. 225.
Beck, S. C., Lacy, J. H., Townes, C. H., Aller, L. H., Geballe, T. R., and Bras, F. 1981, *Ap. J.*, **249**, 592.
Beckwith, S., Evans, N. J., II, Becklin, E. E., and Neugebauer, G. 1976, *Ap. J.*, **208**, 390.
Birkinshaw, M. 1978, *M.N.R.A.S.*, **182**, 401.
Brown, R. L., Knapp, G. R., and Kuiper, T. B. H. 1976, private communication referenced in Beckwith *et al.* (1976), above.
Calvet, N., and Cohen, M. 1978, *M.N.R.A.S.*, **182**, 687.
Deharveng, L. 1974, *Astr. Ap.*, **35**, 63.
Downes, D., Winnberg, A., Goss, W. M., and Johansson, L. E. B. 1975, *Astr. Ap.*, **44**, 243.
Eiroa, C., Elsässer, H., and Lahulla, J. F. 1979, *Astr. Ap.*, **74**, 89.
Evans, N. J., II, Blair, G. N., Harvey, P., Israel, F., Peters, W. L., III, Scholtes, M., de Graauw, T., and Van den Bout, P. 1981, preprint.
Felli, M., Tofani, G., and D'Addario, L. 1974, *Astr. Ap.*, **31**, 431.
Felli, M., and Harten, R. H. 1981, preprint.
Forrest, W. J., McCarthy, J. T., and Houck, J. R. 1979, *Ap. J.*, **233**, 611.
Gillett, F. C., Forrest, W. J., Merrill, K. M., Capps, R. W., and Soifer, B. T. 1975*a*, *Ap. J.*, **200**, 609.
Gillett, F. C., Jones, T. W., Merrill, K. M., and Stein, W. A. 1975*b*, *Astr. Ap.*, **45**, 77.
Glushkov, Y., and Karyagina, Z. V. 1972, *Astr. Circ. USSR*, **711**, 4.
Hackwell, J., and Gehrz, R. 1974, *Ap. J.*, **194**, 49.
Hawley, S. A. 1978, *Ap. J.*, **224**, 417.
Hefele, A., and Hölzle, E. 1980, *Astr. Ap.*, **88**, 145.
Herter, T. L., *et al.* 1981, *Ap. J.*, **250**, 186 (Paper I).
Heydari-Malayeri, M., Testor, G., and Lortet, M. C. 1980, *Astr. Ap.*, **84**, 154.
Israel, F. J. 1977, *Astr. Ap.*, **59**, 27.
Israel, F. J., and Felli, M. 1978, *Astr. Ap.*, **63**, 325.
Israel, F. P., Habing, H. J., and de Jong, T. 1973, *Astr. Ap.*, **27**, 143.
Jones, B., Merrill, R. M., Stein, W., and Willner, S. P. 1980, *Ap. J.*, **242**, 141.
Kwan, J., and Scoville, N. J. 1976, *Ap. J.*, **209**, 102.
Lacasse, M. L., Herter, T., Krassner, J., Helfer, H. L., and Pipher, J. L. 1980, *Astr. Ap.*, **86**, 231.
Lacy, J. H. 1980, in *IAU Symposium 96, Infrared Astronomy*, ed. C. G. Wynn-Williams and D. P. Cruikshank (Dordrecht: Reidel), p. 239.
Lester, D., Dinerstein, H. L., and Rank, D. 1979, *Ap. J.*, **232**, 139.
Lester, D., and Rank, D. 1980, preprint.
Lucas, A. M., Le Squeren, A. M., Kazes, I., and Encrenaz, P. J. 1978, *Astr. Ap.*, **66**, 155.
Martin, A. H. M., and Gull, T. 1976, *M.N.R.A.S.*, **175**, 235.
McCarthy, J. F., Forrest, W. J., and Houck, J. R. 1979, *Ap. J.*, **231**, 711.
———. 1982, *Ap. J.*, submitted.
Peimbert, M., and Torres-Peimbert, S. 1977, *M.N.R.A.S.*, **179**, 217.
Pipher, J. L. 1981, private communication.
Pipher, J. L., Sharpless, S., Savedoff, M. P., Kerridge, S. J., Krassner, J., Schurmann, S., Soifer, B. T., and Merrill, K. M. 1976, *Astr. Ap.*, **51**, 255.
Pipher, J. L., Sharpless, S., Savedoff, M. P., Krassner, J., Varlese, S., and Soifer, B. T. 1977, *Astr. Ap.*, **59**, 215.
Puetter, R. C., Russell, R. W., Soifer, B. T., and Willner, S. P. 1979, *Ap. J.*, **228**, 118.
Russell, R., Soifer, B. T., and Willner, S. P. 1977, *Ap. J.*, **213**, 66.
Simon, M., Righini-Cohen, G., and Fischer, J. 1981, private communication.
Talent, D. L., and Dufour, R. J. 1979, *Ap. J.*, **233**, 888.
Tokunaga, A., and Thompson, R. 1979, *Ap. J.*, **231**, 736.
Wilson, T. L., Bieging, J., and Wilson, W. E. 1979, *Astr. Ap.*, **71**, 205.
Zeilik, M. 1977, *Ap. J.*, **213**, 58.

D. A. BRIOTTA, JR., T. HERTER, and J. R. HOUCK: C. R. S. R., Space Sciences Building, Cornell University, Ithaca, NY 14853

W. J. FORREST, H. L. HELFER, and J. L. PIPHER: Department of Physics and Astronomy, University of Rochester, Rochester, NY 14627

R. J. RUDY: University of Arizona, Steward Observatory, Tucson, AZ 85721

S. P. WILLNER: SAO, Center for Astrophysics, 60 Garden Street, Cambridge, MA 02138

ABUNDANCES IN GALACTIC HII REGIONS, III: G25.4-0.2, G45.5+0.06, M8, S159 and DR22

by

J. L. Pipher,[1,2] H. L. Helfer

University of Rochester

and

T. Herter[1]

Grumman Aerospace Corporation

and

D. A. Briotta Jr., J. R. Houck

Cornell University

and

S. P. Willner[2]

Harvard-Smithsonian Center for Astrophysics

and

B. Jones

University of California, San Diego

Received 1983 August 8;

Accepted April 4, 1984; To appear in October 1, 1984 issue

[1] Visiting Astronomer, Kitt Peak National Observatory, Tucson, AZ. Operated by the Associated Universities for Research in Astronomy, Inc., under contract with the National Science Foundation.

[2] Visiting Astronomer, Cerro Tololo Interamerican Observatory, La Serena, Chile. Operated by the Associated Universities for Research in Astronomy, Inc., under contract with the National Science Foundation.

ABSTRACT

Measurements of the [ArII](6.99μm), [ArIII](8.99μm), [NeII](12.81μm), [SIII](18.71μm), and [SIV](10.51μm) lines are presented for five compact HII regions along with continuum spectroscopy. From these data and radio data we deduce lower limits to the elemental abundances of Ar, S, and Ne. G25.4-0.2 is only 5.5 kpc from the galactic center, and is considerably overabundant in all these elements. G45.5+0.06 is at 7 kpc from the galactic center, and appears to be approximately consistent with solar abundance. S159 in the Perseus Arm, at 12 kpc from the galactic center, has solar abundance, while M8 in the solar neighorhood may be somewhat overabundant in Ar and Ne. DR22, at 10 kpc from the galactic center in the Cygnus arm, is overabundant in Ar. A summary of results from our series of papers to date on abundances is given.

I. Introduction

This is the third paper in a series presenting observations of infrared fine structure line strengths in galactic HII regions for the purpose of assessing abundances in the Galaxy. Hereafter Paper I, II are used to refer to Herter et al. 1981, 1982a, respectively. As we have pointed out before, infrared observations allow one to probe large distances from the Sun or deep within a molecular cloud, although substantial extinction corrections are required in these cases. The weak temperature dependence of the line strengths and the potential for obtaining data on two important ionization states of the argon and sulphur atoms allow direct abundance analysis using the infrared lines.

In this paper we report ground-based and airborne spectroscopic fine structure line observations from 2-30μm for the compact HII region complexes of G25.4-0.2, G45.5+0.06, M8, S159, and DR22. The regions G25.4-0.2 and G45.5+0.06 are near the regions G29.9-0.0 and G45.1+0.1 studied in Paper I. G25.4-0.2, at 5.5 kpc, is the closest HII region to the galactic center studied in this series. The region M8 has been extensively studied at optical wavelengths, allowing direct comparison of infrared and optical abundance estimates. DR22 is near S106 studied in Paper II, and S159 is another example of a Perseus arm HII region (S158 and S156 were studied in Papers I and II respectively). Since Talent and Dufour (1979) have suggested substantial abundance gradients along the Perseus arm, these latter HII regions are of particular interest.

The fine structure lines studied here include the [ArIII] and

[ArII] lines at 8.99μm and 6.99μm; the [SIII] and [SIV] lines at 18.71μm and 10.51μm; and the [NeII] line at 12.81μm. These argon and sulphur ionization states constitute the major ionization states for HII regions with exciting stars of temperature $T_* = 30{,}000$-$45{,}000$K for sulphur and $T_* = 25{,}000$-$40{,}000$K for argon according to simple dust-free ionization structure models (e.g. Lacasse et al. 1980; Lacy 1980). The ionic fraction of NeII is expected to be strongly correlated with the ratio of SIII/SIV (see Herter, Helfer and Pipher, 1983), so that total atomic abundances of argon, sulphur, and, neon can be obtained from these observations.

In section II we present the observational techniques employed, and a brief review of the methods outlined in Papers I and II for estimating and applying extinction corrections and determining ionic and elemental abundances. Individual source data and subsequent abundance estimates are given in section III, and a summary of the abundances from the present work and Papers I and II is presented in section IV.

II. Observations

The data described here were obtained with a variety of infrared systems. Ground-based data were obtained primarily at the Kitt Peak National Observatory (KPNO), Cerro Tololo International Observatory (CTIO) or at the UCSD - U. of Minnesota Mt. Lemmon Observatory using CVF spectrometers with resolutions $\Delta\lambda / \lambda \sim 0.015$. These data, both previously published and new results, are noted in

Table 1. Sampling densities are typically one to two data points per resolution element. Chopper spacings employed for each object are given in §III.C.

The 4-8μm data reported here consist of observations in the [ArII] line and adjacent continuum using the UCSD filter wheel spectrometer with a resolution of $\lambda/\Delta\lambda$ of 0.015 (Russell, Soifer, and Willner 1977; Puetter et al. 1979) on flights of the Kuiper Airborne Observatory (KPO) in July 1980, June and August 1981. For these observations a 27" focal plane aperture was employed, and chopped beam spacing and orientation were chosen to avoid beam cancellation.

The [SIII] 18.71μm line fluxes of G25.4-0.2, S159, and G45.5+0.06 were obtained with a 10-channel cooled-grating spectrometer (McCarthy, Forrest, and Houck, 1979) in July 1980. A focal plane aperture of 30" was used and the spectral resolution was approximately 0.2 μm. Observations of the [SIII] lines of M8 and DR22 were made with a 3-channel cooled-grating spectrometer (Herter et al. 1982b) in August 1981. The focal plane aperture was approximately 20" and the spectral resolution was 0.033μm. For both sets of observations the choice of beam throw was similar to that used with the UCSD instrument.

The observed line fluxes (uncorrected for extinction) are listed in Table 1 along with the beam sizes and references for previously published observations. The line fluxes for all but [ArII] have been derived from a least squares fit to the observations of the form $F_\lambda = a+b\lambda + c\{\exp - [(\lambda-\lambda_c)/\sigma_\lambda]^2\}$, that is

a linear continuum plus unresolved line emission at $\lambda = \lambda_c$, and $\sigma_\lambda \sim 0.6\,\Delta\lambda_{FWHM}$ where $\Delta\lambda_{FWHM}$ was determined from laboratory measurements. We vary a, b, c to minimize $\chi^2 = \Sigma\,(\frac{F_{obs} - F_{model}}{obs\ error})^2$. For [ArII] only one point in the line and one on either side in the adjacent continuum were used to estimate the line flux.

III. Discussion

A) Estimating Extinction

In Paper I we extensively discussed the nature of the extinction correction, and here we will only briefly review the correction techniques and the uncertainties involved. The extinction can be computed from the brightness of the hydrogen emission lines or from the depth of the 9.7μm silicate absorption. In the former method, we can accurately compute the extinction at 2.17μm and 4.05μm by comparing observed and predicted Brackett line fluxes with the free-free radio flux density or by comparing the observed and predicted ratio of the Brackettline fluxes and assuming the form of the extinction law from 2 to 4μm. However the short wavelength extinction cannot be easily extrapolated to the longer wavelengths at which the fine structure lines appear. Alternatively, the 9.7μm silicate extinction (Gillett et al. 1975) can be determined by fitting the absorption spectrum of the 8-13μm continuum radiation with an opacity law τ_λ which fits the optically thin emission from hot dust in the Trapezium. For some sources, unidentified emission features at 7.7, 8.6, and 11.3μm strongly affect the

spectrum. For these sources, a multi-component fit of the form developed by Aitken et al. (1979) and Jones et al. (1980) is used to provide a better estimate of $\tau_{9.7}$.

For each source, all of the available techniques have been used to estimate the extinction. A single extinction law, given in Paper I, was used although there is no guarantee that the extinction law is the same from region to region. The extinctions derived from the different techniques were converted to values of $\tau_{9.7}$ and the mean was computed for each source. The means $\overline{\tau}_{9.7}$ are listed in Table 1, along with their uncertainties. The stated uncertainties in the corrected line fluxes and calculated abundances include the estimated uncertainty in the adopted $\overline{\tau}_{9.7}$.

B) Estimating Abundances

Ionic abundances were estimated by comparison of the corrected line fluxes with radio flux densities, measured at wavelengths short enough that the nebulae are optically thin (Equation 3, Paper I). The electron temperature was assumed to be 7500K and the ratio of electrons to protons 1.15. The electron density was estimated from the radio flux density and source size with an assumed filling factor of 1. New, more reliable and accurate values of the sulphur collision strengths have been employed (Mendoza, 1983) in computation of the ionic abundances, listed in Table 2. Table 3 lists the revised SIII and SIV abundances (using the new collision strengths) for objects studied in Papers I and II.

The prescription for computing total atomic abundances for argon and sulphur from the ArII, ArIII, SIII, and SIV observations was discussed in Paper I. The abundances thus computed, and displayed in Figure 1, are strictly lower limits to the total abundance because

1) other ionization states may be present,

2) clumping may cause us to underestimate ionic abundances, and

3) sources extended with respect to measurement beam sizes lead to exclusion of certain ionic contributions, as discussed in Paper I.

Since only one ionization state of neon was observed (NeII) it is more difficult to calculate the total neon abundance. However, in spherical, uniform models of HII regions employing the OTS approximation with charge exchange included, under the assumption of uniform temperature, it is found that the ionic fraction of NeII/Ne is correlated with the ratio of SIII/SIV, so that the total neon abundance can also be estimated from the NeII measurement (Herter, Helfer, and Pipher 1983).

The mean electron density, distance, and galacto-centric radius for each region are given in Table 4.

C) Individual Sources

G25.4-0.2 = W42

Radio maps of the G25.4-0.2 region show two sources; the one we studied[3]

$^3\alpha_{1950} = 18^h35^m26.^s5$, $\delta_{1950} = -06°48'38"$

has a half power diameter of 10" and total diameter 20". The kinematic distance is 4.7± 0.7 kpc (Reifenstein et al. 1970). It is situated near overabundant HII regions G29.9-0.0 and G30.8-0.0 (Paper I and Lester et al. 1981), which are also within 6 kpc of the galactic center. Felli, Tofani, and D'Addario (1974) give a 10.7 GHz radio flux density for this component of 2.5 Jy; Herter and Krassner (1984) observed the source on the VLA at 5 GHz and confirm the flux density of Felli et al. The diameters and position of Herter and Krassner are listed above. Observations of the 8-13μm spectrum of G25.4-0.2 were obtained on the KPNO 2.1-m telescope in June 1980 with a beam throw of 25" and 14".8 aperture which included 80% of the radio flux. A model II fit to the very deep silicate feature in the 8-13μm spectrum gives $\tau_{9.7} = 5.3\pm0.3$, and the only fine structure line observed was the [NeII] line. Observations of the [SIII] and [ArII] lines were obtained in July 1980 and June 1981 on the KAO, with a 2' beam throw. Abundances were computed assuming $S_\nu = 2.5$ Jy for the [ArII] and [SIII] lines, and $S_\nu = 2.0$ Jy for the [NeII] line.

G45.5+0.06

G45.5+0.06 has been extensively studied in the radio and infrared. Zeilik, Kleinmann, and Wright (1975) mapped this compact HII region at 10.6μm and also presented photometry; in addition, Zeilik and Heckert (1977) mapped the region at 2.2μm with a large

beam (1'). Radio maps by Matthews et al. (1977) at 5 GHz with a resolution of 7" x 35" reveal that G45.5+0.06 consists of three components, a 13" diameter source A of 3.3 Jy radio flux density, and two more diffuse low density components B and C of 26" and 100" respectively. At an adopted kinematic distance of 9.7 kpc (Reifenstein et al.), Matthews et al. conclude that a 47,000K ZAMS exciting star is necessary to ionize component A.

The 8-13μm spectrum, obtained with a 14".8 aperture and a 28" beam throw at the KPNO 2.1-m telescope in June 1980, was taken by offsetting to radio position A of Matthews et al. and peaking up on the [NeII] flux. All three fine structure lines available in this wavelength range are present. There is some indication that the unidentified 11.3μm emission feature may be present. The substantial silicate extinction is reproduced by a model II fit with $\tau_{9.7} = 3.1$, or a multi-component fit of 2.6 if graphite grains are present, and 3.0 if they are not. We adopt $\tau_{9.7} = 2.8 \pm 0.4$, since we do not have 2-4μm data on this source.

The [SIII] and [ArII] line flux measurements were obtained on the KAO in June 1980 and July 1981 respectively, with beam throws of 2'.

Ionic abundances were computed from the corrected line fluxes assuming that component A is the major contribution to the ionized gas. Any contribution from other more diffuse components should have been cancelled out by chopping.

M8

M8 and the surrounding region is one of the most extensively studied HII region/molecular cloud complexes. In the vicinity there is a young cluster (NGC 6530), the 'Hourglass' bright optical HII region, and more extended diffuse optical emission. While 9 Sgr is thought to power much of the optical nebulosity, the O7 star Herschel 36 may power the nearby Hourglass (Thackeray 1950, Woolf 1961). Maps at radio wavelengths show that the radio center coincides with the northern lobe of the Hourglass (Turner et al. 1974, Wink et al. 1975): a high resolution VLA map at 5 GHz (Woodward et al. 1984) is used in the analysis below. Infrared maps by Dyck (1977), Wright et al., Zeilik (1979), Thronson, Loewenstein, and Stokes (1979) and Woodward et al. show peaks at or near the northern Hourglass/Herschel 36 region. An 8-13μm spectrum centered on the narrow 'waist' of the Hourglass was obtained on the KPNO 2.1 m telescope in a 15" aperture with a 60" beam throw in June 1980, and a partial 2-4μm spectrum was obtained on the CTIO 1.5-m telescope in July 1980 in a 9" aperture, with a 30" beam throw. Observations of the [ArII] and [SIII] lines were obtained at KAO in June and August 1981. The extinction to M8 has been estimated by a multicomponent fit to the 8-13μm spectrum as $\tau_{9.7} = 0$. This is in excellent agreement with the visual estimate to the Hourglass of $A_v = 2.4$ assuming Orion-type selective extinction or $A_v = 1.1$ assuming standard selective extinction [Johnson 1967]. Lynds and O'Neil (1982) find $A_v = 3.6$ assuming a standard extinction law. We cannot reliably estimate the extinction from the Brγ flux and VLA radio map

since there is evidence of a possible compact source with partially optically thick Brackett lines in the beam. Hence the corrected line fluxes are taken to be equal to the observed line fluxes. Ionic abundances are computed using the 5 GHz VLA radio flux density estimated for the appropriate beam size (Woodward et al.).

S159A = AFGL3053

S159A was included in the 5 GHz aperture synthesis observations of Perseus arm HII region by Israel (1977). The radio diameter of the compact component is 6" and the optically-thin 5 GHz density is 1.0 Jy. Rossano and Russell (1981) found an extended component as well; in a 4'5 beam at 3.2 GHz, the radio flux density is 2.43 Jy. An exciting star of $\sim$ 35,000K is required to support the radio emission, hence S159A is a fairly low-excitation compact HII region. S159 is near a peak in the CO emission and is at the position of an optically bright wisp as noted by Israel. The 8-13μm spectrum of AFGL3053 was obtained by Merrill (1977) with a 17" beam and a 50" beam throw at Mt. Lemmon in 1976 December; that spectrum shows a substantial [NeII] line as well as very strong 8.6 and 11.3μm unidentified emission features. The [ArII] and [SIII] measurements were obtained on KAO in 1981 June and 1980 July respectively.

Because 8.6μm and 11.3μm features dominate the 8-13μm spectrum, it is necessary to use a multi-component fit to estimate the extinction. We conclude on the basis of the fit that $\tau_{9.7} = 0$, and list the corrected line fluxes equal to the measured line fluxes in Table 1.

Ionic abundances are computed assuming S_ν = 1.0 Jy.

DR 22

DR 22 is one of the 27 sources found in a 5 GHz survey of the Cygnus X complex by Downes and Rinehart (1966). Felli et al. (1974) found DR 22 to be $\sim$16" in size with a 10.7 GHz radio flux density of 3.2 Jy. High resolution radio maps of DR 22 at 2.7 GHz (Krassner et al. 1983) and on the VLA at 5 GHz (Herter and Krassner 1984) yield a size of 22", and the radio flux density can be supported by an exciting star of $\sim$ 37,000K. The 2-4 and 8-13μm spectra of DR 22 were obtained with an 11" aperture with a 53" NS beam throw at the radio peak by Herter (1984), and the [ArII] and [SIII] were data obtained in June and August of 1981. Herter (1984) mapped DR 22 in the Brackett lines and adjacent continua with an 11" beam, and found the extinction in the nebula varied from $\tau_{Br\gamma}$ = 1.4 to 2.7. He deduced that abundance of [NeII] is remarkably constant with position in the nebula. The radio flux density used in the abundance analyses of [NeII], [ArIII], and [SIV] is 1.1 Jy derived from the extinction corrected Brγ and Brα fluxes.

IV. Abundances

We give the ionic abundances computed for each source in Table 2. G25.4-0.2 at 5.5 kpc from the galactic center is overabundant in ArII, SIII, and NeII. Since the half power size of G25.4-0.2 is

smaller than our measurement beam sizes, we can simply add ionic abundances of argon and sulphur to obtain atomic abundances. Because [ArIII] and [SIV] were not detected, we take the ArII and SIII abundances to be equal to the atomic abundances. Since SIII/SIV > 9, we estimate that NeII constitutes $\sim$90% of the neon in the nebula (Herter, Helfer, and Pipher 1983). Thus neon is 2.4-2.7 times standard. Hence G25.4-0.2, like G29.9-0.0, is overabundant compared to standard abundances by approximately a factor of two.

Similarly, G45.5+0.06, at 7 kpc, is also small compared with our measurement beam sizes. We find total abundances of argon and sulfer to be 1.1 and 0.86 times standard abundances respectively. Since the ratio of SIII/SIV is 13 indicating a much softer UV radiation field than that of the single 47,000K star required to support the observed radio flux density, we conclude that most of the neon is NeII, and that the neon abundance is only 0.4 times standard abundance.

S159, a member of the Perseus arm, is 12 kpc from the galactic center, and is also small compared with our measurement beam sizes. It is a low excitation HII region, and most of the argon, sulphur and neon is in the ArII, SIII, and NeII ionic states. Hence atomic abundances of 1, 0.5 and 0.8 are deduced for argon, sulphur and neon respectively, i.e. we find S159 to have approximately standard abundances of these elements.

Both M8 and DR22 are extended with respect to our measurement beams, and are 9 to 10 kpc from the galactic center respectively.

Both M8 and DR22 have been studied in the radio at high resolution by Woodward et al. (1983) and Herter (1984), and these maps are used to compute total Ar and S abundances using the techniques discussed in Paper I. Maps in the [NeII] lines and studies of the extinction have been made for DR22 (Herter). We estimate the atomic abundances of Ne and S in DR22 to be consistent with standard abundances, while DR22 is slightly overabundant in Ar. M8 is apparently overabundant in Ne and Ar.

In figures 1a-d we have plotted the estimated atomic abundances of Ar, S and Ne as well as Ne^+, as compared with solar abundance for the sixteen HII regions we have studied in Papers I, II and the present paper, assuming no uncertainty in R, the galactocentric distance. In these figures, the Ne^+ abundances from Paper I have been adjusted to reflect the standard neon abundance used in Paper II, and these abundances have been converted to total neon abundances using the observed [SIII/SIV] ratios. Despite the fact there is scatter about the solar abundance value of $\sim \pm 1$ unit peak to peak, we immediately can conclude there is no compelling observational evidence for extreme abundance gradients in our Galaxy in these three elements. While there is a slight trend towards decreasing abundance with increasing galacto-centric radius R, the result depends heavily on the few observations obtained to date at $R \leq 6$ kpc. The formal results for argon, neon and sulphur are d log (Ar/H)/dR= -0.06/kpc, $\frac{\text{d log (Ne/H)}}{\text{dR}}$ = -0.19/kpc and $\frac{\text{d log (S/H)}}{\text{dR}}$ = -0.10/kpc respectively. These should be compared with O/H and N/H results

from 8-14 kpc in the solar neighborhood by Peimbert, Torres-Peimbert, and Rayo (1978) who quote gradients in the same units of -0.13 and -0.23 respectively. A recent paper by Shaver et al. (1983), using combined optical and radio observations, deduce oxygen and nitrogen gradients of -0.07, and -0.09 in the same units with very small scatter. Their results for other elements are less certain because of observational difficulties, but they suggest sulphur may have a much smaller gradient. The scatter in the present results is larger than they found for O and N. Talent and Dufour (1979) have derived substantial abundance gradients with galacto-centric distance along a given spiral arm using optical measurements: these determinations exhibit much less scatter than the global studies (both optical and infrared). We have not yet obtained a sufficient infrared sample along a spiral arm to assess these findings.

We must draw attention to W33, the low point at 6 kpc on all four figures. The argon and sulphur measurements lead to the conclusion that W33 is underabundant compared to standard. However, a previous large beam measurement in SIII showed it to be over-abundant (McCarthy, 1980: see Paper I). A second small beam (20") measurement in SIII with chopper throws of 5' and 6' oriented NE to SW yielded results identical to those of Paper I (Herter, private communication). A possible explanation of the small beam SIII measurements is that high density clumps exist in the region: if so the SIII abundance is underestimated. Future plans include

measurement of the [SIII] 33μm line to estimate the density. Aperture synthesis maps of W33 recently published (Ho and Haschick 1981) may help future detailed studies of the region.

V. Conclusion

Abundances measurements for a total of 16 HII regions based on Ar, Ne and S infrared fine structure lines show a slight trend towards decreasing abundances with increasing galacto-centric radius. Region to region scatter at nearly constant radius is, however, as large as the alleged gradient. In particular, we measure low abundances for W33 at small radius, while S158 and S106 have high abundances at larger radii. The latter determinations seem secure, while the determination for W33 is less so.

The major uncertainties in abundance measurements in the infrared include 1) beam size corrections 2) extinction corrections and 3) corrections for unmeasured ionization states. The first two of these might potentially explain the low abundances derived for W33. As noted in §IV, the presence of high density clumps can dramatically affect the SIII emissivity, so that the S abundance would be underestimated (see Herter et al. 1982b). It is imperative that both ionization states of argon and sulphur be measured with the same large (with respect to source diameter) beam size if uncertainties due to item 1) are to be ruled out: an alternative method would be complete maps in the lines. Also, if a greater

number of hydrogen recominbation lines were measured in each region in order to tie down the extinction law, and hence the appropriate extinction for each fine structure line, with the same large beam, the second uncertainty could be alleviated. Finally, empirical relationships concerning the excitation conditions or correcting for the unmeasured ionization states are required. The total neon abundance has been estimated here from a model correlation between the NeII fraction and the [SIII/SIV] ratio, for example.

In spite of the uncertainties, there appear to be real differences between the abundances for different elements. There also appears to be a real spread in element abundances, at least at a galactocentric radius near that of the Sun.

Acknowledgments

It is a pleasure to acknowledge the superlative support staff at KAO, CTIO and KPNO. We thank G. Gull and M. Shure for assistance with the measurements and equipment development. All the authors have been supported in this work by grants from NASA.

Table 1

Observed and Extinction Corrected Line Fluxes

Object	$\bar{\tau}_{9.7}$	Line	Beam (")	Flux[b] (10^{-18} Wcm^{-2})	τ_λ	Corrected Flux (10^{-18} Wcm^{-2})
G25.4-0.2	5.3±0.3	ArII	27	4.0±0.5	1.6±0.1	20±4
		ArIII	15	<0.4	4.2±0.2	<27
		SIII	30	5.0±1.4	3.2±0.2	123±42
		SIV	15	<0.5	4.5±0.3	<45
		NeII	15	20±2	1.9±0.1	130±20
G45.5+0.06	2.8±0.4	ArII	27	4±2	0.8±0.1	8.7±4
		ArIII	15	1.8±0.3	2.2±0.3	16±6
		SIII	30	16±1.5	1.7±0.2	88±19
		SIV	15	2.6±0.4	2.4±0.3	29±10
		NeII	15	12±1	1.0±0.1	33±4
M8	0.0	ArII	27	10±2.5		
		ArIII	15	2.3±0.3		
		SIII	20	26±1		
		SIV	15	<1.2		
		NeII	15	23±2		
		Brγ	9	0.23±.01		
S159	0.0	ArII	27	4.2±0.8		
		ArIII	22	<1.4		
		SIII	30	12±1.3		
		SIV	22	<1.7		
		NeII	22	20±1		
DR22	2.2±0.3	ArII	27	10.7±3	0.7±0.1	21.5±7
		ArIII	11	0.8±0.2[a]	1.8±0.2	4.8±1.6
		SIII	20	17±1	1.3±0.2	62±13
		SIV	11	<1.2[a]	1.9±0.3	<8
		NeII	11	7.1±1.0[a]	0.8±0.1	16±3
		Brγ	11	0.12±.01[a]	2.25±0.3	1.14±0.15
		Brα	11	0.97±.04[a]	1.20±0.15	3.22±0.4

Notes

a. Measurements at peak radio flux position.
b. Uncorrected for extinction.

Table 2
Determination of Ionic Abundances

Object	Line	S_ν (Jy)	$j/n_x^i n_e$ (10^{-22} erg cm^3 s^{-1} sr^{-1})	n_x^i/n_H (10^{-6})	(n_x^i/n_H) (with respect to standard atomic abundance)*
G25.4-0.2	ArII	2.5	3.14	9.0±1.8	1.9±0.4
	ArIII	2.0	7.24	<6.6	<1.4
	SIII	2.5	5.82	30±10	1.8±0.6
	SIV	2.0	25.94	<3.06	<0.2
	NeII	2.0	0.940	243±30	2.4±0.2
G45.5+0.06	ArII	3.3	3.16	2.9±1.5	0.6±0.3
	ArIII	3.3	7.46	2.3±0.9	0.5±0.2
	SIII	3.3	7.67	12±2	0.8±0.2
	SIV	3.3	30.19	1.0±0.4	0.06±0.02
	NeII	3.3	0.961	37±4	0.36±0.03
M8	ArII	1.91	3.16	6.4±1.6	1.4±0.4
	ArIII	0.67	7.46	1.8±0.2	0.38±0.05
	SIII	1.24	7.93	10.2±0.4	0.64±0.24
	SIV	0.67	31.16	<0.25	<0.02
	NeII	0.67	0.961	43±13	1.39±0.08
S159	ArII	1	3.14	4.7±0.9	1.0±0.2
	ArIII	1	7.24	<0.7	<0.2
	SIII	1	5.82	7.5±0.7	0.46±0.05
	SIV	1	25.94	<0.25	<0.01
	NeII	1	0.940	75±4	0.75±0.03
DR22	ArII	3.2[b]	3.17	7.0±2	1.5±0.4
	ArIII	1.1[a]	7.59	2.2±0.5	0.46±0.10
	SIII	3.2[b]	9.32	6.6±1.7	0.42±0.09
	SIV	1.1[b]	33.33	<0.9	<0.06
	NeII	1.1[b]	0.973	60±6	0.60±0.06

*Assumed Standard Abundances: $S/H=1.6\times10^{-5}$; $Ar/H=4.7\times10^{-6}$; $Ne/H=1.0\times10^{-4}$

a. ν=10.7GHz

b. deduced from Brγ flux corrected for extinction.

Table 3

Revised* Sulfur Ionic Abundances $\frac{(n_x^i/n_h)}{(n_x/n_h)\ \text{standard}}$ For Objects From Papers I & II

PAPER	SOURCE	SIV	SIII	GALACTOCENTRIC RADIUS R(kpc)
I	G29.9-0.0	<0.06	1.0±0.39	5
	G12.8-0.2	0.04±0.01	0.22±0.05	6
	G45.1+0.1	0.08±0.03	0.37±0.08	7.5
	G75.84+0.4	0.06±0.006	1.21±0.06	10
	W3IRS1	0.14±0.04	0.67±0.12	12
	NGC7538IRS2	0.01±0.02	0.34±0.17	12.7
II	S88B	<0.07	0.48±0.34	9
	S156	----	1.00±0.18	11.7
	S106	<0.04	0.68±0.14	10
	NGC2170IRS1	<0.01	0.27±0.07	12.5
	M42(20"N^{9},C)	0.09±0.01	0.61±0.06	10.5

*Using the collision strengths of sulphur (Mendoza 1983).

Table 4

Assumed Physical Parameters of Observed Objects

Objects	n_e^{rms} (cm^{-3})	Distance d(kpc)	Galactocentric radius R(kpc)
G25.4-0.2	10^4	4.7±0.7(13.4±0.7) [near and far distances]	6.1
G45.5+0.06 Component A	5800	9.7	7.6
M8 (in a 9" beam)	5000	1.8	8.2
S159	10^4	4.5	11.7
DR22	3400	3.4±1.8	10

REFERENCES

Aitken, D.K., Roche, P.F., Spenser, P.M. and Jones, B. 1979, Ap. J. 233, 60.

Downes, D. and Rinehart, R., 1966, Ap. J. 144, 937.

Dyck, H. M., 1977, A. J. 82, 129.

Felli, M., Tofani, G. and D'Addario, L. R., 1974, Astr. Ap. 31, 431.

Forrest, W. J., McCarthy, J. F. and Houck, J.R., 1979, Ap. J. 233, 611.

Gillett, F.C., Forrest, W.J., Merrill, K.M., Capps, R.W., and Soifer, B.T., 1975 , Ap. J. 200. 609.

Herter, T., Helfer, H.L., Pipher, J.L., Forrest, W.J., McCarthy, J., Houck, J.R., Willner, S.P., Puetter, R.C., Rudy, R.J., 1981, Ap. J. 250, 186, Paper I.

Herter, T., Helfer, H.L., Pipher, J.L., Briotta, D.A. Jr., Forrest, W.J., Houck, J.R., Rudy, R.J. and Willner, S.P., 1982a, Ap. J. 262, 153, (Paper II).

Herter, T., Briotta, D.A., Jr., Gull, G. E., Shure, M. A. and Houck, J. R. 1982b, Ap. J. Letters,259, L25.

Herter, T., Helfer, H.L. and Pipher, J.L., 1983, A.A. Supplements, 51, 195.

Herter, T. 1984, in preparation.

Herter, T. and Krassner, J. 1984, in preparation.

Ho, P.T.P. and Haschick, A.D., 1981, Ap. J. 248, 622.

Israel, F.P. 1977, Astr. Ap. 59, 27.

Johnson, H.L., 1967, Ap. J. 147, 912.

Jones, B., Merrill, K.M., Stein, W., and Willner, S.P., 1980, Ap. J. 242, 141.

Krassner, J., Pipher, J. L., Savedoff, M. P. Soifer, B. T., 1983, A . J. 88, 972.

Lacasse, M.G., Herter, T., Krassner, J., Helfer, H.L. and Pipher, J.L. 1980, Astr. Ap. 86, 231.

Lacy, J. 1980, IAU Symposium #96, Infrared Astronomy, pub. D. Reidel, p. 237.

Lester, D., Dinerstein, H., Werner, M., Watson, D., Genzel, R., Townes, C., Storey, J. and Harvey, P., 1981, B.A.A.S. 13, 808.

Lynds, B.T. and O'Neill, E.J. Jr., 1982, Ap. J., 263, 130.

Matthews, H.E., Goss, W.M., Winnberg, A., and Habing, H.J. 1977, Astr. Ap. 61, 261.

McCarthy, J. F., 1980, Ph.D. thesis, Cornell University.

McCarthy, J. F., Forrest, W. J. and Houck, J. R., 1979, Ap. J. 233, 611.

Mendoza, C., 1982, IAU. Symposium 103 (Reidel).

Merrill, K.M., 1977. in The Interaction of Variable Stars with Their Environment, eds. R. Kippenhahn, J. Rake, W. Strohmeier, IAU Colloquium No. 42 (Bamberg: Veröffentlichunge der Remeis-Sternwarte Bamberg Bd. XI, Nr. 121), p. 446.

Peimbert, M., Torres-Peimbert, S., and Rayo, J. F., 1978, Ap. J. 220, 516.

Puetter, R.C., Russell, R.W., Soifer, B.T. and Willner, S.P. 1979, Ap. J. 228, 118.

Reifenstein, E.C. III, Wilson, T.L., Burke, B.F., Mezger, P.G. and Altenhoff, W.J. 1970, Astr. Ap. 4, 357.

Rossano, G.S. and Russell, R.W. 1981, Ap. J. 250, 227.

Russell, R.W., Soifer, B.T., and Willner, S.P., 1977, Ap. J. (Letters) 217, L149.

Shaver, P.A., McGee, R.X., Newton, L.M., Danks, A.C. and Pottash, S.R., 1983, M.N.R.A.S. 204, 53.

Talent, P.L. and Dufour, R.J., 1979, Ap. J. 233, 888.

Thackeray, A.D., 1950, M.N.R.A.S. 110, 343.

Thronson, H.A., Jr., Loewenstein, R.F., and Stokes, G.M., 1979, A. J. 84, 1328.

Turner, B.E., Balick, B., Cudaback, D.D., Heiles, C. and Boyle, R.J., 1974, Ap. J. 194, 279.

Wink, J.E., Altenhoff and Webster, W.J., Jr., 1975, Astr. Ap. 38, 109.

Woodward, C.E., Pipher, J.L., Helfer, H.L., Sharpless, S., Lacasse, M., Herter, T. Willner, S.P., 1984, in preparation.

Woolf, N.J., 1961, P.A.S.P. 73, 206.

Wright, E.L., Lada, C.J., Fazio, G.G., Kleinmann, D.E. and Low, F.J., 1977, A. J. 82, 132.

Wynn-Williams, C.G., Downes, D. and Wilson, T.L., 1971, Astrophys. Ltrs., 9, 113.

Zeilik, M. II, 1979, A. J. 84, 341.

Zeilik, M. II, and Heckert, P.A., 1977, A. J. 82, 824.

Zeilik, M. II, Kleinmann, D.E., Wright, E.L., 1975, Ap. J. 119, 401.

Figure Captions

1 a. Ratio of $n_x/n_{standard} = (Ne^+/H)/(Ne/H)_{standard}$ as a function of galactocentric radius R; $12+\log(Ne/H)_{standard} = 8.0$.

b. Ratio of $n_x/n_{standard} = (Ne/H)/(Ne/H)_{standard}$ as a function of galactocentric radius R; $12+\log(Ne/H)_{standard} = 8.0$.

c. Ratio of $n_x/n_{standard} = (Ar/H)/(Ar/H)_{standard}$ as a function of galactocentric radius R; $12+\log(Ar/H)_{standard} = 6.67$.

d. Ratio of $n_x/n_{standard} = (S/H)/(S/H)_{standard}$ as a function of galactocentric radius R; $12+\log(S/H)_{standard} = 7.20$.

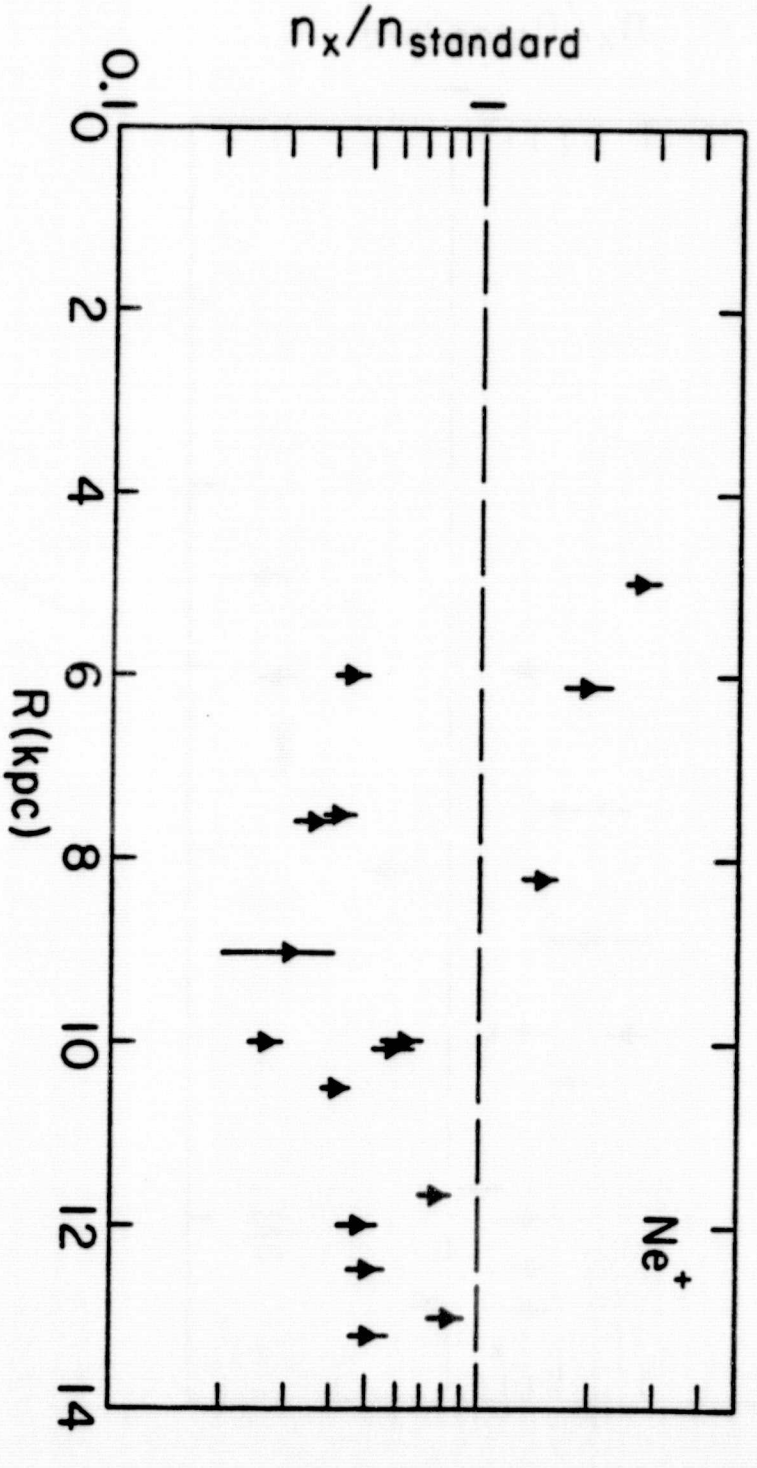

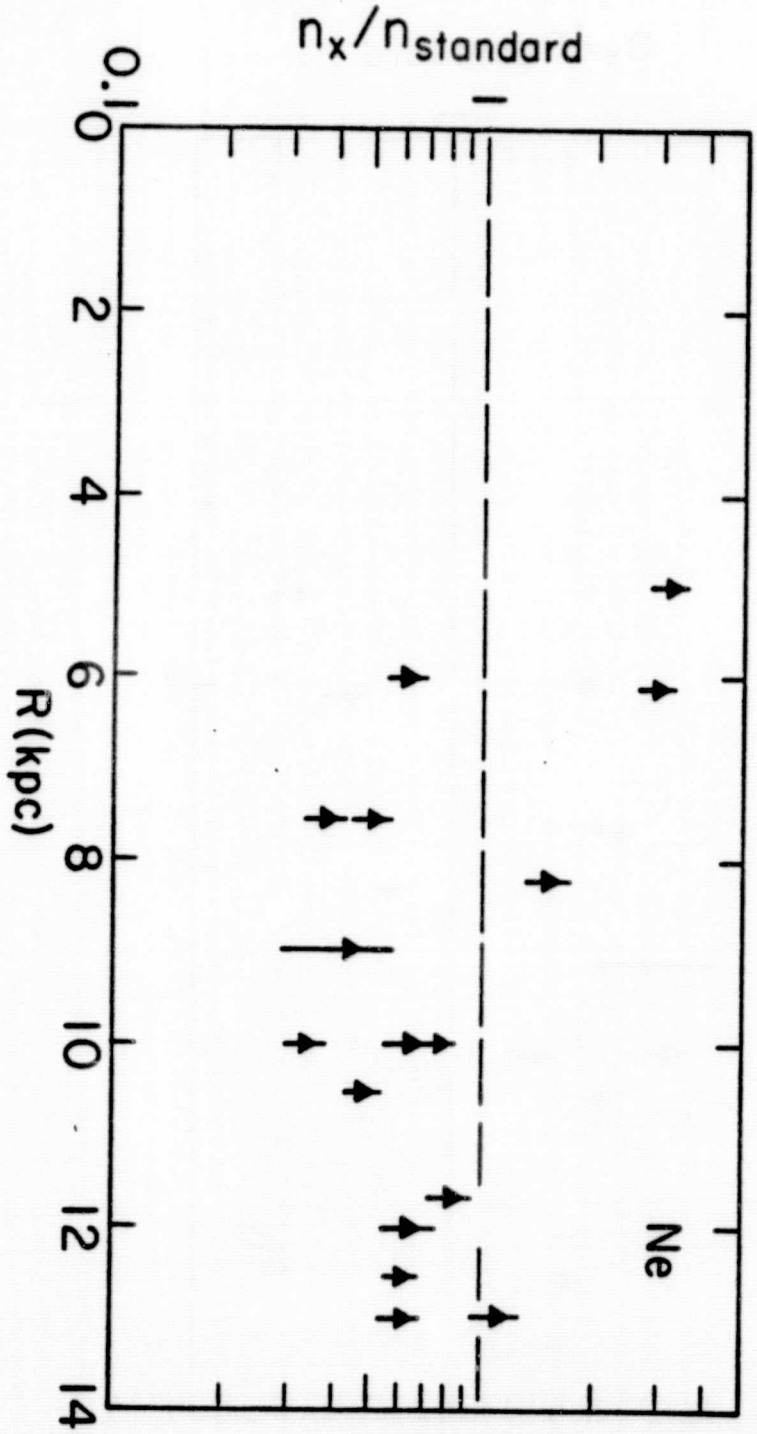

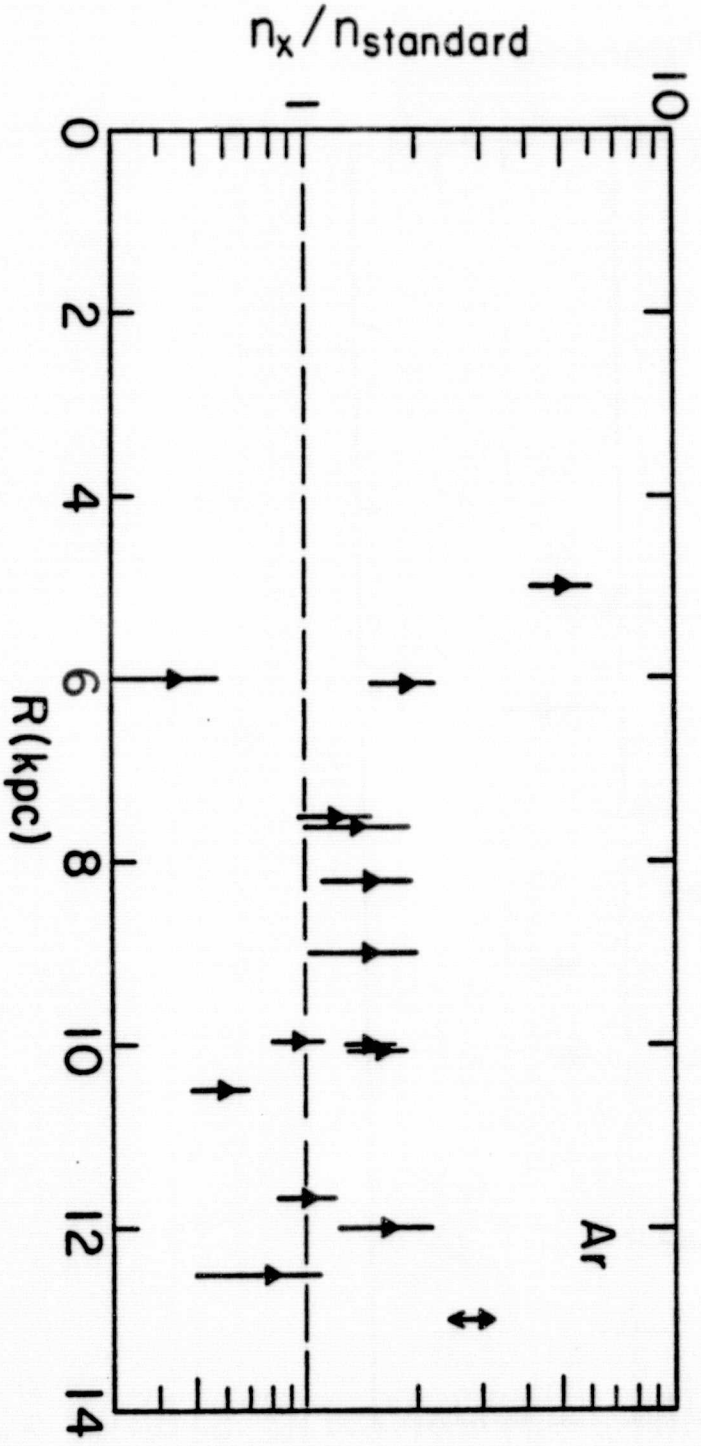

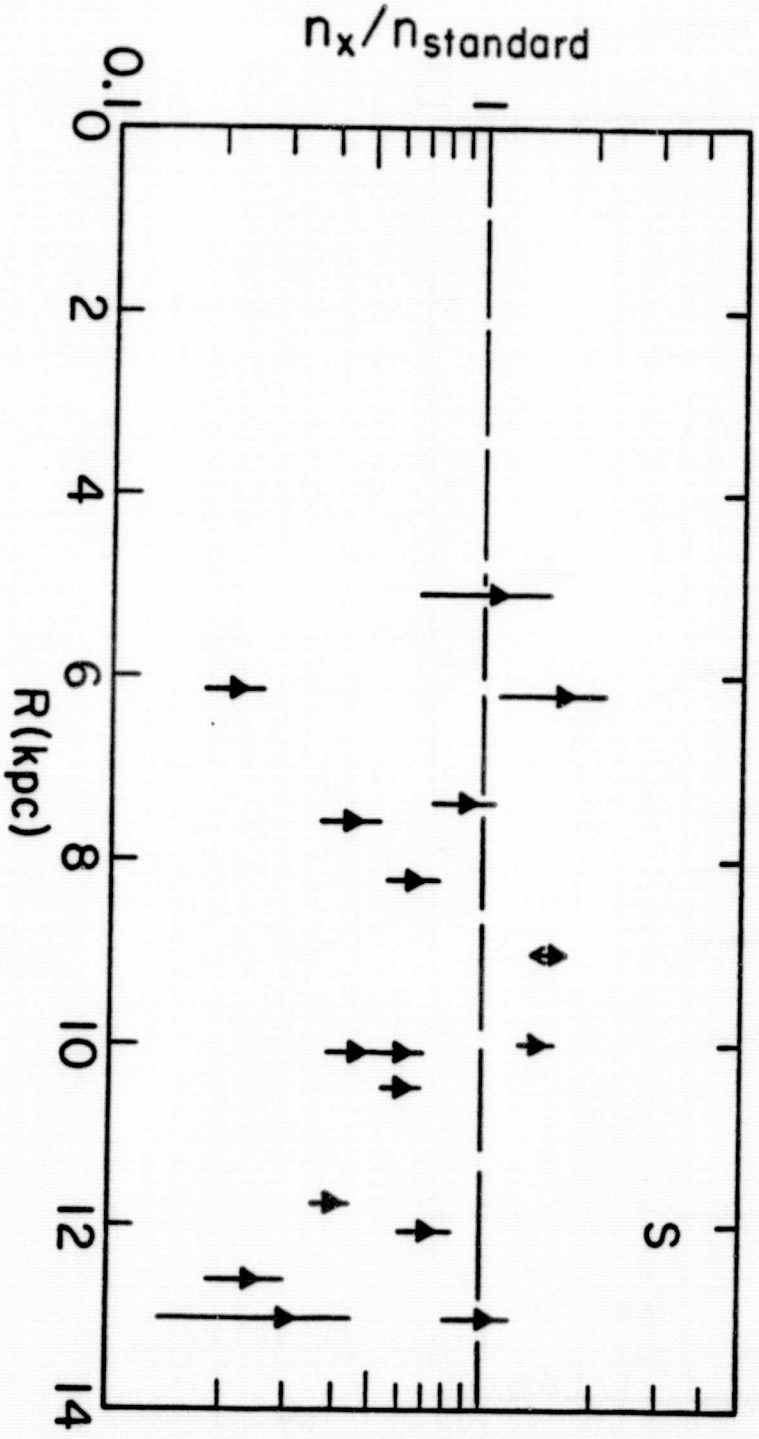

AUTHOR'S ADDRESSES

J. L. Pipher
University of Rochester
Department of Physics and Astronomy
Rochester, NY 14627

H. L. Helfer
University of Rochester
Department of Physics and Astronomy
Rochester, NY 14627

T. Herter
Grumman Aerospace Corporation
Plant 26
Bethpage, NY 11714

D. A. Briotta, Jr.
Cornell University
Department of Astronomy
Space Science Building
Ithaca, NY 14853

J. R. Houck
Cornell University
Department of Astronomy
Space Science Building
Ithaca, NY 14853

S. P. Willner
Harvard-Smithsonian Center for Astrophysics
60 Garden Street
Cambridge, MA 02138

B. Jones
Center for Astrophysics and Space Science
University of California at San Diego
C-011
La Jolla, CA 92093